

AD-766 278

**NONLINEAR SYSTEM MODELING AND ANALYSIS WITH
APPLICATIONS TO COMMUNICATIONS RECEIVERS**

SIGNATRON, INC.

**PREPARED FOR
ROME AIR DEVELOPMENT CENTER**

JUNE 1973

DISTRIBUTED BY:



**National Technical Information Service
U. S. DEPARTMENT OF COMMERCE**

AD-766278

**NONLINEAR SYSTEM MODELING AND ANALYSIS
WITH APPLICATIONS TO
COMMUNICATIONS RECEIVERS**

Edited by
James W. Graham
Vice President

Leonard Ehrman
Senior Consulting Scientist

SIGNATRON, Inc.

SEP 1977

Approved for public release;
distribution unlimited.

This report has been reviewed by the Rome Air Development Center and
is approved.

APPROVED:

John F. Spina

JOHN F. SPINA
Project Engineer

APPROVED:

Joseph J. Naresky

JOSEPH J. NARESKY, Chief
Reliability & Compatibility Division

FOR THE COMMANDER:

Carlo Crocetti

CARLO P. CROCETTI
Chief, Plans Office

If this copy is not needed, return to:
RADC (RBCM), GAFB, N.Y. 13441

ia

UNCLASSIFIED

Security Classification

DOCUMENT CONTROL DATA - R & D

(Security classification of title, body of abstract and indexing annotation must be entered when the overall report is classified)

1. ORIGINATING ACTIVITY (Corporate author) SIGNATRON, Incorporated 27 Hartwell Avenue Lexington, MA 02173		1a. REPORT SECURITY CLASSIFICATION UNCLASSIFIED
		1b. GROUP N/A
3. REPORT TITLE NONLINEAR SYSTEM MODELING AND ANALYSIS WITH APPLICATIONS TO COMMUNICATIONS RECEIVERS		
4. DESCRIPTIVE NOTES (Type of report and inclusive dates) Interim Report - April 1970 - September 1972		
5. AUTHOR(S) (First name, middle initial, last name) James W. Graham Leonard Ehrman		
6. REPORT DATE June 1973	7a. TOTAL NO. OF PAGES 746	7b. NO. OF REFS 0
8a. CONTRACT OR GRANT NO. F30602-70-C-0008 Job Order No.: 45400237	8b. ORIGINATOR'S REPORT NUMBER(S) None 9b. OTHER REPORT NO(S) (Any other numbers that may be assigned this report) RADC-TR-73-178	
10. DISTRIBUTION STATEMENT Approved for public release; distribution unlimited.		
11. SUPPLEMENTARY NOTES None	12. SPONSORING MILITARY ACTIVITY Rome Air Development Center (RBCM) Griffiss Air Force Base, New York 13441	
13. ABSTRACT The objective of the contract was to develop reliable, realistic, and useful mathematical models of communication receivers that must operate in the presence of interfering signals. Major emphasis was placed upon understanding basic phenomena and developing techniques needed to provide a capability of modeling receiver structures for multi-signal inputs. During the study considerable effort was placed upon modeling so that the effects of co-channel and adjacent channel interfering signals having arbitrary modulations in the presence of receiver nonlinearities might be effectively investigated. Therefore, methods of investigating quasi-linear systems having significant frequency selectivity were developed. Matters relating to intermodulation and crossmodulation distortion as well as gain compression, desensitization, and dynamic range were of primary concern. The problem formulation and methods of attack were guided by the desire to develop practical methods that will be effective in an investigation of receiver performance degradation. Associated with these developments was a companion effort to develop effective computer programs that will permit efficient practical application of the basic material presented in this work.		
<p style="text-align: center;">Reproduced by NATIONAL TECHNICAL INFORMATION SERVICE U.S. Department of Commerce Springfield VA 22151</p>		

DD FORM 1 NOV 68 1473

UNCLASSIFIED

Security Classification

if

UNCLASSIFIED
Security Classification

14. KEY WORDS	LINK A		LINK B		LINK C	
	ROLE	WT	ROLE	WT	ROLE	WT
Nonlinear Circuit Analysis Electromagnetic Compatibility Nonlinear Transfer Functions Nonlinear Canonic Models						

UNCLASSIFIED

Security Classification

CONTRIBUTORS

This book is the result of research conducted by the staff of SIGNATRON, Inc. The principal contributors to the study were:

Phillip A. Bello
Charles J. Boardman
Gerald J. Brown
Leonard Ehrman
James W. Graham
S. Ahmed Meer
John O'Donnell

The book was prepared by the editors. Other staff members who provided material particularly helpful in the preparation of specific chapters are acknowledged in the preface.

PREFACE

This book is the result of an intensive theoretical and experimental effort performed by SIGNATRON, Inc., Lexington, Massachusetts, for the Air Force Systems Command, Rome Air Development Center, Griffiss Air Force Base, New York, under Contract F30602-70-C-0008 entitled "Communications Receivers Interference Modeling". Mr. John F. Spina was the cognizant effort engineer at the Rome Air Development Center.

The objective of the contract was to develop reliable, realistic, and useful mathematical models of communication receivers that must operate in the presence of interfering signals. Major emphasis was placed upon understanding basic phenomena and developing techniques needed to provide a capability of modeling receiver structures for multi-signal inputs. During the study considerable effort was placed upon modeling so that the effects of co-channel and adjacent channel interfering signals having arbitrary modulations in the presence of receiver nonlinearities might be effectively investigated. Therefore, methods of investigating quasi-linear systems having significant frequency selectivity have been developed. Matters relating to intermodulation and crossmodulation distortion as well as gain compression, desensitization, and dynamic range have been of primary concern. The problem formulation and methods of attack have been guided by the desire to develop practical methods that will be effective in an investigation of receiver performance degradation. Associated with these developments has been a companion effort to develop effective computer programs that will permit efficient practical application of the basic material presented in this work.

Preceding page blank

It has been necessary and convenient to make a distinction between two types of modeling, namely, nonlinear system function modeling and nonlinear circuit modeling. Nonlinear system function modeling involves extensive application of the Volterra series and the concept of nonlinear system canonic models to develop simplified input-output relationships. Nonlinear circuit modeling and analysis provides a detailed circuit-oriented model in terms of active devices and circuit components. Nonlinear system functions for a particular system can be determined either by a nonlinear circuit analysis or by measurement. Much of the material presented in this book should be viewed in many ways as a research report. Further work continues in its development and practical application. The book will be of interest to communications system engineers and circuit design engineers. Emphasis has been placed upon developing new and systematic methods for investigating and, hopefully, designing equipments intended to function more successfully in a multi-signal electromagnetic interference environment.

The contributions of many individuals to the material presented in this book are gratefully acknowledged. The patient and constructive criticism of our RADC sponsors, particularly Mr. John Spina, Dr. Donald Weiner, and Mr. Jacob Scherer, is appreciated. The work of several present and former SIGNATRON personnel has been particularly helpful in the preparation of the following chapters:

Chapter 2: S.A. Neer, N. Johnson

Chapter 3: P.A. Bello, C.J. Boardman, J.J. Bussgang

Chapter 4: J.O'Donnell, S. Richman

SIGNCAP, the nonlinear circuit analysis program used extensively in our work, was developed by G.J. Brown of SIGNATRON. R. Neal performed most of the solid state device experiments reported in the book. All experimental work on the HF receiver and associated vacuum-tube experiments was performed by Atlantic Research under subcontract to SIGNATRON. Mr. William Duff and Mr. Thomas Roherty were particularly helpful. We also wish to acknowledge the skilled contribution of Mrs. Rita Pavlica and Mrs. Ilse Wegener in the preparation of the manuscript for publication.

Lexington, Massachusetts
May 1973

J.W. Graham
L. Ehrman

**NONLINEAR SYSTEM MODELING AND ANALYSIS
WITH APPLICATIONS TO
COMMUNICATIONS RECEIVERS**

CONTENT.

Chapter 1

Modeling and Analysis of Quasi-Linear Systems

	Page
1.1 Introduction	1
1.2 Background to the Problem	3
1.3 Multiple Input Effects in Nonlinear Systems without Memory	9
1.3.1 Gain Compression and Desensitization	10
1.3.2 Crossmodulation	11
1.3.3 Intermodulation	12
1.4 Analysis of Nonlinear Systems with Memory	13
1.5 An Example of a Nonlinear System with Memory	15
1.6 Alternate Forms of the Volterra Series	24
1.7 Multi-Tone Output Response in Terms of Nonlinear Transfer Functions	27
1.8 Two-Tone Input Example	30
1.9 Frequency-Conversion as a Mild Nonlinearity	36
1.9.1 Equivalent Amplifier Concept	36
1.9.2 Mixer p,q Response	37
1.10 Determining the Nonlinear Transfer Functions H_n for a Multicarrier System	39

Chapter 2

Small Signal Nonlinear Circuit Analysis

2.1 Introduction	40
2.1.1 Frequency Domain Approach	40
2.1.2 Sinusoidal Inputs	41
2.1.3 Applicability of the Volterra Series	46
2.1.4 "Small" and "Large" Signal Criteria and Truncation Error	47
2.2 Nonlinear Circuit Analysis	48
2.2.1 Introduction	48

2.2.2	Single Nonlinear Element Circuit	52
2.2.2.1	Nonlinear Conductance $K(v_2)$	54
2.2.2.2	Current-Controlled Nonlinearity	64
2.2.2.3	Zero-Memory Dependent Nonlinearity	68
2.2.2.4	Nonlinearity with Memory	71
2.2.3	General Single-Input Analysis	73
2.2.3.1	Introduction	73
2.2.3.2	General Procedure for Single-Input Network	75
2.2.3.3	An Example	83
2.2.3.4	Tabulation of Nonlinear Source Terms	87
2.2.4	Recurrence Relations for the Nonlinear Source Term	90
2.2.4.1	Zero-Memory Independent Nonlinearity	94
2.2.4.2	Capacitance-Memory Independent Nonlinearity	97
2.3	Cascading of Networks with Nonlinear Interaction	99
2.3.1	Introduction	99
2.3.2	Cascade Relations for Non-Interacting Systems	100
2.3.3	Nonlinear Interactions in Cascaded Nonlinear Stages	104
2.3.3.1	Nonlinear Transfer Functions of Cascade Stages	105
2.3.3.2	Two Stage Cascade	109
2.3.3.3	Conclusions and Numerical Comparison of Cascade Techniques	124
2.4	Multiple-Input Nonlinear Circuit Analysis	128
2.4.1	Three Node Example	128
2.4.2	Two-Input Volterra Series	131

Chapter 3

Canonic Models for Nonlinear Systems

3.1	Introduction	138
3.2	Nonlinear Response to a Sum of Narrowband Signals	140
3.3	Frequency Power Series Canonic Model	149
3.4	Tapped Delay Line Canonic Model	161
3.5	Frequency Power Series Canonic Model: Sinusoidally Modulated Signals	170
3.5.1	Crossmodulation and Desensitization	170
3.5.2	AM-AM Crossmodulation	172
3.5.2.1	Predetection Spectrum: AM-AM	172
3.5.2.2	Post-Detection Spectrum: AM-AM	178
3.5.2.3	Simplified Assumption Analysis: AM-AM	181

3.5.3	FM-AM Crossmodulation	184
3.5.3.1	Demodulated Spectrum	184
3.5.4	AM-FM and FM-FM Crossmodulation	190
3.6	Simplified Frequency Power Series Canonic Model	194

Chapter 4

Large Excitation Nonlinear Analysis

4.1	Introduction	205
4.2	Large-Excitation Time-Domain Formulation	208
4.2.1	Direct Solution by Numerical Integration	210
4.2.2	Power-Series Solution for a Memoryless Example	210
4.3	Large-Signal Perturbation Method	212
4.3.1	State Equations for Strongly-Driven and Weakly-Driven Equivalent Systems	213
4.3.2	Power-Series Perturbation Solution Example	217
4.3.3	Separation of the Small-Signal Perturbation System into Time-Variant Linear Subsystems	223
4.3.4	Small-Signal Equations for the Time-Variant Nonlinear Transfer Functions	226
4.3.4.1	First-Order Transfer Function	228
4.3.4.2	Second-Order Nonlinear Transfer Function	231
4.3.4.3	Third-Order Nonlinear Transfer Function	233
4.4	Formulation of State Equations	237
4.4.1	First Example	237
4.4.2	A Formal Method	240
4.4.3	A Second Example	242
4.5	Multivariable Formulation of the Perturbation Method	249
4.6	Direct Time-Domain Solution of Nonlinear State Equations	258
4.6.1	Numerical Solution of Nonlinear State Equations	258
4.6.2	Numerical Solution of the Dynamic Operating Point Differential Equation	265
4.6.3	Numerical Solution of the Time-Varying Nonlinear Transfer Function Perturbation Equations	270

Chapter 5
Electronic Device Modeling

5.1	Introduction to Electronic Device Nonlinear Modeling	276
5.2	Semiconductor Diode	277
5.2.1	Ideal Semiconductor Diode	278
5.2.1.1	Static Characteristics	278
5.2.1.2	Junction Depletion-Layer Capacitance	278
5.2.1.3	Avalanche Breakdown	283
5.2.2	Total Equivalent Nonlinear Circuit Model of a Semiconductor Diode	285
5.2.3	Incremental Equivalent Nonlinear Circuit Model of a Semiconductor Diode	288
5.2.4	Examples of Semiconductor Diodes	294
5.2.4.1	Forward Static Characteristics	294
5.2.4.2	Reverse Characteristics	299
5.2.4.3	Switching Characteristics of Junction Diodes	303
5.3	Bipolar Junction Transistor Model	303
5.3.1	Linear Incremental T Model	305
5.3.1.1	Linear T Parameters	305
5.3.1.2	Two-Port Linear Network Parameters	310
5.3.2	Nonlinear Incremental T Model	316
5.3.2.1	Base-Emitter Exponential Nonlinearity	318
5.3.2.2	Avalanche Nonlinearity	324
5.3.2.3	h_{FE} Nonlinearity	328
5.3.2.4	Nonlinear Incremental Current Generator $g(v_2, v_3 - v_1)$	332
5.3.2.5	Collector-Capacitance Nonlinearity	337
5.3.2.6	Emitter-Capacitance Nonlinearity	338
5.3.2.7	Base Resistance r_b	342
5.3.2.8	Collector Resistance r_c	343
5.3.2.9	Capacitances C_1 and C_3	343
5.3.2.10	Parasitic Elements	344
5.3.2.11	Summary of the Bipolar Transistor Nonlinear Incremental Model	344
5.4	Nonlinear Models of Field-Effect Transistors	349
5.5	Nonlinear Charge-Control Model of Bipolar Transistors	350
5.6	Vacuum Tube Nonlinear Models	356
5.6.1	Vacuum Diodes	356
5.6.2	Vacuum Triode	359
5.6.2.1	Vacuum Triode Theory	359
5.6.2.2	Vacuum Triode Measurements	368
5.6.3	Vacuum Pentode	374

5.6.3.1	Vacuum Pentode Theory	374
5.6.3.2	Vacuum Pentode Measurements	380

Chapter 6
Multiple-Tone Input Applications

6.1	Introduction	391
6.2	Power Relationships for Multi-Tone Input Applications	392
6.2.1	First-Order Response	392
6.2.2	Second-Order Response	395
6.2.3	Third-Order Response for Two-Tone Input	397
6.2.4	Fourth-Order Response for Three-Tone Input	399
6.2.5	Summary for Equal-Power Two-Tone Testing	403
6.2.5.1	Two-Tone Test of an Amplifier	403
6.2.5.2	Two-Tone Test of a Small Local Oscillator Mixer	406
6.2.5.3	General Case for n th Order Output	406
6.2.6	Output Powers for High Input Impedance Nonlinear Amplifiers	409
6.3	Small-Signal Input Limit	411
6.4	Single-Stage Untuned Transistor Amplifier	415
6.4.1	First-Order Linear Response	419
6.4.2	Second and Third-Order Intermodulation Distortion for Two-Tone Excitations	423
6.4.2.1	Amplitude Dependence	423
6.4.2.2	Frequency Dependence	428
6.4.3	Excitation of the Untuned Amplifier as a Small-Local Oscillator Mixer	430
6.4.4	Emitter Capacitance Nonlinearity	432
6.4.5	Gain Compression/Expansion	435
6.5	Two-Stage Tuned Amplifier	440
6.5.1	Description of the Two-Stage Amplifier	440
6.5.2	Second and Third-Order Intermodulation Distortion	445
6.5.3	Two-Stage Amplifier Desensitization	450
6.6	Intermodulation Distortion in Vacuum Tubes	453
6.6.1	Untuned Triode Amplifier	453
6.6.2	Untuned Pentode Amplifier	459
6.7	Large-Signal Multi-Tone Input Time-Domain Analysis	465
6.7.1	Two-Tone Time-Domain Analysis	467
6.7.2	Three-Tone Time-Domain Analysis	472
6.7.3	Comparison of Small-Signal Time-Domain Solution Prediction with Nonlinear Transfer Function Prediction and Experimental Measure- ments	474

**6.7.4 Distortion Dependence Upon Local
Oscillator Level**

481

Chapter 7

Communications Receiver Applications

7.1 Solid-State VHF Receiver	492
7.2 Modeling of the Solid-State Receiver	
7.2.1 An Overview of Experimental Modeling	501
7.2.2 Interstage Network Modeling	505
7.2.2.1 Interstage Network Modeling Example	508
7.3 Tuner Modeling	514
7.3.1 Second-Order Nonlinear Transfer Function (Equivalent First-Order Nonlinear Transfer Function)	517
7.3.2 Third-Order Nonlinear Transfer Function (Equivalent Second-Order Nonlinear Transfer Function)	520
7.3.3 Fourth-Order Nonlinear Transfer Function (Equivalent Third-Order Nonlinear Transfer Function)	522
7.4 IF Preamplifier Modeling	524
7.4.1 First-Order Transfer Function Measurement and Prediction	524
7.4.2 Second-Order Nonlinear Transfer Function	526
7.4.3 Third-Order Nonlinear Transfer Function	526
7.5 IF Amplifier Modeling	528
7.5.1 First-Order Transfer Function Measurement and Prediction	534
7.5.2 Third-Order Nonlinear Transfer Function	535
7.6 Detector and AGC Effects	537
7.6.1 The AM Detector	538
7.6.2 FM Detector	541
7.6.3 AGC	544
7.7 Complete Predetection Receiver	547
7.7.1 Equivalent First-Order Nonlinear Transfer Function	549
7.7.2 Equivalent Second-Order Nonlinear Transfer Function	552
7.7.3 Equivalent Third-Order Nonlinear Transfer Function	554
7.8 Gain Compression/Expansion in the VHF Receiver IF Amplifier	561

7.9	Crossmodulation in the VHF Receiver IF Amplifier	567
7.10	Waveform Distortion Due to Crossmodulation, VHF Receiver IF Amplifier	570
7.10.1	Unmodulated Signal; AM Interference	572
7.10.2	AM Desired Signal - AM Interference	577
7.11	Predetection Tapped Delay Line Canonic Modeling, VHF Receiver RF Tuner	583
7.11.1	A Known Test Case	583
7.11.2	Wideband Crossmodulation in the VHF Receiver Tuner	590
7.12	Nominal Receiver Modeling	601
7.12.1	Paramaterizing of the Nominal Tuner	601
7.12.2	Nominal Tuner Results	602
7.12.3	Nominal Receiver Parameter Variations	608
7.13	HF Receiver Modeling	609
7.13.1	Introduction	609
7.13.2	Circuit Model of the Translator	611
7.13.2.1	Linear Passive Interstages	614
7.13.2.2	Operating Point Data	627
7.13.3	Mixer Performance	631
7.13.4	RF Amplifier Performance	633
7.13.5	Complete RF Translator Response	636
7.13.5.1	Simplified Power-Series Modeling of Vacuum Tube Stages	636
7.13.5.2	Translator Nonlinear Transfer Functions	639

Appendix A

SIGNCAP I - Nonlinear Circuit Analysis Computer Program

A.1	Introduction	643
A.2	SIGNCAP Analysis Techniques	645
A.2.1	Nodal Admittance Analysis	645
A.2.2	Segmentation and Cascade Analysis	653
A.2.3	SIGNCAP Processing	655
A.2.4	SIGNCAP Data Preparation	657
A.3	Circuit Elements and Models	659
A.4	SIGNCAP Data Input Structure	
A.4.1	The SIGNCAP Input	662
A.4.1.1	Comment	663
A.4.1.2	Command	663
A.4.1.3	Linear Elements	665
A.4.1.4	Nonlinear Elements	667
A.4.1.5	Solution Control	672

A.4.1.6	Output Control	677
A.5	Examples	679
A.5.1	Single-Stage Transistor Amplifier	679
A.5.2	VHF Receiver	687
Appendix B		
Nonlinear Modeling from Transistor Specification Data		
B.1	Base-Emitter Exponential Nonlinearity	701
B.2	h_{FE} Nonlinearity	701
B.3	Avalanche Nonlinearity	702
B.4	Collector Capacitance Nonlinearity	704
B.5	Emitter Capacitance Nonlinearity	705
B.6	Base Resistance r_b	705
B.7	Collector Resistance	707
B.8	Capacitances C_1 and C_3	707
B.9	Summary of 2N918 Parameters	707
Bibliography		709
Glossary of Principal Symbols		719
Index		729

CHAPTER 1

MODELING AND ANALYSIS OF QUASI-LINEAR SYSTEMS

1.1 Introduction

The radio and intermediate frequency stages of most communications receiving systems serve to amplify the desired signal and reject unwanted signals by employing high gain and frequency selectivity. Thus, the output of an amplifier should be linearly proportional to its input signal, while a frequency converter, or mixer, which is nonlinear with respect to interaction between the RF and local-oscillator inputs, should have an IF output which is linearly proportional to the RF input. Upon close inspection, however, most of these circuits are actually mildly nonlinear. For small enough input signals they appear to be linear, but, as the input signal level increases, the input-output relationship deviates from linearity. If the input signal becomes sufficiently large, the circuit can be driven into highly nonlinear regions of operation, such as saturation and cutoff.

Two methods of analyzing nonlinear systems are developed in this book. The first method is applied to mildly driven nonlinear circuits. They are analyzed by a time-invariant functional series known in mathematics as a Volterra series. The Volterra series is characterized by a set of time-domain functions called nonlinear impulse responses, while in the frequency domain, it is characterized by a set of frequency-domain functions called nonlinear transfer functions. The nonlinear transfer functions and the nonlinear impulse responses form

Fourier transform pairs, in the same manner as do the impulse response and transfer function of a linear system. Circuit analysis techniques have been developed for determining the nonlinear transfer functions of a circuit from its nonlinear equivalent circuit model.

The second method is applied to strongly-driven nonlinear circuits. They are analyzed by employing numerical integration techniques to obtain time-domain solution of the nonlinear differential equations of the circuit. One special case arises when the circuit is driven by several signals of which only one is large and also periodic. This case frequently arises in the analysis of mixer circuits. The strongly-driven circuit can then be considered as being mildly driven by the remaining (small) signals and the results interpreted to define time-varying nonlinear transfer functions for the small signals.

Given the nonlinear transfer functions for the circuit, it is possible to determine the nonlinear input-output relationships for an arbitrary set of small input signals through either a convolutional approach or a Fourier transform approach. Either of these approaches can be time-consuming to implement, even on a high-speed computer. System models have therefore been developed for mildly-driven nonlinear circuits, which permit the circuit output to be computed with a minimum of computational difficulty. These system models are called nonlinear canonic models, and are parameterized by quantities that depend on the nonlinear impulse responses and/or the nonlinear transfer functions of the circuit.

1.2 Background to the Problem

The function of a communication receiver is to amplify a desired radio-frequency signal and, through appropriate detectors, demodulate the information carried by the signal and make it available at the receiver output. The use of demodulation makes the receiver an inherently nonlinear system. Two types of detectors are usually found in receivers. The first is the frequency converter, or mixer, which is used to shift the center frequency of the signal. Mixers can be either large or small-signal nonlinear systems. Receivers usually have at least one stage of conversion, but receivers with as many as three mixer stages are found. Each mixer is a deliberately nonlinear stage, usually followed by an interactive bandpass filter tuned to the mixer's desired output frequency.

The second type of detector is used to demodulate the desired information. The structure of the demodulator is dependent upon the modulation employed at the transmitter. Typical demodulators include envelope detectors, coherent detectors or product demodulators, and limiter-frequency discriminators for FM demodulation. Frequency converters are often referred to as first detectors while demodulators are frequently called second detectors.

The remaining stages of a receiver are normally designed to be linear. However, they are built with electronic components such as transistors or vacuum tubes which are more or less nonlinear. Figure 1.1 shows a simplified block diagram of a single-conversion communications receiver. It is divided into five stages: RF amplifier, mixer, IF preamplifier, IF amplifier, and second detector

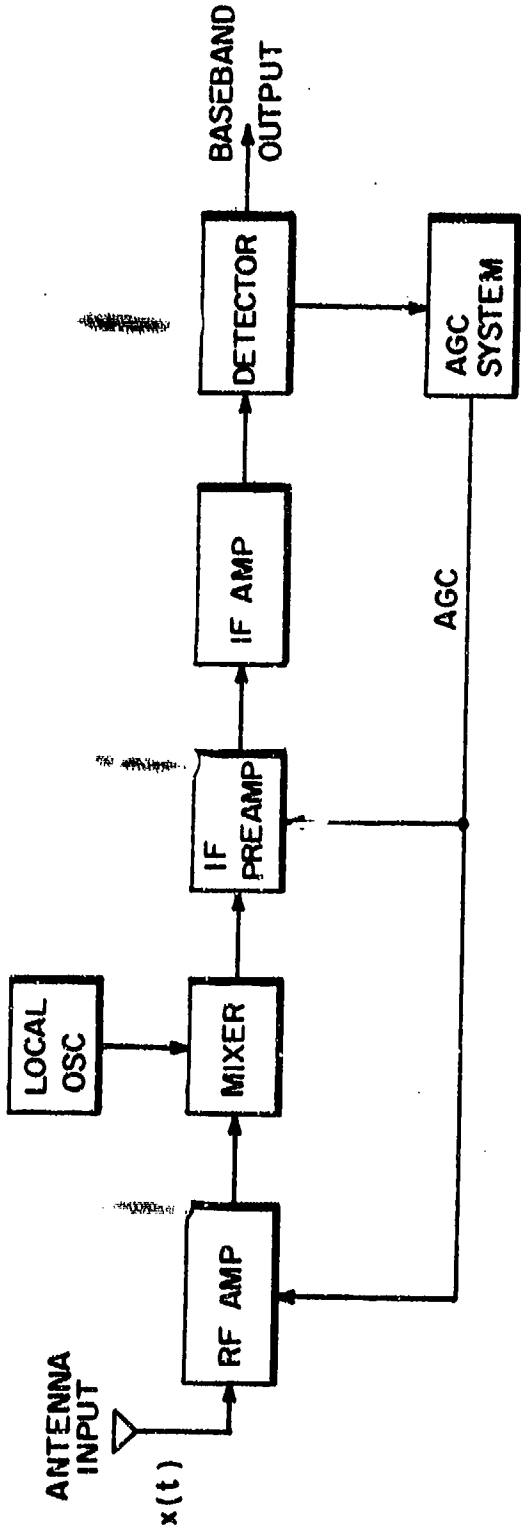
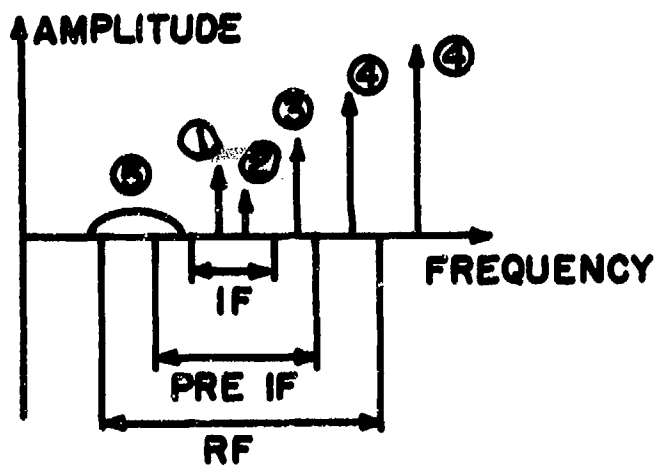


Fig. 1.1. Block Diagram of a Communications Receiver.

and two ancillary but important blocks, the local-oscillator and the AGC system. The AGC controls the RF amplifier and IF pre-amplifier gain generally by varying the operating points of one or more active devices in each amplifier. The nonlinear characteristics of the active devices also change as the operating point is changed. This effect must be included in an adequate receiver model. The antenna gain and impedance are both functions of frequency. This must also be taken into account in the modeling of a receiver.

Although a receiver is tuned to the desired signal frequency, the radio spectrum contains other signals beside the desired one. Figure 1.2 shows typical signals which might be present at the receiver input. The desired signal, 1, falls in the IF passband. A co-channel interferer, 2, is also in the IF passband. An adjacent channel interferer, 3, falls out of the IF passband but in the pre-IF passband. Two out-of-band interferers, both marked 4, fall out of the pre-IF passband but one is in the RF and one is out of the RF band. Signals 1 through 4 are shown as narrowband signals relative to the several receiver bandwidths. The interferer 5 is a wideband interferer with a spectrum spanning the range from out of the RF band to inside the pre-IF band.

Throughout our work we shall be much concerned with methods for effective prediction and accurate analysis of the distortion generated in the receiving system by the nonlinear interaction of multiple-input signals in the physical nonlinearities inherent in the electronic circuits constituting the physical receiving system.



- INPUT
- DESIRED SIGNAL ①**
 - CO-CHANNEL INTERFERENCE ②**
 - ADJACENT CHANNEL INTERFERENCE ③**
 - OUT-OF-BAND INTERFERENCE ④**
 - WIDEBAND INTERFERENCE ⑤**

Fig. 1.2 The Communications Interference Problem.

The approach developed is to perform a frequency-domain analysis of the receiver by using a Volterra functional series (Volterra, 1930). The Volterra series was first applied to nonlinear circuit problems by Wiener (1942). Little application of Wiener's work was made from 1942 until about 1967. At that time Narayanan (1967), working at the Bell Telephone Laboratories, applied the technique to the analysis of transistor amplifier distortion. The work was then extended to the analysis of nonlinear systems with Gaussian inputs, (Maurer, 1968), distortion in cascaded transistor amplifier (Narayanan, 1969), and distortion in feedback amplifiers (Narayanan, 1970). H. Poon (1972) has used Volterra analysis of the charge control transistor model for third-order amplifier distortion studies, and Kuo and Witkowski (1972) have developed a computer program for computing the distortion of amplifier circuits by using Volterra techniques. Volterra analysis has also been used in an experimental cross-modulation characterization of amplifiers (Meyer, 1972). From the late 1950's on, there has been a continuous effort in the application of Volterra analysis to nonlinear system theory. Much of this work has focussed on the problem of noninteracting systems. [Wiener (1958), Brilliant (1958), George (1960), Zames (1960), Parente (1966), Bedrosian and Rice (1971)].

Research in the electromagnetic interference and compatibility field has almost completely dealt with power-series analysis of zero-memory nonlinear systems. When memory has been included in the system, it has been through ad hoc introduction of noninteracting input and output filters. (Einstein, et.al., 1967). It will be shown that the zero-memory nonlinear power-series is a special case of the Volterra series. Although partial

results of the work leading to this book have been reported elsewhere, [SIGNATRON (1971), Bello (1972), Ehrman (1972), O'Donnell (1972), Graham (1972)], this book presents in detail the techniques that have been developed and the results achieved.

The method of analysis used in the study is primarily a frequency domain analysis of the complete nonlinear circuit by using accurate nonlinear device models and including all interaction. The resulting frequency-domain kernels, which we have called nonlinear transfer functions, and their time-domain counterparts, called nonlinear impulse responses, are then used to parameterize nonlinear system models called canonic models. The receiver response to an arbitrary input can be found in either the time or frequency domain through use of the canonic models. By building upon the theoretical and experimental background developed since Volterra's initial work, a unified system of modeling complete nonlinear systems has been developed, implemented, and validated. The development, unification, and application of these techniques to the communication receiver modeling problem was first performed in the effort leading to the material presented in this book. The application of complex signals to the development of the nonlinear system canonic models and the concept of time-varying Volterra series are also new results.

The purpose of the original investigation was to develop methods of modeling communication circuits in a multi-signal environment. Before this work, there were two primary means of predicting the response of a receiver to an arbitrary set of input signals. The first was to use data available in a set of

spectrum-signature measurements. Unfortunately, much of the spectrum signature data can not be extrapolated to the interference problem that must be solved. The second method was to model the receiver by using power series and noninteracting frequency-selective filters, and then perform an analysis of the resulting model. Unfortunately the model is frequently a gross over-simplification of the physical situation and does not and can not be expected to lead to accurate results.

1.3 Multiple Input Effects in Nonlinear Systems without Memory

In almost all cases of interest in communications system analysis, the input to the system is the sum of a desired and one or more interfering signals. These signals interact with the nonlinearities to produce various types of responses. The most common of these responses are given names so that they can be easily referred to, e.g., intermodulation, crossmodulation, compression, and desensitization. In this section we will categorize and give examples of these effects. To begin, consider a nonlinear system represented by the power series:

$$y(t) = \sum_{n=1}^{\infty} a_n x(t)^n. \quad (1.1)$$

The system has no memory since the output at time t depends only on the input at the same instant. Let the input, $x(t)$, be the sum of $S_1(t)$, a desired signal, and $I_2(t)$ and $I_3(t)$, two interferences. The output, $y(t)$ is then:

$$\begin{aligned}
 y(t) = & a_1 [s_1(t) + I_2(t) + I_3(t)] \\
 & + a_2 [s_1(t) + I_2(t) + I_3(t)]^2 \\
 & + a_3 [s_1(t) + I_2(t) + I_3(t)]^3 \\
 & \vdots
 \end{aligned} \tag{1.2}$$

1.3.1 Gain Compression and Desensitization

Now let us specialize Eq. (1.2) to certain cases. First let

$$\left. \begin{aligned}
 s_1(t) &= s_1 \cos \omega_1 t, \\
 I_2(t) &= I_2 \cos \omega_2 t, \\
 I_3(t) &= 0.
 \end{aligned} \right\} \tag{1.3}$$

That is, $s_1(t)$ and $I_2(t)$ are unmodulated tones.

Then:

$$\begin{aligned}
 y(t) = & a_1 [s_1 \cos \omega_1 t + I_2 \cos \omega_2 t] \\
 & + a_2 [s_1^2 \cos^2 \omega_1 t + I_2^2 \cos^2 \omega_2 t + 2s_1 I_2 \cos \omega_1 t \cos \omega_2 t] \\
 & + a_3 [s_1^3 \cos^3 \omega_1 t + 3s_1^2 I_2 \cos^2 \omega_1 t \cos \omega_2 t \\
 & + 3s_1 I_2^2 \cos \omega_1 t \cos^2 \omega_2 t + I_2^3 \cos^3 \omega_2 t] + \dots \\
 = & a_1 s_1 [1 + \frac{3a_3}{4a_1} s_1^2 + \frac{3a_3}{2a_1} I_2^2] \cos \omega_1 t \\
 & + \text{terms at other frequencies.}
 \end{aligned} \tag{1.4}$$

Equation (1.4) demonstrates that the output at the signal frequency is made up of three terms. The first term, of amplitude $a_1 s_1$, is the desired linear response. The second term, of amplitude $\frac{3}{4} a_3 s_1^3$ is the third-order compression term. If the sign of a_3 is opposite that of a_1 , the desired signal output will be smaller than that predicted by linear theory by the amount $\frac{3}{4} a_3 s_1^3$. The third term, of amplitude $\frac{3}{2} a_3 I_2^2 s_1$, is the third-order desensitization term. If the sign of a_3 is opposite that of a_1 the output will be smaller than that predicted by linear theory.

1.3.2 Crossmodulation

Assume:

$$\left. \begin{aligned} s_1(t) &= s_1 \cos \omega_1 t, \\ I_2(t) &= I_2 [1 + m(t)] \cos \omega_2 t; m < 1, \\ I_3(t) &= 0. \end{aligned} \right\} \quad (1.5)$$

That is, $s_1(t)$ is an unmodulated tone, and $I_2(t)$ is an amplitude modulated signal. Then:

$$\begin{aligned} y(t) \approx a_1 s_1 &\left[1 + \frac{3a_3}{4a_1} s_1^2 + \frac{3}{2} \frac{a_3}{a_1} I_2^2 + \frac{3a_3}{a_1} I_2^2 m(t) \right] \cos \omega_1 t \\ &+ \text{terms at other frequencies.} \end{aligned} \quad (1.6)$$

Equation (1.6) includes the desensitization and compression terms of Eq. (1.4) plus a new term, $(3a_3/a_1)I_2^2 m(t)$. The new term represents crossmodulation, that is, a transfer of the modulation from the interference to the desired signal has occurred.

1.3.3 Intermodulation

Assume:

$$\left. \begin{aligned} s_1(t) &= s_1 \cos \omega_1 t, \\ I_2(t) &= I_2 \cos \omega_2 t, \\ I_3(t) &= I_3 \cos \omega_3 t. \end{aligned} \right\} \quad (1.7)$$

That is, the desired signal and two interferences are unmodulated tones. Then

$$\begin{aligned} y(t) = a_1 s_1 &\left[1 + \frac{3a_3}{4a_1} s_1^2 + \frac{3}{2} \frac{a_3}{a_1} (I_2^2 + I_3^2) \right] \cos \omega_1 t \\ &+ a_2 I_2 I_3 [\cos (\omega_2 + \omega_3)t + \cos (\omega_2 - \omega_3)t] \\ &+ \frac{3}{4} a_3 \left[I_2^2 I_3 \cos (2\omega_2 \pm \omega_3)t + I_2 I_3^2 \cos (2\omega_3 \pm \omega_2)t \right] \\ &+ \text{terms at other frequencies.} \end{aligned} \quad (1.8)$$

The terms in Eq. (1.8) at frequencies $\omega_2 \pm \omega_3$ are second-order intermodulation terms. The terms at $2\omega_2 \pm \omega_3$ and $2\omega_3 \pm \omega_2$ are third-order intermodulation terms. If any of the frequency combinations fall in the system passband, they will be processed by the remainder of the system following the nonlinearity in the same manner as the desired signal. Third-order intermodulation can be a serious problem if ω_2 and ω_3 are near the system passband. Second-order distortion is usually a less serious problem in a receiver, since either one or both of the interference frequencies must be far removed from the system passband for $\omega_2 \pm \omega_3$ to equal ω_1 .

The examples given in this section have, for introductory purposes, been in terms of real signals and a zero-memory power-series nonlinearity. In the next section we will introduce the Volterra series and show in later sections that the power-series is a special case.

1.4 Analysis of Nonlinear Systems with Memory

The theory of functionals was developed by Vito Volterra (1930). A series resulting from a functional expansion is a Volterra series. The difference between a function, as found from a power series expansion, and a functional is, by analogy, as follows: A function, f , operates on a set of variables, x , to produce a new set of variables, $f(x)$. A functional operates on a set of functions to produce a new set of functions. Volterra showed that the regular homogeneous functionals of degree n could be written

$$F_n[x(t)] = \int_a^b \int_a^b \dots \int_a^b k_n(\xi_1, \xi_2 \dots \xi_n) x(\xi_1) x(\xi_2) \dots x(\xi_n) d\xi_1 d\xi_2 \dots d\xi_n. \quad (1.9)$$

and that every functional $G[x(t)]$ continuous in the field of continuous functions can be represented by the functional series expansion:

$$\begin{aligned}
 G[x(t)] &= \sum_{n=0}^{\infty} F_n[x(t)] \\
 &= k_0 + \int_a^b k_1(\xi) x(\xi) d\xi \\
 &\quad + \int_a^b \int_a^b k_2(\xi_1, \xi_2) x(\xi_1) x(\xi_2) d\xi_1 d\xi_2 \\
 &\quad + \text{higher order terms.} \tag{1.10}
 \end{aligned}$$

Eq. (1.10) is a Volterra functional series. Convergence conditions have been discussed by Volterra (1930). Wiener (1942) applied the Volterra series in an investigation of a nonlinear circuit response by relating the system input $x(t)$ to the output $y(t)$ by a functional series given by

$$\begin{aligned}
 y(t) &= y_1(t) + y_2(t) + \dots \\
 &= \sum_{n=1}^{\infty} y_n(t), \tag{1.11}
 \end{aligned}$$

where

$$y_1(t) = \int_{-\infty}^{\infty} h_1(\tau) x(t-\tau) d\tau, \tag{1.12}$$

$$y_2(t) = \int_{-\infty}^{\infty} \int_{-\infty}^{\infty} h_2(\tau_1, \tau_2) x(t-\tau_1) x(t-\tau_2) d\tau_1 d\tau_2, \tag{1.13}$$

and, in general,

$$y_n(t) = \int_{-\infty}^{\infty} \dots \int_{-\infty}^{\infty} h_n(\tau_1, \dots, \tau_n) \prod_{i=1}^n x(t-\tau_i) d\tau_i. \tag{1.14}$$

Eq. (1.11) is the input-output functional representation of nonlinear systems upon which much of this book is based. It is a general method and is useful provided the nonlinearities are not excited so violently that the number of terms required become very large. We thus refer to Eq. (1.11) as being applicable to the small-signal nonlinear case. When the required number of terms becomes great we encounter the large-signal nonlinear case, and, to proceed, must use an alternate method of solution based upon the nonlinear differential equations of the system.

The index of the terms of Equation (1.11), n , is called the order of the term. The zero-order term is a DC output in the absence of an input, and can be ignored in our analysis as a fixed bias offset. The first-order term will be identified as the conventional linear response of the system. The higher-order terms are the system nonlinear responses.

1.5 An Example of a Nonlinear System with Memory

Before accepting the Volterra series as a suitable basis for investigating nonlinear physical systems with memory and embarking upon further discussion about the practical applications to communications receivers, it is interesting to consider a simple example. The skeptic will certainly ask what possible physical basis exists for expecting a Volterra series to be a satisfactory input-output relationship for a physical nonlinear system. The complicated terms of the series given by Eq. (1.14) certainly suggest caution before embarking upon a lengthy mathematical treatment. We address this issue by considering a very simple physical example. Our objective is to derive from first principles a series expansion for the input-output relationship and investigate the result to see if it might in fact be a

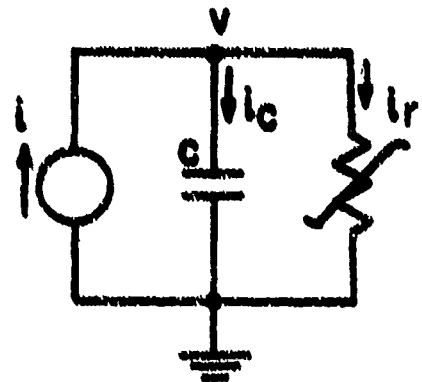
Volterra series. If it is, our skeptic will be less unhappy and be considerably more favorably inclined to accept a Volterra series as a "good" input-output relationship. Of course, the really "hard-nosed" skeptic will not be swayed by our arguments. He will not be convinced until we show him some data from a physical system and compare the data with predictions derived from the theory. Such validation experiments have been performed. We shall come to the details in later chapters of this book.

Figure 1.3 shows a simple nonlinear system with memory, composed of the parallel connection of a current source, a linear capacitor, and a nonlinear resistor. The nonlinear resistor has the no-memory current-voltage relation given by the power series:

$$i_r = \sum_{n=1}^{\infty} k_n v^n. \quad (1.15)$$

Figure 1.4 shows a signal flow graph of the system. The signal flow will now be traced. The current enters at the left-hand node. The capacitor current i_c is integrated in the capacitor to give the charge q ; the charge is multiplied by C^{-1} to give the node voltage v . The resistor current, i_r , is given by the power series $\sum_n k_n v^n$, the first three terms of which are shown. A feedback loop is created when i_r is subtracted from the input current i , resulting in the capacitor current i_c .

Let us next recognize that the resistor current i_r diverted through the resistance and subtracted from the input current i to give the capacitor current i_c can be interpreted as a set of voltage-controlled current sources connected from the voltage node to the ground reference node. Let us examine the system response to an arbitrary input current $i(t)$ with first the first-order voltage-controlled current generator $k_1 v$ present and subsequently examine how the output must be modified as each additional



$$I_r = f(v) = \sum_n k_n v^n$$

Fig. 1.3 A Nonlinear System with Energy Storage.

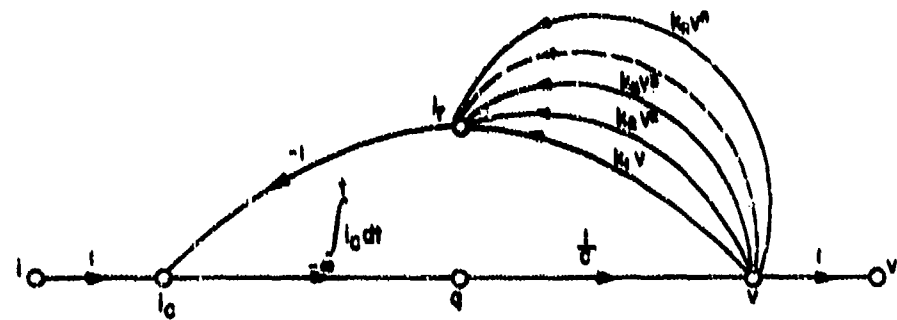


Fig. 1.4 Signal Flow Diagram of the Nonlinear System.

order term is added. With just the first order current generator $k_1 v$ present we have the linear system shown at the top of the signal flow graph in Fig. 1.5. The forward path, relating capacitor voltage to capacitor current, is linear. The first-order (linear) output voltage is obviously given by the convolution integral

$$v_1(t) = \int_{-\infty}^{\infty} h_1(\tau) i(t-\tau) d\tau, \quad (1.16)$$

where $h_1(\tau)$ is the voltage impulse response of the parallel combination C and k_1 to a current source and is given by

$$h_1(\tau) = \frac{1}{C} \exp^{-\frac{k_1 \tau}{C}}. \quad (1.17)$$

Equation (1.16) is identical in form to Eq. (1.12). We have therefore established that the first term in the system voltage response $v_1(t)$ is identical to the first term in the Volterra series as given previously by Eq. (1.12)

Next, consider how the linear portion of the flow graph in Fig. 1.5 must be modified if we add the second voltage-controlled current source $k_2 v^2$ to the system and seek to determine the additional second order response $v_2(t)$ at the output contributed only by the first order voltage v_1 . Clearly, a current source $k_2 v_1^2$ must be added to the first order linear system as shown in Fig. 1.5. This second order current source excites the linear system at the resistor current node. Since the input current source $i(t)$ contains no high-order drive, it does not excite the second order system and therefore does not appear. Therefore the second-order output voltage is given by the convolution of the second-order current source $k_2 v_1^2$ with $g_1(\tau)$, the output voltage impulse response

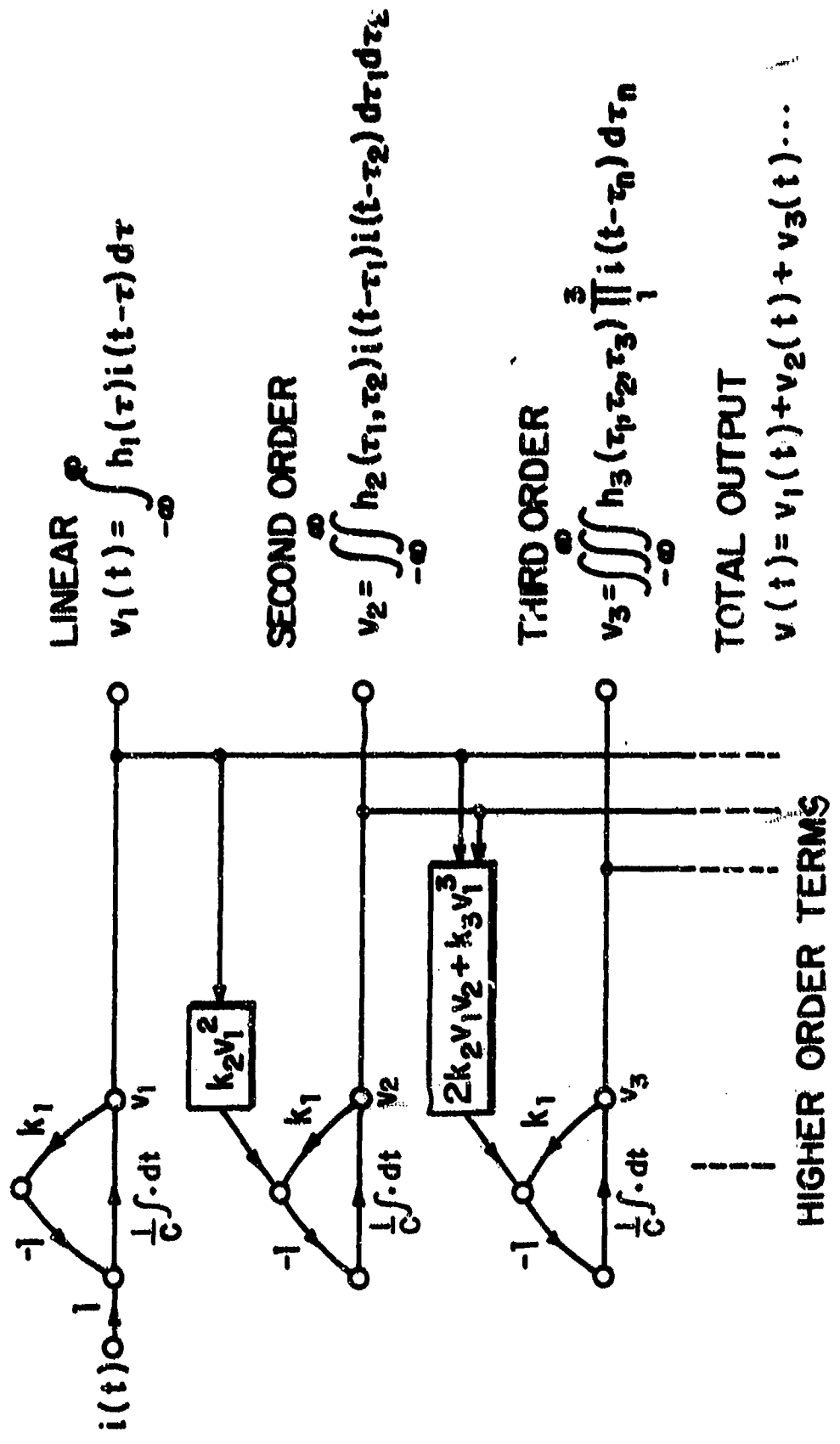


Fig. 1.5 Terms in the Nonlinear Response Expansion.

of the network driven by the second-order current source. From Fig. 1.5 it can be seen that

$$g_1(\tau) = -h_1(\tau), \quad (1.18)$$

which results in

$$v_2(t) = -k_2 \int_{-\infty}^{\infty} h_1(\tau) v_1^2(t-\tau) d\tau. \quad (1.19)$$

If we now substitute Eq. (1.16) for v_1 into Eq. (1.19), we have

$$\begin{aligned} v_2(t) &= \iiint_{-\infty}^{\infty} k_2 h_1(\tau_3) h_1(\tau_1) h_1(\tau_2) \\ &\quad \cdot i[t-(\tau_3+\tau_1)] i[t-(\tau_3+\tau_2)] d\tau_1 d\tau_2 d\tau_3. \end{aligned} \quad (1.20)$$

Letting $\sigma_1 = \tau_3 + \tau_1$ and $\sigma_2 = \tau_3 + \tau_2$, we have

$$v_2(t) = \iint_{-\infty}^{\infty} h_2(\sigma_1, \sigma_2) i(t-\sigma_1) i(t-\sigma_2) d\sigma_1 d\sigma_2, \quad (1.21)$$

where the second-order impulse response is given by

$$h_2(\sigma_1, \sigma_2) = -k_2 \int_{-\infty}^{\infty} h_1(\tau_3) h_1(\sigma_1 - \tau_3) h_1(\sigma_2 - \tau_3) d\tau_3. \quad (1.22)$$

We note that the second-order response $v_2(t)$, as given by Eq. (1.21), is identical in form to the second-order term in the Volterra series as given in Eq. (1.13).

We next determine the third-order voltage response $v_3(t)$. To second order, the voltage appearing at the output node is the sum of v_1 and v_2 . The voltage-controlled current source $k_2 v^2 + k_3 v^3$ driving the linear network is now

$$\begin{aligned}
 k_2 v^2 + k_3 v^3 &= k_2(v_1 + v_2)^2 + k_3(v_1 + v_2)^3 \\
 &= k_2(v_1^2 + 2v_1 v_2 + v_2^2) \\
 &\quad + k_3(v_1^3 + 3v_1^2 v_2 + 3v_1 v_2^2 + v_2^3). \tag{1.23}
 \end{aligned}$$

Equation (1.23) contains terms of many different orders in the excitation $i(t)$. For example, v_1^2 is of second-order in $i(t)$ and has already been accounted for in the computation of the second-order response of $v_2(t)$, while $v_2^3(t)$ is of sixth-order and would be one of the terms used in computing the sixth-order response $v_6(t)$. The third-order term is $2k_2 v_1 v_2 + k_3 v_1^3$. The second-order term $k_2 v_1^2$ has already been accounted for in the second-order response $v_2(t)$.

Now, from Eq. (1.16), we have

$$\begin{aligned}
 k_3 v_1^3 &= k_3 \int_{-\infty}^{\infty} h_1(\tau_1) h_1(\tau_2) h_1(\tau_3) \\
 &\quad \cdot i(t-\tau_1) i(t-\tau_2) i(t-\tau_3) d\tau_1 d\tau_2 d\tau_3, \tag{1.24}
 \end{aligned}$$

and, from Eqs. (1.16) and (1.21)

$$\begin{aligned}
 2k_2 v_1 v_2 &= 2k_2 \int_{-\infty}^{\infty} h_1(\tau_1) h_2(\tau_2, \tau_3) \\
 &\quad \cdot i(t-\tau_1) i(t-\tau_2) i(t-\tau_3) d\tau_1 d\tau_2 d\tau_3, \tag{1.25}
 \end{aligned}$$

and we have, for third-order

$$2k_2 v_1 v_2 + k_3 v_1^3 = \iiint_{-\infty}^{\infty} [2k_2 h_1(\sigma_1) h_2(\sigma_2, \sigma_3) + k_3 h_1(\sigma_1) h_1(\sigma_2) h_1(\sigma_3)] \\ \cdot i(t-\sigma_1) i(t-\sigma_2) i(t-\sigma_3) d\sigma_1 d\sigma_2 d\sigma_3. \quad (1.26)$$

Equation (1.26) is the third-order current source in terms of the system's first and second-order nonlinear impulse responses $h_1(\tau)$ and $h_2(\tau_1, \tau_2)$, as well as the coefficients k_2 and k_3 . This nonlinear source excites the linear network to produce the third-order component of the output voltage

$$v_3(t) = \iiint_{-\infty}^{\infty} g_1(\sigma_4) [2k_2 h_1(\sigma_1) h_2(\sigma_2, \sigma_3) \\ + k_3 h_1(\sigma_1) h_1(\sigma_2) h_1(\sigma_3)] \\ \cdot i[t-(\sigma_4+\sigma_1)] i[t-(\sigma_4+\sigma_2)] i[t-(\sigma_4+\sigma_3)] \\ \cdot d\sigma_1 d\sigma_2 d\sigma_3 d\sigma_4. \quad (1.27)$$

If we let $\tau_1 = \sigma_4 + \sigma_1$, $\tau_2 = \sigma_4 + \sigma_2$ and $\tau_3 = \sigma_4 + \sigma_3$, we have

$$v_3(t) = \iiint_{-\infty}^{\infty} h_3(\tau_1, \tau_2, \tau_3) i(t-\tau_1) i(t-\tau_2) i(t-\tau_3) \\ d\tau_1 d\tau_2 d\tau_3, \quad (1.28)$$

where

$$h_3(\tau_1, \tau_2, \tau_3) = \int_{-\infty}^{\infty} h_1(\sigma_4) [2k_2 h_1(\tau_1 - \sigma_4) h_2(\tau_2 - \sigma_4, \tau_3 - \sigma_4) \\ + k_3 h_1(\tau_1 - \sigma_4) h_1(\tau_2 - \sigma_4) h_1(\tau_3 - \sigma_4)] d\sigma_4. \quad (1.29)$$

Once again comparison of Eq. (1.28) for the third-order term v_3 with the general Volterra series term for $n=3$ in Eq. (1.14) reveals that it is formally identical.

Higher-order responses can be derived in a similar fashion. The current sources of order n can always be written in terms of a power series in voltage v_i , $i=1,2\dots n-1$, and the coefficients k_i , $i=1,2\dots n$. For any given order response, the current excitation is the sum of products of all lower-order excitations which interact to form a source of the desired order. It should be noted that, regardless of the order of the nonlinear response, the response is always a convolution with a linear impulse response. Furthermore, the response of any order is dependent only on the responses of lower order. Thus, the analysis of the nonlinear responses is a bootstrap operation, which allows the determination of a response to be performed in terms of already determined lower-order responses, and allows one to stop the process when the desired order response is known. The nonlinear system model resulting from this process is a Volterra series and is a sum of lower-order responses $v(t) = \sum_n v_n(t) = v_1(t) + v_2(t) + \dots$

The argument presented in this section has been based upon a single nonlinearity. We have shown that a nonlinearity described by a Taylor series and embedded in an otherwise linear network requires a Volterra series to represent the input-output properties of the entire network. Although we have chosen to develop this argument for a simple example, the theory is general and applies to multiple nonlinearities as well as to multiple-port excitation.

1.6 Alternate Forms of the Volterra Series

The general kernel of Eq. (1.14), $h_n(\tau_1, \tau_2, \dots, \tau_n)$, is called a nonlinear impulse response of order n . Its Fourier transform is the nonlinear transfer function of order n , or

$$H_n(f_1, f_2, \dots, f_n) = \iint_{-\infty}^{\infty} \dots \int h_n(\tau_1, \tau_2, \dots, \tau_n) e^{-j2\pi(f_1\tau_1 + f_2\tau_2 + \dots + f_n\tau_n)} d\tau_1 d\tau_2 \dots d\tau_n. \quad (1.30)$$

The nonlinear impulse response of order n is related to the nonlinear transfer function of order n by the inverse Fourier transformation:

$$h_n(\tau_1, \tau_2, \dots, \tau_n) = \iint_{-\infty}^{\infty} \dots \int H_n(f_1, f_2, \dots, f_n) e^{j2\pi(f_1\tau_1 + f_2\tau_2 + \dots + f_n\tau_n)} df_1 df_2 \dots df_n. \quad (1.31)$$

The time-domain output, $y(t)$, of a nonlinear system can be found in terms of the nonlinear transfer functions and the spectrum of the input signal. Equation (1.14) shows that the n -th order term in $y(t)$, $y_n(t)$, can be written as the n -th order convolution of the input, $x(t)$, with the n -th order nonlinear impulse response, $h_n(\tau_1, \tau_2, \dots, \tau_n)$. If Equation (1.31) is substituted into Equation (1.14) and the integration performed over the τ_i , then $y(t)$ is given by

$$y(t) = \sum_n \iint_{-\infty}^{\infty} \dots \int H_n(f_1, \dots, f_n) X(f_1) X(f_2) \dots X(f_n) e^{j2\pi(f_1 + \dots + f_n)t} df_1 df_2 \dots df_n, \quad (1.32)$$

where $X(f)$ is the input signal spectrum.

The spectrum of $y(t)$, $Y(f)$, is the inverse Fourier transform of $y(t)$ and is given by

$$Y(f) = \int_{-\infty}^{\infty} \sum_n \int_{-\infty}^{\infty} \dots \int_{-\infty}^{\infty} H_n(f_1, f_2, \dots, f_n) X_1(f_1) X_2(f_2) \dots X_n(f_n) \\ \cdot e^{j2\pi(f_1 + \dots + f_n)t} df_1 df_2 \dots df_n e^{-j2\pi ft} dt \quad (1.33)$$

$$= \sum_n \int_{-\infty}^{\infty} \dots \int_{-\infty}^{\infty} H_n(f_1, f_2, \dots, f_n) X_1(f_1) X_2(f_2) \dots X_n(f_n) \\ \cdot \int_{-\infty}^{\infty} e^{-j2\pi(f-f_1-f_2-\dots-f_n)t} dt df_1 df_2 \dots df_n. \quad (1.34)$$

However, the unit impulse $\delta(\cdot)$ is defined by the integral relation

$$\int_{-\infty}^{\infty} e^{-j2\pi(f-f_1-f_2-\dots-f_n)t} dt = \delta(f-f_1-f_2-\dots-f_n). \quad (1.35)$$

Substituting Equation (1.35) into Equation (1.34) results in the input-spectrum output-spectrum relationship

$$Y(f) = \sum_n \int_{-\infty}^{\infty} \dots \int_{-\infty}^{\infty} H_n(f_1, \dots, f_n) X(f_1) \dots X(f_n) \\ \delta(f-f_1-f_2-\dots-f_n) df_1 df_2 \dots df_n. \quad (1.36)$$

Equations (1.14), (1.32), and (1.36) are the key time and frequency-domain input/output relations for small-signal nonlinear analysis. They also provide the link for relating nonlinear transfer function analysis to power-series analysis. If the nonlinear system has no memory, then its nonlinear impulse responses and nonlinear transfer functions are given by

$$h_n(\tau_1, \tau_2, \dots, \tau_n) = a_n \delta(\tau_1) \delta(\tau_2) \dots \delta(\tau_n), \quad (1.37)$$

$$H_n(f_1, f_2, \dots, f_n) = A_n, \text{ a constant.} \quad (1.38)$$

The nonlinear impulse response is the product of a constant multiplier a_n and n impulses, and the nonlinear transfer function is a constant A_n , independent of frequency. From (1.31), the two constants a_n and A_n are equal. Substituting Eq. (1.37) into Eq. (1.14) yields:

$$y(t) = \sum_n \iint \dots \int a_n \delta(\tau_1) \delta(\tau_2) \dots \delta(\tau_n) x(t-\tau_1) x(t-\tau_2) \dots x(t-\tau_n) d\tau_1 d\tau_2 \dots d\tau_n \quad (1.39)$$

$$= \sum_n a_n x^n(t) ; \text{ no-memory system,} \quad (1.40)$$

and substituting Equation (1.38) into Equation (1.32) yields

$$y(t) = \sum_n \iint \dots \int a_n x(f_1) x(f_2) \dots x(f_n) e^{j2\pi(f_1 + f_2 + \dots + f_n)t} df_1 df_2 \dots df_n \quad (1.41)$$

$$= \sum_n a_n x^n(t) ; \text{ no-memory system.} \quad (1.42)$$

Thus, $y(t)$ is the same as given by either Eq. 1.40 or 1.42. Furthermore, comparing Eq. (1.40) with Eq. (1.1), it is seen that the zero-memory Volterra series coefficients a_n are equal to the power-series coefficients a_n , thus establishing that the power-series is the special case of the Volterra series for a n-memory system.

1.7 Multi-Tone Output Response in Terms of Nonlinear Transfer Functions

One of the most important multiple signal input waveforms for a nonlinear system characterized by a Volterra series is the sum of several unmodulated tones. If we express these tones in terms of exponentials of complex amplitude A_m and frequency f_m , we have

$$x(t) = \frac{1}{2} \sum_{m=1}^M A_m e^{j2\pi f_m t}. \quad (1.43)$$

Since $x(t)$ must always be real, f_m will include identical positive and negative frequencies, and A_m for a negative frequency will be the complex conjugate of A_m for the positive frequency. A real signal is the sum of a positive-frequency complex signal and its negative-frequency complex conjugate. Alternatively, a real signal is twice the real part of either the positive frequency complex signal or its negative frequency complex conjugate. The frequency spectrum of this $x(t)$ is

$$X(f) = \frac{1}{2} \sum_m A_m \delta(f - f_m), \quad (1.44)$$

where $\delta(f - f_m)$ is a unit impulse at $f = f_m$ in the frequency domain.

Now, we have shown that the system response $y(t)$ may be written in the form

$$y(t) = \sum_n y_n(t), \quad (1.45)$$

where the various $y_n(t)$ are the individual terms in the Volterra series of the system output. Our objective is to determine the

various order responses $y_n(t)$ in terms of the nonlinear transfer functions of the system. For example,

$$y_1(t) = \frac{1}{2} \sum_{m=1}^M A_m H_1(f_m) e^{j2\pi f_m t}, \quad (1.46)$$

by inspection from Eq. (1.43) where $H_1(f_m)$ is the linear transfer function of the system at frequency f_m . The n-th order output can occur at many frequency combinations, depending on the number of complex inputs, M, and the order, n. A general expression for the output frequency, denoted by f_Σ , is

$$f_\Sigma = m_1 f_1 + m_2 f_2 + \dots + m_M f_M, \quad (1.47)$$

where m_1, m_2, \dots, m_M are integers ranging from 0 to n, and

$$\sum_{i=1}^M m_i = n. \quad (1.48)$$

The vector \underline{m} , defined as

$$\underline{m} = [m_1, m_2, \dots, m_M], \quad (1.49)$$

is used extensively throughout the book. We shall show in Chapter 2 that, for $x(t)$ given by Eq. (1.43),

$$y_n(t) = \frac{1}{2} \sum B_n(\underline{m}) H_n e^{j2\pi f_\Sigma t}, \quad (1.50)$$

where

$$B_n(\underline{m}) = \frac{n! A_1^{m_1} A_2^{m_2} \dots A_M^{m_M}}{2^{n-1} m_1! m_2! \dots m_M!}, \quad (1.51)$$

$$H_n = H_n(f_1, \dots, f_{m_1}, \underbrace{f_2, \dots, f_2}_{m_2 \text{ times}}, \dots, \underbrace{f_M, \dots, f_M}_{m_M \text{ times}}). \quad (1.52)$$

There are (see Feller, 1950, p. 52)

$$\binom{M+n-1}{n} \triangleq \frac{(M+n-1)!}{n! (M-1)!}, \quad (1.53)$$

distinguishable combinations of m_i satisfying Eq. (1.48) so that there will be $\binom{M+n-1}{n}$ terms to sum in Eq. (1.50) for each n^{th} order nonlinear response. For example, if there are $M=4$ exponentials in $x(t)$ and we are interested in the $n=2$, or second-order response, we can expect to sum

$$\frac{(4+2-1)!}{2! (4-1)!} = \frac{5!}{2! 3!} = 10 \quad (1.54)$$

terms. For $n=3$, the third-order term, there will be 20 such components.

The essential point to note here is that the complex amplitude of each of the spectral components in Eq. (1.50) is given by the product $B_n(\underline{m}) H_n$ where B_n , given by Eq. (1.51), is dependent upon the input signal amplitudes A_m and is independent of frequency. The frequency dependence of the component is entirely given by H_n , the n^{th} order nonlinear transfer function. It should now be evident that the key step in characterizing the

output terms of a nonlinear system with memory resides in determining the magnitude and phase of the multi-dimensional transfer function H_n . We shall exploit the properties of the nonlinear transfer functions throughout this book.

In Section 1.6 we have pointed out that $H_n = a_n$, the coefficients of a power-series, when the nonlinear system has no memory and can be satisfactorily characterized by the power-series. It follows that the preceding discussion regarding the n^{th} order response components given by Eq. (1.50) applies to and can be used to describe the output terms given by a power series by simply replacing H_n by a_n .

1.8 Two-Tone Input Example

Multi-tone testing of quasi-linear systems is widely employed to characterize the nonlinear distortion. The most important case is two-tone testing. In this section we shall utilize the general results of the previous section and show by an example how to obtain the output terms for a physical system excited by two sinusoids. We have

$$x(t) = \frac{1}{2} \left[A_1 e^{j2\pi f_1 t} + A_2 e^{j2\pi f_2 t} + A_1^* e^{-j2\pi f_1 t} + A_2^* e^{-j2\pi f_2 t} \right], \quad (1.55)$$

where we now identify $M=4$, $A_3=A_1^*$, $A_4=A_2^*$; and $f_3=-f_1$, $f_4=-f_2$ by comparing terms in Eq. (1.55) with Eq. (1.43). Since $M=4$, we have

$$m_1 + m_2 + m_3 + m_4 = n, \quad (1.56)$$

to satisfy for non-negative integer values of m_i for each non-linear order n . We expect there to be four combinations for $n=1$, ten for $n=2$, and twenty for $n=3$.

The first and second-order output components are listed in Table 1.1. The frequency combinations of m_i associated with each response are noted. Note that both negative and positive frequency terms are present and that the complex amplitude of each negative frequency is the complex conjugate of each positive frequency term. The type of nonlinear response is also indicated in the last column of the table. Each of the $n=1$ terms is a linear response. Four of the $n=2$ components are second harmonics and the remainder are second-order intermodulation terms. Two of these are at DC.

The third-order output components are listed in Table 1.2. Again the frequency, complex amplitude, and particular combination of m_i associated with the response is noted. We have also identified in the last column the type of response. Note the presence of terms causing third-order gain compression and desensitization of the linear term at the input frequencies f_1 and f_2 . There is also a set of third-order intermodulation products as well as a set of third harmonics. No DC terms are generated by any odd order n . Also note that for every positive frequency term there is a corresponding negative frequency component with a complex conjugate amplitude. The physical output of such a system is one half the sum of both the positive and negative frequency components and will always be a real time function. Of course, one can take the real part of the positive frequency terms and get the same result.

TABLE 1.1
FIRST AND SECOND-ORDER NONLINEAR RESPONSES

Combination No.	Combination				Frequency of Response	Amplitude of Response	Type of Response
	m_1	m_2	m_3	m_4			
$n = 1$	1	1	0	0	f_1	$A_1 H_1(f_1)$	Linear
	2	0	1	0	f_2	$A_2 H_1(f_2)$	
	3	0	0	1	$-f_1$	$A_1^* H_1(-f_1)$	
	4	0	0	0	$-f_2$	$A_2^* H_1(-f_2)$	
							Second-Order Intermodulation
	1	1	0	0	$f_1 + f_2$	$A_1 A_2^* H_2(f_1, f_2)$	
	2	0	1	0	$f_2 - f_1$	$A_2 A_1^* H_2(f_2, -f_1)$	
	3	0	0	1	$-f_1 - f_2$	$A_1^* A_2^* H_2(-f_1, -f_2)$	
	4	1	0	0	$f_1 - f_2$	$A_1 A_2^* H_2(f_1, -f_2)$	
	5	1	0	1	$f_1 - f_1 = 0$	$ A_1 ^2 H_2(f_1, -f_1)$	
	6	0	1	0	$f_2 - f_2 = 0$	$ A_2 ^2 H_2(f_2, -f_2)$	
$n = 2$	7	2	0	0	$2f_1$	$\frac{1}{2} A_1^2 H_2(f_1, f_1)$	Second Harmonic
	8	0	2	0	$2f_2$	$\frac{1}{2} A_2^2 H_2(f_2, f_2)$	
	9	0	0	2	$-2f_1$	$\frac{1}{2} A_1^{*2} H_2(-f_1, -f_1)$	Second Harmonic
	10	0	0	0	$-2f_2$	$\frac{1}{2} A_2^{*2} H_2(-f_2, -f_2)$	

TABLE 1.2
THIRD-ORDER NONLINEAR RESPONSES.

Combination No.	Combinations				Frequency of Response	Amplitude of Response	Type of Response
	m_1	m_2	m_3	m_4			
1	1	1	0	0	$\epsilon_1 + \epsilon_2 - \epsilon_1 = \epsilon_2$	$\frac{3}{2} A_1^2 A_2 H_3 (\epsilon_1, \epsilon_2, -\epsilon_1)$	
2	0	1	1	1	$\epsilon_2 - \epsilon_1 - \epsilon_2 = -\epsilon_1$	$\frac{3}{2} A_1^* A_2^* H_3 (\epsilon_2, -\epsilon_1, -\epsilon_2)$	
3	1	0	1	1	$\epsilon_1 - \epsilon_1 - \epsilon_2 = -\epsilon_2$	$\frac{3}{2} A_1^2 A_2^* H_3 (\epsilon_1, -\epsilon_1, -\epsilon_2)$	
4	1	1	0	1	$\epsilon_1 + \epsilon_2 - \epsilon_2 = \epsilon_1$	$\frac{3}{2} A_1 A_2^2 H_3 (\epsilon_1, \epsilon_2, -\epsilon_2)$	
5	2	1	0	0	$2\epsilon_1 + \epsilon_2$	$\frac{3}{4} A_1^2 A_2 H_3 (\epsilon_1, \epsilon_1, \epsilon_2)$	
6	0	2	1	0	$2\epsilon_2 - \epsilon_1$	$\frac{3}{4} A_1^* A_2 H_3 (\epsilon_2, \epsilon_2, -\epsilon_1)$	
7	0	0	2	1	$-2\epsilon_1 - \epsilon_2$	$\frac{3}{4} A_1^2 A_2^* H_3 (-\epsilon_1, -\epsilon_1, -\epsilon_2)$	
8	1	0	0	2	$\epsilon_1 - 2\epsilon_2$	$\frac{3}{4} A_1^* A_2^2 H_3 (\epsilon_1, -\epsilon_2, -\epsilon_2)$	
9	2	0	1	0	$2\epsilon_1 - \epsilon_1 = \epsilon_1$	$\frac{3}{4} A_1 A_1^2 H_3 (\epsilon_1, \epsilon_1, -\epsilon_1)$	
10	0	2	0	1	$2\epsilon_2 - \epsilon_2 = \epsilon_2$	$\frac{3}{4} A_2 A_2^2 H_3 (\epsilon_2, \epsilon_2, -\epsilon_2)$	
11	1	0	2	0	$\epsilon_1 - 2\epsilon_1 = -\epsilon_1$	$\frac{3}{4} A_1^2 A_1 H_3 (\epsilon_1, -\epsilon_1, -\epsilon_1)$	
12	0	1	0	2	$\epsilon_2 - 2\epsilon_2 = -\epsilon_2$	$\frac{3}{4} A_2^2 A_2 H_3 (\epsilon_2, -\epsilon_2, -\epsilon_2)$	
13	2	0	0	1	$2\epsilon_1 - \epsilon_2$	$\frac{3}{4} A_1^2 A_2 H_3 (\epsilon_1, \epsilon_1, -\epsilon_2)$	
14	1	2	0	0	$\epsilon_1 + 2\epsilon_2$	$\frac{3}{4} A_1 A_2^2 H_3 (\epsilon_1, \epsilon_2, \epsilon_2)$	
15	0	1	2	0	$\epsilon_2 - 2\epsilon_1$	$\frac{3}{4} A_2^2 A_1 H_3 (\epsilon_2, -\epsilon_1, -\epsilon_1)$	
16	0	0	1	2	$-\epsilon_1 - 2\epsilon_2$	$\frac{3}{4} A_1^2 A_2 H_3 (-\epsilon_1, -\epsilon_2, -\epsilon_2)$	
17	3	0	0	0	$3\epsilon_1$	$\frac{1}{4} A_1^3 H_3 (\epsilon_1, \epsilon_1, \epsilon_1)$	
18	0	3	0	0	$3\epsilon_2$	$\frac{1}{4} A_2^3 H_3 (\epsilon_2, \epsilon_2, \epsilon_2)$	
19	0	0	3	0	$-3\epsilon_1$	$\frac{1}{4} A_1^3 H_3 (-\epsilon_1, -\epsilon_1, -\epsilon_1)$	
20	0	0	0	3	$-3\epsilon_2$	$\frac{1}{4} A_2^3 H_3 (-\epsilon_2, -\epsilon_2, -\epsilon_2)$	

A compact summary of the two-tone responses to third-order is shown in Fig. 1.6. The frequency of the responses is noted along the frequency axis. At the top of the figure we identify the response order and indicate the presence of a response at a particular order by a small circle along the frequency axis. Note that there are multiple responses of various orders at several frequencies. Noted in parentheses beside each circle is the nonlinear order n of the response and combination number from Tables 1.1 and 1.2. The response frequency spectrum is illustrated as a function of frequency at the bottom of the figure. The illustration is a suggestion of what would be observed in a spectrum analyzer.

Finally, let us write out explicitly the terms at a particular output frequency as a further illustration of the interpretation of Fig. 1.6 and Tables 1.1 and 1.2. At frequency f_2 , we have six responses, three at positive frequencies and three at negative. The positives are the linear response (1,2) and the two third-order components (3,1) and (3,10). Hence, at frequency f_2 ,

$$\begin{aligned} y(t) = & \frac{1}{2} [A_2 H_1(f_2) \\ & + \frac{3}{2} |A_1|^2 A_2 H_3(f_1, f_2, -f_1) \\ & + \frac{3}{4} |A_2|^2 A_2 H_3(f_2, f_2, -f_2)] e^{j2\pi f_2 t} + \text{c.c. terms.} \end{aligned} \quad (1.57)$$

The notation "c.c. terms" indicates the complex conjugates, necessary for a real output signal. Alternatively, $y(k)$ is given by

$$\begin{aligned} y(t) = & \text{Re} \{ [A_2 H_1(f_2) + \frac{3}{2} |A_1|^2 A_2 H_3(f_1, f_2, -f_1) \\ & + \frac{3}{4} |A_2|^2 A_2 H_3(f_2, f_2, -f_2)] e^{j2\pi f_2 t} \}. \end{aligned} \quad (1.58)$$

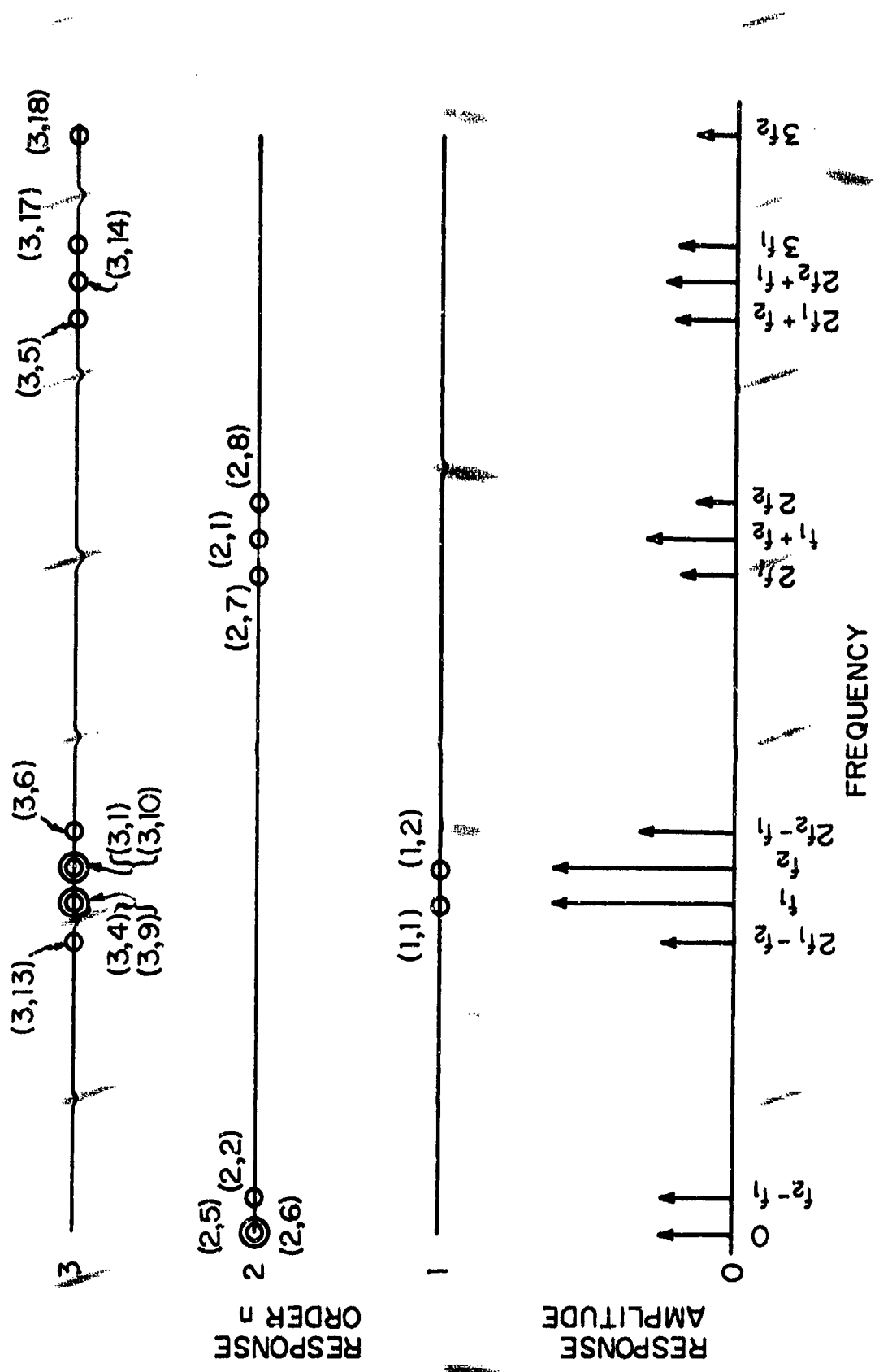


Fig. 1.6. Two-Tone Responses to Third-Order.

The first term is the small-signal linear response, the second term is the desensitization at frequency f_2 , caused by the signal at f_1 , and the third term is the compression of the f_2 term generated by increasing the amplitude A_2 .

1.9 Frequency-Conversion as a Mild Nonlinearity

The process of frequency conversion is basic to communication receivers. Many forward-biased diode, transistor and vacuum tube mixers, and varacter up-converters can be modeled as mildly excited nonlinear devices. The nonlinear analysis described here applies directly to such mixer circuits. Switched-mixers or mixers with large local-oscillator drives are more efficiently treated by large-signal, time-domain techniques.

1.9.1 Equivalent Amplifier Concept

The important difference between a mixer and an amplifier is that the desired output of a mixer is due to the second-order transfer function, and the dominant in-band distortion term is due to the fourth-order transfer function. If the local-oscillator is sufficiently small so that the mixer operates as a small-signal nonlinear system, it can be fully analyzed using time-invariant nonlinear transfer functions. The mixer can be considered to be a nonlinear amplifier with one extra signal, namely the local-oscillator. Consider the case where the input signals are $A_i \exp(j\omega_i t)$, where $i = 1, 2$ for the signals, and 0 for the local-oscillator. The desired output of the amplifier is at frequency f_1 or f_2 , while the desired output of the mixer is at frequency $f_0 - f_1$ or $f_0 - f_2$. For any frequency combination in the amplifier, there will exist at the mixer output a similar frequency combination shifted in frequency by f_0 , and, due to the

nonlinearity, one-order higher than in the amplifier case. This leads to the concept of an equivalent amplifier. A mixer can be considered as an "equivalent amplifier" which incorporates a frequency shift f_0 . The nonlinear transfer functions of the equivalent amplifier can be expressed in terms of those of the mixer, and are functions of the local-oscillator amplitude and frequency. If the mixer nonlinear transfer functions are denoted by $H_{n+1}(f_0, f_1, f_2, \dots, f_n)$ then the corresponding "equivalent amplifier" nonlinear transfer functions, $H_n^{eq}(f_1, f_2, \dots, f_n, f_0)$, are given by:

$$H_n^{eq}(f_1, f_2, \dots, f_n; f_0) = \frac{n+1}{2} A_0 H_{n+1}(f_0, f_1, \dots, f_n). \quad (1.59)$$

The factor $\frac{n+1}{2} A_0$ is a direct consequence of Equation (1.51).

Thus:

$$H_1^{eq}(f_1, f_0) = A_0 H_2(f_0, f_1), \quad (1.60)$$

$$H_2^{eq}(f_1, f_2, f_0) = \frac{3}{2} A_0 H_3(f_0, f_1, f_2), \quad (1.61)$$

$$H_3^{eq}(f_1, f_2, f_3, f_0) = 2A_0 H_4(f_0, f_1, f_2, f_3). \quad (1.62)$$

The use of the equivalent amplifier concept can often simplify receiver analysis.

1.9.2 Mixer p,q Response

In the literature on mixers, one often finds reference to the mixer p,q response. The p,q response is an interaction of the p^{th} multiple of the local-oscillator frequency f_0 and the q^{th} multiple of the signal frequency f_1 to form a mixer output which falls in the IF passband. If both the signal and the local-oscillator are harmonic free, the p,q response y_{p+q} is

$$y_{p+q}(t) = \frac{1}{2} [B_{p+q}(m) H_{p+q} e^{j2\pi(pf_0 + pf_1)} + \text{c.c.}], \quad (1.63)$$

where

$$B_{p+q}(m) = \frac{(p+q)!}{2^{p+q-1} p! q!} A_0^p A_1^q, \quad (1.64)$$

$$H_{p+q} = H_{p+q} \underbrace{(f_0, \dots f_0)}_{p \text{ times}}, \underbrace{(f_1, \dots f_1)}_{q \text{ times}}. \quad (1.65)$$

A_0 = complex amplitude of input local-oscillator at f_0 .

A_1 = complex amplitude of input signal at f_1 .

If the local-oscillator itself has a p^{th} harmonic component of complex amplitude $A_0^{(p)}$ at frequency pf_0 , then the mixer output would be of $q+1$ order:

$$\frac{(q+1)!}{2^q q!} A_0^{(p)} A_1^q H_{q+1}(pf_0, \underbrace{f_1, f_1, \dots f_1}_{q \text{ times}}). \quad (1.66)$$

Since the outputs in (1.63) and (1.66) are at the same frequency, they will add coherently and the resulting amplitude will depend on their relative phases. Thus, the phase of a local-oscillator harmonic, or more fundamentally, the local-oscillator waveform can have a significant effect in determining the amplitude of a p, q response.

It should be cautioned that these results are only for mixers which have a small local-oscillator. Large local-oscillator mixers must be analyzed by other techniques. They will be discussed in Chapter 4.

1.10 Determining the Nonlinear Transfer Functions H_n for a Physical System

Fundamental to the successful application of the nonlinear analysis methods developed in this book is a practical means for determining the nonlinear transfer function H_n for specific systems under investigation. Many communications systems and receivers are relatively large electronic circuits with multiple nonlinearities scattered at many places throughout the system. A systematic nonlinear circuit analysis method designed to efficiently determine H_n is developed in Chapter 2. Successful application of the method requires adequate models of nonlinear devices and circuits as well as access to a digital computer that has been programmed to accurately solve the considerably complicated network equations. The issue of system modeling for input signals of interest is also developed in subsequent chapters. A computer program called SIGNCAP has been developed which solves for the nonlinear transfer functions of an arbitrary circuit containing resistors, inductors, capacitors, transistors, vacuum tubes, and diodes. SIGNCAP is described in Appendix A.

CHAPTER 2

SMALL SIGNAL NONLINEAR CIRCUIT ANALYSIS

2.1 Introduction

2.1.1 Frequency Domain Approach

Small signal nonlinear circuit analysis may be accomplished by use of the Volterra series. The purpose of this chapter is to describe a general technique for obtaining the input-output representation by starting from the incremental nonlinear circuit models. The methods are applicable to any size network.

The time-invariant Volterra series input-output representation of a nonlinear circuit may be given either in the time-domain or in the frequency domain. The frequency domain representation is

$$Y(f) = \sum_{n=1}^{\infty} \int_{-\infty}^{\infty} df_1 \dots \int_{-\infty}^{\infty} df_n \delta(f-f_1-f_2-\dots-f_n) \\ \cdot H_n(f_1, f_2, \dots, f_n) \prod_{p=1}^n X(f_p), \quad (2.1)$$

where $\delta(f)$ is the unit impulse at $f=0$, and $X(f)$ and $Y(f)$ are the frequency spectra of the input $x(t)$ and output $y(t)$ respectively. The H_n are the nonlinear transfer functions. The frequency domain approach developed here will derive the nonlinear transfer functions $H_n(f_1, f_2 \dots f_n)$ by starting with the circuit nonlinear differential equations. This approach was introduced in nonlinear circuit analysis by Weiner (1942). Deutsch (1962) made this work more accessible, while Narayanan (1967) developed it for distortion analysis of broadband amplifiers. We have extended Narayanan's work so that both nominally linear systems

(amplifiers, etc.) as well as nominally nonlinear and multi-input systems (multipliers, mixers, etc.) can be analyzed. Other work concerned with the frequency domain representation of general nonlinear systems has been presented by Barrett (1963), Flake (1963), Parente (1966), Lubbock and Bhansol (1969) and more recently by Bedrosian and Rice (1971). The approach emphasised in this book is to develop general nonlinear circuit analysis methods suitable for computer-aided analysis. Thus the objectives will be to go directly from the network circuit model to the nonlinear transfer functions.

2.1.2 Sinusoidal Inputs

Nonlinear transfer functions can be applied directly in the case of circuits excited by sinusoidal inputs; they are also used to determine the parameters of the nonlinear canonic models developed in detail in Chapter 3.

Consider a nonlinear system excited by the sum of two tones

$$x(t) = \operatorname{Re} \left\{ A_1 e^{j2\pi f_1 t} + A_2 e^{j2\pi f_2 t} \right\}, \quad (2.2)$$

where A_1 and A_2 are complex amplitudes of the tones at frequencies f_1 and f_2 respectively. The output $y(t)$ for the input $x(t)$ is given directly in terms of the nonlinear transfer functions as the sum of the real part of terms such as:

- a. $A_1 H_1(f_1) e^{j2\pi f_1 t}$: Linear response.
- b. $\frac{1}{2} A_1^2 H_2(f_1, f_1) e^{j4\pi f_1 t}$: Second-order sum response at $2f_1$.
- c. $|A_1|^2 H_2(f_1, -f_1)$: Second-order difference response at D.C.

d. $A_1 A_2 H_2(f_1, f_2) e^{j2\pi(f_1 + f_2)t}$: Second-order sum response at $f_1 + f_2$.

e. $\frac{3}{4} A_1^2 A_2^* H_3(f_1, f_1 - f_2) e^{j2\pi(2f_1 - f_2)t}$: Third-order intermodulation response at $2f_1 - f_2$.

In Chapter 1 it was stated that for an input made up of the sum of M tones at frequencies $f_1, f_2 \dots f_M$, the part of the numeric coefficient of $H_n(f_1, f_2 \dots f_n)$ at frequency $m_1 f_1 + m_2 f_2 \dots + m_M f_M$ which is independent of the input signal amplitude is

$$C = \frac{n!}{2^{n-1} m_1! m_2! \dots m_M!}, \quad (2.3)$$

where the m_i are non-negative integers and

$$m_1 + m_2 \dots + m_M = n.$$

Equation (1.51), which defines the total coefficient, $B_n(m)$ of $H_n(f_1, f_2 \dots f_m)$, is C multiplied by the amplitude factor $A_1^{m_1} A_2^{m_2} \dots A_M^{m_M}$. The derivation of Equation (2.3) is straightforward. If the input $x(t)$ is the sum of m complex exponentials

$$x(t) = \frac{1}{2} \sum_{k=1}^M A_k e^{j2\pi f_k t}, \quad (2.4)$$

where f_k will include both positive and negative frequencies and A_k for a negative frequency will be the complex conjugate of A_k for the positive frequency in order to have $x(t)$ real. The nth order output $y_n(t)$ is given by

$$\begin{aligned}
 y_n(t) &= \int_{-\infty}^{\infty} \cdots \int_{-\infty}^{\infty} h_n(\tau_1, \tau_2, \dots, \tau_n) \prod_{i=1}^n x(t-\tau_i) d\tau_i \\
 &= \int_{-\infty}^{\infty} \cdots \int_{-\infty}^{\infty} h_n(\tau_1, \tau_2, \dots, \tau_n) \frac{1}{2^n} \prod_{k=1}^M A_k e^{j2\pi f_k(t-\tau_i)} d\tau_i \\
 &= \sum_{k_1=1}^M \cdots \sum_{k_n=1}^M \frac{1}{2^n} A_{k_1} \cdots A_{k_n} H_n(f_{k_1}, f_{k_2}, \dots, f_{k_n}) \\
 &\quad \cdot e^{j2\pi(f_{k_1} + f_{k_2} + \dots + f_{k_n})t}. \tag{2.5}
 \end{aligned}$$

The time function $y_n(t)$ contains M^n terms. As the indices $k_1, k_2 \dots k_n$ vary over the range 1 through M , many of the terms will be at the same frequency, thus leading to the various nonlinear responses such as intermodulation and harmonic responses, and resulting in a varying number of terms at various particular frequency combinations. For example, for the case $M=6$, the third-order output at the frequency $f_1+f_2+f_3$ is given by

$$\begin{aligned}
 y_3(t) \Big|_{\substack{f=f_1+f_2+f_3 \\ f_1 \neq f_2 \neq f_3}} &= \frac{1}{2^3} A_1 A_2 A_3 \left[H_3(f_1, f_2, f_3) + H_3(f_1, f_3, f_2) \right. \\
 &\quad + H_3(f_2, f_1, f_3) + H_3(f_2, f_3, f_1) + H_3(f_3, f_1, f_2) \\
 &\quad \left. + H_3(f_3, f_2, f_1) \right] e^{j2\pi(f_1 + f_2 + f_3)t} + c.c. \tag{2.6}
 \end{aligned}$$

In Equation (2.6), c.c. indicates the complex conjugate of the term written out fully. In addition, it is assumed that the three frequencies are distinct, that is, $f_1 \neq f_2 \neq f_3$. An intermodulation response with a third-order output at the frequency $2f_1+f_2$ is given by

$$y_3(t) \Big|_{\substack{f=2f_1+f_2 \\ f_1 \neq f_2}} = \frac{1}{2^3} A_1^2 A_2 \left[H_3(f_1, f_1, f_2) + H_3(f_1, f_2, f_1) + H_3(f_2, f_1, f_1) \right] \\ \cdot e^{j2\pi(2f_1+f_2)t} + \text{c.c.} \quad (2.7)$$

Thus there are six terms at $f_1 + f_2 + f_3$, and three terms at $2f_1 + f_2$; at $3f_1$, one would find only one term. The nonlinear transfer functions in Equations (2.6) and (2.7) differ only in the ordering of their arguments, and there are as many nonlinear transfer functions as there are ways of ordering the arguments. If the other terms in the expansion are formed, a similar result is found. Namely, at frequency $m_1 f_1 + m_2 f_2 + \dots + m_M f_M$ there are as many terms as there are ways of forming $m_1 f_1 + m_2 f_2 + \dots + m_M f_M$. There is a result from combinatorial analysis which states (Feller, 1950, p. 32):

Let m_1, m_2, \dots, m_M be non-negative integers such that

$$m_1 + m_2 + \dots + m_M = n. \quad (2.8)$$

The number of ways in which n objects can be divided into m groups of which the first contains m_1 objects, the second m_2 objects, etc., is

$$\frac{n!}{m_1! m_2! \dots m_M!}. \quad (2.9)$$

This quantity is called the multinomial coefficient, and is denoted by $(n; m_1, m_2, \dots, m_M)$. The nonlinear transfer functions of an electrical network are symmetric. As an example of symmetry, consider an unsymmetric second-order nonlinear impulse response $h_2(\tau_1, \tau_2)$, for which $y_2(t)$ is $\iint d\tau_1 d\tau_2 h_2(\tau_1, \tau_2) x(t-\tau_1) x(t-\tau_2)$.

By evaluating the integral twice, using the changes of variable $\tau_1 \rightarrow \xi_1$, $\tau_2 \rightarrow \xi_2$, and $\tau_1 \rightarrow \xi_2$, $\tau_2 \rightarrow \xi_1$, respectively, a symmetric kernel for the system can be shown to be $[h_2(\tau_1, \tau_2) + h_2(\tau_2, \tau_1)]/2$. For an n^{th} order nonlinear impulse response, the symmetrization is performed over the $n!$ time permutations, and the sum is divided by $n!$. The time-domain symmetrization applies also to the frequency-domain nonlinear transfer functions, which are simply multiple-dimensional Fourier transforms of the time-domain impulse responses. In the case of the responses at $f_1 + f_2 + f_3$, and $2f_1 + f_2$, the $y_3(t)$ reduce to

$$y_3(t) \left|_{\substack{f_1 + f_2 + f_3 \\ f_1 \neq f_2 \neq f_3}} = \frac{3! A_1 A_2 A_3}{2^3 1! 1! 1!} H_3(f_1, f_2, f_3) e^{j2\pi(f_1 + f_2 + f_3)t} + \text{c.c.}, \quad (2.10)$$

and

$$y_3(t) \left|_{\substack{2f_1 + f_2 \\ f_1 \neq f_2}} = \frac{3! A_1^2 A_2}{2^3 2! 1!} H_3(f_1, f_1, f_2) e^{j2\pi(2f_1 + f_2)t} + \text{c.c.} \quad (2.11)$$

The output time function $y_n(t)$ is also twice the real part of the first term, or in general

$$\begin{aligned} & \text{n^{th}-order real output} \left|_{\substack{f = m_1 f_1 + m_2 f_2 + \dots + m_M f_M \\ f_1 \neq f_2 \dots \neq f_M}} \right. \\ &= \frac{n!}{2^{n-1} m_1! m_2! \dots m_M!} \operatorname{Re} \left\{ \underbrace{A_1^{m_1} A_2^{m_2} \dots A_M^{m_M}}_{m_1 \text{ times}} H_n \underbrace{(f_1, \dots, f_1, f_2, \dots, f_2, \dots, f_M, \dots, f_M)}_{m_2 \text{ times}} \dots \underbrace{(f_M, \dots, f_M)}_{m_M \text{ times}} \right. \\ & \quad \left. \cdot e^{j2\pi(m_1 f_1 + m_2 f_2 + \dots + m_M f_M)t} \right\}. \quad (2.12) \end{aligned}$$

The numerical coefficient of the real part is C, noted in Equation (2.3).

We now show the application of Equation (2.3) to the five terms given in examples (a) through (e) following Equation (2.2), where the coefficients m_1, m_2, m_3, m_4 relate to the frequencies $f_1, f_2, -f_1, -f_2$, respectively. This results in:

Case	n	m_1	m_2	m_3	m_4	C
a	1	1	0	0	0	$1!/(2^{1-1}1!0!0!0!) = 1$
b	2	2	0	0	0	$2!/(2^{2-1}2!0!0!0!) = 1/2$
c	2	1	0	1	0	$2!/(2^{2-1}1!1!0!0!) = 1$
d	2	1	1	0	0	$2!/(2^{2-1}1!1!0!0!) = 1$
e	3	2	0	0	1	$3!/(2^{3-1}2!1!0!0!) = 3/4$

In the case of non-sinusoidal inputs, the canonic models of the nonlinear system are employed. The canonic models in Chapter 3 are based on a Volterra representation of a nonlinear system, and the parameters of the canonic model are determined from either the nonlinear transfer functions or the time-domain kernels. Obtaining the nonlinear transfer function is the first step in the small-signal nonlinear analysis of nonlinear networks.

2.1.3 Applicability of the Volterra Series

The Volterra series representation is useful only if the series is rapidly convergent, so that only a few nonlinear transfer functions need be determined. Nonlinear systems representable by a convergent Volterra series are called analytic systems. Analytic systems have been defined by Volterra (1930), Brilliant (1958), Parente (1966) and others. An analytic system is one which satisfies three properties: (i) It is deterministic, that is, for a given input signal, the system can have one and only one corresponding output signal. (ii) It is time-invariant, and (iii) the system cannot introduce any abrupt changes in its output.

If such a change is present in the system output, it must be due to a similar abrupt change in the input or its derivatives.

The combinations of non-interacting analytic systems have been studied extensively by Brilliant (1958), George (1959), and Zames (1960). They have shown that analytic systems in cascade, parallel or multiplicative combinations give an overall analytic system. Feedback combinations of analytic systems are analytic except when the feedback makes the system unstable.

In general, determination of analyticity is difficult. Fortunately, in the circuit analysis of interest here we begin with individual circuit elements that will be analytic. Based on the algebra of Volterra systems we then know that with the exception of the unstable feedback case, the overall network is also analytic.

Networks with hysteresis elements (Brilliant 1959), or circuits in a limit-cycle mode are not analytic. However, for a given range of input level, hysteresis elements may be approximated by a Volterra series model.

2.1.4 "Small" and "Large" Signal Criteria and Truncation Error

In a large network with many nonlinear elements the determination of the nonlinear transfer functions over fifth or sixth order becomes inefficient. Given an analytic system and a small enough input signal, the output can be closely approximated by only the first few terms of the Volterra series. An essentially linear or "mildly" nonlinear system also requires only the first few order transfer functions. Thus, small signal nonlinear analysis presented here refers to systems in which only the first few order nonlinear transfer functions are significant. Chapter 4 presents time-variant extensions of the Volterra series and other methods for handling large signals and abrupt or violent nonlinearities.

The error in truncating the Volterra series of a nonlinear circuit has been studied by Flake (1963), Parente (1966), Volterra (1930), Brilliant (1958), George (1959) with few general results. Only in specific examples have useful bounds been obtained on the truncation error. At present the only approach is a brute-force determination of a large number of the higher order terms and then observing their rate of convergence.

Closely related to the truncation error is the range of validity of the nonlinear branch elements in the network. Given a network composed of a variety of nonlinearities combined with linear memory elements, the nonlinear circuit analysis begins by representing the nonlinear elements by a series, usually a Taylor series. The rate of convergence and the truncation error of the network can often be identified by considering the truncation error and the rate of convergence of the Taylor series of the nonlinear elements. This argument extends to nonlinear elements with memory.

2.2 Nonlinear Circuit Analysis

2.2.1 Introduction

In the analysis of nonlinear systems presented in Chapter 1, the nonlinear transfer functions related general input-output mathematical variables. However, when solving a circuit we have to define whether the input and the output are currents or voltage. Thus, the transfer function relating a voltage output to a current input will be different from one relating a voltage-output to a voltage-input.

It is important to note that the nonlinear transfer functions always relate the output voltages or currents to Thevenin generators for voltage excitations, or Norton generators for current excitations. This point is quite important when analyzing circuits which load the sources and make their terminal voltages or currents different from their unloaded values.

Physical interpretation of the input and output variables and the nonlinear transfer function representation is especially desirable since small-signal nonlinear circuit analysis is an extension of the conventional incremental analysis of electronic circuits. The nonlinear circuit models employed here are incremental models developed about a bias or operating point. It will also be found that the linearized equivalent circuit of the network plays an essential role in determining the nonlinear responses of the circuit.

To introduce the approach, first consider the simple circuit shown in Fig. 2.1. A clear understanding of this example aids in understanding more complex circuits which may include several different kinds of nonlinear elements. The circuit in Fig. 2.1 is an incremental nonlinear circuit. All voltages and currents are incremental quantities.

The nonlinear element may be a zero-memory device described by

$$I_2 = K(V_2), \quad (2.13)$$

where I_2 is the total current through the device and V_2 is the corresponding total voltage across it. To proceed with the small-signal analysis, the function $K(V_2)$ is expanded about the operating point V_{20} giving

$$i_2 = \sum_{n=1}^{\infty} K_n v_2^n, \quad (2.14)$$

where K_n are the Taylor series coefficients

$$K_n = \frac{1}{n!} \left. \frac{\partial^n K(V_2)}{\partial V_2^n} \right|_{V_2 = V_{20}}, \quad (2.15)$$

and i_2 and v_2 are the incremental current and voltage.

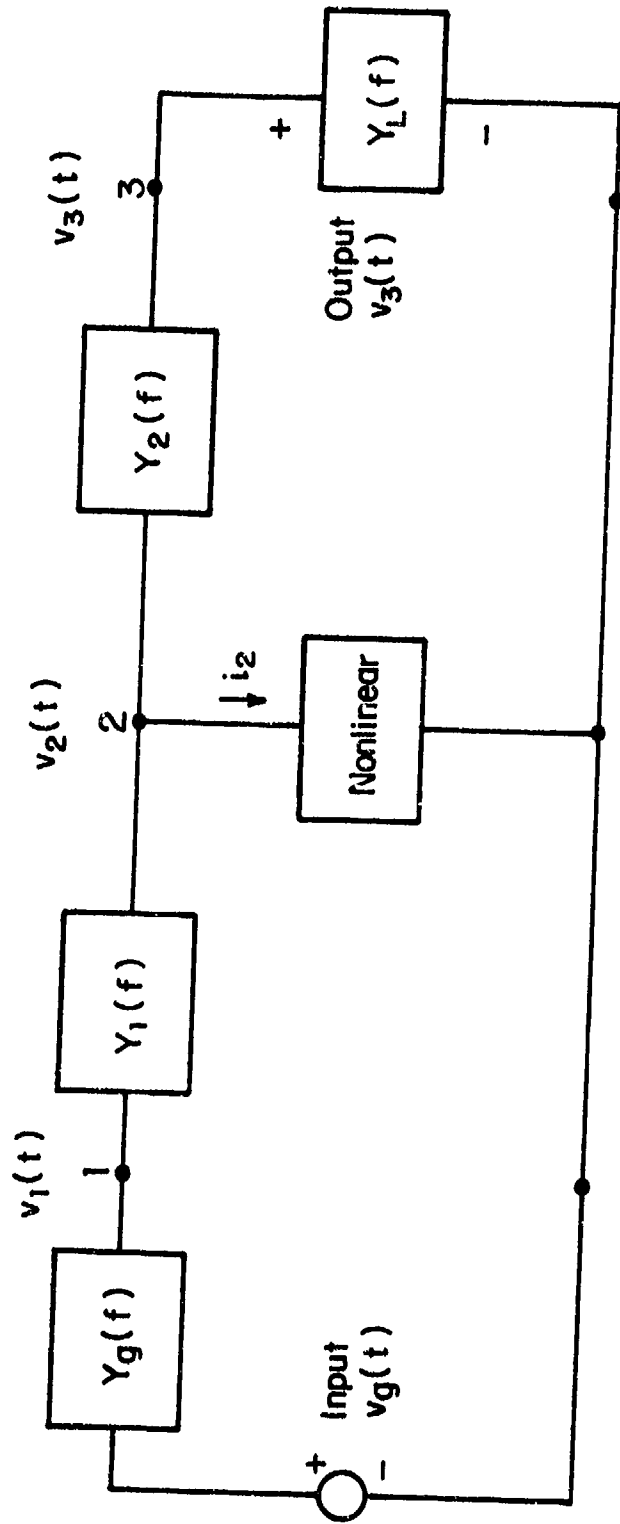


Fig. 2.1. A Simple Incremental Nonlinear Circuit.

In some cases the nonlinear element may be expressed in terms of the current I_2 , or

$$v_2 = R(I_2). \quad (2.16)$$

In this case, the resulting expansion is about the operating point I_{20}

$$v_2 = \sum_{n=1}^{\infty} R_n i_2^n, \quad (2.17)$$

where

$$R_n = \frac{1}{n!} \left. \frac{\partial^n R}{\partial I_2^n} \right|_{I_2 = I_{20}}. \quad (2.18)$$

Whether the nonlinearity is given in the form of Equation (2.13) or Equation (2.16) depends on the model description. The form which the circuit analysis of this chapter takes is a voltage input, voltage output nodal analysis. This has been chosen because it is most convenient for the analysis of electronic circuits, which tend to have many more loops than nodes.

The starting point of the nonlinear analysis is the incremental nonlinear circuit model, with the network structure given, and the input and output variables identified. The nonlinear branch elements in the network may be either zero-memory or a nonlinearity with memory. Additionally, they may be dependent upon variables other than their terminal voltages. The procedure for handling both dependent and independent nonlinearities are presented.

2.2.2 Single Nonlinear Element Circuit

In the circuit shown in Fig. 2.1, the output is the voltage $v_2(t)$ and the input is the generator voltage $v_g(t)$. The generator internal admittance is $Y_g(f)$ and $Y_1(f)$, $Y_2(f)$ and $Y_L(f)$ are linear non-zero memory networks. The purpose of the analysis is to determine the nonlinear transfer functions relating $v_3(t)$ and $v_g(t)$.

Let $C_n(f_1, f_2, \dots, f_n)$ denote the nonlinear transfer functions for the output $v_3(t)$ when the input is $v_g(t)$. If $v_g(t)$ is the sum of the M unit amplitude exponentials

$$v_g(t) = e^{j2\pi f_1 t} + e^{j2\pi f_2 t} + \dots + e^{j2\pi f_M t}, \quad (2.19)$$

the $C_n(f_1, \dots, f_n)$ can then be found in terms of the complex amplitudes of the output at the frequency of interest. Several methods exist for deriving the nonlinear transfer functions. These methods would first reduce the input-output relation between $v_3(t)$ and $v_g(t)$ to a nonlinear differential equation. The Volterra series for $v_3(t)$ can then be substituted into the differential equation and terms of equal order equated. The various methods differ in whether the time-domain Volterra representation is substituted or the frequency domain. The frequency domain approach is the one usually used.

Our frequency domain approach is similar except for the major difference that we are interested in numerical values of the nonlinear transfer function, and want to minimize preliminary work such as reducing the total network to a single differential equation. In the approach used, due to the fact that nonlinear elements can appear at any node, we solve for all independent node voltages or branch currents. Thus we solve the

single-output problem by using a multi-output formulation.

We will consider the following four type nonlinearities in the circuit shown in Fig. 2.1:

(a) Nonlinear conductance

$$i_2 = \sum_{n=1}^{\infty} K_n v_2^n \equiv K(v_2). \quad (2.20)$$

(b) Nonlinear resistance

$$v_2 = \sum_{n=1}^{\infty} R_n i_2^n \equiv R(i_2). \quad (2.21)$$

(c) Dependent nonlinearity which is a function of not only the voltage across it but also the voltage at another node.

$$i_2 = \sum_{m=0}^{\infty} \sum_{\substack{n=0 \\ m \neq n=0}}^{\infty} g_{mn} v_2^m v_3^n \equiv G(v_2, v_3). \quad (2.22)$$

(d) Nonlinearity with memory

$$i_2(t) = \sum_{n=1}^{\infty} \int_{-\infty}^{\infty} d\tau_1 \cdots \int_{-\infty}^{\infty} d\tau_n h_n(\tau_1, \dots, \tau_n) \prod_{m=1}^n v_2(t-\tau_m). \quad (2.23)$$

and $H_n(f_1 \dots f_n)$, the inverse transform of h_n , will be used to denote the nonlinear transfer function of this element.

Following the conventional functional notation, Equation (2.23) may be compactly written as

$$i_2(t) \triangleq H[v_2(t)], \quad (2.24)$$

where the square bracket is used to denote a functional operation.

2.2.2.1 Nonlinear Conductance K(v₂)

Kirchoff current and voltage laws apply to a nonlinear network as well as to a linear network. Thus the circuit equations may be written either as loop or node equations or as a mixed set. When the nonlinearity of Fig. 2.1 is specified as a power series in voltage, the node voltages $v_1(t)$, $v_2(t)$ and $v_3(t)$ are independent voltages. Applying Kirchoff's current law, the circuit node equations in operational notation are:

Node 1

$$Y_g(p) (v_1 - v_g) + Y_1(p) (v_1 - v_2) = 0,$$

Node 2

$$Y_1(p) (v_2 - v_1) + K(v_2) + Y_2(p) (v_2 - v_3) = 0, \quad \left. \right\} \quad (2.25)$$

Node 3

$$Y_2(p) (v_3 - v_2) + Y_L(p) v_3 = 0.$$

The three node equations in Equation (2.25) are time-domain equations. Each equation states that the total current leaving a node is zero. The p is a linear operator, and the various $Y(p)$ are combinations of terms such as Cp for a capacitor, G for a resistor, and $1/(Lp)$ for an inductor. When operating on a voltage, v , they perform the time-domain operations:

$$\begin{aligned} C p v(t) &= C \frac{dv}{dt}, \\ G v(t) &= G v, \\ \frac{1}{Lp} v(t) &= \frac{1}{L} \int_{-\infty}^t v(t) dt. \end{aligned} \quad (2.26)$$

The current through the nonlinearity, $K(v_2)$, is not operated on by any of the $Y(p)$, and is considered separately.

Substituting the power series for $K(v_2)$ into Equation (2.25) and taking the second and higher-order terms to the right-hand side together with the source term we get

$$[v(p)] \begin{bmatrix} v_1 \\ v_2 \\ v_3 \end{bmatrix} = \begin{bmatrix} Y_g(p)v_g \\ -\sum_{n=2}^{\infty} K_n v_2^n \\ 0 \end{bmatrix}. \quad (2.27)$$

where $[Y(p)]$ is the admittance operator matrix of the linearized network

$$[Y(p)] = \begin{bmatrix} Y_g(p) + Y_1(p) & -Y_1(p) & 0 \\ -Y_1(p) & K_1 + Y_1(p) + Y_2(p) & -Y_2(p) \\ 0 & -Y_2(p) & Y_2(p) + Y_L(p) \end{bmatrix}. \quad (2.28)$$

Equations (2.27) and (2.28) are simply matrix restatements of Equation (2.25). Equation (2.27) is still a time-domain equation. To derive the nonlinear transfer functions to third-order, let $v_g(t)$ be the sum of three exponentials of the form given by Eq. (2.19). Denoting the nonlinear transfer functions for $v_1(t)$, $v_2(t)$, and $v_3(t)$ by $A_n(f_1, f_2, \dots, f_n)$, $B_n(f_1, f_2, \dots, f_n)$ and $C_n(f_1, f_2, \dots, f_n)$, respectively, we get in terms of transfer functions A_n ,

$$\begin{aligned}
 v_1(t) = & \sum_{i=1}^3 \left\{ A_1(f_i) e^{j2\pi f_i t} + A_2(f_i, f_i) e^{j4\pi f_i t} \right. \\
 & + A_3(f_i, f_i, f_i) e^{j6\pi f_i t} + \sum_{\substack{j=1 \\ j \neq i}}^3 [A_2(f_i, f_j) e^{j2\pi(f_i + f_j)t} \\
 & \left. + 3A_3(f_i, f_i, f_j) e^{j2\pi(2f_i + f_j)t} \right\} \\
 & + 6A_3(f_1, f_2, f_3) e^{j2\pi(f_1 + f_2 + f_3)t} + O(3), \quad (2.29)
 \end{aligned}$$

where $O(3)$ are terms of higher order than third.

Similarly for $v_2(t)$,

$$\begin{aligned}
 v_2(t) = & \sum_{i=1}^3 \left\{ B_1 e^{j2\pi f_i t} + B_2 e^{j4\pi f_i t} + B_3 e^{j6\pi f_i t} \right. \\
 & + \sum_{\substack{j=1 \\ j \neq i}}^3 (B_2 e^{j2\pi(f_i + f_j)t} + 3B_3 e^{j2\pi(2f_i + f_j)t}) \left. \right\} \\
 & + 6B_3 e^{j2\pi(f_1 + f_2 + f_3)t} + O(3). \quad (2.30)
 \end{aligned}$$

The frequency arguments of the transfer functions are not indicated above since they are clearly defined by the multiplying exponential. An equation similar to (2.29) and (2.30) can be written for v_3 in terms of C_n . Substitution of these expansions on both sides of the node Equation (2.27) gives for the left hand side

$$[Y(p)] = \begin{bmatrix} 3 & j2\pi f_1 t & j2\pi f_2 t & j2\pi(f_1 + f_2 + f_3)t \\ \sum_{i=1}^3 [A_1 e^{j2\pi f_i t} + A_2 e^{j4\pi f_i t} + \dots] + 6A_3 e^{j2\pi(f_1 + f_2 + f_3)t} \\ \sum_{i=1}^3 [B_1 e^{j2\pi f_i t} + B_2 e^{j4\pi f_i t} + \dots] + 6B_3 e^{j2\pi(f_1 + f_2 + f_3)t} \\ \sum_{i=1}^3 [C_1 e^{j2\pi f_i t} + C_2 e^{j4\pi f_i t} + \dots] + 6C_3 e^{j2\pi(f_1 + f_2 + f_3)t} \end{bmatrix}. \quad (2.31)$$

The right-hand side contains the source term and terms involving various powers of the node voltage v_2 . Only terms up to "third-order" exponentials are of interest in these products. The only powers of v_2 contributing up to third-order terms in the right-hand side are the second and third. Thus, squaring v_2 of Eq. (2.26) and writing terms up to third-order gives.

$$\begin{aligned} v_2^2 = & \left[\sum_{i=1}^3 B_1 e^{j2\pi f_i t} \right]^2 + 4 \sum_{\substack{i,j,k=1 \\ i \neq j \neq k}}^3 B_1(f_i) B_2(f_j, f_k) \\ & \cdot e^{j2\pi(f_i + f_j + f_k)t} + 2 \sum_{i,j=1}^3 B_1(f_i) B_2(f_j, f_j) e^{j2\pi(f_i + 2f_j)t} + 0(3). \end{aligned} \quad (2.32)$$

The first term on the right-hand side of Equation (2.32) contains second-order terms at frequencies $2f_i$, and $f_i + f_j$, where $i \neq j$ and i and j take on the values 1, 2, 3. The remaining terms on the right-hand side are third-order terms.

Similarly raising Eq. (2.30) to the third power gives the third-order term in v_2^3 as

$$v_2^3 = \left[\sum_{i=1}^3 B_1 e^{j2\pi f_i t} \right]^3 + O(3), \quad (2.33)$$

Substituting these terms, the right-hand side column vector of Eq. (2.27) up to third-order becomes

$$\begin{bmatrix} Y_g(p) \left[\sum_{i=1}^3 e^{j2\pi f_i t} \right] \\ -K_2 \left[\sum_{i=1}^3 B_1 e^{j2\pi f_i t} \right]^2 - 4K_2 \sum_{\substack{i,j,k=1 \\ i \neq j \neq k}}^3 B_1(f_i) B_2(f_i, f_j) e^{j2\pi(f_i + f_j + f_k)t} \\ -2K_2 \sum_{i,j=1}^3 B_1(f_i) B_2(f_j, f_j) e^{j2\pi(f_i + 2f_j)t} - K_3 \left[\sum_{i=1}^3 B_1 e^{j2\pi f_i t} \right]^3 \\ 0 \end{bmatrix} \quad (2.34)$$

To solve for any order transfer function, e.g., $C_2(f_1, f_2)$, the coefficients of the terms $e^{j2\pi(f_1 + f_2)t}$ on both sides of the

node equations are equated. Since terms in $e^{j2\pi(f_1+f_2)t}$ also arise in conjunction with $A_2(f_1, f_2)$ and $B_2(f_1, f_2)$ we therefore get matrix equations for each order. Starting with first-order, Eq. (2.31) and Eq. (2.34) give

$$[Y(p)] \begin{bmatrix} A_1(f_i) \\ B_1(f_i) \\ C_1(f_i) \end{bmatrix} e^{j2\pi f_i t} = \begin{bmatrix} Y_g(p)e^{j2\pi f_i t} \\ 0 \\ 0 \end{bmatrix}; i = 1, 2, 3. \quad (2.35)$$

Equation (2.35) is a time-domain equation in operator form, which relates the node voltages $A_1(f_i)e^{j2\pi f_i t}$, $B_1(f_i)e^{j2\pi f_i t}$, and $C_1(f_i)e^{j2\pi f_i t}$, to the complex exponential excitation voltage source $Y_g(p)e^{j2\pi f_i t}$. By noting that the operator p is d/dt , Equation (2.35) can be transformed into the frequency-domain for the three first-order nonlinear transfer functions $A_1(f_i)$, $B_1(f_i)$, $C_1(f_i)$.

The first-order transfer functions are then given by

$$\begin{bmatrix} A_1(f_i) \\ B_1(f_i) \\ C_1(f_i) \end{bmatrix} = [Y(f_i)]^{-1} \begin{bmatrix} Y_g(f_i) \\ 0 \\ 0 \end{bmatrix}; i = 1, 2, 3. \quad (2.36)$$

In going from Equation (2.35) to Equation (2.36), the operator p is replaced by $j2\pi f_i$ when operating on a signal at frequency f_i .

Carrying out the differentiation and integration consistent with the operators p and $1/p$, the admittance operator matrix $[Y(p)]$ is replaced by $[Y(f_i)]$, which is the network nodal admittance matrix.

In the second-order case the left-hand side of the node equations becomes

$$[Y(p)] \begin{bmatrix} 2A_2(f_1, f_2) \\ 2B_2(f_1, f_2) \\ 2C_2(f_1, f_2) \end{bmatrix} e^{j2\pi(f_1+f_2)t}$$

$$= 2e^{j2\pi(f_1+f_2)t} [Y(f_1+f_2)] \begin{bmatrix} A_2(f_1, f_2) \\ B_2(f_1, f_2) \\ C_2(f_1, f_2) \end{bmatrix}, \quad (2.37)$$

where the operator p has been replaced by $j2\pi(f_1+f_2)$, and $f_1 \neq f_2$.

In the right-hand side, the term at frequency (f_1+f_2) is

$$\left. -K_2 v_2^2 \right|_{f_1+f_2} = -(2;1,1) K_2 B_1(f_1) B_1(f_2) e^{j2\pi(f_1+f_2)t}, \quad (2.38)$$

where the multinomial coefficient $(2;1,1) = 2$, so that the right-hand side at frequency (f_1+f_2) becomes

$$\begin{array}{l} \text{Right-} \\ \text{hand} \\ \text{side} \end{array} = 2 \begin{bmatrix} 0 & j2\pi(f_1+f_2)t \\ -\hat{K}_2(f_1, f_2)e^{j2\pi(f_1+f_2)t} & 0 \\ f_1+f_2 & 0 \end{bmatrix}. \quad (2.39)$$

where we have defined $\hat{K}_2(f_1, f_2)$ as

$$\hat{K}_2(f_1, f_2) = K_2 B_1(f_1) B_1(f_2). \quad (2.40)$$

Equating the two sides and cancelling $2e^{j2\pi(f_1+f_2)t}$ from both sides we get the equations yielding the second-order transfer functions of the network

$$\begin{bmatrix} A_2(f_1, f_2) \\ B_2(f_1, f_2) \\ C_2(f_1, f_2) \end{bmatrix} = [Y(f_1 + f_2)]^{-1} \begin{bmatrix} 0 \\ -\hat{K}_2(f_1, f_2) \\ 0 \end{bmatrix}. \quad (2.41)$$

It can be easily verified that the equations for the frequency $2f_i$ are the same as above with appropriate change in the frequencies.

In the case of the third-order equations, consider the frequency $(f_1 + f_2 + f_3)$, where $f_1 \neq f_2 \neq f_3$. The left-hand side of the node equations is now

$$\begin{array}{c}
 \text{Left-hand side} \\
 \left| f_1 + f_2 + f_3 \right|
 \end{array}
 = \frac{j2\pi(f_1 + f_2 + f_3)t}{\left\{ Y(f_1 + f_2 + f_3) \right\}} \begin{bmatrix} 6A_3(f_1, f_2, f_3) \\ 6B_3(f_1, f_2, f_3) \\ 6C_3(f_1, f_2, f_3) \end{bmatrix}. \quad (2.42)$$

while in the right-hand side $K_2 v_2^2$ contributes the following term

$$\begin{array}{c}
 K_2 v_2^2 \\
 \left| f_1 + f_2 + f_3 \right|
 \end{array}
 = 2K_2 \left\{ B_1(f_1) \left[B_2(f_2, f_3) + B_2(f_3, f_2) \right] \right. \\
 + B_1(f_2) \left[B_2(f_1, f_3) + B_2(f_3, f_1) \right] \\
 + B_1(f_3) \left[B_2(f_1, f_2) + B_2(f_2, f_1) \right] \left. \right\} \\
 \cdot e^{j2\pi(f_1 + f_2 + f_3)t}. \quad (2.43)$$

The bracket {} term contains all permutations of the three frequencies f_1, f_2 and f_3 . This always occurs in physical circuits since the nonlinear transfer function must be symmetric with respect to all the frequencies. A compact notation for this symmetrization is

$$\overline{B_1(f_1) B_2(f_2, f_3)} \triangleq \frac{1}{6} \left\{ B_1(f_1) \left[B_2(f_2, f_3) + B_2(f_3, f_2) \right] \right. \\
 + B_1(f_2) \left[B_2(f_1, f_3) + B_2(f_3, f_1) \right] \\
 + B_1(f_3) \left[B_2(f_1, f_2) + B_2(f_2, f_1) \right] \left. \right\}. \quad (2.44)$$

Therefore

$$\begin{aligned} K_2 v_2^2 \Big|_{f_1+f_2+f_3} &= 12 K_2 \overline{B_1(f_1) B_2(f_2, f_3)} \\ &= 6 \hat{K}_{23} \overline{B_1(f_1) B_2(f_2, f_3)}, \end{aligned} \quad (2.45)$$

where

$$\hat{K}_{23} = 2K_2 \overline{B_1(f_1) B_2(f_2, f_3)}. \quad (2.46)$$

The term \hat{K}_{23} is a third-order source resulting from an interaction between a linear and a second-order nonlinearity. Thus, there will be third-order products even if the third-order nonlinearity, K_3 , were zero.

The only other term of frequency $(f_1+f_2+f_3)$ comes from the third-order nonlinearity K_3 giving

$$\begin{aligned} K_3 v_2^3 \Big|_{f_1+f_2+f_3} &= (3,1,1,1) K_3 \left\{ \prod_{i=1}^3 B_1(f_i) \right\} e^{j2\pi(f_1+f_2+f_3)t} \\ &\triangleq 6 \hat{K}_3(f_1, f_2, f_3) e^{j2\pi(f_1+f_2+f_3)t}, \end{aligned} \quad (2.47)$$

where $(3,1,1,1) = 6$, and

$$\hat{K}_3 = K_3 \prod_{i=1}^3 B_1(f_i). \quad (2.48)$$

Combining Equations (2.42), (2.43), and (2.47) gives an equation yielding the third-order transfer functions in terms of $\hat{K}_{23}(f_1, f_2, f_3)$ and $\hat{K}_3(f_1, f_2, f_3)$. Thus,

$$\begin{bmatrix} A_3(f_1, f_2, f_3) \\ B_3(f_1, f_2, f_3) \\ C_3(f_1, f_2, f_3) \end{bmatrix} = \left[Y(f_1 + f_2 + f_3) \right]^{-1} \begin{bmatrix} 0 \\ -\hat{K}_{23}(f_1, f_2, f_3) - \hat{K}_3(f_1, f_2, f_3) \\ 0 \end{bmatrix}. \quad (2.49)$$

The general nature of the analysis should now be apparent. Higher-order nonlinear transfer functions can be similarly derived. It may be noted that the n^{th} order transfer functions depend on all the Taylor series coefficients from K_1 to K_n . Additionally, it will be noted that only the first-order transfer functions are required to determine the second-order. Only first and second-orders are required to determine third-order, and in general, only the first through n^{th} order nonlinear transfer functions are required to determine the $n+1^{th}$ order nonlinear transfer function. The analysis determines the nonlinear transfer functions for frequency combinations of the form $f_i + f_j + \dots + f_m$, $i \neq j \neq m$. In using the nonlinear transfer functions to determine input-output relations, they must be evaluated at the frequency combination of interest and premultiplied by the coefficient $B_n(m)$ of Equation (1.51), corresponding to this frequency combination.

2.2.2.2 Current-Controlled Nonlinearity

If the nonlinearity in Figure 2.1 is specified as a power series in current instead of voltage, the node-voltage formulation may again be employed. The nonlinear sources will appear as voltage sources in series with the linearized element, and can be transformed into equivalent Norton current sources. This, it

should be noted, is the same technique used to include linear voltage generators in the node analysis. As an example consider a nonlinear resistor. The power series between v_2 and i_2 for a current-controlled nonlinear resistor is

$$v_2 = \sum_{n=1}^{\infty} R_n i_2^n. \quad (2.50)$$

As the first step, the linear network is solved for v_2 , resulting in $B_1(f_i)$ being found from

$$\begin{bmatrix} A_1(f_i) \\ B_1(f_i) \\ C_1(f_i) \end{bmatrix} = [Y(f_i)]^{-1} \begin{bmatrix} Y_g(f_i) \\ 0 \\ 0 \end{bmatrix}, \quad i=1,2,\dots \quad (2.51)$$

Next, the current through the linearized resistor is computed

$$i_2 \Big|_{f_i} = B_1(f_i)/R_1 e^{j2\pi f_i t}, \quad i=1,2\dots \quad (2.52)$$

Using Equation (2.52) with (2.50) results in

$$i_2^2 \Big|_{f_1+f_2} = 2 \frac{B_1(f_1) B_1(f_2)}{R_1^2} e^{j2\pi(f_1+f_2)t}. \quad (2.53)$$

By analogy with Equations (2.38) - (2.41), a second-order voltage source can then be defined at frequency $f_1 + f_2$

$$v_2|_{f_1+f_2} = R_2 \frac{B_1(f_1) B_1(f_2)}{R_1^2} e^{j2\pi(f_1+f_2)t}, \quad (2.54)$$

and is inserted in series with the linearized resistor. This can be converted into a second-order current source, $\hat{K}_2(f_1, f_2)$, through use of Norton's theorem, or

$$K_2(f_1, f_2) = \frac{1}{R_1} v_2|_{f_1+f_2} \quad (2.55)$$

$$= \frac{R_2}{R_1^3} B_1(f_1) B_1(f_2). \quad (2.56)$$

The second-order node voltages $A_2(f_i, f_j)$, $B_2(f_i, f_j)$, and $C_2(f_i, f_j)$ can be solved from

$$\begin{bmatrix} A_2(f_1, f_2) \\ B_2(f_1, f_2) \\ C_2(f_1, f_2) \end{bmatrix} = [z(f_1+f_2)]^{-1} \begin{bmatrix} 0 \\ -\hat{K}_2(f_1, f_2) \\ 0 \end{bmatrix}. \quad (2.57)$$

With the second-order voltages found, the second-order current through the resistor is

$$i_2(f_i + f_j) = B_2(f_i, f_j)/R_1. \quad (2.58)$$

Using Equations (2.58) and (2.52) in (2.50), the third-order Norton current generator can be written as

$$\hat{K}_{23}(f_1, f_2, f_3) + \hat{K}_3(f_1, f_2, f_3) = 2 \frac{R_2}{R_1^3} \frac{B_1(f_1)B_2(f_2, f_3)}{R_1} + \frac{R_3}{R_1^4} \prod_{i=1}^3 B_1(f_i), \quad (2.59)$$

and the third-order node voltages solved from

$$\begin{bmatrix} A_3(f_1, f_2, f_3) \\ B_2(f_1, f_2, f_3) \\ C_3(f_1, f_2, f_3) \end{bmatrix} = [Y(f_1 + f_2 + f_3)]^{-1} \begin{bmatrix} 0 \\ -\hat{K}_{23}(f_1, f_2, f_3) - \hat{K}_3(f_1, f_2, f_3) \\ 0 \end{bmatrix}. \quad (2.60)$$

The higher-order transfer functions are found in the same manner. It is evident that the equations for the nonlinear transfer functions are formally the same as for the voltage-controlled resistor if the nonlinear current sources, e.g., \hat{K}_{23} and \hat{K}_3 , are properly defined, as in Equations (2.56) and (2.59).

A current-controlled nonlinear inductance can be treated in a similar manner. In this case the functional relation is between voltage and the flux derivative:

$$v_2 = - \frac{d\phi}{dt}, \quad (2.61)$$

where the flux ϕ is given by

$$\phi = \phi(I_2). \quad (2.62)$$

Expanding ϕ in a Taylor series in I_2 and inserting the series into Equation (2.61) results in

$$v_2 = -L_1 \frac{d}{dt} i_2 - L_2 \frac{d}{dt} i_2^2 - L_3 \frac{d}{dt} i_2^3 \dots \quad (2.63)$$

where the L_i are the coefficients of the Taylor series expansion. Using Equation (2.62) in place of Equation (2.50) and carrying out the analysis operations results in nonlinear current sources of the form:

$$\text{Second-Order} \quad \hat{k}_2 = \frac{z_2(f_1+f_2)}{z_1(f_1+f_2)} \frac{B_1(f_1)}{z_1(f_1)} \frac{B_1(f_2)}{z_1(f_2)} \cdot \quad (2.64)$$

Third-Order

$$\begin{aligned} \hat{k}_{23} + \hat{k}_3 &= \frac{2z_2(f_1+f_2+f_3)}{z_1(f_1+f_2+f_3)} \\ &\cdot \frac{B_1(f_1)}{z_1(f_1)} \frac{B_2(f_2, f_3)}{z_1(f_2+f_3)} + \frac{z_3(f_1+f_2+f_3)}{z_1(f_1+f_2+f_3)} \\ &\cdot \prod_{i=1}^3 \frac{B_1(f_i)}{z_1(f_i)} \end{aligned} \quad (2.65)$$

where

$$z_\ell(f_1+f_j \dots) = j2\pi(f_1 + f_j \dots) L_\ell. \quad (2.66)$$

2.2.2.3 Zero-Memory Dependent Nonlinearity

The nonlinearity given by Eq. (2.22) is a dependent nonlinearity since the (i_2, v_2) relation depends on another voltage v_3 . Applying the node equation formulation gives the $[Y(p)]$

$$[Y(p)] = \begin{bmatrix} Y_g(p) + Y_1(p) & -Y_1(p) & 0 \\ -Y_1(p) & g_{10} + Y_1(p) + Y_2(p) & -Y_2(p) + g_{01} \\ 0 & -Y_2(p) & Y_2(p) + Y_L(p) \end{bmatrix}, \quad (2.67)$$

where g_{10} and g_{01} are the linear terms in the power series

$$\begin{aligned} g(v_2, v_3) = & g_{10}v_2 + g_{01}v_3 + g_{20}v_2^2 + g_{11}v_2v_3 \\ & + g_{02}v_3^2 + g_{30}v_2^3 + g_{21}v_2^2v_3 \quad g_{12}v_2v_3^2 + g_{03}v_3^3 \dots \end{aligned} \tag{2.68}$$

It should be noted that dependent nonlinearities cause numerical asymmetry in the Y matrix. Grouping together the terms of order n as $g_n(v_2, v_3)$ gives

$$\begin{aligned} g_2(v_2, v_3) = & g_{20}v_2^2 + g_{11}v_2v_3 + g_{02}v_3^2 \\ g_3(v_2, v_3) = & g_{30}v_2^3 + g_{21}v_2^2v_3 + g_{12}v_2v_3^2 + g_{03}v_3^3 \\ \cdot \\ \cdot \\ \cdot \end{aligned} \tag{2.69}$$

To obtain the second- and third-order transfer functions the series v_2 and v_3 are as usual substituted into $g_2(v_2, v_3)$ and $g_3(v_2, v_3)$ and the coefficient of the frequency of interest isolated. Thus, it can be shown that

$$g_2(v_2, v_3) \left|_{(f_1+f_2)}^{(f_1+f_2)} = 2e^{j2\pi(f_1+f_2)t} \left\{ g_{20} B_1(f_1) B_1(f_2) + g_{02} C_1(f_1) C_1(f_2) + \frac{1}{2} g_{11} \left[B_1(f_1) C_1(f_2) + B_1(f_2) C_1(f_1) \right] \right\}. \quad (2.70)$$

From Eq. (2.70), a second-order current-source $\hat{g}_2(f_1, f_2)$ can be defined as

$$g_2(f_1, f_2) \triangleq g_{20} B_1(f_1) B_1(f_2) + g_{02} C_1(f_1) C_1(f_2) + g_{11} \overline{B_1(f_1) C_1(f_2)}. \quad (2.71)$$

The third order sources can be also defined as follows

$$g_2(v_2, v_3) \left|_{f_1+f_2+f_3}^{f_1+f_2+f_3} = 6e^{j2\pi(f_1+f_2+f_3)t} \left\{ 2g_{20} \overline{B_1(f_1) B_2(f_2, f_3)} + 2g_{02} \overline{C_1(f_1) C_2(f_2, f_3)} + g_{11} \left[\overline{B_1(f_1) C_2(f_2, f_3)} + \overline{B_2(f_1, f_2) C_1(f_3)} \right] \right\} \triangleq 6 \hat{g}_{23}(f_1, f_2, f_3) e^{j2\pi(f_1+f_2+f_3)t}. \quad (2.72)$$

$$g_3(v_2, v_3) \left|_{f_1+f_2+f_3}^{f_1+f_2+f_3} = 6e^{j2\pi(f_1+f_2+f_3)t} \left\{ g_{30} \prod_{i=1}^3 B_1(f_i) + g_{03} \prod_{i=1}^3 C_1(f_i) + g_{21} \overline{B_1(f_1) B_1(f_2) C_1(f_3)} + g_{12} \overline{B_1(f_1) C_1(f_2) C_1(f_3)} \right\} \triangleq 6 \hat{g}_3(f_1, f_2, f_3) e^{j2\pi(f_1+f_2+f_3)t}, \quad (2.73)$$

where $\hat{g}_{23}(f_1, f_2, f_3)$ and $\hat{g}_3(f_1, f_2, f_3)$ are defined by the above equations.

In terms of these nonlinear sources the second- and third-order transfer functions are given by the solution of

$$\begin{bmatrix} A_2(f_i, f_j) \\ B_2(f_i, f_j) \\ C_2(f_i, f_j) \end{bmatrix} = \left[Y(f_i + f_j) \right]^{-1} \begin{bmatrix} 0 \\ -\hat{g}_2(f_i, f_j) \\ 0 \end{bmatrix}, \quad (2.74)$$

$$\begin{bmatrix} A_3(f_i, f_j, f_k) \\ B_3(f_i, f_j, f_k) \\ C_3(f_i, f_j, f_k) \end{bmatrix} = \left[Y(f_i + f_j + f_k) \right]^{-1} \begin{bmatrix} 0 \\ -[\hat{g}_{23}(f_i, f_j, f_k) \\ + \hat{g}_3(f_i, f_j, f_k)] \\ 0 \end{bmatrix}. \quad (2.75)$$

Hence, the form of the transfer function equations are not much more complex than that of the independent nonlinearity, the main difference being the derivation of the nonlinearity sources $\hat{g}_2, \hat{g}_{23} \dots \hat{g}_{ln}$, which becomes complicated with increasing n.

2.2.2.4 Nonlinearity with Memory

A nonlinearity with memory is analyzed by first considering the nonlinearity as an isolated nonlinear system, and then finding its interactions when embedded in the entire network. Thus, its nonlinear transfer functions $H_1(f), H_2(f_i, f_j), H_3(f_i, f_j, f_k)$, etc., are first defined. Then, applying the node equation formulation of Sec. 2.2.2.2, the first-order transfer functions are given by Eq. 2.36), with $[Y(f)]$ given by

$$[Y(f)] = \begin{bmatrix} Y_g(f) + Y_1(f) & -Y_1(f) & 0 \\ -Y_1(f) & H_1(f) + Y_1(f) + Y_2(f) & -Y_2(f) \\ 0 & -Y_2(f) & Y_2(f) + Y_L(f) \end{bmatrix}. \quad (2.76)$$

Note the difference between $[Y(f)]$ here and in Eq. (2.28) is that the conductance K_1 is replaced by a frequency dependent admittance $H_1(f)$.

The second-order transfer functions are given similarly by

$$\begin{bmatrix} A_2(f_i, f_j) \\ B_2(f_i, f_j) \\ C_2(f_i, f_j) \end{bmatrix} = \left[Y(f_i + f_j) \right]^{-1} \begin{bmatrix} 0 \\ -\hat{H}_2(f_i, f_j) \\ 0 \end{bmatrix}, \quad (2.77)$$

where

$$\hat{H}_2(f_i, f_j) = H_2(f_i, f_j) B_1(f_i) B_1(f_j), \quad (2.78)$$

and third-order by

$$\begin{bmatrix} A_3(f_i, f_j, f_k) \\ B_3(f_i, f_j, f_k) \\ C_3(f_i, f_j, f_k) \end{bmatrix} = \left[Y(f_i + f_j + f_k) \right]^{-1} \begin{bmatrix} 0 \\ -\{\hat{H}_{23}(f_i, f_j, f_k) + \hat{H}_3(f_i, f_j, f_k)\} \\ 0 \end{bmatrix}, \quad (2.79)$$

where

$$\hat{H}_{23}(f_i, f_j, f_k) = \frac{2H_2(f_i, f_j + f_k)}{B_1(f_i) B_2(f_j)}, \quad (2.80)$$

$$\hat{H}_3(f_i, f_j, f_k) = H_3(f_i, f_j, f_k) B_1(f_i) B_1(f_j) B_1(f_k). \quad (2.81)$$

Note that $H_2(f_i, f_j + f_k)$ is included in the symmetrization of Eq. (2.80). Nonlinearities with memory occurring in electronic circuits are usually nonlinear capacitors or inductors for which the transfer functions $H_n(\cdot)$ are found by inspection.

2.2.3 General Single-Input Analysis

2.2.3.1 Introduction

In the analysis of a general single-input nonlinear network the main extension from the previous section is the inclusion of multiple nonlinear elements as well as an arbitrary number of nodes. The approach used is the nodal equation formulation, and the transfer function of interest is voltage-input, voltage-output. Communication circuits are usually a ladder structure, and the node equation approach is most efficient.

Given a nonlinear circuit, the assumption of weak excitation of the nonlinearities permits the circuit elements to be represented by the first few terms of a Taylor series expansion around their DC operating point. As the excitation becomes stronger, the number of terms necessary to characterize the system increases making this approach inefficient and the time-domain approach more desirable.

Given a nonlinear incremental circuit, we first derive the incremental current i and voltage v relationships of the elements of the circuit. The following four types of nonlinearities are commonly encountered:

a. No Memory, Independent

$$i = K(v) \stackrel{\Delta}{=} \sum_{n=1}^{\infty} K_n v^n, \quad (2.82)$$

b. No Memory, Dependent

$$i = G(u, v) \stackrel{\Delta}{=} \sum_{m \neq n=0}^{\infty} \sum_{m,n}^{\infty} g_{mn} u^m v^n, \quad (2.83)$$

c. Capacitance Memory, Independent

$$i = \frac{d}{dt} Q(v) \stackrel{\Delta}{=} \frac{d}{dt} \sum_{n=1}^{\infty} \gamma_n v^n, \quad (2.84)$$

d. Inductive Memory, Independent

$$i = \int_{-\infty}^t \Phi(v) dt \stackrel{\Delta}{=} \int_{-\infty}^t dt \sum_{n=1}^{\infty} \varphi_n v^n, \quad (2.85)$$

where v is the incremental voltage across the element through which the incremental current is i . Three of the above nonlinear elements (a), (c) and (d) are independent of voltages and current elsewhere in the network. The nonlinearity (b), however, is a dependent nonlinearity where u is a voltage across another element in the circuit. Such nonlinearities correspond to dependent sources. The memory nonlinearities (c) and (d) are simple forms of the nonlinearity given by the Volterra series of Section 2.2.2.4.

The convergence of the Volterra series representation for a network including only the above nonlinearities and interconnected by linear networks depends on the convergence of the series for each element. If each of the nonlinearities are independently convergent, and the combined network is stable, then the resulting transfer functions will be convergent. In small-signal nonlinear analysis, network stability will seldom be effected by the nonlinearities. If stability is established for the linearized network, it may be assumed to hold for the small-signal nonlinear model. Thus, the analyticity of the network and hence the convergence of the resulting nonlinear transfer functions is easily established by checking that each of the element series are convergent.

2.2.3.2 General Procedure for Single-Input Network

In a nonlinear system with a single input $v_g(t)$ and an output $v_L(t)$, the nonlinear transfer functions $H_n(f_n)$ can be obtained by solving the network with $v_g(t)$ a sum of exponentials given by

$$v_g(t) = \sum_{i=1}^n e^{j2\pi f_i t}, \quad (2.86)$$

where

$$\underline{f_n} = \underline{f_i, f_j, f_k \dots} \quad n \text{ components,} \quad (2.87)$$

$$i, j, k \dots = 1, 2, \dots n.$$

and where $v_L(t)$ up to n 'th order for the above input is given by

$$\begin{aligned}
v_L(t) = & \sum_{i=1}^n H_1(f_i) e^{j2\pi f_i t} + \sum_{i=1}^n \sum_{j=1}^n H_2(f_i, f_j) e^{j2\pi(f_i + f_j)t} \\
& + \sum_{i=1}^n \sum_{j=1}^n \sum_{k=1}^n H_3(f_i, f_j, f_k) e^{j2\pi(f_i + f_j + f_k)t} + \dots \\
& + \sum_{i=1}^n \dots \sum_{n=1}^n H_n(f_i, f_j, f_k \dots) e^{j2\pi(f_i + f_j + f_k \dots)t}.
\end{aligned} \tag{2.88}$$

In our procedure it is of interest to know the coefficient of a given frequency f_Σ in the above series. Thus if f_Σ is given by

$$f_\Sigma = m_1 f_1 + m_2 f_2 + \dots + m_n f_n,$$

where

$$\sum_{i=1}^n m_i = n; m_i = 0, 1, 2, \dots, n, \tag{2.89}$$

the number of terms at frequency f_Σ in Eq. (2.88) can be shown by the multinomial expansion (Abromovitz and Stegun, 1964) to be

$$n! / (m_1! m_2! \dots m_n!).$$

For example the number of terms for $\exp[j2\pi(f_1 + f_2 + f_3)t]$ is 6, for $\exp[j2\pi(f_1 + f_2 + f_3 + f_4)t]$ is 24. For $\exp[j2\pi(4f_1)t]$ there is one term.

To solve for the nonlinear transfer functions of a single

input and single output network, the general approach is to consider all node voltages ($v_1, v_2 \dots v_N$) that control the currents in the nonlinear elements as outputs, together with the actual output node. This means that many nodes connecting only linear elements may be eliminated at a specific set of frequencies by replacing them by their equivalent impedances. For example the linear interstage between transistor amplifiers can be reduced to a π network, eliminating all nodes of the interstage. Having reduced the network to its minimum number of nodes, ($N+1$), we can then represent it as a single input and N output nonlinear system. We will denote by the N component vector $\underline{x}_n(f_n)$ the n -th order nonlinear transfer functions of the network. Thus $\underline{x}_n(f_n)$ and the corresponding node voltage vector $\underline{v}(t)$ can be written as

$$\underline{x}_n(f_n) = \begin{bmatrix} A_n(f_n) \\ B_n(f_n) \\ \vdots \end{bmatrix} : \underline{v}(t) = \begin{bmatrix} v_1(t) \\ v_2(t) \\ \vdots \\ v_N(t) \end{bmatrix}. \quad (2.90)$$

The n -th order transfer function $H_n(f_n)$ of the desired output is one of the components of $\underline{x}_n(f_n)$, usually the last in a typical ladder structure, so that

$$H_n(f_n) = \underbrace{0 \ 0 \ \dots \ 0}_{n-1} \ 1 \ \underline{x}_n(f_n), \quad (2.91)$$

while $A_n(f_n)$ is usually the transfer function of the voltage at the input node.

Using this notation we can very quickly describe the general procedure as three steps:

Step 1

Write the node equations of the network with the input a sum of unit amplitude exponentials at the dummy frequencies $f_1 \dots f_n$. The node equations, assuming that only the four nonlinearities exist, could be written in operational notation as

$$L(p)\underline{v} + K(\underline{v}) + G(\underline{v}) + pQ(\underline{v}) + \frac{1}{p} \Phi(\underline{v}) = \frac{1}{z_g(p)} \begin{bmatrix} n \\ \sum_{i=1}^n e^{j2\pi f_i t} \\ 0 \\ \vdots \\ 0 \end{bmatrix}, \quad (2.92)$$

where p is the differential operator d/dt , and

$L(p)$ is a ($N \times N$) admittance matrix due to the purely linear elements in the network.

$K(\underline{v})$ is an N vector composed of all the zero-memory independent non-linearities of type (a).

$G(\underline{v})$ is an N vector composed of all the zero-memory dependent non-linearities of type (b).

$Q(\underline{v})$ is an N vector composed of all the nonlinear capacitance-memory non-linearities of type (c).

$\Phi(\underline{v})$ is an N vector composed of all the nonlinear inductance-memory non-linearities of type (d).

$z_g(p)$ is the output impedance of the generator $v_g(t)$ assumed connected from the v_1 terminal to the common node.

Step 2

Separate the nonlinear terms into their linear parts and their second- and higher-order parts. Thus the linear part of each one is given by

$$\left. \begin{array}{l} \text{Linear Part } \{K(\underline{v})\} = K_L \underline{v}, \\ \text{Linear Part } \{G(\underline{v})\} = G_L \underline{v}, \\ \text{Linear Part } \{pQ(\underline{v})\} = pQ_L \underline{v}, \\ \text{Linear Part } \left\{ \frac{1}{p} \Phi(\underline{v}) \right\} = \frac{1}{p} \Phi_L \underline{v}, \end{array} \right\} \quad (2.93)$$

where K_L , G_L , Q_L and Φ_L are $N \times N$ constant matrices but are functions of the operating point about which the Taylor series expansion was made.

Thus, the admittance operator matrix $[Y(p)]$ of the corresponding linearized network is

$$[Y(p)] = [L(p) + K_L + G_L + pQ_L + \frac{1}{p} \Phi_L]. \quad (2.94)$$

Thus, the node equations in terms of $[Y(p)]$ can be written as

$$[Y(p)] \underline{v} = \frac{1}{Z_g(p)} \begin{bmatrix} n \\ \sum_{i=1}^n e^{j2\pi f_i t} \\ 0 \\ \vdots \\ 0 \\ 0 \end{bmatrix} + \begin{bmatrix} \text{Vector of second and higher-order terms of } K(\underline{v}), G(\underline{v}), pQ(\underline{v}) \text{ and } \frac{1}{p} \Phi(\underline{v}) \\ \vdots \end{bmatrix}. \quad (2.95)$$

The form of the nonlinear terms on the right-hand side depends on

whether they come from $K(y)$ or $G(y)$, etc. In each case they will have the form given by the four types of nonlinearities. It should be recognized that the nonlinear terms due to each nonlinear element in the network will be separable from nonlinear terms due to any other element.

Step 3

Substitute the nonlinear transfer functions series for each component of y in the above node equations and equate terms of the same exponential frequency on both sides of the equations. The first order transfer functions are again simply the linear solution, and are given by

First-Order Transfer Functions

$$[y(f_i)]_{\underline{x}_1(f_i)} = \begin{bmatrix} \frac{1}{z_g(f_i)} \\ 0 \\ \vdots \\ 0 \end{bmatrix}; i = 1, 2, \dots, n. \quad (2.96)$$

The second and higher order nonlinear transfer functions are again given by the solution of the same linear network, but driven by sources resulting from each nonlinearity. Since the nonlinear terms due to each nonlinear element are separable, multiple nonlinear elements result in a superposition of the source terms due to each nonlinearity. Thus, the equation for the second order can be written as

Second-Order Transfer Functions

$$[\underline{Y}(f_i + f_j)] \underline{X}_2(f_i, f_j) = \begin{bmatrix} \hat{U}_{2a} [\underline{X}_1(f_i), \underline{X}_1(f_j), f_i + f_j] \\ \hat{U}_{2b} [\underline{X}_1(f_i), \underline{X}_1(f_j), f_i + f_j] \\ \vdots \end{bmatrix} \quad \begin{array}{c} \uparrow \\ N \\ \downarrow \end{array}$$

i, j = 1, 2, ... n, (2.97)

where \hat{U}_{2a} , \hat{U}_{2b} are seen to be quadratic functions of components of $\underline{X}_1(f_i)$, $\underline{X}_1(f_j)$ and the frequency $(f_i + f_j)$. In the case of a single nonlinear element \hat{U}_{2a} , \hat{U}_{2b} ... are zero or $\pm \hat{X}_2(f_i, f_j)$ as in Sec. 2.2.2.2. For two or more nonlinear elements $\hat{U}_{2a}, \hat{U}_{2b} \dots$ will include the corresponding second-order sources for each nonlinearity.

Third-Order Transfer Functions

$$[\underline{Y}(f_i + f_j + f_k)] \underline{X}_3(f_i, f_j, f_k) = \begin{bmatrix} \hat{U}_{23} [\underline{X}_1(f_i), \underline{X}_2(f_j, f_k), f_i + f_j + f_k] \\ + \hat{U}_3 [\underline{X}_1(f_i), \underline{X}_1(f_j), \underline{X}_1(f_k), f_i + f_j + f_k] \end{bmatrix},$$

i, j, k = 1, 2, ... n, (2.98)

where both \hat{U}_{23} and \hat{U}_3 are N vectors. The \hat{U}_{23} terms are symmetrized quadratic terms in $\underline{X}_1(f_i)$ and $\underline{X}_2(f_j, f_k)$ and come from the first and second-order interactions in second-order nonlinearities. The \hat{U}_3 terms are cubic terms in $\underline{X}_1(f_i)$, $\underline{X}_1(f_j)$ and $\underline{X}_1(f_k)$ and come from the third-order nonlinearities.

Fourth-Order Transfer Functions

$$[Y(f_i + f_j + f_k + f_l)] \underline{x}_4 = \left[\begin{array}{l} \hat{U}_{24} \overline{(x_1, x_3, x_2, x_2)} + \hat{U}_{34} \overline{(x_1, x_1, x_2)} \\ + \hat{U}_4 \overline{(x_1, x_1, x_1, x_1)} \end{array} \right],$$

$$i, j, k, l = 1, 2, 3 \dots n, \quad (2.99)$$

where for the sake of simplicity the arguments of $\underline{x}_i(f_i)$ have been dropped. Similar to the previous orders we note that \hat{U}_{24} terms come from the second-order nonlinearities, \hat{U}_{34} from the third-order and \hat{U}_4 from the fourth-order.

n^{th} -Order Transfer Functions

The fifth and higher-order transfer functions are given by similar relations. The important point to note is that to determine $\underline{x}_n(f_n)$ only the lower order $\underline{x}_{n-1}, \dots, \underline{x}_1$ have to be determined. Additionally the n^{th} order transfer function depends only on all the lower-order nonlinear coefficients. Thus, in abbreviated notation we can write the general expression for the n^{th} -order transfer function as

$$[Y(f_1 + f_2 + \dots + f_n)] \underline{x}_n(f_n) = \sum_{l=2}^n \hat{U}_{ln}, \quad (2.100)$$

where

$$\hat{U}_{nn} \triangleq \hat{U}_n. \quad (2.101)$$

The $\hat{U}_{\ell n}$ terms may be called the n^{th} -order source terms. We note again that the $\hat{U}_{\ell n}$ function is the same for any frequency combination of the n^{th} -order. The only difference is the substitution in the expression for $\hat{U}_{\ell n}$ the appropriate lower-order transfer functions. For example, the U_n function for the two cases of distinct frequency combination $(f_1 + f_2 + f_3 \dots + f_n)$ and nf_1 are given by

Frequency $(f_1 + f_2 + \dots + f_n)$

$$\hat{U}_{nn} = \hat{U}_{nn}[\underline{x}_1(f_1), \underline{x}_1(f_2), \underline{x}_1(f_3), \dots \underline{x}_1(f_n)], \quad (2.102)$$

Frequency nf_1

$$\hat{U}_{nn} = \hat{U}_{nn}[\underline{x}_1(f_1), \underline{x}_1(f_1), \underline{x}_1(f_1), \dots \underline{x}_1(f_1)]. \quad (2.103)$$

Having completed the above three steps, the nonlinear transfer functions in general would be obtained by a numerical solution of the relevant matrix equations. It should be apparent that the main difficult algebraic exercise in this procedure is determining the source term $\hat{U}_{\ell n}$.

2.2.3.3 An Example

To appreciate the general form of the nonlinear source terms $\hat{U}_{\ell n}$ we will consider the bipolar transistor amplifier model shown in Fig. 2.2. This model is developed in Chapter 5. The four nonlinearities are shown as nonlinear current sources.

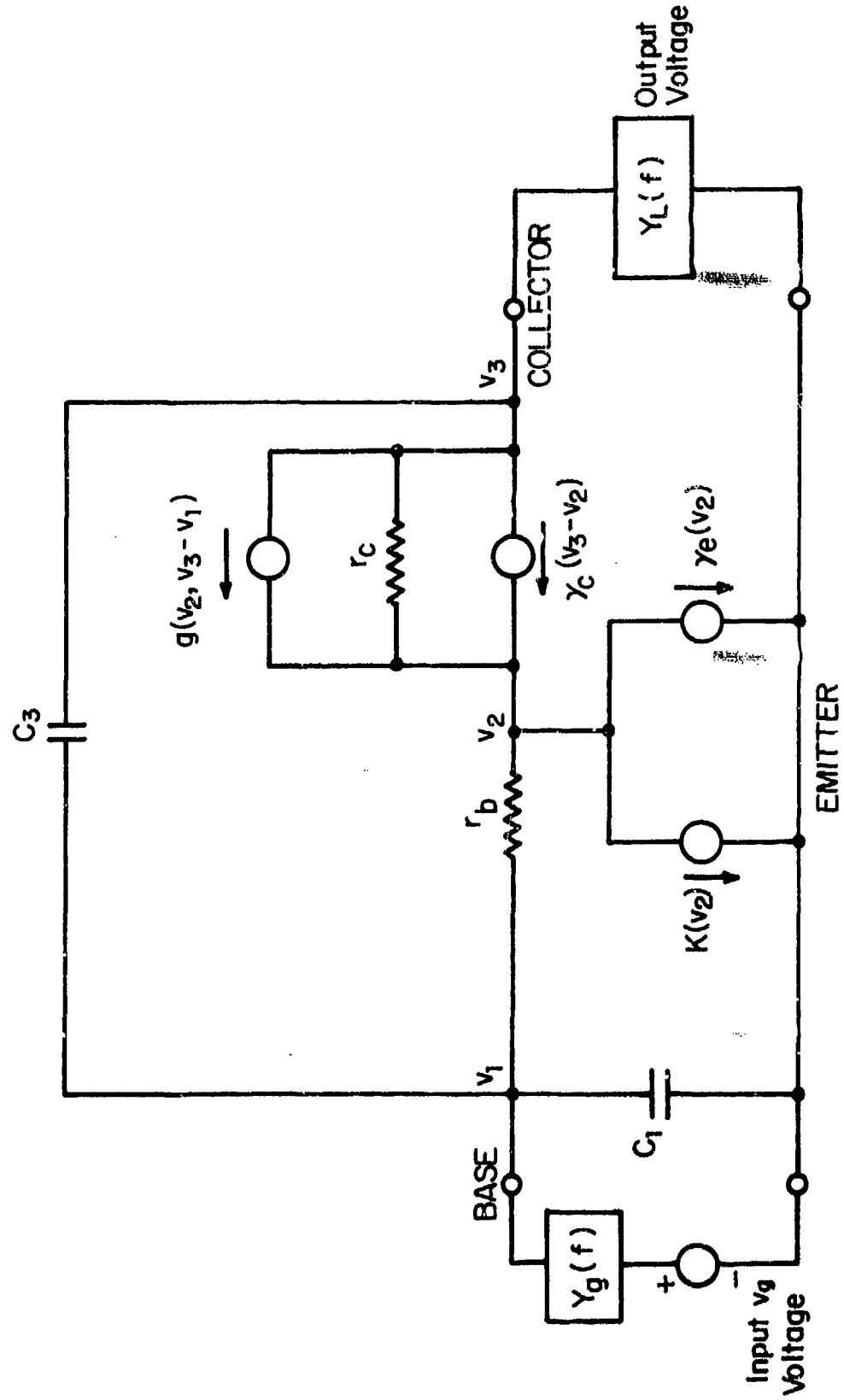


Fig. 2.2. Common-Emitter Nonlinear Incremental Amplifier Model.

$K(v_2)$ is the zero-memory exponential nonlinearity. $\gamma_c(v_3 - v_2)$ and $\gamma_e(v_2)$ are the collector and emitter nonlinear capacitances. The fourth nonlinearity $g(v_2, v_3 - v_1)$ is a zero-memory dependent nonlinearity due to the h_{FE} and avalanche nonlinearity in a bipolar transistor. The node equations of this circuit are in operator notation

$$[Y(p)] \begin{bmatrix} v_1 \\ v_2 \\ v_3 \end{bmatrix} = \frac{1}{Z_g(p)} \begin{bmatrix} v_g(t) \\ 0 \\ 0 \end{bmatrix} + \begin{bmatrix} 0 \\ \sum_{\ell=2}^{\infty} \left\{ g_{\ell}(v_2, v_3 - v_1) + p \gamma_{c:\ell} (v_3 - v_2)^{\ell} - (K_{\ell} + p \gamma_{e:\ell}) v_2^{\ell} \right\} \\ - \sum_{\ell=2}^{\infty} \left\{ g_{\ell}(v_2, v_3 - v_1) + p \gamma_{c:\ell} (v_3 - v_2)^{\ell} \right\} \end{bmatrix}, \quad (2.104)$$

where $g_{\ell}(v_2, v_3 - v_1)$ is the ℓ^{th} order polynomial in v_2 and $(v_3 - v_1)$, $\gamma_{c:\ell}$ and $\gamma_{e:\ell}$ are the ℓ^{th} order coefficients of γ_c and γ_e , respectively, and K_{ℓ} is the ℓ^{th} order coefficient of $K(v_2)$.

The vector $\hat{U}_{\ell n}$ is obtained by substituting the general nonlinear transfer function series of each v_i into the ℓ^{th} term of the above summations and isolating the coefficient of $\exp[j2\pi(f_1 + f_2 + \dots + f_n)t]$. Thus, following notation similar to Section 2.2.3, the general n^{th} order transfer function is given by

$$[Y(f_1 + f_2 + \dots + f_n)] X_n(f_n) = \begin{bmatrix} 0 \\ \sum_{l=2}^n (\hat{g}_{ln} + \hat{\gamma}_{c:ln} - \hat{K}_{ln} - \hat{\gamma}_{e:ln}) \\ \vdots \\ - \sum_{l=2}^{\infty} (\hat{g}_{ln} + \hat{\gamma}_{c:ln}) \end{bmatrix},$$

(2.105)

where the 'nn' coefficients have also been defined with a single subscript, i.e., $\hat{g}_n = \hat{g}_{nn}$, etc.

In terms of the notation of the previous section the source terms \hat{U}_{ln} for these cases are

$$\hat{U}_{ln} = \begin{bmatrix} 0 \\ \hat{g}_{ln} + \hat{\gamma}_{c:ln} - \hat{K}_{ln} - \hat{\gamma}_{e:ln} \\ \vdots \\ -(\hat{g}_{ln} + \hat{\gamma}_{c:ln}) \end{bmatrix}. \quad (2.106)$$

Each of the terms \hat{K}_{ln} , $\hat{\gamma}_{e:ln}$, $\hat{\gamma}_{c:ln}$ and \hat{g}_{ln} can be derived according to the procedure of Sec. 2.2.2. We see that the terms contributed by the various nonlinearities are additive. Thus the form of the terms due to each nonlinearity is the same independent of the number of nonlinearities in the network. Consequently, the nonlinear source terms from the single-element network analysis of Sec. 2.2.2 is applicable to a general nonlinear network by substitution of the corresponding transfer functions.

2.2.3.4 Tabulation of Nonlinear Source Terms

The nonlinear source terms up to fourth-order are listed below. They are applicable to any other network with similar types of nonlinearities. Terms up to third-order are taken directly from Section 2.2.2. The fourth-order terms can be derived similarly.

2.2.3.4.1 Zero Memory Source Terms \hat{K}_{ln}

The source terms for the zero memory nonlinearity $K(v_2)$, with $B_n(f_n)$ the nonlinear transfer function of v_2 , are

$$\hat{K}_2(f_1, f_2) = K_2 B_1(f_1) B_1(f_2), \quad (2.107)$$

$$\hat{K}_{23}(f_1, f_2, f_3) = \overline{2K_2 B_1(f_1) B_2(f_2, f_3)}, \quad (2.108)$$

$$\hat{K}_3(f_1, f_2, f_3) = K_3 \prod_{i=1}^3 B_1(f_i). \quad (2.109)$$

$$\begin{aligned} \hat{K}_{24}(f_1, f_2, f_3, f_4) &= K_2 \left\{ \overline{2B_1(f_1) B_3(f_2, f_3, f_4)} \right. \\ &\quad \left. + \overline{B_2(f_1, f_2) B_2(f_3, f_4)} \right\}, \end{aligned} \quad (2.110)$$

$$\hat{K}_{34}(f_1, f_2, f_3, f_4) = 3K_3 \overline{B_1(f_1) B_1(f_2) B_2(f_3, f_4)}. \quad (2.111)$$

$$\hat{K}_4(f_1, f_2, f_3, f_4) = K_4 \prod_{i=1}^4 B_1(f_i). \quad (2.112)$$

Note that $\hat{K}_n(f_n)$ is the same as $\hat{K}_{nn}(f_n)$.

2.2.3.4.2 Nonlinear Capacitance Source Terms $\hat{\gamma}_{en}$

The source terms for the nonlinearity $\gamma(v_2)$ with $B_n(f_n)$ the nonlinear transfer function of v_2 are

$$\hat{\gamma}_2(f_1, f_2) = j2\pi(f_1 + f_2) \gamma_2 \prod_{i=1}^2 B_1(f_i), \quad (2.113)$$

$$\hat{\gamma}_{23}(f_1, f_2, f_3) = j4\pi(f_1 + f_2 + f_3) \gamma_2 \overline{B_1(f_1)} B_2(f_2, f_3), \quad (2.114)$$

$$\hat{\gamma}_3(f_1, f_2, f_3) = j2\pi(f_1 + f_2 + f_3) \gamma_3 \prod_{i=1}^3 B_1(f_i). \quad (2.115)$$

$$\begin{aligned} \hat{\gamma}_{24}(f_1, f_2, f_3, f_4) &= j2\pi(f_1 + f_2 + f_3 + f_4) \gamma_2 \overline{2B_1(f_1)} B_3(f_2, f_3, f_4) \\ &\quad + \overline{B_2(f_1, f_2) B_2(f_3, f_4)} \end{aligned} \quad (2.116)$$

$$\hat{\gamma}_{34}(f_1, f_2, f_3, f_4) = j6\pi(f_1 + f_2 + f_3 + f_4) \gamma_3 \overline{B_1(f_1) B_1(f_2) B_2(f_3, f_4)}, \quad (2.117)$$

$$\hat{\gamma}_4(f_1, f_2, f_3, f_4) = j2\pi(f_1 + f_2 + f_3 + f_4) \gamma_4 \prod_{i=1}^4 B_1(f_i). \quad (2.118)$$

In applying these expressions to the emitter capacitance $\gamma_e(v_2)$ we replace γ_n by $\gamma_{e:n}$, while for the collector capacitance $\gamma_c(v_3 - v_2)$ we replace γ_n by $\gamma_{c:n}$ and $B_n(f_n)$ by $[C_n(f_n) - B_n(f_n)]$, where $C_n(f_n)$ is the transfer function of v_3 .

The above nonlinear capacitance source terms could also be derived by noting that a nonlinear capacitance is a cascade of a nonlinear no-memory device followed by a linear differential operator.

2.2.3.4.3 Dependent Zero-Memory Source Terms $\hat{g}_{\ell n}$

The source terms for $\hat{g}_{\ell n}(v_2, v_3 - v_1)$ are listed below. The nonlinear transfer functions for v_2 and $(v_3 - v_1)$ are denoted by $B_n(f_n)$ and $T_n(f_n)$, respectively. In the transistor circuit analysis of Sec. 2.2.3.3, $T_n(f_n)$ is the difference $[C_n(f_n) - A_n(f_n)]$.

$$\hat{g}_2(f_1, f_2) = g_{20} \prod_{i=1}^2 B_1(f_i) + g_{11} \overline{B_1(f_1) T_1(f_2)} + g_{02} \prod_{i=1}^2 T_1(f_i), \quad (2.119)$$

$$\begin{aligned} \hat{g}_{23}(f_1, f_2, f_3) &= 2g_{20} \overline{B_1(f_1) B_2(f_2, f_3)} + 2g_{02} \overline{T_1(f_1) T_2(f_2, f_3)} \\ &\quad + g_{11} \left[\overline{B_1(f_1) T_2(f_2, f_3)} + \overline{B_2(f_1, f_2) T_1(f_3)} \right], \end{aligned} \quad (2.120)$$

$$\begin{aligned} \hat{g}_3(f_1, f_2, f_3) &= g_{30} \prod_{i=1}^3 B_1(f_i) + g_{03} \prod_{i=1}^3 T_1(f_i) \\ &\quad + g_{11} \overline{B_1(f_1) B_2(f_2) T_1(f_3)} + g_{12} \overline{B_1(f_1) T_1(f_2) T_1(f_3)}, \\ &\triangleq g_{30} B_1 B_2 B_1 + g_{03} T_1 T_1 T_1 + g_{21} \overline{B_1 B_1 T_1} \\ &\quad + g_{12} \overline{B_1 T_1 T_1}, \end{aligned} \quad (2.121)$$

where the arguments f_i for the transfer functions have been dropped. This simplifies writing the source terms especially for the fourth order which are

$$\begin{aligned}
\hat{g}_{24}(f_1, f_2, f_3, f_4) = & g_{20} \left\{ \overline{2B_1B_3} + \overline{B_2B_2} \right\} \\
& + g_{11} \left\{ \overline{T_1B_3} + \overline{T_3B_1} + \overline{T_2B_2} \right\} \\
& + g_{02} \left\{ \overline{2T_1T_3} + \overline{T_2T_2} \right\}, \tag{2.122}
\end{aligned}$$

$$\begin{aligned}
\hat{g}_{34}(f_1, f_2, f_3, f_4) = & 3g_{30} \overline{B_1B_1B_2} + 3g_{03} \overline{T_1T_1T_2} \\
& + g_{21} \left[\overline{B_1B_1T_2} + 2 \overline{B_1B_2T_1} \right] \\
& + g_{12} \left[\overline{B_2T_1T_1} + 2 \overline{B_1T_1T_2} \right], \tag{2.123}
\end{aligned}$$

$$\begin{aligned}
\hat{g}_4(f_1, f_2, f_3, f_4) = & g_{40} \overline{B_1B_1B_1B_1} + g_{04} \overline{T_1T_1T_1T_1} \\
& + g_{31} \overline{B_1B_1B_1T_1} + g_{13} \overline{B_1T_1T_1T_1} \\
& + g_{22} \overline{B_1B_1T_1T_1}. \tag{2.124}
\end{aligned}$$

2.2.4 Recurrence Relations for the Nonlinear Source Terms

The procedure presented in the previous sections for deriving the nonlinear source terms \hat{K}_{ln} , \hat{g}_{ln} , etc., becomes increasingly complex with increasing order. In this section a recursive method for determining the source terms for the various nonlinearities is derived. We present the method by way of the transistor amplifier example of Section 2.2.3.3, and apply it to obtain the fifth-order nonlinear transfer function.

The three types of source terms considered with reference to the transistor circuit of Sec. 2.2.3 were \hat{K}_{ln} , \hat{q}_{ln} and \hat{g}_{ln} . Since these source terms are independent of one another they will be derived separately.

The recurrence relation between the source terms is based on the property that

$$\left(\sum_{k=1}^N B_k I^k \right)^m = \sum_{n=m}^{mN} G_{m,n} I^n, \quad (2.125)$$

where

$$\begin{aligned} G_{m,n} &= \sum_{i=1}^{n-m+1} B_i G_{m-1, n-i}, \quad n \leq N + m - 1 \\ &= \sum_{i=1}^N B_i G_{m-1, n-i}, \quad n > N + m - 1 \\ &= 0, \quad n > mN, \end{aligned} \quad (2.126)$$

and

$$\begin{aligned} G_{1,n} &= B_n, \quad n = 1, 2, \dots, N \\ &= 0 \quad n > N. \end{aligned} \quad (2.127)$$

To prove this relationship let

$$F_m = \left(\sum_{k=1}^N B_k I^k \right)^m = \sum_{n=m}^{mN} G_{m,n} I^n. \quad (2.128)$$

By the Taylor series theorem

$$G_{m,n} = \frac{1}{n!} \left. \frac{d^n F_m}{dI^n} \right|_{I=0} . \quad (2.129)$$

Since

$$F_m = \left(\sum_{k=1}^N B_k I^k \right) F_{m-1}, \quad (2.130)$$

the derivative of F_m , by Leibnitz's theorem for derivative of a product, gives

$$\frac{d^n F_m}{dI^n} = \sum_{i=0}^N \binom{n}{i} \frac{d^i}{dI^i} \left(\sum_{k=1}^N B_k I^k \right) \frac{d^{n-i}}{dI^{n-i}} F_{m-1}. \quad (2.131)$$

Evaluating at $I=0$ gives

$$\begin{aligned} n! G_{m,n} &= \sum_{i=0}^N \binom{n}{i} (n-i)! G_{m-1,n-i} \left[\left. \sum_{k=1}^N B_k \frac{d^i I^k}{dI^i} \right|_{I=0} \right] \\ &= \sum_{i=0}^N \binom{n}{i} (n-i)! G_{m-1,n-i} [i! B_i], \end{aligned}$$

giving

$$G_{m,n} = \sum_{i=0}^N B_i G_{m-1,n-i}. \quad (2.132)$$

Since B_0 is zero

$$G_{m,n} = \sum_{i=1}^N B_i G_{m-1, n-i}. \quad (2.133)$$

The upper limits on i of Eq. (2.133) are established by noting that

$$B_i = 0, i > N, \text{ and} \quad (2.134)$$

$$G_{m,n} = 0, n < m. \quad (2.135)$$

Eq. (2.134) reduces Eq. (2.133) to

$$G_{m,n} = \sum_{i=1}^N B_i G_{m-1, n-i}; n > N+M-1. \quad (2.136)$$

Equation (2.136) is only true if the last term in the summation $G_{m-1, n-N}$ satisfies Eq. (2.135), i.e.

$$n - N \geq m - 1. \quad (2.137)$$

This proves the second line of Eq. (2.126). If Eq. (2.137) is not satisfied then the upper limit on i is given by

$$\left. \begin{aligned} i &\leq (m-1) \\ &\leq n-N \\ &\leq n-m+1 \end{aligned} \right\}; (n-N) \leq m-1, \quad (2.138)$$

thus proving the first and third lines of the desired recurrence relations, Equation (2.126). This relation is used in the following sections to derive recurrence relations for the nonlinear sources.

2.2.4.1 Zero-Memory Independent Nonlinearity

Let the vector \underline{m} denote the frequency combination of interest f_{Σ} which was defined in Chapter 1 as

$$f_{\Sigma} = m_1 f_1 + m_2 f_2 + \dots + m_M f_M, \quad (2.139)$$

with

$$\sum_{i=1}^M m_i = n; \quad m_i = 0, 1, 2, \dots, n. \quad (2.140)$$

The source term \hat{K}_{ln} is given by substituting the general Volterra series for v_2 into $K_l v_2^l$, isolating the coefficient of $e^{j2\pi f_{\Sigma} t}$, and then dividing it by the number of terms at frequency f_{Σ} which is given by $n!/(m_1! m_2! \dots m_n!)$. Thus

$$\begin{aligned} \hat{K}_{ln} &= \left(\frac{n!}{m_1! m_2! \dots m_M!} \right)^{-1} \text{Coeff of } e^{j2\pi f_{\Sigma} t} \text{ in} \\ K_l \left\{ \sum_{i=1}^M B_1(f_i) e^{j2\pi f_i t} + \sum_{i=1}^M \sum_{j=1}^M B_2(f_i, f_j) e^{j2\pi(f_i + f_j)t} \right. \\ &\quad \left. + \dots \right\}^l, \end{aligned} \quad (2.141)$$

where the $B_n(f_n)$ are the nonlinear transfer functions of the node voltage $v_2(t)$. We use the Coeff of $e^{j2\pi f_{\Sigma} t}$ in {} to mean isolating the coefficient of the term $e^{j2\pi f_{\Sigma} t}$ from the expression contained in the brackets {}. In the absence of any memory, linear or nonlinear, the $B_n(f_n)$ would be frequency independent and \hat{K}_{ln} would be given by

$$\hat{K}_{ln} = \left(\frac{n!}{m_1! m_2! \dots m_M!} \right)^{-1} \text{Coeff of } e^{j2\pi f_{\sum} t} \text{ in}$$

$$K_l \left\{ \sum_{i=1}^n B_i \left(\sum_{j=1}^M e^{j2\pi f_j t} \right)^i \right\}_l. \quad (2.142)$$

We see the relatively simple form of the no-memory expression. The approach we take is to derive \hat{K}_{ln} for the no-memory case. It is then straightforward to convert the expressions to the general memory case as shown below:

<u>Order</u>	<u>No-Memory Terms</u>	<u>Memory Terms</u>
1	B_1	$B_1(f_i)$
2	B_2 B_1^2	$B_2(f_i, f_j)$ $\prod_{i,j} B_1(f_i)$
3	B_3 $B_1 B_2$ B_1^3	$B_3(f_i, f_j, f_k)$ $\frac{B_1(f_i) B_2(f_j, f_k)}{B_1(f_i)}$ $\prod_{i,j,k} B_1(f_i)$

where the bar denotes symmetrization. The general n^{th} order term is similarly obtained.

Using the result of Eq. (2.125) we can write

$$\left(\sum_{i=1}^n B_i I^i \right)^l = \sum_{j=l}^{ln} G_{l,j} I^j, \quad (2.143)$$

with

$$I = \sum_{i=1}^n e^{j2\pi f_i t}, \quad (2.144)$$

where

$$\begin{aligned} G_{l,j} &= \sum_{k=1}^{j-l+1} B_k G_{l-1,j-k} & j \leq n+l-1 \\ &= \sum_{k=1}^n B_k G_{l-1,j-k} & j > n+l-1 \\ &= 0 & j > ln \end{aligned} \quad (2.145)$$

with

$$\begin{aligned} G_{1,j} &= B_j & j = 1, 2, \dots, n \\ &= 0 & j > n. \end{aligned} \quad (2.146)$$

Applying this result to Eq. (2.142) results in

$$\hat{K}_{ln} = \left(\frac{n!}{m_1! m_2! \dots m_M!} \right)^{-1} K_l G_{l,n} \text{ Coeff of } e^{j2\pi f_i \sum t} \text{ in } \{I^n\}. \quad (2.147)$$

From the property of multinomials

$$\text{Coeff of } e^{j2\pi f \sum t} \text{ in } \{I^n\} = \frac{n!}{m_1! m_2! \dots m_M!}, \quad (2.148)$$

so that

$$\hat{K}_{ln} = K_l G_{l,n}. \quad (2.149)$$

We note that $G_{l,n}$ is a linear combination of similar coefficients for lower values of n and l . Thus the higher-order coefficients can be obtained recursively as given by Eq. (2.145) and (2.146). For example the fifth-order sources are

$$\begin{aligned} \hat{K}_{25} &= K_2(2B_1B_4 + 2B_2B_3), \\ \hat{K}_{35} &= K_3(3B_1B_1B_3 + 3B_1B_2B_2), \\ \hat{K}_{45} &= K_4(4B_1B_1B_1B_2), \\ \hat{K}_{55} &= K_5(B_1B_1B_1B_1B_1), \end{aligned} \quad \left. \right\} \quad (2.150)$$

where the B_i are computed at the appropriate frequencies and the expressions symmetrized.

2.2.4.2 Capacitance-Memory Independent Nonlinearity

The form of the expressions for $\hat{Y}_{c:ln}$ and $\hat{Y}_{e:ln}$ of Section 2.2.3 are identical. Thus consider $\hat{Y}_{c:ln}$ which is given by

$$\hat{Y}_{c:ln} = \left(\frac{n!}{m_1! m_2! \dots m_M!} \right)^{-1} j 2\pi f_{\Sigma} \text{ Coeff of } e^{j 2\pi f_{\Sigma} t} \text{ in} \\ Y_{c:l} \left\{ \sum_{i=1}^M T_1(f_i) e^{j 2\pi f_i t} + \sum_{i=1}^M \sum_{j=1}^M T_2(f_i, f_j) e^{j 2\pi (f_i + f_j)t} \right. \\ \left. + \dots \right\}^l, \quad (2.151)$$

where $T_n(f_n)$ are the nonlinear transfer functions of the difference voltage $[v_3(t) - v_1(t)]$ and the factor $j 2\pi f_{\Sigma}$ results from differentiating $e^{j 2\pi f_{\Sigma} t}$. Following the procedure for \hat{K}_{ln} and comparing Eq. (2.142) with Eq. (2.141) shows that $\hat{Y}_{c:ln}$ differs from the \hat{K}_{ln} expression by the factor $j 2\pi f_{\Sigma}$. Thus $\hat{Y}_{c:ln}$ are given by the expressions for \hat{K}_{ln} multiplied by $j 2\pi f_{\Sigma}$, with K_l replaced by $Y_{c:l}$ and B_n replaced by T_n .

The fifth-order expressions for $Y_{c:l5}$ are listed below

$$\begin{aligned} \hat{Y}_{c:25} &= j 2\pi f_{\Sigma} Y_{c:2} (2T_1 T_4 + 2T_2 T_3), \\ \hat{Y}_{c:35} &= j 2\pi f_{\Sigma} Y_{c:3} (3T_1 T_1 T_3 + 3T_1 T_2 T_2), \\ \hat{Y}_{c:45} &= j 2\pi f_{\Sigma} Y_{c:4} (4T_1 T_1 T_1 T_2), \\ \hat{Y}_{c:55} &= j 2\pi f_{\Sigma} Y_{c:5} (T_1 T_1 T_1 T_1 T_1), \end{aligned} \quad (2.152)$$

where, for all terms in Equation (2.152),

$$f_{\Sigma} = f_1 + f_2 + f_4 + f_5. \quad (2.153)$$

The $\hat{Y}_{e:ln}$ are given similarly with e replacing c .

2.3 Cascading of Networks with Nonlinear Interaction

2.3.1 Introduction

The analysis techniques described in the previous sections can be applied to any size network. However, the computations to invert large admittance matrices grows with N^3 , where N is the number of nodes in a network. Therefore, to analyze a large network it is often more efficient to divide the network into segments, and to determine the nonlinear transfer function of each segment separately. The nonlinear transfer function of the overall network can then be found through the use of cascading equations. Segmentation of a network is also desirable in order to investigate the effects of individual stages on the total network.

The maximum size network which can be analyzed on a given computer without the use of cascading depends strongly on the methods used for solving the matrix equations of the form $H_n = Y^{-1} I_n$, where the column vector I_n is the n^{th} order nonlinear current-source vector. By using sparse matrix techniques, such as discussed by Berry (1971), and Hachtel et.al. (1971), much larger networks can be analyzed than if classical matrix-inversion techniques were used. In addition, sparse matrix techniques result in a faster execution time for the matrix equation solution than do classical techniques.

Considerable previous work has been carried out on the algebra of systems represented by nonlinear transfer functions [Barrett (1963), Parente (1966), Brilliant (1955), George (1959)]. Cascade, parallel and feedback arrangements have all been treated.

Unfortunately this work is based on the assumption of no interaction between systems. This considerably limits its application. By returning to the basic nature of the Volterra analysis it has been possible to examine the significance of nonlinear interaction, and determine when it is sufficiently small to be neglected. In many cases incorporation of all interaction makes the cascade approach much more complicated than direct solution of the whole network. Thus segmentation of stages in a network should be done at points where nonlinear interaction is negligible.

In this section we consider the general nonlinear transfer function model for interacting cascaded stages. The derivation is for a two-stage cascade which can be extended to any number of stages. The presentation emphasizes the concepts involved in interaction.

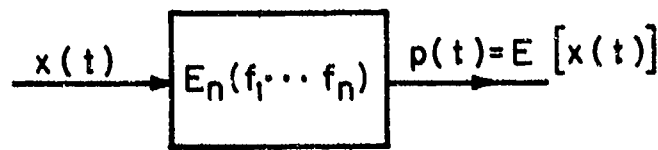
Cascade relations for non-interacting systems will be discussed and followed by a summary of the salient features of the general network analysis of Section 2.2. The demonstration of the effects of linear and nonlinear interaction in a cascade of two networks forms the main body of this section.

2.3.2 Cascade Relations for Non-Interacting Systems

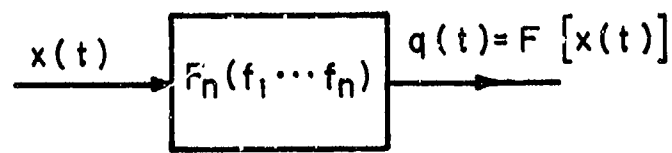
In Figure 2.3 are shown two nonlinear systems with transfer functions $E_n(f_1, \dots, f_n)$ and $F_n(f_1, \dots, f_n)$. When the input to these systems is $x(t)$, their outputs may be expressed

$$p(t) = E[x(t)], \quad (2.154)$$

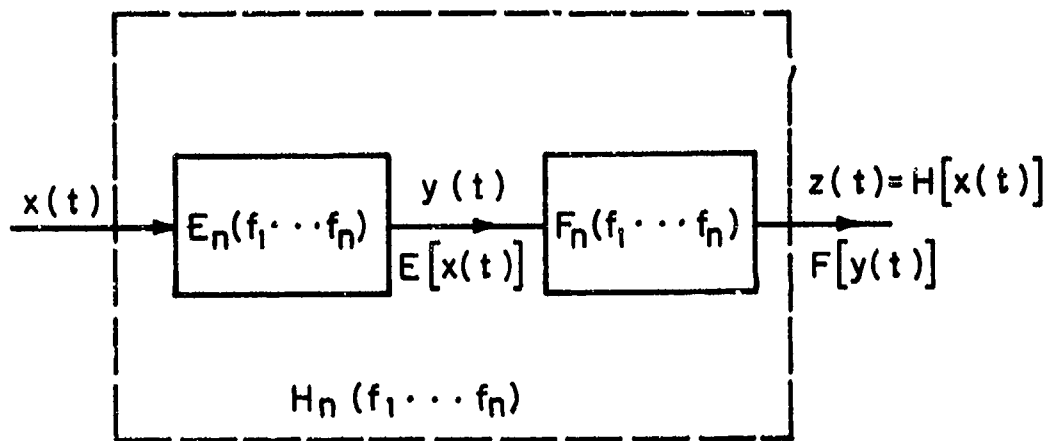
$$q(t) = F[x(t)], \quad (2.155)$$



(a) Nonlinear System with Transfer Functions $E_n(f_1 \cdots f_n)$



(b) Nonlinear System with Transfer Functions $F_n(f_1 \cdots f_n)$



(c) Two Stage Cascade [$H_n(f_1 \cdots f_n)$ is the Transfer Function of the Overall System]

Fig. 2.3. Nonlinear Systems.

where for convenience $E[x(t)]$ is used as denoting the nonlinear operation on $x(t)$ of a system with transfer functions $E_n(f_1, \dots, f_n)$, and similarly for $F[x(t)]$.

Let $H_n(f_1, \dots, f_n)$ be the nonlinear transfer functions of the overall system when these two systems are cascaded, as shown in Fig. 2.3(c). Thus, the output of the overall cascade $z(t)$ may be written as

$$z(t) = H[x(t)]. \quad (2.156)$$

If the two systems are non-interacting, then the output of the first stage $y(t)$ is still given by $E[x(t)]$, while the output $z(t)$ may be written

$$z(t) = F[y(t)] = F[E[x(t)]]. \quad (2.157)$$

The non-interacting cascade relations are obtained by equating Eq. (2.156) and (2.157). The derivation is carried out by substituting the Volterra series representation and equating terms of equal order. The general derivation is cumbersome and hence here we consider some special cases.

(i) First Stage is Linear

If the first stage is linear it is easily shown that

$$H_n(f_1, \dots, f_n) = E_1(f_1) \cdots E_1(f_n) F_n(f_1, \dots, f_n). \quad (2.158)$$

(ii) Second Stage is Linear

When the second stage is linear it is easily shown that

$$H_n(f_1, \dots, f_n) = E_n(f_1, \dots, f_n) F_1(f_1 + \cdots + f_n). \quad (2.159)$$

(iii) Zero-Memory Systems

If both stages are zero-memory each can be represented by a power series

$$p(t) = \sum_{i=1}^{\infty} E_i x^i(t), \quad (2.160)$$

$$q(t) = \sum_{i=1}^{\infty} F_i x^i(t), \quad (2.161)$$

and the cascade output becomes

$$z(t) = \sum_{i=1}^{\infty} F_i \left[\sum_{j=1}^{\infty} E_j x^j(t) \right]^i. \quad (2.162)$$

The overall cascade will also be a zero-memory system representable as

$$z(t) = \sum_{i=1}^{\infty} H_i x^n(t). \quad (2.163)$$

The coefficients H_n to third-order are easily obtained by truncating the summations in Eq. (2.162) up to third-order and equating terms of equal order giving

$$H_1 = F_1 E_1, \quad (2.164)$$

$$H_2 = F_1 E_2 + F_2 E_1^2, \quad (2.165)$$

$$H_3 = F_1 E_3 + 2F_2 F_1 E_2 + F_3 E_1^3, \quad (2.166)$$

(iv) General Cascade Relations

As in the no memory case the cascade relations for a general nonlinear system with memory can be shown to be

$$H_1(f) = F_1(f) E_1(f), \quad (2.167)$$

$$H_2(f_1, f_2) = F_1(f_1 + f_2) E_2(f_1, f_2) + F_2(f_1, f_2) E_1(f_1) E_1(f_2), \quad (2.168)$$

$$\begin{aligned} H_3(f_1, f_2, f_3) &= F_1(f_1 + f_2 + f_3) E_3(f_1, f_2, f_3) \\ &\quad + 2 \overline{F_2(f_1, f_2 + f_3) E_1(f_1) E_2(f_2, f_3)} \\ &\quad + F_3(f_1, f_2, f_3) \prod_{i=1}^3 E_1(f_i). \end{aligned} \quad (2.169)$$

The general expression for $H_n(f_1, \dots, f_n)$ is difficult to obtain and seldom required. However, it should be noted that there is a close analogy between the zero-memory nonlinear systems and the general nonlinear system with memory. This analogy can be used to advantage in deriving and checking the general case.

2.3.3 Nonlinear Interactions in Cascaded Nonlinear Stages

In this subsection we consider the general Volterra series model for interacting cascaded stages. The derivation is for a two stage cascade, which can be extended to any number of stages. To introduce the interaction problem for nonlinear networks we

first summarize the Volterra series analysis of the previous sections. Basic linear circuit theory concepts are then used to show the effects of interaction on the cascade equations.

2.3.3.1 Nonlinear Transfer Functions of Cascade Stages

Figure 2.4(a) shows a circuit with a single nonlinear resistive element whose incremental current i_d as a function of the incremental voltage v_2 is given by

$$i_d = K_1 v_2 + K_2 v_2^2 + K_3 v_2^3 + K_4 v_2^4 + \dots, \quad (2.170)$$

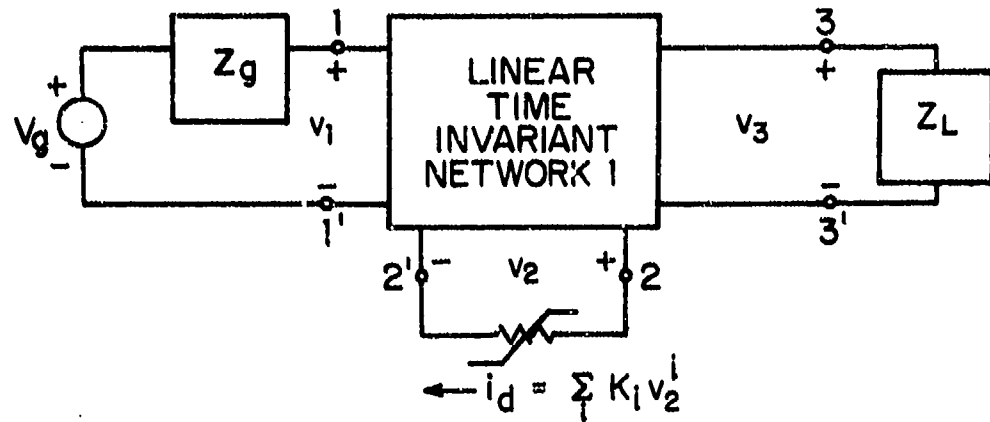
where K_1^{-1} is the incremental linear resistance r_e . The rest of the network is linear time-invariant.

Let us now consider the nonlinear transfer function solution of this network using the methods of Section 2.2. We are only interested in the three external voltages $v_1(t)$, $v_2(t)$ and $v_3(t)$, and their corresponding nonlinear transfer functions $A_n(\cdot)$, $B_n(\cdot)$ and $C_n(\cdot)$ when the input is a voltage v_g .

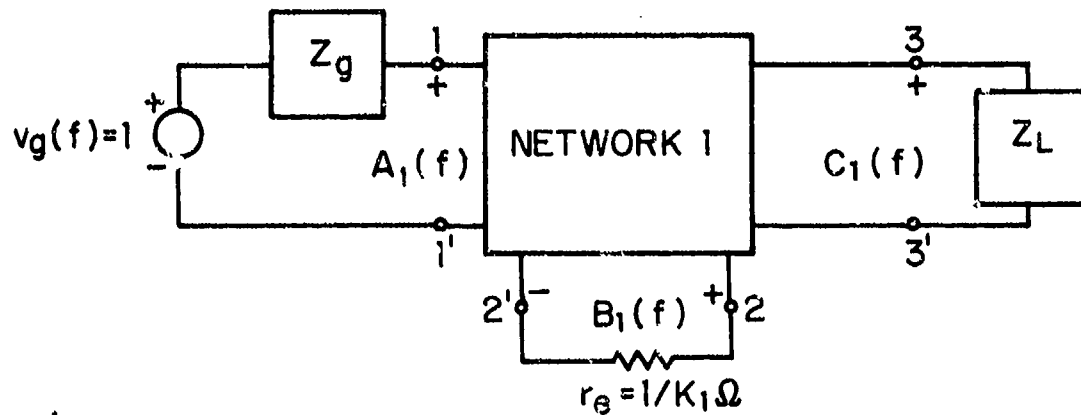
The first-order transfer functions $A_1(f)$, $B_1(f)$ and $C_1(f)$ are obtained by solving the linear network of Fig. 2.4(b) for a unit amplitude input. Note that the nonlinearity in the network of Fig. 2.4(b) is replaced by its incremental resistance r_e .

The second-order transfer functions are obtained again as a solution of the linear network of Fig. 2.4(b) but now the source is a current source of amplitude \hat{K}_2 and frequency $(f_1 + f_2)$ as shown in Fig. 2.5, where \hat{K}_2 is given by

$$\hat{K}_2 = K_2 \prod_{i=1}^2 B_1(f_i). \quad (2.171)$$



(a) Single Nonlinear Element Network



(b) Circuit Determining the First-Order Transfer Functions

Fig. 2.4. Incremental Equivalent Circuits for a Network with a Single Nonlinear Resistive Element.

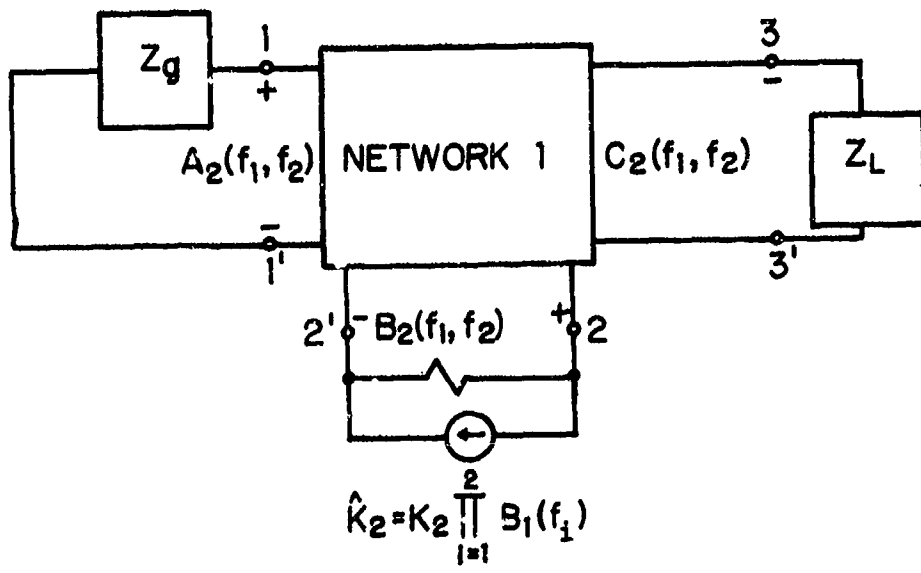


Fig. 2.5. Circuit for Determining the Second-Order Nonlinear Transfer Functions.

The third-order transfer functions are next found by simply replacing the second-order source \hat{K}_2 by the third-order source $\hat{K}_3 + \hat{K}_{23}$, at frequency $(f_1 + f_2 + f_3)$, given by

$$\hat{K}_3 = K_3 \prod_{i=1}^3 B_1(f_i), \quad (2.172)$$

$$\hat{K}_{23} = 2K_2 \frac{B_1(f_1)B_2(f_2, f_3)}{B_1(f_1)B_2(f_2, f_3)}. \quad (2.173)$$

Similarly, for any higher order, the linear network stays the same and only the higher-order sources change. The effect of other nonlinear elements is to introduce additional sources to the linearized network. It is important at this stage to recognize the implications of linearity; use can be made of various circuit theory concepts such as Thevenin and Norton sources and impedances at terminals.

The above outline shows that the basic nature of the small-signal circuit analysis is that the linearized network determines the relationships between the nonlinear transfer functions of a given order. Additionally, and more important from the point of view of interaction, the nonlinearities manifest themselves as sources without changing the linearized network structure. It should therefore be apparent that when nonlinear stages are cascaded, the first-order functions must be those given by the direct application of linear circuit theory. Hence, non-interaction of stages as far as first-order transfer functions are concerned implies that the driving stage output impedance should be much

less than the input impedance of the driven stage. For higher-order transforms this linear interaction must also be taken into account. Additionally, the nonlinear interaction requires the addition of equivalent Thevenin sources from adjacent stages at the terminals of the stage of interest.

2.3.3.2 Two Stage Cascade

In Fig. 2.6(a) a two stage cascade is shown. The first stage is denoted as α and the second as β . If interaction between the stages were negligible, then the nonlinear transfer functions H_n of this cascade are

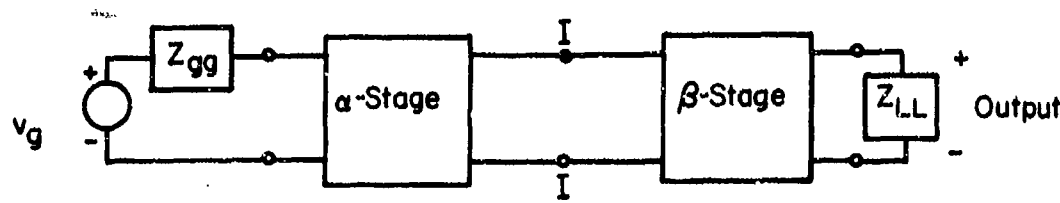
$$H_1(f) = C_1^{\alpha\alpha}(f)C_1^{\beta\beta}(f), \quad (2.174)$$

$$\begin{aligned} H_2(f_1, f_2) &= C_2^{\alpha\alpha}(f_1, f_2)C_1^{\beta\beta}(f_1 + f_2) \\ &\quad + C_1^{\alpha\alpha}(f_1)C_1^{\alpha\alpha}(f_2)C_2^{\beta\beta}(f_1, f_2), \end{aligned} \quad (2.175)$$

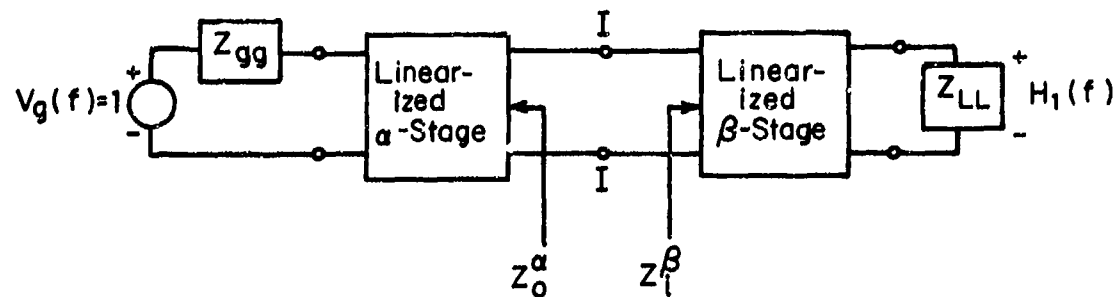
$$\begin{aligned} H_3(f_1, f_2, f_3) &= C_3^{\alpha\alpha}(f_1, f_2, f_3)C_1^{\beta\beta}(f_1 + f_2 + f_3) \\ &\quad + \sum_{i=1}^3 C_1^{\alpha\alpha}(f_i)C_3^{\beta\beta}(f_1, f_2, f_3) \\ &\quad + 2\overline{C_1^{\alpha\alpha}(f_1)C_2^{\alpha\alpha}(f_2, f_3)C_2^{\beta\beta}(f_1, f_2 + f_3)}, \end{aligned} \quad (2.176)$$

where $C_n^{\alpha\alpha}$ are the nonlinear transfer functions of the α stage with its load impedance given by the input impedance Z_i^β of the β stage, while $C_n^{\beta\beta}$ are the nonlinear transfer functions of the second stage with generator impedance assumed zero.

The above equations have a simple physical interpretation. Assuming the two stages do not interact, the first-order transfer function is simply the product of the two transfer functions.



(a) Cascade of Two Nonlinear Stages



(b) Equivalent Circuit Giving the First-Order Transfer Function.

Fig. 2.6. Two Stage Cascade.

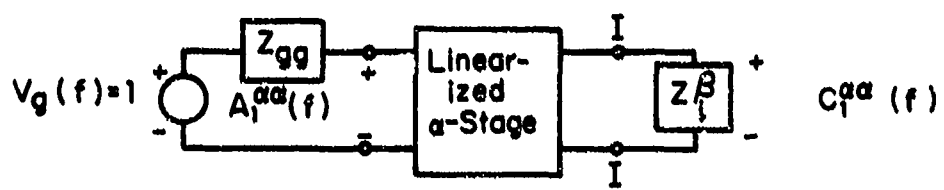
The second-order cascade output will be two contributions: (a) the linear outputs of the α -stage 'distorted' by the second-order nonlinearity of the β -stage, (b) the second-order output of the α -stage linearly transmitted by the β -stage.

The third-order cascade output is similarly determined by accounting for the first, second, and third-order outputs of the α -stage and their resulting transformations in the β -stage. Thus the first-term in Eq. (2.176) is the third-order output of the α -stage linearly transmitted by the β -stage. The second-term in Eq. (2.176) is the β -stage third-order nonlinearity distorting the linear outputs of the α -stage. Finally, the third-term of Eq. (2.176) is the second-order nonlinearity of the β -stage generating an interaction between the linear and second-order outputs of the α -stages.

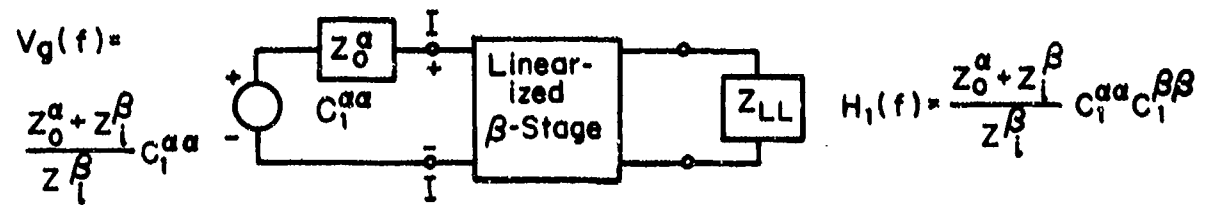
Interaction means that the transfer function of the α and β -stages depend on each other. In the case α and β are linear networks we know that the non-interaction assumption implies that the α -stage output impedance $Z_0^\alpha(f)$ should be much less than $Z_i^\beta(f)$, the input impedance of the β -stage. Thus even the linear case, Eq. (2.174), requires modification for loading. The effects of interaction on each order are considered by solving the combined two stages as a single network.

First-Order Cascade Relationships

The first-order transfer functions of the cascade are obtained by solving the linearized circuit in Fig. 2.6(b), which in turn can be obtained for each stage separately as shown in Fig. 2.7. In Fig. 2.7(b), if the input $V_g(f)$ were of unit amplitude, then the output voltage across the load would be the first-order transfer function of the second stage. However, in



(a) Linear Equivalent Circuit of the First Stage



(b) Linear Equivalent Circuit of the Second Stage

Fig. 2.7. Linear Equivalent Circuits of the First and Second Stages.

Fig. 2.7(b) the input voltage is $C_1^{\alpha\alpha}(z_0^\alpha + z_i^\beta)/z_i^\beta$, the Thevenin equivalent source to the left of the common terminal I, with z_0^α the source Thevenin impedance. The reason this Thevenin source is expressed in terms of output $C_1^{\alpha\alpha}(f)$ rather than the input $V_g(f) = 1$ is to relate the individual stage transfer functions, $C_n^{\alpha\alpha}$ and $C_n^{\beta\beta}$, to H_n , the nonlinear transfer function, as has been done in the non-interacting case. Thus denoting the n^{th} order transfer functions of the two stages by $C_n^{\alpha\alpha}$ and $C_n^{\beta\beta}$, we see that the cascade first-order transfer function is

$$H_1(f) = T_{\alpha\beta}(f)C_1^{\alpha\alpha}(f)C_1^{\beta\beta}(f), \quad (2.177)$$

where

$$T_{\alpha\beta}(f) = \frac{z_0^\alpha(f) + z_i^\beta(f)}{z_i^\beta(f)}. \quad (2.178)$$

In Fig. 2.7(a) we have defined the transfer function at the first stage input by $A_1^{\alpha\alpha}(f)$ when $V_g(f) = 1$. The corresponding notation for the higher-order transfer functions will be $A_n^{\alpha\alpha}$. Similarly, for the second stage of Fig. 2.7(b), the nonlinear transfer functions at the input terminals for unit input amplitude will be denoted by $A_n^{\beta\beta}$. Thus the double superscripts $\alpha\alpha$ and $\beta\beta$ refer to the nonlinear transfer functions of the individual stages considered separately. The purpose of explicitly identifying $A_n^{\alpha\alpha}$ and $A_n^{\beta\beta}$ is that these functions determine the level of interaction for the higher-order cascade.

Second-Order Cascade Relationships

Let us now consider the second-order transfer function of the two stage cascade. Figure 2.8 shows the network whose second-order transfer function is to be found. Since the network is linear, the two stages can be solved individually, with appropriate sources replacing the adjacent stage as shown in Figs. 2.9(a) and 2.9(b).

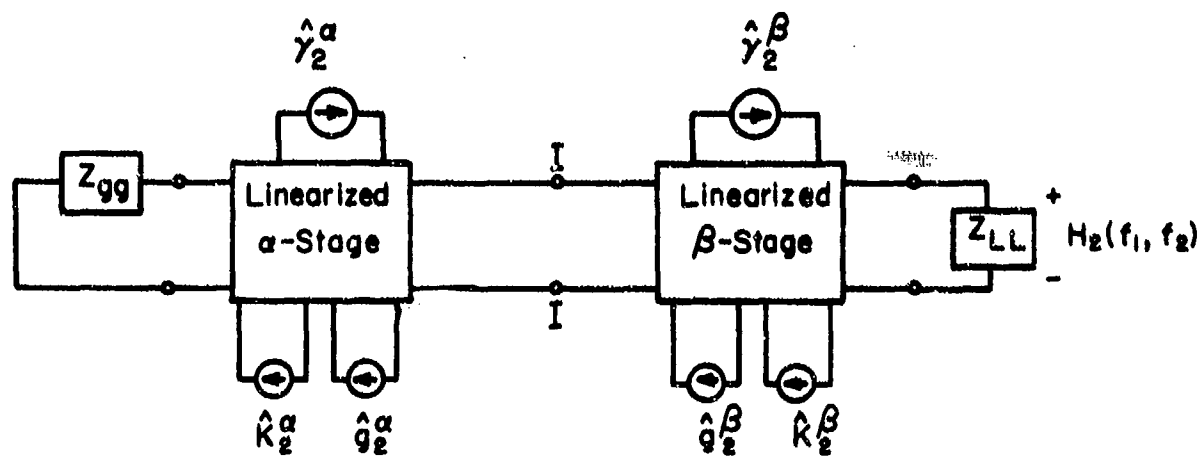


Fig. 2.8. Equivalent Circuit for the Second-Order Transfer Function.

In Fig. 2.8 we have assumed three second-order nonlinearities in each stage as in our previous transistor model for the purpose of pursuing the discussion with familiar parameters. Since each nonlinearity supplies a source which is independent of the other sources of the same order, the existence of one or more sources does not effect the nature of the interaction. Thus we will restrict ourselves to only the K nonlinearity in both stages. Figure 2.8 shows the network to be solved to obtain $H_2(f_1, f_2)$, the nonlinear transfer functions of the full network. The network includes both linear and nonlinear interaction. Furthermore, $H_2(f_1, f_2)$ can be obtained by solving each stage separately as shown in Figs. 2.9(a) and 2.9(b). To do this, the sources $I_2^{\alpha\theta}$ and $I_2^{\beta\theta}$ are determined as follows:

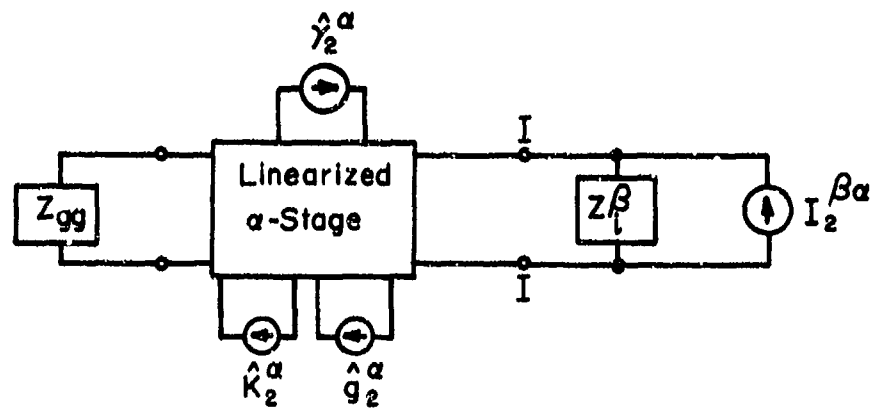
$I_2^{\theta\alpha}$ is the Norton equivalent current source of the network to the right of terminal I in Fig. 2.9(b) when $I_2^{\alpha\theta}$ is set to zero.

$I_2^{\alpha\theta}$ is the Norton equivalent current source of the network to the left of terminal I in Fig. 2.9(a) when $I_2^{\theta\alpha}$ is set to zero.

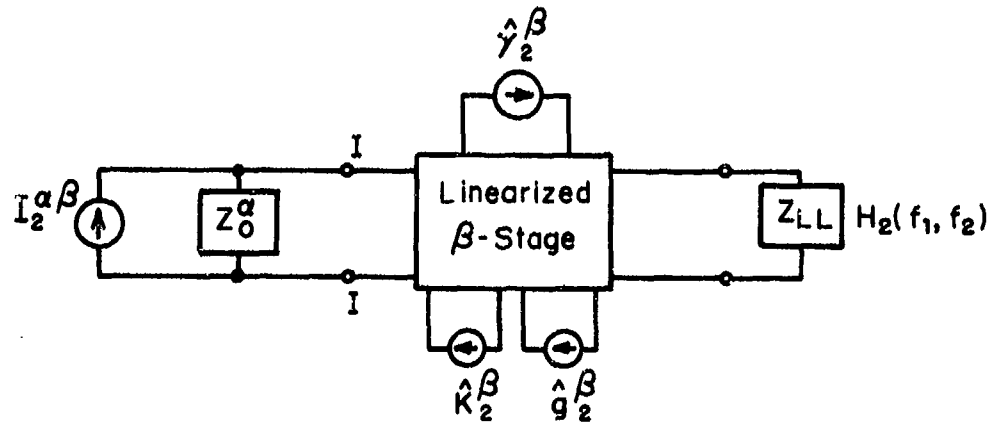
The network and sources K_2^α , g_2^α and γ_2^α of Fig. 2.9(a) with $I_2^{\theta\alpha}$ set to zero are the same network and sources that exist when solving for the transfer functions of the α -stage. Thus, it is easy to show that

$$I_2^{\alpha\theta} = \frac{T_{\alpha\theta}(f_1 + f_2)}{Z_0^\alpha(f_1 + f_2)} C_2^{\alpha\alpha}(f_1, f_2). \quad (2.179)$$

Similarly, in the case of Fig. 2.9(b) with $I_2^{\theta\alpha}$ set to zero, the network and sources, are, within a normalizing factor, the same



(a) Equivalent Circuit of the First Stage



(b) Equivalent Circuit of the Second Stage

Fig. 2.9. Equivalent Circuits for Each Stage in the Cascade for Second Order Transfer Functions.

as exist when solving for the transfer functions of the β -stage alone. The normalization necessary for second-order sources is to multiply the individual β -stage second-order term by

$$\prod_{i=1}^2 T_{\alpha\beta}(f_i) C_1^{\alpha\alpha}(f_i), \quad (2.180)$$

which should be apparent since the first-order input to the β -stage at the frequency f is $T_{\alpha\beta}(f) C_1^{\alpha\alpha}(f)$, and the sources \hat{K}_2^β , \hat{g}_2^β and \hat{v}_2^β are quadratic functions of the first-order terms. Thus, recognizing the effect of Eq. (2.175), it is easily shown that in Fig. 2.9(b) with $I_2^{\beta\beta}$ zero, the voltage at terminals I is given by

$$\prod_{i=1}^2 T_{\alpha\beta}(f_i) C_1^{\alpha\alpha}(f_i) \{A_2^{\beta\beta}(f_1, f_2)\}. \quad (2.181)$$

The resulting value of $I_2^{\beta\alpha}$ is thus

$$I_2^{\beta\alpha} = \frac{T_{\beta\alpha}(f_1 + f_2)}{Z_i^\beta(f_1 + f_2)} \left[\prod_{i=1}^2 T_{\alpha\beta}(f_i) C_1^{\alpha\alpha}(f_i) \{A_2^{\beta\beta}(f_1, f_2)\} \right], \quad (2.182)$$

where $T_{\beta\alpha}(f_1 + f_2)$ is simply the reverse transfer function from β stage to α stage

$$T_{\beta\alpha}(f) = \frac{z_0^\alpha(f) + z_i^\beta(f)}{z_0^\alpha(f)} = \frac{z_i^\beta(f)}{z_0^\alpha(f)} T_{\alpha\beta}(f). \quad (2.183)$$

The second-order nonlinear transfer function of the cascade is obtained from Fig. 2.9(b) by superposition as the sum of the responses to $I_2^{\beta\beta}$ and internal sources of the β -stage as

$$H_2(f_1, f_2) = \{ \underbrace{\sum_{i=1}^2 T_{\alpha\beta}(f_i) C_1^{\alpha\alpha}(f_i)}_{\text{Thevenin Equivalent first-order inputs from a stage}} \} C_2^{\beta\beta}(f_1, f_2)$$

Thevenin Equivalent
first-order inputs
from a stage

$$+ T_{\alpha\beta}(f_1 + f_2) C_2^{\alpha\alpha}(f_1, f_2) C_1^{\beta\beta}(f_1 + f_2).$$

Thevenin Equivalent
second-order input
from a stage

(2.184)

This result is the exact cascade formula for the second-order case including interaction. This result is the same as would be obtained by correcting for the linear loading effect of $T_{\alpha\beta}(f)$. Thus Eq. (2.184) can be obtained by replacing $C_n^{\alpha\alpha}$ in the non-interacting cascade equations as indicated by

$$\left. \begin{aligned} C_1^{\alpha\alpha}(f) &\rightarrow T_{\alpha\beta}(f) C_1^{\alpha\alpha}(f), \\ C_2^{\alpha\alpha}(f_1, f_2) &\rightarrow T_{\alpha\beta}(f_1 + f_2) C_2^{\alpha\alpha}(f_1, f_2), \\ C_3^{\alpha\alpha}(f_1, f_2, f_3) &\rightarrow T_{\alpha\beta}(f_1 + f_2 + f_3) C_3^{\alpha\alpha}(f_1, f_2, f_3). \end{aligned} \right\} \quad (2.185)$$

Equation (2.185) simply expresses the relation that all outputs of the α -stage go through a linear filter $T_{\alpha\beta}(f)$. As the third-order case below will show, Eq. (2.185) is the only modification to the non-interacting cascade equations necessary to account for linear loading or interaction.

It should be observed that the second-stage source $I_2^{\alpha\alpha}$ driving the first-stage is not involved in computing the second-

order cascade formula. However, the second-order terms within the α -stage are changed due to the feedback of $I_2^{\beta\alpha}$. Since the third-order sources due to each nonlinearity are a function of the first and second-order transfer functions across that nonlinearity, $I_2^{\beta\alpha}$ has to be included to compute the α -stage third-order output, which in turn determines the third-order nonlinear transfer function $H_3(f_1, f_2, f_3)$.

Third-Order Cascade Relationships

The third-order transfer functions of the cascade are given by the circuit of Fig. 2.10, and the corresponding equivalent circuits of each individual stage are given by Figs. 2.11(a) and 2.11(b). The interacting sources $I_3^{\alpha\beta}, I_3^{\beta\alpha}, I_{23}^{\alpha\beta}$ and $I_{23}^{\beta\alpha}$ are again determined in the same fashion as for the second-order, i.e.,

$I_{23}^{\beta\alpha} + I_3^{\beta\alpha}$ is the Norton equivalent current source of the network to the right of terminal I in Fig. 2.11(b) when $I_{23}^{\alpha\beta} + I_3^{\alpha\beta}$ is set to zero.

$I_{23}^{\alpha\beta} + I_3^{\alpha\beta}$ is the Norton equivalent current source of the network to the left of terminal I in Fig. 2.11(a) when $I_{23}^{\beta\alpha} + I_3^{\beta\alpha}$ is set to zero.

Again, because of superposition and the independence of all third-order sources, the I_{23} terms depend only on the \hat{K}_{23} , \hat{Y}_{23} and \hat{g}_{23} sources and I_3 terms depend only on the \hat{K}_3 , \hat{Y}_3 and \hat{g}_3 functions.

The network and sources $\hat{K}_{23}^{\alpha} + \hat{K}_3^{\alpha}, \hat{g}_{23}^{\alpha} + \hat{g}_3^{\alpha}$, and \hat{Y}_{23}^{α} of Fig. 2.11(b) with $I_{23}^{\alpha\beta} + I_3^{\alpha\beta}$ set to zero is the same network but different sources than used when solving for the transfer functions of the α -stage alone. The difference is in the sources $\hat{K}_{23}^{\alpha}, \hat{g}_{23}^{\alpha}$ and \hat{Y}_{23}^{α} , due to an additional term from the second-order current $I_2^{\alpha\beta}$ from the second stage which drives the first stage.

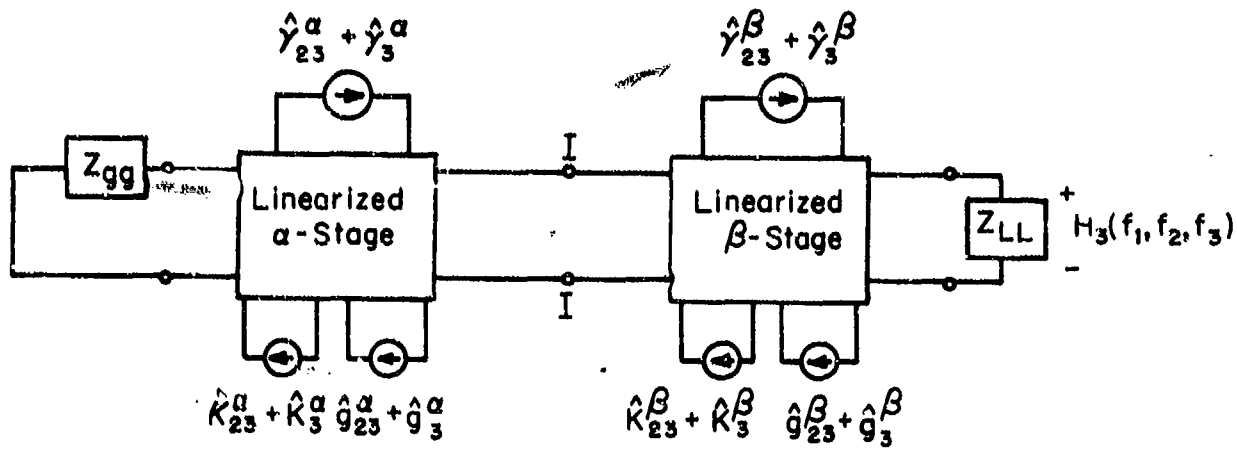
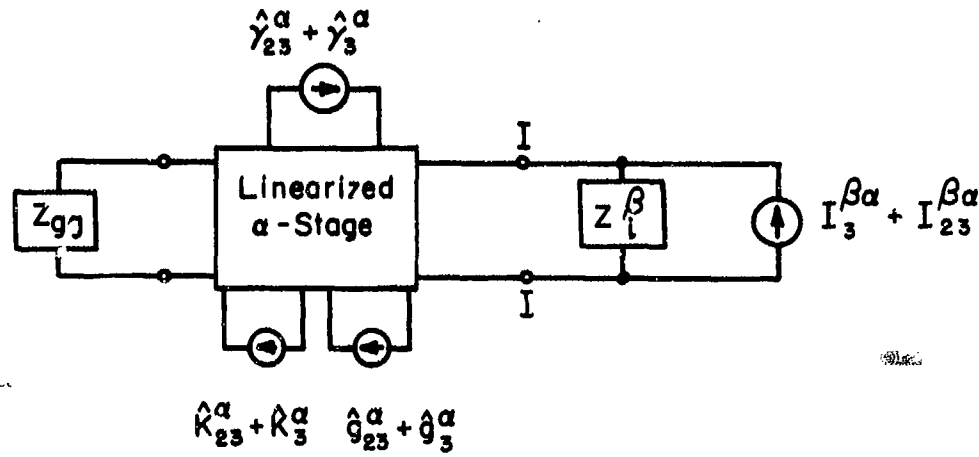
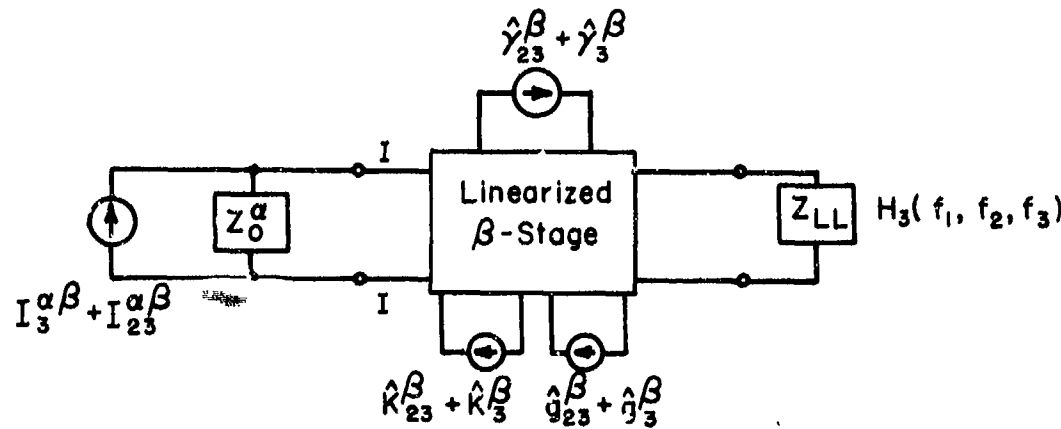


Fig. 2.10. Equivalent Circuit for the Third-Order Transfer Functions.



(a) Equivalent Circuit of the First Stage



(b) Equivalent Circuit of the Second Stage

Fig. 2.11. Equivalent Circuits for Determining the Third-Order Nonlinear Transfer Functions.

With $I_2^{\alpha\beta}$ zero we get

$$I_{23}^{\alpha\beta} + I_3^{\alpha\beta} \Big|_{I_2^{\beta\alpha} = 0} = \frac{T_{\alpha\beta}(f_1 + f_2 + f_3)}{Z_o^\alpha(f_1 + f_2 + f_3)} C_3^{\alpha\alpha}(f_1, f_2, f_3). \quad (2.186)$$

The effect of $I_2^{\beta\alpha}$ is to modify $C_3^{\alpha\alpha}(f_1, f_2, f_3)$ by $\epsilon(I_2^{\beta\alpha})$, i.e.

$$I_{23}^{\alpha\beta} + I_3^{\alpha\beta} = \frac{T_{\alpha\beta}(f_1 + f_2 + f_3) \{C_3^{\alpha\alpha}(f_1, f_2, f_3) + \epsilon(I_2^{\beta\alpha})\}}{Z_o^\alpha(f_1 + f_2 + f_3)}. \quad (2.187)$$

The cascade third-order term $H_3(f_1, f_2, f_3)$ is found from the network of Fig. 2.11(b) by considering the contributions of $(I_{23}^{\alpha\beta} + I_3^{\alpha\beta})$ and the internal β stage sources separately. The contribution to $H_3(f_1, f_2, f_3)$ due to the internal β -stage sources can be viewed as the third-order output resulting from driving the β stage with the sum of exponentials given by

$$v_g(t) = \sum_{i=1}^3 T_{\alpha\beta}(f_i) C_1^{\alpha\alpha}(f_i) e^{j2\pi f_i t} + \sum_{i=1}^3 \sum_{j=1}^3 T_{\alpha\beta}(f_i + f_j) C_2^{\alpha\alpha}(f_i, f_j) e^{j2\pi(f_i + f_j)t}, \quad (2.188)$$

and hence the output nonlinear transfer function in terms of the transfer function of the β stage is given by

$$H_3(f_1, f_2, f_3) \Big|_{(I_{23}^{\alpha\beta} + I_3^{\alpha\beta}) = 0} = \{ \sum_{i=1}^3 T_{\alpha\beta}(f_i) C_1^{\alpha\alpha}(f_i) \} C_3^{\beta\beta}(f_1, f_2, f_3) + 2 \overline{T_{\alpha\beta}(f_i) C_1^{\alpha\alpha}(f_i) T_{\alpha\beta}(f_j + f_k) C_2^{\alpha\alpha}(f_j, f_k) C_2^{\beta\beta}(f_i, f_j + f_k)}. \quad (2.189)$$

Finally including the contribution of $I_{23}^{\alpha\beta}$ and $I_3^{\alpha\beta}$ we get

$$\begin{aligned}
 H_3(f_1 + f_2 + f_3) = & \left\{ \prod_{i=1}^3 T_{\alpha\beta}(f_i) C_1^{\alpha\alpha}(f_i) \right\} C_3^{\beta\beta}(f_1, f_2, f_3) \\
 & + 2 \overline{T_{\alpha\beta}(f_1) C_1^{\alpha\alpha}(f_1) T_{\alpha\beta}(f_j + f_k) C_2^{\alpha\alpha}(f_j, f_k) C_2^{\beta\beta}(f_i, f_j + f_k)} \\
 & + T_{\alpha\beta}(f_1 + f_2 + f_3) \{ C_3^{\alpha\alpha}(f_1, f_2, f_3) + \epsilon(I_2^{\beta\alpha}) \} \quad (2.190) \\
 & \times C_1^{\beta\beta}(f_1 + f_2 + f_3)
 \end{aligned}$$

This is the exact third-order transform of the two stage cascade including interaction. This result, without the $\epsilon(I_2^{\beta\alpha})$ term, is identical to the expression obtained by applying Eq. (2.185) to Eq. (2.176). Therefore, accounting for only linear interaction gives an error in the third-order transfer function.

The term $\epsilon(I_2^{\beta\alpha})$ is not expressible in terms of the individual input and output stage transfer functions as are the rest of the previous cascade expressions. The reason is that $\epsilon(I_2^{\beta\alpha})$ results from second-order interaction between the first-order responses in the α -stage and the $I_2^{\beta\alpha}$ current input at the intermediate terminal I. Thus, consider the K_{23}^α term and let B_n denote the nonlinear transfer function of the voltage across the K^α non-linearity. Then, Eq. (2.173) gives

$$K_{23}^\alpha = 2K_2^\alpha \overline{B_1(f_1) B_2(f_2, f_3)}, \quad (2.191)$$

while, if $I_2^{\beta\alpha}$ is neglected, we get

$$K_{23}^\alpha \Big|_{I_2^{\beta\alpha} = 0} = 2K_2^\alpha \overline{B_1^{\alpha\alpha}(f_1) B_2^{\alpha\alpha}(f_2, f_3)}, \quad (2.192)$$

where $B_n^{\alpha\alpha}$ are the nonlinear transfer functions of the voltage across the K_α nonlinearity for the individual α -stage. Since $B_1(f)$ is the same as $B_1^{\alpha\alpha}(f)$ while $B_2^{\alpha\alpha}$ differs from B_2 due to the source $I_2^{\beta\alpha}$ we can write

$$\hat{K}_{23}^\alpha = \frac{2K_2^\alpha \{B_1^{\alpha\alpha}(f_1)B_2^{\alpha\alpha}(f_2, f_3) + B_1^{\alpha\alpha}(f_1)\tilde{B}_2^{\alpha}(f_2, f_3)\}}{2}, \quad (2.193)$$

where $\tilde{B}_2^{\alpha}(f_2, f_3)$ is the voltage across the K^α nonlinearity due to the excitation $I_2^{\beta\alpha}$ alone. Similar terms will exist in g_{23}^α and γ_{23}^α and their combined effect manifested by $e(I_2^{\beta\alpha})$. If one knows the internal nonlinearities of each stage, $e(I_2^{\beta\alpha})$ can be determined. However, as the discussion has indicated, it involves determining the nonlinear transfer functions of the individual networks for simultaneous excitation at each port.

2.3.3.3 Conclusions and Numerical Comparison of Cascade Techniques

We have shown that the overall nonlinear transfer function of a two-stage cascade cannot be exactly determined from the 'forward' nonlinear transfer function of the individual stages. To determine the correct nonlinear transfer function of the cascade requires solution of the overall network. However, the overall network can be subdivided into the two stages and solved with equivalent Thevenin or Norton sources representing the interaction.

In the case of mildly excited nonlinearities and high forward-gain amplifiers, the nonlinear interaction will frequently be negligible so that only linear interaction needs to be taken into account. Table 2.1 shows computed results for the first three transfer

TABLE 2.1.
COMMON Emitter-Common Base CASCADED NONLINEAR TRANSFER FUNCTIONS

Western Electric Transistor A 2436.

2 = 75

卷之三

Transfer Function	Approximate Cascade (Exact Linear-Loading)						
	Frequency	Order	Exact Cascade Magnitude (dB)	Angle (radians)	Magnitude (dB)	Angle (radians)	
							Change (dB)
f_1	1	27.05	1.64	27.05	1.63	0.00	-0.01
f_2	1	27.77	1.68	27.77	1.67	0.00	-0.01
f_3	1	28.15	4.58	28.15	4.58	0.00	0.00
$f_1 + f_2$	2	29.48	0.24	29.52	0.23	0.04	-0.01
$f_1 - f_3$	2	24.63	3.58	24.67	3.57	0.04	-0.01
$f_2 - f_3$	2	22.39	3.39	22.43	3.38	0.04	-0.01
$f_1 + f_2 - f_3$	3	20.37	4.25	21.17	4.08	0.80	-0.17

functions of a common-emitter and common-base transistor amplifier cascade with $f_1 = 16.6$ MHz, $f_2 = 15.2$ MHz, and $f_3 = 14.5$ MHz. This transistor model is given in Narayanan (1967). The load and generator impedance were 75 ohms. The full nonlinear equations of the cascade have been solved to determine the exact cascade transfer functions. The approximate cascade results in Table 2.1 include the effects of linear interaction but neglect the nonlinear feedback. Comparing the two results, it is seen that the first and second-order functions are essentially in perfect agreement as predicted in Section 2.3.3.2, while the third-order transfer functions differ in magnitude by 0.80 dB and in phase by 0.17 radians. Thus, the cascade equations with impedance corrections can be used in many situations to reliably predict the nonlinear performance of a chain of stages.

Table 2.2 presents the results of a comparison between the non-interacting cascade approach, denoted as the zero-impedance approximation, and the approximate cascade including linear interaction. It is seen that the zero impedance non-interacting cascade differs by up to nearly six dB in the second and third-order functions, showing the need to include the impedance correction for interaction correction.

In conclusion, we note that nonlinear interaction, if significant, is most easily handled by solving the total network. The best approach in the nonlinear analysis of a complete communication receiver is to segment the stages so that it is only necessary to account for linear loading. In summary, the two

TABLE 2.2.
COMMON Emitter-Common Base CASED NONLINEAR TRANSFER FUNCTIONS
Western Electric Transistor A 2436.

		$Z_g = Z_L = 75\Omega$		
Transfer Function	Order	Zero Impedance Cascade (dB)	Approximate Cascade Exact Linear-Loading (dB)	Change (dB)
f_1	1	27.036	27.054	0.018
f_2	1	27.774	27.776	0.002
f_3	1	28.117	28.157	0.040
$f_1 + f_2$	2	31.270	29.525	-1.645
$f_1 - f_3$	2	28.736	24.672	-4.064
$f_2 - f_3$	2	28.313	22.435	-5.878
$f_1 + f_2 - f_3$	3	25.228	21.170	-4.058

important properties of nonlinear interaction that have been derived in this section are:

- 1) The overall second-order transfer function of a cascade is given correctly by the non-interacting cascade expressions as modified only by the linear loading effect.
- 2) The 'forward' nonlinear transfer functions $C_n^{aa}(f_1, \dots, f_n)$ or $C_n^{BB}(f_1, \dots, f_n)$ do not provide sufficient information to solve nonlinearly interacting systems.

2.4 Multiple-Input Nonlinear Circuit Analysis

The Volterra functional series of the output of a single input port system has received more attention in the literature than the case of multiple input ports. However, a variety of nonlinear systems have independent inputs from separate ports or terminals. In this section we show how the nonlinear transfer function analysis is also applicable to multiple port nonlinear networks.

2.4.1 Three Node Example

We show this by a simple physical argument. Equation 2.32 showed that the first-order transfer functions of a three-node linear network were given by

$$\begin{bmatrix} A_1(f_i) \\ B_1(f_i) \\ C_1(f_i) \end{bmatrix} = [Y(f_i)]^{-1} \begin{bmatrix} Y_g(f_i) \\ 0 \\ 0 \end{bmatrix}; i = 1, 2, 3. \quad (2.194)$$

The second-order nonlinear transfer functions were shown by Eq. (2.37) to be given by

$$\begin{bmatrix} A_2(f_1, f_2) \\ B_2(f_1, f_2) \\ C_2(f_1, f_2) \end{bmatrix} = [Y(f_1 + f_2)]^{-1} \begin{bmatrix} 0 \\ -\hat{K}_2(f_1, f_2) \\ 0 \end{bmatrix}, \quad (2.195)$$

where

$$\hat{K}_2(f_1, f_2) = K_2 B_1(f_1) B_1(f_2). \quad (2.196)$$

Higher-order equations could be written, but the argument which will be developed for the second-order case applies directly to the higher-order cases. Similarly, no loss of generality occurs in discussing a three-node, single nonlinearity example.

Equation (2.194) is of the proper form for describing the linearized network when all sources are at node 1 and are of unit amplitude. Now let us consider the case where sources are at all three nodes with complex amplitudes v_1 , v_2 and v_3 , and admittances y_{g1} , y_{g2} , and y_{g3} . For this case, the formulation of the first-order solution is

$$\begin{bmatrix} A'_1(f_i) \\ B'_1(f_i) \\ C'_1(f_i) \end{bmatrix} = [Y(f_i)]^{-1} \begin{bmatrix} v_1(f_i) y_{g1}(f_i) \\ v_2(f_i) y_{g2}(f_i) \\ v_3(f_i) y_{g3}(f_i) \end{bmatrix}, \quad (2.197)$$

where the primed superscript on the first-order solutions denotes the solutions are not the nonlinear transfer functions, per se.,

but instead are scaled linear combinations of the nonlinear transfer functions arising from the superposition of the responses from each of the nodal generators. In addition, the Y matrix would be modified from that of Equation (2.194) by the addition of the generator admittance. As a simple example, one might consider that Equation (2.197) represents a balanced amplifier, with inputs at nodes 1 and 3, and output at node 2. In this case the sum mode response to identical inputs $v_s(f_i)$ would be given by:

$$\begin{bmatrix} A'_1(f_i) \\ B'_1(f_i) \\ C'_1(f_i) \end{bmatrix} = [Y(f_i)]^{-1} \begin{bmatrix} v_s(f_i) Y_g(f_i) \\ 0 \\ v_s(f_i) Y_g(f_i) \end{bmatrix}, \quad (2.198)$$

and the difference mode response to identical but opposite signed inputs $v_s(f_i)$ would be given by

$$\begin{bmatrix} A'_1(f_i) \\ B'_1(f_i) \\ C'_1(f_i) \end{bmatrix} = [Y(f_i)]^{-1} \begin{bmatrix} v_s(f_i) Y_g(f_i) \\ 0 \\ -v_s(f_i) Y_g(f_i) \end{bmatrix}. \quad (2.199)$$

Equations (2.195) and (2.196) show that the second-order response is solely a function of the first-order voltages $B_1(f_1)$ and $B_1(f_2)$. From what port these voltages were established is not of interest, as the first-order solution is linear and superposition holds. It therefore follows that all the nonlinear

transfer functions for a multiple input port circuit can be computed by determining the linear solution with the right-hand column vector of Norton generators appropriate to the port excitations, and then proceeding with the conventional higher-order analysis. If the generator amplitudes are not equal to unity, the transfer functions will be scaled according to the amplitudes and the order of the transfer functions. If the excitations are such that the same frequency does not appear at two different ports, then the analysis can be made with unit amplitude generators, i.e., $V_i(f_i) = 1$. If, on the other hand, the same frequency appears at two or more generators, then the several $V_i(f_i)$ must have the proper phasing and amplitudes, so that the linear response will represent the actual coherent effects.

2.4.2 Two-Input Volterra Series

The Volterra series is a generalization of the Taylor series expansion for representing a nonlinear system. Thus the Volterra series for multiple-input systems is obtained by direct analogy to the corresponding multi-variable Taylor series. A two-input Volterra series is given by

$$c(t) = \sum_{m=0}^{\infty} \sum_{\substack{n=0 \\ m \neq n=0}}^{\infty} \int_{-\infty}^{\infty} d\tau_1 \cdots \int_{-\infty}^{\infty} d\tau_{m+n} h_{mn}(\tau_1, \tau_2, \dots, \tau_{m+n}) \cdot \prod_{i=1}^m x(t - \tau_i) \prod_{j=m+1}^{m+n} y(t - \tau_j), \quad (2.200)$$

where $c(t)$ is the output and $x(t)$ and $y(t)$ the two inputs. The corresponding frequency domain representation is

$$C(f) = \sum_{\substack{m=0 \\ m \neq n=0}}^{\infty} \sum_{n=0}^{\infty} \int_{-\infty}^{\infty} df_1 \dots \int_{-\infty}^{\infty} df_{m+n} H_{mn}(f_1, f_2, \dots, f_{m+n}) \\ \cdot \delta(f - f_1 - f_2 - \dots - f_{m+n}) \prod_{i=1}^m X(f_i) \prod_{j=m+1}^{m+n} Y(f_j),$$

(2.201)

where $H_{mn}(\cdot)$ is the $(m+n)$ -fold transform of $h_{mn}(\cdot)$, and $C(f)$, $X(f)$ and $Y(f)$ are the transforms of $c(t)$, $x(t)$ and $y(t)$ respectively. The formulation for the case of three or more inputs is similar. It should be noted in Eq. (2.201) that the first m frequencies f_1, \dots, f_m correspond to frequencies of the input $x(t)$ and the following frequencies f_{m+1}, \dots, f_{m+n} correspond to the input $y(t)$. To make this frequency relationship explicit let p_1, p_2, \dots represent the frequency variables associated with $x(t)$ and q_1, q_2, \dots the frequency variables associated with $y(t)$. Writing Eq. (2.201) in terms of p_i and q_i gives

$$C(f) = \sum_{\substack{m=0 \\ m \neq n=0}}^{\infty} \sum_{n=0}^{\infty} \int_{-\infty}^{\infty} dp_1 \dots \int_{-\infty}^{\infty} dp_m \cdot \int_{-\infty}^{\infty} dq_1 \dots \int_{-\infty}^{\infty} dq_n \\ \cdot H_{mn}(p_1, \dots, p_m; q_1 \dots q_n) \\ \cdot \delta(f - p_1 - \dots - p_m - q_1 - \dots - q_n) \prod_{i=1}^m X(p_i) \prod_{i=1}^n Y(q_i).$$

(2.202)

We will denote by \underline{f}_{mn} the frequency vector

$$\underline{f}_{mn} = (p_1, p_2, \dots, p_m; q_1, \dots, q_n). \quad (2.203)$$

The most important two-input stage in a receiver is a mixer. One input is the signal and the other the local-oscillator as shown in Fig. 2.12. An amplifier stage may also become a two-input system when an external interference enters the stage at a node other than the input. In Fig. 2.12 $x(t)$ is the input signal and $y(t)$ is the local oscillator.

To determine the nonlinear transfer functions $H_{mn}(\underline{f}_{mn})$ for a given circuit, the node equation formulation for the single input analysis can be applied directly. Each node voltage is now represented as a two-input Volterra series, e.g., $A_{mn}(\underline{f}_{mn})$, $B_{mn}(\underline{f}_{mn})$... etc. The resulting linear transfer functions $H_{10}(p_1)$ and $H_{01}(q_1)$ are given by the solution of the linearized network excited at the appropriate ports by $e^{j2\pi p_1 t}$ and $e^{j2\pi q_1 t}$, respectively. The second and higher-order nonlinear transfer functions are the solution of the linearized network excited by sources such as $\hat{K}_2, \hat{Y}_2, \dots$ etc. resulting from the nonlinearities.

The similarity of the solution to the single-input case is best seen by considering the example of Fig. 2.13. In Fig. 2.13 is shown a two-input network with a single zero-memory nonlinearity. The transfer functions for the voltage $v(t)$ across the nonlinearity will be denoted by $S_{mn}(\underline{f}_{mn})$.

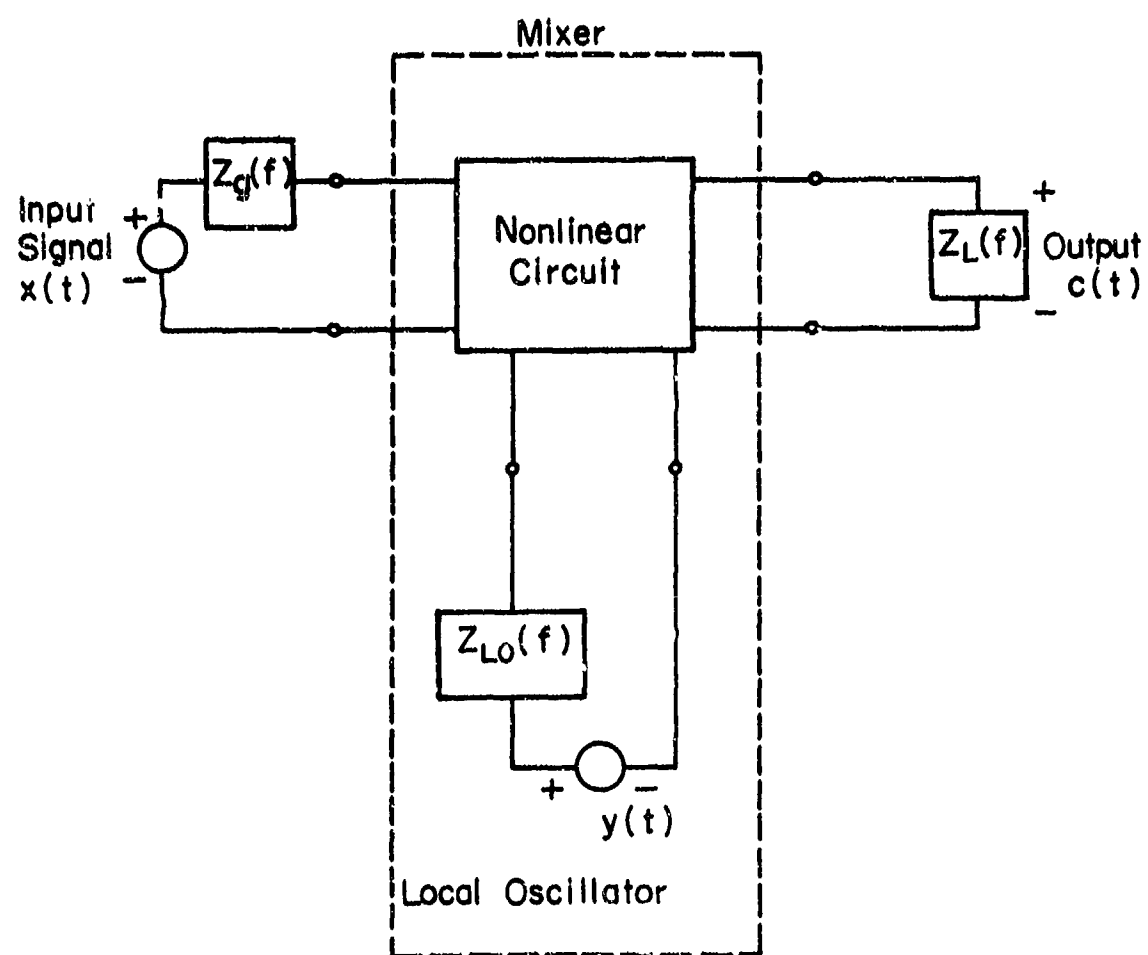


Fig. 2.12. A Two-Input Mixer

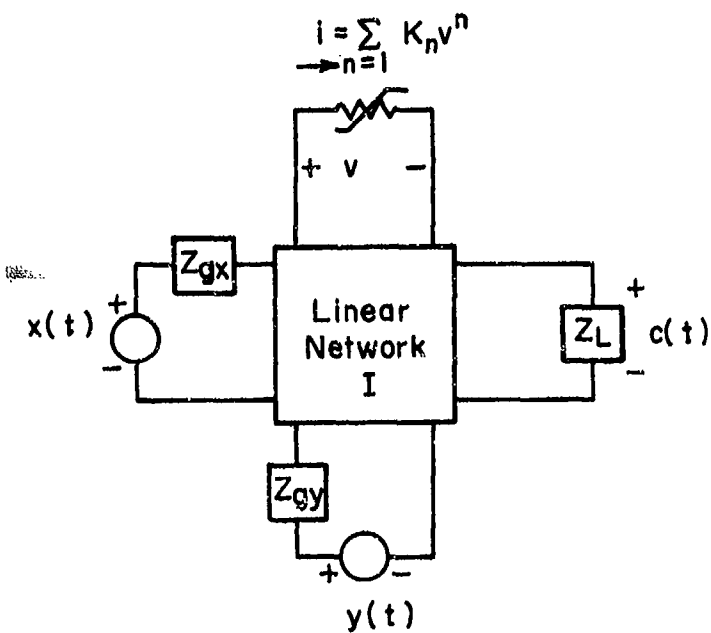


Fig. 2.13. Single Nonlinear Element Circuit with a Multiple Input.

The two first-order transfer functions $H_{10}(p_1)$ and $H_{01}(q_1)$ are given by solving the network of Fig. 2.14. Note that $H_{10}(p_1)$ is the complex amplitude across the load Z_L when $X(p_1)$, the transform of $x(t)$, has a unit amplitude at frequency p_1 . When solving for $H_{10}(p_1)$ the voltage source $y(t)$ is replaced by an ideal short. $H_{01}(q_1)$ is similarly obtained.

The determination of the higher-order nonlinear transfer functions $H_{mn}(f_{mn})$ for a two-input nonlinear circuit is essentially the same as the single-input case. The only difference in the two-input analysis is that the first-order solutions are determined by exciting the corresponding ports separately. In the second and higher-order cases the difference between one or more input port circuits is only in the first-order responses at the nonlinearities. Thus, with the proper accounting for the frequencies originating from each external source, the single-input nonlinear transfer function analysis can be extended to the multiple-input case.

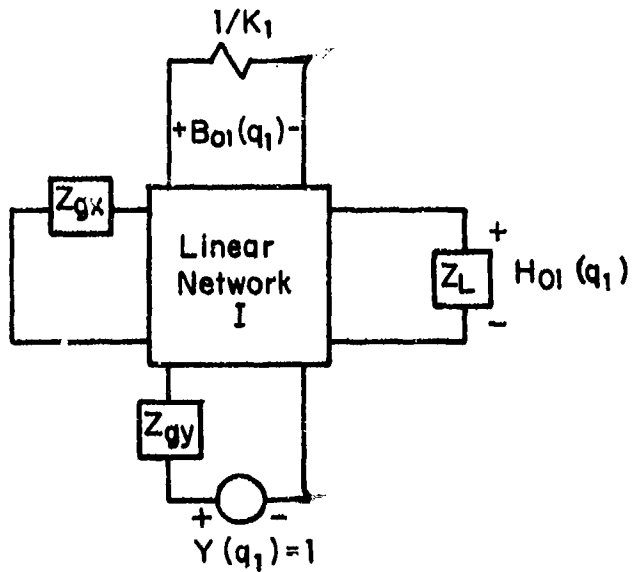
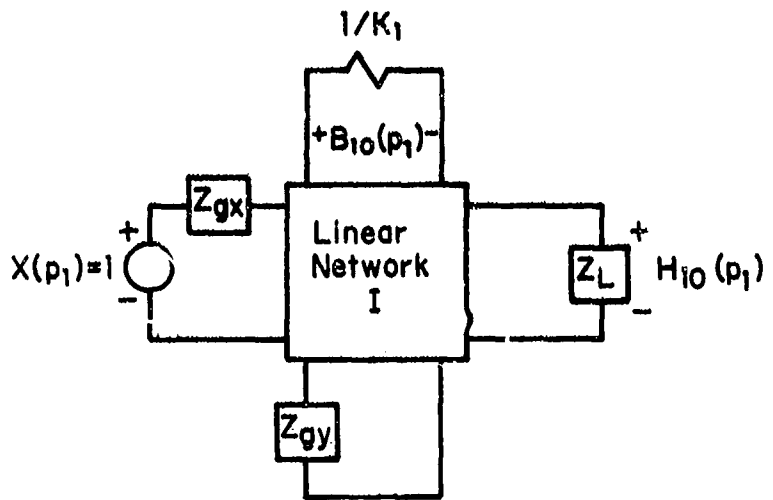


Fig. 2.14. Circuits Giving the First-Order Transfer Functions.

CHAPTER 3

CANONIC MODELS FOR NONLINEAR SYSTEMS

3.1 Introduction

The previous chapters have outlined the nonlinear transfer function approach to the analysis of nonlinear circuits and nonlinear systems. In the special case when the inputs to a time-invariant nonlinear system are discrete tones, the steady-state output also contains discrete tones but at many more frequencies since the nonlinearities generate additional frequency components. For a purely resistive nonlinear circuit each such discrete frequency component at the output would be weighted by a real coefficient characterizing the amplitude of the circuit response. We have shown that for more general circuits, the conventional power series expansion is inadequate. Complex coefficients are needed to properly characterize the amplitudes of the various frequency components. Furthermore, output components of the same order but for different interacting frequencies will have different amplitudes and phases.

In this chapter we are concerned with a situation in which the input to the nonlinear, time-invariant systems are not individual tones but narrowband signals centered about discrete tones. Realistically, this is the most common situation occurring in the communications environment since signals appearing at the input of the receiver are usually modulated on a carrier.

For input signals which are not discrete tones but occupy a certain bandwidth about the carrier frequency, a simple set of complex coefficients is not enough to characterize the behavior of the circuit. The frequency behavior of the circuit may not be

constant and may, in fact, vary across each band of interest. In its full generality the computation of the output involves a multivariate convolution of all the interacting inputs with the multivariate impulse response. Fortunately, in the case of modulated bandpass signals, an approach of intermediate complexity is possible. Broadly speaking, this approach entails representing the nonlinear response by a simple expansion with terms in the expansion added as required to model the input-output behavior of the system. The expansion itself can be interpreted as a specific physical structure, hence this structure is called a canonic model of the circuit (or system). The virtue of the canonic model is that the same basic structure can be used for all members of a class of systems and a class of inputs. The model parameters change from class member to class member. Thus only a few specific quantities must be determined for the actual system in order to properly label the structural elements of its model. These parameters can be either theoretically or experimentally determined. Thus, canonic modeling presented here is an attempt to systematically reduce the information required to characterize a nonlinear system. An important aspect of the canonic modeling is that the models can be refined by adding building blocks to improve the accuracy of the model or simplified by reducing the number of building blocks.

Many canonic models can be developed for linear and nonlinear systems. It should be expected that only a few of these will be of interest since the basis of any useful model is some simplifying constraint on the impulse response duration, bandwidth, or power of the input signals or the nonlinear system response. The use of a Volterra series with a small number of terms implies a power constrained model.

Among the possible models considered, two canonic models have been found particularly useful. These two canonic models, the frequency power series model and the tapped delay line model, will be developed and applied in this chapter. These models incorporate the essential requirements of most systems with mildly-excited nonlinearities. The frequency power series model makes use of the bandwidth constraint, while the tapped delay line model makes use of the impulse response constraint.

3.2 Nonlinear Response to a Sum of Narrowband Signals

In this section we extend the nonlinear transfer function approach by considering specifically the nonlinear ~~response~~ of systems whose inputs are a sum of narrowband zonal signals.

In the analysis of the response of a linear system to narrowband signals it is convenient to use the complex representation of signals. The signal is represented as a low-pass complex envelope modulating a "carrier" frequency. The carrier frequency is for all practical purposes arbitrarily selected within the band. The phase of the carrier tone is also arbitrary. Let the input to the system, $x(t)$, be the sum of K narrowband signals*

$$x(t) = \sum_1^K x_k(t). \quad (3.1)$$

In particular, one of these signals may be the desired signal, and the others may be the interference.

The narrowband representation of the k^{th} component of the input implies low-pass in-phase and in-quadrature components $a(t)$ and $b(t)$ modulating a carrier at the center frequency of the band which we denote by ω_k . Thus

*The list of key symbols used in this chapter can be found in Table 3-7 at the end of the chapter.

$$x_k(t) = a_k(t) \cos 2\pi v_k t - b_k(t) \sin 2\pi v_k t. \quad (3.2)$$

It is convenient to define $z_k(t)$, a slowly-varying complex envelope of $x_k(t)$, such that

$$z_k(t) = a_k(t) + j b_k(t). \quad (3.3)$$

With these definitions it follows that $x_k(t)$, which itself is real, is the real part of the product of the slowly varying $z_k(t)$ and an exponential varying at the carrier frequency

$$x_k(t) = \operatorname{Re} \left\{ z_k(t) e^{j2\pi v_k t} \right\}. \quad (3.4)$$

The real part of a complex variable is also one half of the sum of the variable and its complex conjugate so that

$$x_k(t) = \frac{1}{2} [z_k(t) e^{j2\pi v_k t} + z_k^*(t) e^{-j2\pi v_k t}]. \quad (3.5)$$

Correspondingly, the spectrum of $x_k(t)$ is given by the sum of the positive and negative spectral components centered on v_k and $-v_k$,

$$X_k(f) = \frac{1}{2} [Z_k(f - v_k) + Z_k^*(-f - v_k)], \quad (3.6)$$

where $Z_k(f)$ is the spectrum of $z_k(t)$

$$Z_k(f) = \int_{-\infty}^{\infty} z_k(t) e^{-j2\pi ft} dt. \quad (3.7)$$

Correspondingly

$$z_k(t) = \int_{-\infty}^{\infty} z_k^*(f) e^{+j2\pi ft} df. \quad (3.8)$$

Let $z_0(f) = 0$, and denote $z_k^*(t)$, $z_k^*(-f)$ and $-v_k$ by $z_{-k}(t)$, $z_{-k}(f)$ and v_{-k} , respectively. In this notation, the input spectrum becomes

$$x(f) = \frac{1}{2} \sum_{-K}^K z_k(f - v_k), \quad (3.9)$$

and the input itself can be written as:

$$x(t) = \frac{1}{2} \sum_{-K}^K z_k(t) e^{j2\pi v_k t}. \quad (3.10)$$

We recall from Chapter 1 that the output of the nonlinear system, $y(t)$, can be expanded into a Volterra series

$$y(t) = \sum_n y_n(t) \quad n=1, 2, \dots, \quad (3.11)$$

in which $y_n(t)$, called the component of order n , or n^{th} -order output for short, is given by an n -fold integral

$$y_n(t) = \int_{-\infty}^{\infty} \cdots \int_{-\infty}^{\infty} h_n(\tau_1, \dots, \tau_n) x(t-\tau_1) \cdots x(t-\tau_n) d\tau_1 \cdots d\tau_n, \quad (3.12)$$

where $h_n()$ is the n^{th} -order nonlinear impulse response. Equivalently, $y_n(t)$ is given by

$$y_n(t) = \int_{-\infty}^{\infty} \cdots \int_{-\infty}^{\infty} H_n(f_1, \dots, f_n) \prod_{i=1}^n X(f_i) e^{j2\pi f_i t} df_i, \quad (3.13)$$

where $H_n(\cdot)$ is the n^{th} -order nonlinear transfer function.

With this notation the product of the n input spectra appearing in Equation (3.13) becomes

$$\prod_{i=1}^n X(f_i) = \frac{1}{2^n} \prod_{i=1}^n \sum_{k=-K}^K z_k(f_i - v_k), \quad (3.14)$$

in which the right-hand side is, in fact, the n -fold sum of all the different terms of the form

$$z_{k_1}(f_1 - v_{k_1}) z_{k_2}(f_2 - v_{k_2}) \cdots z_{k_n}(f_n - v_{k_n}), \quad (3.15)$$

with each index k_i ranging from $-K$ to K . Substituting from Equations (3.14) and (3.15) into Eq. (3.13), we thus have for the n^{th} -order component of the output

$$y_n(t) = \frac{1}{2^n} \sum_{m_1=-K}^K \cdots \sum_{m_n=-K}^K p(t; v_{k_1}, \dots, v_{k_n}), \quad (3.16)$$

in which the summand is the multiple integral

$$p(t; v_{k_1}, \dots, v_{k_n}) = \int_{-\infty}^{\infty} \cdots \int_{-\infty}^{\infty} H_n(f_1, \dots, f_n) \prod_{i=1}^n z_{k_i}(f_i - v_{k_i}) \cdot e^{j2\pi f_i t} df_i, \quad (3.17)$$

with the n indices k_i in each such integral taking on any of the $2K$ non-zero integer values from $-K$ to K . The physical interpretation of the integral $p(t; v_{k_1}, \dots, v_{k_n})$ is as follows. In the steady state, a nonlinear system, which has a sum of narrowband zonal frequency components as its input, generates as its output

new narrowband zonal signals centered at all carrier intermodulation frequencies. The integral $P(t; v_{k_1}, \dots, v_{k_n})$, also denoted $P(t; y)$ for short, is then the waveform at $v_{k_1} + v_{k_2} + \dots + v_{k_n}$ attributable to the intermodulation of input components centered at v_{k_1}, \dots, v_{k_n} . The order of the output component is thus, in fact, the number of intermodulating input zones generating this component and can be also termed the order of intermodulation. To find the n^{th} -order output $y_n(t)$, all the intermodulation components of order n must be summed. The sum in Equation (3.16) thus consists of $(2K)^n$ such integrals. Any of these integrals that have the same set of indices $\{k_i\}$ have the same value regardless of the order of indices. Suppose that there are $M \leq n$ distinct v_{k_i} in the argument of $P(t; v_{k_1}, \dots, v_{k_n})$, and each such distinct v_{k_i} occurs m_i times ($m_i = 0, 1, \dots, n$) so that

$$\sum_{i=-K}^K m_i = n. \quad (3.18)$$

There are then

$$\frac{n!}{m_{-K}! m_{-K+1}! \dots m_K!} = (n; m_{-K}, \dots, m_K), \quad (3.19)$$

such terms. Equation (3.19) is the multinomial coefficient $(n; m_{-K}, \dots, m_K)$. Moreover, the different $P(t; y)$ in Equation (3.16) must occur as conjugate pairs in which each v_j is replaced by v_{-j} so that the sum of terms making up $y_n(t)$ is indeed real even if its individual components $P(t; y)$, in general, are not.

We observe that the n -fold integral in Equation (3.17) and its conjugate can be thought of as a waveform which contributes to the frequency component in the vicinity of the sum frequency

$$\nu = \sum_{i=1}^n \nu_{k_i}. \quad (3.20)$$

In general, the component of $y_n(t)$ located in the vicinity of the frequency

$$\nu = \sum_{k=-K}^K m_k \nu_k = \sum_{i=1}^n \nu_{k_i}, \quad (3.21)$$

due to input at a set of frequencies $\underline{\nu} = (\nu_{k_1}, \nu_{k_2}, \dots, \nu_{k_n})$, or any permutation within that set, is given by*

$$y_{n\underline{\nu}}(t) = \frac{(n; m_{-K}, \dots, m_K)}{2^n} [P(t; \underline{\nu}) + P^*(t; \underline{\nu})] \\ = \frac{(n; m_{-K}, \dots, m_K)}{2^{n-1}} \operatorname{Re}\{P(t; \underline{\nu})\}. \quad (3.22)$$

The order of permutation of the component frequencies of $\underline{\nu}$ is immaterial since it does not affect the sum frequency ν or the value of $P(t; \underline{\nu})$. Two sets $\underline{\nu}$ are then distinguishable in this context if they have different components. They are indistinguishable if they have identical components regardless of the order of components within the set. The number of distinguishable sets of n intermodulating zones each of which can be picked out of $2K$ input components is $\binom{2K+n-1}{n}$.

We note that terms of many orders and with different sets of component frequencies can contribute near a particular carrier frequency.

* An alternative notation is $y_n(t; \underline{\nu}) = y_{n\underline{\nu}}(t)$.

For example, consider the input consisting of two narrow-band components at ν_1 and ν_2 and the output generated by a non-linear system in the vicinity of frequency $\nu = 2\nu_1 + \nu_2$. Let the waveform corresponding to all the frequency components of the output in the vicinity of ν be denoted by $y_\nu(t)$. We then have

$$y_\nu(t) = y_{3\underline{a}}(t) + y_{5\underline{b}}(t) + y_{5\underline{c}}(t) + \dots, \quad (3.23)$$

in which $\nu = 2\nu_1 + \nu_2$, $\underline{a} = (\nu_1, \nu_1, \nu_2)$, $\underline{b} = (-\nu_1, \nu_1, \nu_1, \nu_1, \nu_2)$, $\underline{c} = (-\nu_2, \nu_1, \nu_1, \nu_2, \nu_2)$; as mentioned, the order of permutation of the component frequencies in the vectors \underline{a} , \underline{b} and \underline{c} is immaterial. The number of these permutations is taken into account by the value of multinomial coefficients $(n; m_{-K}, \dots, m_K)$ which is $(3; 2, 1) = 3$ for \underline{a} , $(5; 1, 3, 1) = 20$ for \underline{b} , $(5; 1, 2, 2) = 30$ for \underline{c} . Observe that $y_{5\underline{b}}(t)$ and $y_{5\underline{c}}(t)$ represent two different contributions of order five falling into the same frequency region. This indicates the importance of carrying the vector $\underline{\nu}$ in the index of the component of the output.

A convenient way to represent the input-output relation Eq. (3.16) follows when we express the n -th order output $y_n(t)$ and the component of $y_n(t)$ at frequency ν due to the interaction between a set of frequencies $\underline{\nu}$ in terms of their complex envelopes $q_n(t)$ and $q_{n\underline{\nu}}(t)$ respectively.* We have

$$y_n(t) = \operatorname{Re} \left\{ q_n(t) e^{j2\pi\nu t} \right\}, \quad (3.24)$$

$$y_{n\underline{\nu}}(t) = \operatorname{Re} \left\{ q_{n\underline{\nu}}(t) e^{j2\pi\nu t} \right\}. \quad (3.25)$$

A simple change of variables in Eq. (3.17) and substitution into Equation (3.22) yields

*An alternative notation is $q_n(t; \underline{\nu}) = q_{n\underline{\nu}}(t)$.

$$g_{n\underline{\nu}}(t) = \frac{n!}{2^{n-1} m_{-K}! \cdots m_K!} \int_{-\infty}^{\infty} \cdots \int H_n(\xi + \underline{\nu}) \prod_{i=1}^n z_{k_i}(\xi_i) e^{j2\pi\xi_i t} d\xi_i, \quad (3.26)$$

in which $\xi + \underline{\nu}$ denotes the vector $(\xi_1 + \nu_1, \dots, \xi_n + \nu_n)$. Suppose

$h_n(t)$, the n -th order nonlinear impulse response, also has a narrowband representation about the set of frequencies $\underline{\nu}$

$$h_n(t) = \operatorname{Re} \left\{ g_{n\underline{\nu}}(t) e^{j2\pi(\nu_1 t_1 + \cdots + \nu_n t_n)} \right\}. \quad (3.27)$$

The spectrum of the n -th order impulse response, $H_n(f)$, can be expressed as the sum of baseband spectra centered about $\underline{\nu}$ and $-\underline{\nu}$,

$$H_n(f) = \frac{1}{2} \left[G_{n\underline{\nu}}(f - \underline{\nu}) + G_{n\underline{\nu}}^*(-f - \underline{\nu}) \right], \quad (3.28)$$

in which $G_{n\underline{\nu}}(f)$ is the Fourier transform of $g_{n\underline{\nu}}(t)$, $t = (t_1, \dots, t_n)$ and $f = (f_1, \dots, f_n)$.

$$H_n(\xi + \underline{\nu}) = \frac{1}{2} \left[G_{n\underline{\nu}}(\xi) + G_{n\underline{\nu}}^*(-\xi - 2\underline{\nu}) \right]. \quad (3.29)$$

Suppose further that each $z_k(t)$ is bandlimited so that the baseband spectra of the input components do not overlap with the baseband spectrum of the n th-order impulse response centered at $-2\underline{\nu}$, so that

$$G_{n\underline{\nu}}^*(-\xi - 2\underline{\nu}) \prod_{i=1}^n z_{k_i}(f_i) = 0. \quad (3.30)$$

It then follows from Equation (3.26) that the Fourier transform pair for the complex envelope of the n^{th} -order component of the output referred to the set of carrier frequencies $\underline{\nu}$ is

$$q_{n\underline{\nu}}(t) = \frac{n!}{2^n m_{-K} \dots m_K!} \int_{-\infty}^{\infty} \int G_{n\underline{\nu}}(f) \prod_{i=1}^n z_{\kappa_i}(f_i) e^{j2\pi f_i t} df_i, \quad (3.31)$$

in which $\underline{\nu}$ is the set of frequencies which sum to ν as specified by Equation (3.21) and

$$Q_{n\underline{\nu}}(f) = \int_{-\infty}^{\infty} q_{n\underline{\nu}}(t) e^{-j2\pi f_i t} dt. \quad (3.32)$$

These last two equations relate the complex envelopes of input and output signals and are central to the discussion that follows. In addition, we have the relations between the n^{th} -order envelope components and the composite output envelope about ν

$$q_{\nu}(t) = \sum_{n=1}^{\infty} \sum_{\underline{\nu}} q_{n\underline{\nu}}(t), \quad (3.33)$$

$$Q_{\nu}(f) = \sum_{n=1}^{\infty} \sum_{\underline{\nu}} Q_{n\underline{\nu}}(f). \quad (3.34)$$

We are using the notation of $\underline{\nu}$ under the summation to denote that for each n , all the sets $\underline{\nu}$, that differ by other than permutation, are included in the sum.

3.3 Frequency Power Series Canonic Model

In linear analysis of communication channels and receivers, efficiencies of characterization can be achieved through the use of certain "canonic" models. A canonic model originates with approximations to the full mathematical representation of the input-output relationships. These approximations are then interpreted in terms of suitable signal processing structures which can serve as a canonic model for the class of actual systems described by the model. Thus the canonic model will, in general, have a different structure than the actual system but, when assigned proper parameters, will mathematically perform like the actual system. The more restricted the class of systems being modeled, and also the class of input signals, the simpler the canonic model. Examples of canonic models of time-varying linear systems can be found in the work of Zadeh [1950], Kailath [1959], Gersho [1963] and Bello [1963].

In this section we generalize the linear canonic models based on the Taylor series expansion of the linear transfer function of a system about its operating frequency to the multivariate Taylor expansion appropriate to the nonlinear systems. We call this canonic model the Frequency Power Series Canonic Model.

The simplest case occurs when the nonlinear transfer function $H_n(f_1, \dots, f_n)$ can be treated as a constant about the set of frequencies \underline{v} . In such a case the Fourier transforms in Equation (3.26) can all be carried out. Substituting $f_i = \xi_i + v_i$ in the integrand of Equation (3.26) results in

$$q_{n\underline{v}}(t) = \frac{n!}{2^{n-1} m_{-K}! \dots m_K!} \int_{-\infty}^{\infty} \int H_n(\underline{f}) \prod_{i=1}^n z_{k_i}(f_i - v_i) e^{j2\pi(f_i - v_i)t} df_i. \quad (3.35)$$

When $H_n(f)$ is assumed constant and equal to its value at the set of center frequencies, $\underline{\nu}$, we have

$$H_n(f) = H_n(\underline{\nu}). \quad (3.36)$$

For our purposes this relation needs to hold true only over the region of frequencies for which the shifted spectra of the input components, $Z_{k_i}(f_i - \nu_i)$, $i=1, \dots, n$, are non-zero. Recognizing that $H_n(\underline{\nu})$ is a constant and that the n -fold integral of a product of separable factors is the product of n individual integrals, we get from the last two equations that the complex envelope of the output component $y_{n\underline{\nu}}(t)$ is then

$$q_{n\underline{\nu}}(t) = \frac{n!}{2^{n-1} m_{-K}! \dots m_K!} H_n(\underline{\nu}) \prod_{i=1}^n \int_{-\infty}^{\infty} Z_{k_i}(f_i - \nu_i) e^{j2\pi(f_i - \nu_i)t} df_i. \quad (3.37)$$

Since the region of integration is from $-\infty$ to ∞ , a linear change of variables back to $f_i - \nu_i = \xi_i$ conveniently allows each Fourier transform to be carried out, or

$$\int_{-\infty}^{\infty} Z_{k_i}(f_i - \nu_i) e^{j2\pi(f_i - \nu_i)t} df_i = z_{k_i}(t), \quad (3.38)$$

so that the product of these n integrals is simply the product of n out of the $2K$ input components with those components for which ν_k appears m_k times in the argument of $H_n(\underline{\nu})$ also appearing m_k times, i.e.,

$$\prod_{i=1}^n z_{k_i}(t) = \prod_{k=-K}^K z_k^{m_k}(t). \quad (3.39)$$

We conclude that the complex envelope of $y_{n\underline{v}}(t)$ is

$$q_{n\underline{v}}(t) = \frac{n!}{2^{n-1} m_{-K}! \cdots m_K!} H_n(\underline{v}) \prod_{k=-K}^K z_k^{m_k}(t), \quad (3.40)$$

where $\underline{v} = v_{k_1}, v_{k_2}, \dots, v_{k_n}$ and $v = v_{k_1} + \dots + v_{k_n}$. By virtue of Equation (3.24) it follows that $y_{n\underline{v}}(t)$ itself is given by

$$y_{n\underline{v}}(t) = \frac{n!}{2^{n-1} m_{-K}! \cdots m_K!} \operatorname{Re} \left\{ H_n(\underline{v}) \prod_{k=-K}^K z_k^{m_k}(t) e^{j2\pi m_k v_k t} \right\}. \quad (3.41)$$

If $G_{n\underline{v}}(f)$, the baseband version of $H_n(\underline{v})$, is bandlimited so that the tail of the negative part of the spectrum does not extend into the frequency region about $2v$, then it follows from Equation (3.28) that

$$H_n(\underline{v}) = \frac{1}{2} G_{n\underline{v}}(\underline{0}), \quad (3.42)$$

in which $\underline{0} = (0, 0, \dots, 0)$, so that the complex envelope of the output can then be also given in terms of the baseband n^{th} -order response $G_{n\underline{v}}(\underline{0})$,

$$q_{n\underline{v}}(t) = \frac{n!}{2^{n-1} m_{-K}! \cdots m_K!} G_{n\underline{v}}(\underline{0}) \prod_{k=-K}^K z_k^{m_k}(t). \quad (3.43)$$

This equation can also be derived more directly from Equation (3.31) by assuming that $G_{n\underline{v}}(f) = G_{n\underline{v}}(\underline{0})$. The $G_{n\underline{v}}(\underline{0})$, similar to the $H_n(\underline{v})$, are complex coefficients denoting the spectral density of the complex envelope at one set of frequencies.

It should be noted that the index ν on the spectrum of the complex envelope is important as the indication of the set of frequencies to which the envelope is referred. The coefficient, $G_{ny}(0)$, has the argument 0 and would be ambiguous without this subscript.

A simple example that effectively illustrates the application of Eq.(3.28) is to the case of a signal $s_1(t)$ at center frequency ν_1 , and two interfering signals $i_2(t)$ and $i_3(t)$ at center frequencies ν_2 and ν_3 , respectively; i.e.,

$$\begin{aligned} x_1(t) &= \operatorname{Re} \left\{ s_1(t) e^{j2\pi\nu_1 t} \right\} \\ x_2(t) &= \operatorname{Re} \left\{ i_2(t) e^{j2\pi\nu_2 t} \right\} \\ x_3(t) &= \operatorname{Re} \left\{ i_3(t) e^{j2\pi\nu_3 t} \right\}. \end{aligned} \quad (3.44)$$

Some of the more important components specified by Eq. (3.28) for this example are tabulated in Table 3-1. The first three columns of this table give the name of the component as used in interference studies, its frequency region and its complex envelope. Note that the coefficients $H_n(\nu_1, \dots, \nu_n)$ in front of each product are generally complex and are different for a different set of interacting frequencies. This can be contrasted to the conventional approach to a three-tone input in which one would have modeled the nonlinear response by a power series with real coefficients of the same value for components of the output of the same order:

$$y(t) = \sum_{n=1}^{\infty} a_n \left[\operatorname{Re} \left\{ A_1 e^{j2\pi\nu_1 t} + A_2 e^{j2\pi\nu_2 t} + A_3 e^{j2\pi\nu_3 t} \right\} \right]^n. \quad (3.45)$$

TABLE 3.1
SELECTED OUTPUT COMPONENTS FOR A MILDELY NONLINEAR SYSTEM HAVING THREE NARROWBAND INPUTS ($K=3$)

Input Components		Frequency Zone	Volterra Analysis	Conventional Analysis
Desired	v_1		$s_1 = s_1(t)$	A_1
Undesired	v_2		$i_2 = i_2(t)$	A_2
Undesired	v_3		$i_3 = i_3(t)$	A_3
Output Signal Component *		Frequency Zone	Complex Output Envelope $q_{xy}(t)$	Output Power Series Terms
<u>First-Order (n=1)</u>				
Desired	v_1		$H_1(v_1)s_1$	a_1A_1
Adjacent or Co-Channel	v_2		$H_1(v_2)i_2$	a_1A_2
Adjacent or Co-Channel	v_3		$H_1(v_3)i_3$	a_1A_3
<u>Second-Order (n=2)</u>				
Intermodulation	$v_2 + v_3$		$H_2(v_2, v_3)i_2i_3$	a_2A_3
Intermodulation	$v_2 - v_3$		$H_2(v_2, -v_3)i_2i_3$	a_2A_3
<u>Third-Order (n=3)</u>				
Gain "Compression" - Desired Signal	v_1		$3/4 H_3(v_1, v_1, -v_1)s_1^{st}$	$3/4 a_3A_1^2$
Gain "Compression" - Undesired Signal	v_2		$3/4 H_3(v_2, v_2, -v_2)i_2^{st}$	$3/4 a_3A_2^2$
Gain "Compression" - Undesired Signal	v_3		$3/4 H_3(v_3, v_3, -v_3)i_3^{st}$	$3/4 a_3A_3^2$
Cross-Modulation and Desensitization	v_1		$3/2 H_3(v_1, v_2, -v_2)i_2i_3^{st}$	$3/2 a_3A_2A_3$
Cross-Modulation and Desensitization	v_1		$3/2 H_3(v_1, v_3, -v_3)i_2i_3^{st}$	$3/2 a_3A_2A_1$
Intermodulation	$2v_2 - v_3$		$3/4 H_3(v_2, v_2, -v_3)i_2i_3^{st}$	$3/4 a_3A_2^2$
Intermodulation	$2v_3 - v_2$		$3/4 H_3(v_2, v_3, v_3)i_2i_3^{st}$	$3/4 a_3A_2^2$
Intermodulation	$v_1 + v_2 - v_3$		$3/2 H_3(v_1, v_2, -v_3)i_2i_3s_1$	$3/2 a_3A_2A_1$

* Only a few representative components are listed in this table for purposes of illustration.
 In a complete listing of all the distinct permutations of positive and negative frequencies there would be $\binom{6}{1} = 6$ terms of order one, $\binom{7}{2} = 21$ terms of order two and $\binom{8}{3} = 56$ terms of order three.

The amplitudes of the three tones are A_1 , A_2 , and A_3 , and the coefficient a_3 is typically opposite in sign to a_1 , whence the term "compression". The last column in Table 3-1 shows the amplitudes of the various frequency components in this series by way of comparison to the just discussed simple case of frequency power series with a constant nonlinear function.

If the variation of $H_n(f_1, f_2, \dots, f_n)$ from a constant value in the regions around v_1, v_2, \dots, v_n is primarily linear, then H_n can be expanded in a Taylor series containing only the first power of each frequency, namely

$$H_n(\underline{f}) = H_n(\underline{v}) + (f_1 - v_1) \left. \frac{\partial H_n(\underline{f})}{\partial f_1} \right|_{\underline{f}=\underline{v}} + (f_2 - v_2) \left. \frac{\partial H_n(\underline{f})}{\partial f_2} \right|_{\underline{f}=\underline{v}} + \dots + (f_n - v_n) \left. \frac{\partial H_n(\underline{f})}{\partial f_n} \right|_{\underline{f}=\underline{v}} . \quad (3.46)$$

In Equation (3.46) we have again used the vector notation \underline{f} and \underline{v} for convenience, where

$$\underline{f} = (f_1, f_2, \dots, f_n),$$

$$\underline{v} = (v_1, v_2, \dots, v_n),$$

and a vertical bar signifies that the function is evaluated at one point. Figure 3.1 shows a first-order nonlinear transfer function $H_1(f)$, and two spectral regions of center frequencies v_1 and v_2 , and bandwidths B_1 and B_2 . The tangents drawn to $H_1(f)$ at v_1 and v_2 represent the two-term (i.e. constant plus

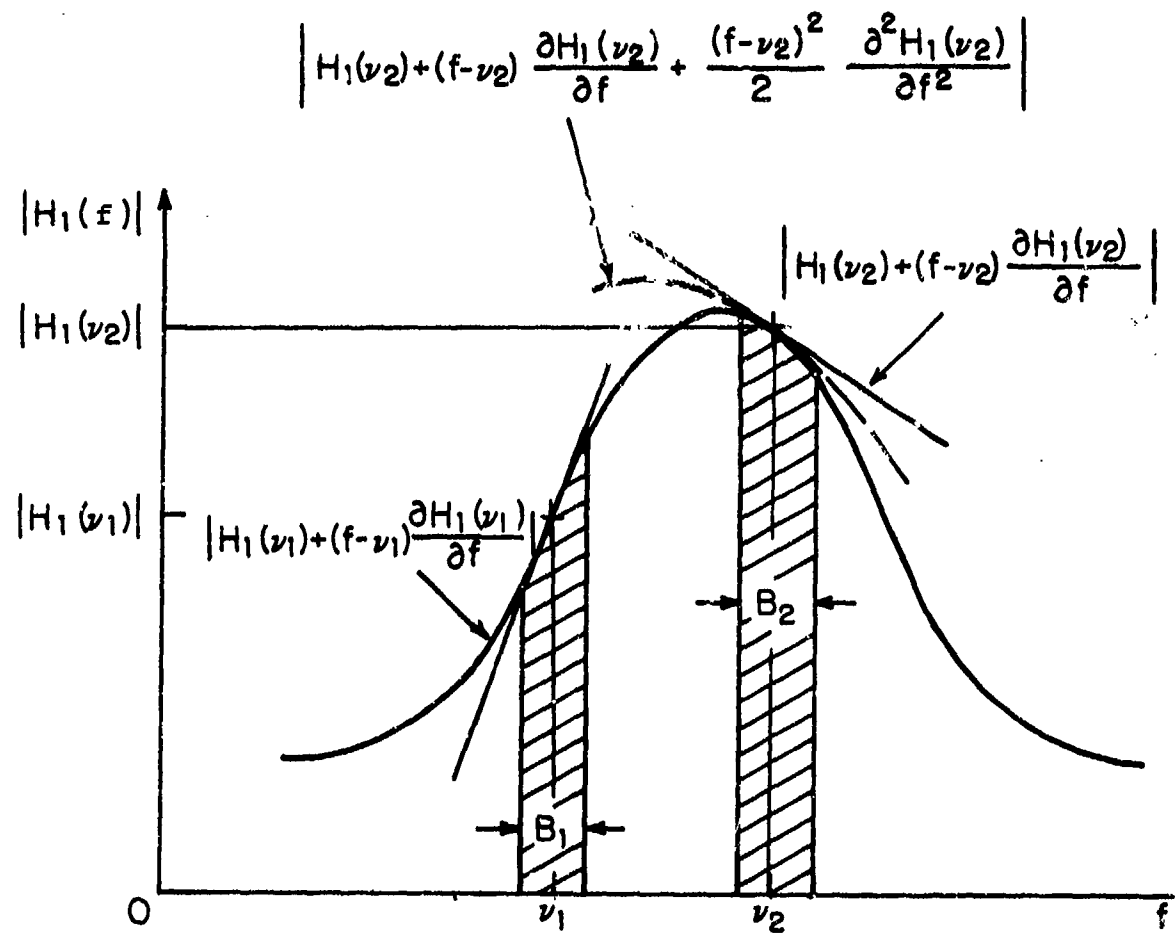


Fig. 3.1. Frequency Power Series Approximation of $H_1(f)$.

one derivative) frequency power series expansion of $H_1(f)$ at these two frequencies. It is seen that the curvature of $H_1(f)$ is such that the two-term representation is better at ν_1 than at ν_2 . A quadratic, or three-term, expansion might be required to adequately represent $H_1(f)$ at ν_2 when the signal bandwidth is B_2 .

Similarly, $G_{ny}(f)$ can be expanded in a Taylor series about 0

$$G_{ny}(f) = G_{ny}(0) + \sum_{i=1}^n f_i \left. \frac{\partial G_{ny}(f)}{\partial f_i} \right|_{f=0} + \dots \quad (3.47)$$

More generally, the p -th order term in the multivariate Taylor series expansion of $G_{ny}(f)$ can be shown in the abbreviated form

$$\frac{1}{p!} \left[f_1 \frac{\partial}{\partial f_1} + f_2 \frac{\partial}{\partial f_2} + \dots + f_n \frac{\partial}{\partial f_n} \right]^p G_{ny}(f) \Big|_{f=0}, \quad (3.48)$$

in which the factor in the square bracket operates on $G_{ny}(f)$. When these operations are carried out individual terms are of the form

$$\frac{1}{p_1! p_2! \dots p_n!} f_1^{p_1} f_2^{p_2} \dots f_n^{p_n} \left. \frac{\partial^p G_{ny}(f_1, f_2, \dots, f_n)}{\partial f_1^{p_1} \partial f_2^{p_2} \dots \partial f_n^{p_n}} \right|_{f=0}, \quad (3.49)$$

in which p_i ranges over all integers from zero to p , and

$$p_1 + p_2 + \dots + p_n = p. \quad (3.50)$$

In general, the full multivariate Taylor series expansion of $G_{ny}(\underline{f})$ is then the multiple sum

$$G_{ny}(\underline{f}) = \sum_{p=0}^{\infty} \sum_{\underline{p}} \frac{1}{p_1! p_2! \dots p_n!} f_1^{p_1} f_2^{p_2} \dots f_n^{p_n} \left. \frac{\partial^p G_{ny}(f_1, \dots, f_n)}{\partial f_1^{p_1} \partial f_2^{p_2} \dots \partial f_n^{p_n}} \right|_{\underline{f}=0}. \quad (3.51)$$

in which \underline{p} denotes the summation over all the permutations of p_i satisfying Equation (3.50). The total number of such permutation is the number of ways in which p objects can be allocated into n cells and is $\binom{n+p-1}{n}$. Thus there are three linear terms and four quadratic terms in the expansion of the third-order nonlinear response ($p=2$, $n=3$).

If we substitute for $G_{ny}(\underline{f})$ in Equation (3.31) its multivariate Taylor series expansion specified above, the integral in Eq. (3.31) becomes

$$q_{ny}(t) = \sum_{p=0}^{\infty} \sum_{\underline{p}} \frac{(m; m_{-K}, \dots, m_K)}{2^n p_1! \dots p_n!} \int_{-\infty}^{\infty} \int \dots \int \left. \frac{\partial^p G_{ny}(\underline{f})}{\partial f_1^{p_1} \partial f_2^{p_2} \dots \partial f_n^{p_n}} \right|_{\underline{f}=0} \cdot \prod_{i=1}^n f_i^{p_i} z_{k_i}(f_i) e^{j2\pi f_i t} df_i. \quad (3.52)$$

Note that the first factor in the integrand is now a constant so that the integrand becomes separable, i.e., the multiple integral of Equation (3.34) becomes now a product of individual integrals because each factor of Equation (3.52) depends only on f_i .

Taking time derivatives of both sides of the Fourier transform relationship Equation (3.49), we observe the relationship

$$(2\pi j)^p \int_{-\infty}^{\infty} f^p Z(f) e^{j2\pi ft} df = \frac{d^p z(t)}{dt^p} = z^{(p)}(t), \quad (3.53)$$

where $z^{(p)}(t)$ defines an abbreviated notation for the p^{th} derivative of $z(t)$. Thus each of the n individual integrals arising in Equation (3.52), after the constant in the integrand is recognized, is proportional to the p^{th} derivative of the waveform $z_i(t)$ denoted by $z_i^{(p)}(t)$. With this notation, the complex envelope of the n -order output component referred to \underline{v} has the expansion

$$a_{n\underline{v}}(t) = \sum_{p=0}^{\infty} \sum_{\substack{(n; m_1, \dots, m_K) \\ p_1! \cdots p_n!}} \frac{\delta^p G_{n\underline{v}}(\underline{f})}{\delta^{p_1} f_1 \delta^{p_2} f_2 \cdots \delta^{p_n} f_n} \Bigg|_{\underline{f}=0} \prod_{i=1}^n \frac{z_i^{(p_i)}(t)}{(2\pi j)^{p_i}}, \quad (3.54)$$

in which the sum is over all the p_1, \dots, p_n whose sum is p and each p_i ranges over all the integers from 0 to p . A great simplification has occurred relative to Eq. (3.31) in that instead of a multiple integration, we now can compute the complex envelope of the n^{th} -order output due to the intermodulation of the input components at \underline{v} as a sum of weighted products of various derivatives of these input components. The weights are time-independent coefficients evaluated at the center frequency of the baseband envelope $f_1 = 0, \dots, f_n = 0$.

This kind of an expansion structures the system as a series of differentiators (to form $z^{(p)}(t)$), and multipliers (to apply the proper complex coefficients) for each product in the sum.

The utility of the frequency power series expansion is predicated on the convergence of the terms in p , so that just the first few terms of the expansion may suffice in generating an adequate approximation. As an example consider the frequency power series canonic model structure for a two-tone input ($K=2$), third order output ($n=3$) and a two-term nonlinear response ($p=0,1$) using the expansion of $H_n(\underline{v})$ about $\underline{v} = (v_1, v_1, v_2)$. In the interest of further simplicity denote the first derivative $dz(t)/dt = z^{(1)}(t)$ by $\dot{z}(t)$.

For this example, if a linear dependence in each input frequency region approximates $H_3(f)$ sufficiently well, the third-order complex envelope of the output component due to the intermodulation of input components at \underline{v} is given by

$$q_{3\underline{v}}(t) = \frac{3}{4} \left[H_3(v_1, v_1, v_2) z_1^2(t) z_2(t) + \frac{2}{2\pi j} \frac{\partial H_3(v_1, v_1, v_2)}{\partial f_1} z_1(t) \dot{z}_1(t) z_2(t) + \frac{1}{2\pi j} \frac{\partial H_3(v_1, v_1, v_2)}{\partial f_3} z_1^2(t) \dot{z}_2(t) \right], \quad (3.55)$$

where $\partial H_3(v_1, v_2, v_3)/\partial f_i, i=1,2,3$, denotes that the derivative of $H_3(f_1, f_2, f_3)$ is evaluated at $f_1=v_1$, $f_2=v_1$, and $f_3=v_2$, and from Eq. (3.42) $H_n(\underline{f})=G_{n\underline{v}}(\underline{f})/2$.

Figure 3.2 shows, in block diagram form, the canonic model of Equation (3.55). The signal flow is from left to right. $z_1(t)$ is differentiated to form \dot{z}_1 . z_1^2 is multiplied by z_2 and their

Complex envelope
of the n-th order
output component
due to intermodu-
lating input zones
at ν

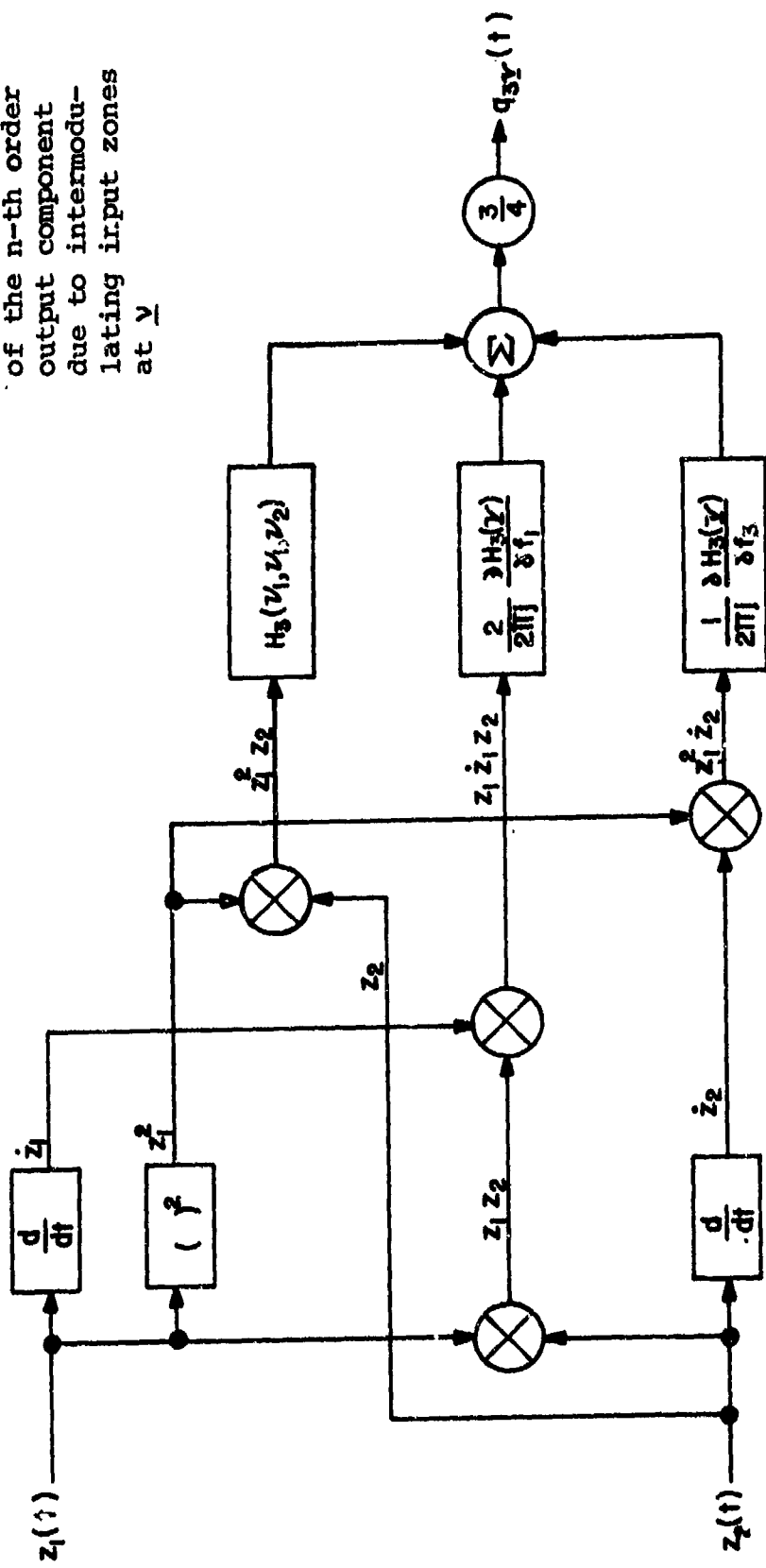


Fig. 3.2. Example of Frequency Power Series Canonic Model
 $n=3$, $k_1=2$, $k_2=1$, $p=0, 1$.

product is multiplied by a complex gain $H_3(v_1, v_1, v_2)$, while $\dot{z}_1 z_1 z_2$ and $z_1^2 \dot{z}_2$ are formed and multiplied by a complex gain $(1/2\pi j) 2 \delta H_3(y)/\delta f_1$ and $(1/2\pi j) \delta H_3(y) \delta f_3$, respectively. The three products are summed, multiplied by 3/4, shifted to the intermodulation product frequency $2v_1 + v_2$, and the real part taken to form $y_{3y}(t)$. The canonic model operations are straightforward numerical processes, as contrasted to the triple integration required if the full integral of Eq. (3.31) were to be carried out. An examination of Equation (3.55) illustrates the addition of perturbation terms to the first term which is a simple intermodulation product with a complex coefficient. These perturbation terms correct the first term to allow for the fact that the spectrum of the multivariate impulse response is not constant over the bandwidths of $z_1(t)$ and $z_2(t)$. The essence of the canonic model representation is that for each y we now need only a set of coefficients to represent effects of a particular nonlinear circuit; the structure of the circuit itself need not be known.

3.4 Tapped Delay Line Canonic Model

The nonlinear transfer function may change too much within the frequency region corresponding to the bandwidths of the input signals for the first few terms of the Taylor series expansion to provide a useful approximation. Under these conditions, we may find recourse to another canonic model based on the representation of the nonlinear impulse response of order n as an expansion using multivariate sampling functions at suitably-spaced periodic intervals. This model is called the Tapped Delay Line Canonic Model because the signal processing structure which relates the input components to the output signal, is a tapped delay line.

If a low-pass complex waveform $g(t)$ is band-limited to the frequency region $|f| \leq B/2$, we denote the resulting band-limited waveform by $\tilde{g}(t)$. The band-limited waveform can be expanded by the sampling theorem as:

$$\tilde{g}(t) = \sum_{-\infty}^{\infty} \tilde{g}(rT) \frac{\sin \pi B(t-rT)}{\pi B(t-rT)}, \quad (3.56)$$

in which $\tilde{g}(rT)$ is the value of $\tilde{g}(t)$ at $t=rT$, commonly known as a sample value, and $T = 1/B$. We denote the interpolation function in Eq. (3.56) by $\text{sinc } B(t-rT)$; that is

$$\text{sinc } y = (\sin \pi y)/\pi y. \quad (3.57)$$

The Fourier transform of $\text{sinc } Bt$ is $(1/B) \text{ Rect}(f/B)$ in which

$$\text{Rect } x = \begin{cases} 1 & |x| < 1/2 \\ 0 & |x| \geq 1/2. \end{cases} \quad (3.58)$$

We shall generally use a tilde (~) to denote a bandlimited version of a function, so that

$$\tilde{G}_{ny}(f) = G_{ny}(f) \prod_{i=1}^n \text{Rect}(f_i/B_i). \quad (3.59)$$

Band-limited functions still follow the Fourier transform relation,

$$\tilde{g}_{ny}(t) = \int_{-\infty}^{\infty} \int_{-\infty}^{\infty} \tilde{G}_{ny}(f) e^{-j2\pi(f_1 t_1 + \dots + f_n t_n)} df. \quad (3.60)$$

Similarly to Eq. (3.50), for a function of multiple variables, limited in bandwidth along each frequency axis, we can use the n-dimensional sampling theorem of Pederson and Middleton (1962).

$$\tilde{g}_{ny}(t_1, \dots, t_n) = \sum_{r_1} \dots \sum_{r_n} \tilde{g}_{ny}(r_1 T_1, \dots, r_n T_n) \prod_{i=1}^n \text{sinc}\left[B_i(t_i - r_i T_i)\right],$$

(3.61)

in which each r_i assumes all integer values and the sampling interval T_i is the reciprocal of the bandwidth B_i in the i -th coordinate, i.e., $T_i = 1/B_i$. The coefficient $\tilde{g}_{ny}(r_1 T_1, \dots, r_n T_n)$ is a sample value of the n -dimensional envelope of the n -th order impulse response at $t_1 = r_1 T_1$, $t_2 = r_2 T_2$ etc. The virtue of expanding $\tilde{g}_{ny}(t)$ in this fashion is that in any n -fold integration in which it appears as a kernel, the kernel g becomes separable and the n integrations can be carried out individually.

Taking the multidimensional Fourier transform of both sides of Eq. (3.61), we now get

$$\tilde{G}_{ny}(\underline{f}) = \sum_{\underline{r}} \tilde{g}_{ny}(\underline{rT}) \prod_{i=1}^n \frac{1}{B_i} (\text{Rect} \frac{f_i}{B_i}) e^{j2\pi r_i T_i f_i},$$

(3.62)

in which \underline{f} and \underline{rT} denote (f_1, \dots, f_n) and $(r_1 T_1, \dots, r_n T_n)$ respectively and the subscript \underline{r} under the summation denotes the multiple sum over r_1, r_2, \dots, r_n each ranging over all integers.

Recall that the narrow-band representation of $h_n(\underline{x})$ defined by Eq. (3.27) implies

$$H_n(\underline{f}) = \frac{1}{2} \left[G_{ny}(\underline{f-y}) + G_{ny}^*(\underline{-f-y}) \right].$$

(3.63)

Thus the integral $P(t, \underline{v})$ of Eq. (3.17) which appears in the expression relating the n -th order output $y_n(t)$ to an input $x(t)$, consisting of the sum of narrowband signals with complex envelopes

$z_{m_i}(t)$, is

$$P(t, \underline{v}) = \frac{1}{2} \int_{-\infty}^{\infty} \cdots \int \left[G_{n\underline{v}}(\underline{f}-\underline{v}) + G_{n\underline{v}}^*(-\underline{f}-\underline{v}) \right] \prod_{i=1}^n z_{k_i}(\underline{f}_i - \underline{v}_{k_i}) e^{j2\pi f_i t} df_i. \quad (3.64)$$

or

$$\begin{aligned} P(t, \underline{v}) &= \frac{1}{2} \int_{-\infty}^{\infty} \cdots \int G_{n\underline{v}}(\underline{\xi}) \prod_{i=1}^n z_{k_i}(\xi_i) e^{j2\pi(\xi_i + v_{k_i})t} d\xi_i \\ &\quad + \frac{1}{2} \int_{-\infty}^{\infty} \cdots \int G_{n\underline{v}}^*(\underline{\xi}) \prod_{i=1}^n z_{k_i}(-\xi_i - 2v_{k_i}) e^{j2\pi(-\xi_i - 2v_{k_i})t} d\xi_i. \end{aligned} \quad (3.65)$$

Assume that each input signal $z_i(t)$ is also bandlimited to a bandwidth no larger than $B_i \ll v_i$, so that

$$G_{n\underline{v}}(\underline{\xi}) \prod_{i=1}^n z_{k_i}(\xi_i) = \tilde{G}_{n\underline{v}}(\underline{\xi}) \prod_{i=1}^n z_{k_i}(\xi_i), \quad (3.66)$$

and

$$G_{n\underline{v}}^*(\underline{\xi}) \prod_{i=1}^n z_{k_i}(-\xi_i - 2v_{k_i}) = 0. \quad (3.67)$$

Substituting from Eq. (3.62) into (3.65) and taking into account the last two equalities, we get

$$p(t; \underline{v}) = \frac{1}{2} \sum_{\underline{r}} \tilde{g}_{n\underline{v}}(\underline{rT}) e^{j2\pi \sum_i v_i t} \prod_{i=1}^n \frac{1}{B_i} \int z_{k_i}(\xi_i) e^{j2\pi \xi_i (t - r_i T_i)} d\xi_i. \quad (3.68)$$

Executing the multidimensional Fourier transform,

$$p(t; \underline{v}) = \frac{1}{2} \sum_{\underline{r}} \tilde{g}_{n\underline{v}}(\underline{rT}) e^{j2\pi \sum_i v_i t} \prod_{i=1}^n \frac{1}{B_i} z_{k_i}(t - r_i T_i). \quad (3.69)$$

Finally, substituting for $p(t; \underline{v})$ in Eq. (3.16)

$$y_n(t) = \frac{1}{2^{n+1}} \sum_{k_1=-K}^K \dots \sum_{k_n=-K}^K \left[\sum_{\underline{r}} \tilde{g}_{n\underline{v}}(\underline{rT}) \prod_{i=1}^n \frac{1}{B_i} z_{k_i}(t - r_i T_i) \right] e^{j2\pi \sum_i v_i k_i t}. \quad (3.70)$$

The right-hand side of Eq. (3.70) contains conjugate component pairs in k_i which makes it a real function of time as is $y(t)$. For a specific frequency set \underline{v} such that $v = -m_{-K} v_{-K} + \dots + m_K v_K$ from Eq. (3.25), the complex envelope of the output of order n referred to \underline{v} becomes

$$q_{n\underline{v}}(t) = \frac{n!}{2^n m_{-K}! \dots m_K!} \sum_{\underline{r}} \frac{\tilde{g}_{n\underline{v}}(\underline{rT})}{B_1 \dots B_n} \prod_{k=-K}^K z_k(t - r_k T_k). \quad (3.71)$$

Again a great simplification has resulted relative to Eq. (3.31) in that a multiple convolution is replaced by the sum of weighted products of the intermodulating input components with various time displacements relative to one another. The last expression serves as the basis for the tapped delay line canonic model. In this model the n -th order response is obtained by passing each complex envelope of the narrowband components of the input through a tapped delay line with taps uniformly spaced at $1/B_i$ intervals, where B_i is the bandwidth of the i -th input component.

All the various products of such delayed envelopes are formed and weighted by a suitable complex coefficient and then added to form the complex envelope of the output of order n for the frequency set $\underline{\nu}$. Clearly, the utility of such a model depends on the convergence of the multiple sum in Eq.(3.71) so that only a finite number of taps need be used. In other words, the coefficient $\tilde{g}_{n\underline{\nu}}(r_1 T_1, \dots, r_n T_n)$ should decrease rapidly for all r_i as the absolute value of r_i increases since the requirement for long delays would render the model impractical. These coefficients are frequency independent and are evaluated at discrete sample points only.

The simplest example that illustrates the tapped delay line canonic model is, of course, the case in which the n^{th} order nonlinear impulse response at a set of frequencies $\underline{\nu}$ can be effectively modeled by a single tap only. This occurs when the system is not dispersive and its frequency response is a constant.

In this case, the complex envelope of the n^{th} order output in the frequency zone centered on $\underline{\nu}$, generated by the input excitations centered on $\nu_1, \nu_2, \dots, \nu_n$, is given by

$$q_{n\underline{\nu}}(t) = \frac{n!}{2^{n-m_{-K}} \cdots m_K!} \frac{\tilde{g}_{n\underline{\nu}}(\underline{\nu})}{B_1 B_2 \cdots B_n} \prod_{k=-K}^K z_k^{m_k}(t - r_k T_k). \quad (3.72)$$

Now, if the envelope of the n^{th} order nonlinear impulse response is constant and bandlimited in each dimension, then the multidimensional Fourier transform relation is found to yield

$$\begin{aligned} \tilde{g}_{n\underline{\nu}}(0) &= \int \cdots \int \tilde{G}_{n\underline{\nu}}(\underline{f}) d\underline{f} = B_1 B_2 \cdots B_n G_{n\underline{\nu}}(0) \\ &= B_1 B_2 \cdots B_n 2H_n(\underline{\nu}). \end{aligned} \quad (3.73)$$

so that $G_{ny}(0) = \tilde{g}_{ny}(0)/B_1 \dots B_n$. Comparing Equation (3.73) for the n -th order output from a single tap model to the Equations (3.40) and (3.43) for a constant transfer function model, it follows that a single tap delay line model is identical to the one-term frequency power series model. Both are applicable when the nonlinear response is not frequency dependent over the respective bandwidths of the input signals. In general, however, each delay line in the model may have more than one tap. We denote the number of taps for z_k by N_k .

Another example, a third-order two-tap canonic model for $\underline{v} = (v_1, v_1, v_2)$; $v = 2v_1 + v_2$, is illustrated in Fig. 3.3. We assume equal bandwidths $B_1 = B_2$ and taps at $T_1 = T_2 = T$. The complex envelope of the third order output for this case is explicitly

$$\begin{aligned}
& \tilde{g}_{3\underline{v}}(t) = \\
& \frac{3T^3}{8} \sum_{r_1=0}^1 \sum_{r_2=0}^1 \sum_{r_3=0}^1 \tilde{g}_{3\underline{v}}(r_1T, r_2T, r_3T) z_1(t-r_1T) z_1(t-r_2T) z_2(t-r_3T) \\
& = \frac{3T^3}{8} \left[\tilde{g}_{3\underline{v}}(0,0,0) z_1^2(t) z_2(t) + 2\tilde{g}_{3\underline{v}}(T,0,0) z_1(t-T) z_1(t) z_2(t) \right. \\
& \quad + \tilde{g}_{3\underline{v}}(T,T,0) z_1^2(t-T) z_2(t) + \tilde{g}_{3\underline{v}}(0,0,T) z_1^2(t) z_2(t-T) \\
& \quad \left. + 2\tilde{g}_{3\underline{v}}(T,0,T) z_1(t-T) z_1(t) z_2(t-T) + \tilde{g}_{3\underline{v}}(T,T,T) z_1^2(t-T) z_2(t-T) \right].
\end{aligned} \tag{3.74}$$

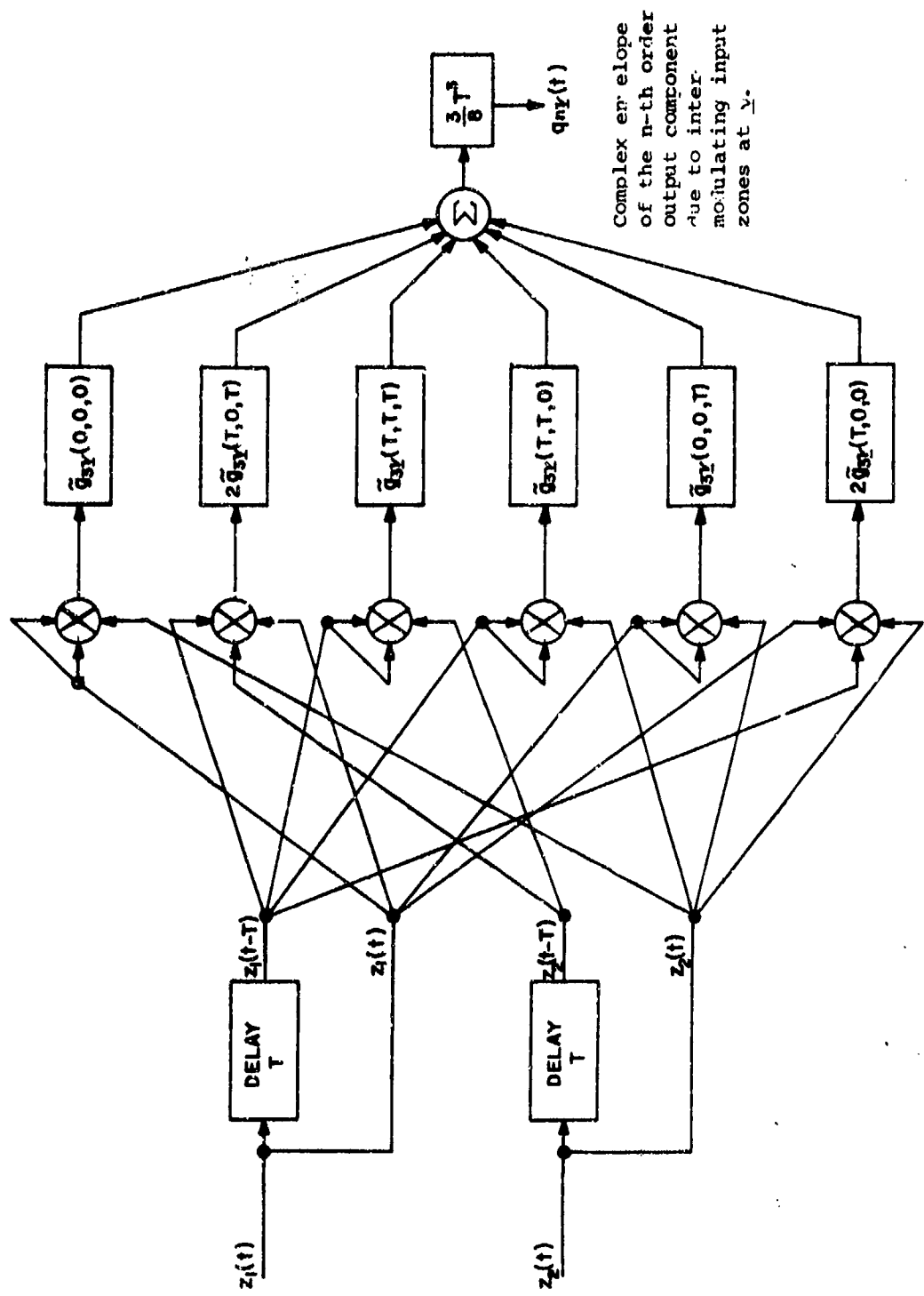


Fig. 3.3. Example of Delay Line Canonic Model: $n = 3$, $k_1 = 2$, $k_2 = 1$
 $T_1 = T_2, N_1 = N_2 = 2$.

Since $n=3$ and $N_1=N_2=2$ there are $2^3=8$ terms to be summed in the triple sum, but some of them are identical because the factor $z_1(t)$ occurs twice ($k_1=2$) in the product. We have the same situation as if we were tossing two identical dice with two faces and one different dice with two faces and counting up distinguishable arrangements; this number is six.

It can be seen that these models become rapidly more complicated as the number of necessary taps is increased. In general, if the delay line for z_{k_i} has N_i taps, then the sum over each r_i in Eq. (3.71) ranges only from 1 to N_i . Moreover, since permutations within the argument of $\tilde{g}_{ny}(rT)$ do not affect its value, some of the terms in the multiple sum in Eq. (3.71) have the same value. The number of ways of placing m_k indistinguishable factors $z_k(t)$ in one of the N_k tap positions is given by the combinatorial coefficient

$$\binom{N_k + m_k - 1}{N_k}. \quad (3.75)$$

Thus if $z_k(t)$ occurs m_k times in the iterated product, the number of distinguishable terms in Eq. (3.71) is

$$\prod_{k=-K}^K \binom{N_k + m_k - 1}{N_k}, \quad (3.76)$$

in which each factor with $m_k = 1$ is unity.

3.5 Frequency Power Series Canonic Model: Sinusoidally Modulated Signals

3.5.1 Crossmodulation and Desensitization

In this section we present the frequency power series canonic model for the case of sinusoidally modulated desired and interfering signals. Specifically, the distortion products which are analyzed are the compression, desensitization, and crossmodulation terms. The canonic model is developed using the constant and first derivative terms. The desired signal frequency is v_1 with complex envelope $z_1(t)$, and the undesired signal is at frequency v_2 with complex envelope $z_2(t)$. Assuming that third-order nonlinearities are dominant, the output complex envelope at frequency v_1 may be expressed as

$$q(t; v_1) = q_1(t; v_1) + \frac{3}{4} q_3(t; v_1, v_1, -v_1) + \frac{3}{2} q_3(t; v_1, v_2, -v_2). \quad (3.77)$$

The first term of Equation (3.77) represents the linear response to the desired signal, the second represents third-order effect involving only the desired signal, i.e., compression, while the last term gives the third-order nonlinear effects involving both signals, i.e., desensitization and crossmodulation. It is assumed for simplicity that the linear undesired signal response at v_2 is out-of-band and, therefore, can be neglected. Including only the first two terms of the frequency power series, the output terms of Equation (3.77) may be represented as

$$q_1(t; v_1) = H_1(v_1) z_1(t) + \frac{1}{2\pi j} \left. \frac{\partial H_1(\underline{f})}{\partial \underline{f}} \right|_{\underline{f}=v_1} \dot{z}_1(t), \quad (3.78)$$

$$\begin{aligned} q_3(t; v_1, v_1, -v_1) &= H_3(v_1, v_1, -v_1) z_1(t) |z_1(t)|^2 \\ &\quad + \frac{1}{2\pi j} \left\{ \left. \frac{\partial}{\partial f_1} H_3(\underline{f}) \right|_{\underline{f}=v_1} \dot{z}_1(t) |z_1(t)|^2 \right. \\ &\quad + \left. \left. \frac{\partial}{\partial f_2} H_3(\underline{f}) \right|_{\underline{f}=v_1} \dot{z}_1(t) |z_1(t)|^2 \right. \\ &\quad + \left. \left. \frac{\partial}{\partial f_3} H_3(\underline{f}) \right|_{\underline{f}=v_1} \dot{z}_1^*(t) z_1^2(t) \right\}, \end{aligned} \quad (3.79)$$

where $\underline{v} = v_1, v_1, -v_1$, and

$$\begin{aligned} q_3(t; v_1, v_2, -v_2) &= H_3(v_1, v_2, -v_2) z_1(t) |z_2(t)|^2 \\ &\quad + \frac{1}{2\pi j} \left\{ \left. \frac{\partial H_3(\underline{f})}{\partial f_1} \right|_{\underline{f}=\underline{v}} \dot{z}_1(t) |z_2(t)|^2 \right. \\ &\quad + \left. \left. \frac{\partial H_3(\underline{f})}{\partial f_2} \right|_{\underline{f}=\underline{v}} z_1(t) \dot{z}_2(t) z_2^*(t) \right. \\ &\quad + \left. \left. \frac{\partial H_3(\underline{f})}{\partial f_3} \right|_{\underline{f}=\underline{v}} z_1(t) z_2(t) \dot{z}_2^*(t) \right\}, \end{aligned} \quad (3.80)$$

where $\underline{v} = v_1, v_2, -v_2$.

The second terms on the right-hand side of the frequency power series, Eqs. (3.78),-(3.80), contain derivatives of the nonlinear transfer functions and the signals. They are significant when the transfer functions cannot be considered flat over the bandwidths of the signals involved, and additionally, are the source of FM crossmodulation. Equations (3.78), (3.79), and (3.80) are general expressions for arbitrary modulation on the desired and undesired signal. In the following sections simple expressions for sinusoidal AM and FM combinations will be developed and simplified for the particularly important situations of small distortion at the post-detector output.

3.5.2 AM-AM Crossmodulation

3.5.2.1 Predetection Spectrum: AM-AM

We now specialize Equations (3.78) - (3.80) to the case of sinusoidally amplitude-modulated desired and interfering signals. The complex envelopes of these signals may be written as

$$z_1(t) = A_1(1 + \alpha_1 \cos 2\pi\mu_1 t), \quad (3.81)$$

$$z_2(t) = A_2(1 + \alpha_2 \cos 2\pi\mu_2 t). \quad (3.82)$$

The symbols α_1 and α_2 represent the modulation indexes of the desired and interfering signals, while μ_1 and μ_2 are the modulating frequencies. With this notation, Eqs. (3.78) - (3.80) may be evaluated explicitly in terms of the signal parameters. In each case a number of frequencies are involved; both the cophasal and quadrature components appear with complex coefficients. Table 3.2 summarizes the frequencies involved in

TABLE 3.2
FREQUENCIES APPEARING IN COMPONENTS OF $q(t; v_1)$

Frequency	$q_1(t; v_1)$	$q_3(t; v_1, v_1, -v_1)$	$q_3(t; v_1, v_2, -v_2)$
dc	x	x	x
μ_1	x	x	x
μ_2			x
$2\mu_1$		x	
$2\mu_2$			x
$3\mu_1$		x	
$\mu_1 + \mu_2$			x
$\mu_1 - \mu_2$			x
$\mu_1 + 2\mu_2$			x
$\mu_1 - 2\mu_2$			x

each of the terms $q_1(t; v_1)$, $q_3(t; v_1, v_1, -v_1)$, and $q_3(t; v_1, v_2, -v_2)$. The equations for these three terms are given in Table 3.3.

We may represent $q(t; v_1)$ as a sum of the form

$$q(t; v_1) = x_o + jy_o + \sum_k \left[(x_{ck} + jy_{ck}) \cos 2\pi f_k t + (x_{sk} + jy_{sk}) \sin 2\pi f_k t \right]. \quad (3.83)$$

The f_k are the frequencies appearing in Table 3.2 and the coefficients may be obtained by summing the appropriate coefficients appearing in Table 3.3 according to Eq. (3.77). The real signal corresponding to the complex envelope $q(t; v_1)$ is given by

$$y(t) = \operatorname{Re} \left\{ q(t; v_1) e^{j2\pi v_1 t} \right\}. \quad (3.84)$$

Inserting Eq. (3.83) into Eq. (3.84) and carrying out the necessary trigonometric manipulations gives the signal structure at the output of the system, or

$$\begin{aligned} y(t) &= x_o \cos 2\pi v_1 t - y_o \sin 2\pi v_1 t \\ &+ \sum_k \left[\frac{x_{ck} + y_{sk}}{2} \cos 2\pi(v_1 + f_k)t \right. \\ &+ \frac{x_{sk} - y_{sk}}{2} \sin 2\pi(v_1 + f_k)t \\ &+ \frac{x_{ck} - y_{ck}}{2} \cos 2\pi(v_1 - f_k)t \\ &\left. - \frac{x_{sk} + y_{ck}}{2} \sin 2\pi(v_1 - f_k)t \right]. \end{aligned} \quad (3.85)$$

TABLE 3.3.
 FREQUENCY POWER-SERIES NONLINEAR CANONIC MODEL EXPRESSIONS
 FOR SINUSOIDAL MODULATION
 AM-AM CASE

$$\begin{aligned}
 q_1(t; v_1) &= A_1 \left[H_1(v_1) + \alpha_1 H_1(v_1) \cos 2\pi\mu_1 t + j\mu_1 \alpha_1 \frac{\partial H_1(\underline{f})}{\partial f} \Big|_{f=v_1} \sin 2\pi\mu_1 t \right] \\
 q_3(t; v_1, v_1, -v_1) &= q_3(t; \underline{v}) = A_1 |A_1|^2 \left[\left(1 + \frac{3\alpha_1^2}{2} \right) H_3(\underline{v}) + 3\alpha_1 \left(1 + \frac{\alpha_1}{4} \right) H_3(\underline{v}) \cos 2\pi\mu_1 t \right. \\
 &\quad \left. + j\mu_1 \alpha_1 \left(1 + \frac{\alpha_1}{4} \right) \sum_{i=1,2,3} \frac{\partial H_3(\underline{f})}{\partial f_i} \Big|_{f=v_1} \sin 2\pi\mu_1 t + \frac{3\alpha_1^2}{2} H_3(\underline{v}) \cos 4\pi\mu_1 t \right. \\
 &\quad \left. + j\mu_1 \alpha_1^2 \sum_{i=1,2,3} \frac{\partial H_3(\underline{f})}{\partial f_i} \Big|_{f=v_1} \sin 4\pi\mu_1 t + \frac{\alpha_1^3}{4} H_3(\underline{v}) \cos 6\pi\mu_1 t \right. \\
 &\quad \left. + j \frac{\mu_1 \alpha_1^3}{4} \sum_{i=1,2,3} \frac{\partial H_3(\underline{f})}{\partial f_i} \Big|_{f=v_1} \sin 6\pi\mu_1 t \right]
 \end{aligned}$$

where $\underline{v} = v_1, v_1, -v_1$.

TABLE 3.3. (Continued)

$$\begin{aligned}
 q_3(t; v_1, v_2, -v_2) = q_3(t; \psi) &= A_1 A_2^2 \left\{ \left(1 + \frac{\alpha_2^2}{2}\right) H_3(\psi) + \alpha_1 \left(1 + \frac{\alpha_2^2}{2}\right) H_3(\psi) \cos 2\pi u_1 t \right. \\
 &\quad \left. + j \alpha_1 \mu_1 \left(1 + \frac{\alpha_2^2}{2}\right) \frac{\partial H_3(\underline{\xi})}{\partial f_1} \Big|_{\underline{\xi}=\psi} \sin 2\pi u_1 t + 2\alpha_2 H_3(\underline{\xi}) \cos 2\pi u_2 t \right. \\
 &\quad \left. + j \alpha_2 u_2 \left[\frac{\partial H_3(\underline{\xi})}{\partial f_2} \Big|_{\underline{\xi}=\psi} + \frac{\partial H_3(\underline{\xi})}{\partial f_3} \Big|_{\underline{\xi}=\psi} \right] \sin 2\pi u_2 t + \alpha_1 \alpha_2 H_3(\psi) \cos 2\pi(u_1 + u_2)t \right\} \\
 &\quad + j \alpha_1 \alpha_2 \left[\mu_1 \frac{\partial H_3(\underline{\xi})}{\partial f_1} \Big|_{\underline{\xi}=\psi} + \frac{\alpha_2}{2} \frac{\partial H_3(\underline{\xi})}{\partial f_2} \Big|_{\underline{\xi}=\psi} + \frac{\alpha_2}{2} \frac{\partial H_3(\underline{\xi})}{\partial f_3} \Big|_{\underline{\xi}=\psi} \right] \sin 2\pi(u_1 - u_2)t \\
 &\quad + \alpha_1 \alpha_2 H_3(\psi) \cos 2\pi(u_1 - u_2)t + j \alpha_1 \alpha_2 \left[u_1 \frac{\partial H_3(\underline{\xi})}{\partial f_1} \Big|_{\underline{\xi}=\psi} - \frac{\alpha_2}{2} \frac{\partial H_3(\underline{\xi})}{\partial f_2} \Big|_{\underline{\xi}=\psi} \right. \\
 &\quad \left. - \frac{\alpha_2}{2} \frac{\partial H_3(\underline{\xi})}{\partial f_3} \Big|_{\underline{\xi}=\psi} \right] \sin 2\pi(u_1 - u_2)t + \frac{\alpha_2^2}{2} H_3(\psi) \cos 4\pi u_2 t \\
 &\quad + j \frac{\alpha_2^2 u_2}{2} \left[\frac{\partial H_3(\underline{\xi})}{\partial f_2} \Big|_{\underline{\xi}=\psi} + \frac{\partial H_3(\underline{\xi})}{\partial f_3} \Big|_{\underline{\xi}=\psi} \right] \sin 4\pi u_2 t
 \end{aligned}$$

TABLE 3.3. (Continued)

$$\begin{aligned}
 & + \frac{\alpha_1 \alpha_2^2}{4} H_3(\underline{\nu}) \cos 2\pi(\mu_1 - 2\nu_2)t + j \frac{\alpha_1 \alpha_2^2}{4} \left[\mu_1 \frac{\partial H_3(\underline{\xi})}{\partial \xi_1} \Bigg|_{\underline{\xi}=\underline{\nu}} + \mu_2 \frac{\partial H_3(\underline{\xi})}{\partial \xi_2} \Bigg|_{\underline{\xi}=\underline{\nu}} \right. \\
 & \quad \left. + \mu_2 \frac{\partial H_3(\underline{\xi})}{\partial \xi_3} \Bigg|_{\underline{\xi}=\underline{\nu}} \right] \sin 2\pi(\mu_1 + 2\nu_2)t + \frac{\alpha_1 \alpha_2^2}{4} H_3(\underline{\nu}) \cos 2\pi(\mu_1 - 2\nu_2)t \\
 & + j \frac{\alpha_1 \alpha_2^2}{4} \left[\mu_1 \frac{\partial H_3(\underline{\xi})}{\partial \xi_1} \Bigg|_{\underline{\xi}=\underline{\nu}} - \mu_2 \frac{\partial H_3(\underline{\xi})}{\partial \xi_2} \Bigg|_{\underline{\xi}=\underline{\nu}} - \mu_2 \frac{\partial H_3(\underline{\xi})}{\partial \xi_3} \Bigg|_{\underline{\xi}=\underline{\nu}} \right] \sin 2\pi(\mu_1 - 2\nu_2)t \}
 \end{aligned}$$

where $\underline{\nu} = \nu_1, \nu_2, -\nu_2$.

The spectral structure of the signal may be obtained immediately from this representation. The amplitude of the carrier is given by

$$\sqrt{x_o^2 + y_o^2}, \quad (3.86)$$

the amplitude of the sideband at $v_1 + f_k$ is given by

$$\frac{1}{2} \sqrt{(x_{ck} + y_{sk})^2 + (x_{sk} - y_{ck})^2}, \quad (3.87)$$

while the amplitude of the sideband at $v_1 - f_k$ is given by

$$\frac{1}{2} \sqrt{(x_{ck} - y_{sk})^2 + (x_{sk} + y_{ck})^2}. \quad (3.88)$$

3.5.2.2 Post-Detection Spectrum: AM-AM

The output of an ideal envelope detector is the magnitude of the complex envelope of the signal applied to the detector. Exact calculation of the detector output corresponding to Eq. (3.83) would result in a form unsuitable for spectral analysis. However, an accurate approximation can be made based on the assumption that the distortion components are small relative to the desired signal. Thus Eq. (3.83) is rewritten in the form

$$q(t; v_1) = (x_o + jy_o) + (x_{cl} + jy_{cl}) \cos 2\pi\mu_1 t + (x_{sl} + jy_{sl}) \sin 2\pi\mu_1 t + e_1(t) + j e_2(t), \quad (3.89)$$

where $\epsilon_1(t)$ and $\epsilon_2(t)$ are the low magnitude distortion terms.

If we let $\phi_o = \tan^{-1} \frac{y_o}{x_o}$ this can also be written in the form

$$q(t; v_1) = \left[\left(x_o^2 + y_o^2 \right)^{\frac{1}{2}} + (x_{c1} + jy_{c1}) e^{-j\phi_o} \cos 2\pi\mu_1 t \right. \\ \left. + (x_{s1} + jy_{s1}) e^{-j\phi_o} \sin 2\pi\mu_1 t \right. \\ \left. + e^{-j\phi_o} \epsilon_1(t) + j e^{-j\phi_o} \epsilon_2(t) \right] e^{j\phi_o}. \quad (3.90)$$

The magnitude is

$$|q(t; v_1)| = \left\{ \left[\left(x_o^2 + y_o^2 \right)^{\frac{1}{2}} + \operatorname{Re}\{(x_{c1} + jy_{c1}) e^{-j\phi_o}\} \cos 2\pi\mu_1 t \right. \right. \\ \left. + \operatorname{Re}\{(x_{s1} + jy_{s1}) e^{-j\phi_o}\} \sin 2\pi\mu_1 t + \epsilon_1(t) \cos \phi_o \right. \\ \left. + \epsilon_2(t) \sin \phi_o \right]^2 + \left[\operatorname{Im}\{(x_{c1} + jy_{c1}) e^{-j\phi_o}\} \cos 2\pi\mu_1 t \right. \\ \left. + \operatorname{Im}\{(x_{s1} + jy_{s1}) e^{-j\phi_o}\} \sin 2\pi\mu_1 t \right. \\ \left. - \epsilon_1(t) \sin \phi_o + \epsilon_2(t) \cos \phi_o \right]^2 \right\}^{\frac{1}{2}}. \quad (3.91)$$

The cosinusoidal component at the signal frequency is predominantly the linear component which is at the same phase angle as the carrier. Thus the phase angle of the cosinusoidal signal

frequency component is approximately equal to that of the carrier:

$$\tan^{-1} \frac{y_{cl}}{x_{cl}} \approx \phi_o. \quad (3.92)$$

Thus the first term in the second bracket of Eq. (3.91) is small. The second term in this bracket will be small as long as frequency selective effects are a small part of the linear transfer function. Thus the second bracket in Eq. (3.91) contains only small terms and its square may be neglected, giving

$$|q(t; v_1)| \approx (x_o^2 + y_o^2)^{\frac{1}{2}} + \operatorname{Re}\{(x_{cl} + jy_{cl})e^{-j\phi_o}\} \cos 2\pi\mu_1 t \\ + \operatorname{Re}\{(x_{sl} + jy_{sl})e^{-j\phi_o}\} \sin 2\pi\mu_1 t + \epsilon_1(t) \cos \phi_o \\ + \epsilon_2(t) \sin \phi_o. \quad (3.93)$$

These approximations are equivalent to retaining only those components of Eq. (3.90) that lie in-phase with the carrier component $x_o + jy_o$. Having established this result it is a simple exercise to complete the spectral analysis of the AM detector output. The amplitude of the desired signal is given by

$$\sqrt{(x_{cl} \cos \phi_o + y_{cl} \sin \phi_o)^2 + (x_{sl} \cos \phi_o + y_{sl} \sin \phi_o)^2}, \quad (3.94)$$

while the amplitude of the k'th distortion component is

$$\sqrt{(x_{ck} \cos \phi_0 + y_{ck} \sin \phi_0)^2 + (x_{sk} \cos \phi_0 + y_{sk} \sin \phi_0)^2}. \quad (3.95)$$

3.5.2.3 Simplified Assumption Analysis: AM-AM

The analysis presented in the preceding section includes a large number of distortion components. In many situations only the crossmodulation component at the undesired modulation frequency μ_2 will be of interest. Furthermore, there are situations where frequency selectivity will not be sufficient to affect the crossmodulation levels; in this case only the first term in the frequency power-series model is required. Therefore, in this section we repeat the analysis of the preceding section with these simplifying assumptions.

Neglecting the second term of the frequency power-series, the linear response may be written

$$q_1(t; v_1) = A_1 H_1(v_1) + a_1 A_1 H_1(v_1) \cos 2\pi\mu_1 t. \quad (3.96)$$

The third-order term involving only the desired signal (compression) $q_3(t; v_1, v_1, -v_1)$ will be neglected entirely; the third-order crossmodulation term can be written as

$$q_3(t; v_1, v_2, -v_2) = 2a_2 A_1 |A_2|^2 H_3(v_1, v_2, -v_2) \cos 2\pi\mu_2 t. \quad (3.97)$$

All contributions from the second term of the frequency power-series and all frequencies other than μ_2 have been ignored. Combining these terms according to Eq. (3.77) gives

$$q(t; \nu_1) = A_1 [H_1(\nu_1) + \alpha_1 H_1(\nu_1) \cos 2\pi\mu_1 t \\ + 3\alpha_2 |A_2|^2 H_3(\nu_1, \nu_2, -\nu_2) \cos 2\pi\mu_2 t]. \quad (3.98)$$

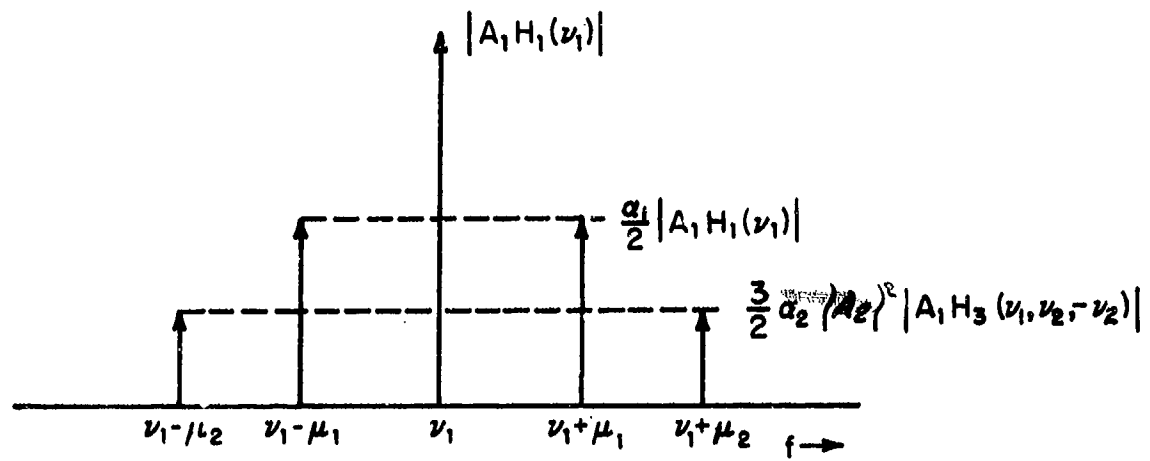
Substitution of these coefficients into Eqs. (3.86), (3.87), and (3.88) gives the spectral structure of the predetection signal, as shown in Fig. 3.4a. Note that corresponding upper and lower sidebands are equal because of the assumed absence of frequency selectivity. The ratio of crossmodulation sideband amplitude to carrier amplitude is given by

$$\frac{3\alpha_2 |A_2|^2 |H_3(\nu_1, \nu_2, -\nu_2)|}{2 |H_1(\nu_1)|}. \quad (3.99)$$

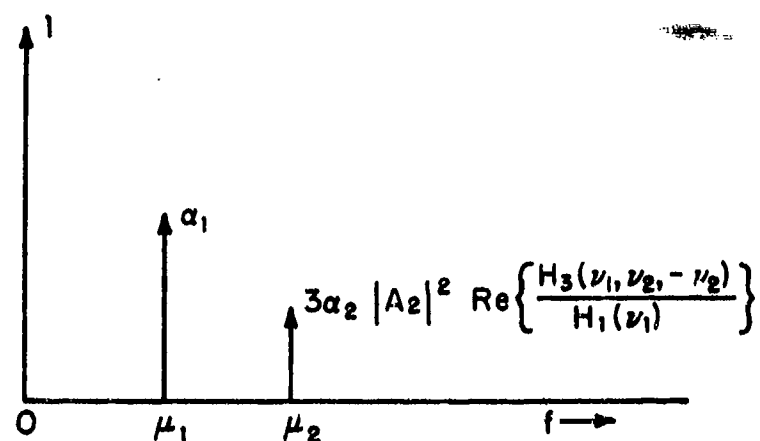
These amplitudes, observed at intermediate frequencies, depend on the magnitudes of $H_1(\nu_1)$ and $H_3(\nu_1, \nu_2, -\nu_2)$ but not on their phases.

The post-detection signal structure for this simplified case may be obtained by substituting the coefficients of Equation (3.98) into Eqs. (3.94) and (3.95). The results, normalized by $|A_1 H_1(\nu_1)|$ to give unit dc amplitude, are shown in Fig. 3.4b. Note that in this case the relative phase of $H_1(\nu_1)$ and $H_3(\nu_1, \nu_2, -\nu_2)$ is significant in determining the crossmodulation level. Relative to the desired signal amplitude, the crossmodulation level is

$$3 \left(\frac{\alpha_2}{\alpha_1} \right) |A_2|^2 \operatorname{Re} \left\{ \frac{H_3(\nu_1, \nu_2, -\nu_2)}{H_1(\nu_1)} \right\}. \quad (3.100)$$



a) IF Spectrum



b) Detector Output Spectrum

Fig. 3.4. Approximate AM-AM Crossmodulation Spectra.

3.5.3 FM-AM Crossmodulation

3.5.3.1 Demodulated Spectrum

In this section a sinusoidally FM modulated desired signal in the presence of a sinusoidally AM modulated interferer is assumed. The complex envelopes of these signals may be written as

$$z_1(t) = A_1 e^{j \frac{\alpha_1}{\mu_1} \sin 2\pi\mu_1 t}, \quad (3.101)$$

and

$$z_2(t) = A_2 (1 + \alpha_2 \cos 2\pi\mu_2 t). \quad (3.102)$$

The instantaneous frequency of the signal corresponding to $z_1(t)$ is $\alpha_1 \cos 2\pi\mu_1 t$; thus α_1 is the peak frequency deviation and (α_1/μ_1) is the modulation index. With these definitions, the terms of the canonic model may be evaluated, as was done in the AM-AM case. The results appear in Table 3.4. It should be observed that all terms include the complex envelope $z_1(t)$ of the desired signal as a multiplicative factor. Thus it is natural to write the complex envelope in the form

$$\begin{aligned} q(t; \nu_1) = z_1(t) & [x_o + jy_o + \sum_k (x_{ck} + jy_{ck}) \cos 2\pi f_k t \\ & + \sum_k (x_{sk} + jy_{sk}) \sin 2\pi f_k t]. \quad (3.103) \end{aligned}$$

TABLE 3.4.

FREQUENCY POWER-SERIES NONLINEAR CANONIC
MODEL EXPRESSIONS FOR SINUSOIDAL MODULATION,
FM-AM CASE

$$q_1(t; \nu_1) = z_1(t) \left[H_1(\nu_1) + \alpha_1 \frac{\partial H_1(\xi)}{\partial f} \Bigg|_{f=\nu_1} \cos 2\pi\nu_1 t \right]$$

$$\begin{aligned} q_3(t; \nu_1, \nu_2, -\nu_2) &= |A_1|^2 e^{-j\nu_2 t} \left[\alpha_3(\underline{\nu}) + \alpha_1 \left[\frac{\partial H_3(\xi)}{\partial f_1} \Bigg|_{\xi=\underline{\nu}} + \frac{\partial H_3(\xi)}{\partial f_2} \Bigg|_{\xi=\underline{\nu}} \right. \right. \\ &\quad \left. \left. - \frac{\partial H_3(\xi)}{\partial f_3} \Bigg|_{\xi=\underline{\nu}} \right] \cos 2\pi\nu_1 t \right] \end{aligned}$$

$$\begin{aligned} q_3(t; \nu_1, \nu_2, -\nu_2) &= |A_2|^2 z_1(t) + \left[\left(1 + \frac{\alpha_2^2}{2} \right) H_3(\underline{\nu}) \right. \\ &\quad \left. + 2\alpha_2 H_3(\underline{\nu}) \cos 2\pi\nu_2 t + j\alpha_2 \mu_2 \sum_{i=2,3} \frac{\partial H_3(\xi)}{\partial f_i} \Bigg|_{\xi=\underline{\nu}} \sin 2\pi\nu_2 t \right. \end{aligned}$$

$$\begin{aligned} &\quad \left. + \frac{\alpha_2^2}{2} H_3(\underline{\nu}) \cos 4\pi\nu_2 t + j \frac{\alpha_2 \mu_2}{2} \sum_{i=2,3} \frac{\partial H_3(\xi)}{\partial f_i} \Bigg|_{\xi=\underline{\nu}} \sin 4\pi\nu_2 t \right] \end{aligned}$$

TABLE 3.4. (Continued)

$$\begin{aligned}
 & + \alpha_1 \left(1 + \frac{\alpha_2^2}{2}\right) \frac{\partial H_3(\underline{f})}{\partial f_1} \Bigg|_{\underline{f}=\underline{v}} \\
 & \quad \cos 2\pi\mu_1 t + \alpha_1 \alpha_2 \frac{\frac{\partial H_3(\underline{f})}{\partial f_1}}{\Bigg|_{\underline{f}=\underline{v}}} \cos 2\pi(\mu_1 + \mu_2) t \\
 & + \alpha_1 \alpha_2 \frac{\partial H_3(\underline{f})}{\partial f_1} \Bigg|_{\underline{f}=\underline{v}} \\
 & \quad \cos 2\pi(\mu_1 - \mu_2) t + \frac{\alpha_1 \alpha_2^2}{4} \frac{\partial H_3(\underline{f})}{\partial f_1} \Bigg|_{\underline{f}=\underline{v}} \\
 & \quad \cos 2\pi(\mu_1 + 2\mu_2) t \\
 & + \frac{\alpha_1 \alpha_2^2}{4} \frac{\partial H_3(\underline{f})}{\partial f_1} \Bigg|_{\underline{f}=\underline{v}} \\
 & \quad \cos 2\pi(\mu_1 - 2\mu_2) t
 \end{aligned}$$

where $\underline{v} = v_1, v_2, -v_2$.

In this case the desired modulation appears in the factor $z_1(t)$ and all of the terms appearing in the bracket, with the exception of $x_o + jy_o$, are the low-level distortion components.

The IF spectrum of the signal corresponding to $q(t; v_1)$ is quite complicated due to the simultaneous presence of frequency and amplitude modulation. The output of an ideal FM demodulator is more accessible. The complex envelope is first written in the form

$$q(t; v_1) = z_1(t)(x_o + jy_o) \left[1 + \sum_k \frac{x_{ck} + jy_{ck}}{x_o + jy_o} \cos 2\pi f_k t + \sum_k \frac{x_{sk} + jy_{sk}}{x_o + jy_o} \sin 2\pi f_k t \right]. \quad (3.104)$$

Making use of the small angle approximation this may be written as

$$q(t; v_1) \approx z_1(t)(x_o + jy_o) e^{j \left[\sum_k \text{Im} \left\{ \frac{x_{ck} + jy_{ck}}{x_o + jy_o} \right\} \cos 2\pi f_k t \right]} e^{j \left[\sum_k \text{Im} \left\{ \frac{x_{sk} + jy_{sk}}{x_o + jy_o} \right\} \sin 2\pi f_k t \right]}. \quad (3.105)$$

Thus the output of an ideal FM demodulator is

$$\begin{aligned} \frac{1}{2\pi} \frac{d}{dt} \text{ARG}[q(t; v_1)] &= \alpha_1 \cos 2\pi\mu_1 t \\ &- \sum_k f_k \frac{x_o y_{ck} - y_o x_{ck}}{x_o^2 + y_o^2} \sin 2\pi f_k t \\ &+ f_k \frac{x_o y_{sk} - y_o x_{sk}}{x_o^2 + y_o^2} \cos 2\pi f_k t \}. \end{aligned} \quad (3.106)$$

The amplitude of the desired signal is

$$\sqrt{\left(\alpha_1 + \mu_1 \frac{x_o y_{s1} - y_o x_{s1}}{x_o^2 + y_o^2}\right)^2 + \left(\mu_1 \frac{x_o y_{cl} - y_o x_{cl}}{x_o^2 + y_o^2}\right)^2}. \quad (3.107)$$

and the amplitude of the k'th distortion component is

$$\frac{f_k}{\sqrt{x_o^2 + y_o^2}} \sqrt{(x_o y_{ck} - y_o x_{ck})^2 + (x_o y_{sk} - y_o x_{sk})^2}. \quad (3.108)$$

3.5.3.2 Simplified Analysis: FM-AM

A simplified analysis of FM-AM crossmodulation will now be made. Using the approximation made in the AM-AM crossmodulation case, the complex envelope of the distorted signal may be written as

$$q(t; v_1) = z_1(t) H_1(v_1) [1 + 3\alpha_2 |A_2|^2 \frac{H_3(v_1, v_2, -v_2)}{H_1(v_1)} \cos 2\pi\mu_2 t]. \quad (3.109)$$

The resulting discriminator output is

$$\alpha_1 \cos 2\pi\mu_1 t - 3\alpha_2 \mu_2 |A_2|^2 \text{Im}\left\{\frac{H_3(v_1, v_2, -v_2)}{H_1(v_1)}\right\} \sin 2\pi\mu_2 t, \quad (3.110)$$

giving the post-detection spectrum shown in Fig. 3.5; the cross-modulation amplitude relative to the desired signal is clearly

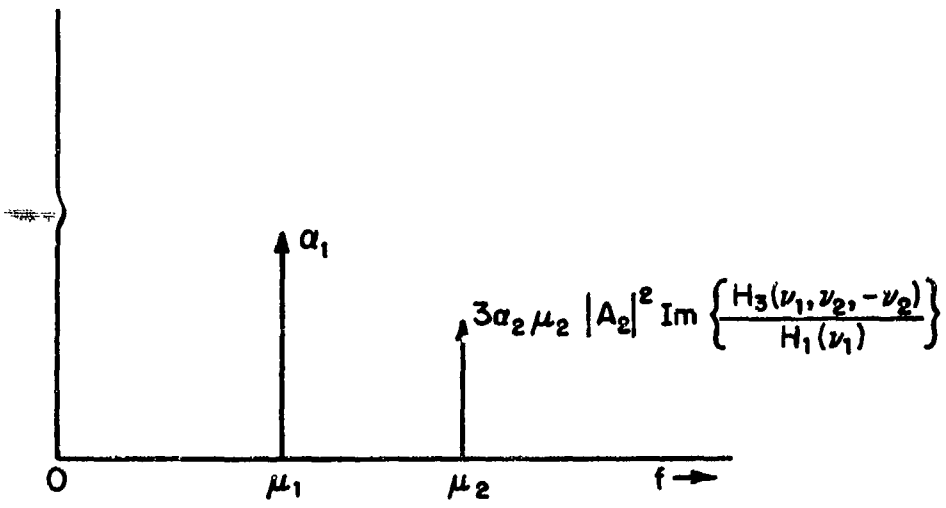


Fig. 3.5. Post Detection Spectrum, AM-FM Case.

$$3\mu_2 \left(\frac{\alpha_2}{\alpha_1}\right) |A_2|^2 \operatorname{Im} \left\{ \frac{H_3(v_1, v_2, -v_2)}{H_1(v_1)} \right\}. \quad (3.111)$$

Just as in the case of the AM detector output, the phase of $H_3(v_1, v_2, -v_2)$ relative to $H_1(v_1)$ appears in the final result.

3.5.4 AM-FM and FM-FM Crossmodulation

The two cases discussed previously both involve an AM interfering signal. The first term on the right-hand side of the frequency power-series shows that crossmodulation arises from a term containing $|z_2(t)|^2$; if $z_2(t)$ is the complex envelope of an FM signal this reduces to a constant so that none of the undesired modulation appears on the desired signal. However, when frequency dependence of the third-order kernels is considered this is no longer the case. Thus the derivative terms of the canonic model will permit calculation of crossmodulation in cases where the undesired signal is FM modulated. The importance of this form of crossmodulation as a source of degradation will depend on the slope of the nonlinear transfer function of the system. In this section we consider the case of an AM or FM desired signal and an FM undesired signal; the next section deals with the case where both signals are FM modulated.

The complex envelopes of the desired and interfering signals may be written in the AM-FM case as

$$z_1(t) = A_1(1 + \alpha_1 \cos 2\pi\mu_1 t), \quad (3.112)$$

and

$$z_2(t) = A_2 e^{j \frac{\alpha_2}{\mu_2} \sin 2\pi\mu_2 t} . \quad (3.113)$$

As before, α_1 is the AM modulation index, α_2 is the peak FM deviation, the μ 's are the modulating frequencies and the A 's are (complex) amplitudes. Since the terms $q_1(t; v_1)$ and $q_3(t; v_1, v_1, -v_1)$ involve only $z_1(t)$, they will be the same as in the AM-AM case. The remaining term of the output complex envelope, $q_3(t; v_1, v_2, -v_2)$, appears in Table 3.5. These terms may be used to calculate the coefficients necessary to evaluate the IF spectrum according to Eqs. (3.86), (3.87), and (3.88). The output of an AM detector may also be calculated from Eqs. (3.94) and (3.95).

In the case of FM-FM signals and interference, the complex envelopes of the input signals are assumed to be

$$z_1(t) = A_1 e^{j \frac{\alpha_1}{\mu_1} \sin 2\pi\mu_1 t} , \quad (3.114)$$

and

$$z_2(t) = A_2 e^{j \frac{\alpha_2}{\mu_2} \sin 2\pi\mu_2 t} . \quad (3.115)$$

The output terms $q_1(t; v_1)$ and $q_3(t; v_1, v_1, -v_1)$, which depend only on $z_1(t)$ will be the same as in the FM-AM case. The remaining term, $q_3(t; v_1, v_2, -v_2)$, has been evaluated and appears in Table 3.6. These terms give the output of an FM detector, using Eqs. (3.107) and (3.108).

TABLE 3.5.

FREQUENCY POWER-SERIES NONLINEAR CANONIC
MODEL EXPRESSIONS FOR SINUSOIDAL MODULATION
AM-FM CASE

$$\left. \begin{array}{l} q_1(t; \nu_1) = \\ q_3(t; \nu_1, \nu_1, -\nu_1) = \end{array} \right\} \text{Same as in AM-AM case.}$$

$$q_3(t; \nu_1, \nu_2, -\nu_2) = q_3(t; \nu) = \alpha_1 |A_2|^2 \left\{ H_3(\nu) + \alpha_1 H_3(\nu) \cos 2\pi\nu_1 t + j\alpha_1 \mu_1 \frac{\partial H_3(\nu)}{\partial f_1} \Big|_{\nu=\nu} \sin 2\pi\nu_1 t \right. \\ \left. + \alpha_2 \left[\frac{\partial H_3(\nu)}{\partial f_2} \Big|_{\nu=\nu} - \frac{\partial H_3(\nu)}{\partial f_3} \Big|_{\nu=\nu} \right] \cos 2\pi\nu_2 t \right. \\ \left. + \frac{\alpha_1 \alpha_2}{2} \left[\frac{\partial H_3(\nu)}{\partial f_2} \Big|_{\nu=\nu} - \frac{\partial H_3(\nu)}{\partial f_3} \Big|_{\nu=\nu} \right] \cos 2\pi(\mu_1 + \mu_2)t \right. \\ \left. + \frac{\alpha_1 \alpha_2}{2} \left[\frac{\partial H_3(\nu)}{\partial f_2} \Big|_{\nu=\nu} - \frac{\partial H_3(\nu)}{\partial f_3} \Big|_{\nu=\nu} \right] \cos 2\pi(\mu_1 - \mu_2)t \right\}$$

where $\nu = \nu_1, \nu_2, -\nu_2$.

TABLE 3.6.

FREQUENCY POWER-SERIES NONLINEAR CANONIC
MODEL EXPRESSIONS FOR SINUSOIDAL MODULATION
FM-FM CASE

$$\left. \begin{array}{l} q_1(t; v_1) = \\ q_3(t; v_1, v_1, -v_1) = \end{array} \right\} \text{Same as in FM-AM case.}$$

$$\begin{aligned} q_3(t; v_1, v_2, -v_2) &= q_3(t; \underline{v}) = \\ z_1(t) |A_2|^2 \left\{ H_3(v) + a_1 \frac{\partial H_3(f)}{\partial f_1} \Bigg|_{f=\underline{v}} \cos 2\pi\mu_1 t \right. \\ &\quad \left. + a_2 \left[\frac{\partial H_3(f)}{\partial f_2} \Bigg|_{f=\underline{v}} - \frac{\partial H_3(f)}{\partial f_3} \Bigg|_{f=\underline{v}} \right] \cos 2\pi\mu_2 t \right\} \end{aligned}$$

where $\underline{v} = v_1, v_2, -v_2$.

3.6 Simplified Frequency Power Series Canonic Model

It is instructive to summarize the essential simplicity of the frequency power series canonic model for a particularly simple yet highly important example. It is assumed that the input to the quasi-linear system consists of a desired signal $\text{Re}[S_1(t)e^{j2\pi f_1 t}]$ together with two interfering signals $\text{Re}[I_2(t)e^{j2\pi f_2 t}]$ and $\text{Re}[I_3(t)e^{j2\pi f_3 t}]$. Each input is a modulated carrier so the complex amplitudes for each are time-varying. If we assume that the bandwidths are not excessive compared to the frequency-selectivity of the system we can retain the significant portion of the canonic model for modulated signals by simply retaining the leading terms in the frequency power series. The leading term can be readily obtained by letting the complex amplitude of the unmodulated signals simply assume a time-dependence.

Summarized in Fig. 3.6 are the several linear and nonlinear responses of our simplified model. The inputs to the system shown in the diagram are the signal complex amplitude $S_1(t)$ and the complex amplitudes $I_2(t)$ and $I_3(t)$ of the two interfering signals. We also show internal equivalent noise referred to the system input. It has been assumed that second-order and terms higher than third-order are negligible. These terms could be added at the cost of considerable complication. It has also been assumed that the signal component at f_1 is of prime interest and attention is to be devoted to signal degradation at or near f_1 , caused by the interference rather than degradation of the interference by the signal. We, therefore, have omitted many third-order terms contributing at or near f_2 and f_3 as well as the gain compression term at f_1 .

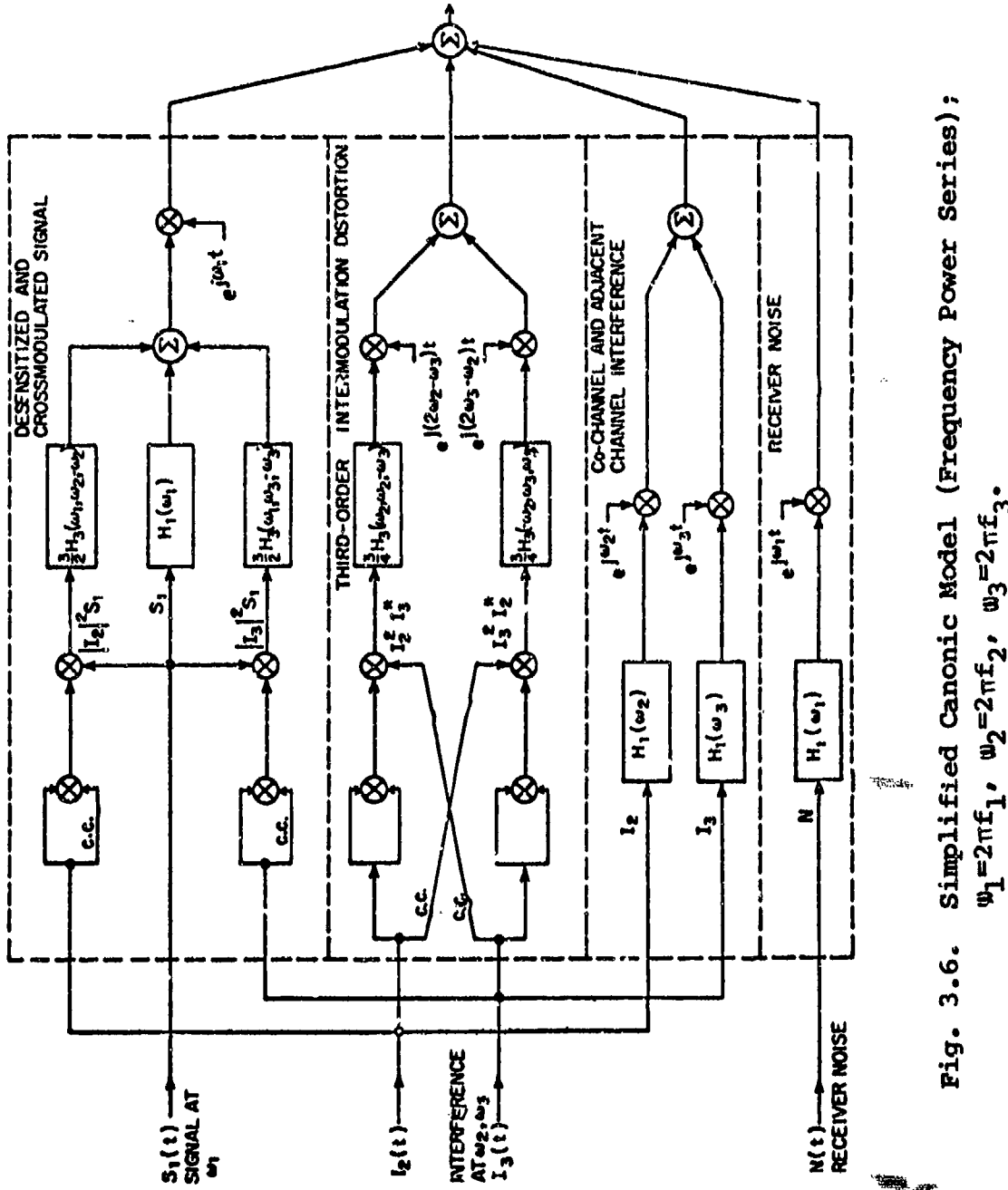


Fig. 3.6. Simplified Canon Model (Frequency Power Series);

$$\omega_1 = 2\pi f_1, \omega_2 = 2\pi f_2, \omega_3 = 2\pi f_3.$$

Consider first the interference situation in a linear system. Except for the receiver noise, the signal linear output is then disturbed only by the linear response of the system to the interference. The output can be written

$$y(t) = \operatorname{Re} [S_1(t) H_1(f_1) e^{j2\pi f_1 t} + I_2(t) H_1(f_2) e^{j2\pi f_2 t} + I_3(t) H_1(f_3) e^{j2\pi f_3 t}], \quad (3.116)$$

where the first term is simply the amplified signal while the last two terms are commonly referred to as co-channel and/or adjacent channel interference. The signal path shows up in Fig. 3.6 as the direct path through the middle of the signal box. The interference is shown in the box next to the bottom of Fig. 3.6. Many investigations of the effects of electromagnetic interference are based entirely upon the effects of the linear interfering terms. The transfer functions included throughout this chapter, as well as those explicitly illustrated in Fig. 3.6, include equivalent amplifier nonlinear transfer functions (See Chapter 1, Section 1.9.1). If the demodulation detector intended to recover the desired modulation contained in $S_1(t)$ follows the system shown in Fig. 3.6, it is frequently convenient to write Eq. (3.116) in the form

$$y(t) = \operatorname{Re}[q(t) e^{j2\pi f_1 t}], \quad (3.117)$$

where the complex envelope $q(t)$ is

$$q(t) = S_1(t) H_1(f_1)$$

$$+ I_2(t) H_1(f_2) e^{j2\pi(f_2-f_1)t}$$

$$+ I_3(t) H_1(f_3) e^{j2\pi(f_3-f_1)t}.$$

(3.118)

The characteristics of the demodulated signal including the effects of the interference are examined by investigating the properties of $q(t)$. For example, $y(t)$ might be the output of a receiver IF amplifier, that is, the predetection receiver output. The post-detection receiver output would be proportional to the envelope of $y(t)$, or $|q(t)|$ for an AM demodulator. The output of coherent demodulators as well as frequency and phase demodulators can be similarly investigated by examining other mathematical operations upon $q(t)$. These operations are frequently large signal nonlinear operations that can not be easily carried out without the assumption of a large signal-to-distortion ratio.

If we next introduce the third-order nonlinear modification to the linear responses that become significant either in distorting the desired signal or in making its detection more difficult in the presence of noise or interference we must add the additional signal and interference components illustrated in Fig. 3.6. (As described earlier, we are illustrating only the first term in the frequency power series canonic model).

Consider first the signal. Instead of just the linear signal we now have at the output at frequency f_1 ,

$$\begin{aligned}
 y(t) \Big|_{f=f_1} &= \operatorname{Re} \left\{ [S_1(t) H_1(f_1) \right. \\
 &\quad + \frac{3}{2} |I_2(t)|^2 S_1(t) H_3(f_1, f_2, -f_2) \\
 &\quad \left. + \frac{3}{2} |I_3(t)|^2 S_1(t) H_3(f_1, f_3, -f_3)] e^{j2\pi f_1 t} \right\}. \\
 & \tag{3.119}
 \end{aligned}$$

This output component is shown in Fig. 3.6 as the output from the signal box at the top of the diagram. The phase of H_3 relative to H_1 is frequently such that the two interfering terms subtract from the first term to reduce the total signal component at f_1 . Hence, the term desensitization. It sometimes happens, however, that the relative phase of H_3 is such that the resultant signal can increase rather than decrease. The presence of modulation on the interference terms $I_2(t)$ and $I_3(t)$ also introduces a transfer of modulations from the interference to the signal via the $|I_2(t)|^2$ and $|I_3(t)|^2$ terms. Therefore, both crossmodulation and desensitization nonlinear effects have a common origin and are thus associated with the same box in Fig. 3.6. Observe that the relative phase of H_3 with respect to H_1 is significant.

The presence of the two interferers at frequencies f_2 and f_3 near the signal frequency f_1 frequently can mask the presence of a weak signal by the third-order intermodulation distortion

terms at $2f_2 - f_3$ or $2f_3 - f_2$. These terms are contributed by the box labeled third-order intermodulation distortion in Fig. 3.6. In particular, the output components are

$$\begin{aligned}
 y(t) &= \\
 &\left| \begin{array}{l} \text{3rd-order} \\ \text{intermo-} \\ \text{dulation} \end{array} \right. \\
 &\text{Re} \left[\frac{3}{4} |I_2(t)|^2 I_3^*(t) H_3(f_2, f_2, -f_3) e^{j2\pi(2f_2-f_3)t} \right. \\
 &\quad \left. + \frac{3}{4} I_2^*(t) |I_3(t)|^2 H_3(-f_2, f_3, f_3) e^{j2\pi(2f_3-f_2)t} \right]. \quad (3.120)
 \end{aligned}$$

If either of these terms is significant relative to the signal term the signal is distorted or, if weak, may be completely masked. A common criterion for adequately low intermodulation distortion is that the intermodulation distortion power be no larger than the receiver noise in some stated bandwidth. Observe that the phase of H_3 in the intermodulation distortion calculation is not of interest since the nonlinear responses are not coherent with the signal at f_1 .

Finally, the demodulation detector output characteristics can be investigated by adding up the several linear and nonlinear components to generate a composite predetection signal. The complex envelope $q(t)$ of this signal can be examined to investigate the post-detection properties of the demodulator output. These ideas can be expanded to include additional terms in the frequency power series or may also be applied to the tapped delay line wideband signal canonic model. Both the

time-domain and frequency-domain structure of the system demodulator output can in principle be examined. Specific examples of several practical situations are developed in associations with the VHF receiver modeling work described in detail in Chapter 7.

Table 3.7
The List of Key Symbols Used in Chapter 3

B_1	bandwidth of the input component $x_1(t)$
B_i	bandwidth of the i -th input component $x_i(t)$
\underline{f}	abbreviation for the vector (f_1, f_2, \dots, f_n)
f_i	the i -th frequency coordinate
$g_{ny}(t_1, \dots, t_n)$	the slowly varying complex envelope of the n -th order nonlinear impulse response to n intermodulating carrier impulses with the ordinates (t_1, \dots, t_n) centered on frequencies v_1, v_2, \dots, v_n
$g_{ny}(t)$	abbreviation for $g_{ny}(t_1, \dots, t_n)$
$G_{ny}(f_1, \dots, f_n)$	multivariate Fourier transform of $g_{ny}(t)$, i.e., the n -fold spectrum of the complex envelope of the n -th order impulse response
$G_{ny}(f)$	abbreviation for $G_{ny}(f_1, \dots, f_n)$
$\tilde{g}_{ny}(t_1, \dots, t_n)$	the envelope $g_{ny}(t)$ after bandlimiting
$\tilde{g}_{ny}(t)$	abbreviation for $\tilde{g}_{ny}(t_1, \dots, t_n)$
$\tilde{G}_{ny}(f_1, \dots, f_n)$	the n -fold spectrum of $\tilde{g}_{ny}(t_1, \dots, t_n)$; i.e., the multivariate spectrum $G_{ny}(f)$ bandlimited in each ordinate to the set of bandwidths (B_1, \dots, B_n)
$\tilde{G}_{ny}(f)$	abbreviation for $\tilde{G}_{ny}(f_1, \dots, f_n)$
$h_n(t_1, \dots, t_n)$	the multivariate impulse response of a nonlinear system
$h_n(t)$	abbreviation for $h_n(t_1, \dots, t_n)$
$H_n(f_1, \dots, f_n)$	multivariate spectrum of the n -th order impulse response with each input having its own frequency ordinate f_1, \dots, f_n
$H_n(t)$	abbreviation for $H_n(f_1, \dots, f_n)$
i	index ranging from 1 to n

Table 3.7 (Continued)

k	index identifying one of the K input components in the one sided spectrum; or the index of input frequency zones, $2K$ in all, in the two-sided spectrum
k_i	index of one of the n factors in the intermodulation product which identifies one of the $2K$ frequency zones
m_k	coefficient denoting the multiplicity of each of the $2K$ waveforms indexed by k , $z_k(t)$, in the intermodulation product
M	number of distinct frequency zones in the intermodulation product
n	order of response, or the number of intermodulating zones
N_i	number of taps in the delay line for each of the n input components in the intermodulation product $z_{k_i}(t)$
N_K	number of taps in the delay line for each of the $2K$ input components $z_k(t)$
o	abbreviation denoting the vector $(0,0,\dots,0)$
p	order of a term in the Taylor series expansion of n -th order impulse response spectrum
p_i	order of the derivative with respect to f_i in the term of order p in the Taylor series expansion
$P(t; v_{k_1}, \dots, v_{k_n})$	product of intermodulation of the n input components at v_{k_1}, \dots, v_{k_n} as it appears at the output in the frequency zone centered on the sum frequency $v_{k_1} + \dots + v_{k_n}$ for a system with n -th order impulse response spectrum $H_n(f_1, \dots, f_n)$

Table 3.7 (Continued)

$\underline{P}(t; \underline{v})$	abbreviation for $\underline{P}(t; v_{k_1}, \dots, v_{k_n})$
$q_v(t) = q(t; \underline{v})$	slowly-varying composite complex envelope at v .
$q_{n\underline{v}}(t) = q_n(t; \underline{v})$	slowly-varying complex envelope of the n-th order nonlinear output component $y_n(t)$ due to intermodulation products of the inputs at v
$Q_{n\underline{v}}(f)$	Fourier transform of $q_{n\underline{v}}(t)$
r_i	ordering number of a tap in the delay line for $z_i(t)$
rect x	rectangular function defined to be unity for $ x < 1/2$ and zero elsewhere
sinc y	$(\sin \pi y / (\pi y))$
\underline{t}	abbreviation for the time coordinates (t_1, \dots, t_n)
T	spacing between taps when all the delay lines have the same tap spacings
t_i	spacing between taps of the delay line of $z_i(t)$
$x(t)$	input waveform
$x_k(t)$	one of the K zonal components of the input waveform
$X(f)$	spectrum of $x(t)$
$X_k(f)$	spectrum of $x_k(t)$
$y(t)$	output waveform
$y_n(t)$	n-th order output component of a nonlinear system
$Y(f)$	spectrum of $y(t)$
$Y_n(f)$	spectrum of $y_n(t)$

Table 3.7 (Continued)

$y_{ny}(t) = y_n(t; \underline{v})$	n-th order output component of a nonlinear system arising out of the intermodulation of input components centered at v_1, v_2, \dots, v_n
$z_k(t)$	complex envelope of $x_k(t)$
$\dot{z}_k(t)$	the first derivative of $z_k(t)$
$z_k^{(p)}(t)$	the p-th derivative of $z_k(t)$
$Z_k(f)$	the spectrum of $z_k(t)$
v	sum frequency of all the intermodulating carriers $v_1 + v_2 + \dots + v_n$
\underline{v}	the set of carrier frequencies (v_1, \dots, v_n)
v_k	carrier frequency of the k-th input component

CHAPTER 4

LARGE EXCITATION NONLINEAR ANALYSIS

4.1 Introduction

The most significant nonlinearities which produce nonlinear distortion in a receiver are found in electronic devices such as transistors and vacuum tubes. The approach to distortion analysis is conditioned by the extent to which the important device nonlinearities are excited. We distinguish between the two cases of mild and strong excitation. Distortion analysis for mild excitation is adequately determined by the use of time-invariant Volterra series. For the determination of distortion under strong excitation conditions we must utilize the total, instead of the incremental small-signal, device models, as well as alternate analysis methods. Four approaches to the analysis of strong-signal nonlinear distortion are possible. These are:

1. Direct Time-Domain Approach

The nonlinear differential equations of the circuit are written, and the circuit is driven by the total input signal. The equations are integrated for a sufficient length of time for all transients to have decayed, and the resulting waveform analyzed by numerical Fourier transform techniques to determine the various frequency components. If the total input signal is periodic, the numerical integration can be speeded up by using Newton-Raphson techniques to find the periodic solution of the nonlinear differential equations.

2. Direct Frequency-Domain Approach (Periodic Solution)

By expressing all appropriate currents and voltages in a Fourier series, a set of nonlinear infinite matrix equations may be written. There will be one set of equations for each frequency component of interest with a nonlinear part of each equation due to the circuit nonlinearity. Solving the system by an iterative method, such as Newton-Raphson, requires two Fourier transforms per step in addition to the arithmetic associated with the iterative method. The method requires the truncation of infinite matrices. Accuracy can not be readily controlled and computation time is large.

3. Time-Variant Volterra Series Perturbation Method
(Time-Domain)

In many cases, the large excitation consists of the sum of a number of small signals plus one large signal such as a local oscillator waveform. The nonlinear differential equations of the circuit are written, and the circuit is driven by the large-signal alone. The resulting time-domain response of the nonlinear circuit is found by numerical integration. Then, using this solution as a time-varying operating point, the small-signals are introduced in a time-domain perturbation analysis of the nonlinear circuit, and the resulting linear differential equations solved in the time-domain for the time-varying nonlinear transfer functions.

4. Time-Variant Volterra Series Perturbation Method
(Frequency-Domain)

The nonlinear circuit is driven by the large-signal and the operating-point response is determined by numerical integration identical to that described in the previous method. The nonlinear transfer functions are, however, determined in the frequency-domain in a manner similar to the mild excitation case. The resulting time-variant nonlinear transfer functions are used to determine the total response to both the strong-input and the small signal. The method requires the truncation of infinite matrices. It has not proved to

be a satisfactory technique because the accuracy of the distortion solution can not be readily controlled, and also because computation time is very large.

The important difference between the direct approach and the time-varying Volterra series approach is that the direct approach attempts to solve the nonlinear state equations for the total excitation while the time-varying Volterra approach solves directly for the small-signal nonlinear responses by a perturbation method. Previous work in frequency-domain large local-oscillator perturbation analysis, as typified by Peterson and Hussey (1939), and Peterson and Llewellyn (1945), was limited to linear equivalent circuits. Of the four approaches, only (1), the direct time-domain and (3), the time-domain time-variant Volterra series, have the requisite accuracy and compatibility to be considered for use in nonlinear distortion analysis. Their application is the subject of this chapter.

Before embarking upon the mathematical details necessary to formulate and solve a general nonlinear problem it is helpful to outline some preliminary requirements. First, the circuit must be described dynamically by a set of ordinary nonlinear differential equations in terms of the state variables of the system. Fundamental introductory material relevant to the state formulation of linear time-varying as well as nonlinear systems of ordinary differential equations is given by Polak and Wong (1970), Schwarz and Friedland (1965), Kim and Meadow (1971), and Zadeh and Desoer (1963). The nonlinear state equations must be numerically solved in order to find time-domain solutions. The differential equations of electronic circuits are of the

class called "stiff" equations" (Callahan, 1972) because they have both long and short time constants. Techniques for solving systems of stiff equations have been developed [Gear (1971)]. Many of the cases which will be discussed will involve determining the periodic solution to nonlinear differential equations. Solutions can be found by applying Newton-Raphson nonlinear iteration techniques as developed by Aprille (1971, 1972).

4.2 Large-Excitation Time-Domain Formulation

The fundamental starting point for the analysis of strongly-driven nonlinear circuits, or systems, is the set of nonlinear differential equations, or state equations, characterizing the nonlinear dynamical behavior of the system. For example, a very simple single-loop nonlinear circuit involving a fixed resistance R , fixed inductance L , and nonlinear resistance in the form of a diode is shown in Fig. 4.1. The circuit stores energy in the inductor magnetic field and, therefore, is a nonlinear circuit with memory. The source voltage u drives the system to produce a loop current j with the instantaneous voltage u_d across the diode nonlinearly related to the instantaneous diode current which is also the loop current j . Direct applications of Kirchoff's voltage law gives the nonlinear ordinary differential, or state equation

$$\frac{dj}{dt} = -\frac{R}{L}j - \frac{u_d(j)}{L} + \frac{u}{L}. \quad (4.1)$$

Thus the single-loop circuit with a single energy storage element results in a scalar state equation in one variable. Solution of the circuit is understood to mean determination of the time-

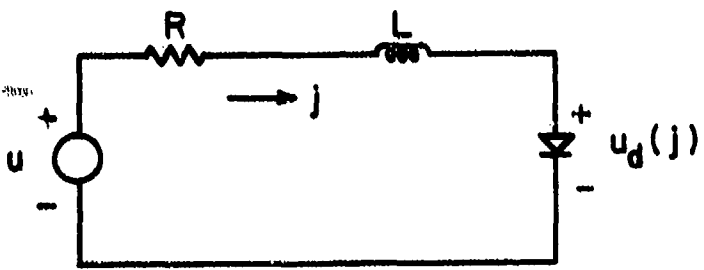


Fig. 4.1. Single-Loop Circuit with Energy Storage.

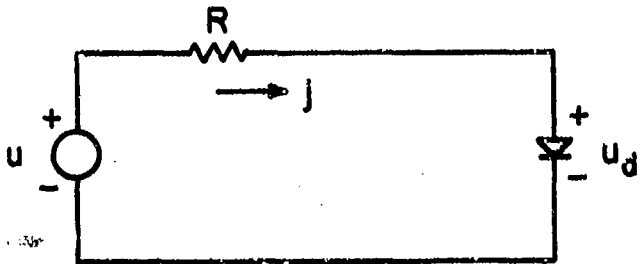


Fig. 4.2. Broadband or Resistive Single-Loop Example.

dependent current j as forced by voltage source u for an initial value of inductor current. The specific nonlinear relationship between diode voltage and current must be known to obtain the solution. For example, for a semiconductor diode

$$j = I_s [e^{\frac{au_d}{kT}} - 1]. \quad (4.2)$$

It is understood that the excitation u is sufficiently large that the problem is a large-signal problem and, therefore, that small signal approximations to Eq. (4.2) are inadequate. A small-signal approximation implies that $au_d \ll 1$, where u_d is the diode total instantaneous voltage.

4.2.1 Direct Solution by Numerical Integration

The direct solution of Eq. (4.1) in the time-domain involves numerical integration performed on a digital computer with sufficient precision to obtain the required result. We shall not embark at this point upon a discussion of numerical solution methods but, instead, will concentrate upon alternative approaches to the strongly-excited system. In the process of doing this we shall subsequently recognize that the direct time-domain numerical analysis methods are also needed to implement perturbation analysis methods. We shall later in the chapter review and discuss a variety of numerical methods for obtaining solutions to the classes of nonlinear differential equations that are of interest.

4.2.2 Power-Series Solution for a Memoryless Example

Small-signal Volterra series methods could be applied to obtain a series solution to Eq. (4.1). A typical example of the difficulties that arise for a strong excitation situation

occurs for the elementary circuit shown in Fig. 4.2. The system is now memoryless and the instantaneous relationship between the input voltage and response current is given by the transcendental equation

$$j = I_s [e^{\alpha(u-Rj)} - 1], \quad (4.3)$$

where we have assumed that Eq. (4.2) describes the nonlinear relationship between diode voltage and current.

Power-series solutions to Eq. (4.3) have been obtained by a number of investigators, e.g., Herishen (1967), and Lotsch (1968). The procedure is to write Eq. (4.3) in the form

$$(j + I_s)e^{\alpha Rj} = I_s e^{\alpha u}, \quad (4.4)$$

and expand the left-hand side in a Taylor series in j about $j=0$. This step is followed by a series reversion [See Abramovitz and Stegun, p. 16(1964)] to obtain j as a power series in terms of the source voltage u . The method has not proved adequate for reasonable values of current j . The reason for this is that, under normal interesting circumstances, $\alpha Rj \gg 1$ and the power-series expansion requires an enormous number of terms for adequate convergence. For example, the requirement for a few terms limits $\alpha Rj \approx 1$ or

$$j \approx \frac{1}{\alpha R}. \quad (4.5)$$

For semiconductor diodes, $\frac{1}{\alpha} \approx 25$ mV. If $R = 1000 \Omega$, the maximum current is limited to 25 μ A. It is not unusual to drive a diode in a mixer application with a peak current of 5 mA through a resistive impedance of 100 ohms. For these values, $\alpha Rj = 20$.

4.3 Large-Signal Perturbation Method

Significant progress can be made towards an analysis of strongly-excited nonlinear communications receivers by extending the nonlinear transfer function concept to strongly-driven networks through recognizing that the large signal driving the system may be a known (and often periodic) excitation while the unknown excitation will frequently be small. An important example arises in the case of frequency-converters or mixers. The local-oscillator level is frequently large while, over the range of significant interest, the input signal is small and arises from a multi-signal environment such that the signal components may consist of several unknown waveforms. One is often interested in the nonlinear distortion properties of a frequency-converter under these circumstances. Typical questions needing to be addressed include how the intermodulation products resulting from a two-tone small-signal excitation depend upon the local-oscillator waveform and drive level. A method is needed that is applicable when there are significant frequency-dependent elements present in the nonlinear system.

The circuit shown in Fig. 4.1 provides a simple example to begin an investigation when the strong-excitation is known and the small-signal excitation is arbitrary. The network has frequency-dependent energy storage. The state equation describing the nonlinear and time-dependent dynamic characteristics of the current $j(t)$ resulting from the voltage excitation $u(t)$ for the nonlinear circuit was given in Eq. (4.1) which can be written in the form

$$L \frac{d}{dt} j(t) = -Rj(t) - u_d(j) + u(t), \quad (4.6)$$

where R and L are constants and $u_d(j)$ expresses the nonlinear dependence of the diode voltage $u_d(t)$ upon the loop current $j(t)$.

We seek a steady-state forced solution of Eq. (4.6) under the assumption that

$$u(t) = v_o(t) + v(t), \quad (4.7)$$

where $v_o(t)$ will be assumed periodic and is the large excitation voltage. Voltage $v(t)$ is a weak excitation with arbitrary time dependence. Both $v_o(t)$ and $v(t)$ are real time functions. Let the period of $v_o(t)$ be T , so that

$$v_o(t) = v_o(t+T). \quad (4.8)$$

4.3.1 State Equations for Strongly-Driven and Weakly-Driven Equivalent Systems

In this section we shall derive two state equations for the system defined by Eq. (4.6). The first equation, called the operating-point state equation, will characterize the current i_o resulting from the strong excitation v_o . The second equation, called the perturbation equation, will characterize the current i resulting from the weak excitation v . It will be shown that the weak-signal state equation depends strongly upon i_o , the solution of the operating-point state equation.

By hypothesis

$$j(t) = i_o(t) + i(t), \quad (4.9)$$

where, as noted above, $i_o(t)$ is the large-signal response and $i(t)$ is the small-signal response. Also, let the diode voltage

$$u_d(i_o + i) = u_d(i_o) + v_d. \quad (4.10)$$

where $u_d(i_o)$ is the diode voltage due to the strong drive v_o and $v_d(t)$ is the additional diode voltage associated with the weak excitation $v(t)$. We may expand $u_d(i_o + i)$ in a Taylor series expansion about the current i_o to obtain

$$u_d(i_o + i) = u_d(i_o) + \left. \frac{\partial u_d}{\partial j} \right|_{j=i_o} i + \left. \frac{1}{2!} \frac{\partial^2 u_d}{\partial j^2} \right|_{j=i_o} i^2 + \dots \quad (4.11)$$

We recognize immediately that v_d is a nonlinear function of current i given by

$$\begin{aligned} v_d(i; i_o) &= u_d(i_o + i) - u_d(i_o) \\ &= r_1(t)i + r_2(t)i^2 + \dots + r_n(t)i^n + \dots, \end{aligned} \quad (4.12)$$

where the coefficients of the Taylor series, given by

$$r_n(t) = \left. \frac{1}{n!} \frac{\partial^n u_d}{\partial j^n} \right|_{j=i_o}, \quad (4.13)$$

are time-varying and depend upon the strong-excitation time-varying current i_o .

With these preliminary results, we may now write the system state equation in the form

$$L \frac{di_o}{dt} + L \frac{di}{dt} = -Ri_o - Ri - u_d'(i_o) - v_d(i; i_o) + v_o + v, \quad (4.14)$$

which may be separated into two differential equations which must be simultaneously satisfied. They are the

Operating-Point Equation (OPE)

$$L \frac{di_o}{dt} = -Ri_o - u_d(i_o) + v_o, \quad (4.15)$$

and the

Perturbation Equation (PE)

$$L \frac{di}{dt} = -Ri - v_d(i; i_o) + v. \quad (4.16)$$

Equation (4.15) is the operating-point equation (OPE) whose solution characterizes the time-varying state of the circuit as driven by the strong excitation v_o . For example, if $v_o(t)$ is a periodic local-oscillator waveform for a mixer, the solution $i_o(t)$ describes the periodic response to the local-oscillator waveform. Note that Eq. (4.15) is a nonlinear differential equation with time-invariant coefficients L and R. The desired solution to periodic excitation v_o is the periodic response i_o .

The second differential equation given by Eq. (4.16) is the nonlinear perturbation equation (FE) whose solution characterizes the response $i(t)$ of the network in Fig. 4.1 to a small-signal excitation, v , while the network is simultaneously being strongly-driven by voltage v_o to produce strong-excitation current i_o . In Fig. 4.3 we show a small-signal equivalent circuit whose response i to voltage v is identical to the solution of the perturbation equation when the nonlinear dependence of the diode

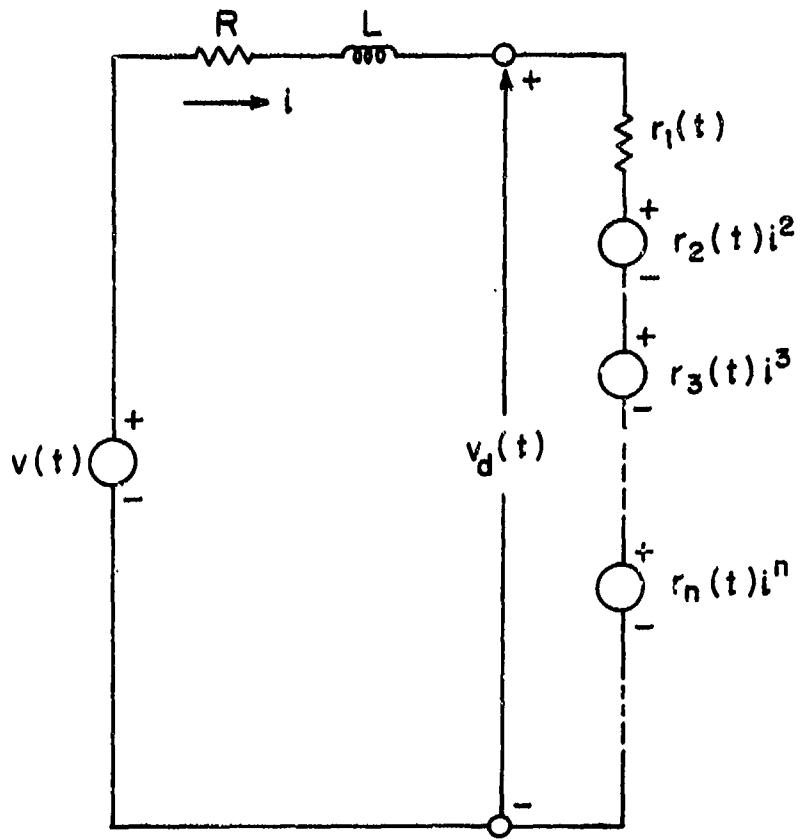


Fig. 4.3. Small-Signal Equivalent Nonlinear Time-Varying Circuit.

voltage v_d is given by the time-varying Taylor series expansion given by Eq. (4.12). The significant fact to observe is that the unknown current i forced by the excitation v requires the solution of a time-varying nonlinear network containing an energy storage element (the inductor). The time-variation is caused by the time-dependent set of coefficients $\{r_1, r_2, \dots, r_n, \dots\}$. The nonlinearity is caused by the dependence upon the current set $\{i, i^2, i^3, \dots, i^n\}$. We are interested in current i when the set of coefficients $\{r_1, r_2, r_3, \dots, r_n, \dots\}$ is periodically time-variant and have been previously determined from Eq. (4.13) by having numerically solved the nonlinear operating-point equation for i_o .

4.3.2 Power-Series Perturbation Solution Example

If we set $L=0$ in both Eqs. (4.15) and (4.16) we have the operating-point equation and perturbation equation applicable to the resistive network shown in Fig. 4.2. For a semiconductor diode characterized by Eq. (4.2), the operating-point equation becomes

$$i_o = I_s [e^{\alpha(v_o - R_i o)} - 1]. \quad (4.17)$$

The solution of this transcendental equation for a known waveform $v_o(t)$ gives the diode operating-point current $i_o(t)$.

For $L=0$, the perturbation equation becomes

$$\begin{aligned} v &= Ri + v_a(i, i_o) \\ &= [R + r_1(t)]i + r_2(t)i^2 \\ &\quad + \dots + r_n(t)i^n + \dots, \end{aligned} \quad (4.18)$$

where $r_n(t)$ is given by Eq. (4.13). For the semiconductor diode we have

$$r_n(t) = \frac{1}{\alpha} \frac{1}{n!} \left. \frac{\partial^n}{\partial j^n} \ln \left[1 + \frac{i}{I_s} \right] \right|_{j=i_o(t)} . \quad (4.19)$$

The power series given by Eq. (4.18) can now be reverted [Ambramovitz and Stegun, p. 16 (1964)] to express the small-signal current i in terms of small-signal source v . The result is

$$i(t) = \sum_{q=1}^{\infty} a_q(t) v(t)^q , \quad (4.20)$$

with the first three time-varying coefficients given by

$$a_1(t) = \alpha \frac{i_o + I_s}{1 + \alpha R(i_o + I_s)} , \quad (4.21)$$

$$a_2(t) = \frac{\alpha^2}{2!} \frac{i_o + I_s}{[1 + \alpha R(i_o + I_s)]^3} , \quad (4.22)$$

$$a_3(t) = \frac{\alpha^3}{3!} \frac{(i_o + I_s)[1 - 2\alpha R(i_o + I_s)]}{[1 + \alpha R(i_o + I_s)]^5} . \quad (4.23)$$

Eq. (4.20) is a solution of the nonlinear resistive diode circuit and is valid for any value of current i_o obtained from the solution for the operating-point, Eq. (4.17). If the large excitation v_o is periodic, i_o is also periodic. A good example arises when v_o is the local-oscillator waveform for a diode mixer. It follows also

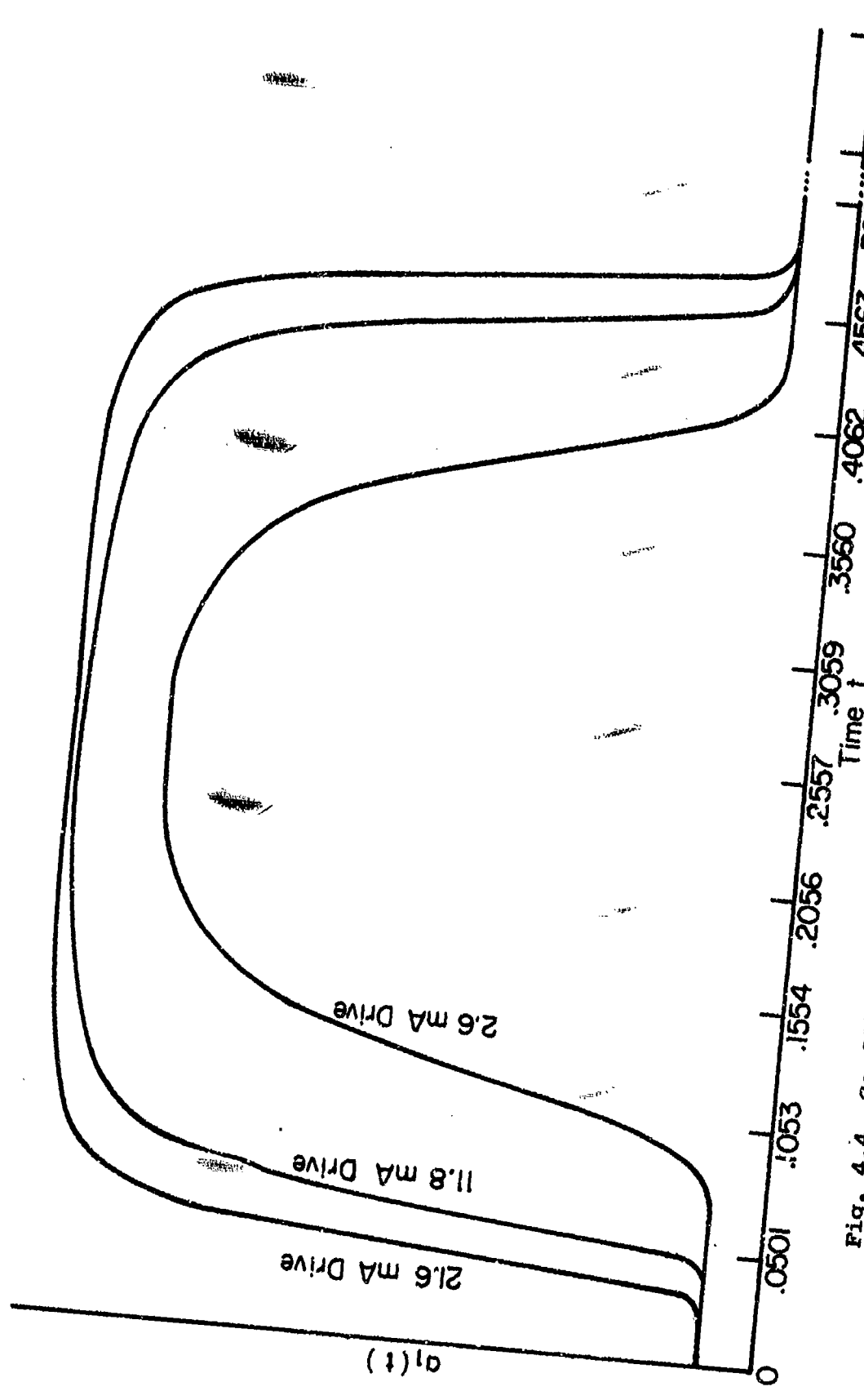
that the time-varying coefficients a_q are also periodic and, therefore, have a Fourier series representation in terms of harmonics of the local-oscillator frequency. Then

$$i(t) = \sum_{q=1}^{\infty} \sum_{p=0}^{\infty} v^q(t) a_{pq} \sin(2\pi p f_o t + \phi_{pq}), \quad (4.24)$$

where a_{pq} and ϕ_{pq} are the amplitude and phase of the Fourier expansion of $v^q(t)$ for the p^{th} harmonic of the local-oscillator frequency f_o .

Figures 4.4, 4.5, and 4.6 show, on a normalized linear scale, the coefficients $a_1(t)$, $a_2(t)$ and $a_3(t)$ for one period of a sinusoidal local-oscillator voltage waveform. Each of the coefficients has been evaluated for three values of local-oscillator peak current, namely, 2.6 mA, 11.8 mA, and 21.6 mA. The effects of increasing the local-oscillator drive are clearly evident. The first-order coefficient, $a_1(t)$, approaches a rectangular pulse, while the second and third-order coefficients approach waveforms which have rapid, impulsive and doublet-like waveforms at the time intervals associated with the sinusoidal local-oscillator voltage passing through zero. If the local oscillator were a square wave, $a_1(t)$ would be a square wave and the spikes would have zero width. Thus the difference in distortion between a square-wave and a sine-wave local oscillator drive is contained in the transition regions. From these waveforms one can clearly see the desirability of operating a diode mixer with a large local-oscillator drive in order to make transition regions as narrow as possible.

Fig. 4.4. Coefficient $a_1(t)$ for Sinusoidal Local Oscillator Waveform.



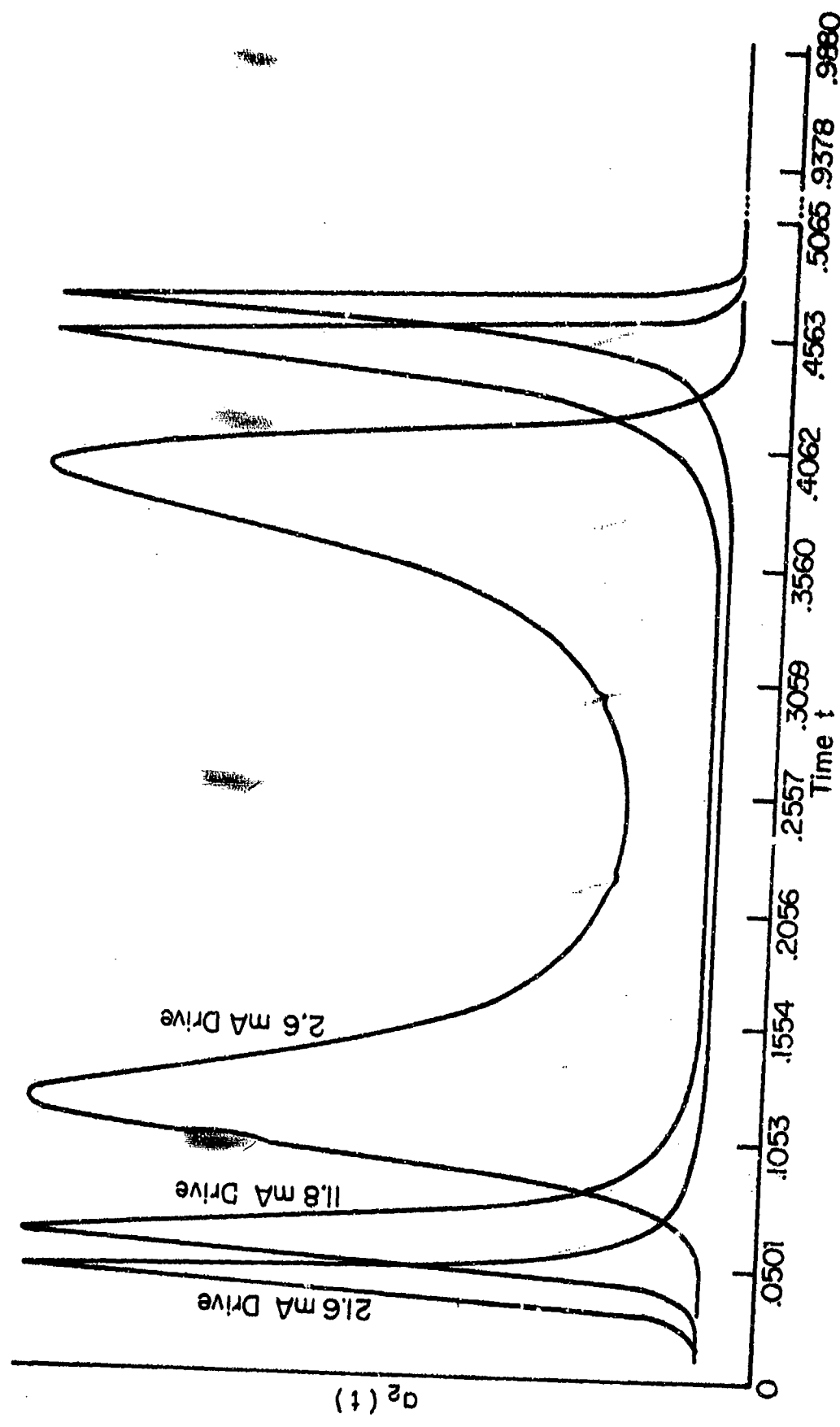


Fig. 4.5. Coefficient $a_2(t)$ for a Sigmoidal Local Oscillator Waveform.

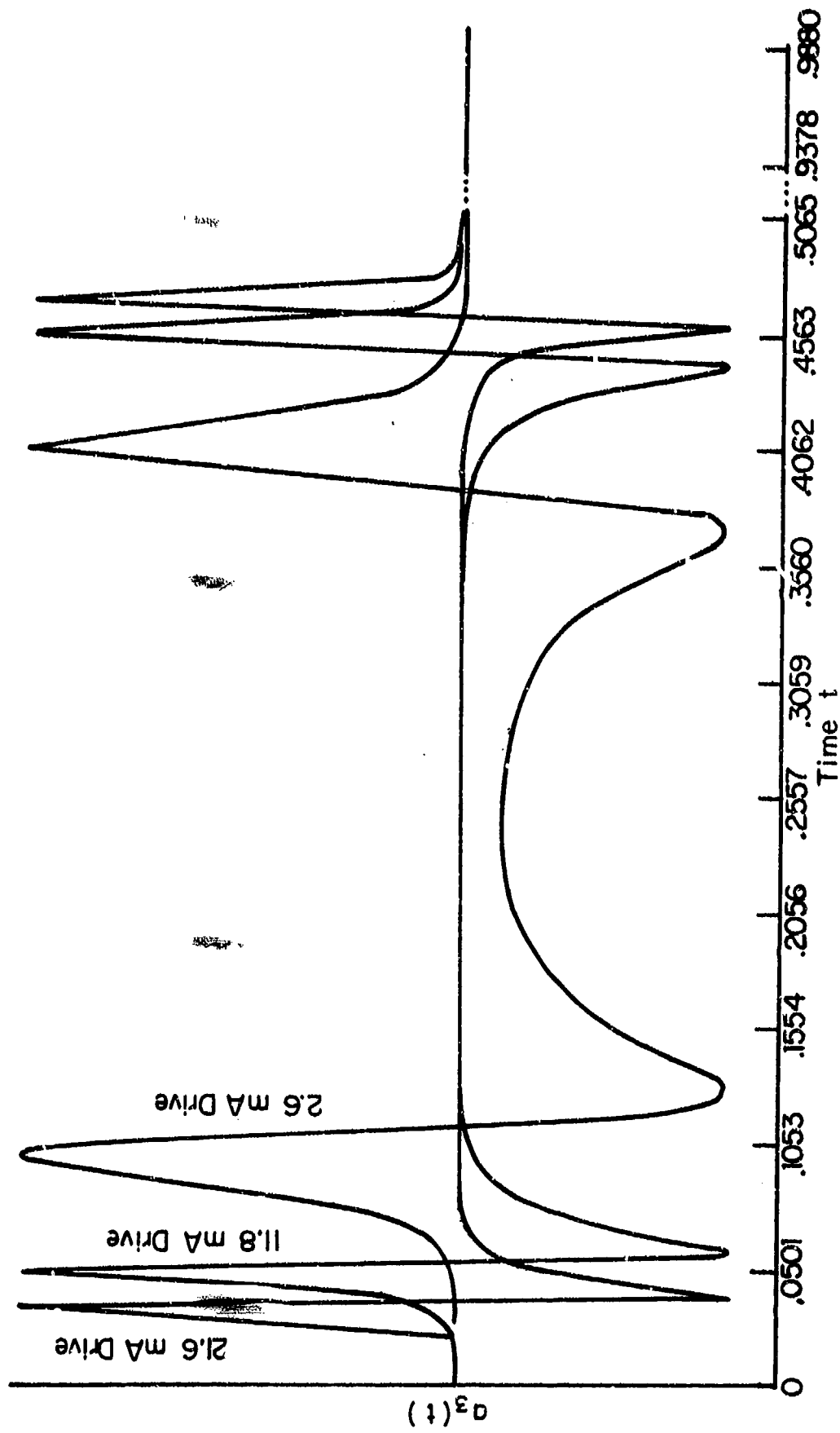


Fig. 4.6. Coefficient $a_3(t)$ for a Sinusoidal Local Oscillator Waveform.

Figures 4.4 through 4.7 also clearly show the desirability of using an integration algorithm which incorporates a variable step size when the nonlinear perturbation equation must be numerically integrated. The time-varying waveforms are divided into regions of little change in which large integration step sizes would be appropriate but there are very significant short intervals in which great activity takes place. A small step size would be needed in such a region.

4.3.3 Separation of the Small-Signal Perturbation System into Time-Variant Linear Subsystems

If there is energy storage ($L \neq 0$) in our simple example as we have described in Section 4.3.1, the solution to the perturbation equation (4.16) can not be written in a power series form as we have done in Section 4.3.2, Eq. (4.18).

We have noted in Section 4.3.1 that the current $i(t)$ is the response of a time-variant nonlinear system having memory. The fact that the circuit has memory necessitates the use of a differential equation approach. The current $i(t)$ can be expanded in a time-variant Volterra functional series

$$i(t) = \sum_n i_n(t), \quad (4.25)$$

where the first order, or linear, term is

$$i_1(t) = \int_{-\infty}^t h_1(t; \tau_1) v(t-\tau_1) d\tau_1. \quad (4.26)$$

The second order term is

$$i_2(t) = \int_{-\infty}^t \int_{-\infty}^t h_2(t; \tau_1, \tau_2) v(t - \tau_1) v(t - \tau_2) d\tau_1 d\tau_2, \quad (4.27)$$

and the general n'th order term is

$$i_n(t) = \int_{-\infty}^t \cdots \int_{-\infty}^t h_n(t; \tau_1 \cdots \tau_n) \prod_{i=1}^n v(t - \tau_i) d\tau_i. \quad (4.28)$$

For the problem at hand, v is the small-signal input and the $i_n(t)$ are the individual order nonlinear responses of the system expressed in terms of the time-variant Volterra kernels h_n .

We shall now show, by employing a decomposition of currents by nonlinear orders as given by Eq. (4.25), that the time-varying nonlinear system can be decomposed into a series of linear time-variant subsystems whose solutions are the nonlinear responses of individual order. This property depends only upon the additive properties of Eq. (4.25) and does not require the use of the integral time-variant expression for the individual terms as given by Eq. (4.28).

We wish to solve the periodically time-varying nonlinear perturbation equation [See Eqs. (4.12) and (4.16)],

$$L \frac{di}{dt} = -Ri - \sum_k r_k(t) i^k + v, \quad (4.29)$$

where

$$i = \sum_n i_n(t). \quad (4.30)$$

We shall seek the solution here for terms including up to third-order nonlinearities. Hence, we are interested in the terms

$$\sum_{k=1}^3 r_k(t)i^k = r_1(t)i + r_2(t)i^2 + r_3(t)i^3, \quad (4.31)$$

where, to third-order nonlinearities,

$$i = i_1 + i_2 + i_3, \quad (4.32)$$

$$i^2 = i_1^2 + 2i_1 i_2, \quad (4.33)$$

$$i^3 = i_1^3. \quad (4.34)$$

To third-order nonlinearities, Eq. (4.29) now reduces to

$$\begin{aligned} L \frac{di_1}{dt} + L \frac{di_2}{dt} + L \frac{di_3}{dt} &= \\ - Ri_1 - Ri_2 - Ri_3 \\ - r_1 i_1 - r_1 i_2 - r_1 i_3 \\ - r_2 i_1^2 - 2r_2 i_1 i_2 \\ - r_3 i_1^3 \\ + v. \end{aligned} \quad (4.35)$$

This result may now be separated into a time-varying linear differential equation for each order nonlinearity. For first-order, we have

$$L \frac{di_1}{dt} = - [R+r_1(t)] i_1 + v. \quad (4.36)$$

For second-order

$$L \frac{di_2}{dt} = - [R+r_1(t)]i_2 - r_2(t)i_1^2. \quad (4.37)$$

For third-order

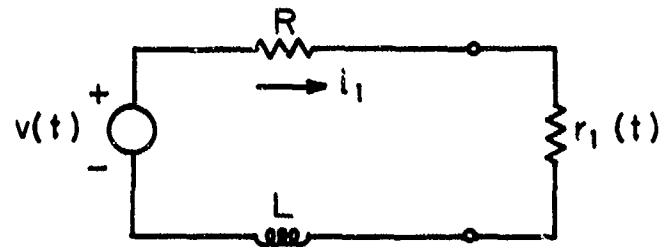
$$L \frac{di_3}{dt} = - [R+r_1(t)]i_3 - 2r_2(t)i_1i_2 - r_3(t)i_1^3. \quad (4.38)$$

For each order nonlinear component of current an equivalent linear time-varying circuit can be drawn, as illustrated in Fig. 4.7. Note the dependent source exciting the second-order circuit. This source is known once the first-order system is solved. In a like manner, the sources exciting the third-order system are known from the solutions of the first and second-order. Note also that interaction between the first and second-order currents excites a third-order current.

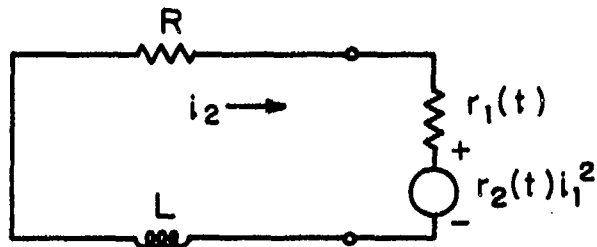
4.3.4 Small-Signal Equations for the Time-Variant Nonlinear Transfer Functions

The time-varying nonlinear small-signal response problem has now been reduced to a set of sub-problems involving the solutions of linear time-varying networks. Since linearity now applies for small signals, the problem can be formulated in a form suitable for arbitrary waveforms. For example, for the linear component of current, we have

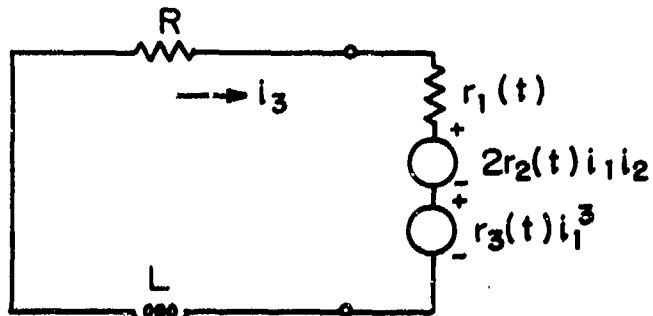
$$i_1(t) = \int_{-\infty}^t h_1(t; \tau_1) v(t-\tau_1) d\tau_1, \quad (4.39)$$



a. First-order linear equivalent circuit.



b. Second-order linear equivalent circuit.



c. Third-order linear equivalent circuit.

Fig. 4.7. Decomposition of the Nonlinear Circuit into Linear Sub-Systems for each Order Nonlinearity.

where $v(t)$ is the small-signal excitation.

Since

$$v(t) = \int_{-\infty}^{\infty} v(f) e^{j2\pi ft} df, \quad (4.40)$$

it is convenient to determine $I_1(f; t)$, the frequency spectrum of $i_1(t)$, by the product form

$$I_1(f; t) = H_1(t; f) v(f), \quad (4.41)$$

where $H_1(t; f)$ is the first-order time-varying nonlinear transfer function. Now $i_1(t)$ can be determined by inversion to the time-domain, or

$$i_1(t) = \int_{-\infty}^{\infty} H_1(t; f) v(f) e^{j2\pi ft} df. \quad (4.42)$$

The question is, of course, how to obtain $H_1(t; f)$ and, for the higher-order nonlinearities, the higher-order nonlinear transfer functions $H_n(t; f_1, f_2, \dots, f_n)$. We shall now show that the subsystem differential equations for various nonlinearities, for example Eqs. (4.36) to (4.38), can be put in a form from which the required H_n can be obtained by numerical integration. The solution is shown to be the periodic solution of a time-varying linear ordinary differential equation.

4.3.4.1 First Order Transfer Function

Let

$$v(t) = E_1(f) e^{j2\pi ft}. \quad (4.43)$$

The first-order component of current for such an excitation is, from Eq. (4.39),

$$i_1(t) = E_1(f)H_1(t;f) e^{j2\pi ft}, \quad (4.44)$$

where

$$H_1(t;f) = \int_{-\infty}^t h_1(t;\tau_1) e^{-j2\pi f\tau_1} d\tau_1. \quad (4.45)$$

Inserting the expression given by Eq. (4.44) into the first-order system differential equation (4.36) and carrying out the indicated differentiation results in

$$\begin{aligned} & L \left[\frac{d}{dt} H_1(t;f) + j2\pi f H_1(t;f) \right] E_1(f) e^{j2\pi ft} \\ &= - [R + r_1(t)] H_1(t;f) E_1(f) e^{j2\pi ft} \\ &+ E_1(f) e^{j2\pi ft}. \end{aligned} \quad (4.46)$$

Cancelling common factors and re-arranging

$$L \frac{d}{dt} H_1(t;f) = - [R + r_1(t) + j2\pi f L] H_1(t;f) + 1. \quad (4.47)$$

Note that the bracketed term in the right-hand side of Equation (4.47) is the time-varying linearized loop impedance. Equation (4.47) is a linear state equation with a time-varying coefficient $r_1(t)$, the solution of which is the time-varying transfer function $H_1(t;f)$. For the case of interest, $r_1(t)$ is periodic and known

from the numerical solution of the operating point equation, Eq. (4.15). Therefore, for any f and known R and L , $H_1(t;f)$ is simply the periodic solution of Equation (4.47), a time-varying ordinary linear differential equation. H_1 is a complex quantity, so both its real and imaginary periodic components are required. Solutions are periodic since we have assumed the strong-signal operating point equation to be periodic.

If the inductor L is zero, the circuit reduces to the resistive diode circuit analyzed in Section 4.3.2, and, from Eq. (4.47), $H_1(t;f)$ is given by

$$H_1(t;f) = \frac{1}{R + r_1(t)}. \quad (4.48)$$

For the semiconductor diode,

$$j(t) = I_s [e^{\alpha u_d(t)} - 1], \quad (4.49)$$

or

$$\ln[j(t) + I_s] - \ln I_s = \alpha u_d(t). \quad (4.50)$$

Using Eqs. (4.13) and (4.50),

$$r_1(t) = \left. \frac{\partial u_d}{\partial j} \right|_{j=i_o} = \frac{1}{\alpha [i_o + I_s]} . \quad (4.51)$$

After substitution in Eq. (4.48), we finally have

$$H_1(t;f) = \frac{\alpha [i_o + I_s]}{1 + \alpha R [i_o + I_s]}. \quad (4.52)$$

This result is identical to the $a_1(t)$ coefficient previously found for the memoryless example in Section 4.3.2.

4.3.4.2 Second-Order Nonlinear Transfer Function

The differential equation giving the second-order nonlinear transfer function can be found when the second-order system is excited by

$$v(t) = E_1 e^{j2\pi f_1 t} + E_2 e^{j2\pi f_2 t}. \quad (4.53)$$

In particular, we are interested in the portion of the second-order response containing the factor $\exp[j2\pi(f_1+f_2)t]$. The response is denoted by $i_2(t; f_1+f_2)$. Inserting Eq. (4.53) into Eq. (4.27) and retaining only the desired frequency term results in

$$i_2(t; f_1+f_2) = 2E_1 E_2 H_2(t; f_1, f_2) e^{j2\pi(f_1+f_2)t}, \quad (4.54)$$

where

$$H_2(t; f_1, f_2) = \int_{-\infty}^t \int h_2(t; \tau_1, \tau_2) e^{-j2\pi f_1 \tau_1} e^{-j2\pi f_2 \tau_2} d\tau_1 d\tau_2. \quad (4.55)$$

From Eq. (4.37) we also need $i_1^2(t)$ to complete the translation to the frequency-domain. Again, only the components of $i_1^2(t)$ containing the factor $\exp[j2\pi(f_1+f_2)t]$ are of interest. For a two-tone input,

$$i_1(t) = E_1 H_1(t; f_1) e^{j2\pi f_1 t} + E_2 H_1(t; f_2) e^{j2\pi f_2 t}, \quad (4.56)$$

from which

$$i_1^2(t; f_1+f_2) = 2E_1 E_2 H_1(t; f_1) H_1(t; f_2) e^{j2\pi(f_1+f_2)t}. \quad (4.57)$$

Finally, substituting Eqs. (4.54) and (4.57) into Eq. (4.37), we obtain

$$L \frac{d}{dt} H_2(t; f_1, f_2) = -[R + r_1(t) + j2\pi(f_1 + f_2)L]H_2(t; f_1, f_2) \\ - r_2(t) H_1(t; f_1) H_1(t; f_2), \quad (4.58)$$

after common factors are cancelled. This equation is also a linear ordinary differential equation with time-varying coefficients. The periodic solution can be obtained by numerical integration for known $r_1(t)$ and $r_2(t)$ for frequencies f_1 and f_2 .

The solution for $L=0$ is

$$H_2(t; f_1, f_2) = -\frac{r_2(t) H_1(t; f_1) H_1(t; f_2)}{R + r_1(t)}. \quad (4.59)$$

Substituting Eq. (4.48) results in

$$H_2(t; f_1, f_2) = \frac{-r_2(t)}{[R + r_1(t)]^3}. \quad (4.60)$$

From Eqs. (4.13) and (4.50),

$$r_2(t) = \frac{1}{2!} \frac{-1}{\alpha[i_o + I_s]^2}. \quad (4.61)$$

Putting $r_1(t)$ from Eq. (4.51) and $r_2(t)$ in Eq. (4.60) gives

$$H_2(t; f_1, f_2) = \frac{2}{2!} \frac{i_o + I_s}{[1 + \alpha P(i_o + I_s)]^3}. \quad (4.62)$$

This result is the same as the $a_2(t)$ coefficient of the second term in the power series solution given in Section 4.3.2.

4.3.4.3 Third-Order Nonlinear Transfer function

The third-order nonlinear transfer function for the system describes the third-order system response when the system is excited by

$$v(t) = E_1 e^{j2\pi f_1 t} + E_2 e^{j2\pi f_2 t} + E_3 e^{j2\pi f_3 t} \quad (4.63)$$

In particular, we are interested in the portion of the third-order response containing the factor $\exp[j2\pi(f_1+f_2+f_3)t]$. This response is denoted by $i_3(t; f_1+f_2+f_3)$. Inserting Eq. (4.63) into the third-order term in Eq. (4.28) and retaining only the desired frequency term results in

$$i_3(t; f_1+f_2+f_3) = 6E_1 E_2 E_3 H_3(t; f_1, f_2, f_3) e^{j2\pi(f_1+f_2+f_3)t}, \quad (4.64)$$

where

$$H_3(t; f_1, f_2, f_3) = \iiint_{-\infty}^t h_3(t; \tau_1, \tau_2, \tau_3) e^{-j2\pi(f_1\tau_1 + f_2\tau_2 + f_3\tau_3)} d\tau_1 d\tau_2 d\tau_3. \quad (4.65)$$

We also need i_1 , i_2 and i_1^3 , the driving terms of Eq. (4.38), to complete the translation of the differential equation to the frequency domain. Again, only components containing the factor $\exp[j2\pi(f_1+f_2+f_3)t]$ are of interest. Since

$$i_1(t) = E_1 H_1(t; f_1) e^{j2\pi f_1 t} + E_2 \overline{H}_1(t; f_2) e^{j2\pi f_2 t} \\ + E_3 H_1(t; f_3) e^{j2\pi f_3 t}, \quad (4.66)$$

the required third-order component of $i_1^3(t)$ is

$$i_1^3(t; f_1 + f_2 + f_3) = 6 E_1 E_2 E_3 H_1(t; f_1) \overline{H}_1(t; f_2) H_1(t; f_3) \\ \cdot e^{j2\pi(f_1 + f_2 + f_3)t}. \quad (4.67)$$

Now, if $f_i \neq f_j \neq f_k$, the component of $i_1(t) i_2(t)$ of interest is

$$12 E_1 E_2 E_3 \overline{H}_1(t; f_i) \overline{H}_2(t; f_j, f_k) e^{j2\pi(f_1 + f_2 + f_3)t}, \quad (4.68)$$

where the overbar indicates a symmetrized nonlinear transfer function. Substituting Eqs. (4.64), (4.67), and (4.68) into Eq. (4.38) results in

$$\begin{aligned} \frac{d}{dt} H_3(t; f_1, f_2, f_3) &= - [R + r_1(t) + 2\pi j(f_1 + f_2 + f_3)L] H_3(t; f_1, f_2, f_3) \\ &\quad - 2r_2(t) \overline{H}_1(t; f_1) \overline{H}_2(t; f_2, f_3) \\ &\quad - r_3(t) H_1(t; f_1) H_1(t; f_2) H_1(t; f_3). \end{aligned} \quad (4.69)$$

Equation (4.69) is a linear ordinary differential equation with time-varying coefficients. As with $H_1(t; f_1)$ and $H_2(t; f_1, f_2)$, the solution for $H_3(t; f_1, f_2, f_3)$ with $L=0$ can be written explicitly and is

$$H_3(t) = \frac{-2r_2(t) H_1(t) H_2(t) - r_3(t) H_1(t)^3}{R + r_1(t)}, \quad (4.70)$$

where the frequency dependencies are omitted since the circuit is broadband. From Eq. (4.59)

$$H_2(t) = \frac{-r_2(t)}{R + r_1(t)} H_1^2(t). \quad (4.71)$$

Substituting Eq. (4.71) into Eq. (4.70) and simplifying

$$H_3(t) = \frac{2r_2^2(t) - r_3(t)[r_1(t) + R]}{[R + r_1(t)]^2} H_1^3(t). \quad (4.72)$$

But

$$r_1(t) = \frac{1}{\alpha(i_o + I_s)}, \quad (4.73)$$

$$r_2(t) = \frac{1}{2!} \cdot \frac{-1}{\alpha(i_o + I_s)^2}, \quad (4.74)$$

$$r_3(t) = \frac{1}{3!} \cdot \frac{2}{\alpha(i_o + I_s)^3}. \quad (4.75)$$

Therefore

$$H_3(t) = \frac{\alpha}{3!} \frac{(i_o + I_s)[1 - 2\alpha R(i_o + I_s)]}{[1 + \alpha R(i_o + I_s)]^5}. \quad (4.76)$$

Equation (4.76) is the same as the $a_3(t)$ coefficient of the third term in the power series solution found in Section 4.3.2.

4.3.3.4 Discussion

Linear ordinary differential equations for the higher-order nonlinear transfer functions may also be obtained by proceeding in a similar manner. From Eqs. (4.47), (4.58), and (4.69), it is seen that the differential equation for the general n^{th} -order time-varying nonlinear transfer function takes the form

$$\begin{aligned} L \frac{d}{dt} H_n(t; f_1, f_2, \dots, f_n) &= -[R + r_1(t) + 2\pi j(f_1 + f_2 + \dots + f_n)L] \\ &\cdot H_n(t; f_1, f_2, \dots, f_n) \\ &+ \text{nonlinear driving sources}, \quad (4.77) \end{aligned}$$

where the nonlinear driving sources are given in terms of the lower-order responses and the $r_n(t)$. The explicit form of the nonlinear driving sources will obey the recurrence relations derived in Section 2.2.4 for the time-invariant nonlinear transfer functions.

To proceed further requires the solution of the linear differential equations with time-varying coefficients derived in this section. Once the transfer functions are found, the various order linear and nonlinear components of current can be found

from Eq. (4.44), (4.54), and (4.64). Our example throughout this chapter has been a particularly simple single-loop situation. The method is, however, quite general but requires formulation in a multi-variable matrix form to accommodate more complex cases. We shall devote the remainder of this chapter to outlining some of these matters as well as outlining several approaches and considerations involved in the numerical solution of the differential equations arising in the formulation.

4.4 Formulation of State Equations

4.4.1 First Example

A more complicated nonlinear circuit example is illustrated in Fig. 4.8. Both the diode current i_d and capacitor C_d are nonlinear functions of the voltage v_d , or

$$i_d = i_d(v_d), \quad (4.78)$$

$$C_d = C_d(v_d). \quad (4.79)$$

An appropriate set of state variables for this network are the capacitor voltage v_d , the inductor current i_3 and the capacitor voltage v_2 . We now proceed to generate the state equations. The nonlinear capacitor current is

$$C_d \frac{dv_d}{dt} = \frac{u - (v_d + v_2)}{R_1} - i_d. \quad (4.80)$$

The inductor voltage is

$$L_2 \frac{di_3}{dt} = v_2. \quad (4.81)$$

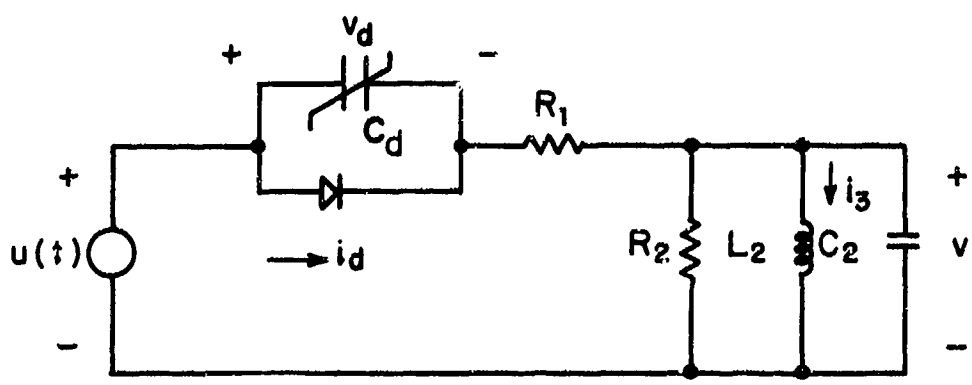


Fig. 4.8. A Multiple-Node Nonlinear Circuit

and, the current through capacitor C_2 is

$$C_2 \frac{dv_2}{dt} = \frac{u - (v_d + v_2)}{R_1} - \frac{v_2}{R_2} - i_3, \quad (4.82)$$

These three equations may now be written in matrix form

$$\begin{bmatrix} \dot{v}_d \\ i_3 \\ \dot{v}_2 \end{bmatrix} = \begin{bmatrix} 0 & 0 & 0 \\ 0 & 0 & \frac{1}{L_2} \\ -\frac{1}{R_1 C_2} & -\frac{1}{C_2} & -\frac{1}{C_2} \left(\frac{1}{R_1} + \frac{1}{R_2} \right) \end{bmatrix} \begin{bmatrix} v_d \\ i_3 \\ v_2 \end{bmatrix} + \begin{bmatrix} -\frac{v_d}{R_1 C_d} - \frac{v_2}{R_1 C_d} + \frac{u}{R_1 C_d} \\ 0 \\ \frac{u}{R_1 C_2} \end{bmatrix}, \quad (4.83)$$

where both i_d and C_d are nonlinear functions of the state variable v_d and the overdot on the left-hand-side signifies the time derivative.

Equation (4.83) is in the form

$$\dot{\underline{x}} = \underline{A} \underline{x} + \underline{f}(\underline{x}, \underline{u}), \quad (4.84)$$

where \underline{x} is the state variable vector and \underline{A} is a constant matrix. The matrix function $\underline{f}(\underline{x}, \underline{u})$ accounts for the nonlinear terms. One can absorb the first term and obtain the normal form of the state equations in matrix form, or

$$\dot{\underline{x}} = \underline{k}(\underline{x}, \underline{u}), \quad (4.85)$$

where \underline{k} is a matrix that is, in general, nonlinearly dependent upon the state variables \underline{x} and network forcing function \underline{u} .

4.4.2 A Formal Method

We next present a more detailed description of how to generate the state equations of more complex networks. The example leads to a set of state equations of the form given by Eq. (4.85). We follow the formal and general methods of Bashkow (1957), Bryant (1962), and Wilson and Massena (1965) for writing the state equations of a network. Definitions required are:

- i) A branch contains a single element only.
- ii) A tree is a subgraph or subnetwork connecting all nodes but having no closed paths or loops.
- iii) A set of links is the set of the remaining branches of the network.
- iv) A proper tree is a tree whose branches contain every ~~capacitive~~ element of the network plus some resistive elements.

We note that a network may contain capacitors in a closed loop or perhaps all trees containing every capacitor also contain inductors. Any capacitor and/or inductor which prevents the formation of the proper tree is called excess. In the state variable network description for a network with excess elements we add a capacitor across each excess inductor and an inductor in series with each excess capacitor. These added elements ultimately are assigned zero value. Based on this formalism, the procedure for writing the state equations follows.

- i) Construct the proper tree for the network and remove all sources by open-circuiting current sources and short-circuiting voltage sources.

- ii) Assign current directions to each tree branch and to each link.

Any link placed on the tree becomes part of a unique closed path. Thus, each link current is equivalent to a mesh current flowing in the path closed by the link, and it is possible to form a current matrix relating the tree branch currents in terms of the link currents as follows:

- a) Label the tree branch current i_a and the link current by I_a .
 - b) If a tree branch is in a given mesh enter a +1(-1) if the tree branch and link currents are in the same (opposite) direction. Enter a zero if the tree branch is not in the mesh.
- iii) Form the voltage matrix as follows:
- a) Label the voltage across each link v_a and the voltage across each branch by V_a where the voltage drop is positive in the same direction as the link currents.
 - b) If a tree branch is in a given mesh enter a +1(-1) if the tree branch voltage drop is in the opposite (same) direction as the link voltage drop. Enter a zero if the tree branch is not in the mesh.
- iv) Form the combined voltage and current matrix using each tree branch current i_a written as $C_a dV_a/dt$ or V_a/R_a and each link voltage v_a written as $L_a dI_a/dt$ or $R_a I_a$.

This matrix still

- a) contains unwanted terms proportional to V_k and I_L on the left,
- b) does not have the sources incorporated, and
- c) has had no remodification due to augmentation.

v) Eliminate unwanted variables.

vi) Remodify the matrix. Across each excess L_a there is an added capacitor C_a which has zero value. Setting C_a to zero, we in general have

$$\pm I_a = \sum_i^r V_i / R_i + \sum_j^s k_j \dot{I}_j, \quad (4.86)$$

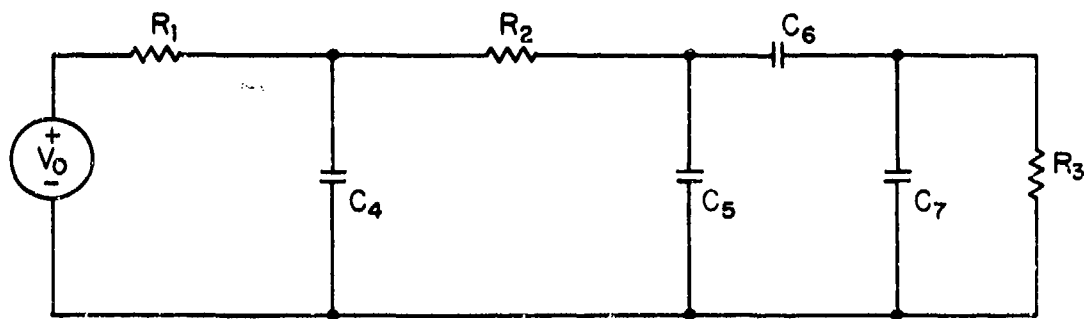
and, since $\pm V_a = L_a \dot{I}_a$,

$$\pm V_a = L_a \left[\sum_i^r R_i \dot{V}_i + \sum_j^s k_j \dot{I}_j \right], \quad (4.87)$$

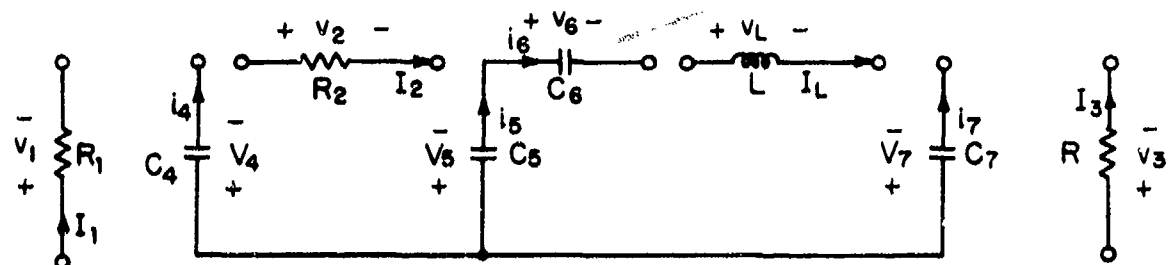
it is possible to eliminate I_a and V_a using \dot{V}_i and \dot{I}_j in terms of undifferentiated quantities. A similar procedure exists for the link inductors L_a placed in series with the excess capacitor C_a .

4.4.3 A Second Example

As an example, consider the network of Fig. 4.9a. One particular proper tree which may be drawn is shown in Fig. 4.9b. Capacitor C_6 is excess, and the links are R_1 , R_2 , R_3 and L , where L has been added in series with C_6 . The current matrix equation is formed using the branch currents as state variables. In particular, meshes are formed by placing the links containing I_1 , I_2 , I_3 and I_L into the circuit one at a time. The first row of the current matrix defines the branch current i_4 , and contains -1, 1, 0 and 0, since I_1 and I_2 are opposite and in the same direction, respectively, as i_4 and I_3 and I_L are in other meshes. The total current matrix equation is given by



(a) Given Circuit



(b) Proper Tree and Links (C_6 is excess capacitor)

Fig. 4.9. Circuit Example.

$$\begin{bmatrix} i_4 \\ i_5 \\ i_6 \\ i_7 \end{bmatrix} = \begin{bmatrix} -1 & 1 & 0 & 0 \\ 0 & -1 & 0 & 1 \\ 0 & 0 & 0 & 1 \\ 0 & 0 & -1 & -1 \end{bmatrix} \begin{bmatrix} I_1 \\ I_2 \\ I_3 \\ I_L \end{bmatrix}. \quad (4.88)$$

Next the voltage matrix equation is formed. In particular, closing the mesh with R_2 results in v_4 having the same polarity and v_5 the opposite polarity that v_2 has, while v_6 and v_7 are out of the mesh. Therefore, row 2 of the matrix contains -1, 1, 0, 0. The total voltage matrix equation is

$$\begin{bmatrix} v_1 \\ v_2 \\ v_3 \\ v_L \end{bmatrix} = \begin{bmatrix} 1 & 0 & 0 & 0 \\ -1 & 1 & 0 & 0 \\ 0 & 0 & 0 & 1 \\ 0 & -1 & -1 & 1 \end{bmatrix} \begin{bmatrix} v_4 \\ v_5 \\ v_6 \\ v_7 \end{bmatrix}. \quad (4.89)$$

The two matrix equations are now combined by substituting, in general, $i_a = C_a \dot{v}_a$ or $i_a = V_a / R_a$, $v_a = L_a \dot{i}_a$ or $v_a = R_a I_a$) and including the source $V_0(t)$. This results in

$$\begin{bmatrix} i_4 \\ i_5 \\ i_6 \\ i_7 \\ v_1 - v_0(t) \\ v_2 \\ v_3 \\ v_L \end{bmatrix} = \begin{bmatrix} C_4 \dot{v}_4 \\ C_5 \dot{v}_5 \\ C_6 \dot{v}_6 \\ C_7 \dot{v}_7 \\ R_1 I_1 - v_0 \\ R_2 I_2 \\ R_3 I_3 \\ L \dot{i}_L \end{bmatrix} = \left[\begin{array}{c|ccccc} & -1 & 1 & 0 & 0 \\ 0 & 0 & -1 & 0 & 1 \\ & 0 & 0 & 0 & 1 \\ & 0 & 0 & -1 & -1 \\ \hline 1 & 0 & 0 & 0 & 0 \\ -1 & 1 & 0 & 0 & 0 \\ 0 & 0 & 0 & 1 & 0 \\ 0 & -1 & -1 & 1 & 0 \end{array} \right] \begin{bmatrix} v_4 \\ v_5 \\ v_6 \\ v_7 \\ I_1 \\ I_2 \\ I_3 \\ I_L \end{bmatrix}. \quad (4.90)$$

The state variables which are to be eventually retained are v_4 , v_5 , and v_7 . First, v_1 , v_2 , and v_3 are eliminated by setting

$$v_1 = R_1 I_1 = v_4 + v_0, \quad (4.91)$$

so that

$$I_1 = G_1 v_4 + G_1 v_0, \quad (4.92)$$

where G_i is equal to $1/R_i$. Similarly

$$I_2 = -G_2 v_4 + G_2 v_5, \quad (4.93)$$

and

$$I_3 = G_3 v_7, \quad (4.94)$$

so that the matrix differential equation reduces to

$$\begin{bmatrix} c_4 \dot{v}_4 \\ c_5 \dot{v}_5 \\ c_6 \dot{v}_6 \\ c_7 \dot{v}_7 \\ L \dot{I}_L \end{bmatrix} = \begin{bmatrix} -(G_1 + G_2) & G_2 & 0 & 0 & 0 \\ G_2 & -G_2 & 0 & 0 & 1 \\ 0 & 0 & 0 & 0 & 1 \\ 0 & 0 & 0 & -G_3 & -1 \\ 0 & -1 & -1 & 1 & 0 \end{bmatrix} \begin{bmatrix} v_4 \\ v_5 \\ v_6 \\ v_7 \\ I_L \end{bmatrix} + \begin{bmatrix} -G_1 \\ 0 \\ 0 \\ 0 \\ 0 \end{bmatrix} v_0. \quad (4.95)$$

Next I_L and v_6 are eliminated. Since $L \dot{I}_L = -v_5 - v_6 + v_7$ and $L = 0$, $v_6 = -v_5 + v_7$ which is used to eliminate v_6 . Thus, using $I_L = c_6 \dot{v}_6$

$$\dot{v}_6 = I_L / c_6 = -\dot{v}_5 + \dot{v}_7, \quad (4.96)$$

which is used to eliminate I_L . Substituting Eq. (4.96) into Eq. (4.95) results in

$$\begin{bmatrix} c_4 \dot{v}_4 \\ -c_6 \dot{v}_7 + (c_6 + c_5) \dot{v}_5 \\ -c_6 \dot{v}_5 + (c_6 + c_7) \dot{v}_7 \end{bmatrix} = \begin{bmatrix} -(G_1 + G_2) & G_2 & 0 \\ G_2 & -G_2 & 0 \\ 0 & 0 & -G_3 \end{bmatrix} \begin{bmatrix} v_4 \\ v_5 \\ v_7 \end{bmatrix} + \begin{bmatrix} -G_1 \\ 0 \\ 0 \end{bmatrix} v_0. \quad (4.97)$$

Finally the latter two equations

$$-c_6 \dot{v}_7 + (c_6 + c_5) \dot{v}_5 = g_2 v_4 - g_2 v_5, \quad (4.98)$$

and

$$-c_6 \dot{v}_5 + (c_6 + c_7) \dot{v}_7 = -g_3 v_7, \quad (4.99)$$

are solved simultaneously for \dot{v}_5 and \dot{v}_7 . Defining

$$D \equiv c_5 c_6 + c_5 c_7 + c_6 c_7, \quad (4.100)$$

the resulting state differential equations are

$$\begin{bmatrix} \dot{v}_4 \\ \dot{v}_5 \\ \dot{v}_7 \end{bmatrix} = \begin{bmatrix} -(g_1 + g_2)/c_4 & g_2/c_4 & 0 \\ g_2(c_6 + c_7)/D & -(c_6 + c_7)g_2/D & -c_6 g_3/D \\ g_2 c_6/D & -g_2 c_6/D & -(g_3 c_6 + g_3 c_5)/D \end{bmatrix} \begin{bmatrix} v_4 \\ v_5 \\ v_7 \end{bmatrix} + \begin{bmatrix} -g_1/c_4 \\ 0 \\ 0 \end{bmatrix} v_0. \quad (4.101)$$

In order to show the effect of a nonlinearity, consider that R_2 is a nonlinear function of v_5 and v_4 . Then Equation (4.101) can be written in the general matrix form

$$\dot{\underline{x}}(t) = \underline{A} \underline{x}(t) + \underline{G} \underline{f}(\underline{x}, \underline{u}) + \underline{D} \underline{u}(t) = \underline{k}(\underline{x}, \underline{u}), \quad (4.102)$$

where

$$\underline{x} = \begin{bmatrix} v_4 \\ v_5 \\ v_7 \end{bmatrix}, \quad (4.103)$$

$$\underline{A} = \begin{bmatrix} -G_1/v_4 & 0 & 0 \\ 0 & 0 & -C_6 G_3/D \\ 0 & 0 & -(G_3 C_6 + G_3 C_5)/D \end{bmatrix}, \quad (4.104)$$

$$\underline{G} = \begin{bmatrix} -\frac{1}{C_4} \\ (C_6 + C_7)/D \\ C_6/D \end{bmatrix}, \quad (4.105)$$

$$\underline{f(x,u)} = (v_4 - v_5) G_2, \quad (4.106)$$

$$\underline{D} = \begin{bmatrix} -G_1/C_4 \\ 0 \\ 0 \end{bmatrix}, \quad (4.107)$$

$$\underline{u}(t) = v_0. \quad (4.108)$$

The matrices in Equation (4.102 have the following interpretation: \underline{A} is a square matrix, containing all the linear circuit elements, while the vector $\underline{f(x,u)}$ accounts for all nonlinear elements. In this case, there is only one nonlinearity, and the vector reduces to a scalar. Vectors \underline{G} and \underline{D} , which are in the general case rectangular matrices, account for the way nonlinearities and inputs, respectively, affect the state variables. The vector $\underline{u}(t)$, which in this case is a scalar, is the vector of voltage sources.

Equation (4.102) can be also written in the normal form given by Equation (4.85), that is, $\dot{\underline{x}} = \underline{k}(\underline{x}, \underline{u})$.

4.5 Multivariable Formulation of the Perturbation Method.

In Section 4.3, the essential steps involved in determining the small-signal responses of a nonlinear system which is also excited by a strong periodic waveform have been presented in some detail. The example developed was a single-loop circuit that permitted formulation of the problem and its solution for a system having memory in simple form. In the general case, however, nonlinear systems are not limited to single state variables. Examples discussed in Section 4.4 are examples of multivariable state equations. In this section we shall indicate the extension of the formulation to circuits having many state variables. The appropriate mathematical formulation is in terms of matrices, and free use will be made of such formulation. As in the simpler example from Section 4.3 we shall obtain an operating point equation (OPE) and a small-signal perturbation equation (PE). The OPE is nonlinear and has a periodic forcing function. The PE is also nonlinear but can be decomposed into a set of linear time-varying differential equations.

Very often the input to a receiver stage, or even the receiver itself, is the sum of a strong signal and a much weaker signal. For that particular case it is possible to break the network solution into two solutions. The first solution, due to the large signal, will result in a time-varying operating point while the second solution, due to the small signal, will result in what are called perturbations about the operating point.

As is the case for all of the solution methods we must first describe the particular network under analysis by a system of state variable equations as given in Section 4.4. The general form of the state differential equations for a time-invariant nonlinear circuit as given by Eq. (4.102), is

$$\dot{\underline{x}}(t) = \underline{A} \underline{x}(t) + \underline{G} \underline{f}(\underline{x}, \underline{u}) + \underline{D} \underline{u}(t) = \underline{k}(\underline{x}, \underline{u}). \quad (4.109)$$

\underline{A} is a matrix which accounts for all linear circuit elements while the $\underline{f}(\underline{x}, \underline{u})$ vector accounts for all of the nonlinear elements and vector $\underline{u}(t)$ for all the input or forcing functions. Very often when the state variable equation is written \underline{A} is time-varying. Rectangular matrices \underline{G} and \underline{D} describe the way in which nonlinearities and inputs, respectively, affect the state variables.

Equation (4.109) is converted into two sets by a perturbation procedure. One set is formally identical to the original system except that its solution gives the circuit operating locus. The solution of the second set gives the small signal behavior, as influenced by the operating locus.

In order to avoid extensive complication we make the simplifying assumption that all small-signal inputs appear at the same input port and may therefore be lumped into one small input. For example, this assumption is true for a mixer where the large signal may appear at a second input port. This assumption is made in order to simplify the presentation and does not effect the generality of the technique.

We begin the perturbation method by breaking up the input $\underline{u}(t)$ into the small and large signal components. Formally, for the general case, the input vector is written as

$$\underline{u}(t) = \underline{u}_o(t) + \Delta \underline{u}(t), \quad (4.110)$$

so that the matrix D in Eq. (4.109) will have two corresponding column vectors \underline{d}_2 and \underline{d}_1 and we may write

$$D \underline{u}(t) = [\underline{d}_1 \underline{d}_2] \begin{bmatrix} \underline{u}_o(t) \\ \Delta \underline{u}(t) \end{bmatrix}. \quad (4.111)$$

In the particular case where the small and large signals are $u_2(t)$ and $u_1(t)$, respectively, we have

$$\underline{u}_o(t) = \begin{bmatrix} u_1(t) \\ 0 \end{bmatrix}, \quad (4.112)$$

and

$$\Delta \underline{u}(t) = \begin{bmatrix} 0 \\ u_2(t) \end{bmatrix}. \quad (4.113)$$

The network solution vector $\underline{x}(t)$ is also written in the form

$$\underline{x}(t) = \underline{x}_o(t) + \Delta \underline{x}(t), \quad (4.114)$$

where $\Delta \underline{x}(t)$ is the perturbation solution while $\underline{x}_o(t)$ gives the time-varying operating point solution. Substituting Eq. (4.111) and (4.114) into Eq. (4.109),

$$\begin{aligned}
 \dot{\underline{x}}_o(t) + \Delta \dot{\underline{x}}(t) &= \underline{A} \left[\underline{x}_o(t) + \Delta \underline{x}(t) \right] \\
 &+ \underline{Gf} \left[\underline{x}_o(t) + \Delta \underline{x}(t), \underline{u}_o(t) + \Delta \underline{u}(t) \right] \\
 &+ \underline{D} \left[\underline{u}_o(t) + \Delta \underline{u}(t) \right].
 \end{aligned} \tag{4.115}$$

Substituting the definition of the differential of $f(\underline{x}, \underline{u})$

$$\begin{aligned}
 \Delta f[\underline{x}_o(t), \Delta \underline{x}(t), \underline{u}_o(t), \Delta \underline{u}(t)] &= \\
 f[\underline{x}_o(t) + \Delta \underline{x}(t), \underline{u}_o(t) + \Delta \underline{u}(t)] - f[\underline{x}_o(t), \underline{u}_o(t)],
 \end{aligned} \tag{4.116}$$

into Eq. (4.115), we may separate Eq. (4.115) into two equations:

$$\dot{\underline{x}}_o(t) = \underline{A} \underline{x}_o(t) + \underline{Gf} [\underline{x}_o(t), \underline{u}_o(t)] + \underline{d}_1 \underline{u}_o(t), \tag{4.117}$$

which is the operating point equation (OPE) and

$$\Delta \dot{\underline{x}}(t) = \underline{A} \Delta \underline{x}(t) + \underline{G} \Delta f[\underline{x}_o, \Delta \underline{x}, \underline{u}_o, \Delta \underline{u}] + \underline{d}_2 \Delta \underline{u}(t), \tag{4.118}$$

which is the perturbation equation (PE).

Equations (4.117) and (4.118) are the statement of the multi-variable time-varying nonlinear transfer function problem. In the OPE, only the strong excitation, which is applied to the original circuit, is present. The OPE is a set of time-invariant nonlinear equations, the solution of which is the system of time-varying operating points about which the perturbations occur.

The time-varying operating points applied to the perturbation equation, Eq. (4.118), result in a system of time-varying nonlinear equations. The solution to the perturbation equation can be approximated by use of time-varying Volterra functionals, the more terms of which are included, the better is the solution. The solution of the multivariate perturbation equation follows the same techniques as were used in solving Eq. (4.16), that is, a Taylor series expansion is made of Eq. (4.118), vector driving terms are inserted, and systems of equations of equal order are formed.

Physically, the n^{th} -order response of a network does not depend upon the inclusion of higher-order responses. For example, the linear perturbation solution, which is the response of the small-signal linear equivalent circuit, is the same no matter how many terms are assumed in the mathematical expansions of Δf and Δx . Similarly, the second-order response is independent of any higher-order response through the second-order nonlinear behavior of the circuit. Due to the choice of expansion in Volterra functionals, each higher-order nonlinear response is the result of excitation of the linearized system with inputs which are created from combinations of lower-order responses. Once again we remark that the linearized circuit is time-varying due to and determined by the strong signal response, $x_o(t)$. In the case where the strong-signal input, $u_1(t)$ is arbitrary, it is not possible to explicitly determine the Volterra kernels. However, in the special case where the strong-signal input is periodic, although of an arbitrary known waveshape, and the small-signal input is a sum of sinusoids, Eq. (4.118) may be converted to a form in which a vector of time-varying nonlinear

transfer functions, $H_k(t; f_1, \dots, f_k)$ are obtained as solutions. The time-varying operating point solution, $x_o(t)$, will be periodic. $x_o(t)$ can be found numerically either by the Newton-Raphson techniques (Aprille and Trick, 1972) or by integrating Eq. (4.117) until the steady-state is reached. The order-separated equations needed to determine the total perturbation solution will also be periodic as well as time-varying. The solution is a direct matrix-vector analog of the techniques developed in Section 4.3 for the single-loop case. While the derivation is complex and will not be presented, the final result can be easily stated.

The perturbation equation for the single-loop network was shown to be

$$\frac{di}{dt} = -\frac{R}{L} i - \frac{1}{L} v_d(i, i_o) + \frac{v}{L}, \quad (4.119)$$

where $v_d(t)$ is the diode perturbation voltage due to the weak excitation, v . From Eq. (4.12), $v_d(i, i_o)$ was shown to be equal to

$$v_d(i, i_o) = r_1(t) i + r_2(t) i^2 + \dots, \quad (4.120)$$

with the result that

$$\frac{di}{dt} = -\left(\frac{R}{L} + \frac{r_1(t)}{L}\right) i + \sum_{n=2}^{\infty} \frac{r_n(t)}{L} i^n + \frac{v}{L}. \quad (4.121)$$

From Eq. (4.119), the time-varying linear differential equations for the nonlinear transfer functions were found to be

$$\dot{H}_1(t; f) = - \left[\frac{R}{L} + \frac{r_1(t)}{L} + j2\pi f \right] H_1(t; f) + \frac{1}{L}, \quad (4.122)$$

$$\begin{aligned} \dot{H}_2(t; f_1, f_2) &= - \left[\frac{R}{L} + \frac{r_1(t)}{L} + j2\pi(f_1 + f_2) \right] H_2(t; f_1, f_2) \\ &\quad - \frac{r_2(t)}{L} H_1(t; f_1) H_1(t; f_2), \end{aligned} \quad (4.123)$$

$$\begin{aligned} \dot{H}_3(t; f_1, f_2, f_3) &= - \left[\frac{R}{L} + \frac{r_1(t)}{L} + j2\pi(f_1 + f_2 + f_3) \right] H_3(t; f_1, f_2, f_3) \\ &\quad - 2 \frac{r_2(t)}{L} \overline{H_1(t; f_1) H_2(t; f_2, f_3)} \\ &\quad - \frac{r_3(t)}{L} \prod_{i=1}^3 H_1(t; f_i). \end{aligned} \quad (4.124)$$

In the multistate case, the perturbation equation as given by Eq. (4.118), is

$$\Delta \dot{\underline{x}}(t) = \underline{A} \Delta \underline{x}(t) + \underline{G} \Delta \underline{f} (\underline{x}_o, \Delta \underline{x}, \underline{u}_o, \Delta \underline{u}) + \underline{d}_2 \Delta \underline{u}(t), \quad (4.125)$$

and the desired solution will be a vector time-varying nonlinear transfer function, $\underline{H}_n(t; f_1, f_2 \dots f_n)$, where the components of \underline{H}_n are the time-varying nonlinear transfer functions of the state variables. Associated with \underline{H}_n will be the operating-point state-variable vector \underline{x}_o . Comparing Equations (4.119) and (4.125), we identify the analogous quantities

- (i) $i \leftrightarrow x_i$,
- (ii) $- R/L \leftrightarrow \underline{A}$,
- (iii) $- 1/L v_d(i, i_o) \leftrightarrow \underline{G} \Delta \underline{f} (\underline{x}, \underline{x}_o, \underline{u}_o, \Delta \underline{u})$,
- (iv) $v/L \leftrightarrow \underline{d}_2 \Delta \underline{u}(t)$,

and state the differential equations satisfied by the time-varying nonlinear transfer functions to be

$$\dot{\underline{H}}_1(t; f) = [\underline{A} + \underline{GF}_1(\underline{x}_0) - j2\pi f \underline{I}] \underline{H}_1(t; f_1) + \underline{d}_2, \quad (4.126)$$

$$\begin{aligned} \dot{\underline{H}}_2(t; f_1, f_2) = & [\underline{A} + \underline{GF}_1(\underline{x}_0) - j2\pi(f_1 + f_2) \underline{I}] \underline{H}_2(t; f_1, f_2) \\ & + \underline{GF}_2(\underline{x}_0) \text{ col} [\underline{H}_{1,i}(t; f_1) \underline{H}_{1,i}(t; f_2)], \end{aligned} \quad (4.127)$$

$$\begin{aligned} \dot{\underline{H}}_3(t; f_1, f_2, f_3) = & [\underline{A} + \underline{GF}_1(\underline{x}_0) - j2\pi(f_1 + f_2 + f_3) \underline{I}] \underline{H}_3(t; f_1, f_2, f_3) \\ & + 2\underline{GF}_2(\underline{x}_0) \text{ col} [\overline{\underline{H}_{1,i}(t; f_1)} \underline{H}_{2,i}(t; f_2, f_3)] \\ & + \underline{GF}_3(\underline{x}_0) \text{ col} [\underline{H}_{1,i}(t; f_1) \underline{H}_{1,i}(t; f_2) \underline{H}_{1,i}(t; f_3)]. \end{aligned} \quad (4.128)$$

Equations (4.126) through (4.128) can be formally derived. In writing the equations, we have used the notation:

$\underline{F}_i(\underline{x}_0)$ = i-th coefficient matrix in the Taylor series expansion of $\underline{F}(\underline{x}_0)$.

$\underline{H}_{n,i}$ = i-th component of n-th order nonlinear transfer function vector.

$\text{col} []$ = a column vector, the i-th row of which is given by the term in the bracket.

\underline{I} = identity matrix.

Equations (4.126) through (4.128) are each a linear, time-varying, periodic system of differential equations the solution of which is the vector time-varying nonlinear transfer function of desired order. The equations for the higher-order nonlinear transfer functions can be developed using these equations as a guide, plus the recursion relations of Section 2.2.3 to define the nonlinear sources.

Equations (4.126) through (4.128) also assume that each component of $\Delta f(x_0)$ is a function of only one component of x , so that each row of $E_n(x_0)$ has only one non-zero element. The effect of this assumption is shown in the post-multiplication by the column vectors in the single components of H_n . In the most general case, where this restriction is removed, the Taylor series expansion of H_n , and the subsequent analysis, would utilize appropriately higher dimensional matrices and driving terms. The form of the solution would, however, remain unchanged.

4.6 Direct Time-Domain Solution of Nonlinear State Equations

In Section 4.4 it was shown that the equations describing nonlinear circuits could be formulated as nonlinear state equations. One means of finding the large-excitation, multi-input signal response of a circuit is to solve the nonlinear differential equations with the circuit excited by all signals. The various spectral components in the circuit output can then be found by performing a Fourier analysis of the time-domain solution to the differential equations. The Fourier analysis can be performed using the fast Fourier transform algorithm of Cooley and Tukey (1965). We will be concerned next with the problem of numerically evaluating the solution of a nonlinear differential equation, and the related problem of finding a periodic solution when the input excitation is periodic.

4.6.1 Numerical Solution of Nonlinear State Equations

The equation

$$F(t; x, x', x'', \dots x^{(p)}) = 0, \quad (4.129)$$

is a differential equation of order p. A function $x(t)$ such that:

$$F[t, x(t), x'(t), x''(t), \dots x^{(p)}(t)] = 0, \quad (4.130)$$

for all t over which F is defined is a solution of the differential equation. In order to have a unique solution to a p-order differential equation, p conditions are required. If the function x and its first $p-1$ derivatives are defined at one point, the problem of finding $x(t)$ is called an initial value problem. If $x(t)$ and/or some of the derivatives are specified at several points, the problem is called a boundary value problem.

The numerical evaluation of differential equations is done through the use of numerical integration. The first important attribute of an integration method is its order: a method is of order k if the truncation error is $O(h^{k+1})$ where h is the integration step size. Thus the higher the order of a method, the more accurate the results for a fixed step size h .

Methods which essentially extrapolate from past values provide a formula which gives the next value of the state vector explicitly. By contrast, implicit methods have formulas in which \underline{x}_n is given not only in terms of past values but also in terms of $\dot{\underline{x}}_n$. A general implicit integration rule is given by [Gear 1970, p. 112]

$$\alpha_0 \underline{x}_n = h \beta_0 \dot{\underline{x}}_n + \sum_{j=1}^k (\alpha_j \underline{x}_{n-j} + h \beta_j \dot{\underline{x}}_{n-j}), \quad (4.131)$$

where $\alpha_0 = 1$, h is the step size, and the subscript n denotes the n -th time step. Thus, in implicit methods, β_0 is non-zero; in explicit methods, β_0 is uniquely zero. An iterative method must be used to solve for \underline{x}_n ; a formula which provides a first approximation, $\underline{x}_n^{(C)}$, as a starting point for the integration formula, is called a predictor, while the integration formula itself is called the corrector. Many schemes exist in which the number of corrector iterations is fixed, or a modifier is used after the predictor so that the corrector is evaluated only once.

Methods may be single step, or multistep, depending on whether the method uses information from one or more previous mesh points. The number of steps in Equation (4.130) is the index, k . Runge-Kutta methods of any order are single step; predictor-corrector

methods are multistep. If the order of the predictor is q , and the order of the corrector is r , then, after m iterations, the error is $O(h^{q+m+1}) + O(h^{r+1})$. Thus, if $q = r-1$, only two corrector iterations are required before the predictor-corrector accuracy is limited by the order of the corrector.

An extremely important aspect of an integration formula is its stability, which can be determined only if the method is linear. Because the integration method is a linear difference approximation to the actual nonlinear differential equation, there is a truncation, or discretization, error which is generated at each step. The total error in the solution can be shown to be the solution of a linear difference equation with the truncation error as a forcing function; it is the stability of the error difference equation which must be guaranteed if the total error in the numerical solution is to remain bounded. Because the numerical integration scheme amounts to solving a linear difference equation, it is possible, through choice of the discrete time step size, to have unstable poles in the difference equation without there being unstable poles in the original differential equations. Since the numerical stability of an integration formula is dependent upon the properties of the system being integrated, it is usual to assume a scalar test system of the form

$$\dot{x} = -\lambda x. \quad (4.132)$$

The philosophy is that for a sufficiently small time step h , the dynamic behavior of x in $\dot{x} = f(x)$ is well approximated by

$$x = x(t_n) + \delta x, \quad (4.133)$$

where

$$\delta \dot{x} = \left. \frac{\partial f}{\partial x} \right|_{x(t_n)} \delta x. \quad (4.134)$$

Thus, in the scalar case, we have

$$-\lambda \approx \left. \frac{\partial f}{\partial x} \right|_{x(t_n)} \quad (4.135)$$

while, in the vector case, $-\lambda$ is the largest magnitude eigenvalue of the matrix

$$\underline{A} = \left. \frac{\partial \underline{f}}{\partial \underline{x}} \right|_{\underline{x}(t_n)}, \quad (4.136)$$

The matrix \underline{A} of Eq. (4.136) is the Jacobian matrix of the system. For linear difference schemes, the poles of the total solution error difference equation are functions of $h\lambda$, and for a stable formula, the conditions on $h\lambda$ such that all poles of the total solution error difference equation are within or on the unit circle must be determined.

The classic textbook by Henrici (1962) provides the fundamental background and details of most linear integration schemes. The stability properties of the most well known linear methods can be determined from the plots given by Lomax (1967), which show that classical numerical integration methods tend to have restrictively small stability regions, e.g., for fourth-order Runge-Kutta, $|h\lambda| \leq 2.6$ for stability, while for the Hamming modified predictor-corrector, $|h\lambda| \leq 0.6$. Systems of equations with widely separated time constants are called "stiff equations". These arise frequently in the analysis of electronic circuits, where coupling networks may have long time constants, while parasitic elements may cause short time constants. In integrating stiff equations with these methods, stability is insured only by estimating the largest magnitude eigenvalue and restricting h in accordance with the stability boundary for the method.

Besides the difficulty of performing this estimation, there is the additional burden that the solution component represented by this largest magnitude pole is frequently not of interest, as it usually belongs to some high-frequency parasitic mode. Thus, standard integration methods can be exceedingly inefficient. The most desirable property of a numerical scheme would be numerical stability for all stable λ ; in this case h could be chosen to satisfy some truncation error requirement on an important solution component without the danger of inducing numerical instability due to the high-frequency parasitic modes. Any method which possesses numerical stability for all values of $h\lambda$ whenever λ has a negative real part is said to be A-stable (Dahlquist, 1963); no linear multistep method of order greater than two can be A-stable, and any linear A-stable method must be implicit. It is discouraging that A-stable methods cannot be of order greater than two. The need for higher-order methods arises from the relationship between order and truncation error. Because the solution function is being approximated by a polynomial, there is, as in a Taylor's series approximation, a truncation error which is $O(h^{k+1})$ where k is the order of the method. Only by the use of higher order methods can the step size h be made large and the truncation error small simultaneously.

By relaxation of the stability requirement, Gear (1971) has developed certain high-order implicit formulas for orders one through six. Only the first and second order formulas are stable for all $h\lambda > 0$; the remainder are stable in the shaded region shown in Fig. 4.10. They are called stiffly stable formulas in order to differentiate them from A-stable formulas. Gear's formulas are stiffly stable for $D \approx 6$ and $\theta \approx 0.5$. The basic justification for the sufficiency of stiff stability lies in the assumption

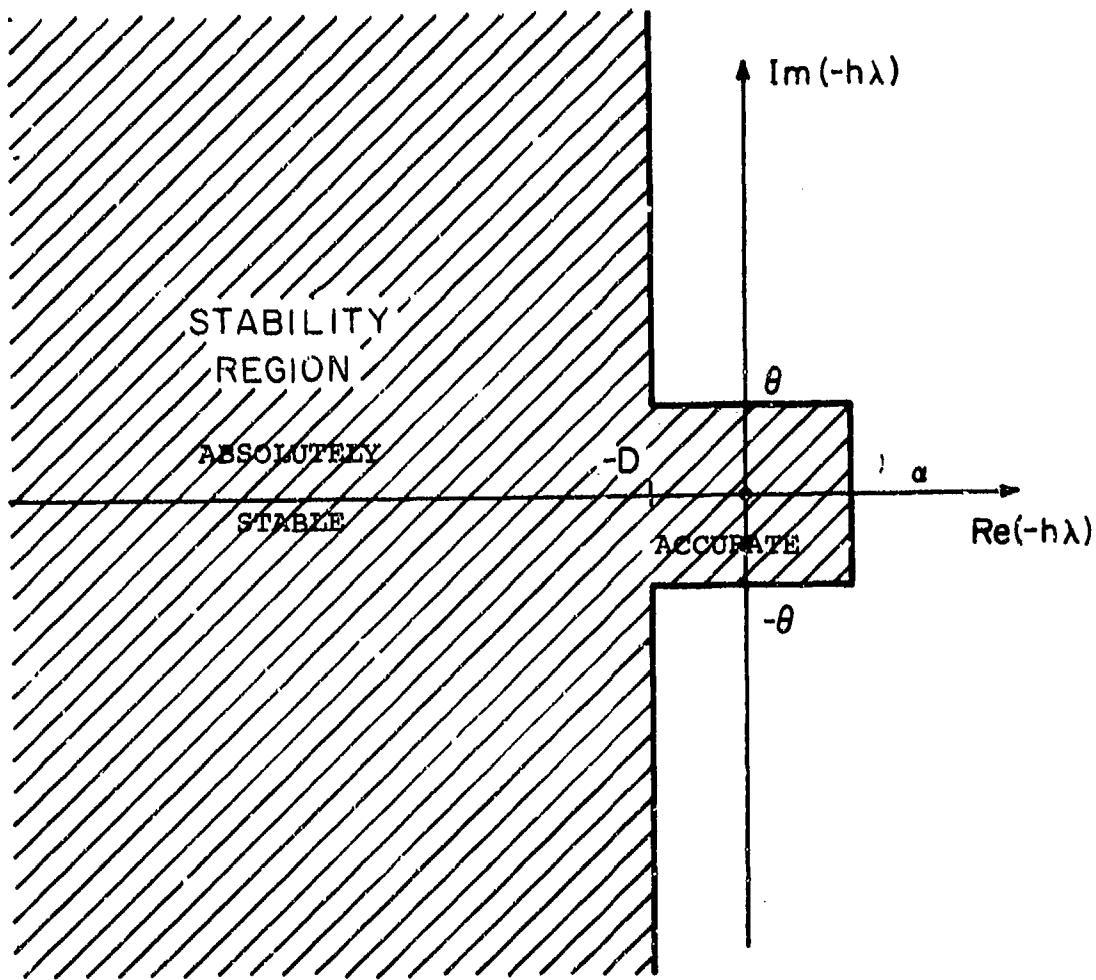


Fig.4.10. Regions of Stable Integration for Gear's Higher-Order Integration Formulas from (Gear, 1971, p.214).

that large magnitude eigenvalues correspond to parasitic modes which affect the total solution but little; it is not necessary that the method be accurate for such parasitic modes, but only that it be stable for such modes. On the other hand, high accuracy is desired for modes corresponding to smaller magnitude λ 's so that h must therefore be small; the result is that for $h\lambda$ small in magnitude, the stability region need not be too large, since accuracy is the dominant concern. In programming the formulas, the step size and the order of the integration formula are changed as needed. To minimize the running time it is desired to make h as large as possible, consistent with the desired accuracy; for a fixed h , increased accuracy results from the use of a higher order formula. Gear (1971) presents a complete discussion of stiffly-stable predictor-corrector techniques, and includes a FORTRAN program for performing the numerical integration of a set of N ordinary first-order differential equations. As part of the program, there is an algorithm which automatically changes the step size and order of the integration routine so that the error is kept within a prescribed amount while maintaining a fast execution time. In applying the variable step, use is made of the Nordseick vector (Nordseick, 1962). The predictor used in the routine is a Pascal triangle, and the program allows for three corrector iterations at the smallest step size before failure of convergence is declared.

4.6.2 Numerical Solution of the Dynamic Operating Point Differential Equation

In the previous sections we have presented considerable detail regarding the single-variable and multi-variable formulation of a perturbation method of solving strongly driven nonlinear networks. Two multi-variable differential equations must be solved to obtain specific results for any particular nonlinear circuit example. First, the operating point must be determined by obtaining a numerical solution of the nonlinear state equations of the system when the system is strongly driven with a periodic excitation. There are very efficient methods of determining the periodic solution. This section describes the Newton-Raphson iterative procedure of determining the time-varying operating point, $\underline{x}_o(t)$, when the strong signal input, $u_1(t)$, is periodic. After the periodic operating point has been determined, the periodic derivative matrices (Taylor series coefficient matrices), F_i , which are a function of $\underline{x}_o(t)$, can be determined and hence the time-varying nonlinear transfer functions $H_n(t; f)$ may be computed. Numerical techniques for determining H will be described in Section 4.6.3. We now describe the method for obtaining the periodic solution of a set of nonlinear differential equations characterizing the system state.

The general nonlinear system state equations are given by

$$\dot{\underline{x}} = \underline{f}(\underline{x}, t). \quad (4.137)$$

After presenting the method we will specialize the results to the operating point equation. Our goal is to determine the periodic solution of Eq. (4.137).

Let \underline{a} be the initial condition vector of the periodic solution of period T . We must determine \underline{a} such that one period later the same initial conditions occur [i.e., $\underline{x}(t_0+T, \underline{a}) = \underline{x}(t_0, \underline{a}) = \underline{a}$]. We have selected $t=t_0$ as the initial condition time and, for simplicity, now set $t_0=0$. We shall develop here the Newton-Raphson iteration procedure that is needed.

The problem is restated as follows. Given the initial condition vector \underline{a} at time $t=t_0$, where we now arbitrarily choose $t_0=0$, determine \underline{a} such that the vector equation

$$\underline{c}(\underline{a}) = \underline{x}(T, \underline{a}) - \underline{a} = \underline{0}, \quad (4.138)$$

is satisfied. Physically, all (4.138) implies is that T seconds after the initial time the solution is back to the initial conditions.

Let us assume that \underline{a}^k is the k 'th approximation to the root of $\underline{c}(\underline{a})=\underline{0}$. We wish to determine $\underline{\varepsilon}^k$ such that $\underline{c}(\underline{a}^k + \underline{\varepsilon}^k) = \underline{0}$. Expanding $\underline{c}(\underline{a})$ about \underline{a}^k gives, to the first degree,

$$\underline{c}(\underline{a}^k + \underline{\varepsilon}^k) = \underline{c}(\underline{a}^k) + \underline{c}_{\underline{a}}(\underline{a}^k) \underline{\varepsilon}^k, \quad (4.139)$$

where $\underline{c}_{\underline{a}}(\underline{a}^k)$ is a matrix of the form

$$\underline{c}_{\underline{a}}(\underline{a}^k) = \frac{\partial \underline{c}(\underline{a})}{\partial \underline{a}} \Big|_{\underline{a}^k} = \begin{bmatrix} \frac{\partial c_1}{\partial a_1} & \frac{\partial c_1}{\partial a_2} & \dots \\ \frac{\partial c_2}{\partial a_1} & \frac{\partial c_2}{\partial a_2} & \dots \\ \vdots & \vdots & \ddots \\ \vdots & \vdots & \ddots \end{bmatrix}_{\underline{a}=\underline{a}^k}. \quad (4.140)$$

In order for $\underline{\alpha}^k + \underline{\epsilon}^k$ to be a root, it is necessary for $c(\underline{\alpha}^k + \underline{\epsilon}^k)$ to be equal to zero. Thus $\underline{\epsilon}^k$ is obtained by setting (4.139) equal to zero. We find that

$$\underline{\epsilon}^k = -[\underline{c}_{\underline{\alpha}}(\underline{\alpha}^k)]^{-1} \underline{c}(\underline{\alpha}^k). \quad (4.141)$$

Since we only used the linear term to obtain Eq.(4.139) it is clear that $\underline{\alpha}^k + \underline{\epsilon}^k$ is not necessarily the desired root of $\underline{c}(\underline{\alpha}) = 0$. It is a closer approximation than $\underline{\alpha}^k$, however, so that we make it the next guess for $\underline{\alpha}$, $\underline{\alpha}^{k+1}$. The Newton iteration formula is thus

$$\underline{\alpha}^{k+1} = \underline{\alpha}^k - [\underline{c}_{\underline{\alpha}}(\underline{\alpha}^k)]^{-1} \underline{c}(\underline{\alpha}^k) \quad (4.142)$$

Using (4.138) we find that

$$\underline{c}_{\underline{\alpha}}(\underline{\alpha}^k) = [\underline{x}_{\underline{\alpha}}(T, \underline{\alpha}^k) - \underline{I}], \quad (4.143)$$

where the matrix $\underline{x}_{\underline{\alpha}}$ is given by

$$\underline{x}_{\underline{\alpha}}(T, \underline{\alpha}^k) = \begin{bmatrix} \frac{\partial \underline{x}_1(T, \underline{\alpha})}{\partial \alpha_1} & \frac{\partial \underline{x}_1(T, \underline{\alpha})}{\partial \alpha_2} & \dots \\ \frac{\partial \underline{x}_2(T, \underline{\alpha})}{\partial \alpha_1} & \frac{\partial \underline{x}_2(T, \underline{\alpha})}{\partial \alpha_2} & \dots \\ \vdots & \vdots & \ddots \\ \vdots & \vdots & \ddots \end{bmatrix} \quad (4.144)$$

$\underline{\alpha} = \underline{\alpha}^k.$

and the superscript k implies the k'th iteration.

The iteration relationship then becomes

$$\underline{a}^{k+1} = \underline{a}^k - [\underline{x}_{\underline{a}}(T, \underline{a}^k) - \underline{I}]^{-1} [\underline{x}(T, \underline{a}^k) - \underline{a}^k], \quad (4.145)$$

which is the iteration relationship for the initial state vector.

Before the iteration procedure of (4.145) may be used it is necessary to develop a method for computing the matrix $\underline{x}_{\underline{a}}(T, \underline{a}^k)$. We do this by means of a result from differential equation theory [Coddington, 1955, p. 349]. The original system differential equation $\dot{\underline{x}} = \underline{f}(\underline{x}, t)$ is rewritten as

$$\dot{\underline{x}}(t, \underline{a}) = \underline{f}[\underline{x}(t, \underline{a}), t], \quad (4.146)$$

where we have shown explicit dependence upon t and the initial condition \underline{a} . Eq. (4.146) is clearly a vector equation. However, taking $\partial/\partial \underline{a}$ of both sides and letting $\underline{a} = \underline{a}^k$ gives

$$\dot{\underline{x}}_{\underline{a}}(t, \underline{a}^k) = \underline{f}_{\underline{x}}[\underline{x}(t, \underline{a}^k), t] \underline{x}_{\underline{a}}(t, \underline{a}^k), \quad (4.147)$$

which is now a matrix differential equation. The "chain" rule has been applied here so that $\underline{f}_{\underline{x}}$ is given by

$$\underline{f}_{\underline{x}} = \begin{bmatrix} \frac{\partial f_1}{\partial x_1} & \frac{\partial f_1}{\partial x_2} & \dots \\ \frac{\partial f_2}{\partial x_1} & \frac{\partial f_2}{\partial x_2} & \dots \\ \vdots & \vdots & \ddots \\ \vdots & \vdots & \ddots \\ \vdots & \vdots & \ddots \end{bmatrix}, \quad (4.148)$$

and (4.147) may alternately be written

$$\frac{\partial \dot{x}}{\partial g} = \frac{\partial f}{\partial x} \cdot \frac{\partial x}{\partial g}. \quad (4.149)$$

We observe that the matrix $\underline{x}_g(t, \underline{g}^k)$ is a solution of the matrix differential equation (4.147). Noting that

$$\underline{x}_g(0, \underline{g}^k) = \underline{I}, \quad (4.150)$$

since $\underline{x}(0, \underline{g})$ is the initial condition vector \underline{g} , we conclude that $\underline{x}_g(t, \underline{g}^k)$ is by definition the state transition matrix of the linear system

$$\dot{y} = \underline{f}_x[t, \underline{x}(t, \underline{g}^k)]y. \quad (4.151)$$

\underline{f}_x is simply the first derivative matrix of $f(\underline{x})$ given by $\underline{F}_1 = \frac{\partial f}{\partial \underline{x}}$. We therefore solve Eq (4.151) at time T to determine $\underline{x}_g(T, \underline{g}^k)$.

We now consider the application of this iteration procedure to the operating point equation. The period T is the period of the strong input function, $u_1(t)$. Corresponding to the initial condition $\underline{x}_o(0) = \underline{g}^k$, Eq.(4.117) is integrated for $0 \leq t \leq T$, to obtain $\underline{x}_o(t, \underline{g}^k)$. The matrix linear system (4.151) to be integrated is

$$\dot{y} = \left\{ \underline{A} + \underline{G} \underline{F}_1 [\underline{x}_o(t, \underline{g}^k)] \right\} y. \quad (4.152)$$

By a suitable choice of integration method, the state transition matrix of (4.152) can be obtained for $0 \leq t \leq T$. We need only

the matrix evaluated at $t=T$, namely, $[\partial \underline{x}_o(T, \underline{a}) / \partial \underline{a}]_{\underline{a}=\underline{a}^k}$, to perform the next Newton iteration, or

$$\underline{a}^{k+1} = \underline{a}^k - \left[\frac{\partial \underline{x}_o(T, \underline{a})}{\partial \underline{a}} \Big|_{\underline{a}=\underline{a}^k} - I \right]^{-1} \left[\underline{x}_o(T, \underline{a}^k) - \underline{a}^k \right], \quad (4.153)$$

When the iteration has converged, the periodic operating point $\underline{x}_o(t)$, corresponding to the strong periodic excitation, $u_1(t)$, has been obtained. This solution will exist and be unique as long as the derivative matrix of $\underline{x}_o(T, \underline{a})$ is non-singular. This condition will occur as long as the linearized circuit has no periodic solutions of the same period, T .

4.6.3 Numerical Solution of the Time-Varying Nonlinear Transfer Function Perturbation Equations

There is one technique which must be presented so that all of the cases we expect to encounter in the communications receiver can be handled efficiently. The task is to determine the nonlinear transfer functions from the set of differential equations (4.126) through (4.128). In these equations we find that, since there is direct dependence on the time-varying operating point, $\underline{x}_o(t)$, both the state matrix and the forcing functions are periodic with period T . The periodicity of the state matrix is due to the presence of $F_1 [\underline{x}_o(t)]$. The periodicity of the forcing functions shall be demonstrated before concluding this subsection.

Each nonlinear transfer function, $H_n(t, f)$, is the solution vector of a system of linear periodic differential equations. The forcing function is obtained from the solution of the system

of equations of lower order. Thus each $\underline{H}_n(t; f)$ is obtained as the periodic solution of a system of equations which may be put in the general form

$$\dot{\underline{z}}(t) = \underline{B}(t)\underline{z}(t) + \underline{y}(t). \quad (4.154)$$

Here $\underline{y}(t)$ is the complete set of forcing functions and the linear circuit, represented by $\underline{B}(t)$, is time-varying. For example, if we consider $\underline{H}_3(t; f)$ in (4.128) we see that $\underline{B}(t)$ and $\underline{y}(t)$ would be, respectively, equal to

$$\underline{B}(t) = \{\underline{A} + \underline{GF}_1[\underline{x}_0(t)] - j2\pi(f_1 + f_2 + f_3) \underline{I}\}, \quad (4.155)$$

$$\begin{aligned} \underline{y}(t) = & \frac{2}{3} \underline{GF}_2(\underline{x}_0) \text{ col}[H_{1,i}(t; f_1) H_{2,i}(t; f_2, f_3) \\ & + H_{1,i}(t; f_2) H_{2,i}(t; f_1, f_3) + H_{1,i}(t; f_3) H_{2,i}(t; f_1, f_2)] \\ & + \underline{GF}_3(\underline{x}_0) \text{ col}[H_{1,i}(t; f_1) H_{1,i}(t; f_2) H_{1,i}(t; f_3)]. \end{aligned} \quad (4.156)$$

It is clear in (4.155) that, since $\underline{x}_0(t+T) = \underline{x}_0(t)$ and, therefore, $E_1[\underline{x}_0(t+T)] = E_1[\underline{x}_0(t)]$, we have

$$\underline{B}(t+T) = \underline{B}(t). \quad (4.157)$$

We now reason the periodicity of the forcing function, $\underline{v}(t)$. In (4.126) the forcing function, $\underline{v}(t)$, is equal to \underline{d}_2 . Since \underline{d}_2 is constant it is trivially periodic. In (4.127) the forcing function is a function of $\underline{F}_2(\underline{x})$, which is periodic with period T , and $\underline{H}_1(t; f)$. But $\underline{H}_1(t; f)$ is the periodic solution, of period T , from the first order nonlinear periodic differential equation. Therefore, combining \underline{F}_2 and \underline{H}_1 maintains the periodicity and the forcing function in this case is also of period T . In addition, the solution to the equation $\underline{H}_2(t; f)$ is periodic with period T . Looking at the forcing function in (4.156) we see dependence on \underline{F}_2 , \underline{F}_3 , \underline{H}_1 and \underline{H}_2 , all of which are periodic with period T . Therefore, we may now conclude, in general, that the forcing functions of (4.126) through (4.128) are all periodic so that

$$\underline{v}(t+T) = \underline{v}(t). \quad (4.158)$$

Since it is clear how $\underline{B}(t)$ and $\underline{v}(t)$ are determined from Eqs. (4.126) through (4.128) we proceed to describe the method for solving the general linear periodic system of differential equations described by Eq. (4.154).

Solution of linear equations is well known and may be given in terms of the system transition matrix, $\underline{\Phi}(t, \tau)$, which is determined by $\underline{B}(t)$. The problem, however, which we consider is to have an efficient method of solution for the periodic case. The known solution is [Schwarz and Friedlander, (1965), p. 114].

$$\underline{z}(t) = \underline{\Phi}(t, t_0) \underline{z}(t_0) + \int_{t_0}^t \underline{\Phi}(t, \tau) \underline{v}(\tau) d\tau, \quad (4.159)$$

where t_0 is the initial time. There are many techniques for determining the state transition matrix. However, in general, $\underline{\Phi}(t, \tau)$ cannot be calculated analytically. In the solution method which we have chosen we seek that set of initial conditions, $\underline{z}^P(t_0)$, such that $\underline{z}(t_0 + T)$, one period later, is identical to the initial conditions. In this fashion we determine the solution with period T . If $\underline{z}(t_0 + T) = \underline{z}^P(t_0)$, then

$$\underline{z}^P(t_0) = \underline{\Phi}(t_0 + T, t_0) \underline{z}^P(t_0) + \int_{t_0}^{t_0 + T} \underline{\Phi}(t_0 + T, \tau) \underline{v}(\tau) d\tau, \quad (4.160)$$

or, equivalently

$$\underline{z}^P(t_0) = [\underline{I} - \underline{\Phi}(t_0 + T, t_0)]^{-1} \int_{t_0}^{t_0 + T} \underline{\Phi}(t_0 + T, \tau) \underline{v}(\tau) d\tau. \quad (4.161)$$

In order for this solution to exist, the indicated matrix inverse must exist. Physically, the state transition matrix $\underline{\Phi}(t, t_0)$ describes the impulse responses of (4.154) when the system is excited by a set of impulses at time $t=t_0$. Therefore, each diagonal element of $\underline{\Phi}(t, t_0)$ is a solution function with $\underline{v}(t)$ identically zero. Let us assume that, without the periodic input $\underline{v}(t)$ applied, the unforced system has a solution of period T . This would imply that $\underline{\Phi}(t_0 + T, t_0) = \underline{\Phi}(t_0, t_0)$. By definition, $\underline{\Phi}(\tau, \tau)$ is equal to the identity matrix, so that $\underline{z}(t_0) = \underline{z}(t_0)$ in (4.159). As a result, the matrix $[\underline{I} - \underline{\Phi}(t_0 + T, t_0)]$ is singular. Therefore, the solution exists and is unique only if the unforced periodic system has no solution of period T . Physically, we expect the system described in general by (4.154) to have only damped responses in the absence of any excitation. Thus, (4.161) will give the periodic solution. The procedure is as follows:

- i) With zero initial conditions, $\underline{z}(t_0)=0$, obtain the state transition matrix $\underline{\Phi}(t, t_0)$ for $t_0 \leq t \leq t_0 + T$ by using numerical integration. Simultaneously, we obtain the integral $\int_{t_0}^t \underline{\Phi}(t, \tau) \underline{v}(\tau) d\tau$ for $t_0 \leq t \leq t_0 + T$.

Since we are using numerical integration on the computer we actually progress in time by steps. If h is the step size and is constant then we would find $\underline{\Phi}(kh, 0)$ for $k=0, 1, \dots, T/h$. Since the numerical procedure uses variable step sizes we symbolically write $k=0 \rightarrow T/h$ to mean $\underline{\Phi}(kh, t_0)$ is determined at the appropriate time points between $t=0$ and $t=T$.

- ii) Using (4.161) find the solution $\underline{z}^P(t_0)$. Actually, the most efficient computational methods will solve

$$[\underline{I} - \underline{\Phi}(t_0 + T, t_0)] \underline{z}^P(t_0) = \int_{t_0}^{t_0 + T} \underline{\Phi}(t_0 + T, \tau) \underline{v}(\tau) d\tau, \quad (4.162)$$

rather than find the actual inverse.

- iii) Using $\underline{z}^P(t_0)$ and the time histories of $\underline{\Phi}(t, t_0)$ and $\int_{t_0}^{t_0+t} \underline{\Phi}(t, \tau) \underline{v}(\tau) d\tau$, compute the periodic solution vector $\underline{z}^P(t_0 + t)$ for $0 \leq t \leq T$. Actually, we find $\underline{z}^P(t_0 + kh)$ for $k=0 \rightarrow T/h$, as explained above.

Hence, knowing $\underline{z}^P(kh)$ between $t=0$ and $t=T$ uniquely defines the total solution $\underline{z}(t)$.

As we indicated in the above subsections on time domain methods, the step size, h , is variable and chosen automatically, according to the particular integration method, in order to provide a desired accuracy in $H_n(t; f)$. By contrast, a frequency-domain approach would require, somehow, the determination of the number of Fourier coefficients to be used. Should H_n have a region

of rapid variation it would be necessary to solve for a large number of Fourier coefficients no matter how small that region is. The time-domain solution would require a small step size only in the region of rapid variation. In that region computation would be slow. But the speed will be made up in slow variation regions. The time-domain solutions which we have described will therefore be both more accurate and more efficient than a frequency domain solution approach.

CHAPTER 5
ELECTRONIC DEVICE MODELING

5.1 Introduction to Electronic Device Nonlinear Modeling

Fundamental to the successful application of the nonlinear system modeling and circuit analysis methods developed in this book are accurate nonlinear models for the active devices employed in the system. Device models of most interest will be commonly used in active regions where the device operation is quasi-linear about an operating point established by circuit bias. It is necessary to make a distinction between total and incremental nonlinear circuit models. Total models interrelate the total instantaneous voltages, currents, and/or charges in the device. Such models are required for operating point and large-signal circuit analyses. They are also the starting point for the development of incremental nonlinear models in a quasi-linear small-signal analysis. In the development of the nonlinear incremental models individual total instantaneous nonlinear relationships will be expanded in a Taylor series in the time domain about circuit static operating-points in order to form the nonlinear dynamic incremental models. The leading term in the Taylor series is linear. A circuit model containing only the leading term for each nonlinearity is the familiar linear incremental circuit model commonly utilized in small-signal analysis and design. Additional terms from the Taylor series can be added to form nonlinear incremental models. For example, three terms from the series are needed for a third-order model.

It is desirable to have device models that can be utilized wherever they may be biased in the normal active region. This is

accomplished primarily by seeking mathematical relationships relating the device model parameters to the operating bias points. The reason this objective is desirable is it enables the prediction of nonlinear effects as the operating point may change, for example, by an AGC control voltage. We shall also find that, given a mathematical model, far fewer parameters will frequently be necessary to characterize the nonlinear incremental model than a complete set of Taylor series coefficients for every operating point.

The models we seek must also be capable of accurately predicting distortion levels in the presence of much larger input signals causing the distortion. For example, third-order effects may be 60 dB below the input signals generating the distortion.

There are many possible electronic devices that may be employed in communication systems that introduce physical nonlinearities causing distortion and signal degradations. We shall be primarily concerned with bipolar transistors and vacuum tubes.

5.2 Semiconductor Diode

It is the objective of this section to review the electrical characteristics of semiconductor diodes and to present a reasonably accurate total as well as incremental nonlinear equivalent electrical circuit for a physical diode. An excellent elementary review of basic pn junction diode properties can be found in Gray (1964). Our presentation begins with a summary of ideal diode static and dynamic characteristics. Several examples of characteristics for an actual metal-semiconductor junction diode are shown. Examples of departures from the ideal diode for both forward and reverse bias conditions are illustrated.

5.2.1 Ideal Semiconductor Diode

5.2.1.1 Static Characteristics

The total static, or DC current I , through an ideal semiconductor junction diode is an exponential function of the total voltage, V , across the junction and is given by

$$I = I_s \left[e^{\frac{qV}{kT}} - 1 \right], \quad (5.1)$$

where

I_s = saturation current

q = magnitude of charge of an electron =
 1.602×10^{-19} coulomb

k = Boltzmann constant = 1.380×10^{-23} joule
per degree Kelvin

T = absolute temperature in degrees Kelvin.

At room temperature ($T = 290^\circ\text{K}$), $\frac{kT}{q}$ is 25 millivolts. Eq. (5.1) is shown for low-level junction voltages on a normalized linear current scale in Figure 5.1. The forward current characteristics of the ideal diode are shown on a semi-log scale in Figure 5.2.

Note that the characteristics approach the straight line $\exp\left[\frac{qV}{kT}\right]$ for large $\frac{qV}{kT}$. The straight line intersects the normalized current scale for $V = 0$ at the saturation current. This fact can be useful in determining I_s from data measured in the forward current region of the diode.

5.2.1.2 Junction Depletion-Layer Capacitance

The semiconductor junction region of the ideal diode is a space charge layer or dipole layer of charge density. The

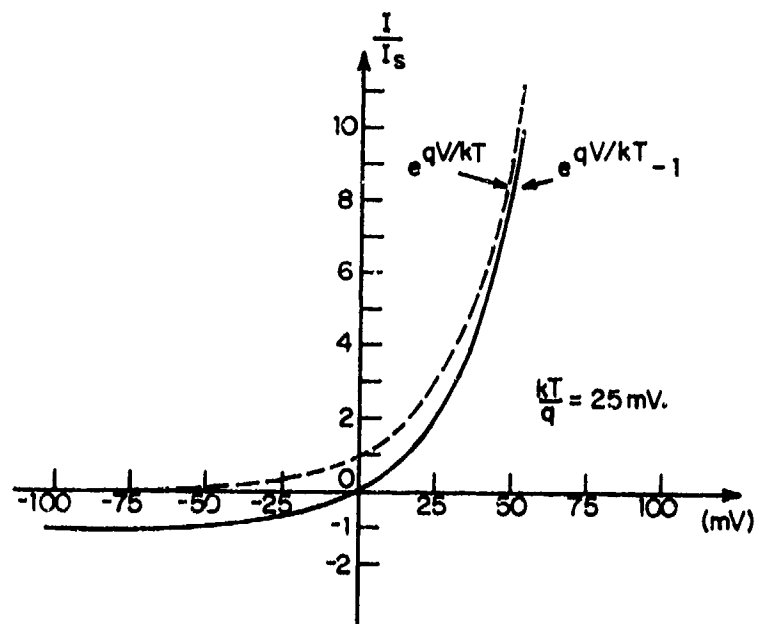


Fig. 5.1. Ideal Diode Characteristics.

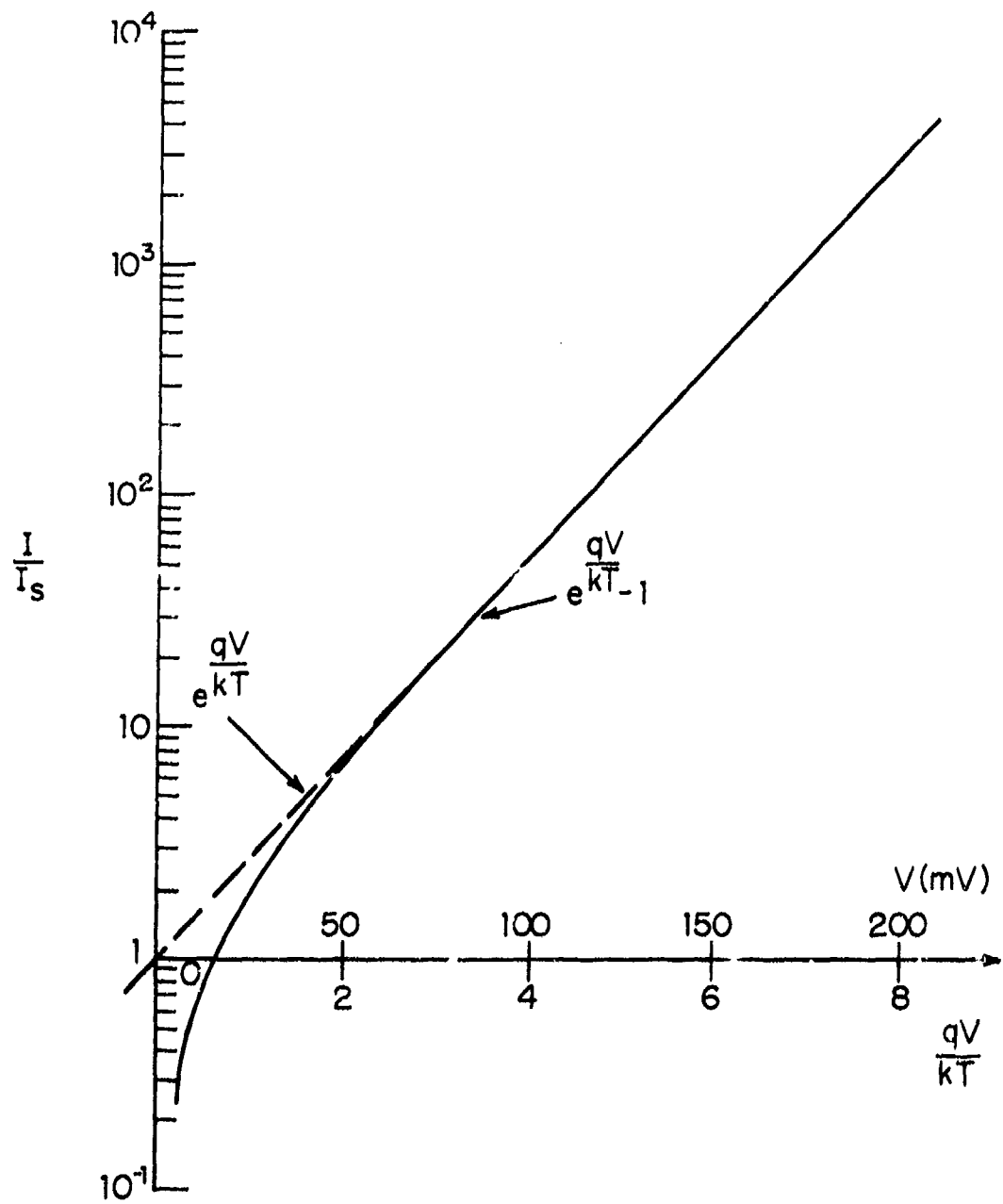


Fig. 5.2. Ideal Diode Forward Current Characteristics.
($kT/q = 25$ mV for voltage scale).

charge stored in either half of this dipole layer depends upon the bias voltage. Therefore, the junction capacitance is a function of the voltage applied to the junction as well as the distribution of charge for a fixed voltage. The theoretical value of this capacitance for the ideal reverse-biased diode in terms of the total voltage V at the junction is given by

$$C(V) = \frac{C(0)}{\left[1 - \frac{V}{\phi}\right]^\mu}, \quad (5.2)$$

where

- $C(0)$ = capacitance for $V = 0$
- V = total externally applied voltage
- ϕ = internal barrier potential
- μ = $\begin{cases} 1/2; & \text{abrupt junction} \\ 1/3; & \text{graded junction} \end{cases}$

In terms of elastance $S = \frac{1}{C}$,

$$\frac{S(V)}{S(0)}^{\frac{1}{\mu}} = 1 - \frac{V}{\phi}. \quad (5.3)$$

This form of Eq. (5.2) is useful for determining the internal potential and the junction type. The value of $1/\mu$ causing the left hand side of Eq. (5.3) to plot linearly as a function of junction voltage V establishes μ . This is illustrated in Figure 5.3 for the abrupt junction. The intercept of the straight line $1 - \frac{V}{\phi}$ with the horizontal axis of the curve gives the internal potential ϕ .

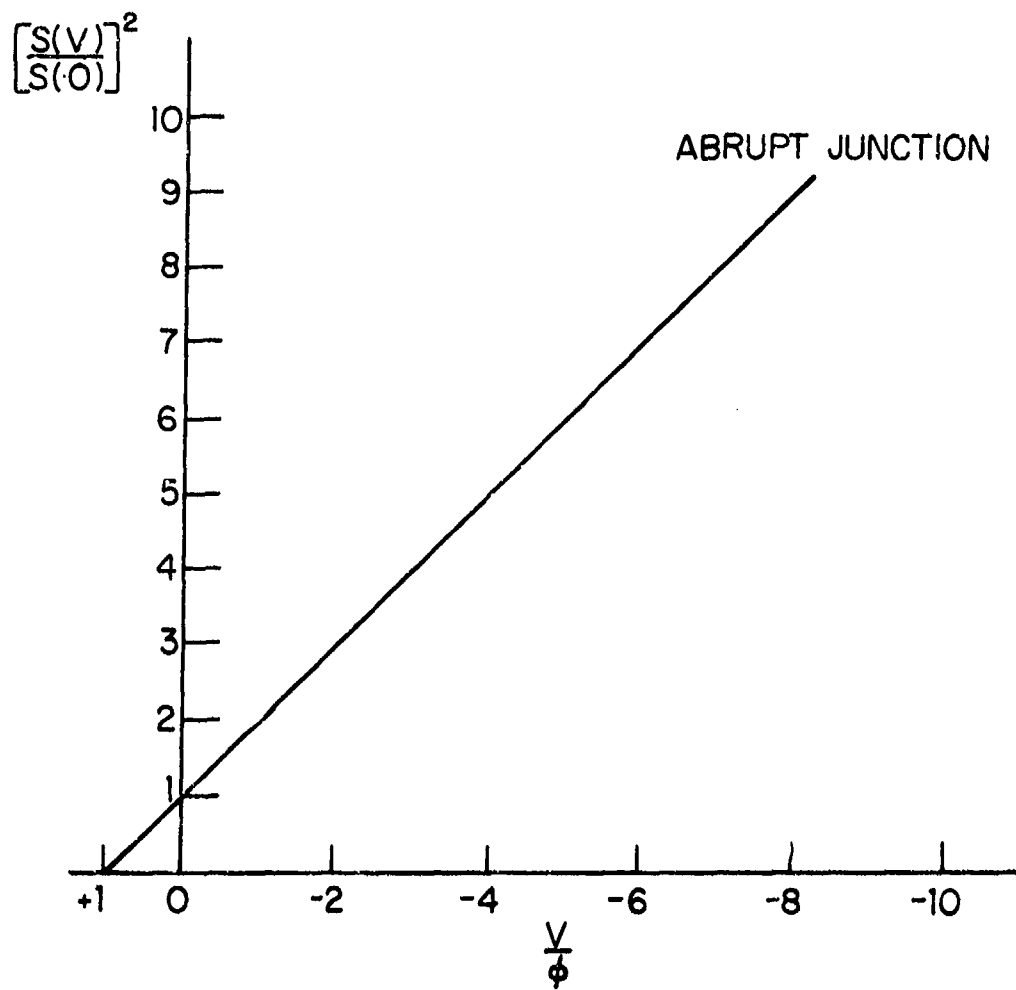


Fig. 5.3. Normalized (Elastance)² Voltage Dependence upon Junction.

The space-charge-layer capacitance accounts for most of the junction capacitance when the junction is reverse biased. When the junction is forward biased, charge carriers are drawn across the junction. If the lifetime of the carriers is much greater than the period of the applied signal, the carriers will appear to cause a second capacitance known as the diffusion capacitance which is in parallel with the space-charge-layer capacitance. The magnitude of the diffusion capacitance is proportional to the diode current.

5.2.1.3 Avalanche Breakdown

Hot-carrier and pn junction diodes, when reverse-biased, exhibit an effect known as avalanche breakdown or current multiplication. Avalanche current multiplication occurs when the electric field in the space-charge-layer of the diode is large enough so that carriers traversing the space-charge region acquire sufficient energy to break covalent bonds. Defining a multiplication factor M , the total reverse current becomes I_s^M instead of I_s . M has been experimentally found to be of the form [Miller, 1965]

$$M = \frac{1}{1 - (V/V_{BD})^\eta}, \quad (5.4)$$

where V_{BD} = breakdown voltage. A curve of M for several values of η as a function of V/V_{BD} is shown in Figure 5.4. Avalanche multiplication occurs only in a reverse-biased junction.

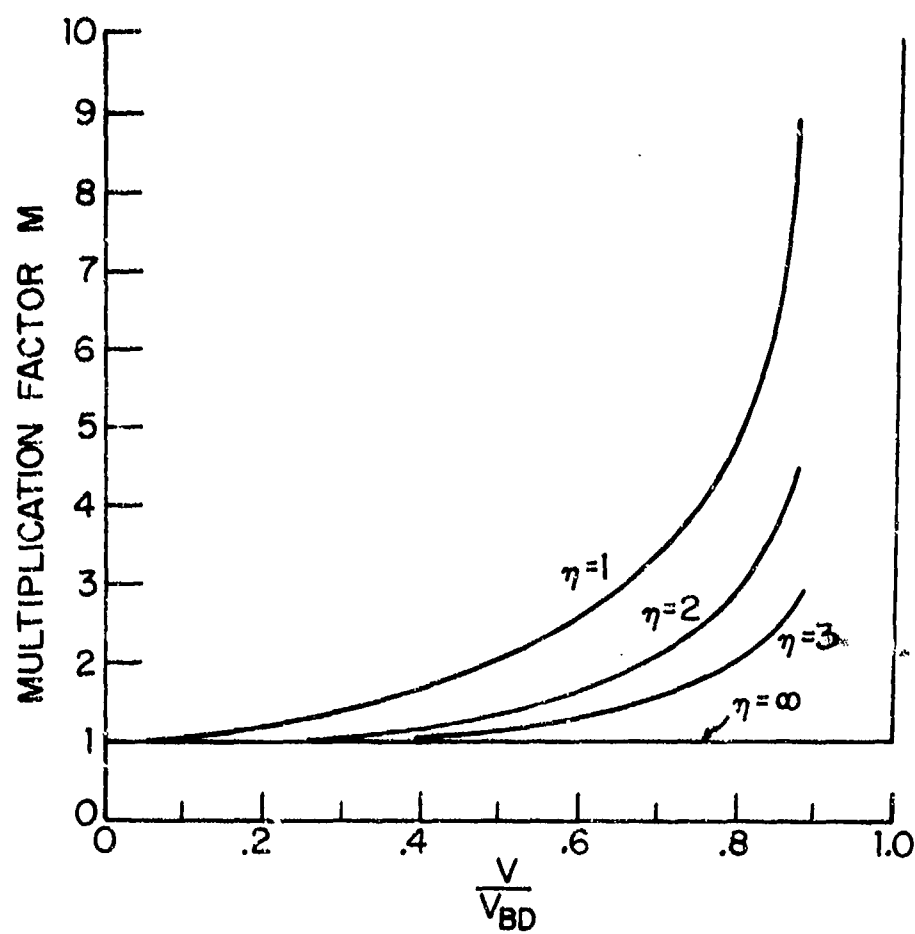


Fig. 5.4. Avalanche Breakdown Current Multiplication Factor M .

5.2.2 Total Equivalent Nonlinear Circuit Model of a Semiconductor Diode

Total equivalent nonlinear circuits of semiconductor diodes are summarized in this section. The total equivalent nonlinear circuit for a forward-biased diode is shown in Fig. 5.5. The nonlinear voltage-dependent current source is the exponential diode model with the quality factor n added to the exponent. A fixed series resistance R_s has been added. Inductance L is internal lead inductance while C is case capacitance associated with the diode package. The capacitance C_j is the sum of the diffusion and the space-charge capacitances. The diffusion capacitance is absent in hot-carrier diodes. The model will frequently be reduced to R_s in series with the current generator $I(V)$. The reverse-biased total equivalent circuit is shown in Fig. 5.6. The nonlinear voltage-dependent current source $I(V)$ models the effect of avalanche breakdown. Capacitance $C(V)$ models the depletion-layer capacitance. R_s is again a fixed series resistance. L and C are, respectively, lead inductance and package capacitance. The reverse-biased total model also will frequently be simplified to just R_s in series with $C(V)$.

Typical values for the Schottky-barrier diode are $I_s = 10\text{nA}$, $n = 1.05$, $R_s = 10 \Omega$, $C(0) = 0.8 \text{ pF}$, $\phi = 0.45 \text{ V}$, $\mu = \frac{1}{2}$, $L = 3 \text{ nH}$, $C = 0.15 \text{ pF}$, with $V_{BD} = -35 \text{ V}$, so that $C(V)$ is restricted to reverse bias less than 35 V.

There are other important parameters associated with diode models which are of interest in receiver design. These include the incremental circuit model parameters which are implicit in the total model. Equivalent noise source models [Van der Ziel,

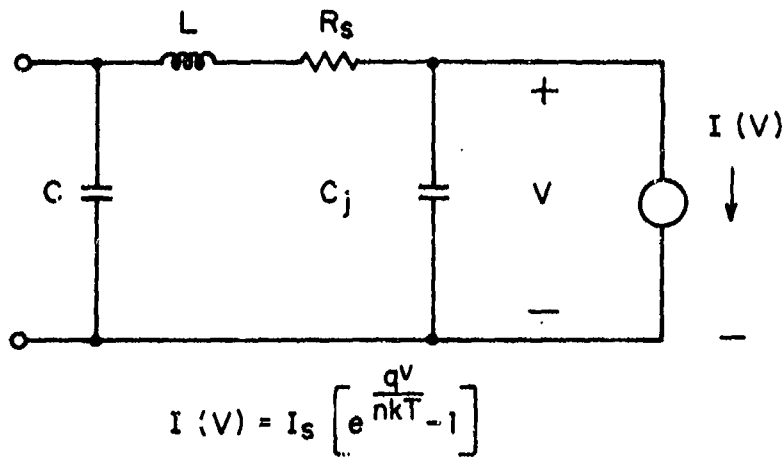
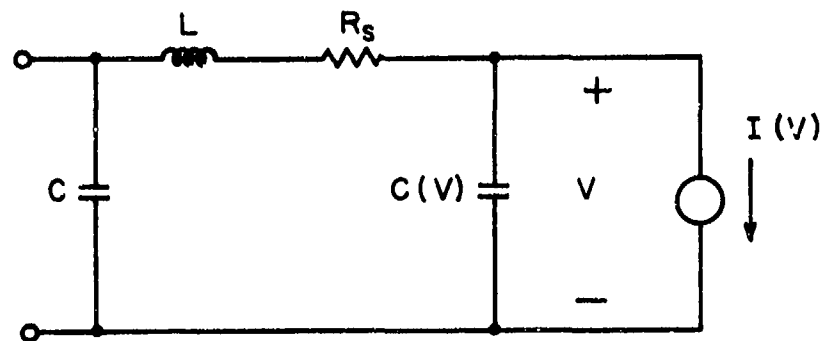


Fig. 5.5. Forward-Biased Total Equivalent Nonlinear Circuit of a Semiconductor Diode. [V > 0].



$$I(V) = \frac{I_s}{1 - \left(\frac{V}{V_{SD}}\right)^\eta}$$

$$C(V) = \frac{C(0)}{\left(1 - \frac{V}{\phi}\right)^\mu}$$

Fig. 5.6. Reverse-Biased Total Equivalent
Nonlinear Circuit of a Semiconductor
Diode [$V < 0$].

1970] are of interest for dynamic range studies. The total equivalent models in Figs. 5.5 and 5.6 do not include the effects of minority carrier storage accounting for the current waveforms for the pn junction when the diode is used in a switching mode. The models presented here are satisfactory for hot-carrier diodes used as switches because such diodes have very short switching mode recovery times.

5.2.3 Incremental Equivalent Nonlinear Circuit Model of a Semiconductor Diode

In this section we summarize the incremental equivalent nonlinear semiconductor model, based on the total models of Figures 5.5 and 5.6. In normal small-signal applications where the incremental models are valid, diodes are either operated at a forward-bias as in a biased-mixer, or at a reverse-bias, as in a varactor converter. Thus, there are two distinct small-signal semiconductor models.

In the case of the forward-biased diode, the primary nonlinearity is the exponential diode junction. This is a zero-memory nonlinearity characterized by

$$I = I_s \left[e^{\frac{qV}{nkT}} - 1 \right], \quad (5.5)$$

where n is the ideality factor for the diode. The incremental model for a forward-bias of V_D , an incremental voltage of v_d volts, a forward-bias current of I_D , and an incremental current of i_d is given by:

$$I_D + i_d = I_s \left[e^{\frac{qV_D}{nkT}} e^{\frac{qv_d}{nkT}} - 1 \right]. \quad (5.6)$$

As long as qv_d/nkT is less than unity, the exponential can be expanded in a Taylor's series and truncated after a small number of terms:

$$e^{\frac{qv_d}{nkT}} = 1 + \frac{qv_d}{nkT} + \frac{1}{2!} \left(\frac{qv_d}{nkT} \right)^2 + \frac{1}{3!} \left(\frac{qv_d}{nkT} \right)^3 \dots \quad (5.7)$$

Substituting Eq. (5.7) into Eq. (5.6)

$$\begin{aligned} I_D + i_d &= I_s \left[\exp\left(\frac{qv_D}{nkT}\right) - 1 \right] \\ &+ I_s e^{\frac{qv_D}{nkT}} \left[\frac{qv_d}{nkT} + \frac{1}{2!} \left(\frac{qv_d}{nkT} \right)^2 + \frac{1}{3!} \left(\frac{qv_d}{nkT} \right)^3 \dots \right]. \end{aligned} \quad (5.8)$$

The forward bias current, I_D , is given by:

$$I_D = I_s \left[\exp\left(\frac{qv_D}{nkT}\right) - 1 \right] \approx I_s e^{\frac{qv_D}{nkT}}. \quad (5.9)$$

Therefore,

$$i_d = I_d \left(\frac{q}{nkT} \right) v_d + \frac{1}{2!} I_d \left(\frac{q}{nkT} \right)^2 v_d^2 + \frac{1}{3!} I_d \left(\frac{q}{nkT} \right)^3 v_d^3 \dots \quad (5.10)$$

Equation (5.10) is the mathematical model of the incremental nonlinear resistive diode. When a diode is to be modeled as a linear resistance r_d , the value of r_d is the reciprocal of the coefficient of the linear term in Eq. (5.10), or

$$r_d \triangleq \frac{nkT}{qI_D}. \quad (5.11)$$

Since n is of the order of unity and kT/q is approximately 25 mV at room temperature,

$$r_d \approx \frac{25}{|I_D|} \text{ ohms, } I_D \text{ in mA.} \quad (5.12)$$

The forward-biased diode is generally operated sufficiently below its cut-off frequency so that the nonlinearities associated with the junction capacitance can be neglected, and the junction capacitance can be represented by a fixed capacitor. The incremental nonlinear circuit model of the forward-biased diode is shown in Figure 5.7. The model shows the nonlinearities as controlled current sources where

$$K_t = \frac{1}{t!} I_d \left(\frac{q}{nKT} \right)^t. \quad (5.13)$$

In the case of the reverse-biased diode, the primary nonlinearity is the nonlinear junction capacitance $C(V)$. The avalanche multiplication factor is of more importance in transistors than in conventional diodes, and will be considered in greater detail in the transistor model. Capacitance $C(V)$ is given by

$$C(V) = \frac{C(0)}{[1 - V/\phi]^\mu}. \quad (5.14)$$

The charge stored in the capacitor is

$$\begin{aligned} Q(V) &= \int_0^V C(v) dv \\ &= \frac{\phi}{\mu-1} \frac{C(0)}{[1 - V/\phi]^{\mu-1}}. \end{aligned} \quad (5.15)$$

The Taylor's series expansion of Equation (5.15) around an operating point V_C is

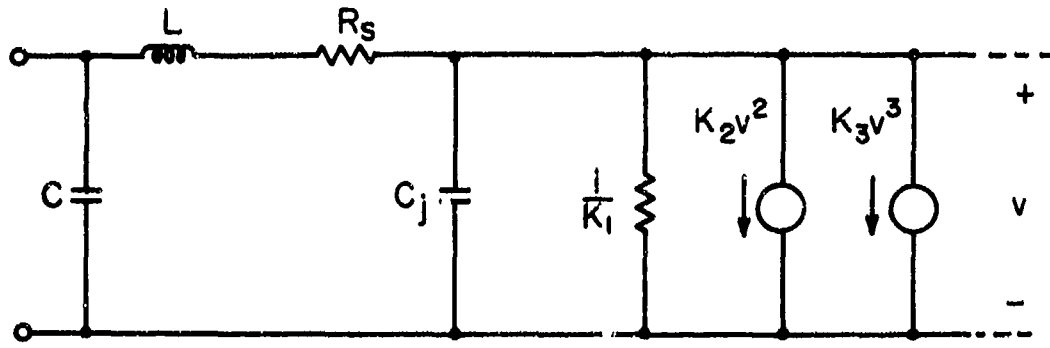


Fig. 5.7. Forward-Biased Incremental Nonlinear Circuit of a Semiconductor Diode.

$$Q(V_C + v_c) = C(V_C) \left[\frac{(\phi - V_C)}{(\mu - 1)} + v_c + \frac{\mu v_c^2}{2! (\phi - V_C)} + \frac{\mu(\mu+1)v_c^3}{3! (\phi - V_C)^2} \dots \right]. \quad (5.17)$$

The incremental capacitor current i_c is the derivative of the total charge with respect to time. Since V_C is constant, the incremental capacitor current is given by the time derivative of v_c in Equation (5.17). Hence

$$i_c = C(V_C) \frac{dv_c}{dt} + \frac{\mu C(V_C)}{2! (\phi - V_C)} \frac{dv_c^2}{dt} + \frac{\mu(\mu+1)C(V_C)}{3! (\phi - V_C)^2} \frac{dv_c^3}{dt} \dots \quad (5.18)$$

Equation (5.18) is the mathematical model of the incremental nonlinear capacitance current. The first term is a linear capacitor of value $C(V_C)$, and the terms in v_c^n represent the n^{th} -order nonlinearities. The incremental nonlinear circuit model of the reverse biased diode is shown in Figure 5.8. The model shows the nonlinearities as controlled current sources, with coefficients γ_ℓ . From Equation (5.17) the γ_ℓ are equal to

$$\gamma_\ell = \frac{\mu(\mu+1)\dots(\mu+\ell-2)}{\ell! (\phi - V_C)^{\ell-1}} C(V_C); \quad \ell \geq 2. \quad (5.19)$$

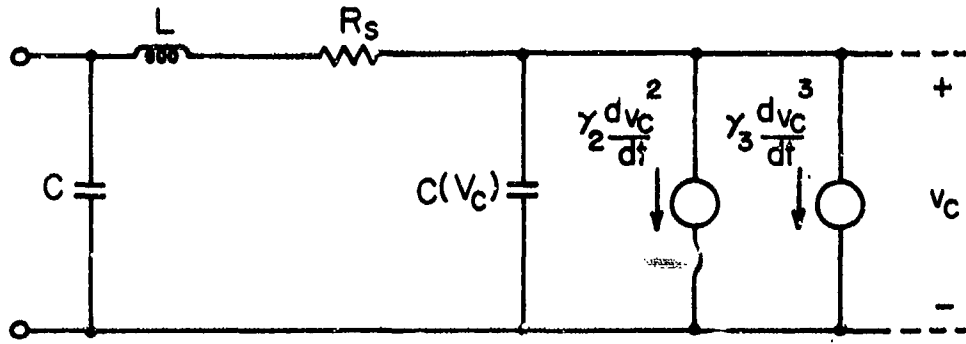


Fig. 5.8. Reverse-Biased Nonlinear Incremental Model of a Semiconductor Diode.

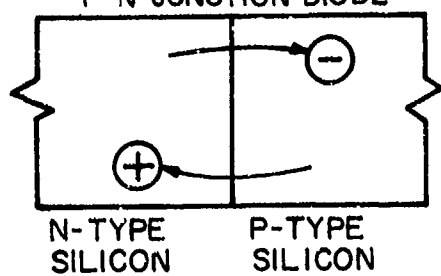
5.2.4 Examples of Semiconductor Diodes

There are three main categories of semiconductor diodes, namely, the pn junction diode, the point-contact diode, and the Schottky barrier, or hot-carrier diode. Figure 5.9 shows the idealized construction of these diodes. The point-contact diode, the first semiconductor diode to be developed, has little application in communication receivers. The pn junction diode is used in both mixers and detector circuits as well as a varactor. The hot-carrier diode is a simple metal-semiconductor interface. When forward-biased, current flows because of majority carrier injection from the semiconductor into the metal. Hot-carrier diodes are free of both the long reverse recovery time and diffusion capacitance of the pn junction diode. Hot-carrier diodes have electrical characteristics that, in many respects, come close to the ideal-diode properties described in Section 5.2.1. Hot-carrier diodes are also used extensively in receiver mixers and detectors. Actual data from several diode devices will be used in the remainder of this section to illustrate various differences between ideal diodes and their physical counterpart.

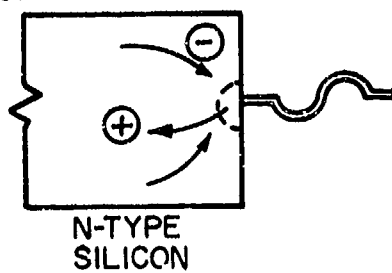
5.2.4.1 Forward Static Characteristics

Typical forward current versus forward voltage characteristics of a hot-carrier diode are shown in Fig. 5.10. The median curve differs from the ideal diode characteristic shown in Figure 5.2 in two significant ways. First, the actual diode terminal voltage is not exponentially related to terminal current, since the data deviates at high current levels considerably from the straight line that is tangent to

P-N JUNCTION DIODE



POINT CONTACT DIODE



SHOTTKY BARRIER DIODE

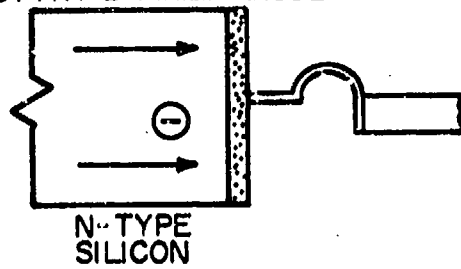


Fig. 5.9. P-N, Point Contact, and Schottky Diode Comparison.

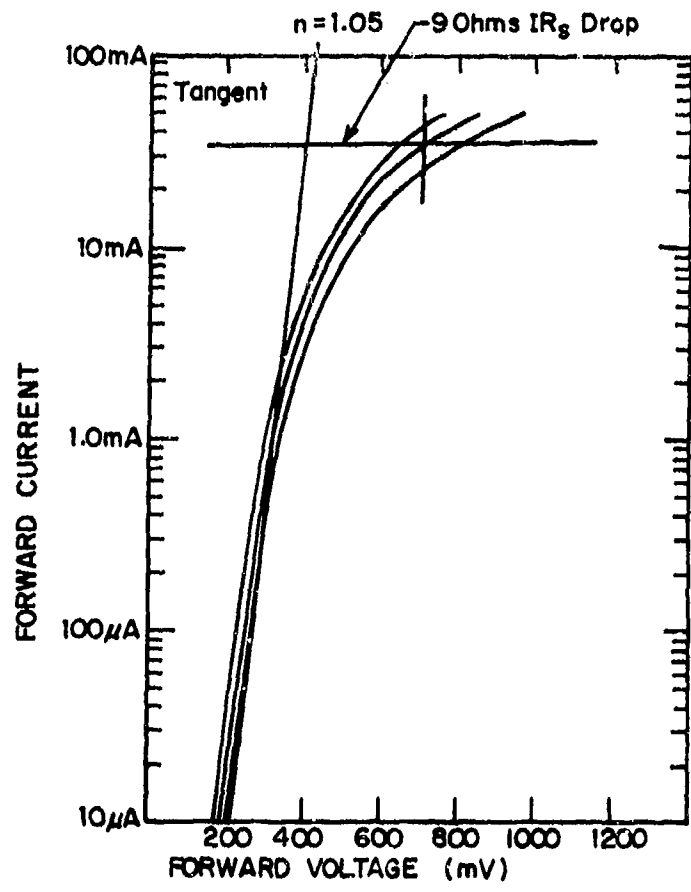


Fig. 5.10. HP 2302 Typical Minimum, Median, and Maximum Forward Current vs. Forward Voltage at $T_A = 25^\circ\text{C}$.

the low current data. In the example shown in Figure 5.10, approximately 9 ohms of fixed series resistance accounts for the extra voltage drop at the diode terminals. The slope of the straight line drawn tangent to the low current data is

$$n = \frac{q}{kT} \frac{\left| V_1 - V_2 \right|}{\ln \left| \frac{I_1}{I_2} \right|}, \quad (5.20)$$

when the diode forward characteristic is expressed by

$$I = I_s \left[e^{\frac{qV}{nkT}} - 1 \right]. \quad (5.21)$$

For the data in Figure 5.10, $n = 1.05$. The factor n , called the diode ideality factor, is a measure of the extent to which the physical diode differs from the ideal diode for which $n = 1$.

The saturation current I_s can also be estimated from the forward current characteristic. For diode currents approximated by the straight line region in Fig. 5.10 we have

$$I = I_s \exp \left[\frac{qV}{nkT} \right]. \quad (5.22)$$

For $I = 10 \mu A$ and $V = 200 \text{ mV}$, this gives $I_s \approx 6.1 \text{ nA}$ for the HP 2302 diode.

The static characteristics of a junction diode are also strongly dependent upon temperature. Illustrated in Fig. 5.11 are forward I-V characteristics for typical hot-carrier diodes at three different temperatures. Thermal coefficients for several fixed current levels are noted on the curves. Circuit models of diodes must include temperature dependence if they are to accurately represent physical diodes over large environmental temperature ranges.

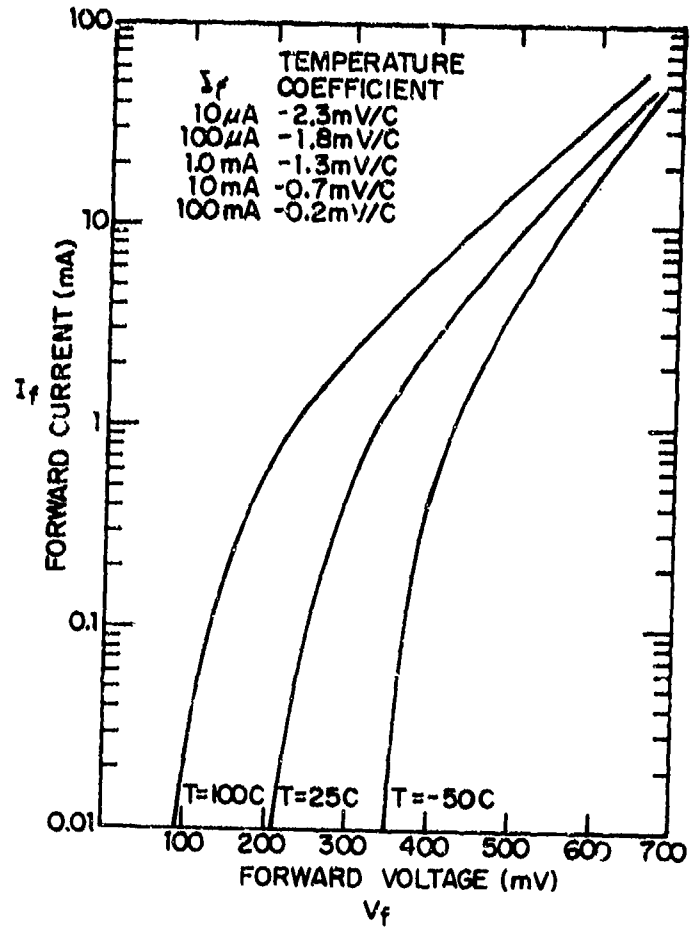


Fig. 5.11. I-V Curve Showing Typical Temperature Variation for HP 2300 Series Hot Carrier Diodes.

5.2.4.2 Reverse Characteristics

5.2.4.2.1 Static Characteristics

Typical reverse-current static characteristics for the HP 2300 series hot-carrier diode are shown in Fig. 5.12. The data are essentially linear on the semi-log graph which suggests an exponential dependence upon reverse voltage. In Section 5.2.4.1, I_s for the HP 2302 was estimated to be about 6.1 nA.

The static reverse-voltage characteristic for the ideal diode gives I_s as the reverse current. The data for the HP 2302 diode in Fig. 5.12 shows that reverse current varies exponentially between 20 and 80 nanoamperes over the 0 to 15 V reverse voltage range. Clearly, the ideal diode model is invalid for this particular diode in the reverse bias region. Although it does not show in the data on Fig. 5.12, the reverse breakdown voltage for the HP 2300 series diodes is greater than 30 V.

5.2.4.2.2 Junction Capacitance

Typical junction capacitance as a function of reverse voltage data are shown in Fig. 5.13 for the HP 2300 series hot-carrier diode. The hot-carrier diode is theoretically an abrupt-junction diode. Data taken from Fig. 5.13 are plotted in Fig. 5.14 in the form of $(\text{elastance})^2$ versus reverse junction voltage to test the agreement with the ideal reverse voltage junction capacitance discussed in Section 5.2.1.2. A straight line reasonably fits the data, to confirm the abrupt junction property. The internal barrier potential is seen to be about 1.5 volts. It is evident that the ideal junction diode reverse voltage capacitance reasonably models the actual diode junction capacitance.

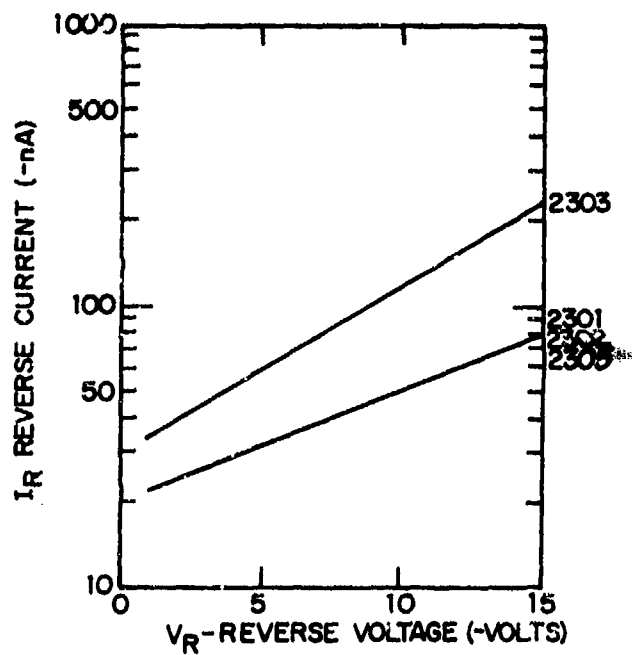


Fig. 5.12. HP 2300 Series Typical Reverse Current
vs. Reverse Voltage at $T_A = 25^\circ\text{C}$.

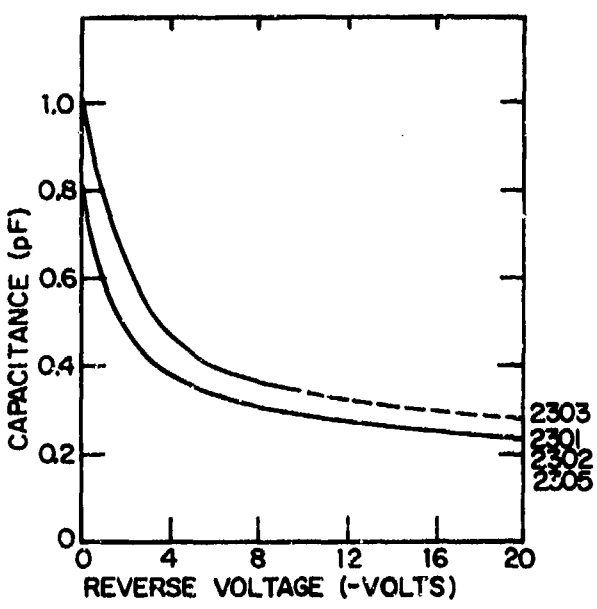


Fig. 5.13. HP 2300 Series Typical Capacitance vs.
Reverse Voltage at $T_A = 25^\circ\text{C}$.

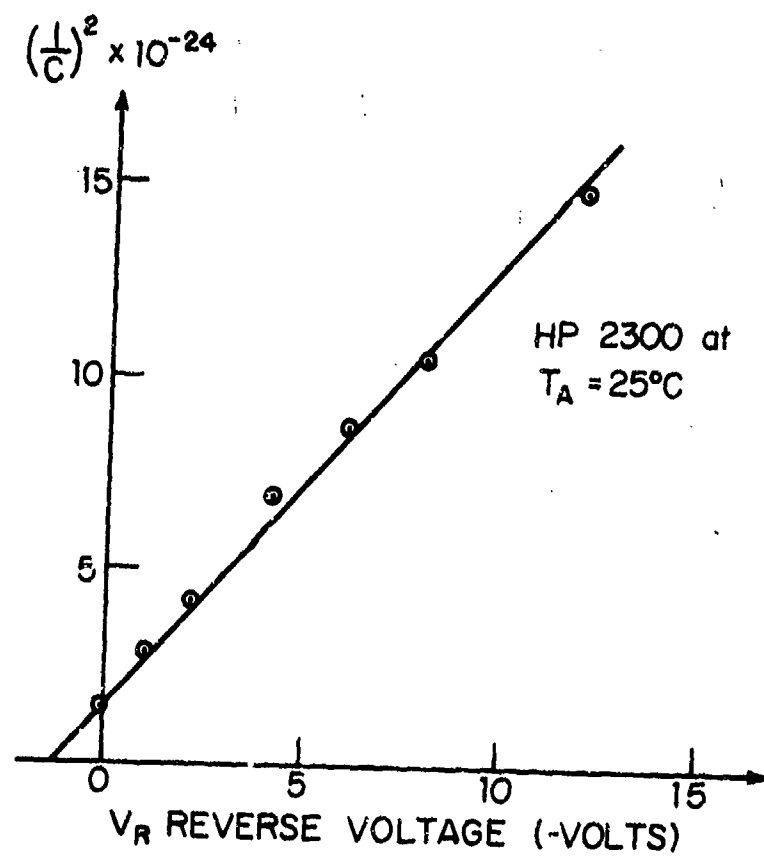


Fig. 5.14. $(Elastance)^2$ vs. Reverse Voltage.

5.2.4.3 Switching Characteristics of Junction Diodes

The switching characteristics of junction diodes are not generally adequately accounted for by the static I-V curves or by the reverse junction capacitance data such as that illustrated previously in Section 5.2.4. Shown in Fig. 5.15 are sketches of high speed oscilloscope traces of diode current response to sinusoidal voltage drive on a pn junction and on a hot-carrier diode. Note that the turn-off current waveform is significantly different than the turn-on transient for the pn junction diode. The hot-carrier diode does not exhibit this effect since it has virtually no storage of minority carriers. Diodes are sometimes deliberately designed to emphasize the storage mechanism to produce, for some applications, desirable switching current impulses. Data for a step-recovery diode is illustrated in Fig. 5.16. Step-recovery diodes are abrupt-junction silicon diodes used for harmonic generation applications.

Care must be exercised in modeling the semiconductor diode if the application requires a model to account for the switching transition region from forward to reverse-voltage conditions under dynamic conditions. Fortunately, the most commonly used high-speed diode for mixers, the Schottky-barrier diode, exhibits a very minimum of non-ideal switching characteristics.

5.3 Bipolar Junction Transistor Model

There are many different transistor models that are specialized to different operating conditions. One of the oldest models, that of Ebers-Moll (1954), represents the transistor by two sets of diodes and current generators, one for the base-emitter junction, and the other for the base-collector junction. Other large signal models which have been developed include the Linvill (1958) lumped model, and the Beaufoy-Sparkes (1957) charge-control model.

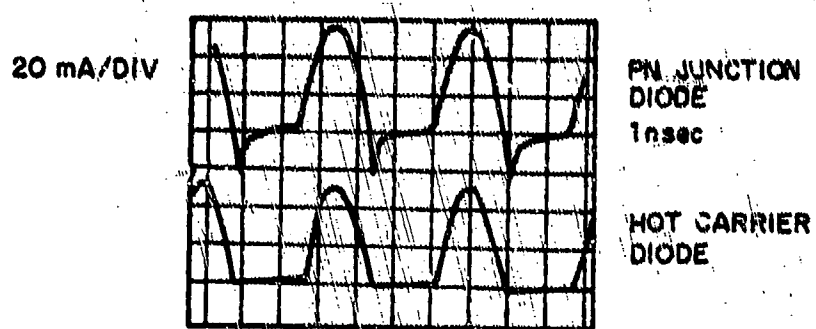


Fig. 5.15. Switching Characteristic of Hot Carrier and P-N Diodes.

Top: High Speed P-N with 1 nsec Recovery Time

Bottom: Hot Carrier Diode
Horizontal: 10 nsec/div.
Vertical: 20 mA/div.

Applied Signal: 30 MHz

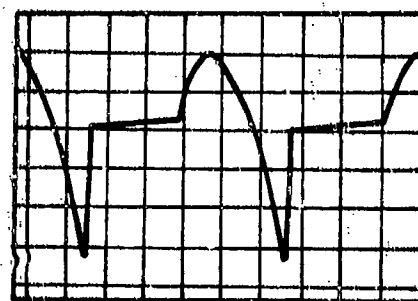


Fig. 5.16. Switching Characteristic of a Step-Recovery Diode.

A good review of these models can be found in Hamilton, et.al. (1964). In general, large-signal models are used in the solution of transient or switching circuit problems.

Small-signal transistor models have been developed for transistors over significant frequency ranges. The most common models are the hybrid-pi model and the T model. Discussions of these models can be found in Searle, et.al. (1964), Thornton, et.al. (1966), and Gartner (1960). A review of microwave transistors using both these models can be found in Cooke (1971). The charge-control model has also been applied to small-signal modeling, and good results have been reported by Gummel and Poon, (1970), Poon and Meckwood (1972), and Poon (1972). The nonlinear-T, utilizing a linear emitter capacitance, was applied to amplifier distortion analysis by Narayanan (1967). We shall use the nonlinear-T with the addition of a nonlinear emitter capacitance.

In this section, we will review the incremental model of the bipolar junction transistor, and note the physical source of each of its components. As part of this, we indicate which elements in the model are operating-point dependent. Following this, we show the generalization of the linear incremental T model to the nonlinear incremental model. For each of the elements in the nonlinear model we describe a method or methods of experimentally determining numerical values. In addition, examples of numerical values obtained from transistor specification sheets are described in Appendix B.

5.3.1 Linear Incremental T Model

5.3.1.1 Linear T Parameters

The linear incremental T model of the bipolar junction transistor is shown in Fig. 5.17. The linear incremental model has nine parameters. These are:

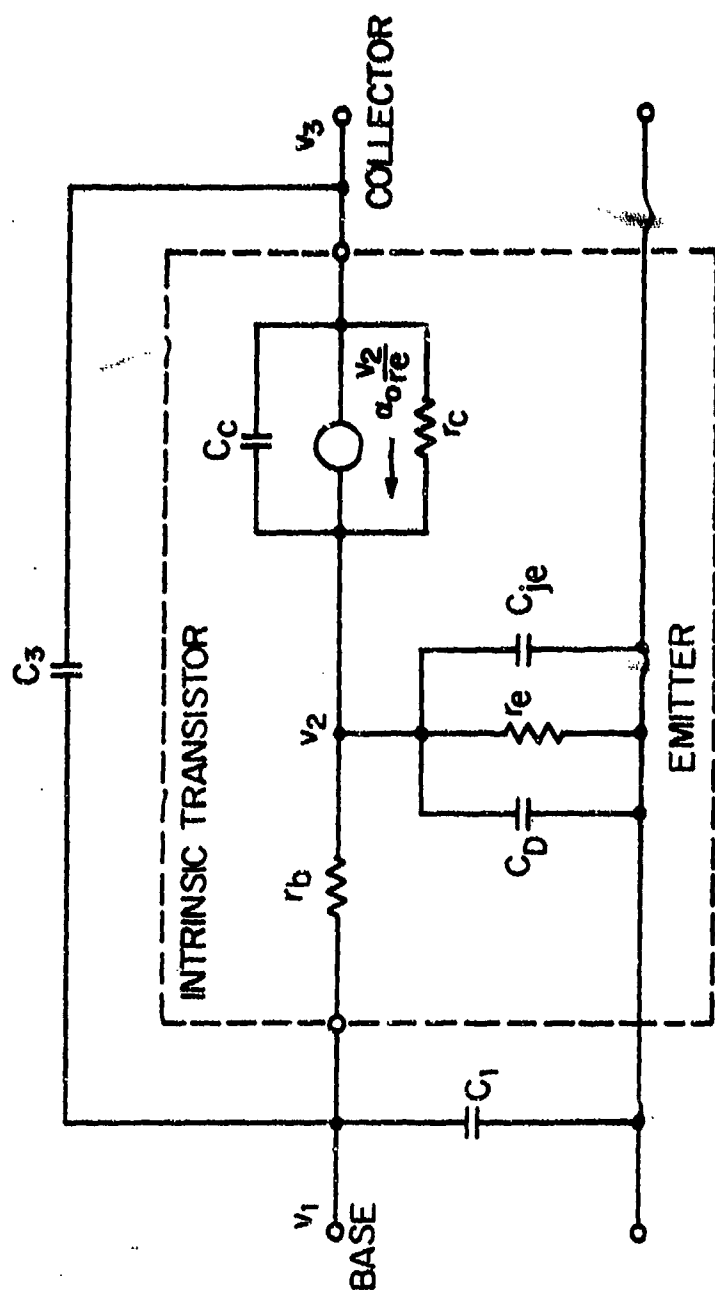


Fig. 5.17. Linear Incremental-T Transistor Model.

1. Base-Emitter Resistance r_e

The base-emitter resistance r_e represents the incremental resistance of the forward-biased base-emitter junction. The incremental resistance r_e is a nonlinear function of the emitter current; r_e varies inversely with the emitter bias current.

2. Base-Spreading Resistance, r_b

Resistance r_b is the base-spreading resistance due to the finite resistivity of the base region. Resistance r_b is known to be frequency dependent and at high frequencies tends to approach a constant value. It is assumed constant and independent of the operating point in our model.

3. Collector Resistance, r_c

Resistance r_c is the collector resistance. Physically it arises as a base-width modulation effect produced by incremental collector-junction bias. It is a large resistance which generally takes on importance only for high frequencies or large load impedances. It is assumed independent of the operating point.

4. Capacitance C_1

Capacitance C_1 is the header capacitance between the base and emitter terminals. It is a small capacitance, generally on the order of several pF, and is independent of the transistor operating point.

5. Capacitance C_D

Capacitance C_D is the diffusion capacitance associated with the storage in the base region of minority charge carriers injected into the base region by the forward-biased emitter junction. The diffusion capacitance is directly dependent upon the

emitter bias current. Consequently, the product $r_e C_D$ is nearly constant over a wide operating range since r_e is inversely dependent upon bias current. At sufficiently high current levels, this product determines the transistor cut-off frequency.

6. Capacitance C_{je}

Capacitance C_{je} is the space charge layer capacitance associated with the forward-biased emitter junction, and is equivalent to the diode capacitance described in Section 5.2. It is dependent on the bias voltage, is independent of the current, and, at sufficiently low current levels, may be greater than C_D . When this occurs, the product $r_e C_{je}$ is the determining factor for the transistor cut-off frequency.

7. Capacitance C_c

Capacitance C_c , often called the varactor capacitance, is the reverse-biased collector junction capacitance. C_c is nonlinearly dependent upon the voltage across the junction as described in Section 5.2.1.2. C_c , as shown in the linear equivalent circuit, is the first term in the power series expansion of the capacitance nonlinearity.

8. Capacitance C_3

Capacitance C_3 is physically due to two effects, one the collector-base header capacitance, and the other the so-called overlap capacitance. The overlap capacitance is physically due to the portion of the collector-base junction capacitance which lies outside of the active region of the base and is therefore not charged through the base impedance. Although, strictly speaking, C_3 is a function of the operating point it is considered a constant in the incremental model.

9. Current Gains α_o and h_{fe}

The dependent current generator in the collector circuit of Fig. 5.17 has a value $\alpha_o v_2 / r_e$. The parameter α_o is the low-frequency small-signal current gain, that is, the ratio of the short-circuit incremental collector current to the incremental emitter current. It is both current and voltage dependent, and thus must be evaluated at a specific operating point. The value α used in the linear T model is the first term in its power series expansion. It can alternatively be defined in terms of the low-frequency small signal common-emitter current gain h_{fe} , and is equal to $h_{fe} / (1 + h_{fe})$.

The definition of the current source as $\alpha_o v_2 / r_e$ has an implicit frequency dependence since v_2 / r_e is the incremental current through the emitter resistance r_e which is shunted by the capacitances C_D and C_{je} . Thus, the voltage v_2 will show the frequency cut-off due to the $r_e C_D$ and $r_e C_{je}$ products. Alternatively the dependent current generator can be defined as

$i_{et} \alpha_o / (1 + j f / f_\alpha)$, where i_{et} is the sum of the incremental current through r_e , C_D , and C_{je} , and f_α^{-1} is set equal to $2\pi r_e (C_D + C_{je})$. The two definitions are then equivalent. The frequency f_α is the current-generator half-power frequency. Related to f_α is f_β , the common-emitter half-power frequency, and f_T , the frequency at which the common-emitter current gain is unity. These frequencies are related: $f_\alpha = f_T = h_{fe} f_\beta$.

These nine parameters determine the linear incremental model of the transistor from a circuit point of view. However, the transistor can be looked upon as a linear two-port network, and described in terms of y , h , z , etc., matrices. In particular, the transistor device incremental measurements can be best made in terms of the h parameters and the y parameters.

5.3.1.2 Two-Port Linear Network Parameters

The linear incremental model of a transistor can be characterized as a two-port four terminal network. As such, many conventional parameter sets can be used to describe its behavior. Consider the general linear network shown in Fig. 5.18 with incremental input and output voltages v_1 and v_2 , and incremental input and output currents i_1 and i_2 . The y-parameter formulation is given by

$$i_1 = y_i v_1 + y_r v_2 \quad (5.23)$$

$$i_2 = y_f v_2 + y_o v_1 \quad (5.24)$$

which can be written in matrix form as

$$\begin{bmatrix} i_1 \\ i_2 \end{bmatrix} = \begin{bmatrix} y_i & y_r \\ y_f & y_o \end{bmatrix} \begin{bmatrix} v_1 \\ v_2 \end{bmatrix}. \quad (5.25)$$

The y-parameters are:

y_i = input admittance for short-circuited output

y_r = reverse transfer admittance for short-circuited input

y_f = forward transfer admittance for short-circuited output

y_o = output admittance for short-circuited input

A second parameter set, the h-parameters, is given by

$$v_1 = h_{i1} i_1 + h_{r2} v_2, \quad (5.26)$$

$$i_2 = h_{f1} i_1 + h_{o2} v_2. \quad (5.27)$$

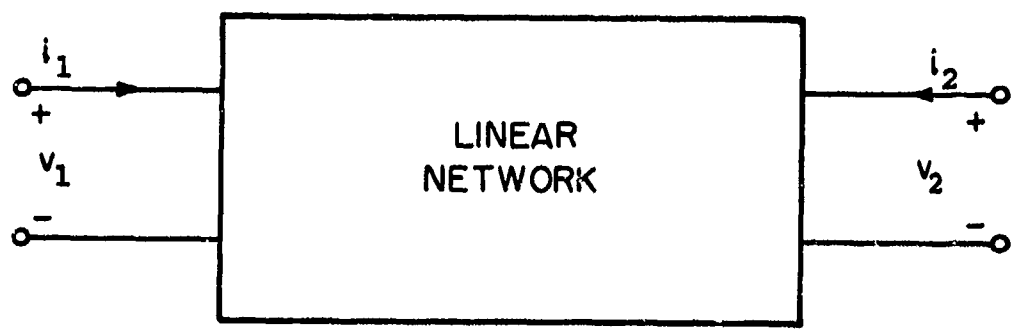


Fig. 5.18. Linear Two-Port Network.

or

$$\begin{bmatrix} v_1 \\ i_2 \end{bmatrix} = \begin{bmatrix} h_i & h_r \\ h_f & h_o \end{bmatrix} \begin{bmatrix} i_1 \\ v_2 \end{bmatrix}. \quad (5.28)$$

The h-parameters are:

- h_i = small-signal short-circuit input impedance,
 h_r = small-signal open-circuit reverse voltage,
transfer ratio
 h_f = small-signal short-circuit forward current
transfer ratio,
 h_o = small-signal open-circuit output admittance.

The h- and y-parameters are related in the following manner:

$$\left. \begin{array}{l} h_i = 1/y_i \quad h_r = -y_r/y_i \\ h_f = y_f/y_i \quad h_o = \Delta_y/y_i \end{array} \right\}, \quad (5.29)$$

where $\Delta_y = y_i y_o - y_r y_f$.

and

$$\left. \begin{array}{l} y_i = 1/h_i \quad y_r = -h_r/h_i \\ y_f = h_f/h_i \quad y_o = \Delta_h/h_i \end{array} \right\}, \quad (5.30)$$

where $\Delta_h = h_i h_o - h_r h_f$.

It is notationally more convenient to refer to parameters by matrix notation, for which we redefine the parameter subscripts as:

$$\begin{aligned} i &\rightarrow 11 \\ r &\rightarrow 12 \\ f &\rightarrow 21 \\ o &\rightarrow 22. \end{aligned} \tag{5.31}$$

or, for example, h_i becomes h_{11} , h_r becomes h_{12} , h_f becomes h_{21} , and h_o becomes h_{22} . Additionally, subscripts e, b, c are used to denote common emitter, base, and collector parameters.

The input and output impedances of the linear incremental model of the transistor terminated in an impedance Z_L and driven from an impedance Z_g can be written from a knowledge of the h- or y-parameters. These impedances are:

$$Z_{in} = \frac{1+y_{22}Z_L}{y_{11}+\Delta_y Z_L} = \frac{h_{11}+\Delta_h Z_L}{\Delta_h + h_{22}Z_L}, \tag{5.32}$$

$$Z_{out} = \frac{1+y_{11}Z_g}{y_{22}+\Delta_y Z_g} = \frac{h_{11}+Z_g}{\Delta_h + h_{22}Z_g}. \tag{5.33}$$

The modeling of UHF transistors presents a new set of problems. The frequency range of interest extends to, at least, 1 GHz. Special test jigs and measurement techniques suitable for use at UHF must be employed. Model parameterization requires use of S parameters. This comes about because the short and open-circuits needed for y, z, or h-parameter measurements cannot be reliably established in the region above 100 MHz. The matched terminations of an S parameter measurement can be established and maintained into the microwave region. Consider the linear network shown in Fig. 5.19. The two sets of wave variables, (a_1, b_1) , and (a_2, b_2) , represent the incident and reflected waves at the terminals of the network, and are defined by:

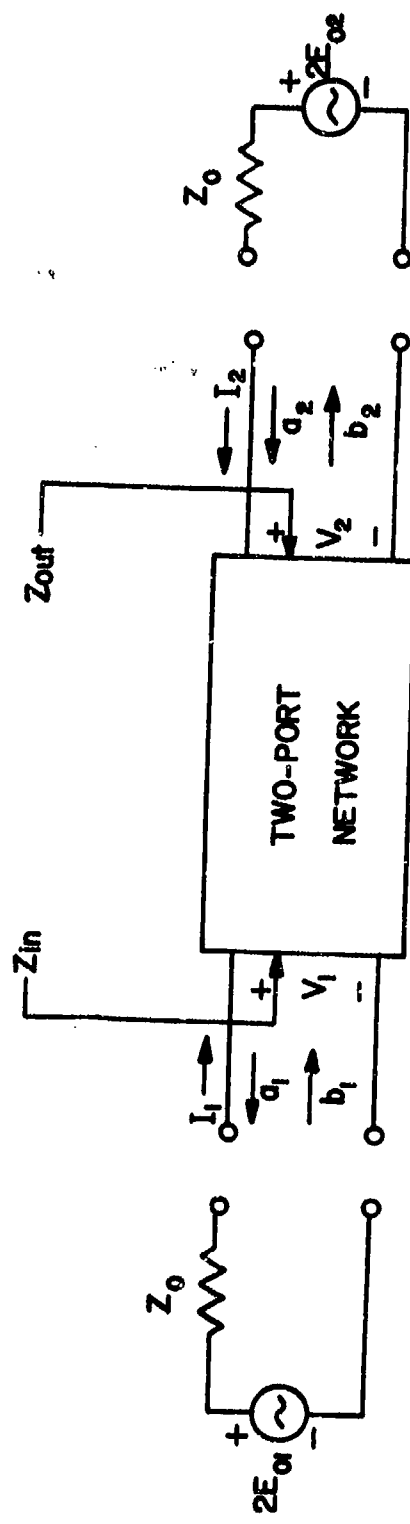


Fig. 5.19. Power Waves and a Two-Port Network.

$$\left. \begin{aligned} a_i &= \frac{1}{2} \left[\frac{v_i}{\sqrt{Z_0}} + \sqrt{Z_0} I_i \right], \quad i = 1, 2 \\ b_i &= \frac{1}{2} \left[\frac{v_i}{\sqrt{Z_0}} - \sqrt{Z_0} I_i \right], \quad i = 1, 2 \end{aligned} \right\}, \quad (5.34)$$

where Z_0 is positive real. The squares of a_i and b_i have the dimensions of power, and are known as power waves. They are related by the scattering matrix elements as follows:

$$\begin{bmatrix} b_1 \\ b_2 \end{bmatrix} = \begin{bmatrix} s_{11} & s_{12} \\ s_{21} & s_{22} \end{bmatrix} \begin{bmatrix} a_1 \\ a_2 \end{bmatrix}. \quad (5.35)$$

The parameters s_{11} and s_{22} are the reflection coefficients at the input and output ports, while s_{12} and s_{21} are the reverse and forward transmission coefficients, respectively. The scattering parameters s_{11} and s_{22} can be measured by exciting the two-port network with a_2 equal to zero, and s_{22} and s_{12} can be measured by exciting the network with a_1 equal to zero. Thus, working in a matched system with the network connected to the source and load by transmission lines of characteristic impedance Z_0 , the S parameter measurements can be made.

S parameters, while simple to measure, do not lead directly to device parameter values. However, the z, y, and h matrices, from which device parameters can be determined, can be easily written in terms of the S matrix. Computer programs can be written to derive the desired parameter set in terms of the S parameters. As an example, consider the measurement of f_T for a transistor. The frequency f_T is defined as the frequency at which the extrapolated value of incremental current gain h_{fe} is unity; f_T is an inferred, not a measured, quantity. In the h

matrix notation, h_{fe} is the h_{21} component, measured in the common-emitter connection, and can be expressed in terms of the S-parameters as

$$h_{21} = \frac{-2 s_{21}}{[1-s_{11}][1+s_{22}] + s_{12}s_{21}}. \quad (5.36)$$

Thus, if the common-emitter S parameters are measured as a function of frequency, h_{21} can be computed at the same frequency points and, finally, f_T found.

5.3.2 Nonlinear Incremental T Model

In this section, we describe the nonlinear incremental T model for the bipolar junction transistor. This model is shown in Fig. 5.20, and is the basic transistor model used in this book for small-signal nonlinear distortion analysis. The model differs from the linear incremental model in the following important aspects:

1. The base-emitter resistor r_e has been replaced by the nonlinear incremental current generator $K(v_2)$, for the base-emitter junction exponential nonlinearity.
2. The collector capacitor C_c has been replaced by the nonlinear incremental current generator $\gamma_c(v_3-v_2)$.

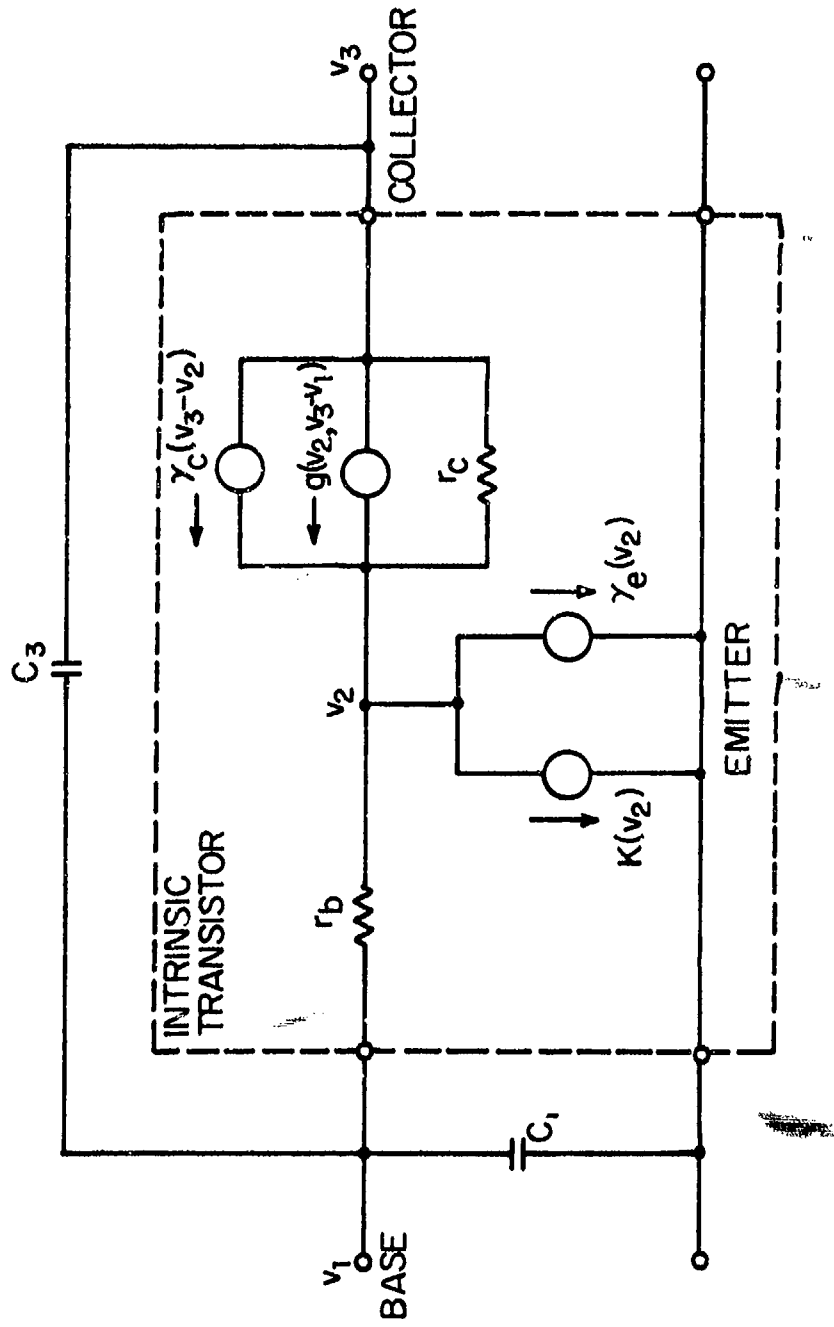


Fig. 5.20. Nonlinear Incremental T Transistor Model.

3. The collector current source $\alpha_{C_2} v_e / r_e$ has been replaced by the nonlinear incremental dependent current generator $g(v_2, v_3 - v_1)$, which includes both the h_{FE} nonlinearity and the avalanche nonlinearity.
4. Capacitors C_D and C_{je} have been combined into a nonlinear capacitor, represented by the nonlinear incremental current generator $\gamma_e(v_2)$.

We shall examine how the nonlinear elements in the model are defined, and outline methods of determining the model parameters. We begin with the nonlinear parameters using data taken in the measurement of a 2N2950 transistor. The 2N2950 is a NPN silicon annular transistor used for power and driver applications to 100 MHz. The particular 2N2950 which is used as the example in this section is the mixer transistor in the VHF receiver which is modeled in Chapter 7. The modeling of a 2N918, a NPN double-diffused silicon planar epitaxial transistor used as a UHF oscillator and amplifier is presented in Appendix B.

5.3.2.1 Base-Emitter Exponential Nonlinearity

The base-emitter junction is a semiconductor junction, and, like the diode of Section 5.2, has an exponential current-voltage relation. This relation is evident if one writes the large-signal static equations for the transistor. A suitable form are the Ebers-Möll equations, where we define:

I_{EO} = reverse saturation current of the emitter junction
with the collector open, $e^{qV_2/kT} \ll 1$, $I_C = 0$

I_{CO} = reverse saturation current of the collector junction
with the emitter open, $e^{-q(V_3-V_2)/kT} \ll 1$, $I_E = 0$

α_N = current gain in normal operation

α_I = current gain in inverted operation

Then, the equations for I_E , the total emitter current, and I_C ,
the total collector current, are:

$$I_E = -\frac{I_{EO}}{1-\alpha_N \alpha_I} \left[e^{\frac{qV_2}{kT}} - 1 \right] + \frac{\alpha_I I_{CO}}{1-\alpha_N \alpha_I} \left[e^{\frac{-q(V_3-V_2)}{kT}} - 1 \right], \quad (5.37)$$

$$I_C = \frac{\alpha_N I_{EO}}{1-\alpha_N \alpha_I} \left[e^{\frac{qV_2}{kT}} - 1 \right] - \frac{I_{CO}}{1-\alpha_N \alpha_I} \left[e^{\frac{-q(V_3-V_2)}{kT}} - 1 \right]. \quad (5.38)$$

The Ebers-Moll model is shown in Fig. 5.21. Equations (5.37)
and (5.38) are the Ebers-Moll equations for a NPN transistor
in a common-emitter connection. The Ebers-Moll model is a con-
venient total model of the transistor, as it shows the two
diodes which make up a junction transistor, as well as their
associated current generators. In the nonlinear T model shown
in Fig. 5.20, we have included the base resistor r_b which is
omitted from the Ebers-Moll model. Under normal operating
conditions, $qV_2/kT > 0$ and $-q(V_3-V_2)/kT \ll -1$, that is, the
emitter junction is forward biased and the collector junction
is reverse-biased. In this case, α_E reduces to

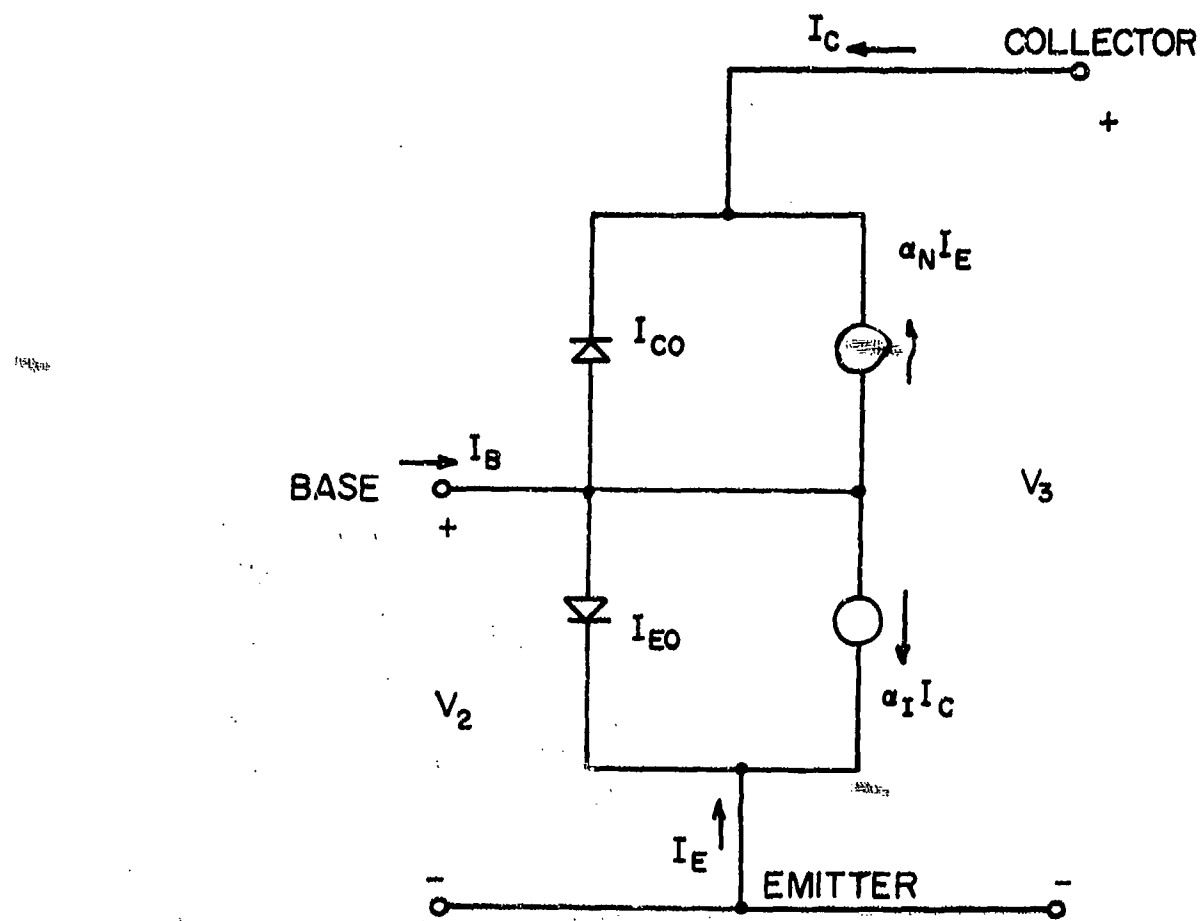


Fig. 5.21. NPN Ebers-Moll Model (Common-Emitter).

$$I_E = -\frac{I_{EO}}{1-\alpha_N \alpha_I} \left[e^{\frac{qv_2/kT}{N}} - 1 \right] - \frac{\alpha_I I_{CO}}{1-\alpha_N \alpha_I}. \quad (5.39)$$

or

$$I_E = A \left[\exp \left(\frac{qv_2}{kT} \right) - 1 \right] + B. \quad (5.40)$$

The additive term B in Eq. (5.40) is normally very small and can be neglected. In this case, Eq. (5.40) takes the same form as Eq. (5.5), and, as shown in Section 5.2.3 the incremental emitter current can be written as a power series in the incremental voltage v_2 to give the nonlinear incremental current model

$$-i_e = K(v_2) = K_1 v_2 + K_2 v_2^2 + K_3 v_2^3 + \dots \quad (5.41)$$

In Equation (5.41), the positive direction for i_e is defined from the reference node to the base node. If B is not small, we still get the same result for $K(v_2)$ since B is independent of v_2 . The coefficient of the first term, K_1 , is the linear incremental conductance and is given by

$$K_1 = \frac{q|I_E|}{kT}, \quad (5.42)$$

where I_E is the emitter bias or operating point current. If Eq. (5.41) were truncated after the linear term, K_1^{-1} would be interpreted as r_e , the equivalent incremental resistance of the base-emitter diode. It should also be noted that $K(v_2)$ is defined as the incremental current associated with the zero-memory exponential nonlinearity, and does not include the incremental current associated with $C_2 = C_D + C_{je}$ in Fig. 5.17.

A diode ideality factor should also be introduced into the emitter current Eq. (5.40) to account for imperfect junctions. At high current levels, a factor $n=1+m$ where m is of the order of 0.4 can occur. The plus sign applies for a pnp while the minus sign applies to npn transistors. Imperfect emitter junctions will have $n \neq 1$ even at low current levels. Therefore, the Taylor series coefficients K_t for the emitter junction current I_E are operating point dependent in a manner identical with the semiconductor diode coefficients as given by Eq. (5.13), or

$$K_t = \frac{1}{t!} |I_E| \left(\frac{q}{nkT} \right)^t, \quad (5.43)$$

where the emitter bias current I_E replaces the diode bias current and n is the ideality factor. As a practical matter it is only necessary to obtain the ideality factor n for the base-emitter junction characteristics to employ the incremental model. The bias current I_E is known explicitly from a given collector bias current I_C and the DC beta given by $h_{FE} = \frac{I_C}{I_B}$ since

$$I_E = -I_C \left[\frac{1+h_{FE}}{h_{FE}} \right]. \quad (5.44)$$

Measurements of the base-emitter static I-V characteristic should be made at zero base current conditions to avoid voltage drops in any DC base resistance that may be present. The internal junction emitter-base voltage is the desired parameter. The base-emitter junction static characteristic measured on the 2N2950 transistor are shown in Fig. 5.22. Note that experimental data points lie on straight lines to confirm that the emitter current is exponentially dependent upon the base-emitter voltage.

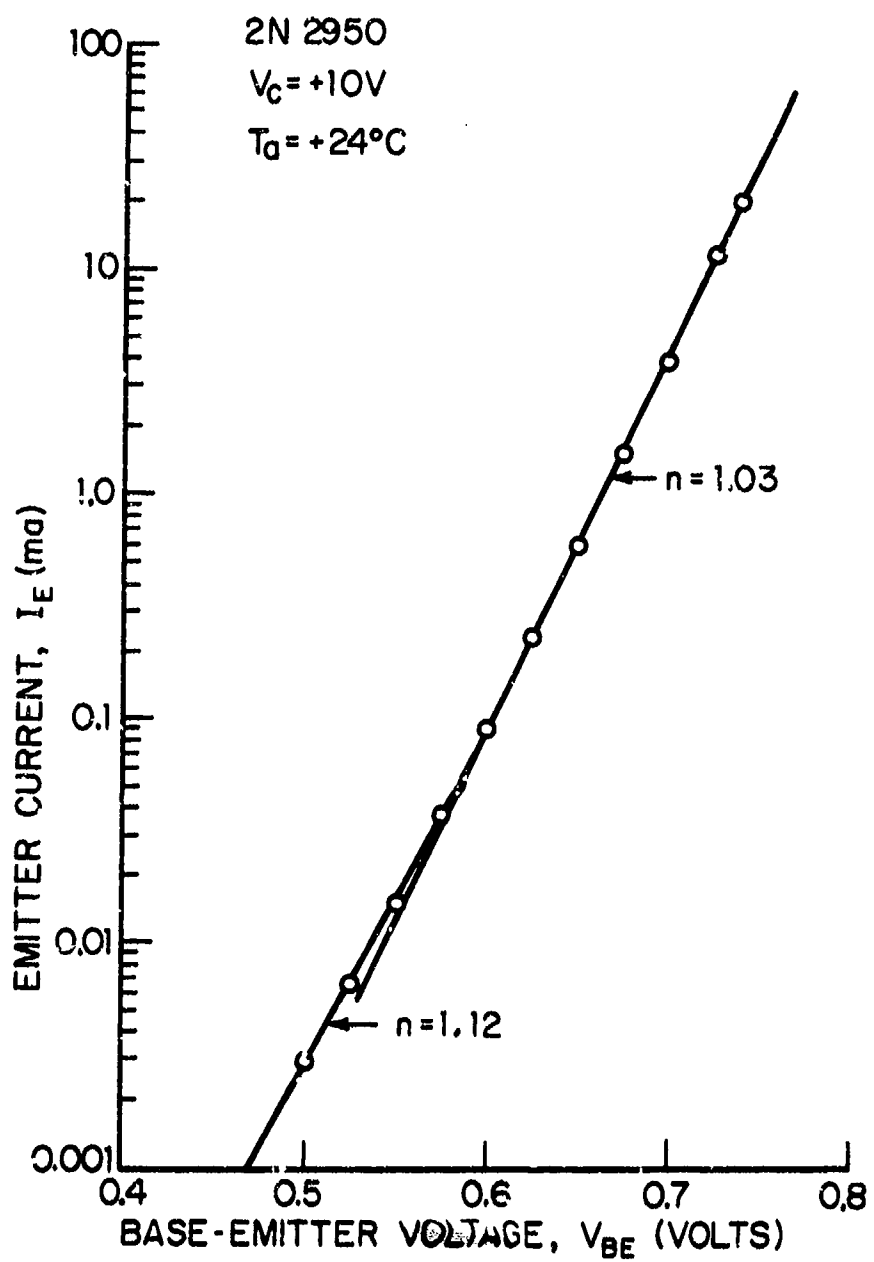


Fig. 5.22. Forward-Biased Base-Emitter Junction Characteristics of 2N2950.

5.3.2.2 Avalanche Nonlinearity

The first nonlinear mechanism effecting the dependent current source $g(v_2, v_3 - v_1)$ in Figure 5.20 is avalanche multiplication of collector current. The collector characteristics of a transistor are modified at large collector voltages by avalanche multiplication of charge carriers in the collector space-charge layer.

In the common-base connection, the pre-breakdown avalanche process is usually described in terms of a collector-current multiplication factor M given by

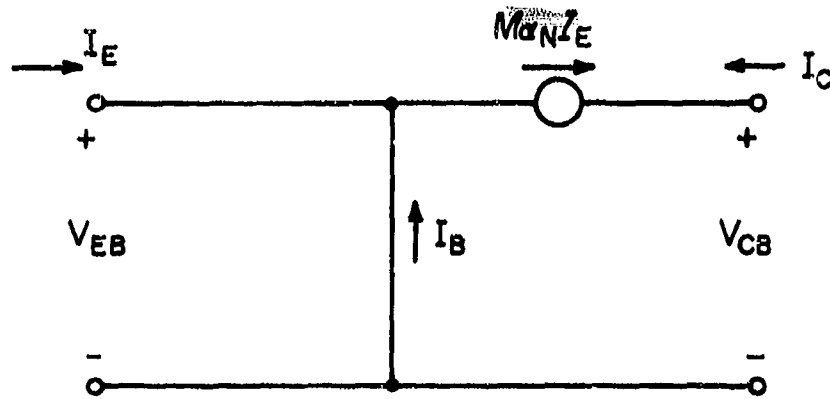
$$M = \frac{1}{1 - \left(\frac{V_{CB}}{V_{CBO}}\right)^\eta}, \quad (5.45)$$

where

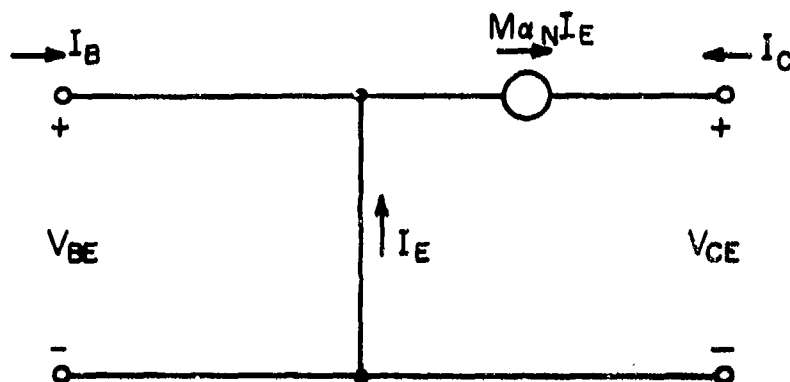
V_{CB} = DC collector-to-base voltage = $v_3 - v_1$ for the common-emitter connection,

V_{CBO} = avalanche voltage = collector-to-base breakdown voltage for zero emitter current.

Figure 5.23 shows simplified common-emitter and common-base total equivalent circuits for the NPN transistor avalanche multiplication effect. These circuits have been derived from the Ebers-Moll model of Fig. 5.21 by replacing the base-emitter and base-collector diodes by short-circuits and open-circuits respectively, which are active-quadrant operating point idealizations. The multiplication factor M defined by Eq. (5.45) is introduced in Fig. 5.23a as a multiplier associated with the dependent total current generator $M_a I_E$ from the Ebers-Moll model shown in Fig. 5.21. The factor M accounts for the



a. Simplified NPN Common-Base Total Circuit with Avalanche Multiplication.



b. Simplified NPN Common-Emitter Total Circuit with Avalanche Multiplication.

Fig. 5.23. Simplified NPN Total Circuits Including Avalanche Multiplication.

avalanche multiplication effect of V_{CB} in the common-base collector family. In order to define the avalanche nonlinearity the exponent η and the collector avalanche voltage V_{CBO} must be measured. The most direct way to find the avalanche voltage is to reverse-bias the base-collector junction (through a current-limiting series resistor) and increase the voltage until avalanche occurs; this defines the breakdown voltage V_{CBO} .

The avalanche voltage may also be found from measurements of the common-emitter collector I-V family. The value of collector-to-emitter voltage for which the CE collector family appears to have a "breakdown" is not the avalanche voltage (which is defined in terms of a CB measurement) but is called the sustaining voltage, V_{CEO} , or the value of collector-to-emitter voltage for which the common-emitter incremental forward-current-gain at zero base current becomes infinite.

It is not sufficient, however, to know only V_{CEO} . The dependent current generator to be utilized in the nonlinear incremental equivalent circuit for the transistor is developed in terms of the avalanche voltage V_{CBO} and the exponent η , so we must have a simple relationship between data obtained from the common-emitter collector family and the avalanche factor M defined by Eq. (5.45).

In Fig. 5.23b we have redrawn the total equivalent circuit with avalanche effect included in a common-emitter configuration. From the simplified Ebers-Moll circuit we have

$$I_C = - (I_B + I_E) = -M\alpha_N I_E. \quad (5.46)$$

Eliminating I_E , we have for the total collector current

$$I_C = \frac{M\alpha_N}{1-M\alpha_N} I_B. \quad (5.47)$$

The incremental current gain

$$\frac{dI_C}{dI_B} = \frac{\alpha_N}{1-\alpha_N} \quad (5.48)$$

becomes very large when α_N approaches unity. Thus it is sufficient to examine the current ratio

$$\frac{I_C}{I_B} = \frac{\frac{\alpha_N}{1-x^\eta}}{1 - \frac{\alpha_N}{1-x^\eta}} ; \quad x = \frac{V_{CB}}{V_{CBO}} , \quad (5.49)$$

or

$$I_C = \frac{I_B \alpha_N}{1-\alpha_N} \cdot \frac{1}{1 - \frac{x^\eta}{1-\alpha_N}} . \quad (5.50)$$

The first factor in Eq. (5.50) is the collector current in the absence of avalanche and the second factor represents the effect of avalanche multiplication upon collector current for the common-emitter connection. The current gain is infinite when

$$x^\eta = \left[\frac{V_{CB}}{V_{CBO}} \right]^\eta = 1 - \alpha_N . \quad (5.51)$$

Since $V_{CB} \approx V_{CE}$, the special value of V_{CE} satisfying Eq. (5.51) is the collector sustaining voltage V_{CEO} . Solving for V_{CBO} , we have

$$V_{CBO} = V_{CEO} \cdot (1-\alpha_N)^{-\frac{1}{\eta}} . \quad (5.52)$$

The exponent η can be found by accurately fitting the second factor of Eq. (5.50) to a set of experimental collector curves.

It is to be noted that the transistor is not actually in avalanche breakdown when the common-emitter collector voltage is V_{CEO} . Instead, the avalanche multiplication factor is such to generate an infinite incremental current gain region for moderately low V_{CE} .

The measured common-emitter collector family for the 2N2950 in the avalanche multiplication region is shown in Fig. 5.24. A curve fit is shown near the $I_B = 1.0$ mA curve. We obtain the parameters $V_{CBO} = 140$ V and $\eta = 4.6$ from this fit.

5.3.2.3 h_{FE} Nonlinearity

The $g(v_2, v_3 - v_1)$ nonlinearity in Fig. 5.20 also includes the h_{FE} nonlinearity, which is a relationship between I_C , the collector current, and I_B , the base current for low collector voltage in a region free of avalanche effects. The ratio of these two quantities is

$$h_{FE} \stackrel{\Delta}{=} \frac{I_C}{I_B}. \quad (5.53)$$

The Ebers-Moll model for very small collector voltage predicts that h_{FE} is a constant since α_N is a constant. (See Eq. 5.47 for $M=1$.) Experimentally it has been observed that h_{FE} is not constant and can be approximated by

$$\frac{I_C}{I_B} = \frac{h_{FE\max}}{1 + a \log^2\left(\frac{I_C}{I_{C\max}}\right)}. \quad (5.54)$$

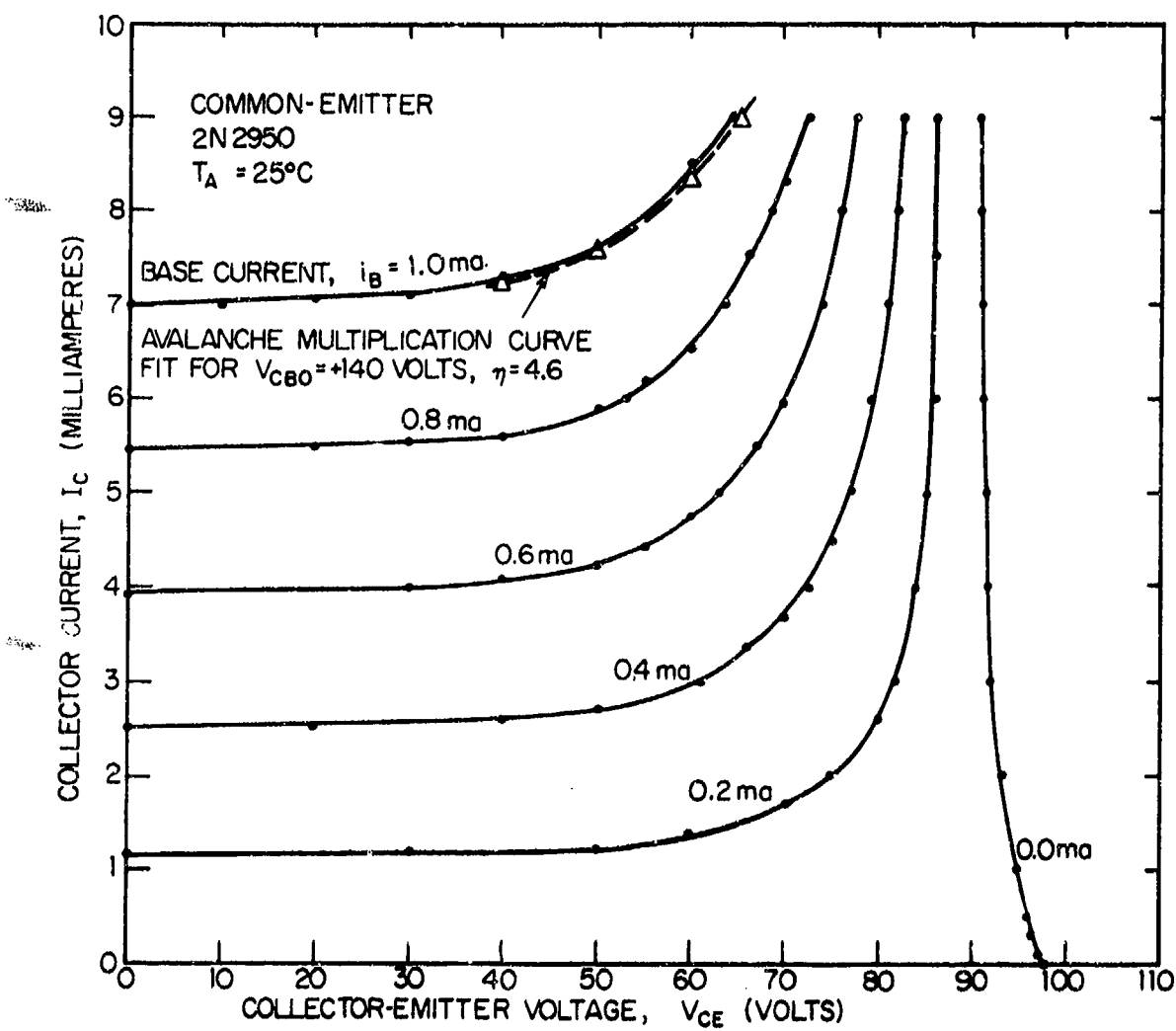


Fig. 5.24. Common-Emitter Collector Characteristics of 2N2950 in Avalanche Multiplication Region.

Consequently, α_N is dependent upon collector current I_C . From this relationship, h_{FE} peaks at I_C equal to $I_{C_{max}}$, and decreases for larger and smaller values of I_C .

The small-signal common-emitter current gain, h_{fe} is given by

$$h_{fe} = \frac{dI_C}{dI_B} = \frac{h_{FE_{max}}}{1 + a \log^2\left(\frac{I_C}{I_{C_{max}}}\right) + 2a \log e \log \frac{I_C}{I_{C_{max}}}} \quad . (5.55)$$

Equation (5.55) shows that, while h_{fe} equals $h_{FE_{max}}$ at I_C equal to $I_{C_{max}}$, in general h_{fe} is not equal to h_{FE} . The maximum of h_{FE} generally occurs at a value of I_C at which high-level injection becomes important, e.g., when the m discussed in relation to the exponential nonlinearity assumes a nonzero value. The current ratio h_{FE} can be measured in at least two ways. The first technique is to simply measure the static common-emitter characteristics on a transistor curve tracer, and then plot h_{FE} (or I_C/I_B) from these measured characteristics. The measurement of h_{FE} must be made at a sufficiently low voltage for avalanche effects to be negligible. The second technique is to make a pulsed measurement of h_{FE} . This has the advantage that higher peak currents can be measured, which may be necessary to find $I_{C_{max}}$ while keeping the temperature effects to a minimum. Again, the measurement should be made at a low collector voltage. The temperature sensitivity of h_{FE} should be considered in defining receiver experiments. Measured data from the 2N2950 are shown in Fig. 5.25. Observe that several points obtained by fitting the algebraic expression for h_{FE} to the data are shown.

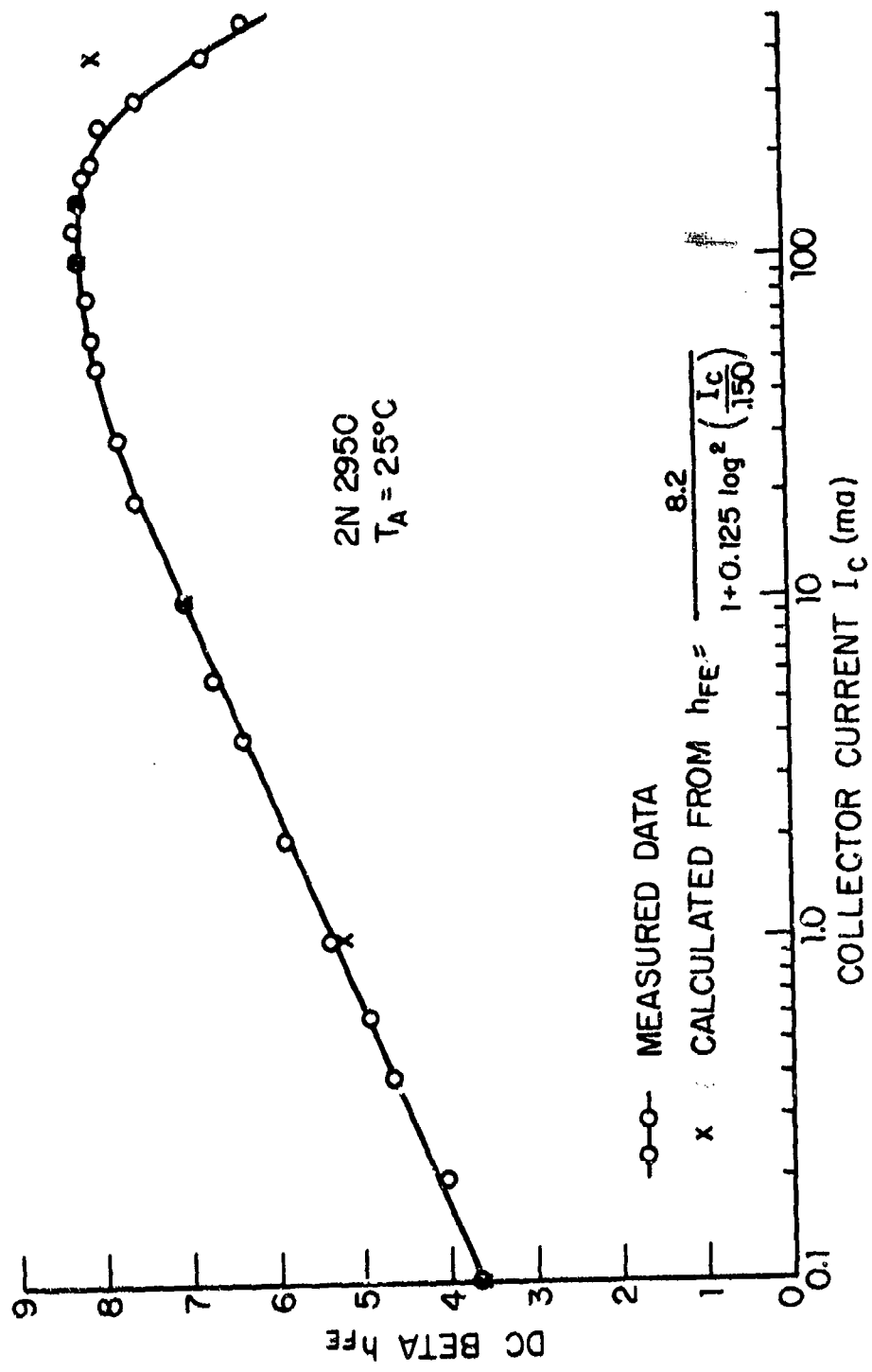


Fig. 5.25. DC Beta, $h_{FE} = I_c/I_B$ Nonlinearity.

The parameters $h_{FE}^{max} = 8.2$, $I_{Cmax} = 150$ mA, and $a = 0.125$ provide an accurate fit except at very large collector current values.

5.3.2.4 Nonlinear Incremental Current Generator $g(v_2, v_3 - v_1)$

The discussion of the h_{FE} nonlinearity in Section 5.3.2.3 and avalanche multiplication factor M in Section 5.3.2.2 has introduced the constants associated with the h_{FE} and M expressions given by Equations (5.45) and (5.54). The dependent current generator $g(v_2, v_3 - v_1)$ contains both the h_{FE} and avalanche nonlinear effects directly and the $K(v_2)$ nonlinearity indirectly through the dependence upon the emitter current. The method of combining these three nonlinearities to give the multi-variable Taylor series expansion and, thus, the incremental nonlinear current generator $g(v_2, v_3 - v_1)$ from the

$$I_C = -Ma_N I_E, \quad (5.56)$$

total dependent current generator in the modified Ebers-Moll model is outlined in this section. The Ebers-Moll generator (See Fig. 5.21 and 5.23b) has been modified by introducing the avalanche multiplication factor M which is a nonlinear function of $V_3 - V_1$, the DC collector-to-base voltage. It has also been modified by recognizing that

$$a_N = \frac{h_{FE}(I_C)}{1+h_{FE}(I_C)}, \quad (5.57)$$

is not a constant, but is nonlinearly-dependent upon the collector current I_C . Our objective is to determine i_c , the incremental component of I_C . The dependent generator g is simply the incremental component i_c which we shall show can be expressed in terms of the incremental node voltages v_2 and $v_3 - v_1$.

First, we recognize that we can re-arrange Eq. (5.56) by making use of Eq. (5.57) to obtain

$$I_C \frac{1+h_{FE}(I_C)}{h_{FE}(I_C)} = -MI_E. \quad (5.58)$$

The left hand side of this equation is dependent upon I_C and can be expanded in a Taylor series about the DC operating bias I_{CO} to obtain

$$I_C \frac{1+h_{FE}}{h_{FE}} = I_{CO} \frac{1+h_{FE}(I_{CO})}{h_{FE}(I_{CO})} + \sum_{n=1}^{\infty} a_n i_c^n, \quad (5.59)$$

where

$$a_n = \frac{1}{n!} \left. \frac{\partial^n}{\partial I_C^n} \left[I_C \frac{1+h_{FE}}{h_{FE}} \right] \right|_{I_{CO}}. \quad (5.60)$$

The total emitter current can also be decomposed into its operating point value I_{EO} and the incremental component i_e , or

$$I_E = I_{EO} + i_e, \quad (5.61)$$

and, similarly,

$$M = M_o + m, \quad (5.62)$$

where M_o is the operating-bias value of M and m is the incremental variation in M caused by variation in the collector-to-base operating-point voltage $V_3 - V_1$. It follows that

$$\begin{aligned} i_{CO} &= \frac{1+h_{FE}(I_{CO})}{h_{FE}(I_{CO})} + \sum_{n=1}^{\infty} a_n i_c^n \\ &= -M_o I_{EO} - [m I_{EO} + M_i_e]. \end{aligned} \quad (5.63)$$

Equating incremental terms, we obtain

$$\sum_{n=1}^{\infty} a_n i_c^n = z, \quad (5.64)$$

where

$$z = -[m I_{EO} + M_i_e], \quad (5.65)$$

and

$$\begin{aligned} I_{EO} &= I_E \left| \begin{array}{l} I_C = I_{CO} \end{array} \right\} \\ M_o &= M \left| \begin{array}{l} V_3 - V_1 \end{array} \right\} \end{aligned} \quad (5.66)$$

Also,

$$m = \sum_{i=1}^{\infty} M_i (V_3 - V_1)^i. \quad (5.67)$$

where

$$M_i = \frac{1}{i!} \left. \frac{\partial^i M}{\partial (V_3 - V_1)^i} \right|_{V_3 - V_1}. \quad (5.68)$$

The Taylor series expansion in Eq. (5.64) can now be rewritten as a power series in current (Abramowitz and Stegun, 1964, p.16) to get a series for the incremental current generator

$$i_c = \sum_{q=1}^{\infty} a_q z^q \triangleq g(v_2, v_3 - v_1), \quad (5.69)$$

where the first-three coefficients a_q are

$$\begin{aligned} a_1 &= \frac{1}{a_1}, \\ a_2 &= \frac{-a_2}{a_1^3}, \\ a_3 &= \frac{2a^2 - a_1 a_3}{a_1^5}. \end{aligned} \quad (5.70)$$

The a coefficients are given by Eq. (5.60). The first three terms of the expansion are of the form

$$g(x, y) = g(v_2, v_3 - v_1) \cong g_1 + g_2 + g_3, \quad (5.71)$$

where

$$g_1(v_2, v_3 - v_1) = g_x v_2 + g_y (v_3 - v_1). \quad (5.72)$$

$$g_2(v_2, v_3 - v_1) = \frac{1}{2!} g_{xx} v_2^2 + g_{xy} v_2 (v_3 - v_1) + \frac{1}{2!} g_{yy} (v_3 - v_1)^2, \quad (5.73)$$

$$\begin{aligned} g_3(v_2, v_3 - v_1) &= \frac{1}{2} g_{xxy} v_2^2 (v_3 - v_1) + \frac{1}{2} g_{xyy} v_2 (v_3 - v_1)^2 \\ &\quad + \frac{1}{3!} g_{yyy} (v_3 - v_1)^3 + \frac{1}{3!} g_{xxx} v_2^3. \end{aligned} \quad (5.74)$$

The various g coefficients are partial derivatives which can be worked out directly from the expansion coefficients given in Eqs. (5.43), (5.60), (5.68), and (5.71).

Higher-order terms may be added if they are of interest. In the practical application of the nonlinear incremental model, only the constants given as $h_{FE_{max}}$, $I_{C_{max}}$, etc., are required as inputs to the computer program used to determine the input/output distortion characteristics of a transistor amplifier.

5.3.2.5 Collector-Capacitance Nonlinearity

The other nonlinear incremental current generator in the collector circuit is the collector capacitance current source

$$\gamma_c(v_3 - v_2) = \gamma_1 \frac{d}{dt} (v_3 - v_2) + \gamma_2 \frac{d}{dt} (v_3 - v_2)^2 + \dots \quad (5.75)$$

The first coefficient γ_1 is the first derivative of the nonlinear charge characteristic of the reverse-biased collector junction at the operating point and is, therefore, the collector-junction capacitance, C_c .

In Section 5.2.3, Eq. (5.14) for the voltage-variable junction capacitance of a reverse-biased junction diode was given. In the normal reversed-bias mode of collector operation, the magnitude of the junction voltage $|V|$ is much greater than the barrier voltage ϕ . Eq. (5.14) then becomes

$$C(V) \approx C(0) \left(\frac{\phi}{|V|} \right)^\mu \quad (5.76)$$

$$\approx k |V|^{-\mu}. \quad (5.77)$$

where $k = C(0) \phi^\mu = C [|V| = 1]$. It follows that the collector-base junction capacitance for the bipolar transistor is given by

$$C_c = \gamma_1 = k |V_3 - V_2|^{-\mu}; \quad |V_3 - V_2| \gg \phi, \quad (5.78)$$

where $V_3 - V_2$ is the reverse-bias voltage across the collector-to-base junction. This will be very nearly V_{CE} at the operating point bias. An incremental measurement of the linear current through the base-collector capacitor will determine C_c . To relate this to conventional transistor measurements, consider the h-parameter set. In particular, if h_{22b} , the common-base h_{22} is measured, it will be approximately

$$h_{22b} \approx \frac{1}{r_C} + j 2\pi f (C_c + C_3). \quad (5.79)$$

The measurement should be made at a frequency such that the impedance of C_c is of the same order as r_c . Thus

$$C_c = \frac{1}{2\pi f} \operatorname{Im}(h_{22b}) - C_3. \quad (5.80)$$

If $\operatorname{Im}(h_{22b})$ is measured for a range of collector-base voltages and C_c is plotted on logarithmic paper, μ is the slope of the graph and k is the value (extrapolated if necessary) at V equal to one volt. Experimental data for the collector-to-base capacitance C_c nonlinearity of the 2N2950 are shown in Fig. 5.26. Also shown is a curve fit for the theoretical functional dependence expected. From this data we have the parameters $k = 25.0 \text{ pF}$, $\phi = 0.4 \text{ V}$, and $\mu = 0.348$. The value of ϕ is seen to be sufficiently small at normal operating voltages that it can be set equal to zero.

5.3.2.6 Emitter-Capacitance Nonlinearity

The last nonlinear parameter to be evaluated in the nonlinear incremental equivalent circuit model is the nonlinear base-emitter capacitance source $v_e(v_2)$. The base-emitter capacitance is the parallel combination of the diffusion capacitance and the space-charge layer capacitance. It can be determined by measuring f_T , the frequency at which the extrapolated common-emitter current gain goes to unity, or f_a , the frequency at which the common-base current gain goes to 0.707. The two cutoff frequencies f_T and f_a are essentially the same. The frequency cutoff mechanism in the model is the $r_e C_2$ product, and C_2 is given by

$$C_2 = \frac{1}{2\pi f_T r_e}. \quad (5.81)$$

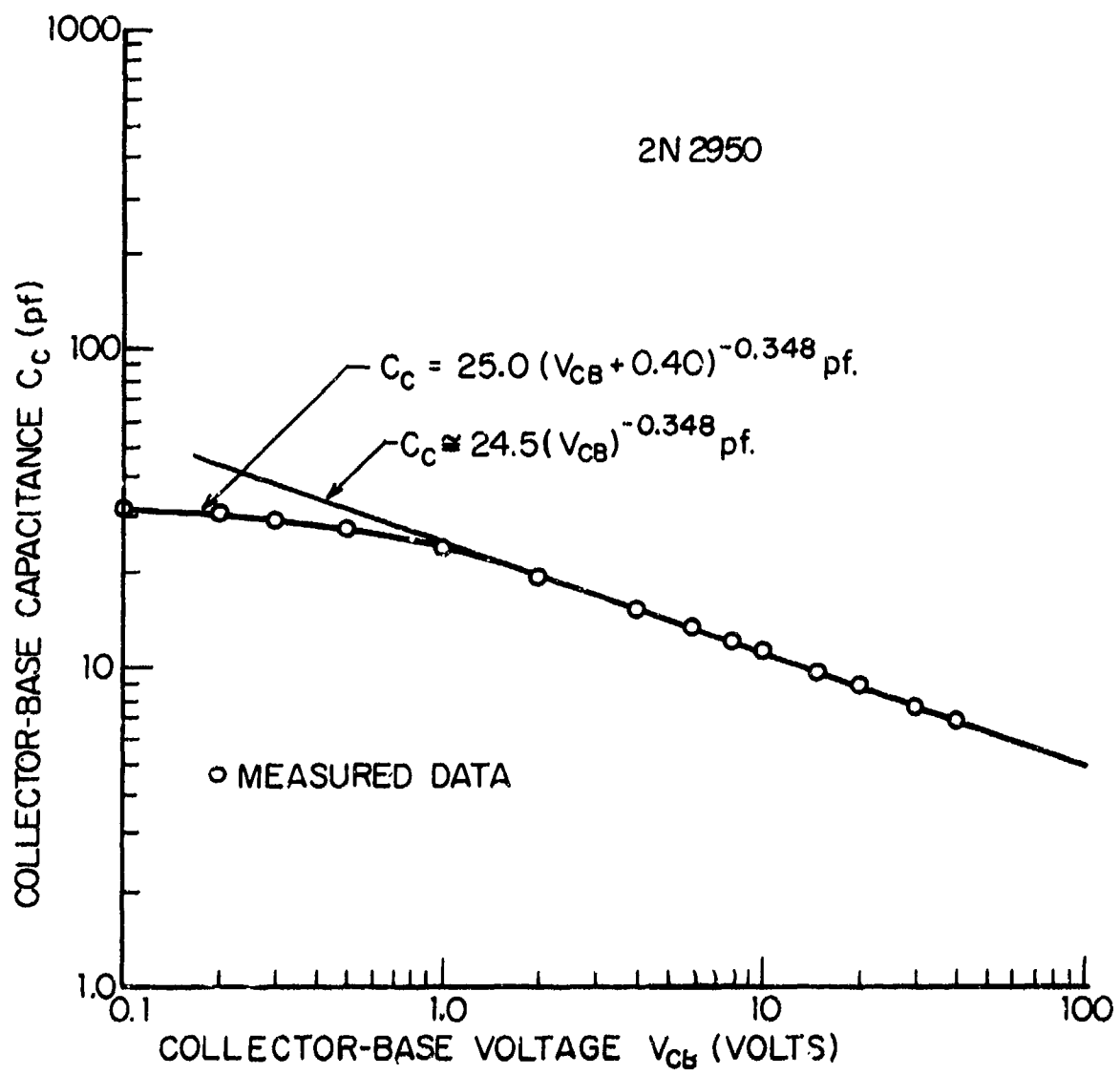


Fig. 5.26. Collector-Base Reverse Bias Capacitance C_c for 2N2950.

The space-charge layer capacitance is a function of the base-emitter voltage. In forward bias, this voltage remains nearly constant over a wide current range. Thus the space-charge layer capacitance is nearly a constant. At low-to-moderate values of emitter current, the diffusion capacitance varies linearly with the emitter current. Since r_e varies inversely with the emitter current, as long as the diffusion capacitance is much greater than the space-charge capacitance, the cutoff frequency will be constant independent of the emitter current. At sufficiently low currents, when the diffusion capacitance is less than the space-charge capacitance, the cutoff frequency will vary linearly with the emitter current. At high values of emitter current the diffusion capacitance can increase faster than the emitter current, thus causing the cutoff frequency to decrease. The cutoff frequency is also a function of collector bias, which is not included in this model.

Figure 5.27 shows the measured emitter capacitance of the 2N2950 transistor. The capacitance of the forward-biased emitter junction is seen to have a linear slope of 60 pF/mA and an intercept of 330 pF. The 330 pF represents the space-charge capacitance. The total emitter junction capacitance can be written as

$$C_2 = C_{je} + C'_d I_E, \quad (5.82)$$

where C_{je} is the space-charge capacitance, and C'_d is the proportionality factor relating diffusion capacitance to emitter current.

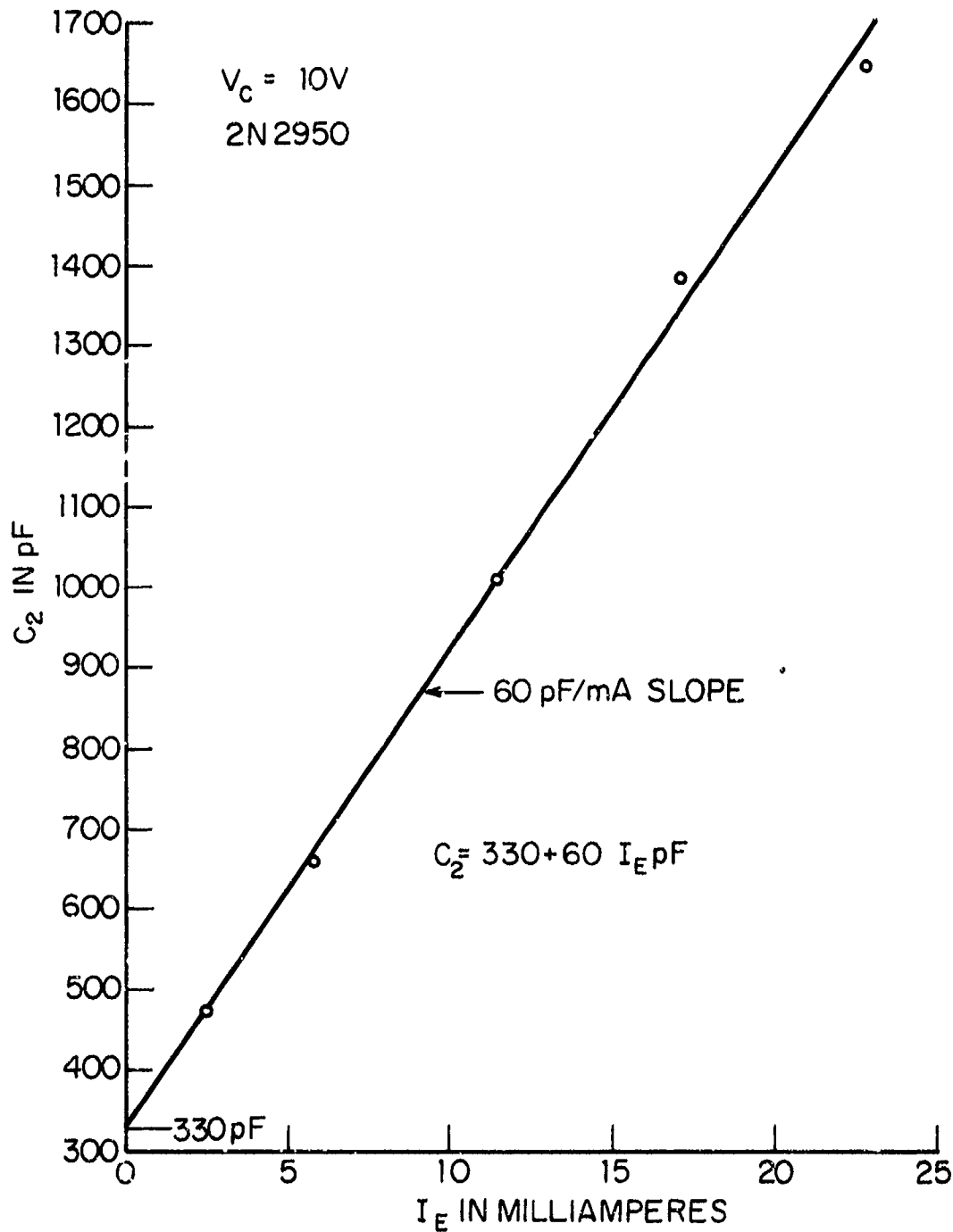


Figure 5.27. Base-Emitter Junction Forward-Bias Capacitance. 2N2950

5.3.2.7 Base Resistance r_b

The remaining two resistive elements in the nonlinear incremental model are essentially independent of operating point bias values and will be limited to the linear term in the incremental model.

Resistance r_b is the incremental linear base-spreading resistance due to the finite resistivity of the base region, and can be determined from h-parameter measurements. r_b will show a slight variation with collector voltage and may change under high injection current conditions and should therefore be measured at the desired operating point. Using the subscript b to represent common base:

$$h_{11b} = r_e \parallel c_2 + r_b (1-\alpha), \quad (5.83)$$

where $r_e = \frac{kT}{q|I_E|}$

\parallel means "in parallel with",

$$\alpha = \alpha_0 / (1 + j\omega/\omega_\alpha).$$

Therefore, r_b can be found from h_{11b} measured at a sufficiently high frequency that $r_b(1-\alpha) \gg r_e \parallel c_2$. Since $h_{11} = 1/y_{11}$, a y-parameter measurement can also be used to determine r_b . Either technique may be complicated by the existence of parasitic capacitance. For the 2N2950, r_b is 10.1 ohms.

High frequency transistors, which have narrow base regions, tend to have large base resistances, and the accurate determination of r_b by the measurement of high frequency parameters may be difficult. An alternate technique, which has been used with good results, consists of inserting the transistor into a test

amplifier and in measuring its low-frequency insertion gain. If all circuit parameters except r_b are known, r_b can be deduced from the circuit model and the measured insertion gain.

5.3.2.8 Collector Resistance r_c

Resistance r_c is the collector resistance. Physically it arises as a base-width modulation effect produced by incremental collector junction bias. It is a large resistance which generally is important only at high frequencies or large load impedances. r_c can be determined from common-base h-parameter measurements:

$$r_c = 1/\text{Re}(h_{22b}). \quad (5.84)$$

For the 2N2950, r_c is 635 kΩ.

5.3.2.9 Capacitances C_1 and C_3

C_1 is the header capacitance between the base and emitter terminals. It is a small capacitance, of the order of several pF, and is independent of the transistor operating point. Capacitance C_3 is physically due to the portion of the collector which "overlaps" the emitter, hence the name "overlap capacitance". C_3 may have some voltage dependence.

C_3 can be determined by measurement of the common-emitter reverse transfer admittance for incrementally short-circuited input, y_{12e} . By definition

$$y_{12e} = \left. \frac{di_1}{dv_2} \right|_{v_1 = 0}. \quad (5.85)$$

At a sufficiently high frequency, somewhat above the β cutoff frequency, the transistor is short-circuited by C_3 , and

$$y_{12e} \approx -j\omega C_3. \quad (5.86)$$

This region can be found by plotting $|y_{12e}|$ as a function of frequency and examining asymptotic slopes.

Capacitance C_1 can be determined by a measurement of y_{11e} , the input admittance for incrementally short-circuited output. The measurement should be made at the desired operating point and at a frequency somewhat higher than that required to measure C_3 .

The definition of y_{11e} is

$$y_{11e} = \left. \frac{di_1}{dv_1} \right|_{v_2 = 0}, \quad (5.87)$$

and, at sufficiently high frequency,

$$y_{11e} \approx j\omega(C_1 + C_3). \quad (5.88)$$

As with C_3 , the asymptotic region can be found by plotting $|y_{11e}|$ as a function of frequency.

For the 2N2950, C_1 is negligible and C_3 is 1.5 pF.

5.3.2.10 Parasitic Elements

A transistor may have parasitic elements, e.g. series inductance or shunt capacitance depending on the construction of the transistor. The 2N2950 is fabricated in a TO-102 case, has three leads and a stud mounting. The collector is connected to the case; the mounting stud is insulated from the case. This results in a parasitic capacitance of 4.0 pF between the collector and the stud.

5.3.2.11 Summary of the Bipolar Transistor Nonlinear Incremental Model

In summary, the nonlinear T incremental model for the bipolar transistor has five sources of nonlinearities which are included as four sets of incremental controlled current generators. These are:

$K(v_2)$: Base-emitter exponential nonlinearity,

$g(v_2, v_3 - v_1)$: Avalanche and h_{FE} nonlinearity,

$\gamma_C(v_3 - v_2)$: Collector capacitance nonlinearity,

$\gamma_e(v_2)$: Emitter capacitance nonlinearity.

Each of these can be expanded in a Taylor series in an equivalent circuit form as shown in Fig. 5.28. Each of the current generators has been decomposed into three parallel generators for the linear, second-order, and third-order current sources. Higher order nonlinearities may be included as further generators. The circuit model emphasizes the fact that we are concerned with the normal active quadrant, that is, neither in cutoff nor in saturation.

The linear incremental T model of a transistor is shown in Fig. 5.29. The model includes the case-stud capacitance C_{CG} , found in the 2N2950. A comparison of Figs 5.28 and 5.29 shows that the linear model contains only the first term of the expansion of each nonlinear generator.

A summary of the parameters necessary to characterize the nonlinear and linear frequency dependent incremental model of the bipolar transistor are listed in various categories in Table 5.1. The numerical values are for the 2N2950 sample evaluated at $T_A = 25^\circ\text{C}$. Linear parameters are evaluated at the $V_C = 10$ volts, $I_C = 10$ milliamperes operating point. Note that 17 parameters are involved in the nonlinear model while 9 are necessary in the linear model.

It is also sometimes possible to characterize the nonlinear parameters of a bipolar transistor from manufacturer's specification data sheets. An example is worked out in Appendix B for the 2N918 transistor.

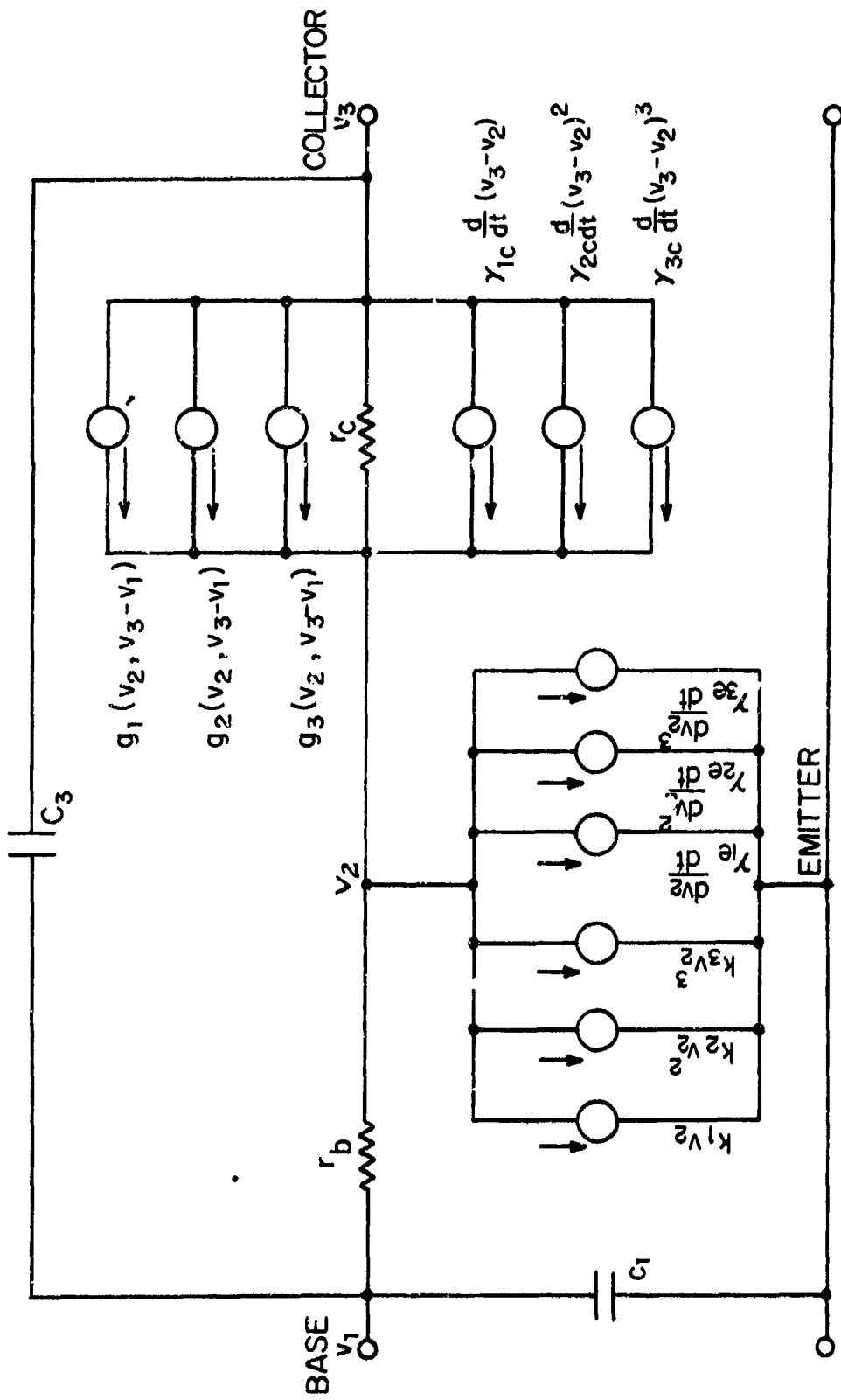


Fig. 5.28. Controlled-Current Generator Third-Order Incremental Nonlinear-T Equivalent Circuit of a Bipolar Transistor.

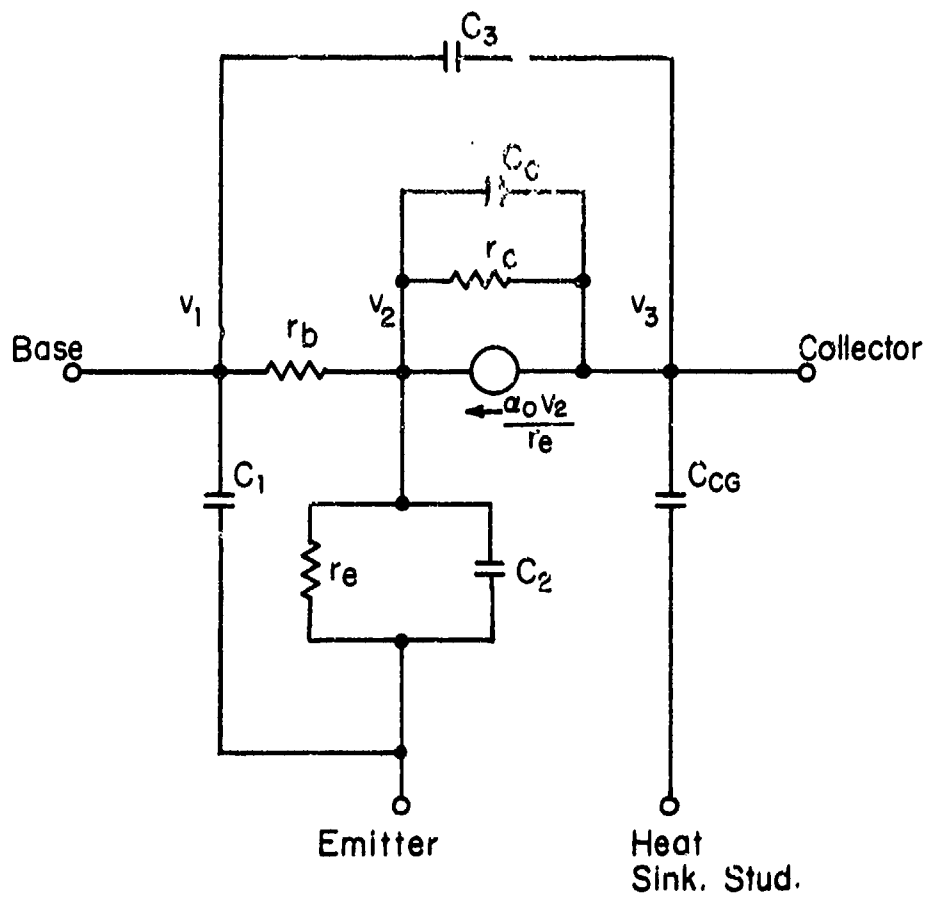


Figure 5.29. Linear Incremental Equivalent Circuit of 2N2950.

Table 5.1
 TABLE OF 2N2950 MODEL PARAMETERS FOR NONLINEAR AND LINEAR INCREMENTAL MODELS
 AT $T_A = 25^\circ\text{C}$ and $V_C = 10\text{V}$, $I_C = 10 \text{ mA}$

Description	Nonlinear Parameters	Linear Parameters
Emitter Junction-Forward Biased		
Conductance	$I_E = 11.4 \text{ mA}; n = 1.03$	$r_e = 2.3 \text{ ohms}$
Capacitance	$C_{je} = 330 \text{ pF}; C_d' = 60 \text{ pF/mA}$	$C_2 = 1040 \text{ pF}$
Collector Junction-Reverse Biased		
Conductance	$r_c = 635 \text{ k}\Omega$	$r_c = 635 \text{ k}\Omega$
Capacitance	$k = 25.0 \text{ pF}; \phi = 0.4 \text{ volt}; \mu = 0.348$	$C_c = 11.1 \text{ pF}$
Dependent Source		
h_{FE}	$h_{FE_{max}} = 8.2, I_{C_{max}} = 150 \text{ mA}; a = .125$	$a_0 = .882$
Avalanche	$V_{CBO} = 140 \text{ volts}; \eta = 4.0$	
Base	$r_b = 10.1 \Omega$	$r_b = 10.1 \Omega$
Other		
Emitter-base capacitance	$C_1 = \text{neg}$	$C_1 = \text{neg}$
Collector-base capacitance	$C_3 = 1.5 \text{ pF}$	$C_3 = 1.5 \text{ pF}$
Collector-heat sink capacitance	$C_{CG} = 4.0 \text{ pF}$	$C_{CG} = 4.0 \text{ pF}$

5.4 Nonlinear Models of Field-Effect Transistors

The state of the art in modeling field effect transistors, both MOSFET and JFET, is less advanced than is bipolar junction transistor modeling. This is due to several factors:

- 1) Extensive availability and use of FET's is a relatively new phenomenon;
- 2) The first-order theory of the device predicts no (or very little) important distortion effects at the normal frequencies of use;
- 3) The important effects (which do experimentally show up) therefore arise from primarily more complicated second-order physical factors which tend to be structure-sensitive;
- 4) There is a large variety of physical structure, from JFETS through MOSFETS, over which the second-order parameters vary greatly;
- 5) It may not be possible to find a single "generic model" (like the Integral Charge-Control Model of Gummel and Poon, 1970, for bipolar transistors), out of which all the important cases can be selected merely by measuring a limited number of critical parameters.

As a consequence, at the present time there are no well-developed theoretical nonlinear FET models ready for immediate use. However, experimentally developed models are available. Good results in distortion prediction have been achieved in the VHF and low UHF bands. It is generally agreed that the first-order large signal theoretical models are inadequate for the prediction of third-order nonlinear distortion.

Miller and Meyer (1971) do, however, obtain excellent results for the prediction of crossmodulation at frequencies up to 450 MHz on the basis of a 30 point measurement of incremental transconductance as a function of gate-to-source voltage V_{GS} . The measured data was fitted by an 8th-order Taylor series and integrated analytically to obtain a nonlinear relationship between the static drain current I_D and gate voltage V_G . Fifth order terms were found to be significant. The large signal total model employed by Miller and Meyer is shown in Fig. 5.30 where the total static drain current $I_D = f(V_G)$ depends nonlinearly upon V_G . The gate-to source capacitance $C_{GS}(V_G)$ was found to be voltage dependent and experimentally approximated by

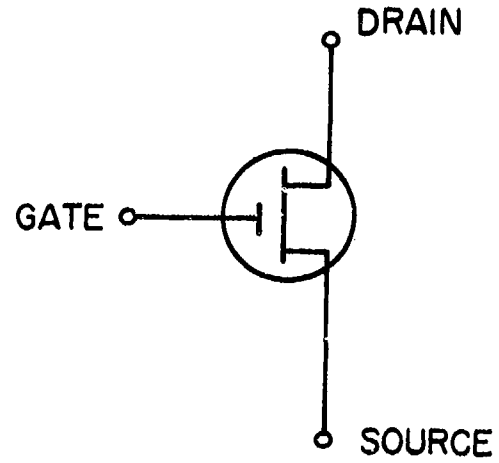
$$C_{GS} = C_{GS}(0) [1 + bV_G], \quad (5.89)$$

where $C_{GS}(0)$ and b are constants. Both R_S and C_{GD} were observed to be nearly constant.

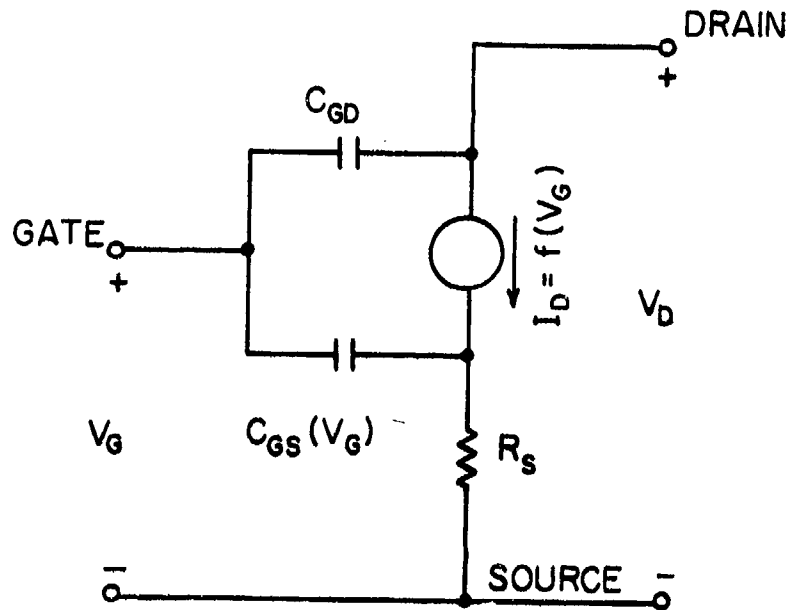
Miller and Meyer's use of the model involved Fourier analysis of the large-signal time domain solution for a resistive embedding of the model. Application of the Volterra series analysis was not attempted but it is clear that straightforward application of the device modeling techniques will give the nonlinear incremental equivalent model. Fair (1972) recently investigated harmonic distortion in JFET's by employing a power-series equivalent circuit model. Lindholm (1971) has employed charge-control theory in modeling field-effect transistors.

5.5 Nonlinear Charge-Control Model of Bipolar Transistors

There are two physical phenomena not included in the nonlinear T bipolar transistor model presented in Section 5.3 of potential importance at higher power levels which should be added to the model. These are:



(a) FET Circuit Symbol.



(b) Total Voltage/Current Equivalent Model (Miller and Meyer, 1971).

Fig. 5.30. FET Large Signal Model.

- 1) At large collector voltage swings, the base narrows as the collector space charge layer widens toward the emitter junction to add a current-dependence to both the collector resistance and the collector capacitance. Alternatively, base transit time decreases with increased voltage. This effect is known as the Early effect.
- 2) At large collector currents the base push-out effect, which effectively widens the base into the collector body region (or, alternatively increases base transit time with increased current), is a result of the increased neutralizing charge of minority carriers injected into the collector space-charge layer.

Both of these effects tend to produce, on one hand, a curvature of the collector characteristics before the avalanche multiplication process sets in to produce similar variations at higher voltages; and, on the other hand, a variation of output capacitance with current that is not expected from the previous models. In addition, f_T is made voltage, as well as current dependent. Accordingly more distortion may well be expected from these processes at lower load impedance levels than would be anticipated otherwise.

In order to include these effects in a consistent manner, it is also expected that modification should be made of some of the other nonlinearities presently included in the model. Accordingly it becomes most reasonable to adopt a rather different and considerably more complete model of the transistor; in particular the so-called Integral Charge-Control Model of Bipolar Transistors, described by Gummel and Poon (1970). The model has been applied very successfully to the calculation of second and third order distortions (including intermodulation) at output frequencies as high as 75 MHz in a resistively terminated transistor with $f_T \approx 2$ GHz.

The essence of the model (which is analytical rather than topological) is the recognition that in the modern bipolar junction transistor the dominant "longitudinal" current I_{CC} from emitter body to collector body, composed of carriers which are minorities in the base region (electrons for an NPN transistor), is practically unaffected by the slight amount of recombination

involved in the structure. It contains, however, many of the major device nonlinearities. By neglecting recombination, Gummel showed for a one dimensional transistor that I_{cc} is proportional to

$$\frac{\exp(qV'_{eb}/kT)}{Q_b} - \frac{\exp(qV'_{cb}/kT)}{Q_b}, \quad (5.90)$$

where V'_{eb} and V'_{cb} are the voltages at the "internal" emitter-base and collector-base contacts, and Q_b is the entire base charge given by

$$Q_b = Q_{bo} + Q_e + Q_c + B\tau_f I_f + \tau_r I_r. \quad (5.91)$$

Q_{bo} is the equilibrium total stored charge in the base, Q_e the emitter junction stored charge, Q_c the same for the collector junction, $B\tau_f I_f$ represents a forward diffusion-capacitance charge storage, and $\tau_r I_r$, correspondingly, an inverse storage. The factor B describes base push out, which in the normal active region of operation increases with $|I_c|$ and decreases with $|V_{cb}|$.

Equation (5.90) becomes the usual Ebers-Moll result when $Q_b = Q_{bo}$, but otherwise Q_b provides the mechanism for including many of the important nonlinearities which are less violent than the exponentials.

The base current I_b does not have as simple a form as I_{cc} , and is much more structure-sensitive:

$$I_b = I_{be_1} + I_{be_2} + I_{bc} - I_A. \quad (5.92)$$

The various components, as well as I_{cc} , are shown in Fig. 5.31. Generally,

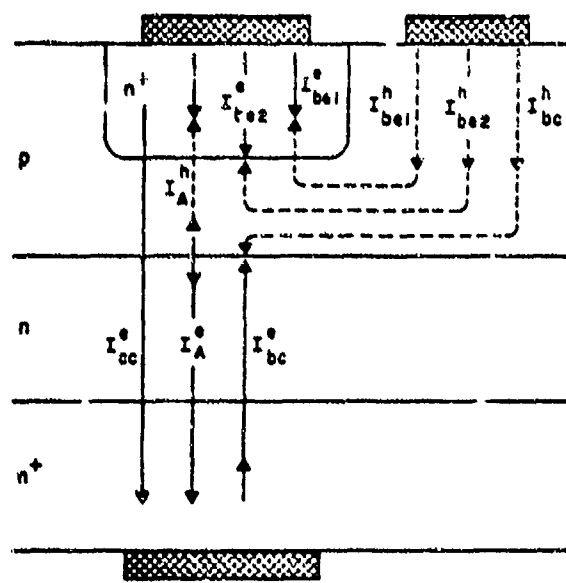


Fig. 5.31. Particle Currents in an NPN Transistor
 (From H.C. Poon, IEEE Trans. Electronic Devices, June 1972).

$$\left. \begin{array}{l} (a) I_{be_1} \sim [\exp(qV'_{eb}/kT) - 1] \\ (b) I_{be_2} \sim [\exp(V'_{eb}/n_e kT) - 1]; 1 \leq n_e \leq 2 \\ (c) I_{bc} \sim [\exp(qV'_{cb}/n_c kT) - 1]; 1 \leq n_c \leq 2 \end{array} \right\}, \quad (5.93)$$

and I_A is based on analysis of the avalanche multiplication phenomenon.

The net result of the integral charge control model is that equations can be written for the collector current, base charge, and base current:

$$\left. \begin{array}{l} I_c = f(V'_{eb}, V'_{cb}, Q_b, I_c) \\ Q_b = g(V'_{eb}, V'_{cb}, I_c) \\ I_b = h(V'_{eb}, V'_{cb}, I_c) \end{array} \right\}. \quad (5.94)$$

Unlike our previous device models, the equations are implicit and cannot be used to represent individual elements in the device model. However, the transistor can, through the use of Eq. (5.94), be represented as a nonlinear two-port. The linear y-parameters are, as usual, the first derivative terms. The current sources in the higher-order nonlinear representation are found through utilizing higher-order terms of the Taylor's series expansion of (5.94), along with the same nonlinear circuit analysis techniques outlined in Chapter 2. The integral charge-control model employed by Gummel and Poon is, as might be expected, considerably more complex than the nonlinear T model outlined in Section 5.3. For example, some 31 parameters are required to characterize the model instead of the 17 for the nonlinear T.

5.6 Vacuum Tube Nonlinear Models

There are still many communication systems in use that employ vacuum tubes. Our model of such devices is a modified form of the classical space-charge limited 3/2 power law.

The 3/2 power law model states that the current-voltage relation for a vacuum diode is

$$i_s = G e^{3/2}, \quad (5.95)$$

where

i_s = total space current (cathode current),

G = a "constant" called the perveance,

e = plate-cathode total voltage.

The incremental model is found by expanding Eq. (5.95) in a Taylor series around the operating bias. The first term in the series represents the linear model, and the higher-order terms represent the nonlinear terms of the model. Multi-grid tubes are modeled by replacing the voltage e by e_{eq} , an equivalent diode voltage. Corrections must be made in the model for the space-charge potential and the operating-point dependence of some of the so-called constants of the tube. Good supplementary background material can be found in Spangenberg (1948), and M.I.T. E.E. Staff (1943).

5.6.1 Vacuum Diodes

The instantaneous total plate current i_b of a vacuum diode in the space-charge limited region is related to the instantaneous total plate-to-cathode voltage e_b by

$$i_b = G e_b^{3/2}, \quad (5.96)$$

where G , a constant called the perveance, is dependent upon the tube geometry. If the diode is biased at the operating point (I_{b0}, E_{b0}) , we have

$$I_{b0} + i_p = G(E_{b0} + e_p)^{3/2}, \quad (5.97)$$

where i_p and e_p are the incremental plate current and plate voltage relative to the operating bias point. Expanding in a Taylor series about the operating point and solving for the incremental plate current, we have

$$i_p = K_1 e_p + K_2 e_p^2 + K_3 e_p^3 + K_4 e_p^4 + \dots, \quad (5.98)$$

where

$$\left. \begin{aligned} K_1 &= \frac{3}{2} G E_{b0}^{1/2} \\ K_2 &= \frac{3}{8} G E_{b0}^{-1/2} \\ K_3 &= \frac{-1}{16} G E_{b0}^{-3/2} \\ K_4 &= \frac{3}{128} G E_{b0}^{-5/2} \end{aligned} \right\}. \quad (5.99)$$

The vacuum diode in the $3/2$ power-law space-charge limited region is equivalent to a nonlinear resistor. The general form of the coefficient is

$$K_n = \frac{1}{n!} \left(\frac{3}{2}\right) \left(\frac{3}{2} - 1\right) \cdots \left[\frac{3}{2} - (n-1)\right] G E_{b0}^{(3/2-n)}. \quad (5.100)$$

The nonlinear incremental circuit model for the diode is shown in Fig. 5.32. A plate-to-cathode capacitance C_{pk} has been added to model the high-frequency vacuum diode.

A triode, with the signal grid connected to the cathode, is electrically a diode. Similarly, a pentode, with the signal grid and suppressor connected to the cathode, and the screen

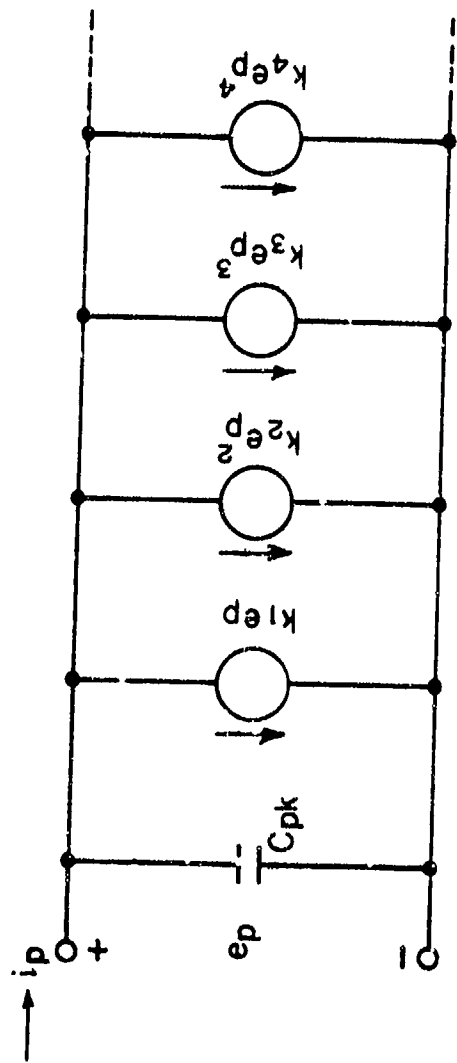


Fig. 5.32. Nonlinear Incremental Circuit Model of a High Frequency Vacuum Diode.

connected to the plate, is a diode. Fig. 5.33 shows the measured diode-connected plate characteristics of a 12AT7 triode and three pentodes, the 6DG6, 6AH6, and 5763 with the current axis being the two-thirds power of current; the two-thirds exponent serves to remove the curvature caused by the 3/2 power law. From Fig. 5.33 it is seen that the 3/2 power law is valid. Two of the curves, the 5763 and the 12AT7, go through the origin of the graph. The 6AH6 and 6DC6, however, have zero current intercepts of 7.5 volts and -7.0 volts, respectively. This offset is due to the effects of the space-charge of the tube, and can be modeled by defining a potential ϕ which is added to the diode plate-cathode voltage or

$$i_b = G(e_b + \phi)^{3/2}. \quad (5.101)$$

The potential $e_b + \phi$ is referred to as an equivalent diode voltage.

5.6.2 Vacuum Triode

5.6.2.1 Vacuum Triode Theory

The total space current of an ideal vacuum triode (see Fig. 5.34) operated in the normal space-charged limited region is given by

$$i_s = G(e_c + e_b/\mu)^{3/2}, \quad (5.102)$$

where G = permeance, a parameter dependent upon geometry,

$i_s = i_c + i_b$ = total space current, the sum of grid current and plate current,

e_c = total grid-to-cathode voltage,

e_b = total plate-to-cathode voltage,

μ = amplification factor, a constant dependent upon geometry.

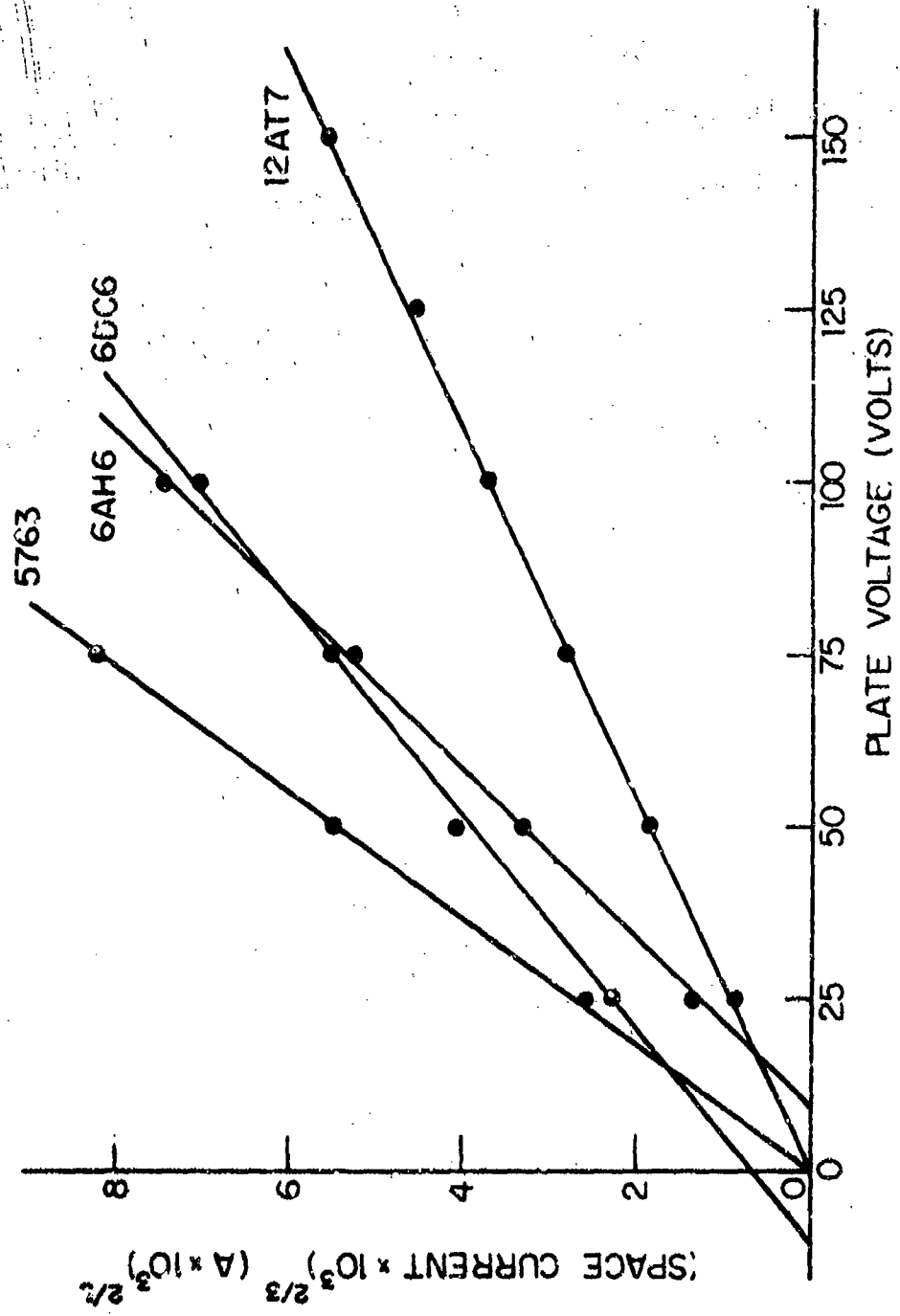


Fig. 5.33. Diode Connection Space Current Characteristics of Several Vacuum Tubes.

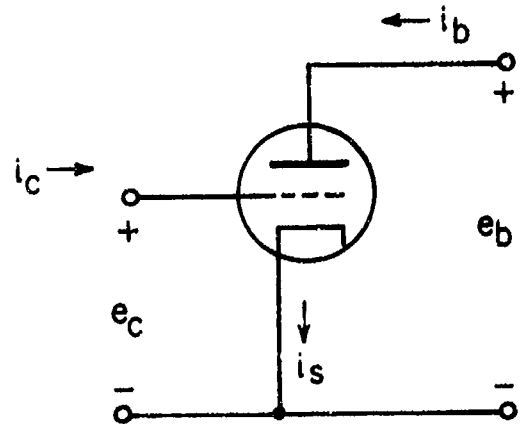


Fig. 5.34. Vacuum Triode.

Normally, the triode is operated in the negative grid region and grid current is negligible. The space current is then entirely plate current and

$$i_b = G(e_c + e_b/\mu)^{3/2}; \quad e_c \leq 0. \quad (5.103)$$

If μ and G are essentially constant in the normal operating region, the primary nonlinearity is the 3/2 power law. Since both the grid voltage and plate voltage are variable, the total plate current i_b given by Eq. (5.103) must be expanded in a two-variable Taylor's series about the operating bias point to determine the incremental plate current i_p dependence upon incremental grid voltage e_g and incremental plate voltage e_p . If the operating point plate voltage is E_{b0} and grid voltage E_{c0} , then the related plate bias current is given by

$$I_{b0} = G [E_{c0} + \frac{E_{b0}}{\mu}]^{3/2}. \quad (5.104)$$

The incremental plate current i_p becomes

$$i_p = \sum_{n=1}^{\infty} \frac{1}{n!} \left[e_g \frac{\partial}{\partial e_c} + e_p \frac{\partial}{\partial e_b} \right]^n \left[e_c + e_b/\mu \right]^{3/2} \Big|_{\begin{array}{l} e_c = E_{c0} \\ e_b = E_{b0} \end{array}}. \quad (5.105)$$

The partial derivative operator can be expanded in a binomial series to give

$$\left[e_g \frac{\partial}{\partial e_c} + e_p \frac{\partial}{\partial e_b} \right]^n = \sum_{j=0}^n \binom{n}{j} \left[e_g \frac{\partial}{\partial e_c} \right]^{n-j} \left[e_p \frac{\partial}{\partial e_b} \right]^j. \quad (5.106)$$

Using Eq. (5.106) to expand Eq. (5.105) produces a general two-variable Taylor series expansion of the incremental plate current. The nonlinear as well as linear dependence upon incremental grid and plate voltages is then established. The first four terms of the triode plate current expansion are given in Table 5.2, under the assumption that G and μ are constant.

The first term of the incremental plate current is given by

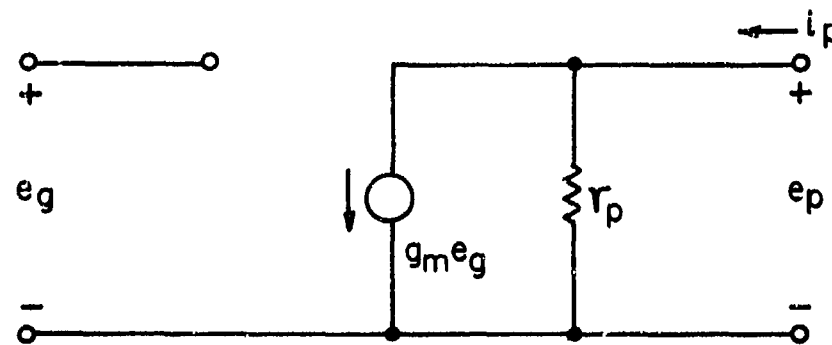
$$i_p = g_m e_g + \frac{1}{r_p} e_p , \quad (5.107)$$

where the transconductance $g_m = (3/2)G[E_{c0} + \frac{E_{b0}}{\mu}]^{1/2}$ and plate resistance $r_p = \mu/g_m$. Eq. (5.107) is the linear incremental relationship describing the triode and leads directly to the familiar linear incremental equivalent circuits illustrated in Fig. 5.35. If we add the interelectrode capacitances of the triode to the linear low-frequency equivalent circuit we obtain the familiar high-frequency equivalent circuit illustrated in Fig. 5.36.

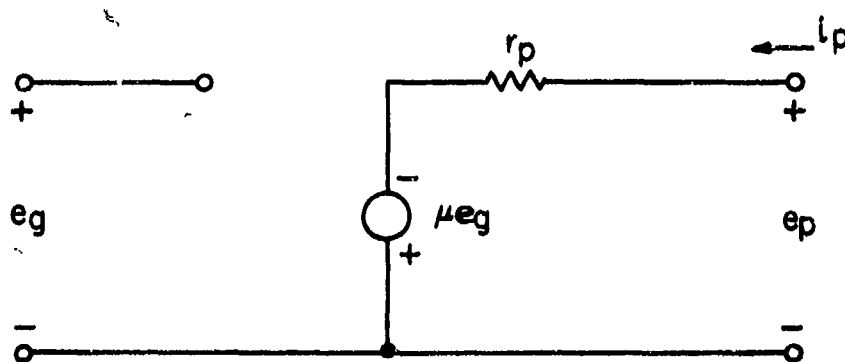
The nonlinear incremental equivalent circuit to the fourth order for the ideal vacuum triode is illustrated in Fig. 5.37. The low-frequency nonlinear model is represented by the series of controlled current sources that are given in Table 5.2. These sources are dependent upon the incremental grid and plate voltages e_g and e_p . We have also added the interelectrode capacitances to the model to obtain the high-frequency form of the nonlinear incremental model. The nonlinear incremental equivalent circuit has three nodes, i.e., the grid, plate, and cathode. All incremental voltages have been defined with respect to the cathode.

TABLE 5.2
First Four Terms of Ideal Triode Expansion

<u>Order</u>	<u>Term</u>
1	$g_1(e_g, e_p) = \frac{3}{2} G [E_{CO} + E_{BO}/\mu]^{1/2} [e_g + e_p/\mu]$ $= g_m e_g + \frac{1}{r_p} e_p$
2	$g_2(e_g, e_p) = \frac{3}{8} G [E_{CO} + E_{BO}/\mu]^{-1/2} [e_g^2 + 2e_g e_p/\mu + (\frac{e_p}{\mu})^2]$
3	$g_3(e_g, e_p) = -\frac{1}{16} G [E_{CO} + E_{BO}/\mu]^{-3/2}$ $\bullet [e_g^3 + 3e_g(\frac{e_p}{\mu}) + 3e_g(\frac{e_p}{\mu})^2 + (\frac{e_p}{\mu})^3]$
4	$g_4(e_g, e_p) = \frac{3}{128} G [E_{CO} + E_{BO}/\mu]^{-5/2}$ $\bullet [e_g^4 + 4e_g^3(\frac{e_p}{\mu}) + 6e_g^2(\frac{e_p}{\mu})^2 + 4e_g(\frac{e_p}{\mu})^3 + (\frac{e_p}{\mu})^4]$



a) Thevenin current source equivalent circuit.



b) Thevenin voltage source equivalent circuit.

Fig. 5.35. Low-Frequency Linear Incremental Equivalent Circuit of a Vacuum Triode.

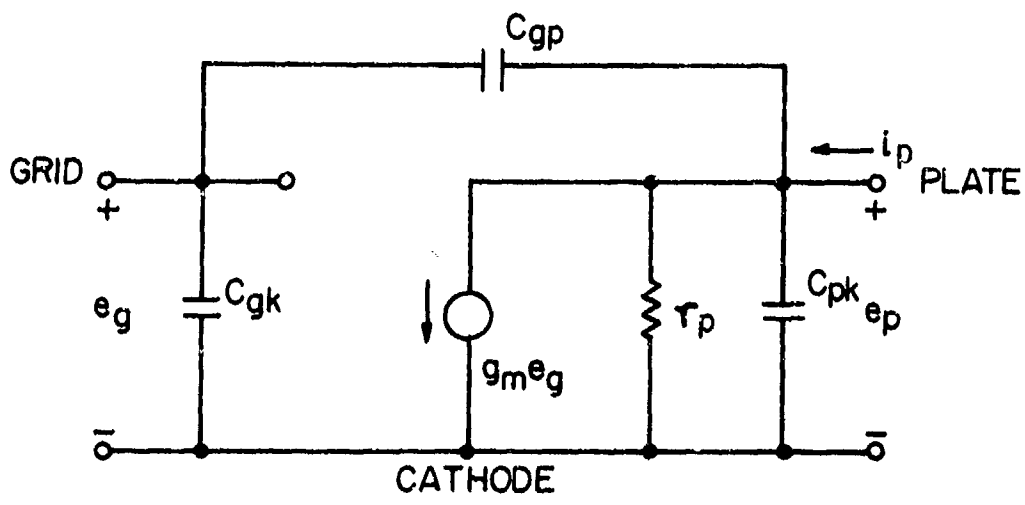


Fig. 5.36. High Frequency, Linear Incremental
Equivalent Circuit of a Vacuum Triode.

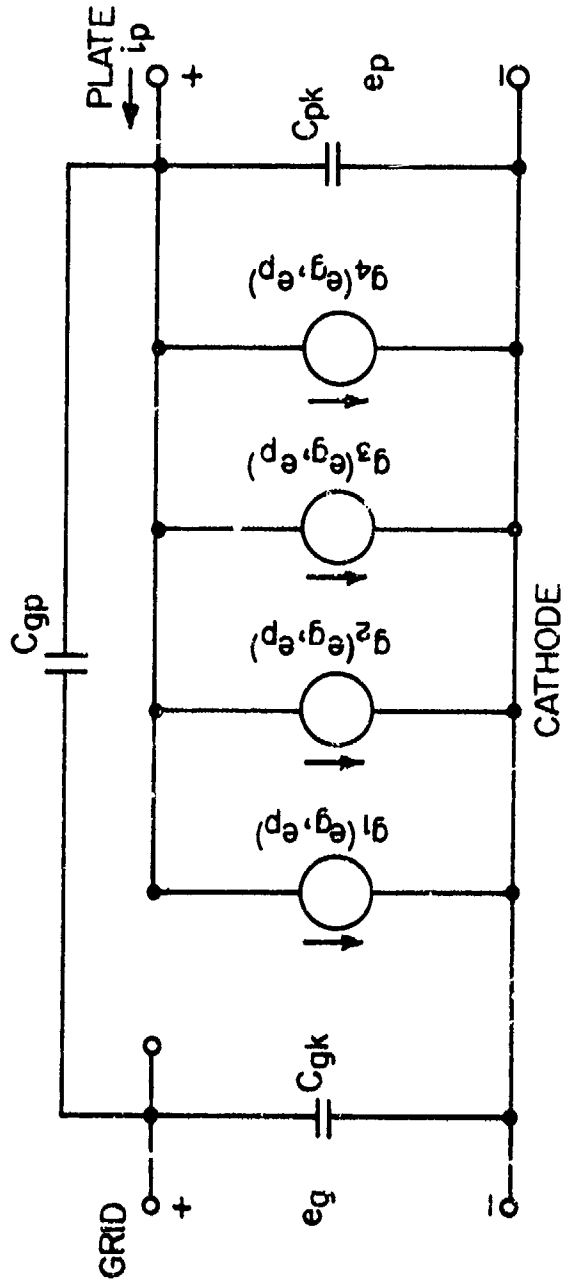


Fig. 5.37. High Frequency Nonlinear Incremental Equivalent Circuit of a Vacuum Triode. (Fourth-Order).

5.6.2.2 Vacuum Triode Measurements

A 12AT7 triode was measured in the laboratory in order to examine the applicability of Eq. (5.102). The measured characteristic curves are shown in Fig. 5.38 for one section of the tube. An inspection of the curves shows that they are relatively parallel for $i_b > 2.5$ mA, indicating nearly constant parameters for higher currents. However, for lower currents the curves become non-parallel and increasingly more horizontal as the grid voltage becomes more negative. Thus the tube parameters are changing in these regions.

As a further investigation of the triode, one can plot $i_b^{2/3}$ as a function of e_b . From Eq. (5.102)

$$i_b^{2/3} = G^{2/3} \left(e_c + e_b / \mu \right). \quad (5.108)$$

Therefore, in the range in which G , and μ are constant, there is a linear relation between $i_b^{2/3}$ and e_b . Figure 5.39 shows the $(i_b^{2/3}, e_b)$ relation for one section of the 12AT7. The $(i_b^{2/3}, e_b)$ curves are straight lines for i_b greater than about 2.5 mA, confirming our assumption of constant parameters in this range. However the curves are not parallel; they seem to have a decreasing slope as e_c decreases. Since the slope is $G^{2/3}/\mu$, the inference is that either G decreases with e_c , or μ increases with e_c . The data of Fig. 5.39 are somewhat coarse, as the grid voltage curves are taken at 1 volt intervals. One can, however, estimate the perveance from the data if we assume that G and μ are locally constant. Thus,

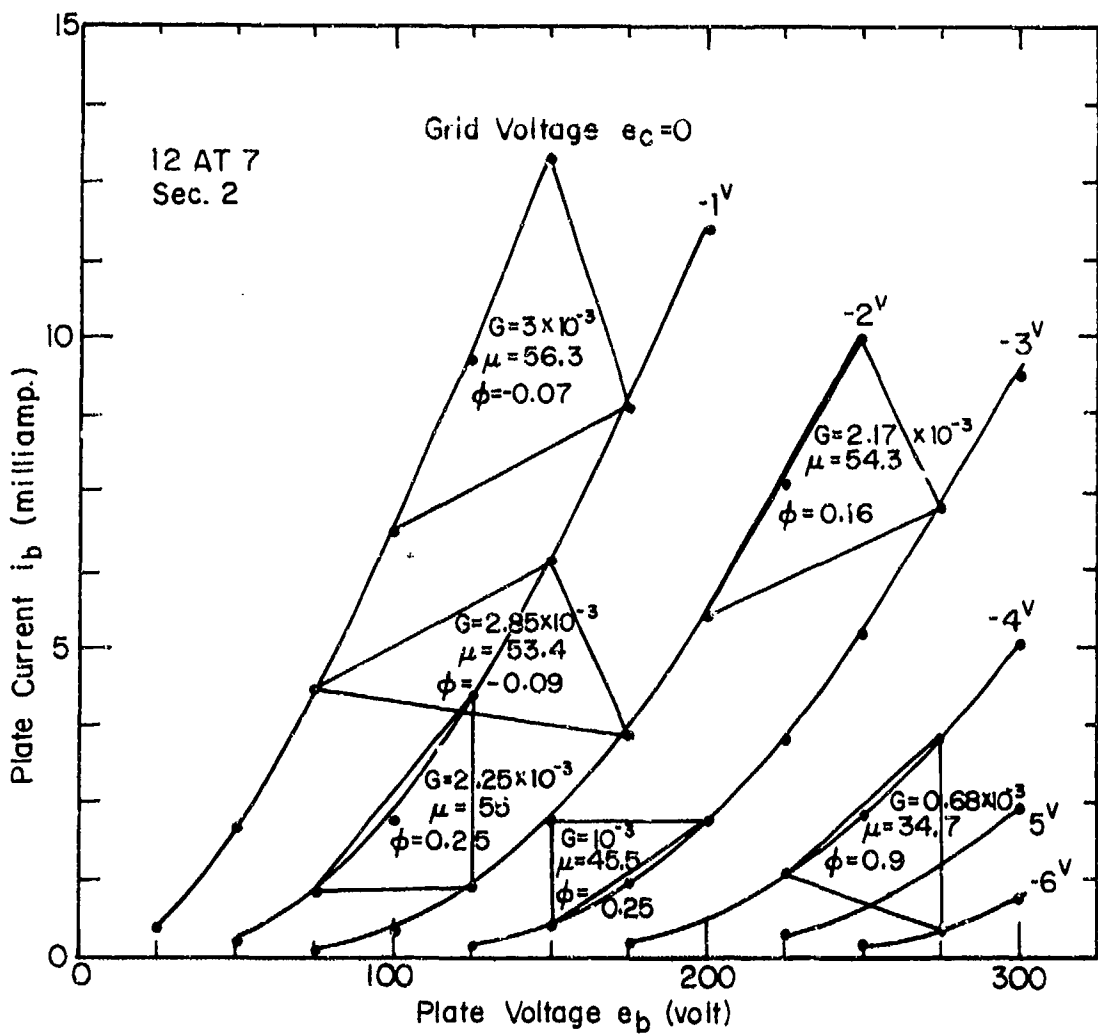


Fig. 5.38. Triode Characteristic Cruves.

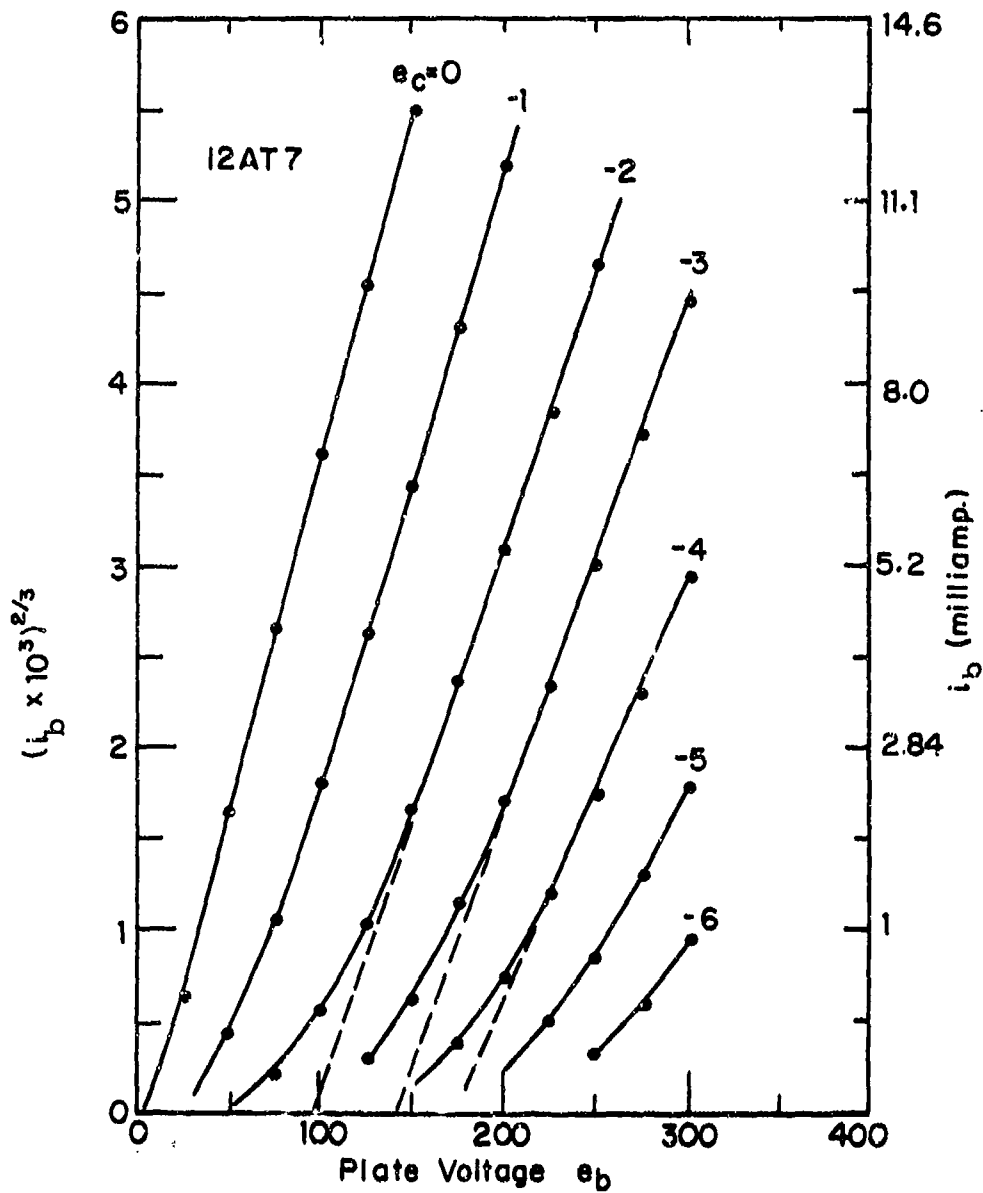


Fig. 5.39. $i_b^{2/3}$ versus e_b : 12AT7.

from Eq. (5.102), G can be estimated in two ways or

$$G \approx \left(\frac{\Delta(i_s^{2/3})}{\Delta e_c} \right)^{3/2} \quad |_{e_b = \text{constant}}, \quad (5.109a)$$

and

$$G \approx \left(\frac{\Delta(i_s^{2/3})}{\Delta e_b} \mu \right)^{3/2} \quad |_{e_c = \text{constant}}. \quad (5.109b)$$

G , evaluated through the use of both techniques for the data shown in Fig. 5.38 is shown on Fig. 5.40. It is seen that the permeance is, indeed, linearly-dependent on the grid voltage, and takes the form

$$G \approx 3.35 \times 10^{-3} \left(1 - e_c/E_{c \max} \right), \quad (5.110)$$

where $E_{c \max} \approx -6.2V$.

This result shows that there is another nonlinearity to be considered in triode analysis over and above the $3/2$ power nonlinearity; that is, G must be considered as a variable in equation (5.105).

Returning now to Fig. 5.39, we note a second point of interest, namely that the $e_c = 0$ curve does not go through the point $e_b = i_c = 0$, as required by Eq. (5.103). Instead, it is offset by approximately 5 volts. This is due to the space-charge voltage of the tube. In Equation (5.103) it is assumed that the emitted electrons start with zero velocity from a point of zero

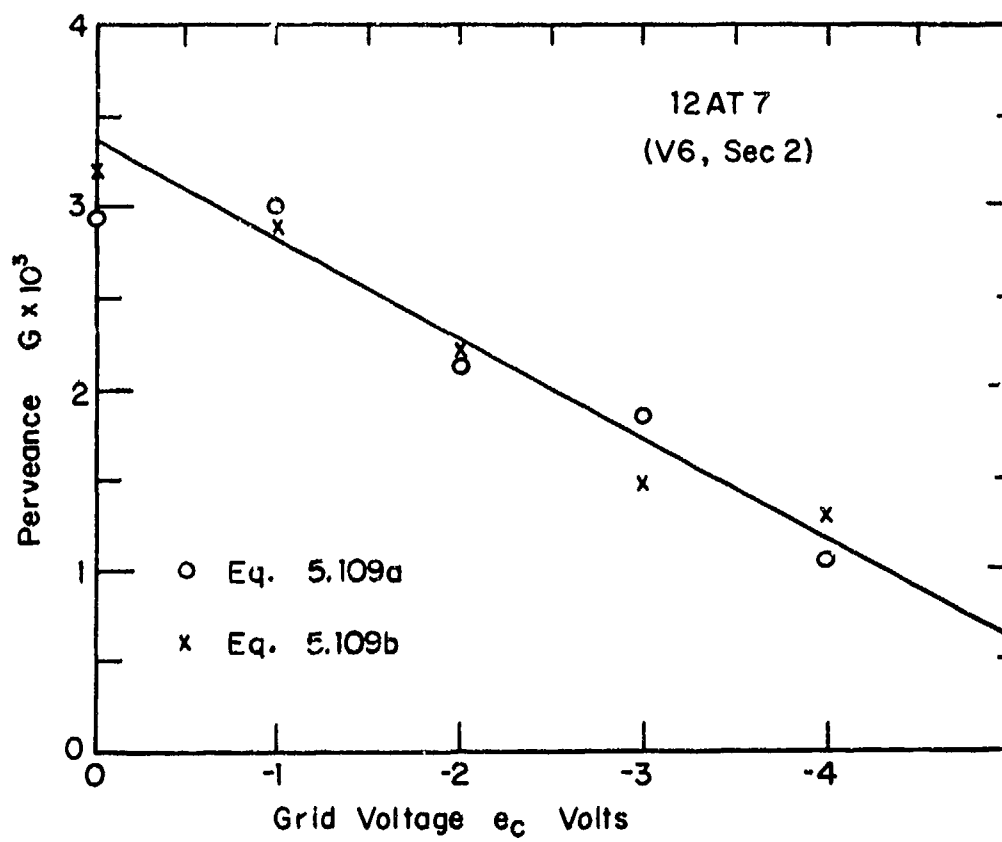


Fig. 5.40. Variation of Pervenance with Grid Voltage

potential. In space-charge limited operation the electrons leave the cathode with a Maxwellian distribution of velocity and, near the actual cathode, a virtual cathode is formed which acts like an ideal cathode. The effects of this can be added to Eq. (5.103) by defining a potential, ϕ , which is added to the grid voltage, resulting in

$$i_b = G(e_c + \phi + e_b/\mu)^{3/2}. \quad (5.111)$$

Given a consistent set of (i_b, e_c, e_b) , Eq. (5.111) contains three unknowns, G , ϕ , and μ . Thus, if (I_b, E_c, E_b) are measured at three reasonably close points, we might make the assumption that G , ϕ , and μ are locally constant and solve the set of simultaneous equations. If we denote the measured points by a subscript i , $i=1,2,3$, the solution for G , ϕ , μ is given by:

$$\begin{aligned} \frac{1}{\mu} & \left[\frac{I_{b1}^{2/3} - I_{b3}^{2/3}}{I_{b1}^{2/3} - I_{b2}^{2/3}} (E_{b1} - E_{b2}) - (E_{b1} - E_{b3}) \right] \\ & = -(E_{c1} - E_{c2}) \frac{I_{b1}^{2/3} - I_{b3}^{2/3}}{I_{b1}^{2/3} - I_{b2}^{2/3}} + (E_{c1} - E_{c3}). \end{aligned} \quad (5.112a)$$

$$G^{-2/3} = \frac{[(E_{b1} - E_{b2})/\mu + (E_{c1} - E_{c2})]}{(I_{b1}^{2/3} - I_{b2}^{2/3})}, \quad (5.112b)$$

$$\phi = -E_{c1} - E_{b1}/\mu + (I_{b1}/G)^{2/3}. \quad (5.112c)$$

Equations (5.112a-c) were solved for several operating regions of the 12AT7. The resulting values of μ, G, ϕ are shown in Fig. 5.38 in the triangle formed by the 3 points used to solve Eq. (5.112-c). It is seen that at higher currents, μ is indeed nearly constant, while G is less so. The value of ϕ varies, but is small. For the lower current ranges, G, ϕ , and μ vary considerably. Thus, the required triode model nonlinearities are the 3/2 power law, the varying perveance, and a nonzero potential ϕ based on the operating point.

5.6.3 Vacuum Pentode

5.6.3.1 Vacuum Pentode Theory

The schematic symbol for a vacuum pentode is illustrated in Fig. 5.41. Electrode total voltages and currents are defined in the diagram. The suppressor is normally tied to the cathode. The screen grid is normally biased positively while the control grid is negative with respect to the cathode. The generalized 3/2 power law relationship is

$$i_s = G (e_{eq})^{3/2}, \quad (5.113)$$

where

$$i_s = \text{total space current} = i_{c1} + i_{c2} + i_{c3} + i_b. \quad (5.114)$$

G = a parameter called the perveance,

e_{eq} = equivalent diode voltage for a pentode,

$$= e_{c1} + \frac{e_{c2}}{\mu_{12}} + \frac{e_{c3}}{\mu_{13}} + \frac{e_b}{\mu_{1b}}. \quad (5.115)$$

The several μ 's are ideally constants. In particular

μ_{1j} = voltage gain between grids 1 and j ,

μ_{1b} = voltage gain between grid 1 and plate.

Since the screen grid is positive with respect to grid 1, part of the space-current is intercepted by the screen.

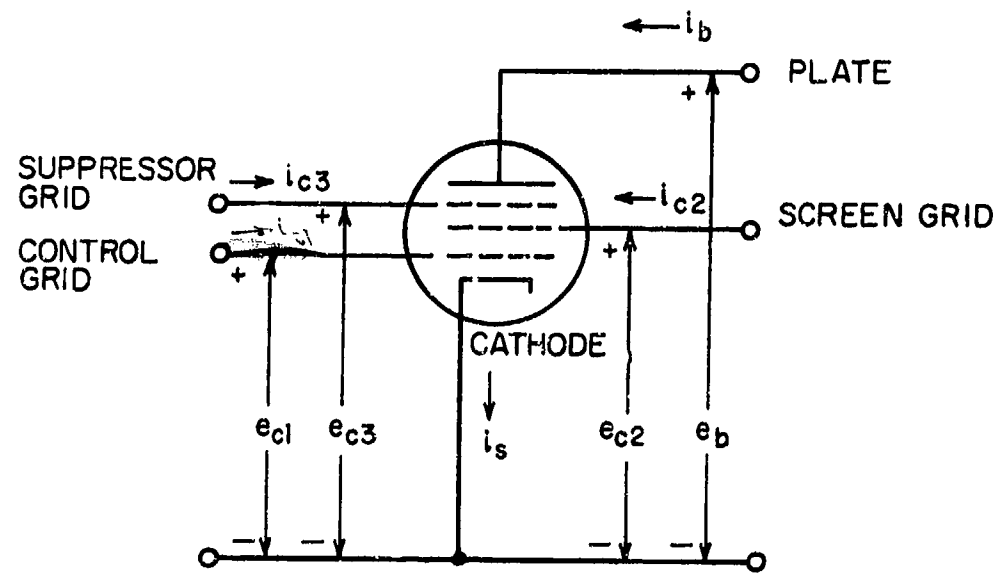


Fig. 5.41. Vacuum Pentode.

The ratio of the plate to screen grid current, i_b/i_{c2} , is empirically given by

$$\frac{i_b}{i_{c2}} = D \left[\frac{e_b}{e_{c2}} \right]^m, \quad (5.116)$$

where D and m are parameters of the tube.

Note that $i_{c1} = i_{c3} = 0$ when the control grid voltage is negative and the suppressor voltage is less positive than the screen voltage. Combining the pentode equations we find that the total plate current i_b is given by

$$i_b = G \left[e_{c1} + \frac{e_{c2}}{\mu_{12}} + \frac{e_{c3}}{\mu_{13}} + \frac{e_b}{\mu_{lb}} \right]^{3/2} \frac{D \left[\frac{e_b}{e_{c2}} \right]^m}{1 + D \left[\frac{e_b}{e_{c2}} \right]^m}. \quad (5.117)$$

If we connect the suppressor grid to the cathode, then $e_{c3} = 0$. Note that the physical effect of the screen grid is to make the plate current nearly independent of plate voltage since $e_{c2}/\mu_{12} \gg e_b/\mu_{lb}$. Therefore

$$i_b \approx G \left[e_{c1} + \frac{e_{c2}}{\mu_{12}} \right]^{3/2} \frac{D \left[\frac{e_b}{e_{c2}} \right]^m}{1 + D \left[\frac{e_b}{e_{c2}} \right]^m}, \quad (5.118)$$

in the negative grid region of a pentode whose suppressor grid is connected to the cathode. Total plate current is a function of three voltage variables, e_{c1} , e_{c2} , and e_b . The parameters are G, μ_{12} , D, and m.

If we now assume that each total voltage is given by

$$e_{c1} = E_{10} + e_{g1}, \quad (5.119)$$

$$e_{c2} = E_{20} + e_{g2}, \quad (5.120)$$

$$e_b = E_{b0} + e_p. \quad (5.121)$$

where e_{g1} , e_{g2} , and e_p are incremental voltages and E_{10} , E_{20} , E_{b0} are bias voltages, the total plate current now becomes

$$i_b = I_{b0} + i_p, \quad (5.122)$$

where

$$\begin{aligned} I_{b0} &= \text{plate bias current} \\ &= G \left[E_{10} + \frac{E_2}{\mu_{12}} \right]^{3/2} - \frac{D \left[\frac{E_{b0}}{E_{20}} \right]^m}{1 + D \left[\frac{E_{b0}}{E_{20}} \right]^m}, \end{aligned} \quad (5.123)$$

and

$$\begin{aligned} i_p &= \text{incremental plate current} \\ &= \sum_{n=1}^{\infty} \left\{ \frac{1}{n!} \left[e_{g1} \frac{\partial}{\partial e_{c1}} + e_{g2} \frac{\partial}{\partial e_{c2}} + e_p \frac{\partial}{\partial e_b} \right] \right. \\ &\quad \left. \cdot G \left[e_{c1} + \frac{e_{c2}}{\mu_{12}} \right]^{3/2} \frac{D \left[\frac{e_b}{e_{c2}} \right]^m}{1 + D \left[\frac{e_b}{e_{c2}} \right]^m} \right\} \Big|_{\substack{e_{c1} = E_{10} \\ e_{c2} = E_{20} \\ e_b = E_{b0}}} \end{aligned} \quad (5.124)$$

Normally, the screen grid of the pentode is well by-passed at desired responses so that the incremental voltage e_{g2} is zero. However, if the screen should not be adequately bypassed at a frequency generated by nonlinear interaction, or the screen is utilized as a local-oscillator input in a mixer application, we should retain the effects of incremental variation in screen voltage.

An additional factor which must be considered occurs in the so-called variable μ pentode. In this case, the control grid is deliberately constructed so that μ_{12} , instead of being a constant, is a function of e_{c1} . This is a possible source of distortion.

These considerations lead to Eq. (5.124) as a representation of the pentode incremental nonlinear plate current. Equation (5.124) is complicated by two factors - namely, the appearance of e_p and e_{g2} in both factors of the operand, and the occurrence of $\mu_{12}(e_{c1})$ in the denominator of the first factor. Symbolically, they are controlled-current sources, that is,

$$i_p = g_1(e_{g1}, e_{g2}, e_p) + g_2(e_{g1}, e_{g2}, e_p) + \dots \\ + g_n(e_{g1}, e_{g2}, e_p), \quad (5.125)$$

where

$$g_n(e_{g1}, e_{g2}, e_p) = \frac{1}{n!} \left[e_{g1} \frac{\partial}{\partial e_{c1}} + e_{g2} \frac{\partial}{\partial e_{c2}} + e_p \frac{\partial}{\partial e_b} \right]^n$$

$$\cdot G \left[e_{c1} + \frac{e_{c2}}{\mu_{12}} \right]^{3/2} \frac{D \left[\frac{e_b}{e_{c2}} \right]^m}{1+D \left[\frac{e_b}{e_{c2}} \right]^m} \quad \begin{array}{l} e_{c1} = E_{10} \\ e_{c2} = E_{20} \\ e_b = E_{b0} \end{array}$$

(5.126)

The first term represents the linear incremental current source and the plate resistance while the higher-order terms contribute nonlinear responses.

Typically, $m \ll 1$, so that the plate and screen currents have only a slight dependence on the plate voltage. This accounts for the nearly infinite plate resistance of a pentode. The dependence of the current division on the total plate and screen voltages is, however, a source of nonlinear distortion which must be considered in pentode analysis.

The screen current similarly has the incremental nonlinear representation:

$$i_{g2} = \sum_{n=1}^{\infty} \left\{ \frac{1}{n!} \left[e_{g1} \frac{\partial}{\partial e_{c1}} + e_{g2} \frac{\partial}{\partial e_{c2}} + e_p \frac{\partial}{\partial e_b} \right]^n \right. \right. \quad (5.127)$$

$$\left. \cdot G \left[e_{c1} + \frac{e_{c2}}{\mu_{12}} \right]^{3/2} \frac{1}{1+D \left[\frac{e_b}{e_{c2}} \right]^m} \right\} \quad \begin{array}{l} e_{c1} = E_{10} \\ e_{c2} = E_{20} \\ e_b = E_{b0} \end{array}$$

The nonlinear incremental equivalent circuit to third order for the pentode as implied by Eq. (5.125) and (5.127) is illustrated in Fig. 5.42. The series of current sources g_n are in the plate circuit. They are dependent upon the control grid voltage e_{g1} and screen grid voltage e_{g2} when the screen is inadequately by-passed. The series of current sources k_n are in the screen circuit. They are dependent upon the control grid voltage e_{g1} and the incremental screen voltage e_{g2} .

In Fig. 5.43 we illustrate the pentode linear incremental equivalent circuit with the un-bypassed screen. Inter-electrode capacitances may be added to the equivalent circuit to create a useful high frequency model.

5.6.3.2 Vacuum Pentode Measurements

As with the vacuum triode, Equation (5.113) is an approximation to the actual pentode characteristic. Experimental data, which we shall show in this section, indicates both that the perveance depends on the screen voltage and that there is a non-zero space-charge voltage. Thus, for the pentode, one can write:

$$i_s = G_0 [1 - e_c/E_{c_{\max}}] [\phi + e_c + e_2/\mu]^{3/2}, \quad (5.128)$$

where e_c is grid 1 voltage and e_2 is screen voltage.

Laboratory measurements were performed on a number of pentodes in order to test the validity of Equation (5.128). In this section we will examine in detail the results of the measurements on one pentode, a 6AH6, and summarize the results of measurements on two other types, the 6DC6 and the 5763.

The 6AH6 is a sharp-cutoff pentode. The measured plate characteristics of a 6AH6 are shown in Fig. 5.44, for a screen voltage of 100 volts. Note the almost horizontal curves for

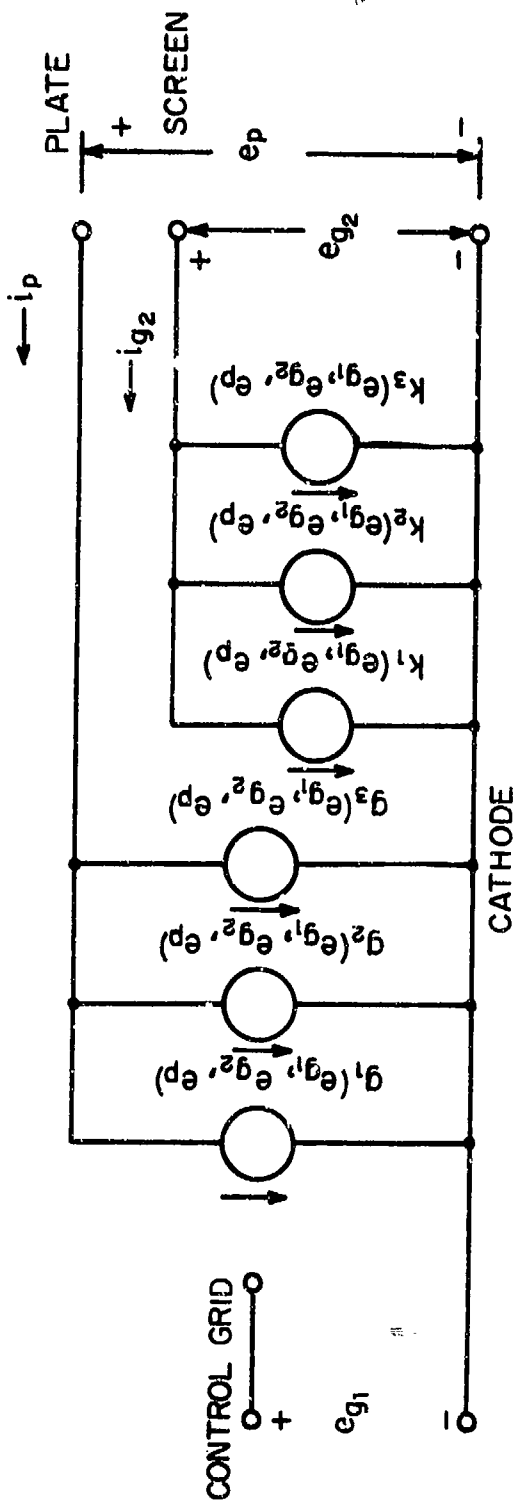


Fig. 5.42. Nonlinear Incremental Equivalent Circuit of a Vacuum Pentode. (Third-order).

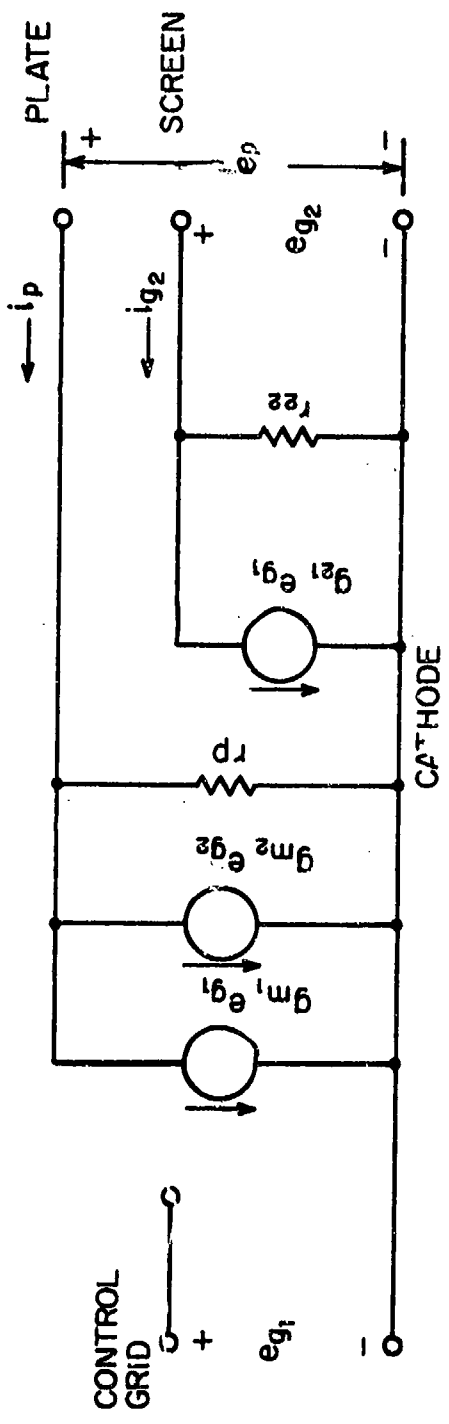


Fig. 5.43. Linear Incremental Equivalent Circuit of a Pentode with Unbypassed Screen.

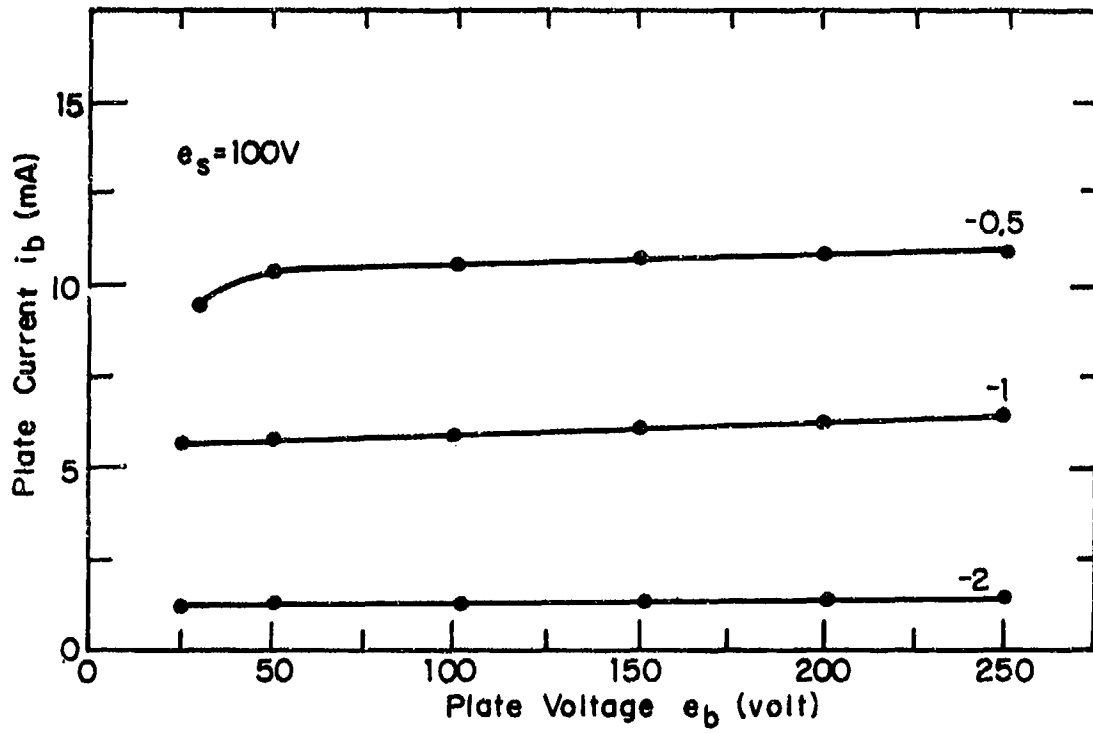


Fig. 5.44. Pentode Characteristic 6AH6.

constant grid voltage, indicative of a very high plate resistance. The triode-connected characteristics of this tube, that is, screen connected to plate, are shown in Fig. 5.45. As a further investigation of the pentode, one can plot $(i_b + i_2)^{2/3}$ as a function of e_b , as shown in Fig. 5.46. It is seen that the 3/2 power law holds down to 1 mA, well into the curved regions of the triode curves. The zero bias curve does not go through the origin, indicating a need to add a correction for the effect of space-charge potential. The variation of perveance with control grid voltage is shown in Fig. 5.47. This variation is seen to be linear, with cutoff at about -5 volts. The current division between screen and plate currents in the triode connection is plotted in Fig. 5.48. The division of currents is seen to be nearly independent of grid voltage. The current division in the pentode connection is shown in Fig. 5.49; a slight dependence is seen on the grid voltage and the ratio of the plate-to-screen voltage.

Figures 5.44 - 5.49 show that the three-halves power law model, when modified for the non-constant perveance and the effects of space-charge potential, is a good model for the 6AH6 pentode. The results found in modeling the 5763 and 6DC6 were similar. Table 5.3 summarizes the parameters measured for these three tube types. The operating points at which these were modeled are also shown. In the electrode capacitance values are also included.

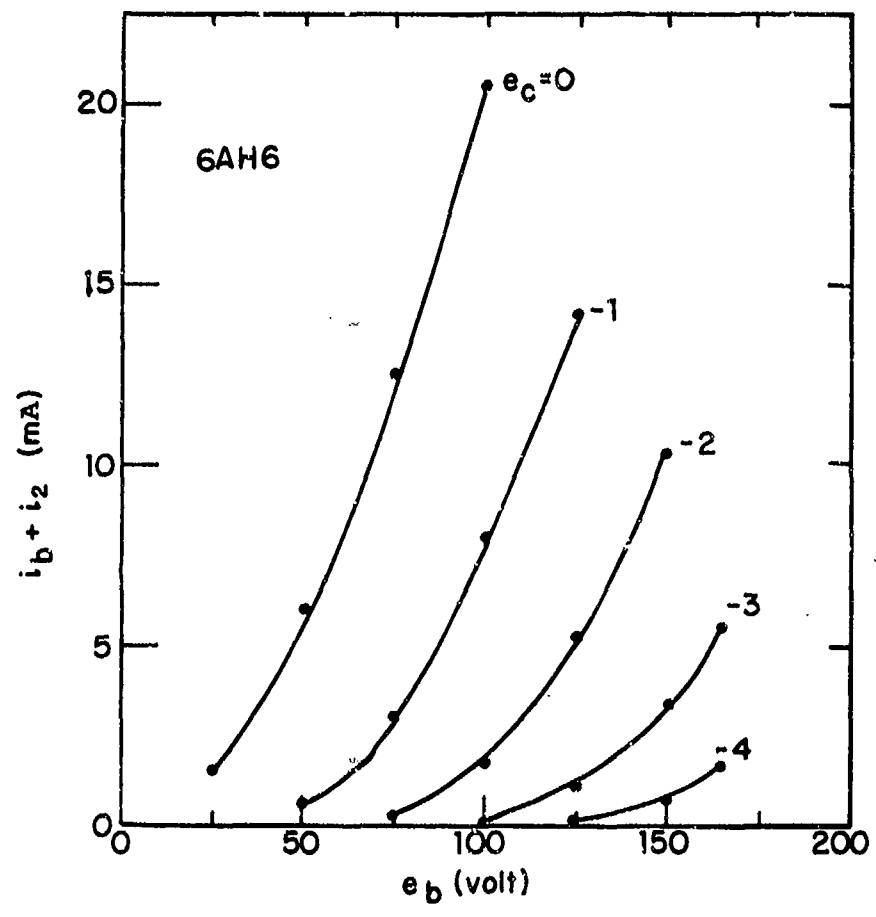


Fig. 5.45. Triode Characteristic - 6AH6.

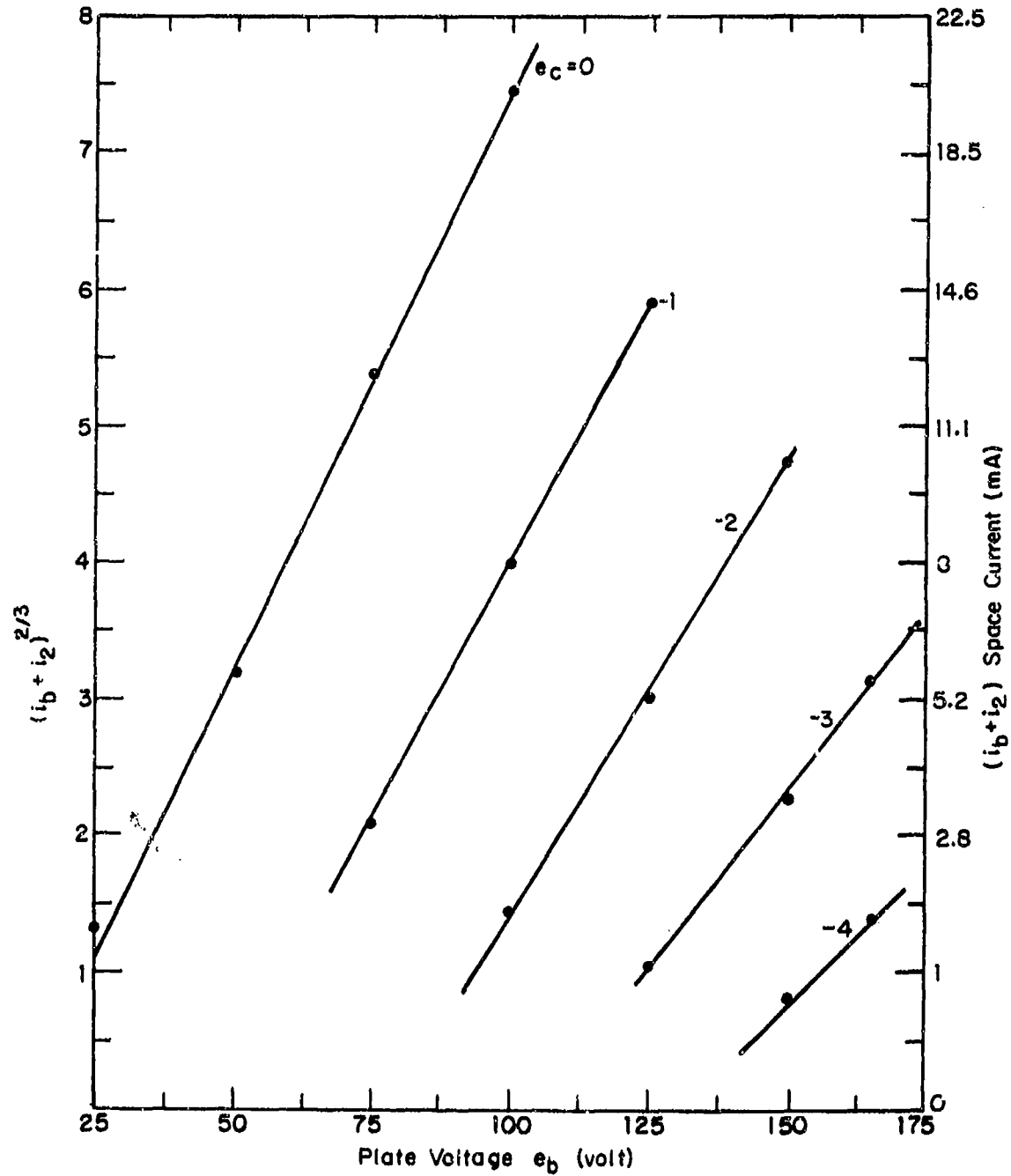


Fig. 5.46. $(i_b + i_2)^{2/3}$ Triode Characteristics 6AH6 Pentode.

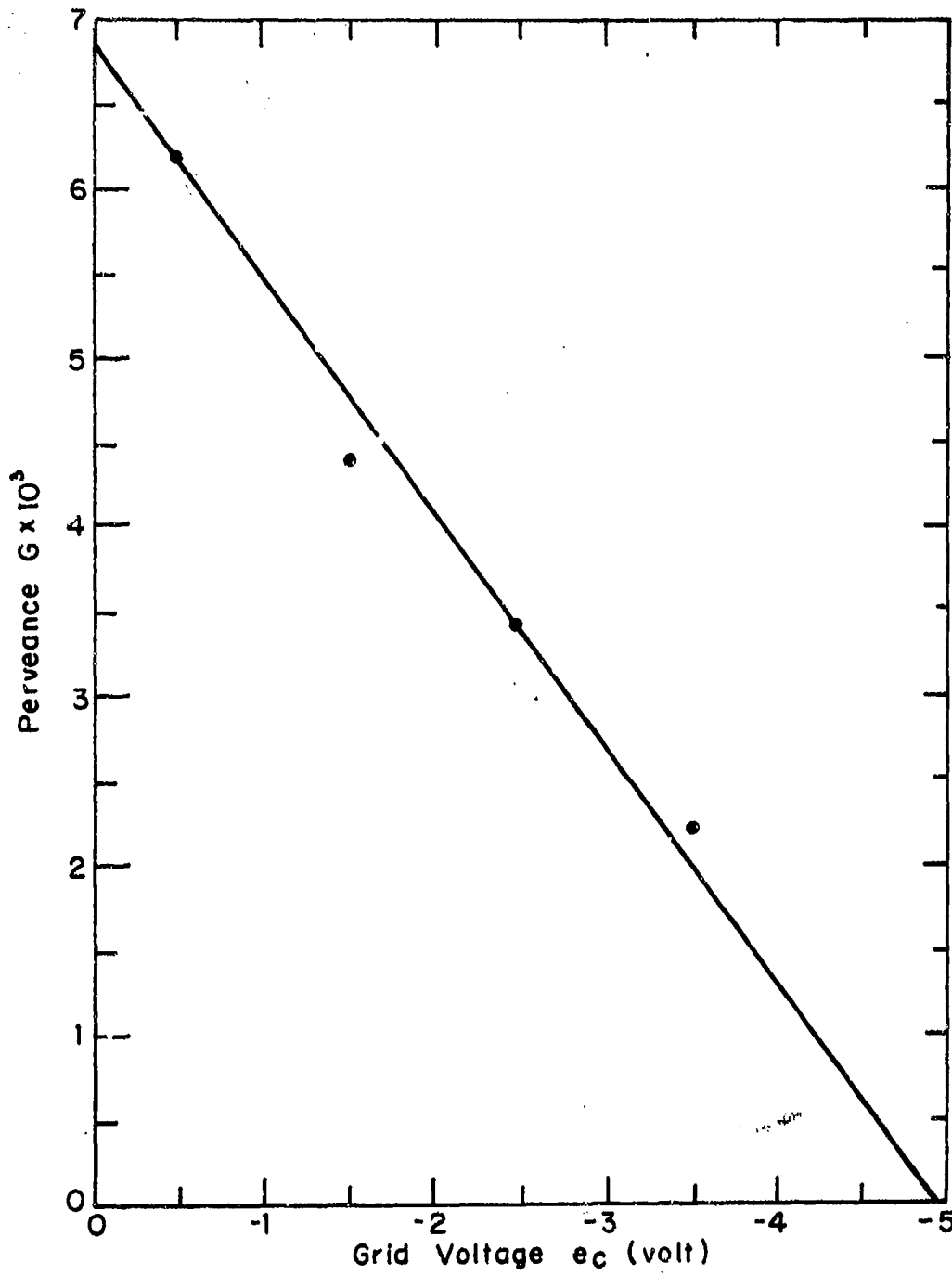


Fig. 5.47. Pervenance Variation with Grid Voltage:
6AH6 Pentode.

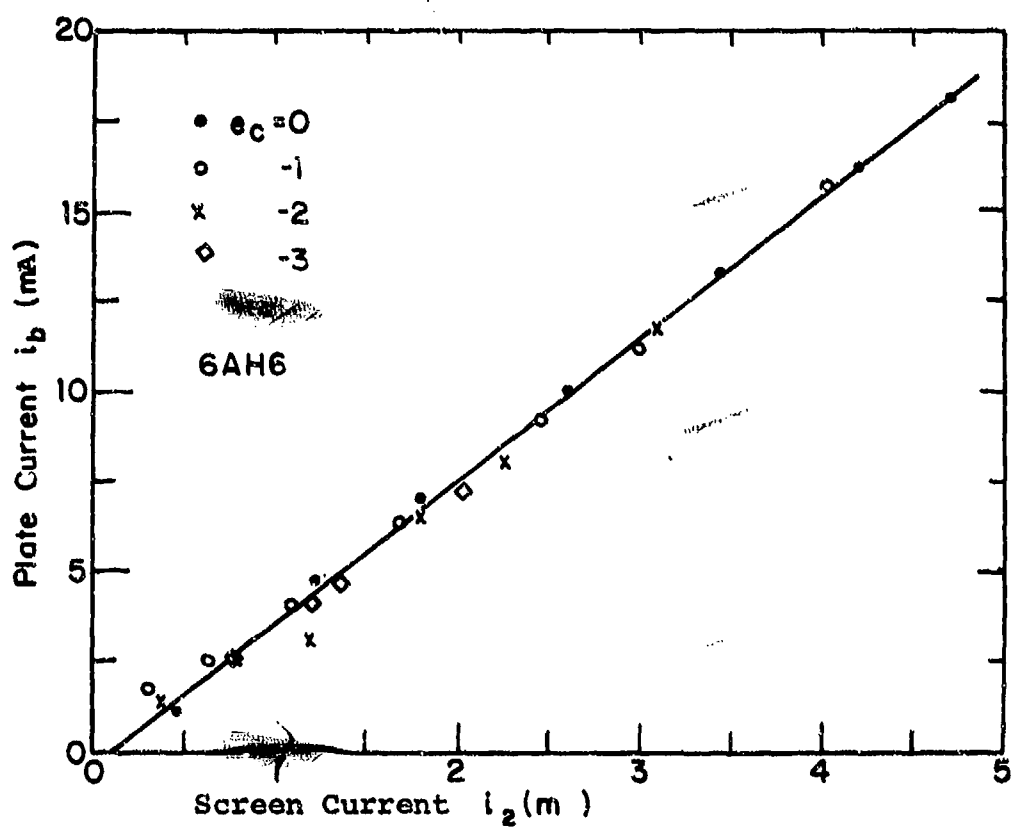


Fig. 5.48. 6AH6 Current Division - Triode Connection

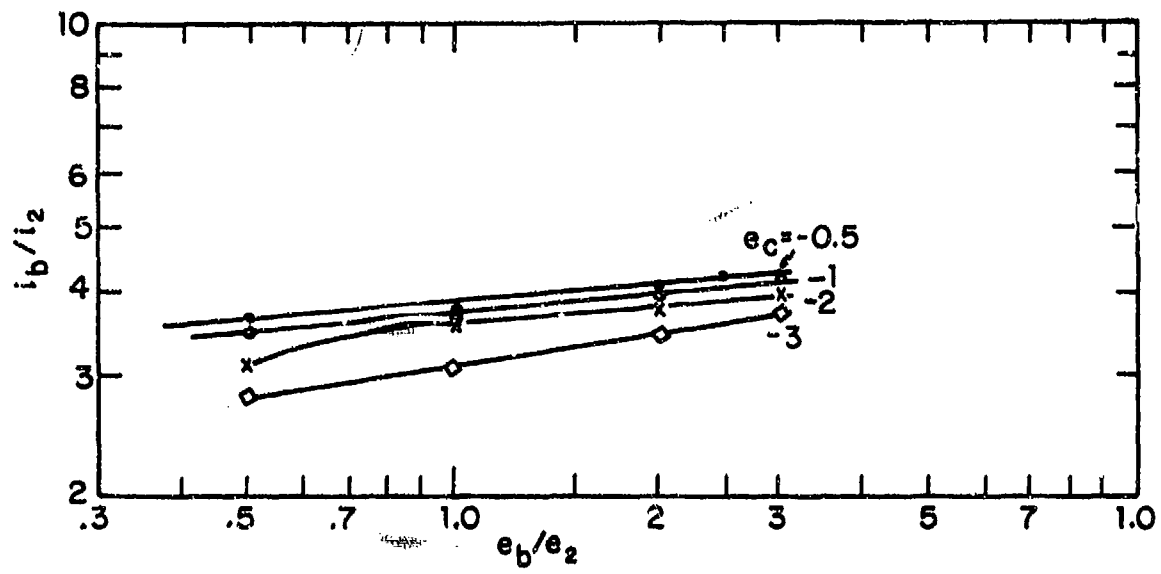


Fig. 5.49. Current Division, 5AH6 Pentode.

Table 5.3
Pentode Model Parameters

Parameter	6AH6	6DC6	5763	Units
Operating Points				
E_{c0}	-2.0	-1.0	-6.0	V
E_{b0}	129.6	91.2	187	V
E_{20}	135.8	84.0	203	V
I_{b0}	5.7	8.9	3.9	mA
I_{20}	0.15	3.1	0.47	mA
Model Parameters				
G_0	6.85×10^{-3}	3.95×10^{-3}	2.0×10^{-3}	$AV^{-3/2}$
μ	38.5	39.4	13.8	
D	4.0	2.8	9.0	
m	0.088	0.11	2.0	
E_{c0}	-2.0	-1.0	-6.0	V
$E_{c\max}$	-5.0	-7.6	-48.0	V
ϕ	-0.04	0.98	0.6	V
E_{20}	135.8	84.0	203	V
E_{b0}	129.6	91.2	187	V
C_{gk}	12	6.5	9.5	pF
C_{pg}	0.02	0.02	0.3	pF
C_{pk}	4.7	2.0	4.5	pF

CHAPTER 6

MULTIPLE-TONE INPUT APPLICATIONS

6.1 Introduction

One of the most important applications of the nonlinear transfer function is the prediction of the nonlinear distortion responses of a quasi-linear system that has been excited by multiple unmodulated input tones. By far the most commonly employed method of investigating and evaluating a quasi-linear system involves excitation of the system by two equal amplitude tones. In this chapter we shall concentrate upon a fairly complete study of multiple-tone excitation analysis with particular attention focused upon formulating the problem in terms of practical engineering quantities. We shall be most concerned about decibel power relationships and the practical prediction and interpretation of a nonlinear system output as measured by a spectrum analyzer. Various simple examples have been worked out with the theoretical predictions compared with laboratory measurements from the actual modeled circuit. Emphasis is placed upon simple circuits so that confidence in the methods and the validity and limitations of the electronic device models introduced in Chapter 5 can be obtained. Most of our concern will be with intermodulation distortion nonlinear responses although gain compression, desensitization, and spurious responses for unmodulated tonal inputs are relevant. Matters concerned with modulation distortion and the transfer of modulation to other tones (cross-modulation) are more properly studied in association with nonlinear canonic model applications. Although most of this chapter is devoted to small-signal excitation, we also describe in some detail the results of a large-signal time-domain analysis of a simple test amplifier.

circuit and compare the time-domain analysis results with both measurements and predictions based upon the nonlinear transfer function determined from a model analysis using SIGNCAP.

6.2 Power Relationships for Multi-Tone Input Applications

In this section we shall examine the intermodulation distortion power relationships describing the output power from a quasi-linear system characterized by nonlinear transfer functions. The formulation will be for multitone small-signal excitation with particular emphasis placed upon the important two and three tone input cases. The special case of equal-power two-tone inputs will be of particular practical interest.

In Fig. 6.1 we list several responses for a nonlinear amplifier excited by two tones in terms of nonlinear transfer functions. Observe that the input is the open-circuit voltage source $v_s(t)$ behind the source impedance Z_s . The output is $v_o(t)$ across the load impedance Z_L . It is assumed that the source and load impedances are linear. The source and load impedances must be used to determine the nonlinear transfer functions.

6.2.1 First-Order Response

The first-order output voltage for a sinusoidal open-circuit excitation voltage amplitude V_1 is $V_1 H_1(f)$ where $H_1(f)$ is the first-order transfer function. It is readily demonstrated that the power p_1 delivered to load impedance Z_L is given by

$$p_1 = g_T p_a, \quad (6.1)$$

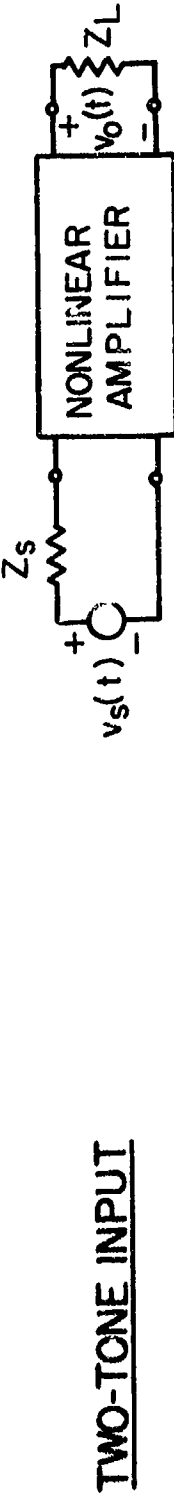
where

$$p_1 = \frac{1}{4} \frac{Z_L + Z_L^*}{|Z_L|^2} |v_o|^2,$$

$$p_a = \frac{1}{4} \frac{|V_1|^2}{Z_s + Z_s^*} = \text{source available power},$$

g_T = transducer gain $\triangleq \frac{\text{delivered power}}{\text{available power}}$,

$$= \frac{(Z_L + Z_L^*)(Z_s + Z_s^*)}{|Z_L|^2} |H_1|^2. \quad (6.2)$$



SINUSOIDAL AT ω_1, ω_2 .

$$v_s(t) = \operatorname{Re}[V_1 e^{j\omega_1 t} + V_2 e^{j\omega_2 t}]$$

OUTPUTS

FIRST ORDER AT ω_1 AND ω_2 :

$$v_o(t) = \operatorname{Re}[V_1 H_1(\omega_1) e^{j\omega_1 t} + V_2 H_1(\omega_2) e^{j\omega_2 t}]$$

SECOND ORDER AT $\omega_1 - \omega_2$

$$v_o(t) = \operatorname{Re}[V_1 V_2^* H_2(\omega_1, -\omega_2) e^{j(\omega_1 - \omega_2)t}]$$

THIRD ORDER AT $2\omega_1 - \omega_2$:

$$v_o(t) = \operatorname{Re}\left[\frac{3}{4} V_1^2 V_2^* H_3(\omega_1, \omega_1, -\omega_2) e^{j(2\omega_1 - \omega_2)t}\right]$$

Fig. 6.1. Examples of Nonlinear Amplifier Responses in Terms of Nonlinear Transfer Functions.

It is frequently desired to express power in decibels relative to a reference power p_x . If the reference power is 1 milliwatt, then the decibel power unit is dBm. Thus, defining

$$P_1 \triangleq 10 \log \frac{P_1}{P_x}, \quad (6.3)$$

$$P_a \triangleq 10 \log \frac{P_a}{P_r}, \quad (6.4)$$

where $P_r = 10^{-3}$ watts, results in

$$P_1 = P_a + G_T \text{ (dBm)}, \quad (6.5)$$

where

$$G_T \triangleq 10 \log_{10} g_T \text{ (dB)}$$

$$\begin{aligned} &= 20 \log |H_1| \\ &+ 10 \log_{10} \frac{(Z_L + Z_L^*) (Z_S + Z_S^*)}{|Z_L|^2}. \end{aligned} \quad (6.6)$$

The special case $Z_L = Z_S = 50$ ohms is commonly encountered in practical measurements. Under these circumstances transducer gain G_T reduces to insertion gain G_I and we have the useful result

$$P_1 = P_a + G_I \text{ (dBm)}, \quad (6.7)$$

where

$$G_I = 20 \log_{10} |H_1| + 6 \text{ dB}. \quad (6.8)$$

Identical relationships apply to each output linear response for multiple tone inputs.

6.2.2 Second-Order Response

The amplitude of a typical second-order response at $f_1 + f_2$ in terms of the second-order nonlinear transfer function is $V_1 V_2 H_2$. It is readily demonstrated that p_2 , the second-order response power delivered to the output load Z_L at $f_1 + f_2$ is given by

$$p_2 = m_2 p_{a1} p_{a2}, \quad (6.9)$$

where

p_{a1} = available power (watts) from source at frequency f_1 ,

p_{a2} = available power (watts) from source at frequency f_2 ,

$$m_2 = 4 |H_2|^2 (Z_S + Z_S^*) \Big|_{f=f_1} (Z_S + Z_S^*) \Big|_{f=f_2} \frac{Z_L + Z_L^*}{|Z_L|^2} \Big|_{f=f_1 + f_2} \text{ (watts)}^{-1}. \quad (6.10)$$

Our objective now is to cast Eq. (6.9) in a decibel form with the reference power p_r set equal to one milliwatt so that the result will be a suitable expression with power expressed in dBm. Special care must be exercised to properly interpret such a form. We begin by defining

$$p_2 \stackrel{\Delta}{=} 10 \log_{10} \frac{p_2}{p_r}, \quad (6.11)$$

$$p_{a1} \stackrel{\Delta}{=} 10 \log_{10} \frac{p_{a1}}{p_r}, \quad (6.12)$$

$$p_{a2} \stackrel{\Delta}{=} 10 \log_{10} \frac{p_{a2}}{p_r}, \quad (6.13)$$

$$M_2 \stackrel{\Delta}{=} 10 \log_{10} p_r m_2, \quad (6.14)$$

and note that Eq. (6.9) can be written in the form

$$\frac{p_2}{p_r} = (p_r m_2) \left(\frac{p_{a1}}{p_r} \right) \left(\frac{p_{a2}}{p_r} \right), \quad (6.15)$$

where p_r is the reference power level. It follows from the definitions that

$$P_2 = P_{a1} + P_{a2} + M_2. \quad (6.16)$$

Let us now further note that we may write

$$p_r = \frac{|v_r|^2}{Z_r + Z_r^*}, \quad (6.17)$$

where v_r is a reference voltage and Z_r a reference impedance. For example, let us select the reference power level p_r at 10^{-3} watts and the reference voltage level at 1 volt. The reference impedance term $Z_r + Z_r^*$ is then $|v_r|^2/p_r = 10^3$ ohms.

Utilizing Eqs. (6.10) and (6.17), we have

$$M_2 = 20 \log_{10} |v_r| |H_2| + 6.02 \\ + 10 \log_{10} \frac{(Z_s + Z_s^*)|_{f_1} (Z_s + Z_s^*)|_{f_2} (Z_L + Z_L^*)|_{f_1 + f_2}}{(Z_r + Z_r^*) |Z_L|^2|_{f_1 + f_2}} \text{ dB.} \quad (6.18)$$

Note that the logarithmic operations are upon dimensionless quantities by virtue of defining the reference voltage v_r and impedance Z_r . For p_r chosen as 1 mW,

$$P_2 = P_{a1} + P_{a2} + 20 \log_{10}(1)|H_2| + 6.02$$

$$+ 10 \log_{10} \frac{(Z_S + Z_S^*)|_{f_1} (Z_S + Z_S^*)|_{f_2} (Z_L + Z_L^*)|_{f_1 + f_2}}{10^3 |Z_L|^2 |_{f_1 + f_2}} \text{ dBm.} \quad (6.19)$$

This form is valid for power expressed in decibels relative to one milliwatt (dBm).

If we specialize now to $Z_S = Z_L = 50$ ohms, we note that

$$M_2 = 20 \log_{10}(1)|H_2| + 2.04, \quad (6.20)$$

and

$$P_2 = P_{a1} + P_{a2} + 20 \log_{10} |H_2| + 2.04 \text{ dBm.} \quad (6.21)$$

The notation $(1)|H_2|$ has been dropped and replaced by $|H_2|$ but a one volt reference is implied.

One further comment is appropriate. When H_2 is evaluated using the nonlinear circuit analysis software, the quantity $(1)^2 H_2$ volts has been evaluated since unit voltage exponentials are the assumed excitation. The $(1)^2$ factor has been suppressed. If we refer to $|H_2|$ in decibels, we mean $20 \log_{10} |H_2|$.

6.2.3 Third-Order Response for Two-Tone Input

We have from Fig. 6.1 the voltage amplitude $3/4 v_1^2 v_2^* H_3$ for the third-order intermodulation response with two-tone excitation. In a manner similar to that for second-order delivered output power, we find that the third-order output power p_3 delivered to load Z_L at frequency $2f_1 - f_2$ can be written in the form

$$p_3 = m_3 p_{a1}^2 P_{a2}, \quad (6.22)$$

where

p_{a1} = power available in watts from the source at frequency f_1 ,

p_{a2} = power available in watts from the source at frequency f_2 ,

$$m_3 = \frac{3^2 |H_3|^2 (Z_S + Z_S^*)^2}{|Z_L|^2} \left| \frac{(Z_S + Z_S^*)}{2f_1 - f_2} \right| \frac{(Z_L + Z_L^*)}{|Z_L|^2} (watts)^{-2}. \quad (6.23)$$

If we now introduce the reference power $p_r = \frac{|v_r|^2}{(Z_r + Z_r^*)}$, Eq. (6.22) can be written in the form

$$\frac{p_3}{p_r} = p_r^2 m_3 \left(\frac{p_{a1}}{p_r} \right)^2 \left(\frac{p_{a2}}{p_r} \right). \quad (6.24)$$

Defining

$$P_3 \triangleq 10 \log_{10} \frac{p_3}{p_r}, \quad (6.25)$$

$$P_{a1} \triangleq 10 \log_{10} \frac{p_{a1}}{p_r}, \quad (6.26)$$

$$P_{a2} \triangleq 10 \log_{10} \frac{p_{a2}}{p_r}, \quad (6.27)$$

$$M_3 \triangleq 10 \log_{10} p_r^2 m_3, \quad (6.28)$$

we have, from Eq. (6.22)

$$P_3 = 2 P_{a1} + P_{a2} + M_3, \quad (6.29)$$

where

$$M_3 = 20 \log_{10} |v_r|^2 |H_3| + 9.54$$

$$+ 10 \log_{10} \frac{(z_s + z_s^*)^2 |f_1 (z_s + z_s^*)| f_2 (z_L + z_L^*) |_{2f_1 - f_2}}{(z_r + z_r^*)^2 |z_L|^2 |_{2f_1 - f_2}}. \quad (6.30)$$

Eqs. (6.29) and (6.30) can now be specialized to give dBm by letting $p_r = 10^{-3}$ watts, setting $|v_r| = 1$ volt, and again noting that $z_r + z_r^* = 10^3$ ohms for these references.

For the special case $Z_S = Z_L = 50$ ohms, we finally obtain

$$P_3 = 2P_{a1} + P_{a2} + 20 \log_{10} |H_3| - 4.44 \text{ dBm}, \quad (6.31)$$

where the reference voltage $v_r = 1$ volt is suppressed in the notation and all powers are expressed in decibels relative to one milliwatt, or dBm.

6.2.4 Fourth-Order Response for Three-Tone Input

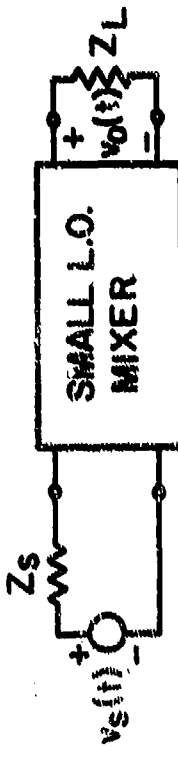
The procedure for expressing the output delivered power in decibels relative to one milliwatt is now clear. The final situation of interest at this time is the fourth-order response for three-tone inputs at frequencies f_1, f_2 and f_0 . Three-tone inputs are shown in Fig. 6.2. The response at $f_0 - (2f_1 - f_2)$ is the equivalent third-order intermodulation response term for a small-signal mixer with the local oscillator at frequency f_0 . From Fig. 6.2, the voltage amplitude of such a response is $3/2 v_0 (v_1^*)^2 v_2 H_4$.

By inspection we can write for the power p_4 delivered to an output load impedance Z_L ,

$$P_4 = m_4 P_{a1}^2 P_{a2} P_{a0}, \quad (6.32)$$

where

P_{a1} = power in watts available from source
at frequency f_1 .



THREE-TONE INPUT

SINUSOIDAL AT $\omega_0, \omega_1, \omega_2$.

$$v_s(t) = \operatorname{Re}[V_0 e^{j\omega_0 t} + V_1 e^{j\omega_1 t} + V_2 e^{j\omega_2 t}]$$

OUTPUTS

FIRST ORDER

$$v_o(t) = \operatorname{Re}[V_0 H_1(\omega_0) e^{j\omega_0 t} + V_1 H_1(\omega_1) e^{j\omega_1 t} + V_2 H_1(\omega_2) e^{j\omega_2 t}]$$

SECOND ORDER AT $\omega_0 - \omega_1, \omega_0 - \omega_2$:

$$v_o(t) = \operatorname{Re}[V_0 V_1^* H_2(\omega_0, -\omega_1) e^{j(\omega_0 - \omega_1)t} + V_0 V_2^* H_2(\omega_0, -\omega_2) e^{j(\omega_0 - \omega_2)t}]$$

FOURTH ORDER AT $\omega_0 - (2\omega_2 - \omega_1)$; $\omega_0 - (2\omega_1 - \omega_2)$:

$$\begin{aligned} v_o(t) = & \operatorname{Re}\left\{\frac{3}{2} V_0 V_1 (V_2^*)^2 H_4(\omega_0, \omega_1, -\omega_2, -\omega_2) e^{j[\omega_0 - (2\omega_2 - \omega_1)]t}\right. \\ & \left. + \frac{3}{2} V_0 (V_1^*)^2 V_2 H_4(\omega_0, -\omega_1, -\omega_1, \omega_2) e^{j[\omega_0 - (2\omega_1 - \omega_2)]t}\right\} \end{aligned}$$

Fig. 6.2. Examples of Small Local-Oscillator Mixer Responses
in terms of Nonlinear Transfer Functions.

P_{a2} = power in watts available from source
at frequency f_2 .

P_{a0} = power in watts available from source
at frequency f_0 .

and

$$M_4 = 144 |H_4|^2 (Z_S + Z_{S^*}) \left\{ \frac{(Z_S + Z_{S^*})^2}{f_0} \right\}_{f_1} \left(Z_S + Z_{S^*} \right) \left| \frac{Z_L + Z_{L^*}}{f_2} \right| \left| \frac{Z_L + Z_{L^*}}{2} \right| \left(\text{watts} \right)^{-3} \\ f_0 - (2f_1 - f_2). \quad (6.33)$$

Introducing the reference power $p_r = |v_r|^2 / (Z_r + Z_{r^*})$ we obtain

$$P_{a0} = 2P_{a1} + P_{a2} + P_{a0} + M_4, \quad (6.34)$$

where

$$P_4 = 10 \log_{10} \frac{P_4}{p_r}, \quad (6.35)$$

$$P_{a1} = 10 \log_{10} \frac{P_{a1}}{p_r}, \quad (6.36)$$

$$P_{a2} = 10 \log_{10} \frac{P_{a2}}{p_r}, \quad (6.37)$$

$$P_{a0} = 10 \log_{10} \frac{P_{a0}}{p_r}, \quad (6.38)$$

$$M_4 = 10 \log_{10} p_r^3 m_4 = 20 \log_{10} |v_r|^3 |H_4| + 21.58$$

$$\begin{aligned}
& + 10 \log_{10} \left[\frac{(Z_S + Z_S^*) \mid f_0 \mid (Z_S + Z_S^*)^2 \mid f_1}{(Z_S + Z_S^*)^3} \right. \\
& \cdot \left. \frac{(Z_S + Z_S^*) \mid f_2 \mid (Z_L + Z_L^*) \mid f_0 - (2f_1 - f_2)}{|Z_L|^2 \mid f_0 - (2f_1 - f_2)} \right]. \tag{6.39}
\end{aligned}$$

Specializing for reference power level $p_r = 1$ milliwatt at reference voltage level $v_r = 1$ volt and terminating impedance $Z_S = Z_L = 50$ ohms, we obtain

$$P_4 = 2P_{a1} + P_{a2} + P_{a0} + 20 \log_{10} |H_4| - 2.40 \text{ dBm.} \tag{6.40}$$

Each power is now in dBm and we again have suppressed the 1 volt factor in the term involving $|H_4|$.

6.2.5 Summary for Equal-Power Two-Tone Testing

It is useful to further simplify the results of the previous sections to specialize them for equal power two-tone testing of an amplifier and for two-tone testing of a mixer where the local oscillator plays the role of the third tone. The following results are valid for 50 ohm source and load impedance only.

6.2.5.1 Two-Tone Test of an Amplifier

It will be assumed that the input tones have equal available power P_a .

First-Order

From Eq. (6.7) and (6.8),

$$P_1 = P_a + 20 \log_{10} |H_1| + 6 \text{ dBm.} \quad (6.41)$$

Second-Order

From Eq. (6.21),

$$P_2 = 2P_a + 20 \log_{10} |H_2| + 2.04 \text{ dBm.} \quad (6.42)$$

Third-Order

From Eq. (6.31),

$$P_3 = 3P_a + 20 \log_{10} |H_3| - 4.44 \text{ dBm.} \quad (6.43)$$

These equations are shown graphically in Fig. 6.3 which shows the delivered output power for a nonlinear system excited by the sum of equal power tones as a function of the available input power in each tone. When plotted on a dB scale, the separate order outputs will have slopes equal to their orders, e.g., a third-order output will have a slope of three up to a certain input power, called P_{lim} . Above P_{lim} , higher-order effects will cause the response to deviate from this line.

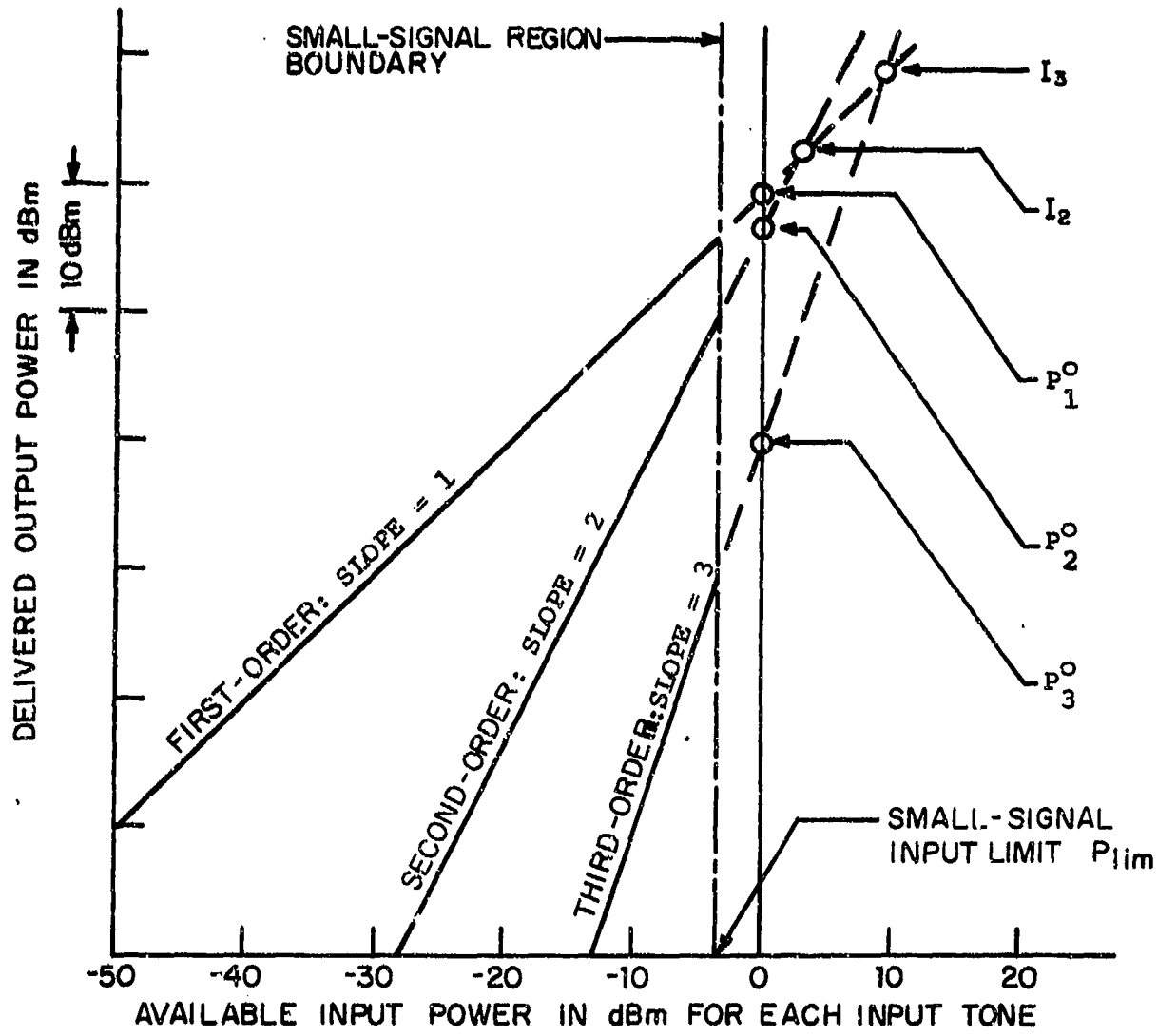


Fig. 6.3. Two-Tone Intermodulation Distortion Power Relationships.

If the straight lines are extended, the higher-order terms will intercept the first-order term. The output power at which the (extended) n^{th} -order term intercepts the (extended) first-order is called the n^{th} -order intercept, I_n . The intercept is based on an extrapolation of the well-behaved small-signal region into the large-signal effects region. Also shown in Fig. 6.3 are levels P_1^O , P_2^O , P_3^O ; these are the output powers for 0 dBm input power. Specific values for these intercepts and 0 dBm ordi-nates are given in Table 6.1 for 50 ohm source and load impedances.

Table 6.1

Significant Parameters of Two-Tone
Intermodulation Nonlinear Responses
for a 50 Ohm System

Zero dBm Input Ordinates

a) First Order

$$P_1^O = 20 \log_{10} |H_1| + 6 \text{ dBm}$$

b) Second Order

$$P_2^O = 20 \log_{10} |H_2| + 2 \text{ dBm}$$

d) Third Order

$$P_3^O = 20 \log_{10} |H_3| - 4.4 \text{ dBm}$$

Intercepts

a) Second Order

$$I_2 = 40 \log_{10} |H_1| \\ - 20 \log_{10} |H_2| + 10 \text{ dBm}$$

b) Third Order

$$2I_3 = 60 \log_{10} |H_1| \\ - 20 \log_{10} |H_3| + 22.4 \text{ dBm}$$

6.2.5.2 Two-Tone Test of a Small Local Oscillator Mixer

It will be assumed that each of the two-tone input signals have equal available power P_a , that the local oscillator available power is P_{a0} , and that $Z_s = Z_L = 50$ ohms.

Equivalent First-Order (Second-Order)

From Eq. (6.21) for each input tone,

$$P_1 = P_a + P_{a0} + 20 \log_{10} |H_2| + 2.04 \text{ dBm.} \quad (6.44)$$

The mixer conversion (transducer) gain is the $P_a = 0$ dBm input intercept.

Equivalent Third-Order (Fourth-Order)

From Eq. (6.40) with two-tone excitation,

$$P_3 = 3P_a + P_{a0} + 20 \log_{10} |H_4| - 2.40 \text{ dBm.} \quad (6.45)$$

These equations are illustrated graphically in Fig. 6.4. The "0 dBm input" output power levels are noted. They are linearly dependent upon the available local-oscillator power for a small-local oscillator mixer. Finally, note again that these simple results are valid for source and load impedances equal to 50 ohms.

6.2.5.3 General Case for n^{th} -Order Output

In the general case for an n^{th} -order output with multi-tone excitation one can write:

$$P_n = \sum_{i=1}^n P_{ai} + P_n^o \text{ dBm,} \quad (6.46)$$

where

$$P_n^o = 20 \log_{10} |H_n| + C_n,$$

and C_n is a constant which depends on the source and load impedance and the frequency combination. Table 6.2 shows C_n (for a 50 ohm system) computed for commonly found frequency combinations.

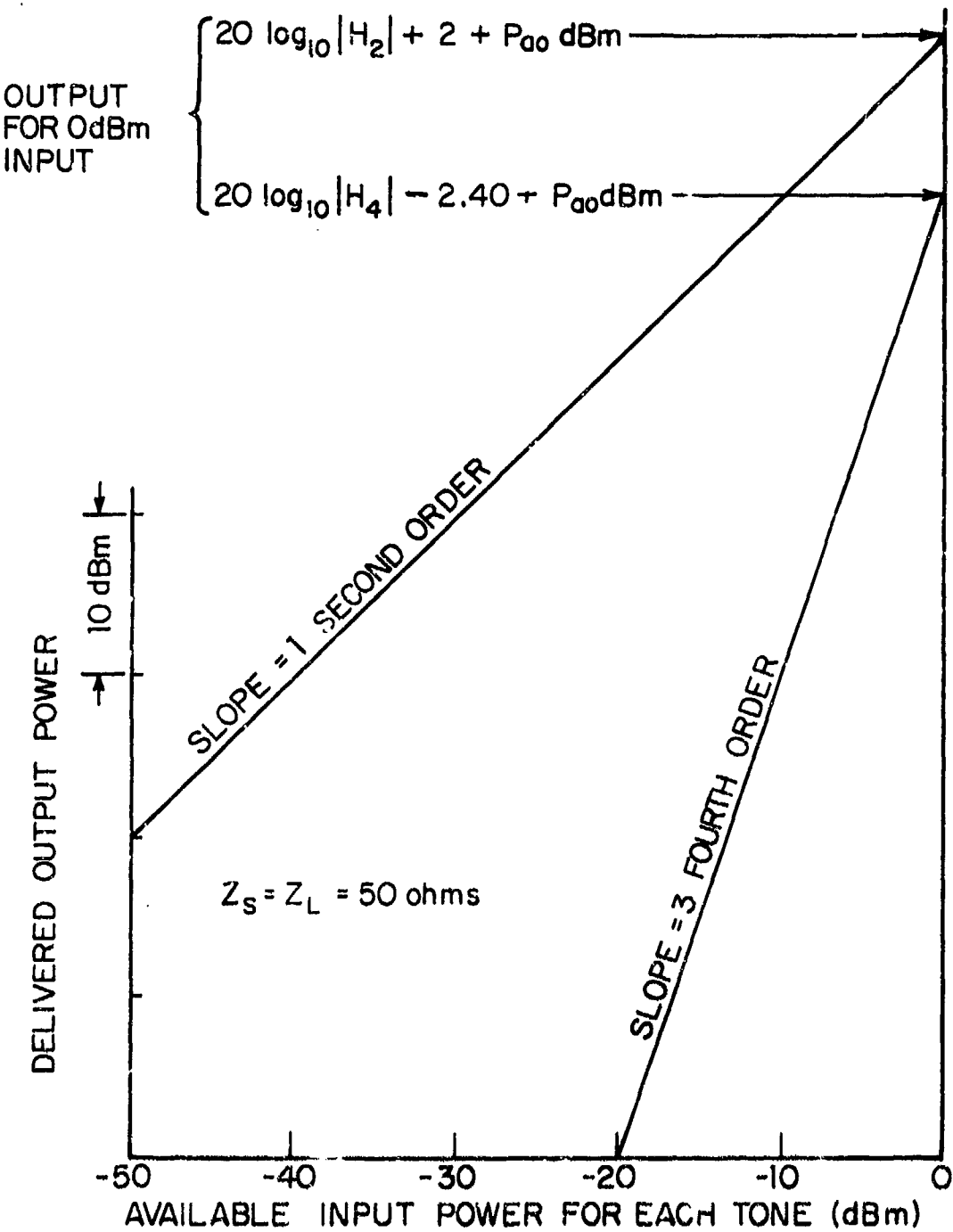


Fig. 6.4. Graphical Presentation of Equal-Power Two-Tone Testing Output Response for a Small Local-Oscillator Mixer.

Table 6.2

Some Common Coefficients C_n for a 50 Ohm System

<u>Order</u>	<u>Frequency Combination</u>	<u>C_n (dB)</u>
1	f_1	+ 6.0
2	$f_1 + f_2$	+ 2.0
2	$2f_1$	- 4.0
3	$f_1 + f_2 + f_3$	+ 1.6
3	$2f_1 + f_2$	- 4.4
3	$3f_1$	-14.0
4	$f_1 + f_2 + f_3 + f_4$	+ 3.6
4	$2f_1 + f_2 + f_3$	- 2.4
4	$2f_1 + 2f_2$	- 8.4
4	$3f_1 + f_2$	-18.0
4	$4f_1$	-24.0

6.2.6 Output Powers for High Input Impedance Nonlinear Amplifiers

For practical purposes the input impedance of certain electronic circuits is so high that it may be assumed infinite. In addition, such circuits have nonlinear transfer functions that are independent of the source impedance. Vacuum tube and field-effect transistor amplifiers are examples. It is, therefore, of interest to express the power delivered to a load at the various order nonlinear responses in terms of the input RMS voltage E_{IN} . The system under study is shown in Fig. 6.5. It is readily demonstrated that the output powers at f_1 , f_1-f_2 , and $2f_1-f_2$, respectively, are given for a 50 ohm load, by

First Order at $f = f_1$

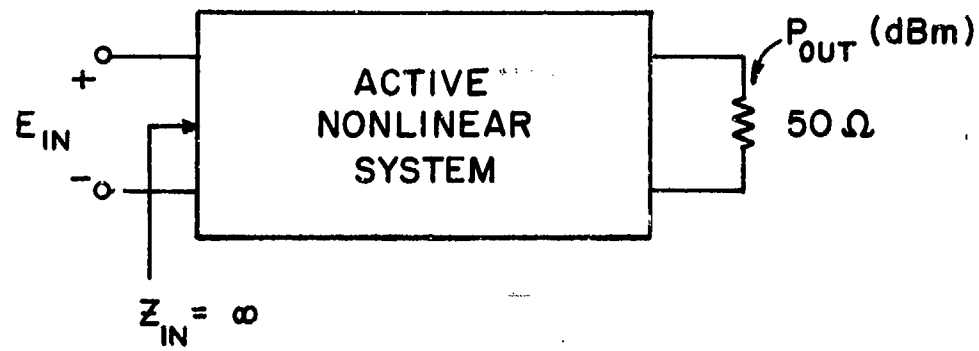
$$P_1 = 20 \log_{10} |H_1(f_1)| + 20 \log_{10} |E_{IN}| + 13 \text{ dBm}, \quad (6.47)$$

Second Order at f_1-f_2

$$P_2 = 20 \log_{10} |H_2(f_1, -f_2)| + 40 \log_{10} |E_{IN}| + 16 \text{ dBm}, \quad (6.48)$$

Third Order at $2f_1-f_2$

$$P_3 = 20 \log_{10} |H_3(f_1, f_1, -f_2)| + 60 \log_{10} |E_{IN}| + 16.5 \text{ dBm}. \quad (6.49)$$



E_{IN} IS RMS

Fig. 6.5. Nonlinear System with Very High Input Impedance.

6.3 Small-Signal Input Limit

In conjunction with Fig. 6.3 we have referred to a small-signal input power P_{lim} below which the small-signal quasi-linear system theory is an accurate representation of the physical system. At input signal levels greater than P_{lim} , higher-order terms are needed. For example, third-order and higher odd-order terms are needed to correct the linear response. This leads to the introduction of desensitization and compression effects. Similarly, third-order intermodulation components need to be corrected with fifth and higher odd-order terms. Second-order effects need to be corrected with fourth and higher even-order terms. There are at least two distinct methods of establishing an approximate value for P_{lim} . First, the model for the physical nonlinearity can be examined to determine an approximate value for the signal level above which the Taylor series expansion can not be expected to converge rapidly. If such a level can be found the input power generating the level can be established from the first-order linear model. We shall examine such an approach in this section. An alternative approach is to evaluate the correction term in terms of the higher-order nonlinear transfer function by an analysis of the complete system nonlinear incremental model. For example, one might establish that the input signal power for which 0.5 dB of gain compression is incurred is a suitable measure for P_{lim} . We shall also examine this possibility later in this chapter.

The small-signal nonlinear transfer function analysis is based on two assumptions. The first is that the input excitation is sufficiently small that the number of terms used in the Volterra series expansion is adequate to characterize the system. The second assumption is that the nature of the nonlinearity remains constant over its entire operating range. We will examine these assumptions separately.

First, consider the assumption that the number of terms is sufficient to characterize the system. We will not consider the

convergence properties of the Volterra series. Instead, we consider the Taylor's series expansion of a nonlinear device used in the circuit analysis by noting that an n^{th} -order Volterra series expansion requires that all nonlinearities be expanded to n^{th} -or r . For bipolar transistor circuits the resistive nonlinearity of the base-emitter junction is the dominant nonlinearity. Thus, the junction voltage can be used as a measure of the small-signal limit. From Chapter 5, Eq. (5.41) we have the Taylor series expansion of the emitter junction incremental current in terms of the junction incremental voltage v_2 given by

$$\begin{aligned} -i_e &= K(v_2) = I_E \left(e^{\frac{qv_2}{kT}} - 1 \right) \\ &= I_E \left[\left(\frac{qv_2}{kT} \right) + \frac{1}{2!} \left(\frac{qv_2}{kT} \right)^2 + \frac{1}{3!} \left(\frac{qv_2}{kT} \right)^3 + \dots \right. \\ &\quad \left. + \frac{1}{n!} \left(\frac{qv_2}{kT} \right)^n + \dots \right]. \end{aligned} \quad (6.50)$$

If the series is truncated after the n^{th} term the error in the approximation to $K(v_2)$ becomes of interest. The normalized truncation error is defined as the remainder R_N of the series divided by the value of the function being expanded. The $K(v_2)$ nonlinearity is a function of qv_2/kT , where kT/q is approximately 25 mV at room temperature and v_2 is the junction voltage. Curves of normalized truncation error are shown in Fig. 6.6 for truncation after three and four terms. Note that the error at 25 millivolts is approximately 10 percent for three terms and about 1 percent for four terms. Normalized truncation errcr is quite sensitive to qv_2/kT . It provides a positive measure of the maximum levels of emitter-junction voltage permissible for a reasonable expectation that a given order of approximation can adequately account for a component nonlinearity when small-signal distortion estimates are of interest. One would expect that, at $v_2 = kT/q = 25$ millivolts, the Volterra series representation

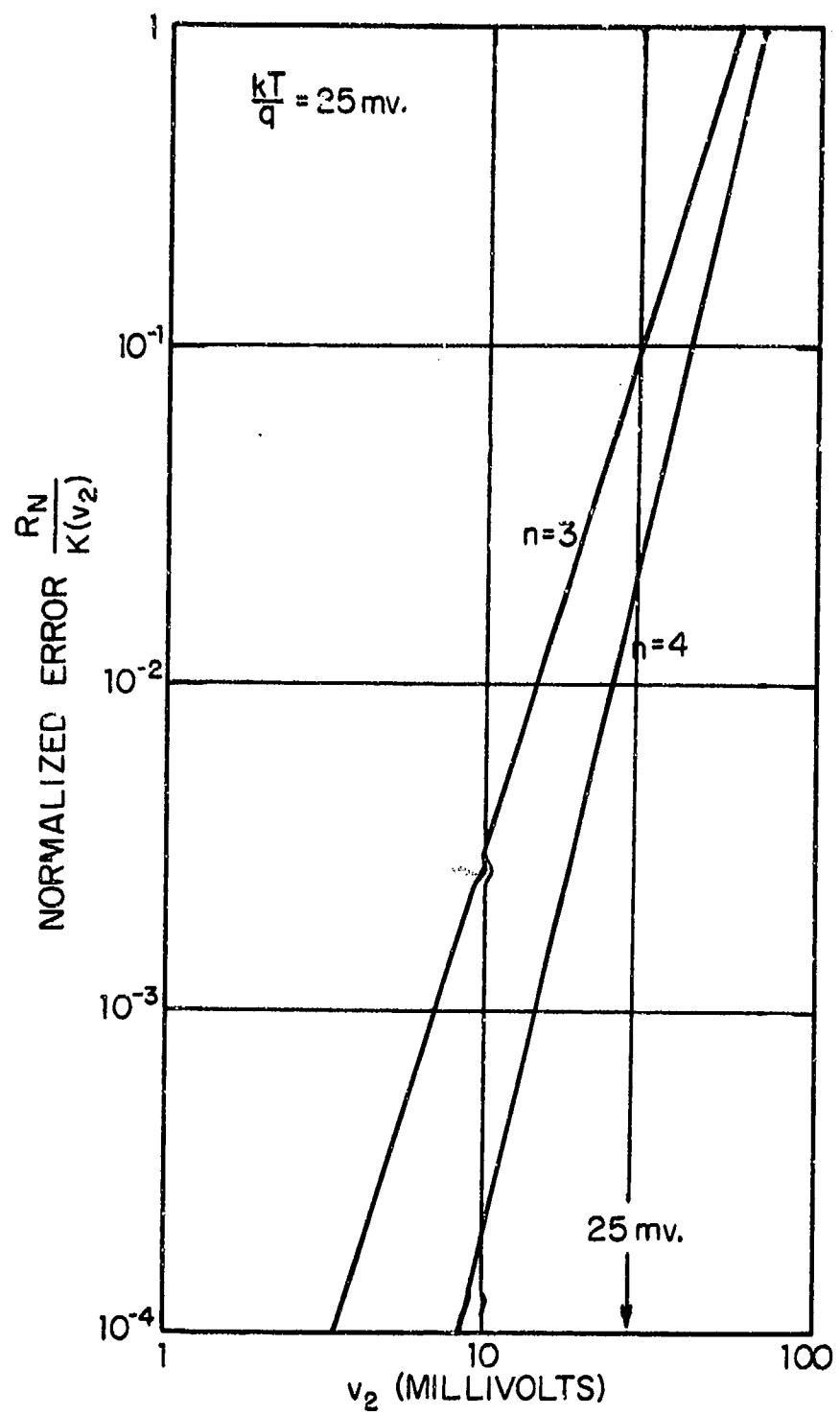


Fig. 6.6. Normalized Truncation Error.

would begin to require the inclusion of terms of higher-order than the third or fourth. Experimental data supports this expectation. The normalized truncation errors for other nonlinearities in the device nonlinear incremental model could also be determined in a similar manner.

Next consider the second assumption, namely, that the nature of the nonlinearity remains constant over the entire operating range. If a circuit is driven into cutoff or saturation, this assumption is violated unless cutoff or saturation is part of the device model. In order to include such effects the Taylor series expansion must include an impractically large number of terms. There is no reason to expect satisfactory results with hard nonlinearities, or with piecewise-linear circuit models. Instead, an alternate analysis technique must be used.

The one technique which can be used for both small-signal and large-signal analysis and allows for even the most violent of nonlinearities is the large signal time-domain solution outlined in Chapter 4. Time-domain solutions involve the numerical integration of state-variable differential equations. A comparison of such an approach with the small-signal quasi-linear approach will be presented later in this chapter.

6.4 Single-Stage Untuned Transistor Amplifier

In Chapter 5 the parameters characterizing the nonlinear T model of a particular bipolar transistor, the 2N2950, were developed from theoretical models of individual nonlinear physical processes. Specific values for the 17 needed parameters, determined from measurements on a 2N2950 sample, have been listed in Table 5.1. In this and subsequent sections we shall use the 2N2950 bipolar transistor that has been modeled in a variety of circuit applications to illustrate how the nonlinear transfer functions are used to determine nonlinear responses of a physical circuit. In particular, we shall show in detail how to determine the small-signal quasi-linear responses of a single-stage untuned amplifier used both as an amplifier and as a small-local oscillator mixer. A detailed comparison of predicted responses based upon the theory will be made with actual values determined from laboratory measurements. A fairly extensive two and three-tone excitation analysis of the amplifier will also be presented for large signal excitation. Figure 6.7 shows the test circuit for which the analysis and measurements to be described were made. The operating-point collector voltage is 10 V, collector current is 10 mA, and the 2N2950 model parameters are those given in Table 5.1. The source and load impedances are 50 ohms. Other linear elements are noted in the circuit diagram. The incremental circuit model for the amplifier is shown in Fig. 6.8. Element values and node numbering for a computer-aided analysis using SIGNCAP I for tone inputs at 2.5 and 3.0 MHz are given in Table 6.3. Further details regarding SIGNCAP are included in Appendix A. Transfer functions for a third-order nonlinear

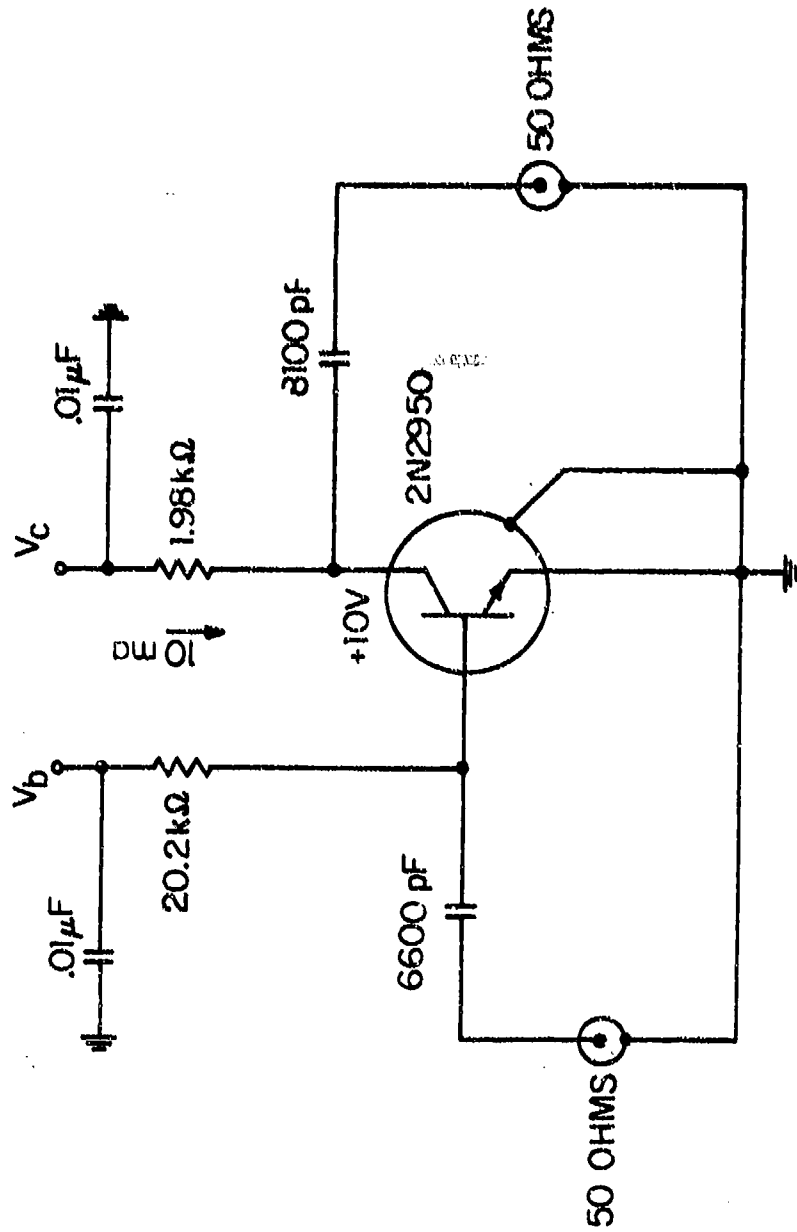


Fig. 6.7. Schematic of 2N2950 Common-Emitter Amplifier Test Circuit.

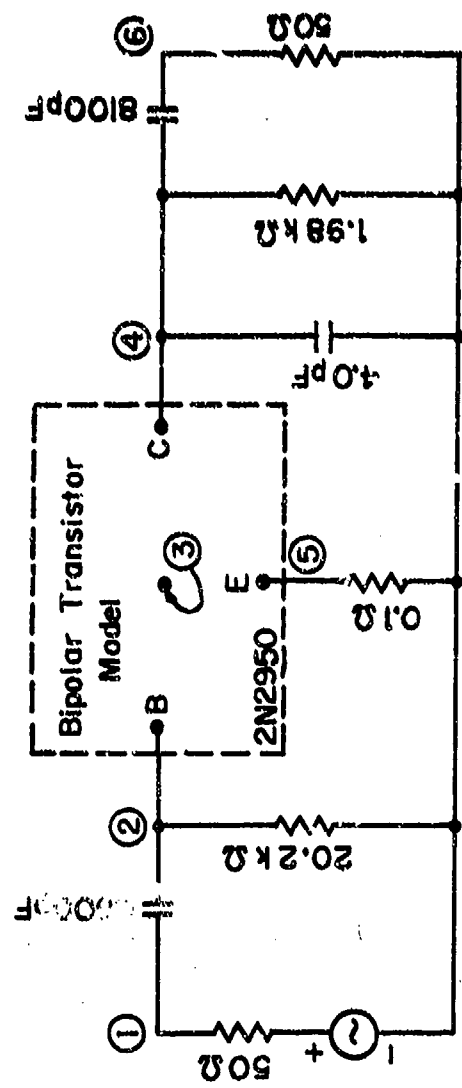


Fig. 6.8. Incremental Circuit Model of Single-Stage Untuned Amplifier.

Table 6.3.

SIGNCAP I Coding for Single-Stage
Amplifier. ($f_1 = -2.5$ MHz, $f_2 =$
 3.0 MHz, $f_3 = 3.0$ MHz).

```
*START SEGMENT
*GENERATOR
NODE    1
FR      1          -2.5E6
FR      2          3.0E6
FR      3          3.0E6
IM      50.
*PASSIVE COMPONENTS
C   1    2.6600.E-12
R   2        20.2E3
R   4        1.98E3
C   4    6.8100.E-12
R   6        50.
R   5        .01
C   4        4.E-12
*TRANSISTOR
NODE    2
        4.6        9.27        140.       .348
        .0100      .150        .125       8.2
        25.0E-12    1.03      330.E-12  60.E-09
        10.1      635.E3
        0.           .           .           1.5E-12
*END SEGMENT
*END
```

analysis are listed in Table 6.4. The linear responses and second-order difference term as well as a third-order intermod and gain compression term are included in the table. Similar results for a third-order analysis with two-tone inputs at 30 and 51.4 MHz are given in Table 6.5.

6.4.1 First-Order Linear Response

The first test of a circuit model is the small-signal single-tone frequency response. This can be most conveniently examined by comparing the predicted and measured insertion gain of the amplifier. From Eq. (6.8) and the value for H_1 tabulated in Tables 6.4 and 6.5, we have

$$G_I = \begin{cases} 12.7 + 6 = 18.7 \text{ dB; } f = 2.5 \text{ MHz,} \\ 12.4 + 6 = 18.4 \text{ dB; } f = 3.0 \text{ MHz,} \\ 1.6 + 6 = 7.6 \text{ dB; } f = 30 \text{ MHz,} \\ -2.6 + 6 = 3.4 \text{ dB; } f = 51.4 \text{ MHz.} \end{cases} \quad (6.51)$$

These values together with other predicted values based upon the linear model can be compared with experimentally measured values of insertion gain as presented in Fig. 6.9. The linear frequency response is fairly broadband with a low-frequency 3 dB cut-off at about 300 kHz and a high-frequency cut-off near 9 MHz. There is excellent agreement between measured and predicted insertion loss from below 100 kHz to over 100 MHz. The linear frequency response could also be predicted from any linear circuit analysis program capable of analyzing the linear equivalent circuit of the amplifier. A manual calculation is, of course, also possible.

Table 6.4
 Single-Stage Untuned Amplifier Nonlinear Transfer Functions at
 $f_1 = -2.5$, $f_2 = 3.0$, $f_3 = f_2$ MHz

Order and Type	Nonlinear Transfer Function	Magnitude		Phase (Degrees)	Frequency (MHz.)
		Ratio	Decibels (dB)		
<u>First Order</u>	$H_1(f_1)$	4.32	12.7	187*	2.5
	$I_1(f_2)$	4.17	12.4	156	3.0
<u>Second Order</u>					
	$H_2(f_1, f_2)$	5.95	15.5	170	0.5
<u>Third Order</u>					
	$H_3(f_1, f_2, f_2)$	24.5	27.8	332	3.5
Intermodulation	$H_3(f_2, f_2, -f_2)$	34.6	30.7	355	3.0
	Gain Compression				

* Note that f_1 is negative. For $f_1 = 2.5$ MHz, phase is -187° .

Table 6.5

Single-Stage Untuned Amplifier Nonlinear Transfer Functions at
 $f_1 = -30.0$, $f_2 = 51.4$, $f_3 = f_2$ MHz

Order and Type	Nonlinear Transfer Function	Magnitude		Phase (Degrees)	Frequency (MHz.)
		Ratio	Decibels (dB)		
<u>First Order</u>	$H_1(f_1)$	1.20	1.6	262*	30.0
	$H_1(f_2)$	0.832	-2.6	86	51.4
<u>Second Order</u>					
	$H_2(f_1, f_2)$	0.251	-12.0	165	21.4
<u>Third Order</u>	$H_3(f_1, f_2, f_2)$	0.146	-16.7	258	72.8
	$H_3(f_2, f_2, -f_2)$	0.075	-22.5	272	51.4

* Note that f_1 is negative.

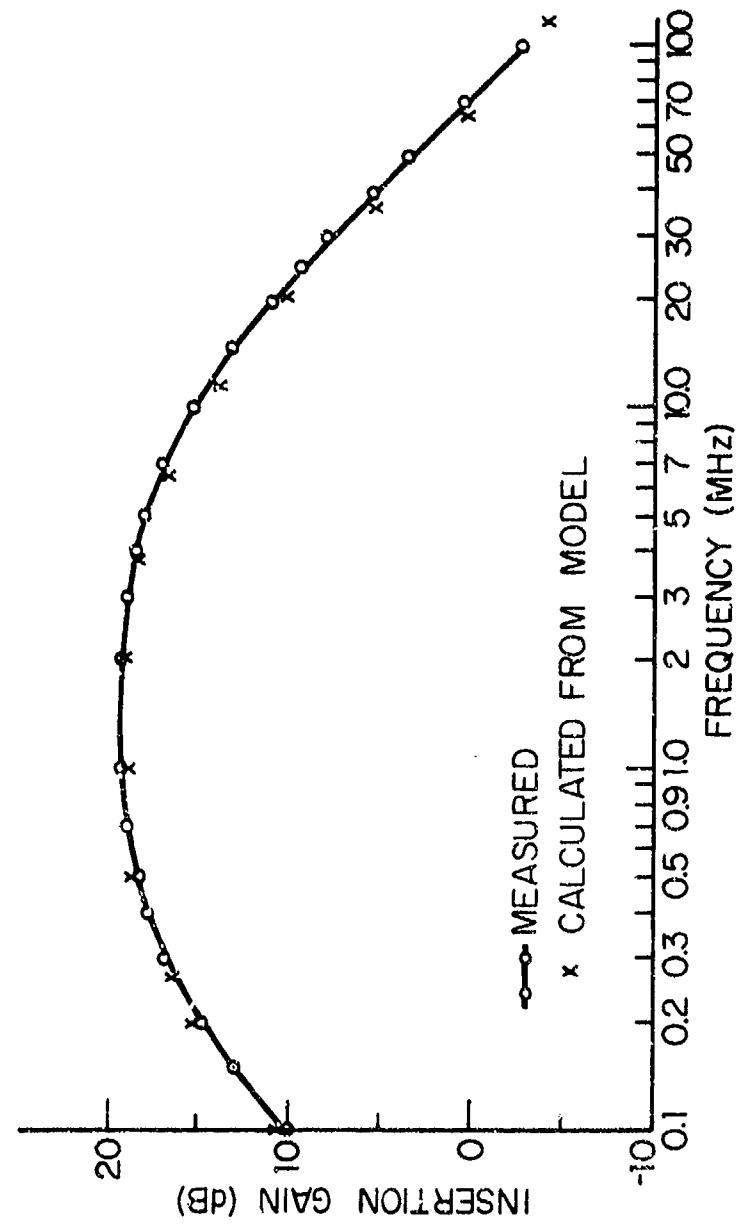


Fig. 6.9. Insertion Gain 2N2950 Common-Emitter Amplifier.

6.4.2 Second and Third-Order Intermodulation Distortion for Two-Tone Excitations

6.4.2.1 Amplitude Dependence

The second and third-order intermodulation distortion non-linear transfer functions are listed in Table 6.4 for excitation at -2.5 and 3.0 MHz. If we assume equal strength two-tone excitation we have, from Eq. (6.42), the second-order power at 0.5 MHz given by

$$\begin{aligned} P_2 &= 2P_a + 15.5 + 2.0 \\ &= 2P_a + 17.5 \text{ dBm}, \end{aligned} \quad (6.52)$$

and the third-order at 3.5 MHz, from Eq. (6.43), given by

$$\begin{aligned} P_3 &= 3P_a + 27.8 - 4.4 \\ &= 3P_a + 23.5 \text{ dBm}. \end{aligned} \quad (6.53)$$

Eq. (6.52) and (6.53) together with the linear response power at -2.5 MHz, given by

$$\begin{aligned} P_1 &= P_a + 12.7 + 6 \\ &= P_a + 18.7 \text{ dBm}, \end{aligned} \quad (6.54)$$

are shown in Fig. 6.10 as theoretical results. Also plotted in the figure are measured values of the delivered output power for the linear, second, and third-order intermodulation components.

The second and third-order intercept values are noted in Fig. 6.10. Equations for predicting intercept have been given in Table 6.1. For the second-order intercept

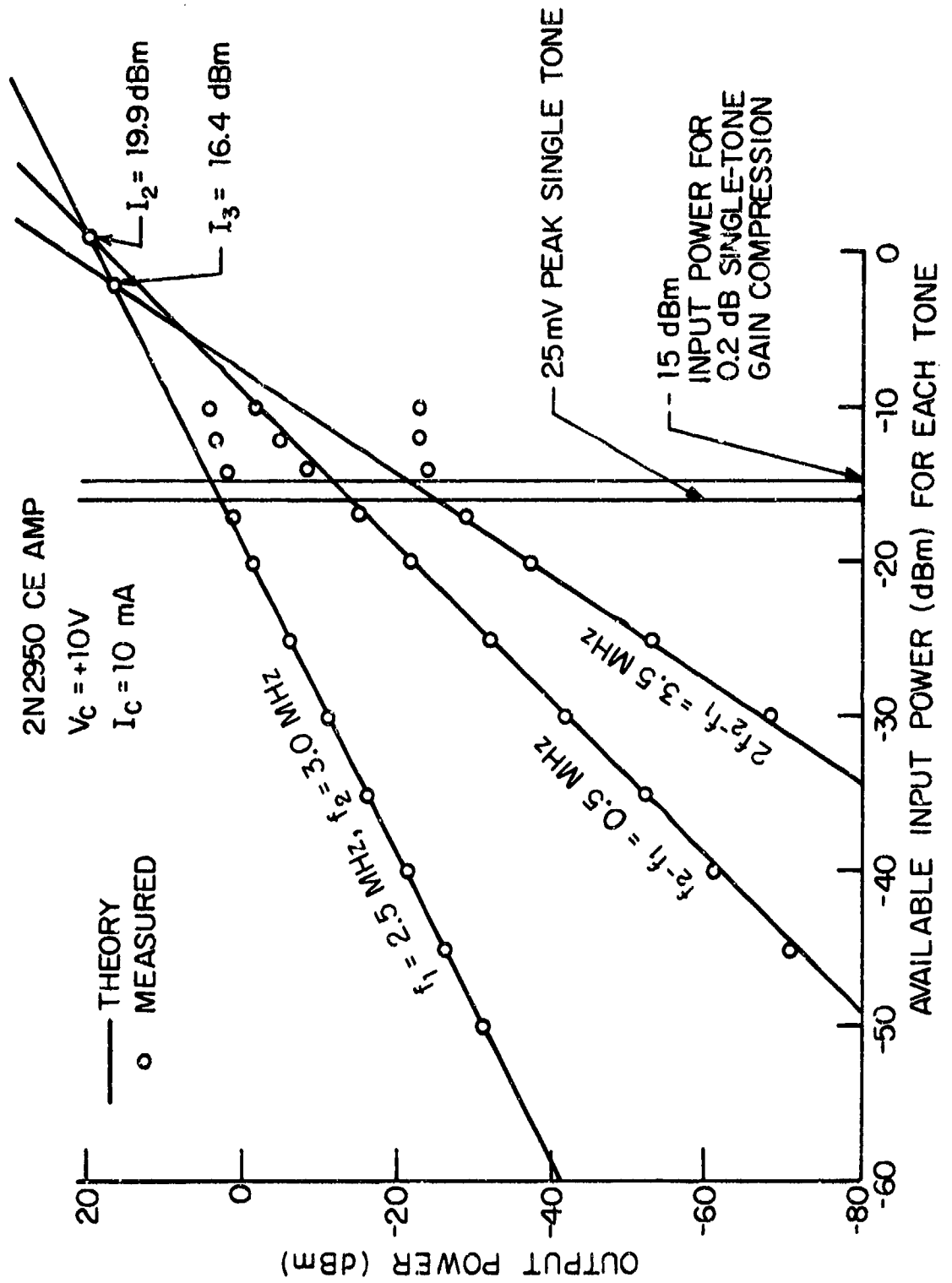


Fig. 6.10. Comparison of Predicted and Measured Two-Tone Distortion Products for 2N2950 Common-Emitter Amplifier ($f_1=2.5 \text{ MHz}$, $f_2=3.0 \text{ MHz}$).

$$\begin{aligned} I_2 &= 2(12.7) - 15.5 + 10 \\ &= 19.9 \text{ dBm}, \end{aligned} \quad (6.55)$$

and third-order intercept

$$\begin{aligned} I_3 &= \frac{1}{2} \left[3(12.7) - 27.8 + 22.4 \right] \\ &= 16.4 \text{ dBm}. \end{aligned} \quad (6.56)$$

Similar theoretical predictions and measured data for two-tone excitations at -30 and 51.4 MHz are presented in Fig. 6.11.

The theoretical curves shown in the figures are not straight line fits to the experimental data but are mathematical predictions based upon nonlinear circuit model analysis of the actual power output at the particular frequencies of interest. The predictions were made by direct analysis of the nonlinear incremental circuit model of the nonlinear amplifier. Nonlinearities to third-order were included in the prediction. The agreement between measurement and prediction is excellent over the range of model validity. For the mid-band data shown in Fig. 6.10, the model ceases to make accurate predictions at inputs above about -16 dBm, while for the data in Fig. 6.11 the model ceases to make accurate predictions above inputs at about -5 dBm. We have previously noted in Section 6.3 that a reasonable criteria for validity range is the input signal level for which the base-emitter junction incremental voltage exceeds kT/q or about 25 millivolts at room temperature. Figure 6.12 presents a set of curves showing the peak value of the first-order or linear terms for a single-tone input at the several frequencies of interest. Observe that the 25 millivolt level is reached at -16 dBm input

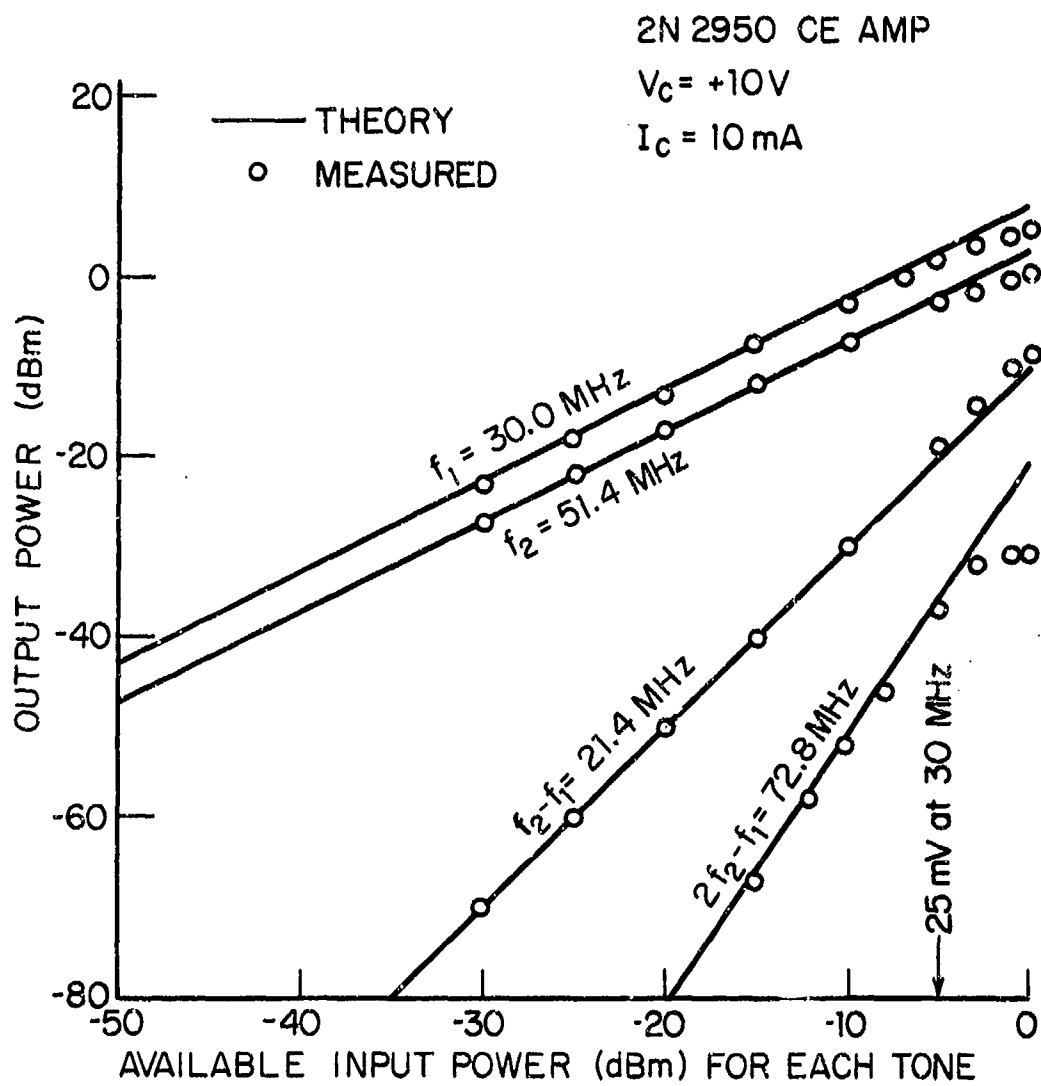


Fig. 6.11. Comparison of Predicted and Measured Two-Tone Distortion Products for 2N2950 Common-Emitter Amplifier.

($f_1 = 30 \text{ MHz}$, $f_2 = 51.4 \text{ MHz}$)

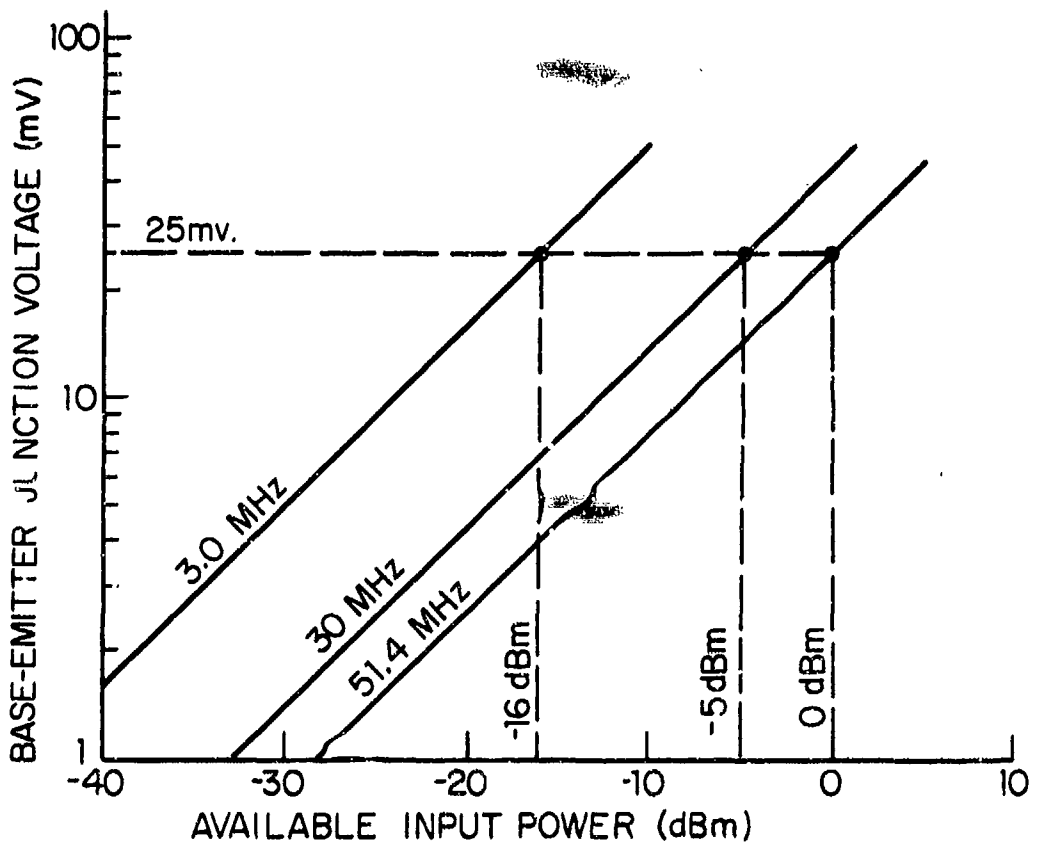


Fig. 6.12. Base-Emitter Junction Incremental Peak Voltage for 2N2950 Common-Emitter Amplifier.

at 3 MHz. This value is noted in Fig. 6.10. Also shown on Figure 6.10 is the measured single-tone input power at which 0.2 dB compression occurs in the amplifier. It is quite close to the power corresponding to the 25 mV criterion. Above these input levels the experimental data deviates significantly from the small-signal prediction. A similar conclusion can be reached for two-tone excitations at 30 and 51.4 MHz. The 30 MHz tone reaches the 25 millivolt level at -5 dBm input. The data presented in Fig. 6.11 ceases to follow the small-signal theory prediction above about such an input level.

6.4.2.2 Frequency Dependence

The dependence of second and third-order responses upon the input available power has been examined and compared with measurement in the previous section. It is also important to determine the frequency-dependence of the intermodulation as the input tones are moved about in frequency. One simple way to explore this is to measure the output intermodulation power in the small-signal region as the frequencies f_1 and f_2 are changed, and deduce from the measured output power what the appropriate nonlinear transfer function must have been. For example, if we write Eq. (6.42) for second-order intermod in the form

$$20 \log_{10} |H_2| = P_2 - 2P_a - 2.0 \text{ dB}, \quad (6.57)$$

an experimental estimate of $|H_2|$ (in dB) can be found by utilizing measured values of P_2 (dBm) obtained from the small-signal region for known values of available input power P_a (dBm). A comparison of measured and predicted values of the second-order nonlinear transfer function $|H_2|$ obtained by this method is shown in Fig. 6.13. The two-tones exciting the single-stage untuned amplifier were separated by 0.5 MHz as they moved across the range of f_2 .

2N2950 CE AMP
 $f_1 = f_2 - 0.5 \text{ MHz}$

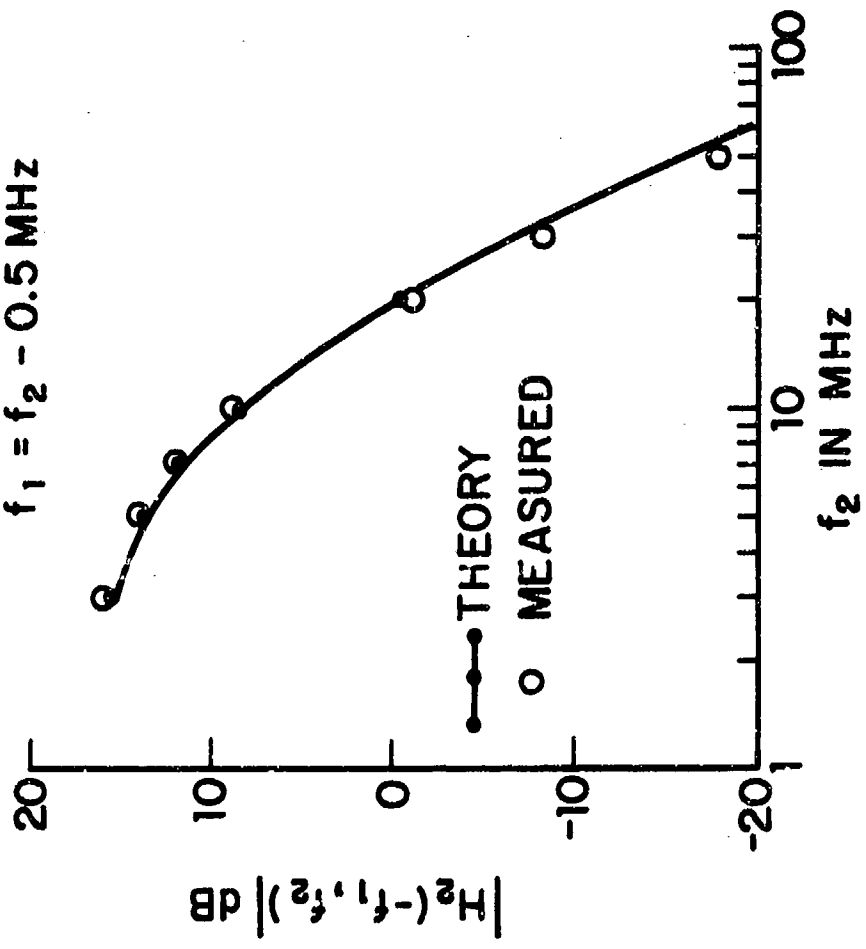


Fig. 6.13. Second-Order Nonlinear Transfer Function
for the CE 2N2950 Amplifier.

The third-order intermod transfer function $|H_3|$ (dB) can similarly be estimated from experimental measurements by putting Eq. (6.43) in the form

$$20 \log_{10} |H_3| = P_3 - 3P_a + 4.4 \text{ dB}, \quad (6.58)$$

and measuring P_3 in the small-signal region for known values of input P_a . The results for such an experiment on the untuned single-stage amplifier are shown in Fig. 6.14. Both the third and second-order transfer functions are in good agreement with predictions based upon the circuit incremental model.

6.4.3 Excitation of the Untuned Amplifier as a Small-Local Oscillator Mixer

Amplifier stages can frequently be used as frequency converters, or mixers, by adding the local-oscillator waveform to the input signal and utilizing the inherent nonlinearities in the stage to generate desired conversion products. If the local-oscillator drive level as well as the input signal level are confined to the small-signal excitation region the output nonlinear responses will be predictable from the small-signal nonlinear transfer functions. In particular, if f_0 is the local-oscillator frequency at 51.4 MHz, and f_1 and f_2 are input signal frequencies at 30.0 and 29.8 MHz, respectively, the second-order responses at $f_0 - f_1 = 21.4$ MHz and $f_0 - f_2 = 21.6$ MHz are desired mixer responses while fourth-order responses at $f_0 - (2f_1 - f_2) = 21.2$ MHz and $f_0 - (2f_2 - f_1) = 21.8$ MHz are undesired intermodulation distortion terms. The second-order response is given by Eq. (6.44) and the intermodulation term is given by Eq. (6.45). A comparison between predicted and measured responses for the untuned 2N2950

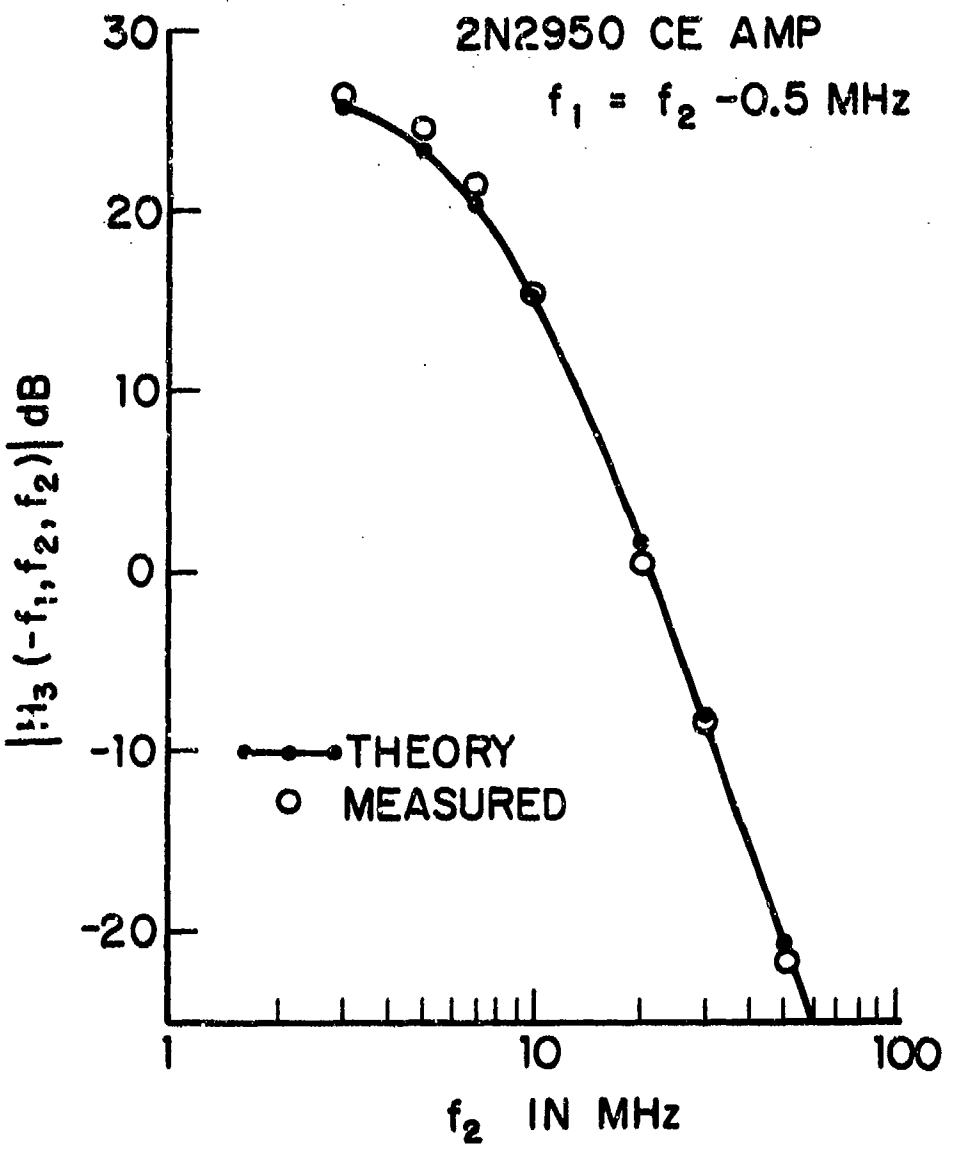


Fig. 6.14. Third-Order Nonlinear Transfer Function for the CE 2N2950 Amplifier.

single-stage circuit is shown in Fig. 6.15. The local-oscillator available power at 51.4 MHz was held constant at -5 dBm to insure small-signal level excitation which, from Fig. 6.12, can be expected to be exceeded at about 0 dBm for 51.4 MHz. The prediction is seen to be in good agreement with measurement.

6.4.4 Emitter Capacitance Nonlinearity

In Chapter 5, Section 5.3.2.6, the emitter junction capacitance of the bipolar junction was noted to be primarily a diffusion capacitance nonlinearity dependent upon emitter junction current. The nonlinear distortion predictions for the untuned amplifier have been made with this nonlinearity part of the device model. It is interesting to examine the specific effects of this particular nonlinearity by predicting the nonlinear transfer functions of the untuned 2N2950 amplifier in its absence, and comparing the results to those obtained including it. Below the 3 dB high-frequency cut-off region its effects are small since the diffusion current is very small. Above the 3 dB cut-off frequency its effects are significant, particularly with respect to even-order nonlinear effects of importance in mixer applications. A list of transfer function magnitudes, expressed in dB, is presented in Table 6.5. The first three entries are values of the first-order, or linear transfer functions. The linear responses are, of course, not dependent upon the nonlinear model. The second and fourth-order transfer functions H_2 and H_4 are significantly influenced by the diffusion capacitance nonlinearity while the third-order transfer function H_3 is only influenced in a minor manner. Since the small local-oscillator mixer output and third-order intermodulation distortion are directly dependent, respectively,

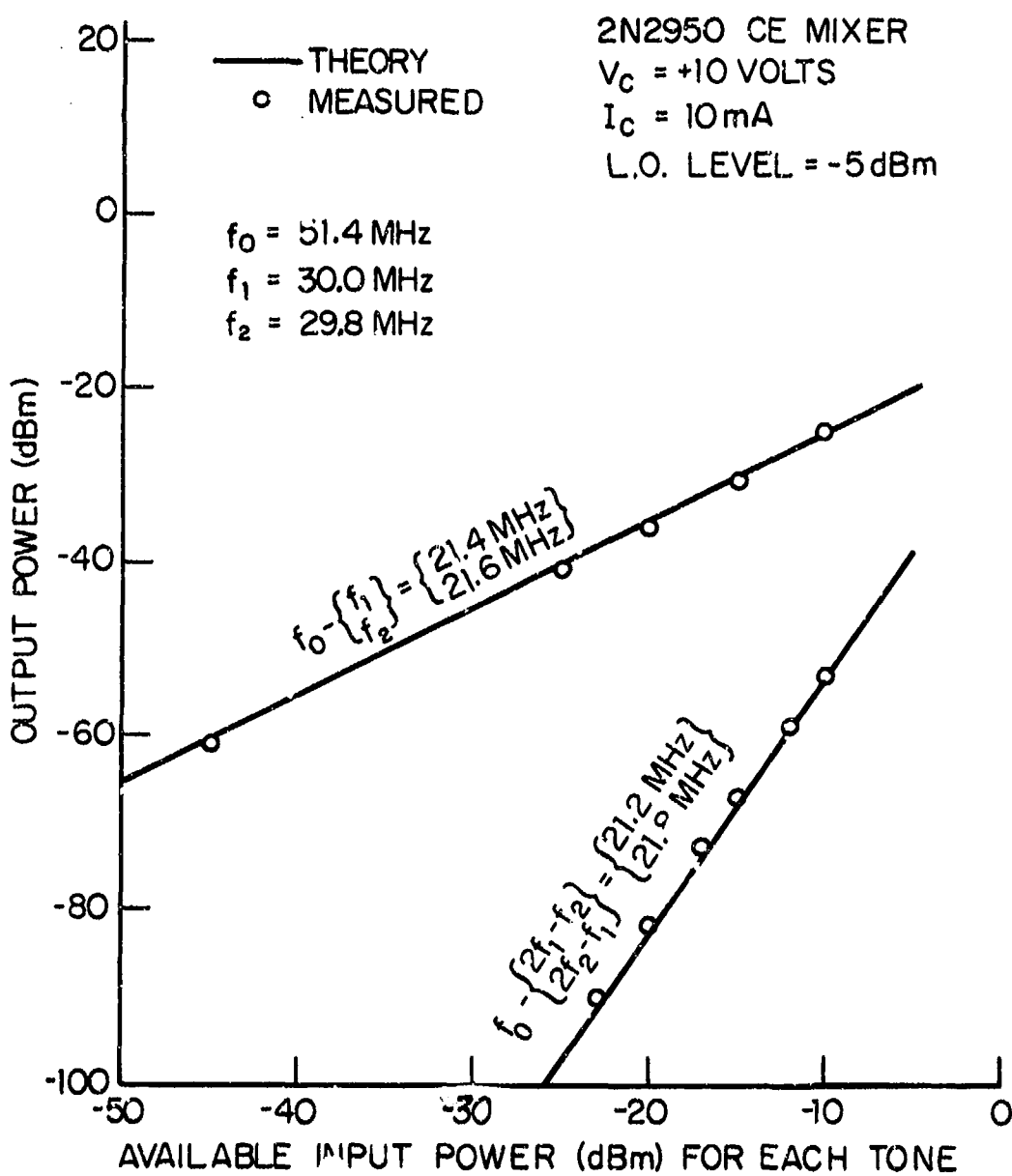


Fig. 6.15. Comparison of Predicted and Measured Two-Tone Distortion Products for Common-Emitter Mixer. L.O. = -5 dBm

TABLE 6.5

NONLINEAR TRANSFER FUNCTION MAGNITUDES (IN dB) FOR
OUT-OF-BAND EXCITATION. (2N2950 CE. AMP.)

$$f_0 = 51.4 \text{ MHz}$$

$$f_1 = 30.0 \text{ MHz}$$

$$f_2 = 29.8 \text{ MHz}$$

NONLINEAR TRANSFER	FREQ. MHz	WITHOUT E-B DIFFUSION NONLINEARITY	WITH E-B DIFFUSION NONLINEARITY
$H_1(f_0)$	51.4	-3.1 dB	-3.1 dB
$H_1(f_1)$	30.0	+1.4	+1.4
$H_1(f_2)$	29.8	+1.4	+1.4
$H_2(f_0, -f_2)$	21.6	-3.4	-11.9
$H_3(f_0, f_1, -f_2)$	51.6	-13.1	-13.3
$H_4(f_0, f_1, -f_2, -f_2)$	21.8	-10.8	-15.5

upon H_2 and H_4 , the nonlinear diffusion capacitance is of special importance in transistor mixer circuits. It is interesting to note that adding the diffusion capacitance nonlinearity to the circuit model results in a decrease in the even-order transfer functions H_2 and H_4 .

6.4.5 Gain Compression/Expansion

Gain compression or expansion is an effect which may be observed in amplifiers. It is possible to predict this phenomenon using small-signal theory involving third-order nonlinear transfer functions. We first review the relevant theory and then compare prediction with measurement for the 2N2950 single-stage amplifier.

According to the small-signal nonlinear theory outlined in Section 1.8, the complex amplitude of the output signal of a system excited by a single tone of amplitude A at frequency f is

$$A H_1(f) + \frac{3}{4} A |A|^2 H_3(f, f, -f) + \dots \text{(higher order terms)}. \quad (6.59)$$

The observed gain is the ratio of output amplitude to input amplitude. From Eq. (6.59) the magnitude of this ratio is

$$|H_1(f)| \left[\left[1 + \frac{3}{4} |A|^2 \operatorname{Re} \left\{ \frac{H_3(f, f, -f)}{H_1(f)} \right\} \right]^2 + \left[\frac{3}{4} |A|^2 \operatorname{Im} \left\{ \frac{H_3(f, f, -f)}{H_1(f)} \right\} \right]^2 \right]^{1/2}. \quad (6.60)$$

Gain compression or expansion appears as the second factor in Eq. (6.60). In many cases H_3 is real and it will be possible to drop the last term of the second factor so that the gain "compression" factor becomes

$$\left[1 + \frac{3}{4} |A|^2 \operatorname{Re} \left\{ \frac{H_3(f, f, -f)}{H_1(f)} \right\} \right]. \quad (6.61)$$

The initial effect observed as signal level is increased will be expansion if the sign of $\operatorname{Re}\{H_3/H_1\}$ is positive and compression if the sign is negative. The cases in which the approximation involved in (6.61) is inaccurate are those where $H_3(f, f, -f)$ and $H_1(f)$ are nearly in quadrature.

Equation (6.61) permits calculation of predicted compression/expansion for small-signal levels.

The gain compression/expansion factor in dB, x , is

$$x = 20 \log_{10} \left[1 + \frac{3}{4} |A|^2 \operatorname{Re} \left\{ \frac{H_3}{H_1} \right\} \right], \quad (6.62)$$

where the arguments of H_3 are $f, f, -f$, and of H_1 is f . Equation (6.62) can be expressed as a natural logarithm, and then expanded under the assumption that x is small. Thus:

$$x = 8.68 \ln \left[1 + \frac{3}{4} |A|^2 \operatorname{Re} \left\{ \frac{H_3}{H_1} \right\} \right] \approx 8.68 \left[\frac{3}{4} |A|^2 \operatorname{Re} \left\{ \frac{H_3}{H_1} \right\} \right]. \quad (6.63)$$

The factor A in Equation (6.63) is the peak voltage amplitude of the open-circuit source, i.e., the Thevenin source voltage driving the nonlinear circuit. The available power from that generator, assuming a 50 ohm source impedance, is then

$$P_a = \frac{A^2}{400} \text{ watts.} \quad (6.64)$$

Inserting Equation (6.64) into Equation (6.63), and solving for P_a in terms of x results in

$$P_a = \frac{x}{2.604 \operatorname{Re} \left\{ \frac{H_3}{H_1} \right\}} \text{ mW.} \quad (6.65)$$

Expressing P_a in dBm,

$$P = 10 \log_{10} P_a,$$

$$= 10 \log_{10} \left[x \operatorname{Re} \left\{ \frac{H_1(f)}{H_3(f, f, -f)} \right\} \right] - 4.2 \text{ dBm.} \quad (6.66)$$

The error in calculating P from Equation (6.66) is about 1/4 dB for 1 dB compression or expansion.

The gain compression characteristics of the single-stage untuned amplifier example have been measured and compared with prediction for both in-band and out-of-band excitation. The results for in-band at 3 MHz are shown in Fig. 6.16. The theoretical curve was calculated using the nonlinear transfer function data from Table 6.4. Compression characteristics for the amplifier at 51.4 MHz are shown in Fig. 6.17. The theoretical curve was calculated using the nonlinear transfer function values from Table 6.5. The theoretical results predict reasonably well the actual compression values for small amounts of compression.

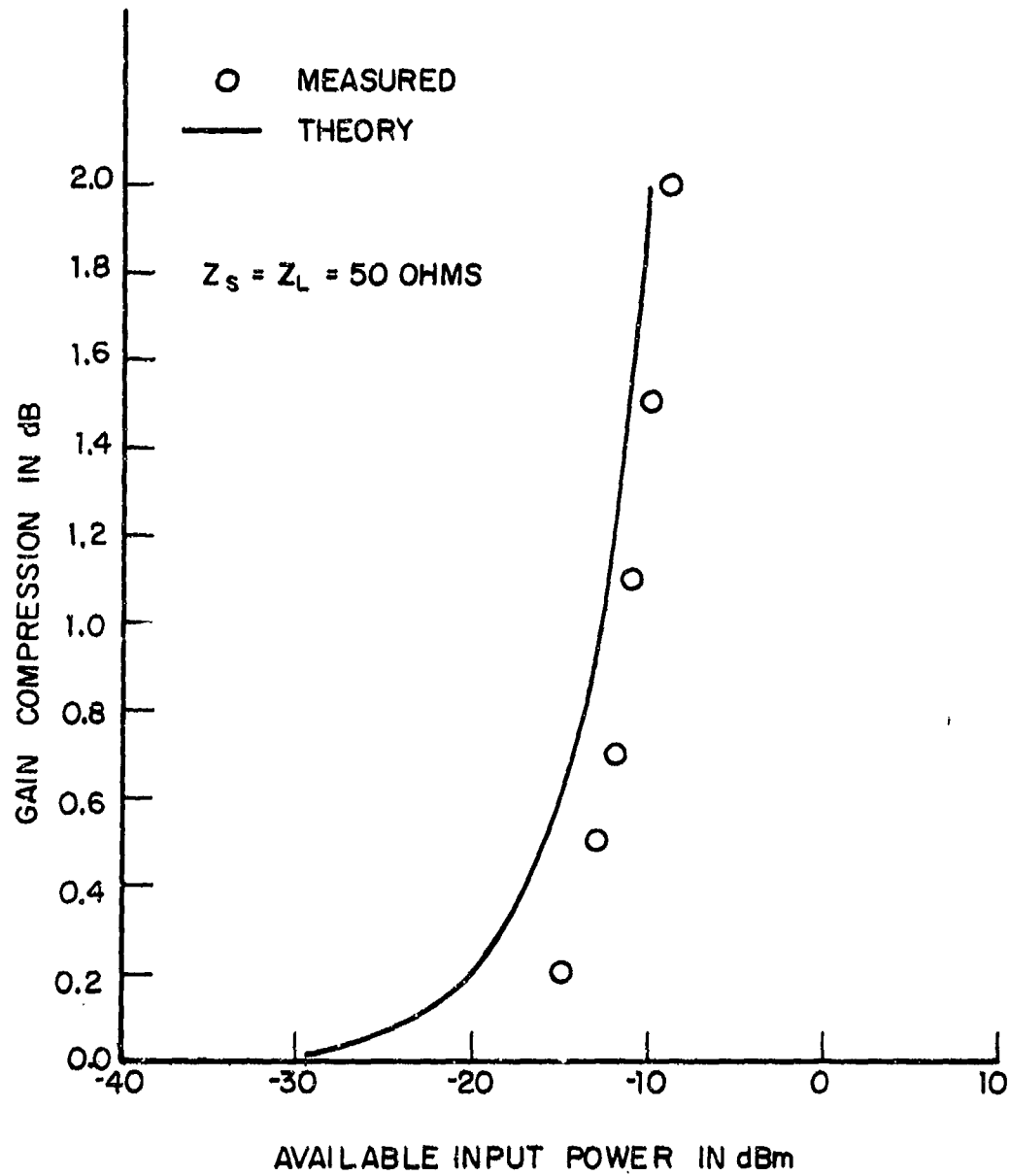


Fig. 6.16. Gain Compression Curve for 2N2950
Test Amp. $f = 3.0 \text{ MHz.}$

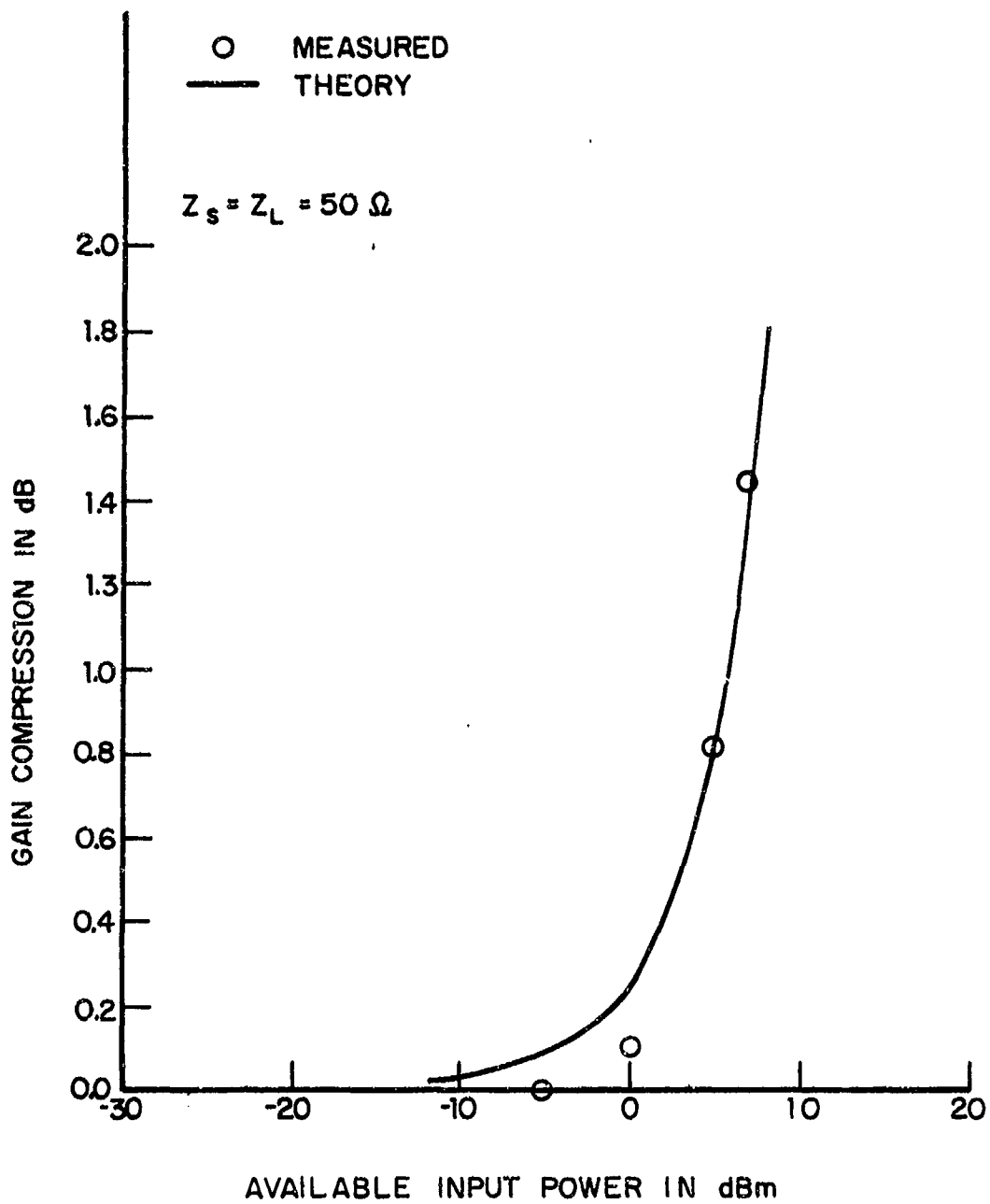


Fig. 6.17. Gain Compression Curve for 2N2950
Test Amp. $f = 51.4$ MHz.

6.5 Two-Stage Tuned Amplifier

6.5.1 Description of the Two-Stage Amplifier

The single-stage untuned amplifier example of multi-tone testing described in detail in Section 6.4 illustrates the basic application of two and three-tone testing to small-signal nonlinear amplifiers. The untuned amplifier is an example of a nonlinear device imbedded in a network in which only a minor frequency-dependent interaction occurs with the imbedding network. In this section we examine in some detail a two-stage tuned amplifier where the interaction with the frequency-dependent networks is strong. The circuit for the amplifier is shown in Fig. 6.18. The first stage is a 2N2950 common-emitter amplifier driving a low-pass interstage network. The second stage is a SA395 common-base amplifier driving a tuned load. The insertion gain of the amplifier is shown in Fig. 6.19. The bandwidth is about 2 MHz. Both measured data and theoretical predictions from the linear circuit model of the amplifier are in good agreement. Model parameters for the two transistors at their DC operating points are given in Tables 6.6 and 6.7. Observe that the 2N2950 operating point is different from that employed in the single stage amplifier. Other circuit values needed in the analysis are given in the schematic. The source and load impedances were 50 ohm. SIGNCAP I coding for linear as well as nonlinear analysis to determine the nonlinear transfer functions will not be given here but sufficient information is given in Fig. 6.18 and Tables 6.6 and 6.7 for the analysis to be accomplished. Selected results from such an

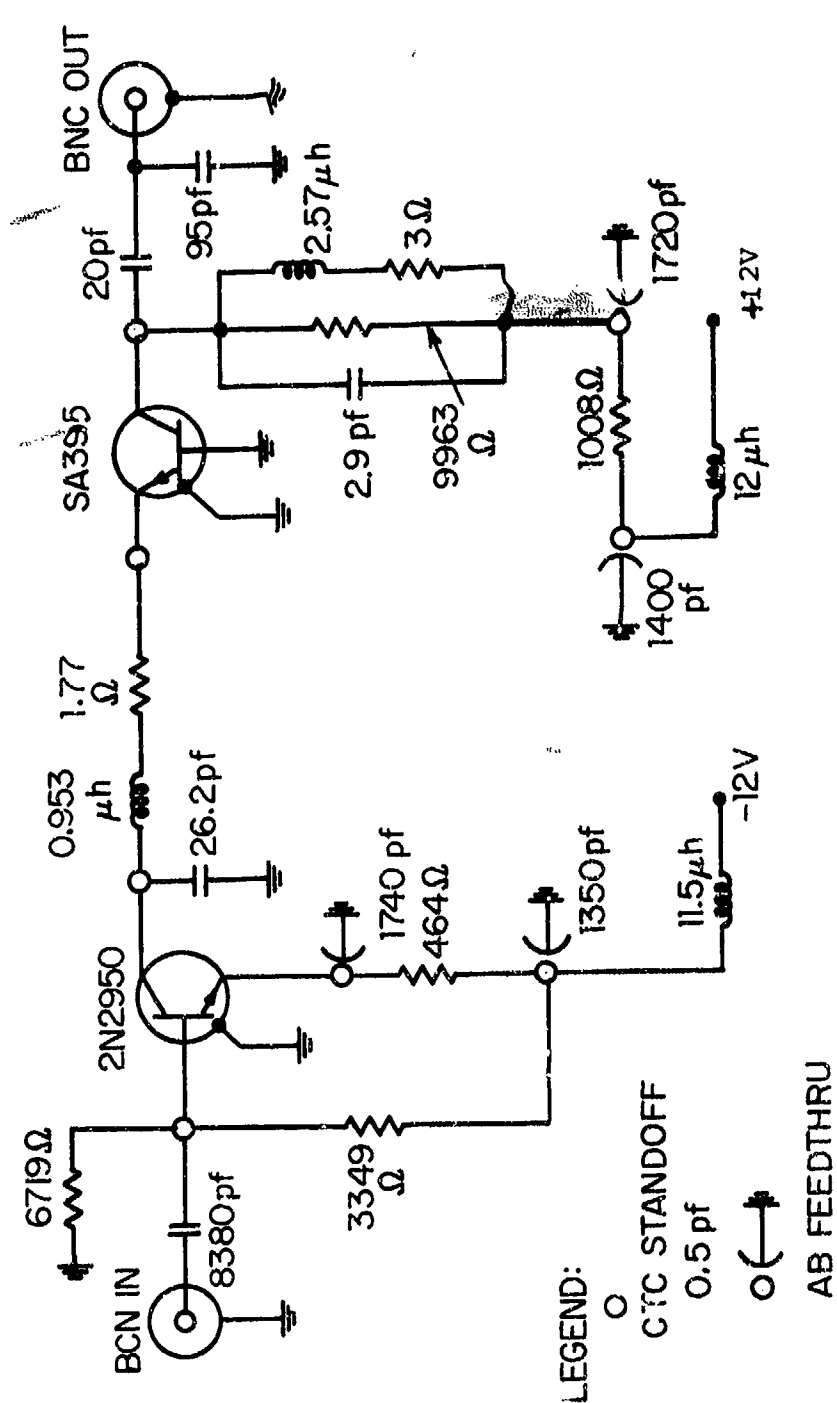


Fig. 6.18. Schematic of Two-Stage Tuned Amplifier

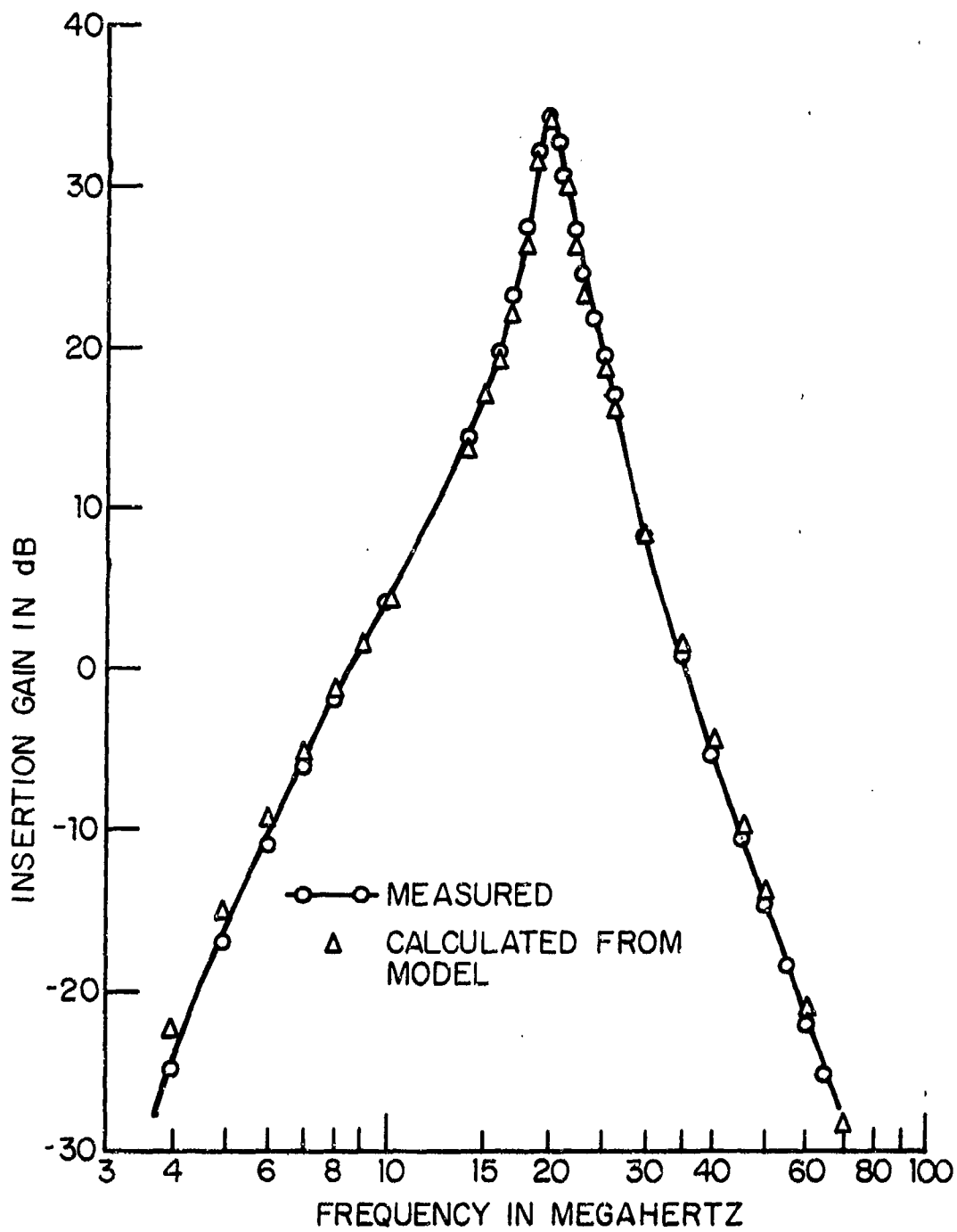


Fig. 6.19. Comparison of Two-Stage Tuned Amplifier Measured and Calculated Insertion Gain.

Table 6.6
 2N2950 MODEL PARAMETERS FOR NONLINEAR AND LINEAR INCREMENTAL MODELS
 AT $T_A = 25^\circ\text{C}$ AND $V_{CB} = 9.3$ V, $I_C = 3.7$ mA.

Description	Nonlinear Parameters	Linear Parameters
Emitter Junction-Forward Biased		
Conductance	$I_E = 4.2$ mA; $n = 1.0$	$r_e = 6.04$ ohms
Capacitance	$C_{je} = 340$ pF; $C_D' = 59.1$ pF/mA	$C_2 = 594$ pF
Collector Junction-Reverse Biased		
Conductance	$r_c = 635$ k Ω	$r_c = 635$ k Ω
Capacitance	$\kappa = 24.5$ pF; $\phi = 0.4$ volt; $\mu = .348$	$C_c = 9.73$ pF
Dependent Source		
h_{FE}	$h_{FE\max} = 8.2$, $I_{C\max} = 150$ mA; $a = .125$	$a = .877$
Avalanche	$V_{CBO} = 140$ volts; $n = 4.6$	
Base	$r_b = 10.1$ Ω	$r_b = 10.1$ Ω
Other		
Emitter-base capacitance	$C_1 = 0$	$C_1 = 0$
Collector-base capacitance	$C_3 = 1.5$ pF	$C_3 = 1.5$ pF
Collector-base sink capacitance	$C_{CG} = 4.0$ pF	$C_{CG} = 4.0$ pF

Table 8.7
SA395 MODEL PARAMETERS FOR NONLINEAR AND LINEAR INCREMENTAL MODELS
AT $T_A = 25^\circ\text{C}$ AND $V_{CB} = 9.6 \text{ V}$, $I_C = 3.7 \text{ mA}$

Description	Nonlinear Parameters	Linear Parameters
Emitter Junction-Forward Biased		
Conductance	$I_E = 3.8 \text{ mA}; n = 1.0$	$r_e = 6.88 \text{ ohms}$
Capacitance	$C_{je} = 25 \text{ pF}; C_D^I = 7.5 \text{ pF/mA}$	$C_2 = 53.3 \text{ pF}$
Collector Junction-Reverse Biased		
Conductance	$r_c = 200 \text{ k}\Omega$	$r_c = 200 \text{ k}\Omega$
Capacitance	$\kappa = 1.4 \text{ pF}; \mu = .086$	$C_c = 1.15 \text{ pF}$
Dependent Source		
h_{FE}	$h_{FE\max} = 51.4, I_{C\max} = 20 \text{ mA}; a = 0.30$	$a = .981$
Avalanche	$V_{CBO} = 50.0 \text{ volts}; n = 4.5$	
Base	$r_b = 90 \Omega$	$r_b = 90 \Omega$
Other		
Emitter-base capacitance	$C_1 = 0$	$C_1 = 0$
Collector-base capacitance	$C_3 = 0 \text{ pF}$	$C_3 = 0 \text{ pF}$
Collector-base sink capacitance	$C_{CG} = 0 \text{ pF}$	$C_{CG} = 0 \text{ pF}$

analysis are listed in Table 6.8. For example, the midband insertion gain from Eq. (6.8) and Table 6.8 is

$$G_I = 28.0 + 6.0 = 34.0 \text{ dB} . \quad (6.67)$$

6.5.2 Second and Third-Order Intermodulation Distortion

The frequency dependence of the second and third-order intermodulation distortion nonlinear transfer functions for the two-stage tuned amplifier is quite different from the ~~un~~tuned amplifier example discussed in Section 6.4. The theoretical values of H_2 and H_3 for several different two-tone input frequency combinations are given in Table 6.8. These values together with additional values calculated by SIGNCAP can be compared with experimental estimates of H_2 and H_3 . The experimental estimates were obtained from distortion measurements and reduced as previously described in conjunction with Eq. (6.57) and (6.58).

The second-order nonlinear transfer function is most conveniently determined by a two-tone test in which tones of frequencies f_1 and f_2 are used to drive the amplifier, and the response at $f_1 + f_2$ is measured. Figure 6.20 shows the second-order nonlinear transfer function of the two-stage tuned amplifier under the condition that $f_1 + f_2$ was equal to 19.75 MHz, the center frequency of the amplifier. The transfer function varies by some 35 dB over the 750 KHz to 80 MHz range, peaking at 10, 30, and 55 MHz, and having minima at about 20 and 42 MHz. At low-frequency, the transfer function has a 20 dB/decade slope.

Table 6.8
Two-Stage Tuned Amplifier Nonlinear Transfer Functions

Order and Type	Nonlinear Transfer Function	Input Frequency (MHz)		Magnitude (dB)	Phase (Degrees)
		f_1	f_2		
<u>First Order</u>	$H_1(f_1)$	19.75		28.0	117
<u>Second-Order</u>					
Intermodulation	$H_2(f_1, f_2)$	9.0	10.7	47.9	163
Intermodulation	$H_2(-f_1, f_2)$	35.0	15.25	33.6	202
Intermodulation	$H_2(-f_1, -f_2)$	49.75	30.0	19.8	171
<u>Third-Order</u>					
Intermodulation	$H_3(f_1, f_2, f_3)$	9.75	5.0	51.6	283
Intermodulation	$H_3(-f_1, f_2, f_3)$	10.25	15.0	62.5	255
Intermodulation	$H_3(-f_1, -f_2, f_3)$	60.25	40.0	23.9	303
Desensitization	$H_3(f_1, f_2, -f_2)$	19.75	24.75	47.3	314
Desensitization	$H_3(f_1, f_2, -f_1)$	19.75	29.75	38.0	303
Desensitization	$H_3(f_1, -f_2, -f_2)$	19.75	34.75	28.0	267
Desensitization	$H_3(f_1, -f_2, -f_1)$	19.75	39.75	32.6	219
Desensitization	$H_3(f_1, f_2, -f_1)$	19.75	49.75	27.8	237

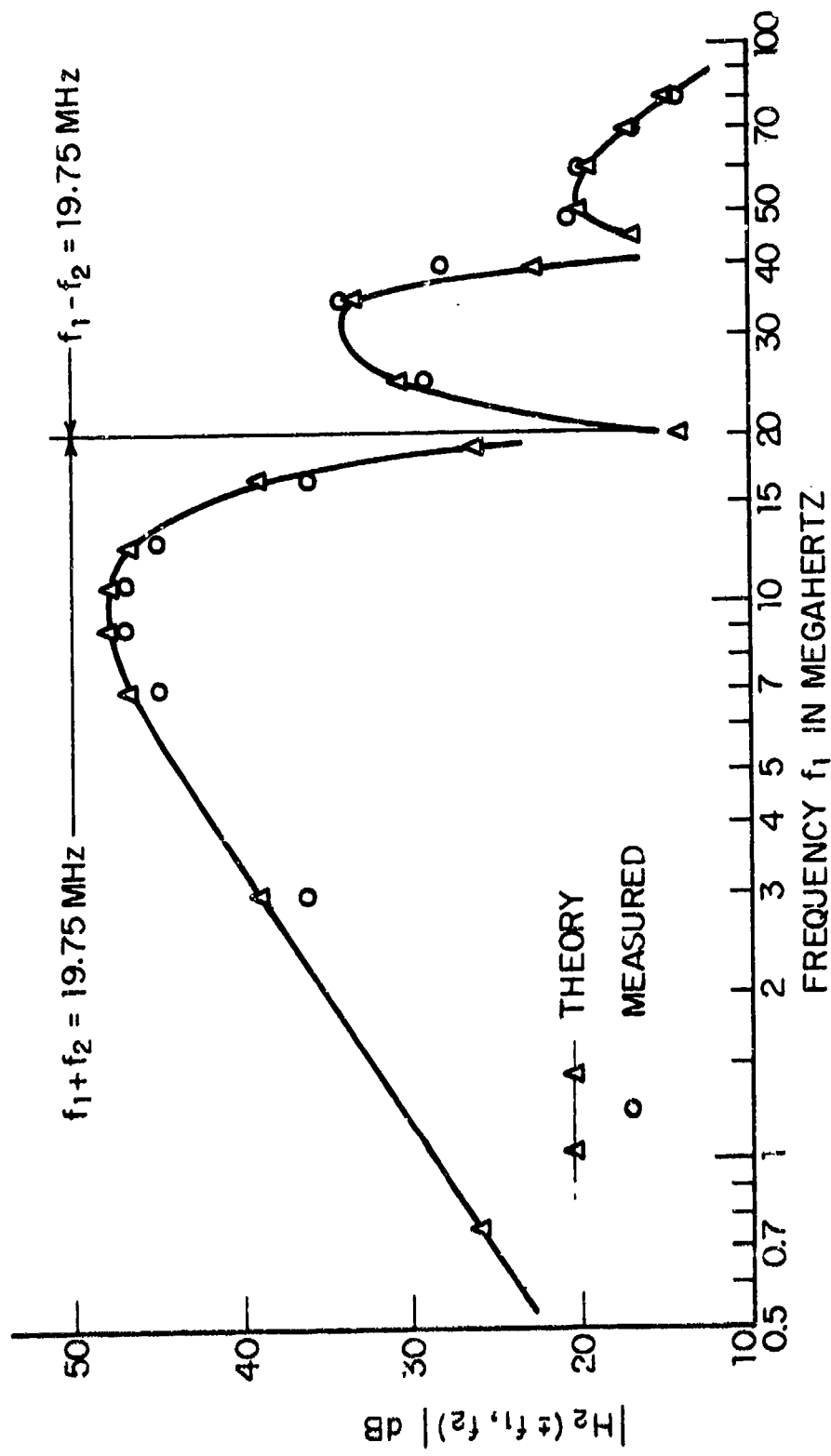


Fig. 6.20. Second-Order Nonlinear Transfer Function for the Two-Stage Tuned Amplifier Cascade.

The points plotted below 19.75 MHz are associated with sum frequency terms, i.e., $f_1 + f_2$. Since the designations f_1 and f_2 are arbitrary for a sum frequency, the value of the second-order nonlinear transfer function will be symmetrical about $19.75/2 = 9.975 \approx 10$ MHz.

The null at 19.75 MHz has a simple explanation. Since the f_1 input tone is 19.75 MHz at this frequency, f_2 must be zero and the lack of a DC response causes the null. The null near $f_1 = 42$ MHz is caused by an internal resonance associated with the interstage network.

The third-order nonlinear transfer function is also conveniently determined by a two-tone test, in which tones at frequencies f_1 and f_2 are used as inputs, and the nonlinear response at frequency $2f_2 \pm f_1$ is measured.

The measured and predicted third-order nonlinear transfer functions for the two-stage tuned amplifier are shown on Fig. 6.21. The transfer function covers a 50 dB interval with good agreement between measured and predicted values throughout the range. The measurement was made by varying f_1 and f_2 so that $2f_2 \pm f_1 = 19.75$ MHz. For frequencies below $19.75/2$ MHz, the response is a sum response, that is, $2f_2 + f_1 = 19.75$ MHz. At $f_2 = 19.75/2$ MHz f_1 is again zero and the null occurs because of the lack of a DC response in the linear transmission. The null at about 28 MHz is caused by the internal resonance associated with the interstage network.

The conclusion one can reach is that the model does successfully predict the rather complicated frequency dependence of both second and third order intermodulation distortion. Although we have not presented here curves similar to Fig. 6.10

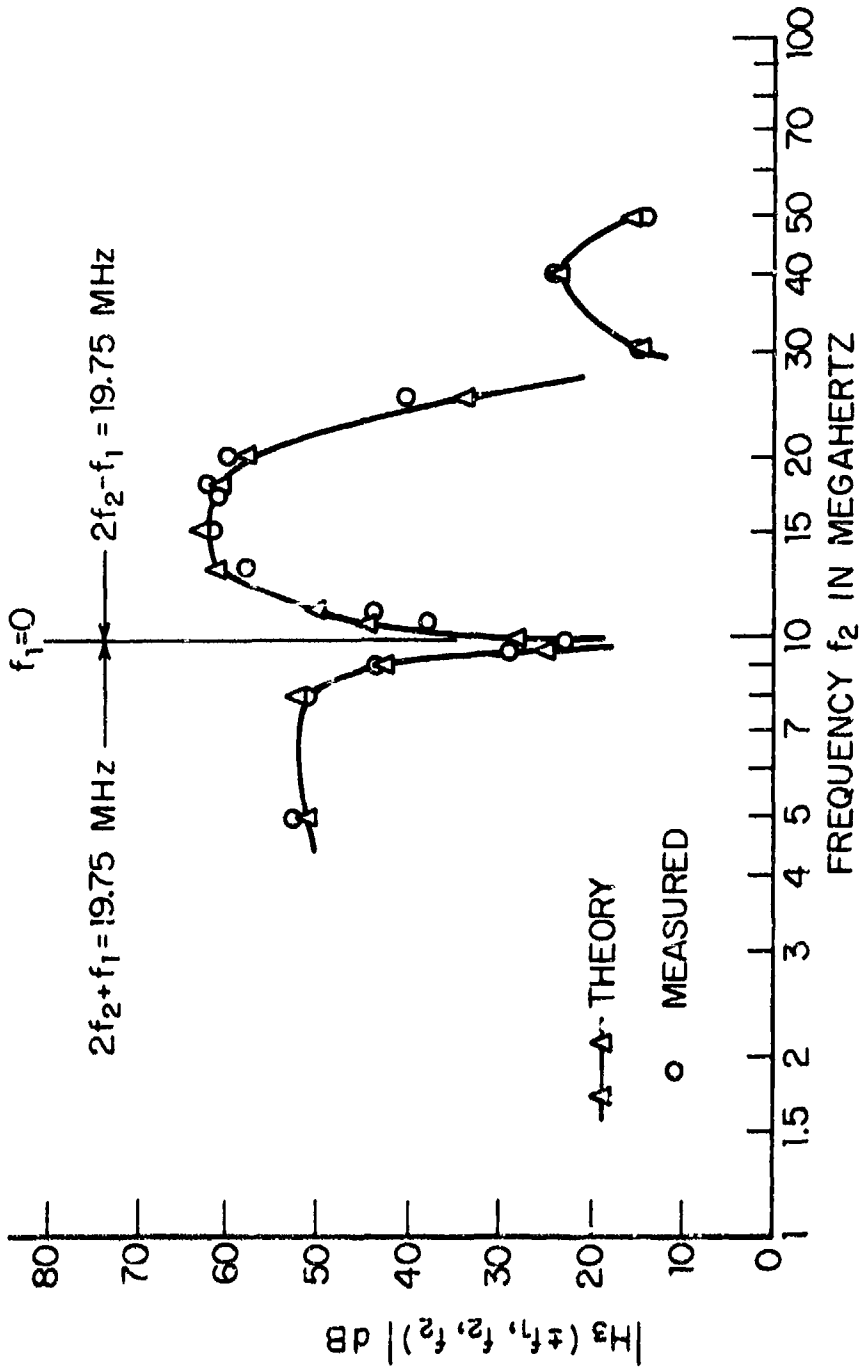


Fig. 6.21. Third-Order Nonlinear Transfer Function for the Two-Stage Tuned Amplifier Cascade.

for input amplitude dependence such results have been found to be in good agreement with prediction and are, in fact, the source of data used to experimentally estimate H_2 and H_3 .

6.5.3 Two-Stage Amplifier Desensitization

Based on the success in predicting the third-order intermodulation distortion of the two-stage amplifier, one would expect that desensitization, also a third-order effect, can be predicted with good accuracy. In this section we examine the measured and predicted values of desensitization, and discuss the results and their implication.

If the input to a nonlinear system be the sum of a desired signal of frequency f_1 and complex envelope S_1 , and an undesired signal of frequency f_2 and complex envelope I_2 , then V_0 , the complex envelope of the output of the system at frequency f_1 , is, from Section 1.8,

$$V_0 = H_1(f_1)S_1 + \frac{3}{2} H_3(f_1, f_2, -f_2) S_1 |I_2|^2, \quad (6.68)$$

where H_3 is the third-order desensitization term.

If H_3 is 180° out of phase with H_1 , V_0 will decrease with increasing I_2 . This is the desensitization effect, whereby the response of a system at the desired frequency f_1 is decreased by the component at f_2 . It is a third-order effect, but it is also sensitive to the phase of H_3 relative to H_1 . If H_3 and H_1 are in phase, then there will be expansion instead of a desensitization.

An experiment was run using the two-stage tuned amplifier with the desired signal an unmodulated tone at -55 dBm at the

center tuned frequency 19.75 MHz, and the second input also an unmodulated tone varied in both power and frequency. Figure 6.22 shows the desensitization of the amplifier at 19.75 MHz for inputs at frequencies of 24.75, 29.75, 34.75, 39.75, and 49.75 MHz. Both measured (solid curve) and predicted desensitization data are shown. It is seen that the onset of desensitization is well predicted for the 24.75, 29.75 and 34.75 MHz cases. It is further seen that at 39.75 MHz, an expansion, not a desensitization, is predicted; a desensitization is, however, measured. The predictions were made using the transfer function from Table 6.8. Four vertical lines are shown on Fig. 6.22, corresponding to the input power at which the base-emitter voltage of the second stage transistor (SA395) is 25 mV at the second input frequency. This represents the boundary between small and large-signal effects. For powers somewhat lower than that which produces 25 mV, small-signal theory is applicable while large signal analysis is required for higher power. The onset of desensitization is in the small-signal region and is predicted well. For 24.75, 29.75, and 34.75 MHz, predicted desensitization of 1 dB corresponds approximately to the 25 mV boundary. Thus, the desensitization predictions above this region are not expected to be valid. This example shows the interaction between small and large signal effects, as well as showing the applicability of the simple 25 mV criterion. It also illustrates that prediction of desensitization must be undertaken with care. The onset of the effect is predicted but the amount of desensitization, when significant, may be a large signal nonlinear effect.

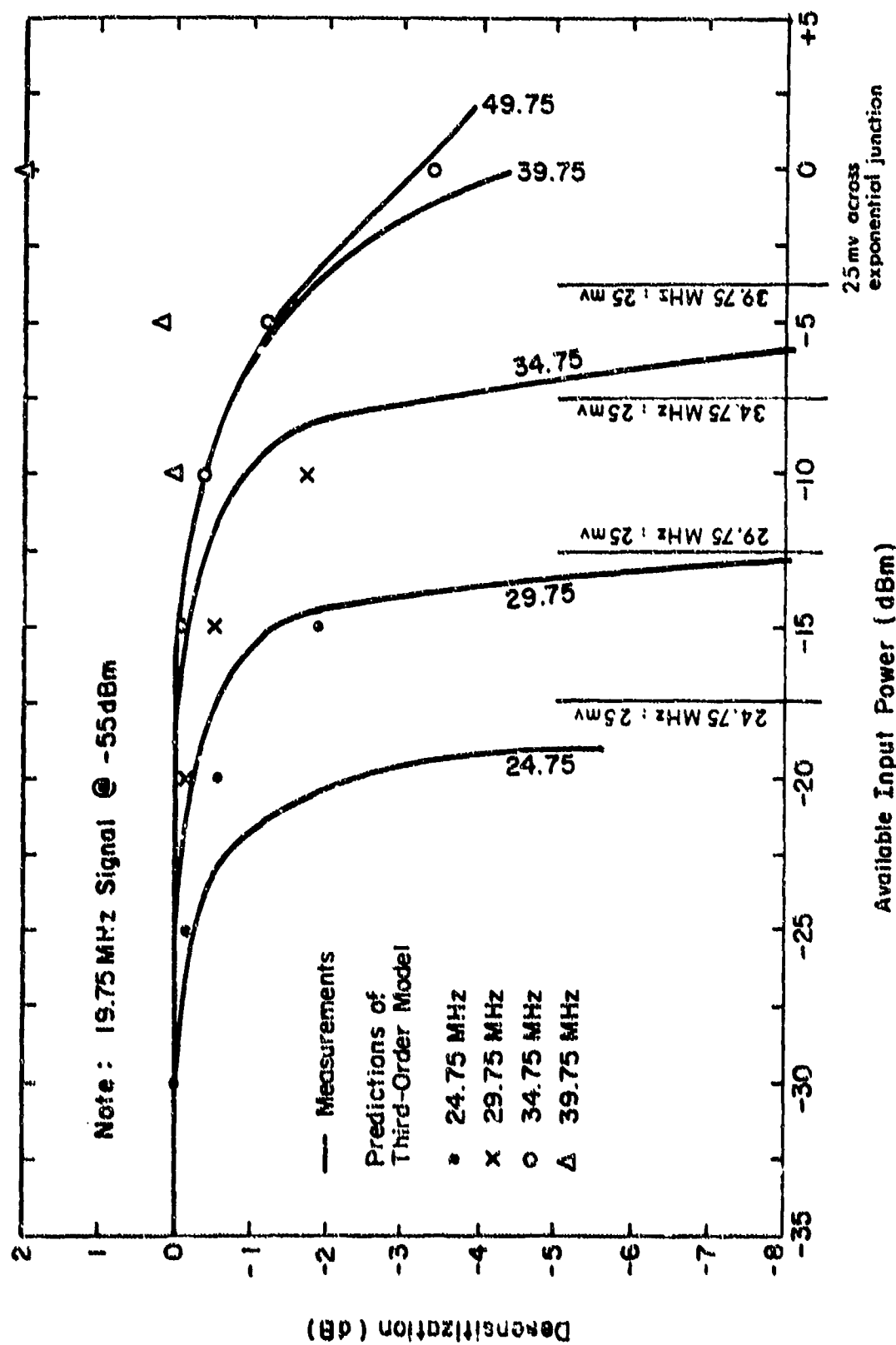


Fig. 6.22. Measured and Predicted Desensitization.
 Two Stage Amplifier

6.6 Intermodulation Distortion in Vacuum Tubes

6.6.1 Untuned Triode Amplifier

Two-tone testing of a triode is a useful technique for establishing the validity of triode model parameters in addition to providing a technique for measurement of intermodulation distortion. The triode test circuit is shown in Fig. 6.23. One half of a 12AT7 triode was utilized in the measurements in a relatively broadband untuned test circuit. Model predictions and laboratory measurements were made with 50 ohm sources and loads. The nonlinear incremental circuit model is shown in Fig. 6.24. The triode nonlinear model was developed in Section 5.6.2.1. Parameters for the 12AT7 as well as the operating point are listed in Table 6.9. The triode is the same unit whose static characteristics were previously described in Section 5.6.2.2.

The linear voltage gain, or $|H_1(f)|$, the first-order transfer function magnitude, is shown in Fig. 6.25 together with measured data at selected frequencies. Model prediction and measurement are seen to be in good agreement.

A comparison of predicted and measured intermodulation distortion output power for two-tone excitation at 100 and 330 kHz is shown in Fig. 6.26. The predictions are seen to be in relatively good agreement with measurements. Note that the input tone level is expressed in RMS voltage rather than available source power. The RMS voltage E_{IN} is noted in Fig. 6.24 as the incremental RMS grid voltage. For practical purposes E_{IN} is the open-circuit Thevenin source voltage at 100 and 300 kHz.

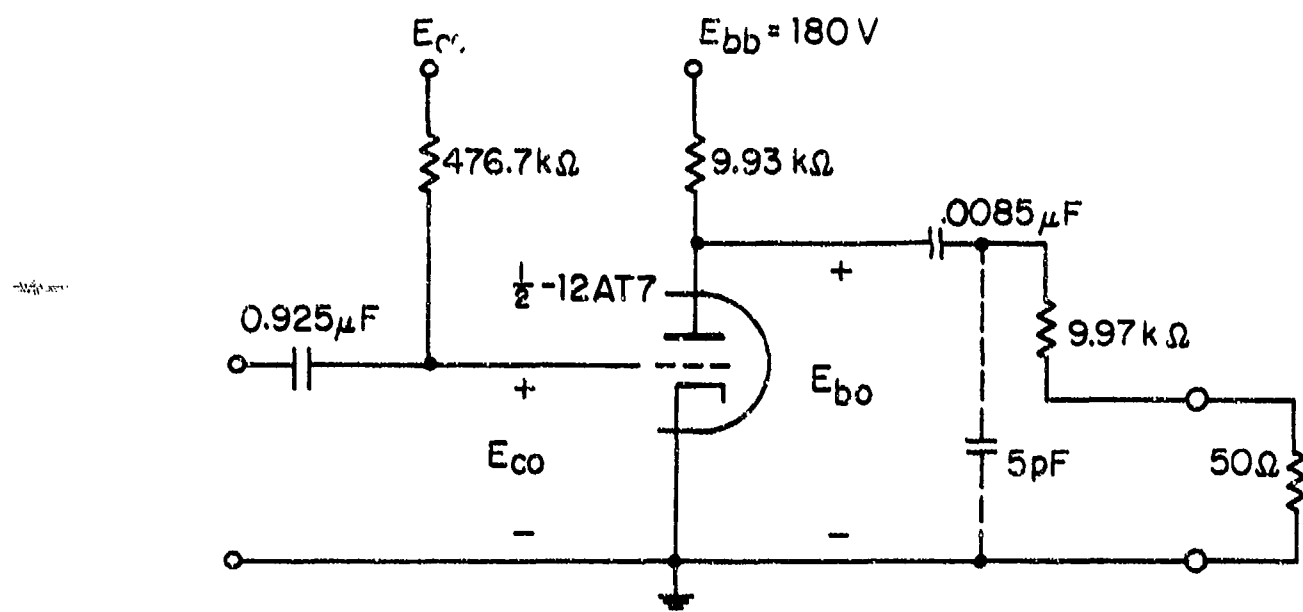


Fig. 6.23. Triode Test Circuit.

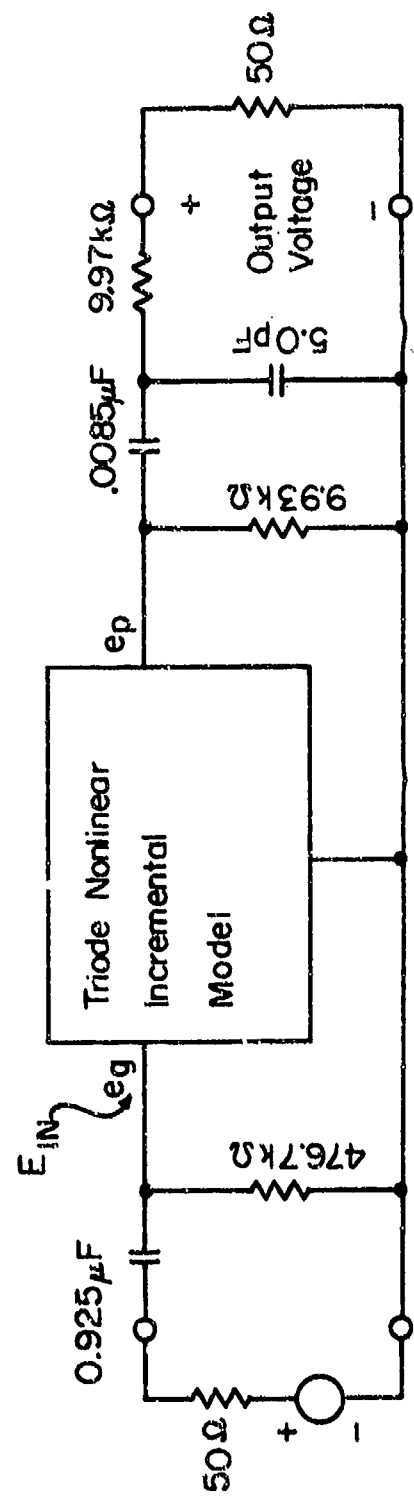


Fig. 6.24. Triode Test Circuit Incremental Model.

TABLE 6.9
12AT7 Triode Model Parameters

Operating Point

$$E_{c0} = -1.0 \text{ v}$$

$$E_{b0} = 136 \text{ v}$$

$$I_{b0} = 4.43 \text{ mA}$$

Model Parameters

$$G_0 = 3.35 \times 10^{-3} \text{ ampere (volt)}^{-3/2}$$

$$\mu = 53.4$$

$$E_{c_{\max}} = -6.2 \text{ v}$$

$$E_{c0} = -1.0 \text{ v}$$

$$E_{b0} = 136 \text{ v}$$

$$\phi = -0.09 \text{ v}$$

$$C_{gk} = 2.2 \text{ pF}$$

$$C_{pg} = 1.5 \text{ pF}$$

$$C_{pk} = 1.5 \text{ pF}$$

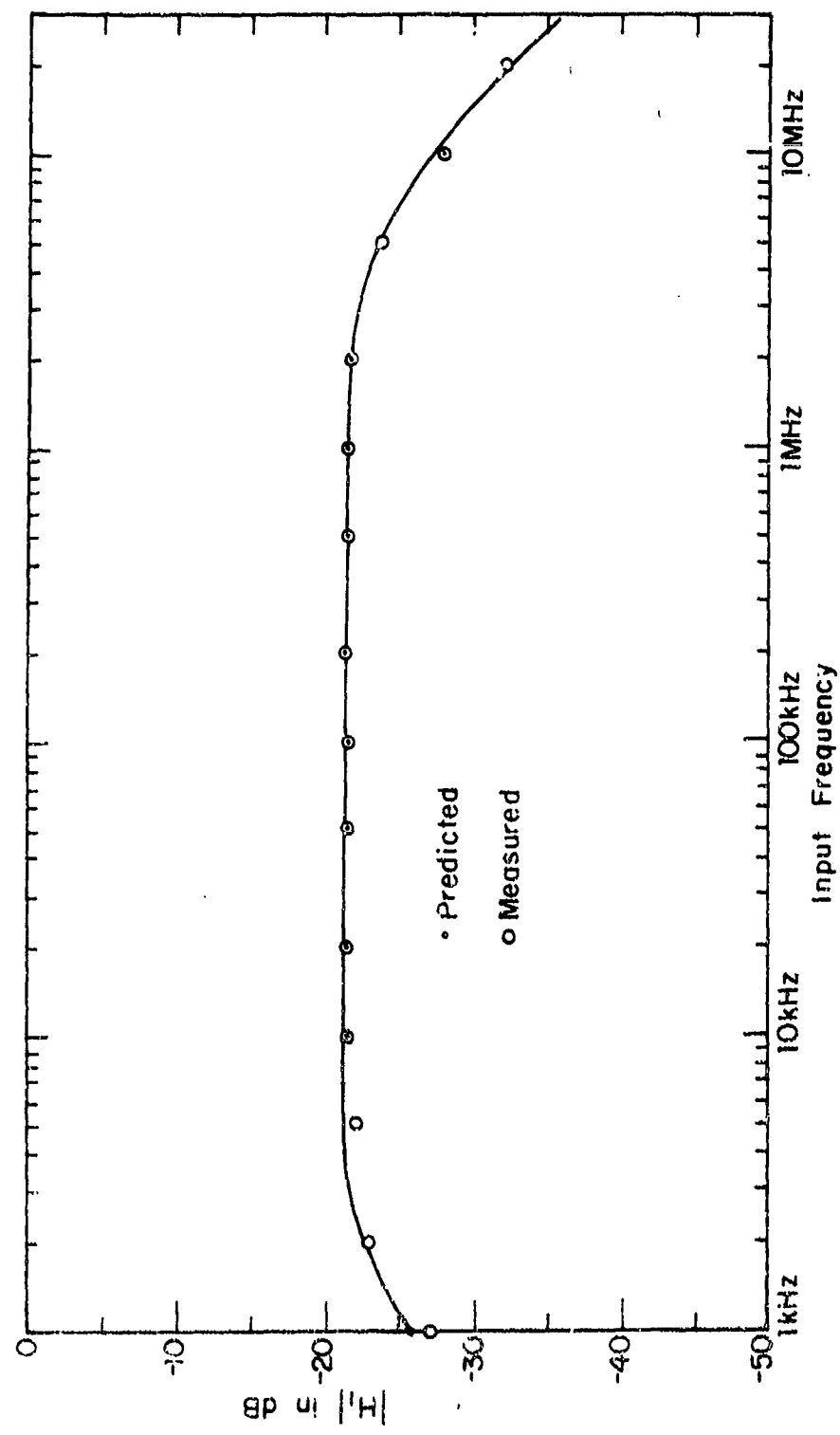


Fig. 6.25. 12AT7 triode First-Order transfer Function.

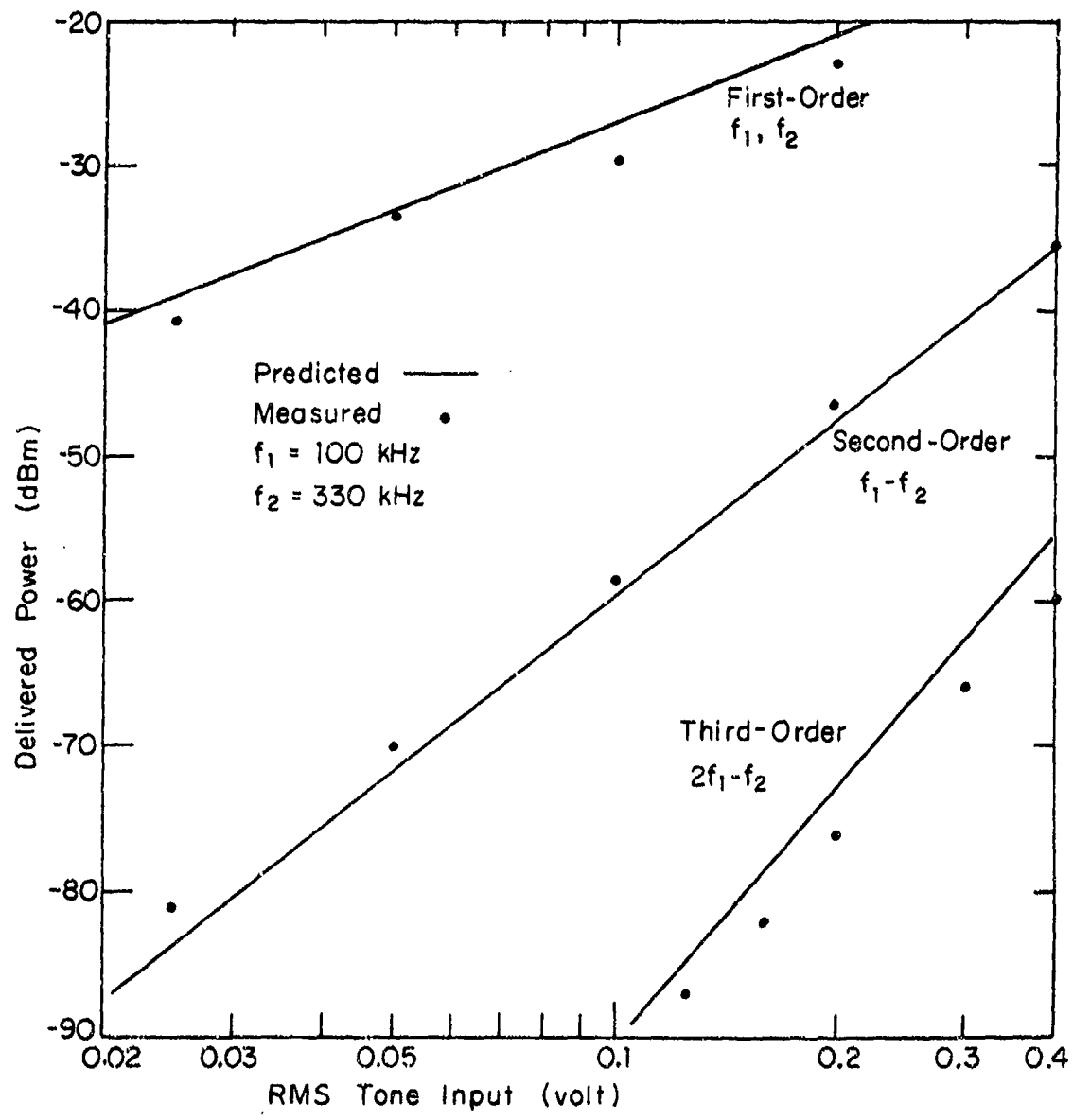


Fig. 6.26. Comparison of Predicted and Measured 12AF7 Triode Intermodulation Distortion.

since the grid input impedance is so high for the triode. Under these circumstances one can readily relate the delivered output power to the computed nonlinear transfer function H_1 , H_2 , and H_3 and the RMS input voltage E_{IN} through Eq. (6.47) - (6.49) which have been developed specifically for this purpose. Application of the triode model in other circuits is straightforward. Transfer functions are readily determined by employing SIGNCAP as outlined in Appendix A.

6.6.2 Untuned Pentode Amplifier

In this section we shall briefly review the results of a prediction and comparison with measurement of intermodulation distortion for three different vacuum pentodes. A relatively broadband untuned test amplifier circuit was employed to reveal the device nonlinear characteristics without the masking effects of tuned loads. Results for tuned load situations will be implicit in a later chapter devoted to modeling of vacuum tube receivers. The test circuit used for the untuned amplifier is shown in Fig. 6.27. Circuit element values for the three different pentodes that were modeled are noted in Table 6.10. We have previously given in Table 5.3 the model parameters and operating-bias points utilized in the study.

The measured and predicted intermodulation output power for the first three nonlinear responses of the three pentodes are shown in Figs. 6.28 through 6.30. All measurements were made with two equal-power input tones, one at 100 kHz and the other at 330 kHz. It is seen that the predictions are in fair agreement with the measurements for the 6AH6 and 5763, as well

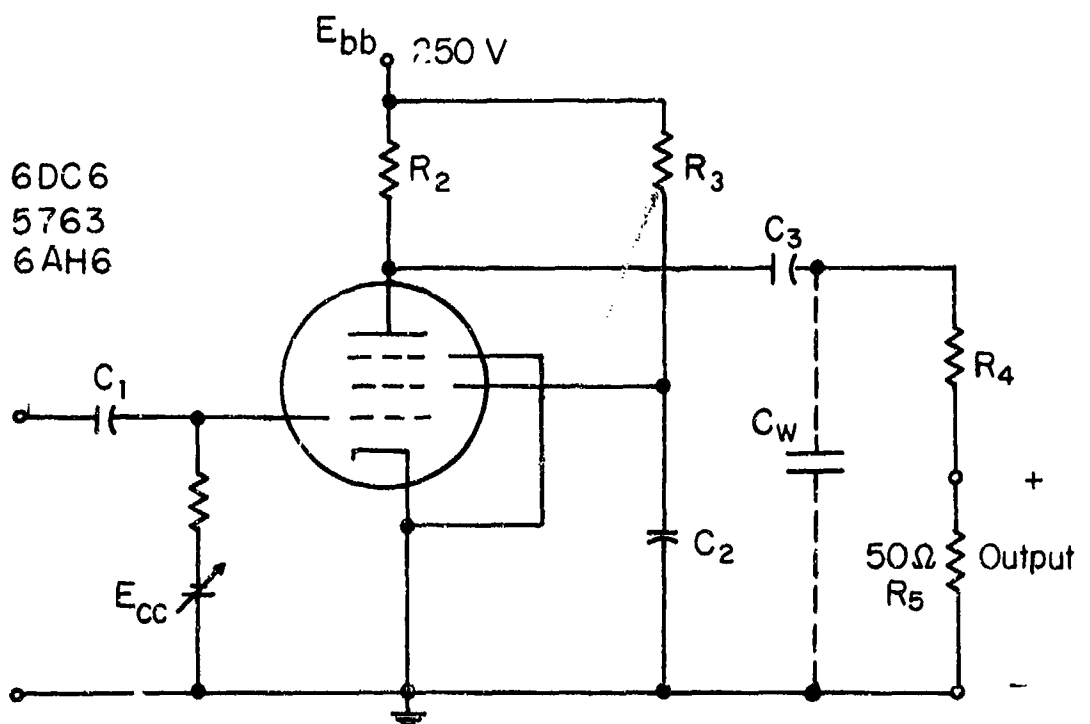


Fig. 6.27 Pentode Test Circuit

TABLE 6.10
Pentode Test Circuit Element Values

Type Component	6DC6	5763	6AH6
R ₁	102.6 kΩ	103.5 kΩ	100 kΩ
R ₂	9.99 kΩ	1.61 kΩ	9.85 kΩ
R ₃	31.1 kΩ	9.94 kΩ	30.1 kΩ
R ₄	9.84 kΩ	9.69 kΩ	10.04 kΩ
R ₅	50 Ω	50 Ω	50 Ω
C ₁	0.95 μF	0.96 μF	0.99 μF
C ₂	0.048 μF	0.0406 μF	0.0581 μF
C ₃	0.0113 μF	0.0098 μF	0.01205 μF
C _w	5 pF	5 pF	5 pF

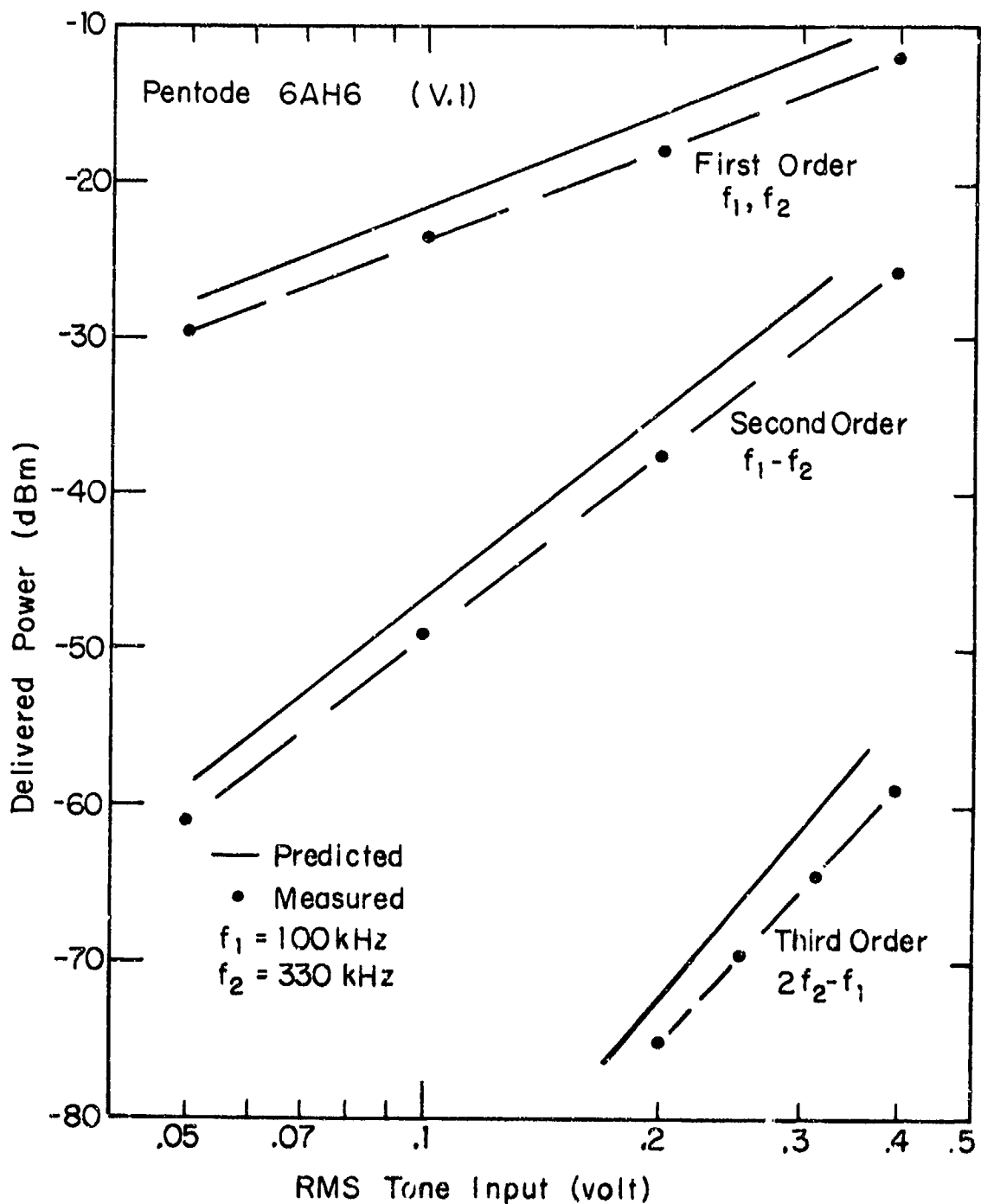


Fig. 6.28 Comparison of Predicted and Measured 6AH6 Pentode Intermodulation Distortion.

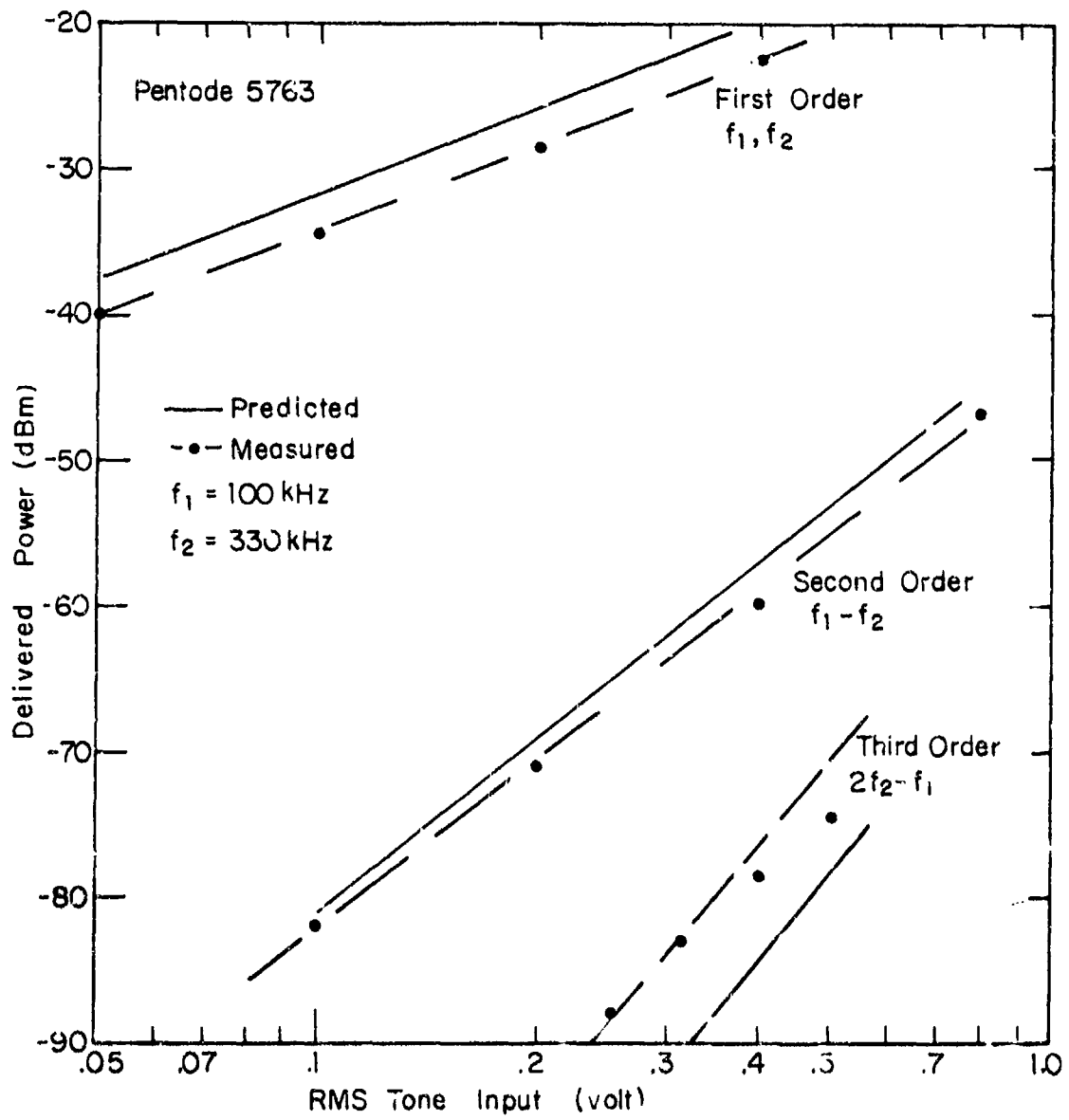


Fig. 6.29. Comparison of Predicted and Measured 5763 Pentode Intermodulation Distortion.

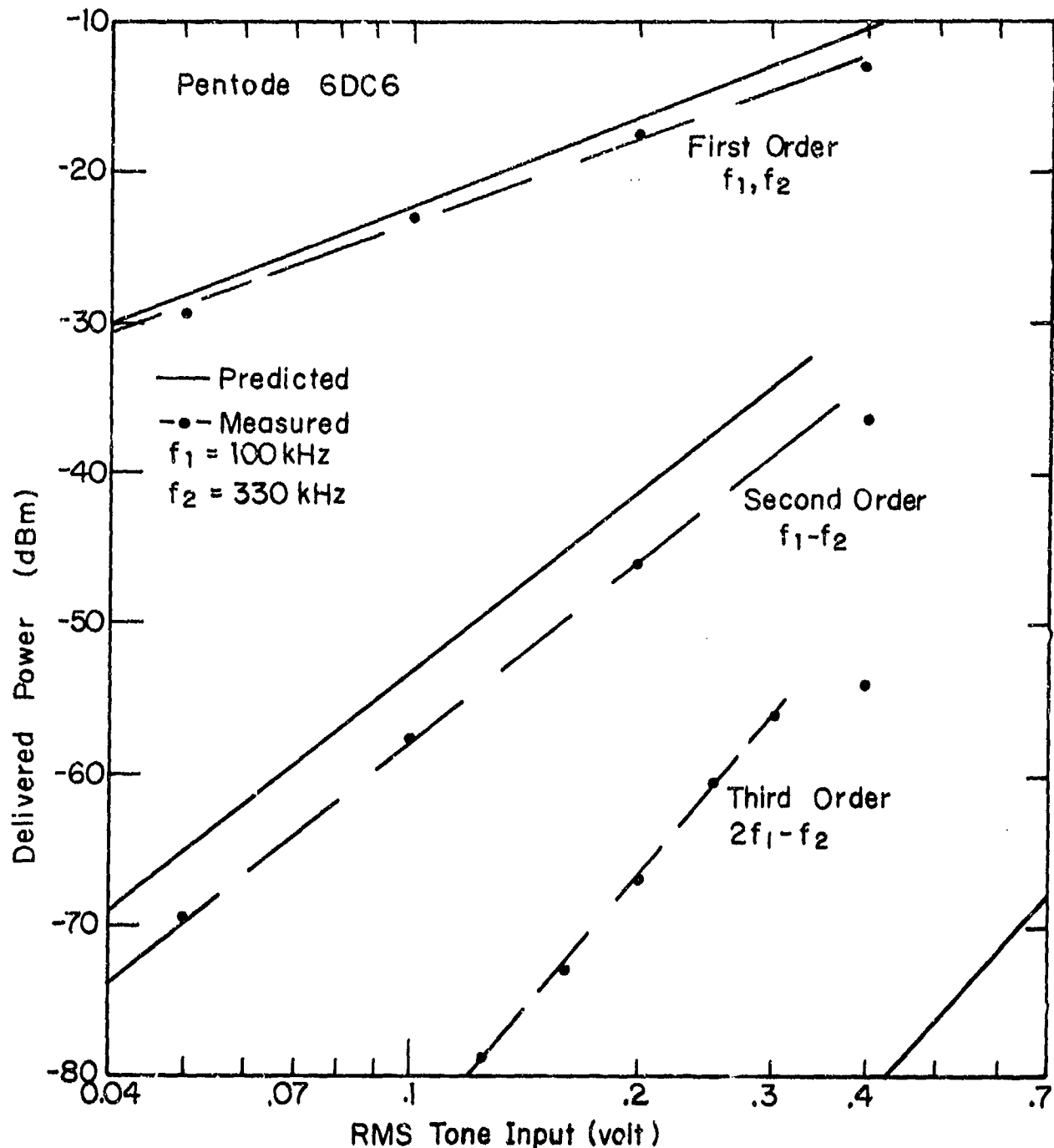


Fig. 6.30 Comparison of Predicted and measured 6DC6 Pentode Intermodulation Distortion.

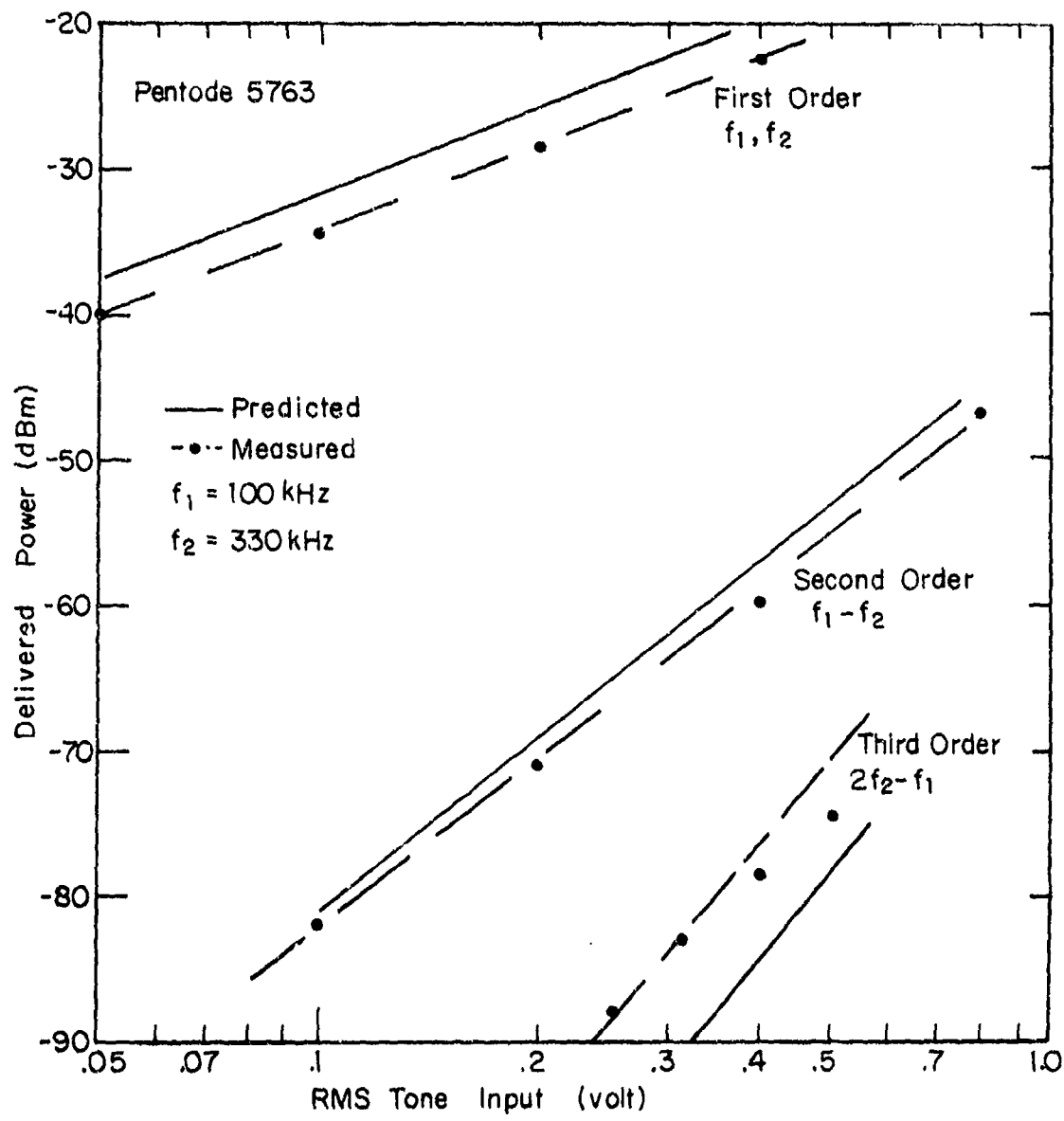


Fig. 6.29. Comparison of Predicted and Measured 5763 Pentode Intermodulation Distortion.

as for the first and second-order responses of the 6DC6, but are unsatisfactory for the third-order response of the 6DC6. The reason for this is uncertain. It is interesting to note that the first and second-order responses of the 6DC6 are essentially independent of the current-division parameter m , while the third-order response depends strongly upon m . This is shown in Table 6.11 where the experimentally determined values of H_1 , and H_2 , and H_3 are compared with predictions for several values of m , the exponential factor in the current division nonlinearity. It is evident that near $m = 0.11$, the value of m found in the analysis of the 6DC6 characteristics (see Table 5.3, Chapter 5), the third-order response is predicted to have a null. For smaller values of m , e.g. $m=0$, and larger values, e.g. 0.2 or 0.5, the agreement between the measured and predicted third-order nonlinear transfer function is much better. This result illustrates the fact that caution should be employed when using the pentode model in the vicinity of a distortion null region.

6.7 Large-Signal Multi-Tone Input Time-Domain Analysis

In Section 6.4 we illustrated the application of small-signal analysis methods to determine the nonlinear transfer functions of a single-stage bipolar transistor (2N2950) amplifier. We found that model predictions agreed well with experimental predictions over a wide range of frequencies provided the input tones exciting the network were not too strong. The circuit studied was shown in Fig. 6.7. Typical mid-band intermodulation distortion levels were compared with prediction in Fig. 6.10. In this section we present further results complementing the small-signal modeling and analysis by extending the

TABLE 6.11
Effect of m on 6PC6 Pentode Nonlinear Transfer Functions

	$ H_1(f_1) $	$ H_2(f_1, -f_2) $	$ H_3(f_1, f_1, -f_2) $
Measured	-16 dB	-34 dB	-41.5 dB
Predicted			
$m = 0$	-15.50 dB	-28.56 dB	-58.51 dB
.05	-15.49	-28.79	-64.88
.10	-15.48	-29.01	-85.08
.11	-15.48	-29.06	-75.20
.20	-15.46	-20.50	-57.86
.50	-15.41	-31.17	-46.14

model to large signals and describing the results of a large-signal time-domain analysis. Both two and three-tone excitation examples have been investigated. The two-tone results presented in Section 6.7.1 extend the small-signal results of Section 6.4.2 while the three-tone results presented in Section 6.7.2 extend the results of Section 6.4.3 to include a mixer with a large local-oscillator.

6.7.1 Two-Tone Time-Domain Analysis

The two-tone intermodulation distortion products for the 2N2950 untuned test circuit (Fig. 6.7) have been presented earlier in this chapter in Figs. 6.10 and 6.11. The distortion products were found to be predicted accurately by small-signal nonlinear theory in the small-signal range. Predictions based upon small-signal analysis in the large-signal region were found to be poor. In Chapter 4 we examined several large-signal analysis methods and, particularly, noted that the nonlinear state equations for a system could be numerically integrated and large-signal performance predicted provided effective numerical integration techniques were used. This time-domain method has been used to predict the large-signal performance of the 2N2950 test circuit. Figure 6.31 shows the nonlinear total circuit model used in the analysis. The two inductors were included to model the test fixture parasitic inductance. The four nonlinearities included in the analysis were the base-emitter resistive nonlinearity $k(v_2)$, the base-emitter diffusion capacitance $C_2(v_2)$, the collector current generator nonlinearity $g(v_2)$, and the nonlinear collector capacitance $C_y(v_3)$. The avalanche effect was not included in the model. The h_{FE} nonlinearity, included in Fig. 6.31 by the dependent current generator $g(v_2)$, is given in the implicit form

$$g(v_2) = k(v_2) \cdot \frac{9.2}{9.2 + \frac{1}{8} \log_{10}^2 \frac{g(v_2)}{0.150}} . \quad (6.69)$$

After some experience with the computational results, it was observed that there was no significant effect on the predicted distortion levels when a constant h_{FE} was used. Accordingly, all results to be reported were obtained with

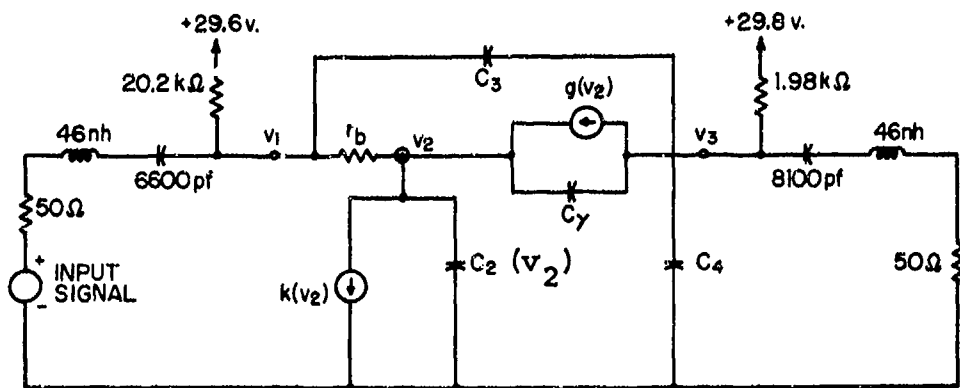
$$h_{FE} = 0.882, \quad (6.70)$$

and

$$g(v_2) = 0.892 [k(v_2)]. \quad (6.71)$$

Figure 6.32 shows the measured and predicted results for two equal tones at 2.5 and 3.0 MHz, while Fig. 6.33 shows the results for two equal tones at 30.0 and 51.4 MHz. To obtain the results, the state equations were integrated for 2 μ sec after the driving voltage was applied in order to allow the transients to settle, and then integrated for an additional time to achieve the desired spectral resolution. Because the numerical integration technique used a nonuniform time step, the set of time samples obtained was converted by interpolation into a set of uniformly spaced samples before the spectral analysis was performed.

The data shown in the figures illustrate the results which careful modeling and numerically-accurate large-signal analysis can achieve. Three sets of data are shown on each figure. The solid lines are the theoretical results predicted by small-signal theory. The measured output powers (shown by the circles) and the predicted output power using the large-signal theory (triangles) are shown in the figures. It is seen that the agreement between the measurements and both small and large-signal predictions is quite good in the small-signal region. In the large-signal region, the large signal



2N2950 PARAMETERS

$$r_b = 10.1\Omega \quad k(v_2) = 10^{-6} \exp(37.76v_2 - 18.12) \text{ ma.}$$

$$C_3 = 1.5 \text{ pf} \quad C_2 = 340.0 (1 + 174 k(v_2)) \text{ pf}$$

$$C_4 = 4.0 \text{ pf} \quad C_Y = 21.2 (v_3^{-348}) \text{ pf} \quad v_2 = 0.726 \text{ v.} \quad v_3 = 10.0 \text{ v.}$$

$$g(v_2) = 0.882 k(v_2)$$

OPERATING POINT

COLLECTOR CURRENT = 10.0 ma.

BASE CURRENT = 1.43 ma.

Fig. 6.31. Model of 2N2950 Test Circuit for Large Signal Analysis.

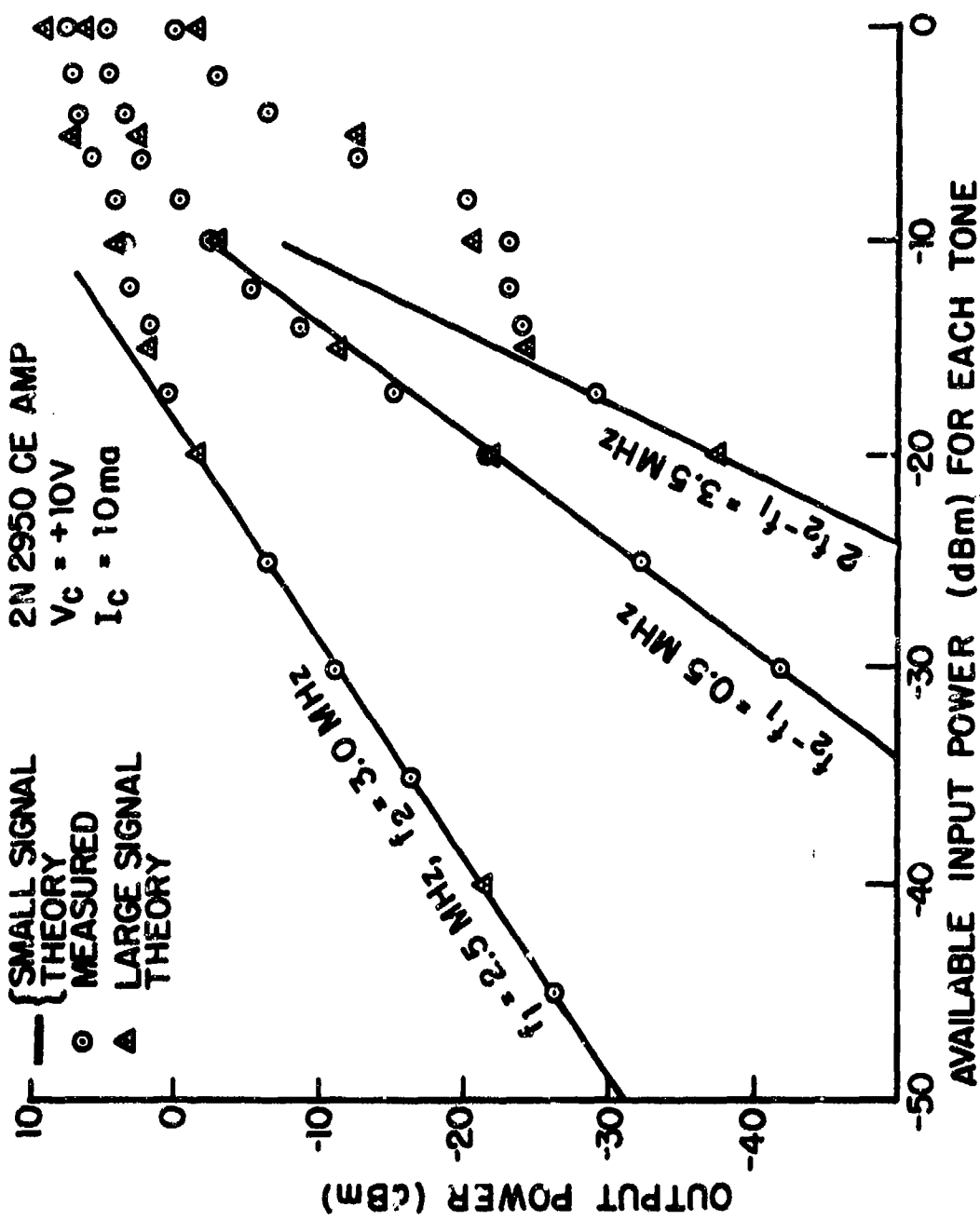


Fig. 6.32. Comparison of Large-Signal Time-Domain Solutions with Experimental Data for Inputs at 2.5 and 3.0 MHz.

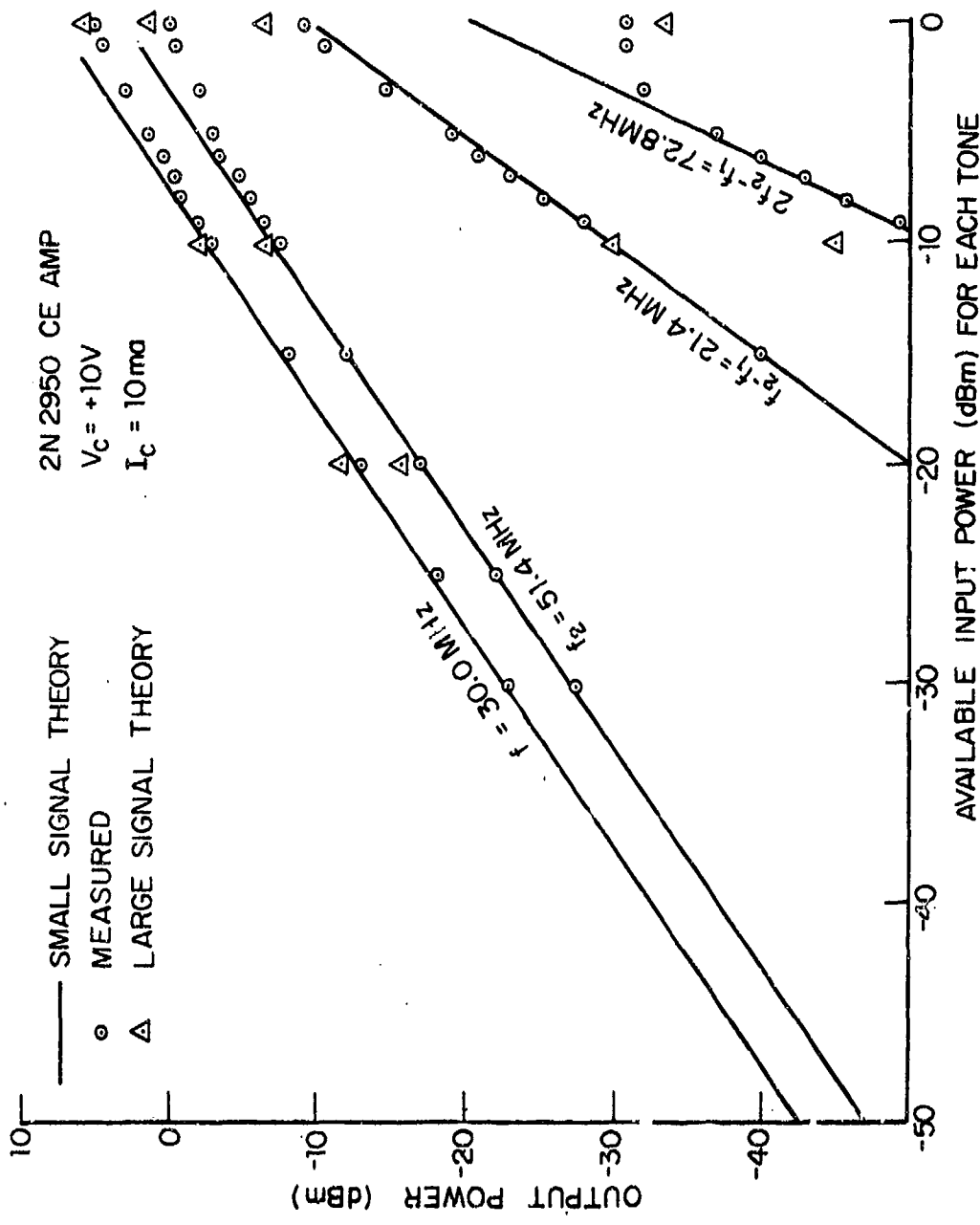


Fig. 6.33. Comparison of Large-Signal Time-Domain Solution with Experimental Data for Inputs at 30 and 51.4 MHz.

predicted output power tracks the measured output power well. One should not jump to the conclusion that small signal methods are not needed, however. The small-signal accuracy and computer solution time as well as ease in formulating the problem and obtaining a solution are far more attractive.

6.7.2 Three-Tone Time-Domain Analysis

The results presented next apply to three-tone test conditions identical to the situation described in Section 6.4.3 for mixer operation but now for a large local oscillator at 51.4 MHz. Two tones at 29 and 30 MHz were maintained at the same input level, while a third-tone, the local oscillator was varied in level. Because numerical computation of spectral information is accomplished by a Fourier series analysis, all output products will be harmonics of some fundamental frequency whose period determines the duration of the computed time-domain waveform. To keep computation time to a reasonable value, 1.0 MHz was selected as the fundamental. With an allowance of 2.0 ~~usec~~ of steady-state behavior to be analyzed, a single run of the ~~longer~~ signal time-domain program covered 3.0 ~~usec~~ of circuit time. To reflect the frequency range of interest, and to provide the 1.0 MHz fundamental, the two signal tones were set at 29 MHz and 30 MHz, respectively, and the local oscillator was set at 50 MHz.

Time-domain predictions of output power from the model as well as measured values from the test-circuit are tabulated in Table 6.12. Included in the table are first-order responses at 29, 30 and 50 MHz, second-order responses at 1, 20, and 21 MHz, and a third-order term at $2(50)-30 = 70$ MHz. Various combinations of input levels are included. Levels span the range from large to small signal excitation

Table 6.12
Measured and Time-Domain Predictions of Three-Tone Tests

Input Freq.	Available Input Power (dBm)										
	50 MHz			+6			0			-5	
	-20	-10	-20	-10	-20	-10	-20	-10	-20	-10	-20
Output	Delivered Output Power (dBm)										
Freq. (MHz)											
1 Meas.	-20.2	-40.7	-17.6	-38.2	-19.0	-40.4	-19.6	-41.2	-20.0	-41.6	
1 Pred.	-26.61	-42.21	-21.97	-43.21	-24.11	-42.59	-24.70	-43.22	-24.98	-46.66	
70 Meas.	-11.4	-21.1	-17.6	-28.2	-23.0	-33.9	-28.6	-39.6	-39.1	-50.1	
70 Pred.	-11.62	-21.31	-16.66	-27.4	-22.86	-33.02	-28.15	-38.46	-38.26	-49.74	
21 Meas.	-11.2	-20.8	-17.6	-28.2	-23.0	-33.9	-28.6	-39.6	-39.1	-50.1	
21 Pred.	-11.33	-21.08	-16.37	-27.4	-22.57	-32.81	-27.87	-38.17	-37.99	-49.44	
22 Meas.	-47.0		-54.5	-84.5	-58.5		-61.5				
22 Pred.	-48.60		-59.21	-73.90	-52.40		-55.31				
79 Meas.	-4.7	-14.8	-3.2	-13.0	-2.65	-12.3	-2.4	-12.15	-2.4	-12.1	
79 Pred.	-4.94	-14.85	-2.84	-12.36	-2.08	-11.76	-1.87	-11.56	-1.78	-11.41	
30 Meas.	-5.0	-15.1	-3.5	-13.2	-2.8	-12.6	-2.7	-12.4	-2.6	-12.3	
30 Pred.	-5.21	-15.12	-3.12	-12.64	-2.36	-12.03	-2.15	-11.83	-2.06	-11.68	
50 Meas.	+6.8	+7.0	+2.2	+2.7	-2.0	-1.7	-7.5	-7.0	-16.6	-16.9	
50 Pred.	7.17	+7.41	+2.93	3.54	-1.54	-1.15	-6.41	-6.03	-16.36	-15.90	
70 Meas.	-30.0	-39.0	-33.0	-42.0	-52.0	-53.0	-63.0	-73.0	-84.0		
70 Pred.	-27.88	-35.72	-30.60	-38.74	-39.38	-48.88	-49.07	-58.68	-68.48	-78.88	

NOTE: At each frequency the top row is measured value and the lower row is time-domain prediction.

at 50 MHz while the excitation at 29 and 30 MHz was maintained below the large signal region. Inspection of the tabulated data suggests good agreement over most of the table entries. For example, in Fig. 6.34 the output at 29 MHz is plotted as a function of input 50 MHz power. There is good agreement between measured and the time-domain prediction. Observe the gain reduction (desensitization) at 29 MHz caused by increasing the 50 MHz drive. Also shown in the figure is the small-signal prediction using SIGNCAP with the third-order desensitization correction included.

In Fig. 6.35 the output at 50 MHz is shown as a function of 50 MHz input drive. Again measurement and time-domain prediction are in good agreement. Note the gain-compression onset occurring at about -5 dBm input that is well predicted by the time-domain analysis but not well predicted in the large signal region by the small signal result. Similar observations are noted for the second-order output at 21 MHz shown in Fig. 6.36 and third-order output at 70 MHz shown in Fig. 6.37.

6.7.3 Comparison of Small-Signal Time-Domain Solution Prediction with Nonlinear Transfer Function Prediction and Experimental Measurements

A suitable basis for comparing small-signal predicted and measured distortion products for a nonlinear system for relatively large quantities of data can be based upon the general n-tone result given earlier in this chapter in Eq. (6.46), or

$$P_n = \sum_{i=1}^n P_{ai} + P_n^o. \quad (6.72)$$

The 29 MHz and 30 MHz Input Tones
are both at -10 dBm available power.

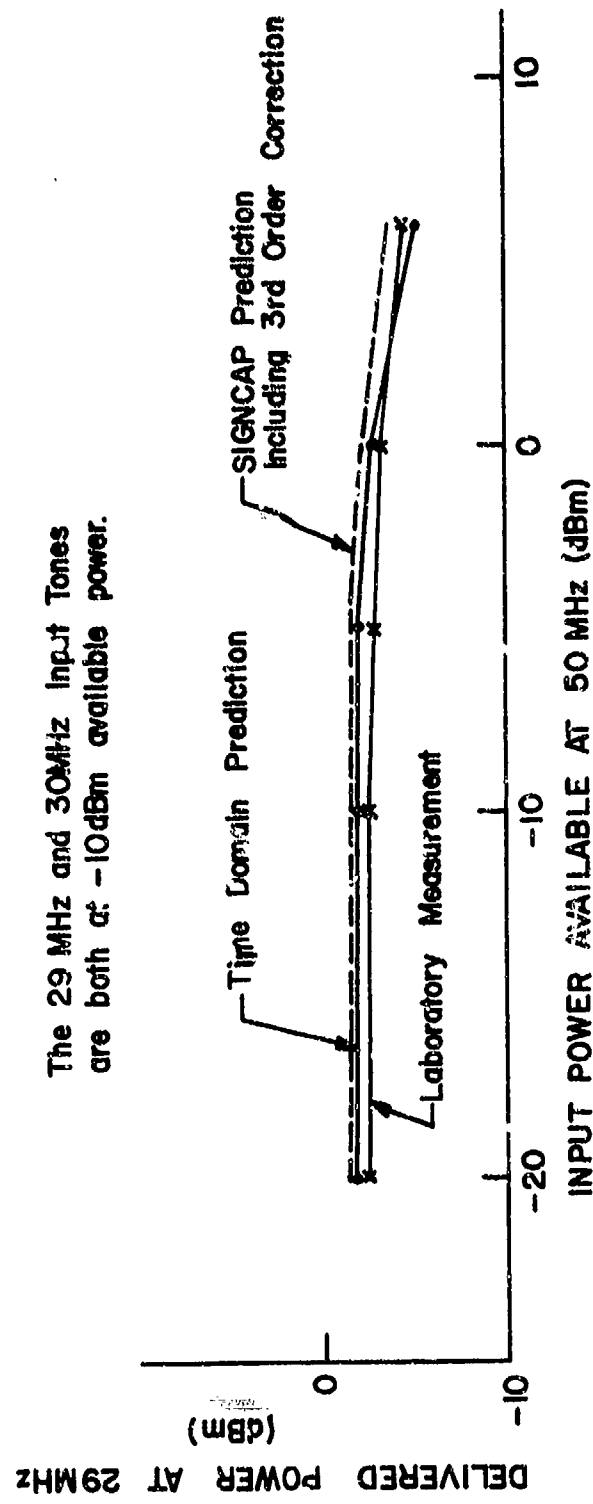


Fig. 6.34. Predicted and Measured First-Order Response at 29 MHz.

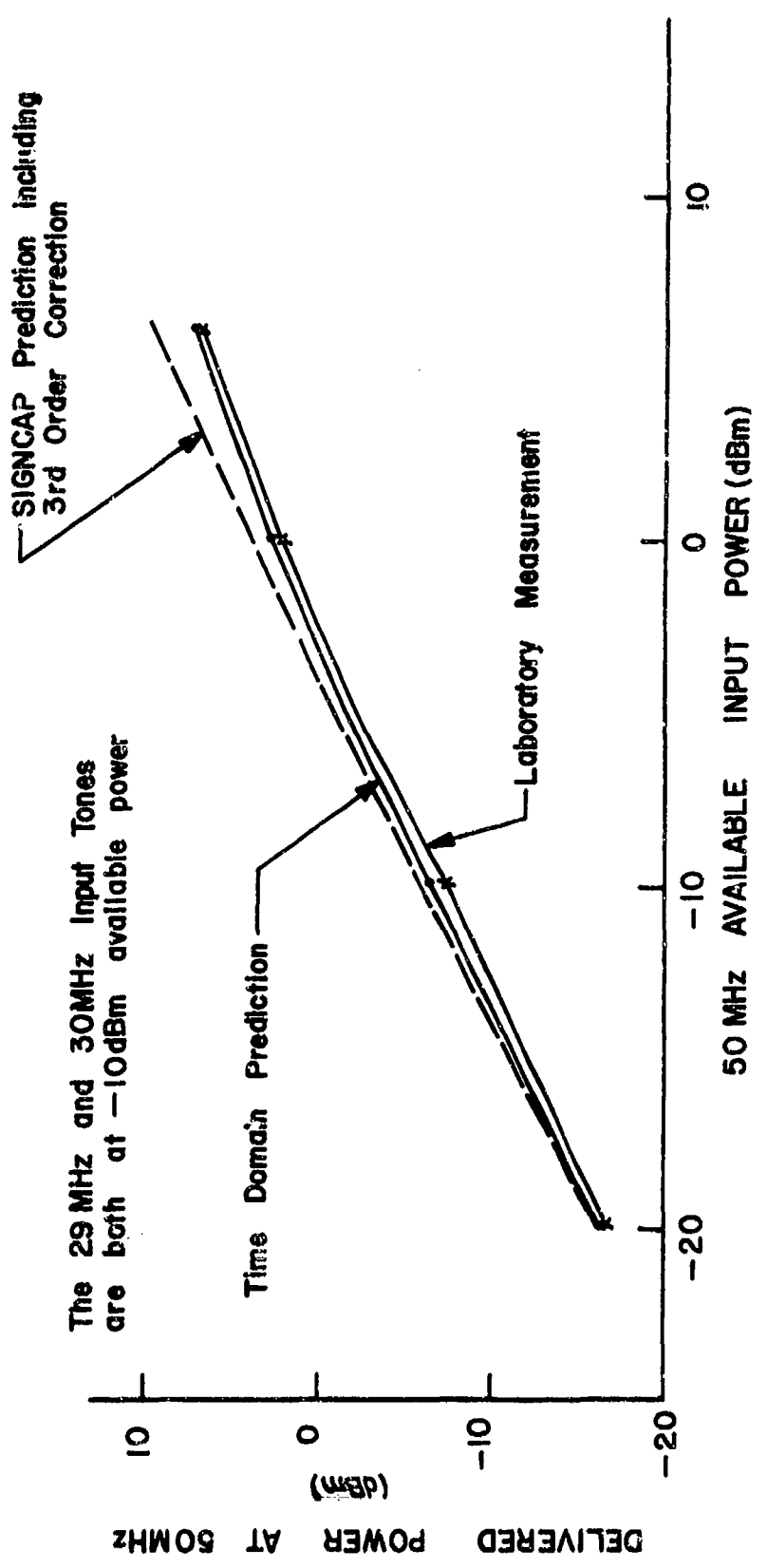


Fig. 6.35. Predicted and Measured First-Order Response at 50 MHz.

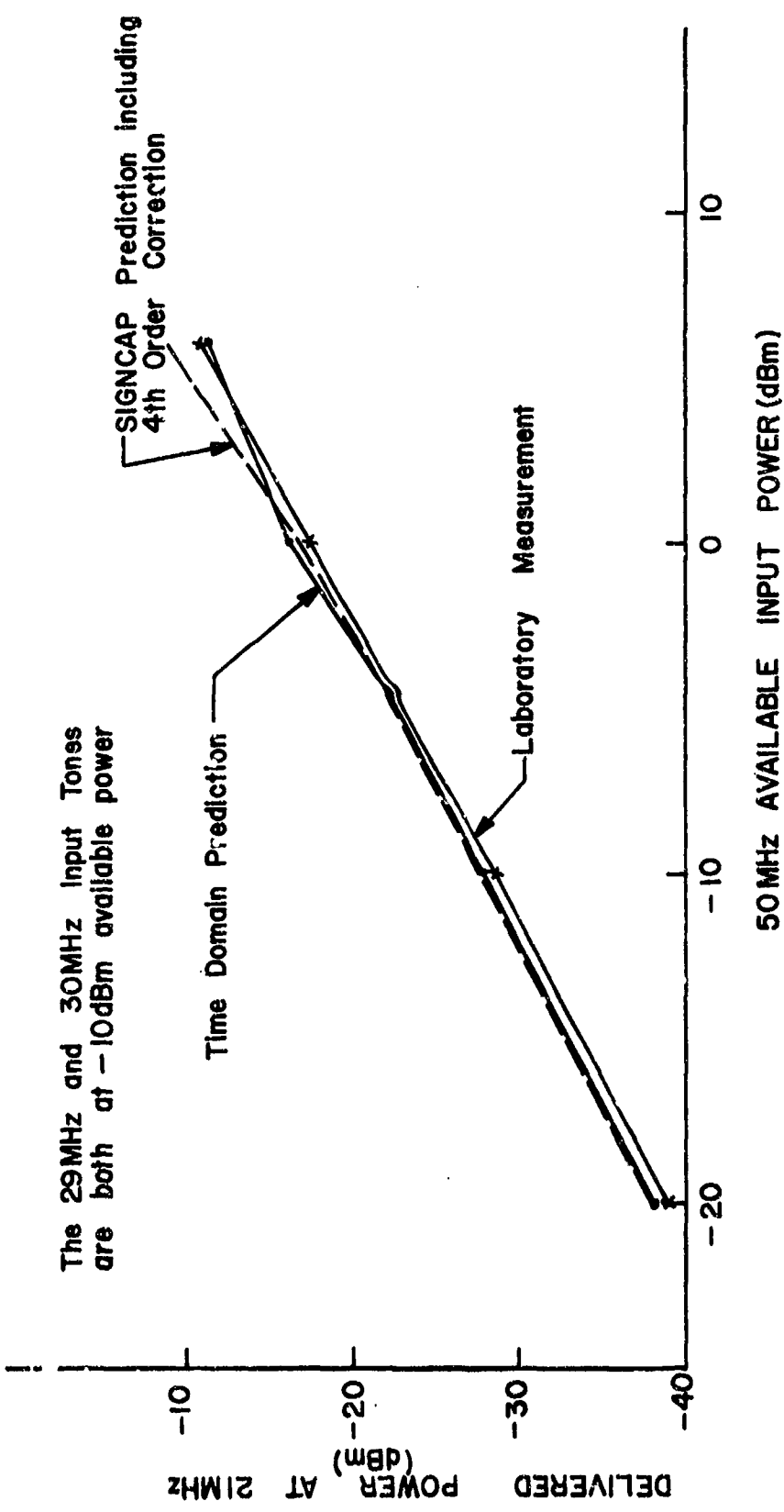


Fig. 6.36. Predicted and Measured Second-Order Response at 21 MHz as a Function of LO Power.

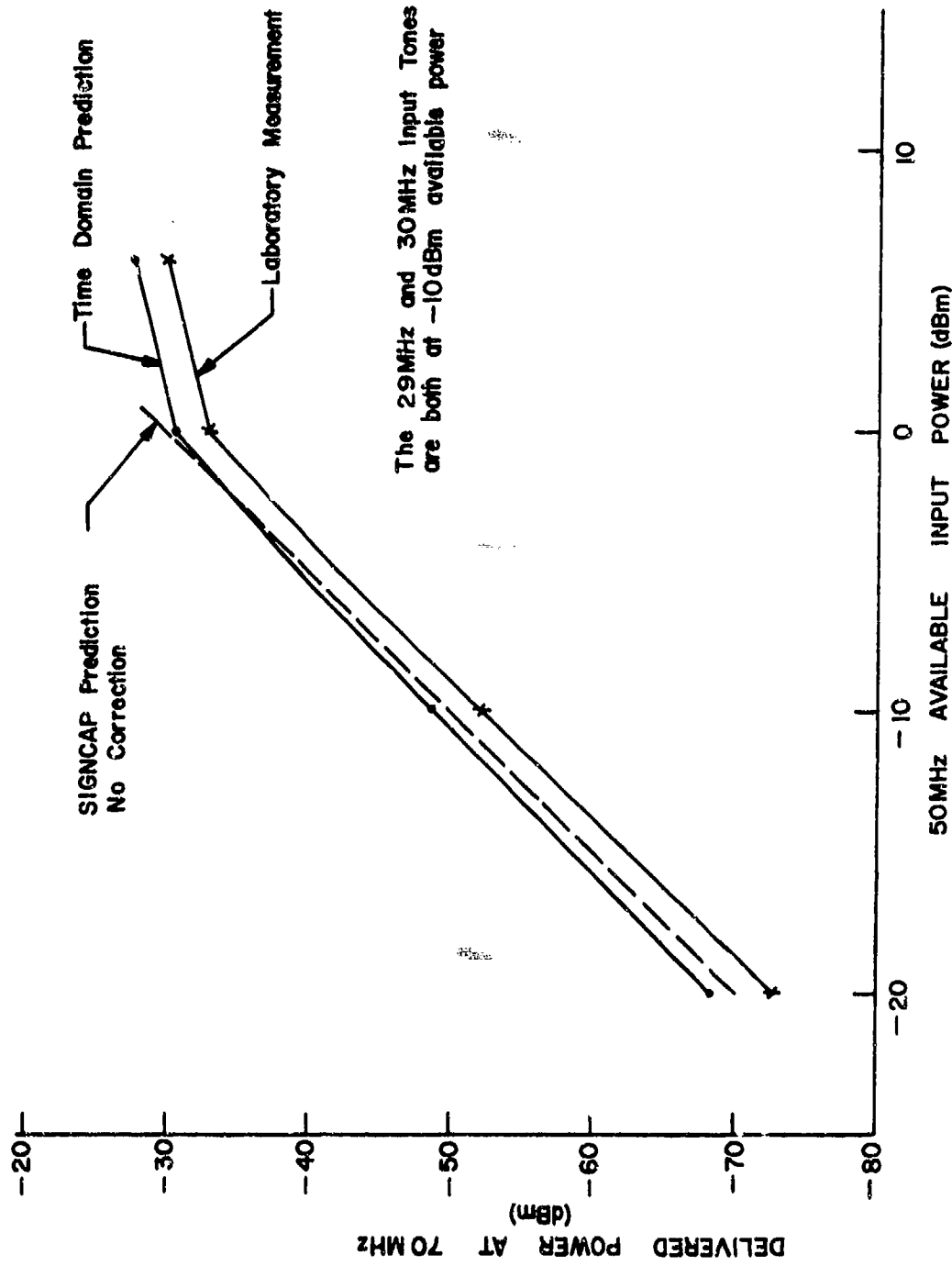


Fig. 6.37. Predicted and Measured Third-Order Response at 70 MHz as a Function of LO Power.

P_n^o is the n^{th} -order output power in dBm, $\sum P_{ai}$ is the sum of the input powers contributing to the n^{th} order output and P_n^o is the "0 dBm"-input output power characterizing the nonlinear system for the small-signal region. For both experimental data and time-domain solutions for particular output spectral responses, P_n^o can be estimated from

$$P_n^o = P_n - \sum_{i=1}^n P_{ai} \text{ dB}, \quad (6.73)$$

while for predictions of P_n^o from the small-signal nonlinear transfer function analysis we have the theoretical relationship

$$P_n^o = 20 \log_{10} |H_n| + C_n \text{ dB}, \quad (6.74)$$

where H_n is the nonlinear transfer function for the spectral component in question and C_n is given in Table 6.2.

For three-tone excitation at 29, 30, and 50 MHz, there are a great many output products from the 2N2950 test circuit.

The raw data for the time-domain derived values P_n^o are given in Table 6.13. The 0.00 entries in the table represent points which were edited out as being in error, primarily due to background noise in the computed spectrum of the time-domain waveform. In addition, it was determined from the computed results, all of which are not included in Table 6.13, that a 50 MHz local-oscillator level of -5 dBm with both signals at -10 dBm represents the limit of the mild excitation regime; stronger local-oscillator drives cause the transistor to be in a large-signal state.

Table 6.13

Time-Domain Predicted P_n^o Used to Obtain Results of Table 6.15

Input Freq.	Input Available Power (dBm)				
	50 MHz	-5	-10	-20	
29 30 MHz	-20	-10	-20	-10	-20
Output Freq. (MHz)	P_n^o (dBm)				
1	0.00	-4.70	-3.22	-4.98	-6.66
8	-14.21	-15.08	-13.82	-15.11	-14.83
9	-8.32	-9.17	-8.45	-9.25	0.00
10	0.00	-15.44	-15.23	-15.47	-15.15
19	-16.51	-16.13	0.00	-14.69	0.00
20	-8.00	-8.15	-8.46	-8.26	0.00
21	-7.72	-7.87	-8.17	-7.99	0.00
22	-15.30	-15.31	-13.29	-14.16	0.00
28	0.00	-9.34	-9.45	-9.35	-9.27
29	8.24	8.13	8.44	8.22	8.59
30	7.97	7.85	8.17	7.94	8.32
31	-9.66	-9.64	-9.76	-9.66	0.00
38	-16.80	-15.99	-14.75	-15.56	0.00
39	-14.20	-16.77	-13.03	-15.77	0.00
40	-24.78	-24.04	-20.41	0.00	0.00
41	-19.78	-21.37	-20.91	-20.38	0.00
49	-8.11	-8.15	-8.25	-8.16	-8.59
50	3.86	3.59	3.97	3.64	4.10
51	-8.21	-8.18	-8.52	-8.14	0.00
58	-8.41	-8.78	-9.20	-9.02	0.00
59	-2.74	-3.27	-3.46	-3.54	-4.72
60	-9.06	-9.28	-9.67	-9.51	0.00
70	-18.54	-19.07	-18.68	-18.48	-18.88
71	-18.36	-18.86	-18.52	-18.11	-18.93
78	-14.68	-15.02	-14.87	-14.11	0.00
79	-7.36	-7.29	-7.82	-7.42	0.00
80	-7.65	-7.51	-8.09	-7.65	0.00
81	0.00	-14.85	-14.57	-14.11	0.00
87	-18.85	-18.75	-17.82	-18.59	-18.83
88	0.00	-9.43	-8.59	-9.48	-10.32
89	-8.43	-9.73	-9.21	-9.73	-10.40
90	-18.02	-19.65	-19.84	-19.35	-19.99
100	-18.03	-17.57	-18.43	-17.61	-19.39
108	-13.20	-13.55	0.00	-13.56	-14.05
109	-7.16	-7.88	0.00	-7.89	-8.70
110	0.00	-14.18	0.00	-14.01	-14.49

In Table 6.14 we list in detail the calculation of P_n^o for each of the many output frequencies when Eq. (6.74) is utilized to determine P_n^o from an analysis using SIGNCAP to calculate the nonlinear transfer functions H_n . The component frequencies as well as the order of the product are noted in the table listings.

Finally, in Table 6.15 we bring together the results in Table 6.13 and 6.14 to obtain a comparison of P_n^o for each output product obtained by the time-domain solution and the nonlinear transfer function method.

The time-domain results were analyzed to obtain P_n^o for several different input power levels. Because the large number (five) of mild excitation conditions for which time-domain computation was performed, the mean and standard deviation σ of the resulting P_n^o were computed. The results are displayed in Table 6.15 where the one-sigma interval is bounded by mean-plus-sigma and mean-minus-sigma values. The maximum discrepancy between SIGNCAP predicted P_n^o and time-domain mean values is 2 dB, with many predictions agreeing to within less than 0.5 dB.

The laboratory measurement results were processed in the same fashion as the time-domain predictions to produce mean values for the nonlinear response P_n^o . The results are displayed in Table 6.16.

6.7.4 Distortion Dependence Upon Local Oscillator Level

We turn now from comparisons of small signal results to an interpretation of the data supplied by the time-domain solutions, particularly, for large LO drives. From the many time-domain computer

Table 6.14
'0 dBm' Input Distortion Power P^o from SIGNCAP

PRODUCT FREQ. (MHz)	COMPONENT FREQUENCIES (MHz)	H's FROM SIGNCAP ANALYSIS (dB)	CONSTANT C_n^+ (dB)	P^o_n (dB)	ORDER OF PRODUCT
1	30-29	-5.92	+2.04	-3.88	2
8	29+29-50	-10.17	-4.44	-14.61	3
9	29+30-50	-10.49	+1.58	-8.91	3
10	30+30-50	-10.49	-4.44	-14.93	3
19	29-30-30+50	-12.07	-2.38	-14.45	4
20	50-30	-11.13	+2.04	-9.09	2
21	50-29	-10.88	+2.04	-8.84	2
22	50+30-29-29	-11.87	-2.38	-14.25	4
28	29+29-30	-0.55	-4.44	-10.99	3
29	29	2.22	+6.	+8.22	1
30	30	1.94	+6.	+7.94	1
31	30+30-29	-6.86	-4.44	-11.30	3
38	29+29+30-50	-11.76	-2.38	-14.14	4
39	30+30+29-50	-12.02	-2.38	-14.40	4
40	50+50-30-30	-16.47	-8.4	-24.9	4
41	50+50-29-30	-16.22	-2.38	-18.60	4
49	29+50-30	-11.06	+1.58	-9.48	3
50	50	-2.38	+6.	+3.62	1
51	30+50-29	-11.08	+1.58	-9.50	3
58	29+29	-6.85	-4.	-10.85	2
59	29+30	-7.13	+2.04	-5.09	2
60	30+30	-7.41	-4.	-11.41	2
70	50+50-30	-15.58	-4.44	-20.02	3
71	50+50-29	-15.32	-4.44	-19.76	3
78	50+29+29-30	-12.18	-2.38	-14.56	4
79	50+29	-11.52	+2.04	-9.48	2
80	50+30	-11.80	+2.04	-9.76	2
81	50+30+30-29	-12.45	-2.38	-14.83	4
87	29+29+29	-6.52	-4.	-20.52	3
88	29+29+30	-6.81	-4.44	-11.25	3
89	30+30+29	-7.09	-4.44	-11.53	3
90	30+30+30	-7.37	-4.	-21.37	3
100	50+50	-16.23	-4.	-20.23	2
108	29+29+50	-11.24	-4.44	-15.68	3
109	30+29+50	-11.53	+1.58	-9.95	3
110	30+30+50	-11.81	-4.44	-16.25	3
139	50+30+30+29	-13.06	-2.38	-15.44	4

[†]This constant modification factor (C_n^+) is based on a 50 ohm system. (See Table 6.2).

Table 6.15

Comparison of Time-Domain and SIGNCAP Predictions

FREQUENCY (MHZ)	P_n^o from Time Domain Analysis (dBm)	ONE-SIGMA INTERVAL	MEAN	P_n^o FROM SIGNCAP ANALYSIS (dBm)
1	(-6.11 , -3.67)	-4.89	-3.88	
8	(-15.12 , -14.10)	-14.61	-14.61	
9	(-9.21 , -8.38)	-8.80	-8.91	
10	(-15.46 , -15.19)	-15.32	-14.93	
19	(-16.56 , -14.99)	-15.78	-14.45	
20	(-8.39 , -8.05)	-8.22	-9.09	
21	(-8.10 , -7.77)	-7.94	-8.84	
22	(-15.36 , -13.67)	-14.51	-14.25	
28	(-9.42 , -9.29)	-9.35	-10.99	
29	(8.16 , 8.49)	8.32	8.22	
30	(7.88 , 8.22)	8.05	7.94	
31	(-9.73 , -9.63)	-9.68	-11.30	
38	(-16.52 , -15.03)	-15.77	-14.14	
39	(-16.38 , -13.51)	-14.94	-14.40	
40	(-24.99 , -21.17)	-23.08	-24.90	
41	(-21.20 , -20.02)	-20.61	-18.60	
49	(-8.43 , -8.08)	-8.25	-9.48	
50	(3.64 , 4.03)	3.83	3.62	
51	(-8.41 , -8.11)	-8.26	-9.50	
58	(-9.15 , -8.56)	-8.85	-10.85	
59	(-4.20 , -2.90)	-3.55	-5.09	
60	(-9.61 , -9.15)	-9.38	-11.41	
70	(-18.95 , -18.51)	-18.73	-20.02	
71	(-18.86 , -18.25)	-18.56	-19.76	
78	(-15.02 , -14.32)	-14.67	-14.56	
79	(-7.68 , -7.27)	-7.47	-9.48	
80	(-7.94 , -7.51)	-7.73	-9.76	
81	(-14.82 , -14.20)	-14.51	-14.83	
87	(-18.95 , -18.18)	-18.57	-20.52	
88	(-10.07 , -8.84)	-9.45	-11.25	
89	(-10.15 , -8.85)	-9.50	-11.53	
90	(-20.08 , -18.66)	-19.37	-21.37	
100	(-18.88 , -17.54)	-18.21	-20.23	
108	(-13.89 , -13.29)	-13.59	-15.68	
109	(-8.45 , -7.36)	-7.91	-9.95	
110	(-14.43 , -14.03)	-14.23	-16.25	

Table 6.16

Measured P_n^o and SIGNCAP Predictions

OUTPUT FREQUENCY (MHZ)	MEASUREMENT DERIVED P_n^o (dBm)	SIGNCAP
		Derived P_n^o (dBm)
1	(-1.60 , -1.20)	-3.88
20	(-9.79 , -8.73)	-9.09
21	(-9.79 , -8.73)	-8.84
22	(-21.50 , -21.50)	-14.25
29	(7.60 , 7.84)	8.22
30	(7.33 , 7.63)	7.94
50	(2.75 , 3.37)	3.62
70	(-23.63 , -22.37)	-20.02

runs which were done, twenty cases were selected for analysis. Because in each case there was available the complete output spectrum (dc to 512 MHz in steps of 1 MHz) it was possible to select only those distortion products, up to fourth-order, which were present to a significant degree in each of the twenty cases. It must be realized that for low enough levels some of the third and fourth-order products were swamped by the background computational noise, and that for the higher signal levels there would be significant fifth and higher-order products. Nevertheless, in order to avoid undue complexity it was decided to consider only products up to fourth-order, and limited to 110 MHz (products above 110 MHz are chiefly related to harmonics of the 50 MHz LO and hence appear mostly at higher LO levels.

The raw numbers, culled from the time-domain computed spectra, are presented in Table 6.17. Each of these predictions of a distortion product level is readily converted to P_n^O with the result given in Table 6.18. By analysis of the behavior of P_n^O we can appreciate the role of the LO drive level.

In order to better display the results listed in Table 6.18, they have been grouped according to the order of the distortion product and plotted as a function of LO level. We have selected the results for 29 and 30 MHz at -10 dBm, used Eq. (6.73) to extrapolate the data to equivalent 0 dBm input signal levels for computing P_n^O , and plotted P_n^O as a function of the 50 MHz level in Figures 6.38, 6.39 and 6.40. First we note that the apparently anomalous behavior of the 90 MHz output distortion P_n^O in Fig. 6.39 is due to a strong fifth-order distortion product composed as (50+50+50-30-30) and due to the strong LO drive. In fact, in the computed spectrum for 50 MHz at +5 dBm, and 29 and 30 MHz at -10 dBm, there were equally strong fifth-order products at

Table 6.17

Time Domain Predictions of Output Distortion Power

Input Freq. MHz	Input Available Power (dBm)									
	+6		0		-5		-10		-20	
29 MHz	-10	-20	-10	-20	-10	-20	-10	-20	-10	-20
Output Freq. (MHz)	Output Delivered Power (dBm)									
1	-26.61	-42.21	-21.97	-43.21	-24.11	-42.69	-24.70	-43.22	-24.98	-46.64
8	-47.65	-64.36	-37.15	-55.18	-40.21	-59.21	-45.08	-63.82	-55.11	-74.83
9	-41.70	-61.67	-30.73	-49.32	-34.30	-53.32	-39.17	-58.45	-49.25	-71.38
10	-48.82	-62.49	-38.12	-54.77	-40.84	-59.25	-45.44	-65.23	-55.47	-75.15
19	-49.40	-66.59	-56.26	-77.25	-53.65	-81.51	-56.13	-90.15	-64.69	-85.21
20	-11.62	-21.31	-16.66	-27.74	-22.86	-33.01	-28.15	-38.40	-38.26	-49.74
21	-11.33	-21.04	-16.37	-27.45	-22.57	-32.72	-27.87	-34.17	-37.94	-49.44
22	-48.60	-71.49	-59.21	-73.90	-52.40	-80.30	-56.31	-83.29	-64.16	-82.68
28	-60.31	-64.21	-44.33	-70.62	-39.56	-68.57	-39.34	-69.45	-39.35	-69.27
29	-4.94	-14.85	-2.	-12.36	-2.08	-11.76	-1.87	-11.56	-1.78	-11.41
30	-5.21	-15.12	-3.42	-12.64	-2.36	-12.03	-2.15	-11.83	-2.06	-11.68
31	-59.83	-79.22	-45.06	-71.00	-39.95	-69.66	-39.64	-69.76	-39.63	-70.53
38	-47.56	-67.95	-60.92	-79.19	-53.43	-81.80	-56.99	-84.75	-65.56	-86.52
39	-48.57	-66.46	-56.38	-86.38	-54.68	-79.20	-56.71	-83.03	-65.77	-90.63
40	-39.16	-60.18	-61.78	-65.89	-59.62	-74.78	-64.04	-80.41	-75.87	-89.44
41	-32.91	-52.60	-60.51	-60.94	-53.30	-69.78	-61.37	-80.91	-80.38	-84.78
49	-39.48	-52.51	-29.99	-47.87	-33.29	-53.11	-38.15	-58.25	-48.16	-68.59
50	7.17	7.41	2.93	3.54	-1.54	-1.14	-6.41	-6.03	-16.36	-15.90
51	-39.35	-54.00	-30.05	-48.17	-33.29	-53.21	-38.18	-56.52	-48.14	-69.26
58	-31.25	-51.23	-27.53	-47.49	-28.34	-48.41	-28.78	-49.20	-29.02	-50.46
59	-25.60	-45.45	-21.56	-41.69	-22.71	-42.74	-23.27	-43.46	-23.54	-44.72
60	-31.62	-52.47	-28.10	-48.20	-28.87	-49.06	-29.28	-49.67	-29.51	-51.01
70	-27.88	-35.72	-30.60	-38.74	-39.38	-48.54	-49.07	-58.68	-68.48	-78.81
71	-27.63	-35.52	-30.24	-38.50	-39.03	-48.36	-48.86	-58.82	-68.11	-78.93
78	-47.82	-67.44	-57.50	-85.57	-52.04	-79.68	-51.02	-84.87	-61.11	-89.51
79	-10.68	-20.39	-15.90	-26.83	-21.97	-32.36	-27.29	-37.82	-37.42	-48.34
80	-10.95	-20.65	-16.16	-27.11	-22.22	-32.65	-27.51	-38.09	-37.65	-49.19
81	-47.77	-78.89	-60.51	-77.72	-52.11	-76.70	-54.85	-84.57	-64.11	-84.61
87	-65.02	-76.27	-54.86	-79.05	-49.63	-78.85	-48.75	-77.82	-48.59	-78.43
88	-56.29	-72.87	-44.39	-70.67	-39.77	-67.35	-39.43	-68.59	-39.48	-70.32
89	-59.78	-72.96	-44.80	-70.85	-40.11	-68.43	-39.73	-69.21	-39.73	-70.40
90	-43.84	-59.02	-55.33	-84.60	-50.92	-78.02	-49.65	-79.84	-49.38	-79.94
100	-4.36	-3.83	-16.41	-17.68	-27.36	-28.03	-37.57	-38.43	-57.61	-59.59
108	-45.68	-64.84	-35.71	-53.65	-38.87	-58.20	-43.51	NA	-63.56	-74.05
109	-40.09	-62.21	-29.31	-47.75	-32.95	-52.16	-37.81	NA	-47.89	-68.70
110	-45.48	-61.49	-36.38	-54.51	-39.44	-57.79	-44.18	NA	-54.01	-74.49

Entries in table are output level, in dBm, for 50 MHz L.O. and tones at 29 and 30 MHz. Input levels are in dBm available. Note that 29 and 30 MHz are always at the same level.

Table 6.18
Time Domain Prediction of P_n^o

Input Freq. (MHz)	Input Available Power (dBm)									
	+6	0	-5	-10	-20	-10	-20	-10	-20	-20
50 MHz	-10	-20	-10	-20	-10	-20	-10	-20	-10	-20
29 and 30 MHz	-10	-20	-10	-20	-10	-20	-10	-20	-10	-20
Output Freq. (MHz)	P_n^o dB									
1	-6.61	-2.21	-1.97	-3.21	-4.11	-2.69	-4.70	-3.22	-4.98	-6.66
8	-33.65	-30.36	-17.45	-15.18	-15.21	-14.21	-15.08	-13.82	-15.11	-14.83
9	-27.70	-27.67	-10.73	-9.32	-9.30	-8.32	-9.17	-8.45	-9.25	-11.38
10	-34.82	-28.49	-18.12	-10.77	-15.84	-14.25	-15.44	-15.23	-15.47	-15.15
19	-25.40	-12.59	-26.26	-17.25	-18.65	-16.51	-16.13	-20.15	-14.69	-5.21
20	-7.62	-7.31	-6.66	-7.74	-7.86	-8.00	-8.15	-8.46	-8.26	-9.74
21	-7.33	-7.04	-6.37	-7.45	-7.57	-7.72	-7.87	-8.17	-7.94	-9.44
22	-24.60	-17.49	-29.21	-13.90	-17.40	-15.30	-15.31	-13.29	-14.16	-2.68
28	-30.31	-4.21	-14.33	-10.62	-9.56	-8.57	-9.34	-9.45	-9.35	-9.27
29	5.06	5.15	7.16	7.64	7.92	8.24	8.13	8.44	8.22	8.59
30	4.79	4.88	6.88	7.36	7.64	7.97	7.85	8.17	7.94	8.32
31	-29.83	-19.22	-15.06	-11.00	-9.95	-9.66	-9.64	-9.76	-9.66	-10.53
38	-23.56	-13.95	-30.92	-19.19	-18.43	-16.80	-15.99	-14.75	-15.56	-6.52
39	-24.57	-12.46	-26.38	-26.38	-19.68	-14.20	-16.77	-13.03	-15.77	-10.68
40	-31.16	-32.18	-4.78	-25.49	-29.62	-24.78	-24.04	-20.41	-15.87	-9.44
41	-24.91	-24.60	-40.51	-20.90	-23.30	-19.78	-21.37	-20.91	-20.38	-4.78
49	-25.48	-18.51	-9.09	-7.87	-8.29	-8.11	-8.15	-8.25	-8.16	-8.59
50	1.17	1.41	2.93	3.54	3.46	3.86	3.59	3.97	3.64	4.10
51	-25.35	-20.00	-10.05	-8.17	-8.29	-8.21	-8.18	-8.52	-8.14	-9.26
58	-11.25	-11.23	-7.53	-7.49	-8.34	-8.41	-8.78	-9.20	-9.02	-10.46
59	-5.60	-5.48	-1.56	-1.69	-2.71	-2.74	-3.27	-3.46	-3.54	-4.72
60	-11.62	-12.47	-8.10	-8.20	-8.87	-9.06	-9.28	-9.67	-9.51	-11.01
70	-29.88	-27.72	-20.60	-18.74	-19.38	-18.54	-19.07	-18.68	-18.48	-18.48
71	-29.63	-27.52	-20.24	-18.50	-19.03	-18.36	-18.86	-18.52	-18.11	-18.93
78	-23.82	-33.44	-27.80	-25.57	-17.04	-14.68	-15.02	-14.87	-14.11	-9.51
79	-6.68	-6.39	-6.90	-6.83	-6.97	-7.34	-7.29	-7.82	-7.42	-8.94
80	-6.95	-6.65	-6.16	-7.11	-7.22	-7.65	-7.81	-8.09	-7.65	-9.19
81	-23.77	-24.89	-30.61	-17.72	-17.11	-11.70	-14.85	-14.57	-14.11	-8.61
87	-35.02	-16.27	-21.46	-19.05	-19.63	-18.45	-18.75	-17.82	-18.59	-18.83
88	-26.29	-12.67	-14.39	-10.67	-9.77	-7.34	-9.43	-9.49	-9.48	-10.32
89	-29.78	-12.96	-14.80	-10.85	-10.11	-8.43	-9.73	-9.21	-9.73	-10.40
90	-13.84	0.98	-25.33	-24.60	-20.92	-18.02	-19.65	-19.84	-19.35	-19.94
100	-16.36	-15.83	-16.41	-17.68	-17.36	-18.03	-17.57	-18.43	-17.61	-19.39
108	-31.68	-30.84	-15.71	-13.65	-13.87	-13.20	-13.51	NA	-13.56	-14.05
109	-26.09	-28.21	-9.31	-7.75	-7.95	-7.14	-7.81	NA	-7.89	-8.70
110	-31.48	-27.49	-16.36	-14.51	-14.44	-12.79	-14.18	NA	-14.01	-14.40

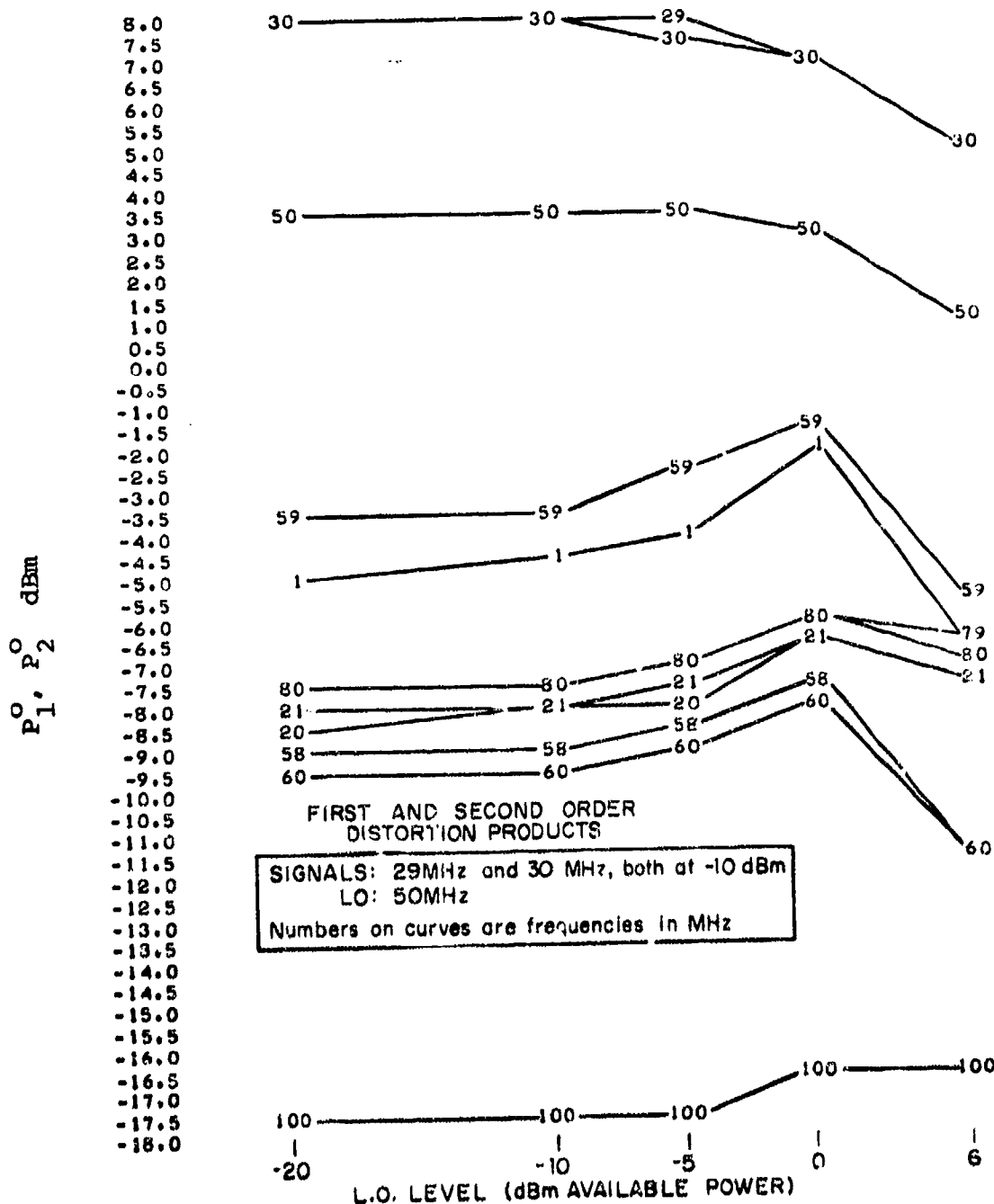


Fig. 6.38. First and Second-Order Outputs P_1^o , P_2^o as a Function of L.O. Level.

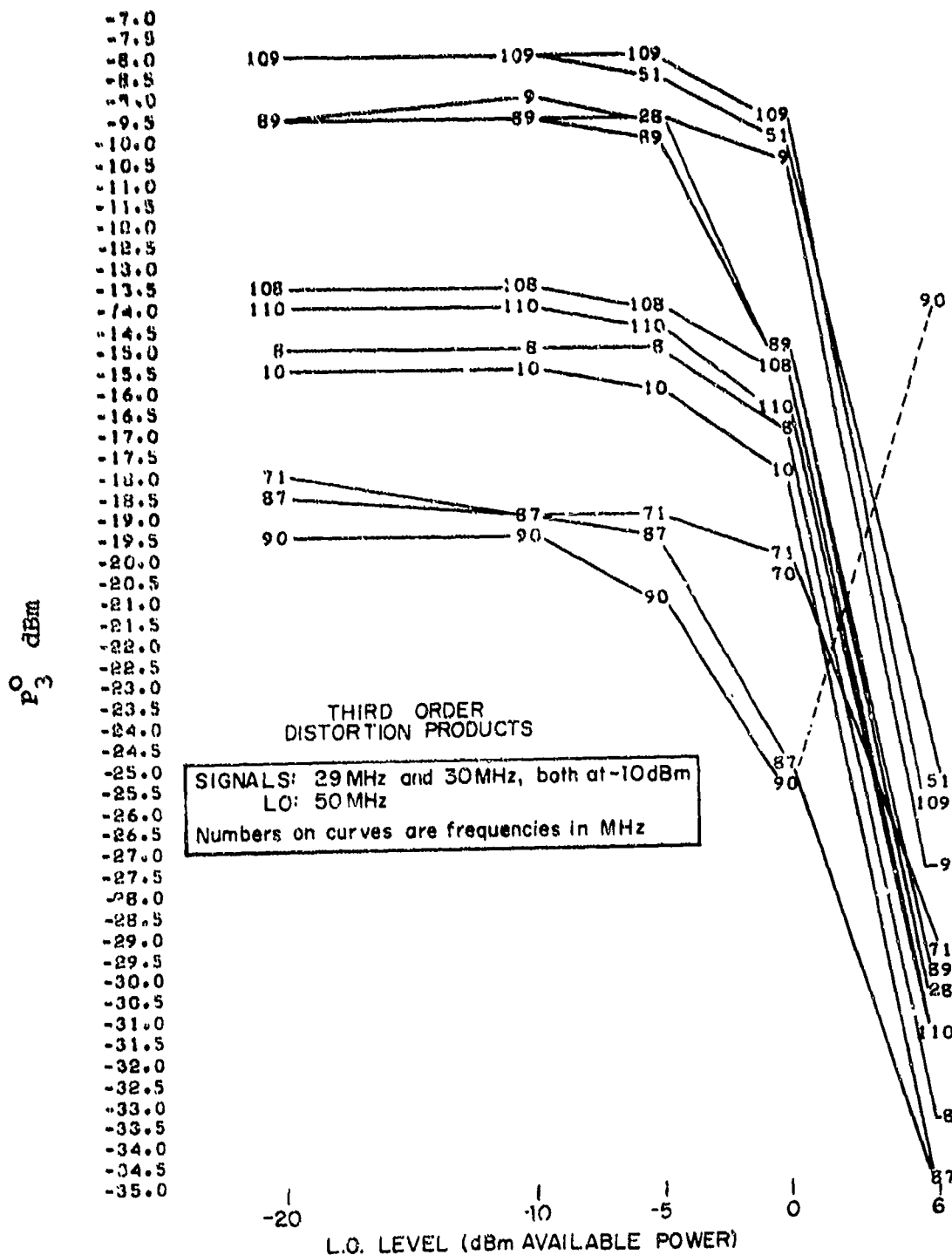


Fig. 6.39. Third-Order Output P_3^o as a Function of L.O. Level

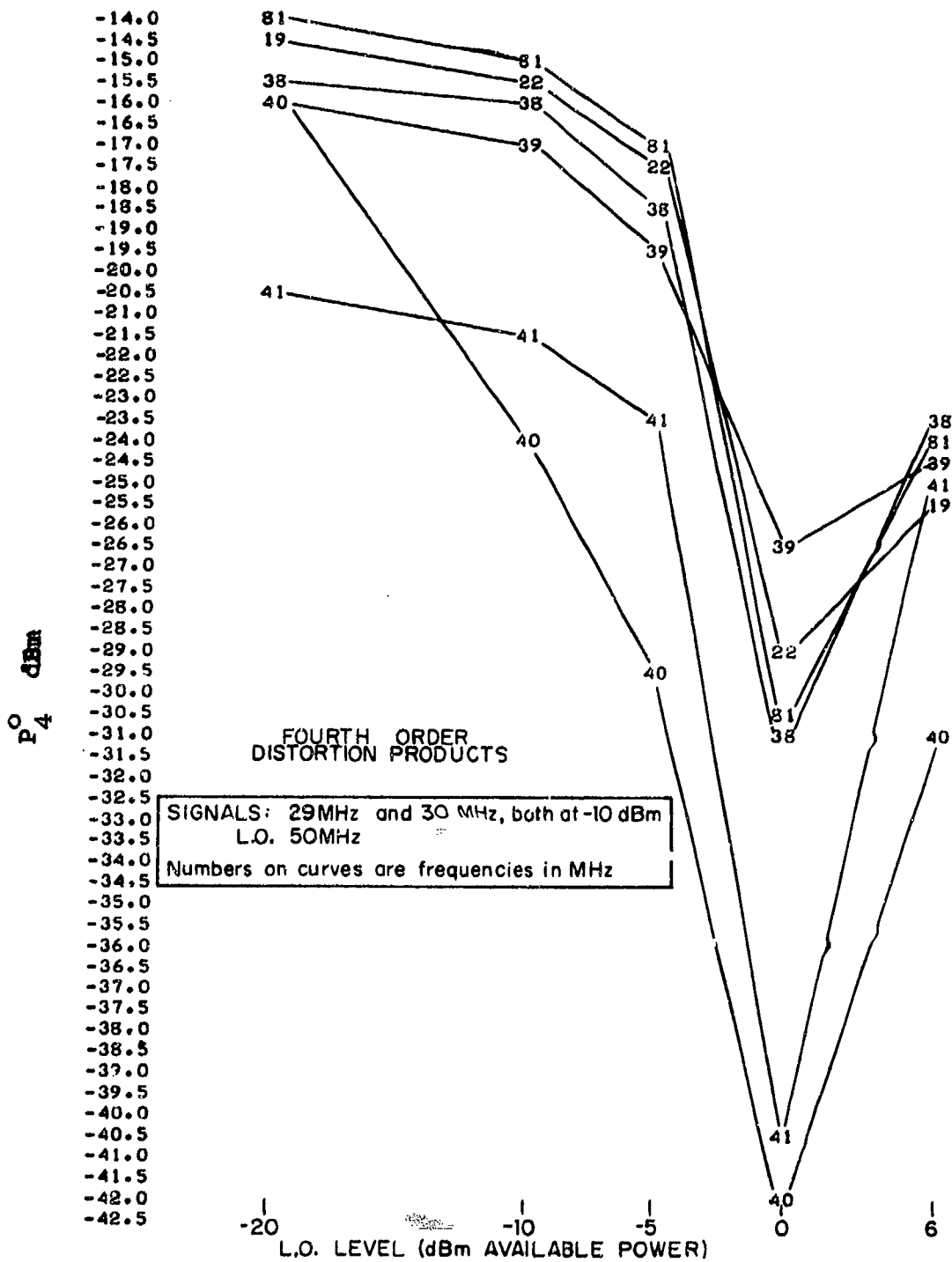


Fig. 6.40.. Fourth Order Output P_4^O as a Function of L.O. Level

$91 = 50+50+50-30-29$ and $92 = 50+50+50-29-29$ MHz. Some of the observations relative to Figs. 6.38 to 6.40 as the local-oscillator level is increased are:

1. There is an expected gain compression for first order.
2. The second-order curves show expansion followed by compression.
3. There is a uniform and large decrease for all third-order products, and a large decrease for fourth-order followed by a significant increase.
4. The grouping of products is related to the frequency sets, i.e., $(f_1 \pm f_2)$ and $(2f_1 \text{ or } 2f_2)$, constituting different groups

CHAPTER 7

COMMUNICATIONS RECEIVER APPLICATIONS

The nonlinear transfer function theory and the device modeling of the preceding chapters allow the nonlinear modeling of complete communications receivers. In this chapter two receivers are modeled. The first receiver is a solid-state single-conversion VHF receiver. The second receiver is a triple-conversion vacuum tube HF receiver.

7.1 Solid-State VHF Receiver

The block diagram of the receiver is shown in Figure 7.1. Figure 7.2 shows a detailed block diagram of the tuning head, which includes the RF amplifier, mixer, local-oscillator, and 21.4 MHz preamplifier. The nominal tuning head characteristics are listed in Table 7.1.

In signal-flow order, the tuner contains four transistors, i.e., Q1, Q2, Q4, and Q3. Transistors Q1 and Q2 provide RF amplification while Q4 and Q3 form a cascode mixer-amplifier. Q5 is the local oscillator, the frequency of which is above the signal frequency. Transistors Q3 and Q4 are the same transistors used in the two-stage amplifier of Section 6.5. The schematic of the tuner is shown in Figure 7.3. There are five interstage networks in the signal path. Interstage network 1, from the RF input to the base of Q1, is a mechanically tunable double-tuned RF preselector network. Interstage network 2, between Q1 and Q2, is a fixed low-pass network which cuts off at about 100 MHz. It serves to further reject high frequency interference. Interstage network 3, between Q2 and Q4, is again a mechanically

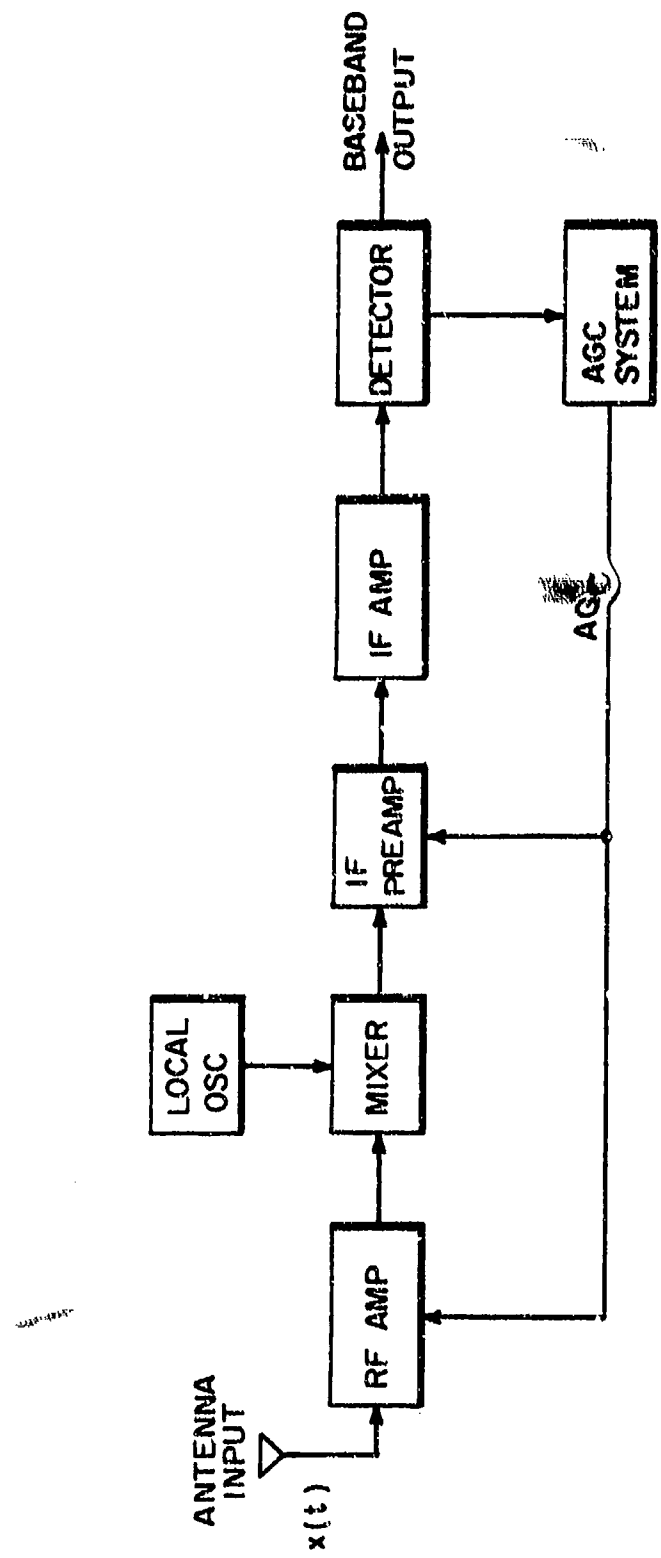


Fig. 7.1 Simplified Block Diagram of the VHF Communications Receiver.

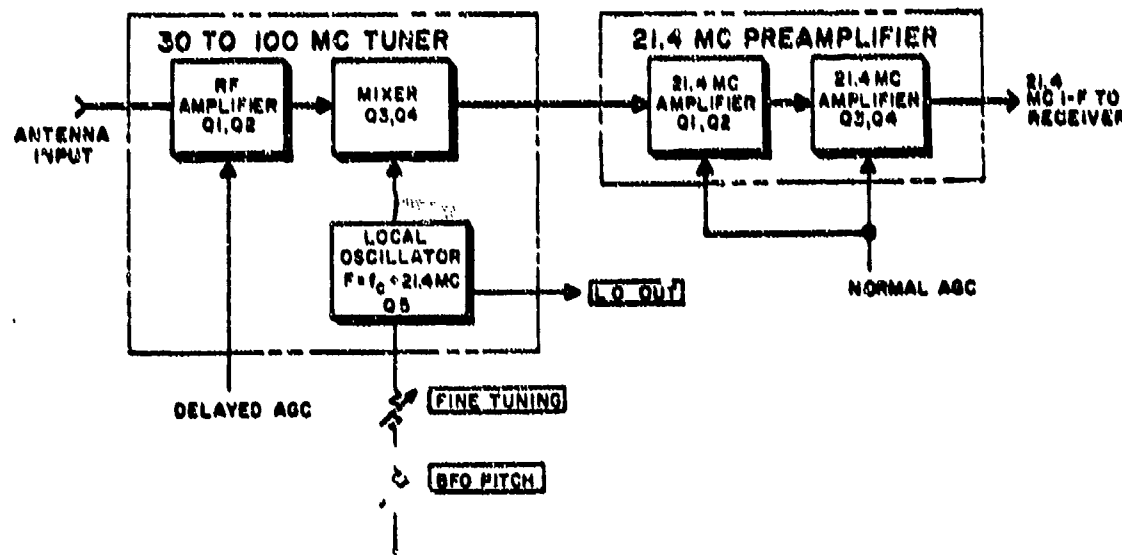


Fig. 7.2 Tuning Head Block Diagram.

UNLESS OTHERWISE SPECIFIED
ALL RESISTOR VALUES ARE IN OHMS, 5% MAX
* TRANSISTOR CASE OR DS MUST BE ISOLATED FROM GROOVE BY
LEADS NEAR SAWTOOTH TURNING ON THE TRANSISTOR CASE.

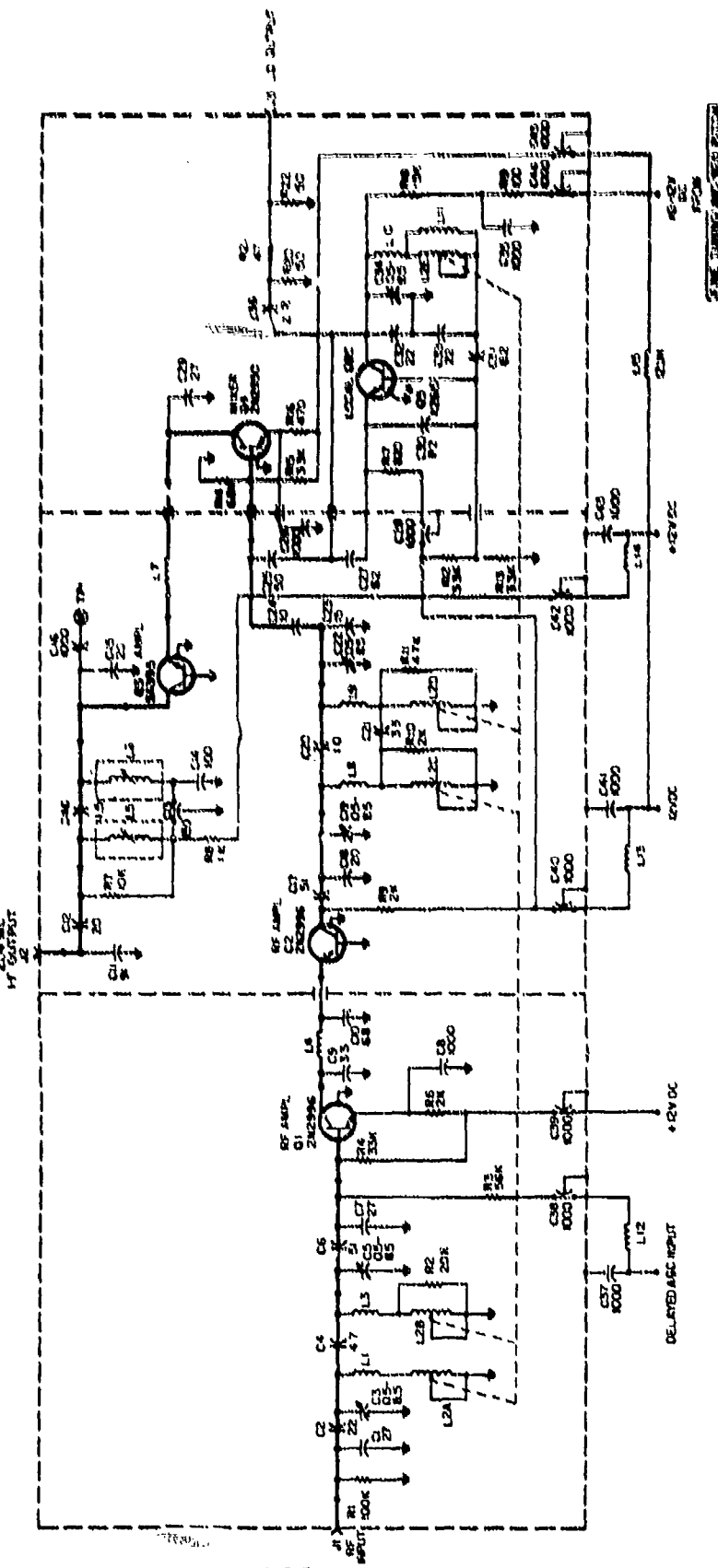


Fig. 7.3 30-100 MHz RF Tuning Head

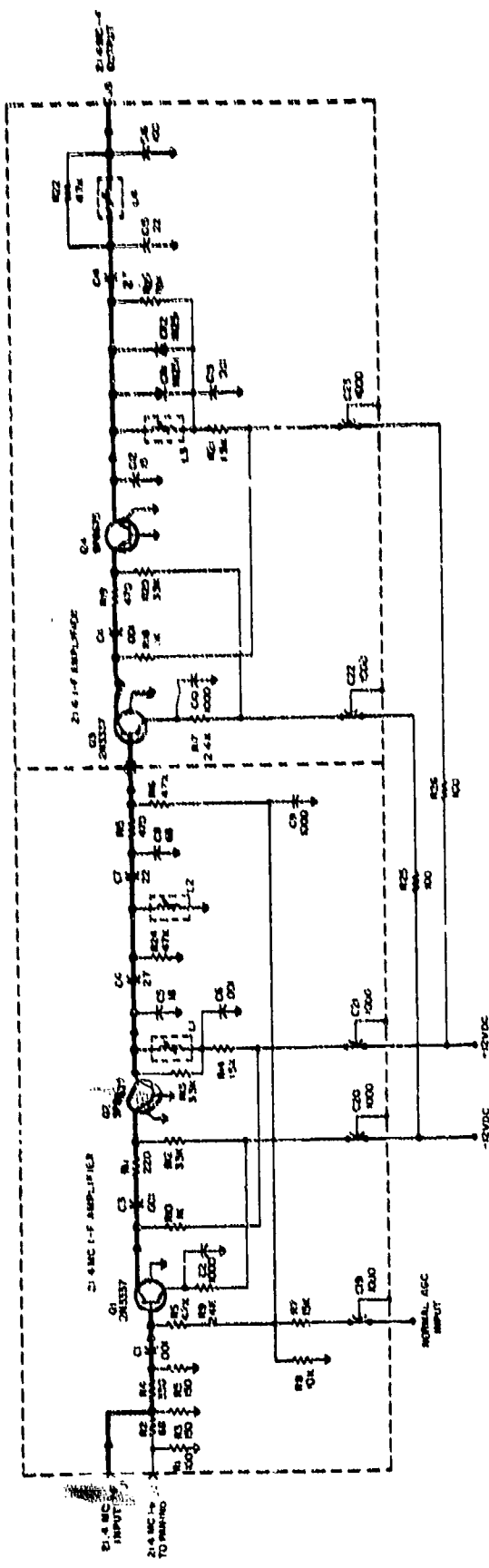
TABLE 7.1
Solid State Receiver Tuning Head Characteristics

Frequency Coverage	30-100 Mc
Noise Figure	4.5 dB maximum (30 to 90 Mc) 5.5 dB maximum (90 to 100 Mc)
Intermediate Frequency	21.4 Mc
IF Rejection	56 dB minimum below 40 Mc 60 dB minimum above 40 Mc
Image Rejection	60 dB minimum

adjustable double-tuned RF filter. This network, along with interstage 1, provides the principal tunable selectivity over the 30 to 100 MHz band. Since mixing is accomplished in Q4, the desired output of Q4 is at the 21.4 MHz IF. Thus interstage network 4, between Q4 and Q3, is a low-pass network which cuts off near the intermediate frequency. Since the local-oscillator is 21.4 MHz above the desired signal, this filter also decreases local-oscillator feedthrough into subsequent stages. The last network, interstage number 5, is between the output of Q3 and the IF output. It is a fixed-frequency double-tuned circuit tuned to the 21.4 MHz IF.

The schematic diagram of the preamplifier is shown in Fig. 7.4. The amplifier contains four transistors. The input network provides a resistive broadband load to the RF tuner output. Broadband RC networks are also used to couple the CE and CB stages of the two cascode amplifiers, involving Q1, Q2, and Q3, Q4. Frequency selectivity is provided by the tuned circuits between Q2 and Q3, and at the output of Q4.

ALL RESISTOR VALUES ARE IN OHMS.
ALL CAPACITOR VALUES ARE IN MICRO FARADS.



21.4 MC PREAMPLIFIER PR-21.4
Fig. 7.4 Schematic Diagram of the 21.4 MHz Preamplifier

There are two diodes, CR1 and CR2, in the collector circuit of Q4. These diodes form a symmetric clipper, and prevent overdriving of subsequent stages due to large signals. The diodes are unbiased and the diode current, therefore, is extremely small. Unless the voltage across the diodes is many times kT/q , they can be omitted. This has been confirmed experimentally.

The preamplifier is physically located on the RF tuner chassis, and has, as an input signal, the output of the mixer. Its output, in turn, is the input to the IF amplifier. It will be seen in a later analysis of the IF amplifier that the input network to the IF amplifier is a resistive network, similar to that at the input to the preamplifier.

The preamplifier has AGC applied to two common-emitter stages, Q1 and Q3. The AGC voltage is developed from the AM detector output, and is increasingly positive for a signal of increasing power. Since Q1 and Q3 are NPN transistors, the AGC is a forward-acting AGC. The AGC is not applied to the two common base stages, Q2 and Q4. They are DC decoupled from the common-emitter stages by capacitors C3 and C11.

The IF amplifier which was used in the receiver had a 500 KHz bandwidth and 21.4 MHz center frequency. A block diagram of the IF amplifier circuit module is shown in Fig. 7.5. In addition to the two-stage IF amplifier, the AM detector and FM limiter-discriminator are contained on the module. The schematic of the amplifier is shown in Fig. 7.6. The entire IF amplifier is fabricated on one printed circuit module. The module contains ten transistors, all of them being

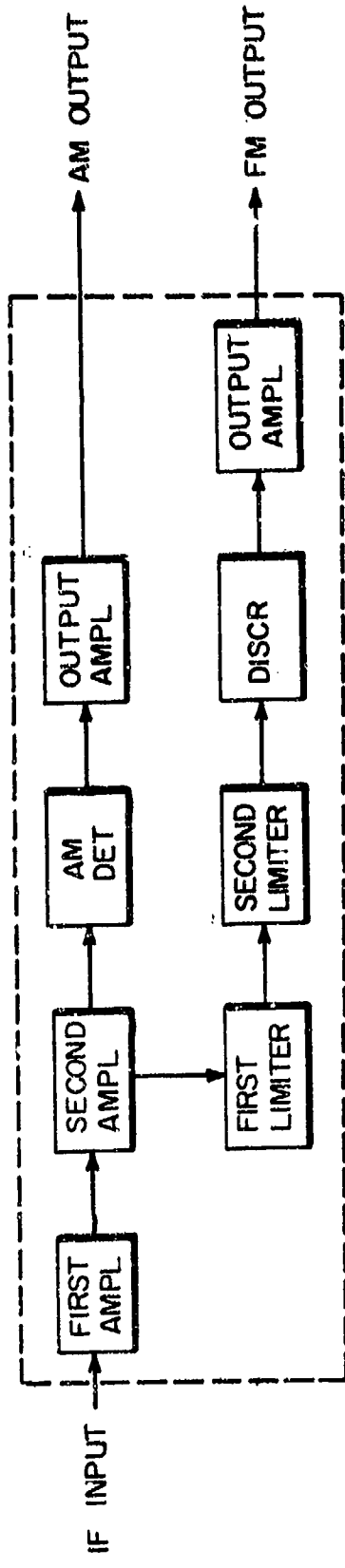


Fig. 7.5 Block Diagram of Wideband IF Amplifier and Detectors.

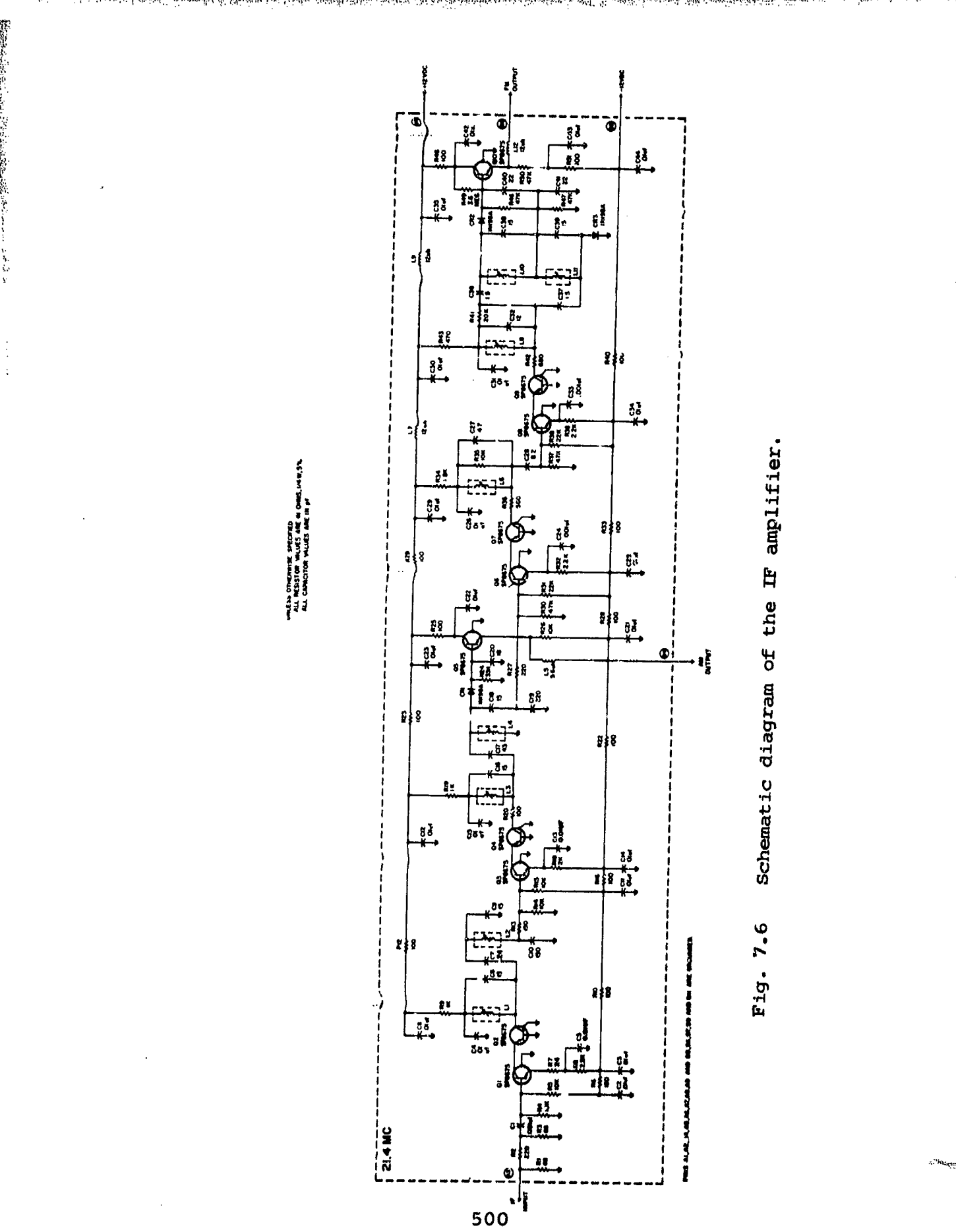


Fig. 7.6 Schematic diagram of the IF amplifier.

specially designated by the manufacturer as SP8675. Measurements indicate them to be medium-gain, medium-frequency transistors with betas of about 40, and alpha-cutoff frequencies of about 100 MHz. Transistors Q1-Q2, and Q3-Q4 form cascode pairs. The input network to Q1 is a broadband RC network which serves as a constant impedance load to the IF preamplifier. Two tuned interstage networks, one between Q2 and Q3 and the other at the output of Q4, provide the IF selectivity. The AM detector is composed of the peak-detector CRL and emitter-follower Q5. The FM detector is composed of two stages of cascode limiting, Q6-Q7 and Q8-Q9, a discriminator (the network between Q9 and Q10) and an emitter-follower Q10.

7.2 Modeling of the Solid-State Receiver

7.2.1 An Overview of Experimental Modeling

In this section we outline the steps involved in modeling the receiver. Bear in mind that the information about the tuner available at the outset is normal instruction manual data. The tuner is also available for physical measurements.

To model the interstage networks, it is necessary to establish values for each of the network elements. The schematic diagrams give the nominal values of the components. The values of the tunable elements are not shown. In addition, parasitic elements that may be present are not shown. Measurements are needed, therefore, to permit the networks to be parameterized.

There are a number of ways in which the networks could be parameterized. First, each element could be removed from the receiver and measured on an appropriate RF bridge. This approach

could result in network misalignment and possible destruction of the components being measured. It was not attempted. A second approach is to consider each interstage network as an entity, and measure its transmission parameters in situ. This has the distinct advantage that the networks undergo a minimum of dissection in their analysis, and that the networks can be measured by familiar techniques. Some of the measurements which might be made are:

- a. insertion gain
- b. Y or Z parameter
- c. scattering parameters.

Insertion gain measurements are an attractive technique since the basic network structure is known. If insertion gain is measured as a function of frequency, the unknown elements can be determined by choosing values for the unknown elements, predicting the network insertion gain using a linear network analysis program, and refining the estimate until the predicted insertion gain is sufficiently close to the measured. The Y and Z parameters are more difficult to measure. They require that short and open circuits be established at the network ports. Scattering parameters may also be used to characterize lumped networks. The insertion gain technique is preferred, at least through VHF. The measurement is made in two steps. First, the generator is calibrated by measuring P_1 , the delivered power to a 50Ω load from a 50Ω generator. The generator is connected to the load through a 50Ω cable, so the load need not be right at the generator terminals. Next, the network under test is connected to the generator, and its output brought through a 50Ω coaxial cable to a 50Ω termination. P_2 , the power delivered to the load by the network is then measured.

The insertion gain is $P_2 - P_1$ assuming that the powers are in a consistent set of logarithmic units such as dBm's. It was found that the network topology is well represented by the schematic diagrams in the design range of the network. Out of band, however, responses are measured which require the inclusion of parasitic elements. These can be modeled with reasonable effectiveness if the analyst takes sufficient care. An example of this is discussed in Section 7.2.2.

Each of the signal-processing transistors - twelve in all - was unsoldered and removed from the receiver, and its parameters measured. As a check on the correctness of the transistor parameterization, two-tone measurements were made of the second and third-order nonlinear transfer functions of all transistors, as well as their insertion gains. All of the measurements were made in 50 ohm test fixtures. Predictions of the nonlinear transfer functions were made with SIGNCAP. Upon confirmation of the modeling, the transistors were resoldered into their circuits. The removal and replacement of the transistors was non-destructive, and easily accomplished by a skilled electronics technician.

With the interstage networks and the transistors modeled, the next step was the modeling of the three sections of the receiver. Using 50 ohm sources and loads, insertion gain and swept frequency two-tone nonlinear transfer function measurements were made of the tuner, IF preamplifier, and IF amplifier. The basic instruments used to measure the available and delivered powers were a vector voltmeter and a spectrum analyzer. Input tones were combined by means of a 50 ohm hybrid junction. The points at which the outputs were measured were the C11-C12

junction of the tuner, R22-C16 junction of the preamplifier, and the input to Q6 of the IF amplifier. The last point was selected instead of the more obvious selection of the AM detector input, because the detector input is a high-impedance point which does not provide a convenient monitoring point for the laboratory measurements. Predictions of the various nonlinear transfer functions were made using SIGNCAP. When needed, measurements and predictions were also made at interior points in the circuits. It was generally found that slight adjustments had to be made to the previously modeled network parameters in order to match predicted overall responses with measured responses. Transistor parameters, however, were left unchanged.

When the modeling of the tuner, IF preamplifier, and IF amplifier was completed, the three units were connected and measurements made on the overall receiver. Predictions of the overall receiver were made using the SIGNCAP predictions* of the three units, combined with simple cascading theory.

During all of the measurements, the receiver was tuned to 45 MHz on the front dial. Since the intermediate frequency is 21.4 MHz, the nominal local-oscillator frequency is 66.4 MHz.

The sinusoidal local oscillator amplitude at the collector of Q5 was measured to be 2.9 volts RMS. Analysis shows that this causes the mixer to operate in the borderline region between small and large local-oscillator mixer theory since the peak local-oscillator voltage across the mixer transistor internal base-emitter junction is computed to be 29.4 millivolts. All measurements were made with the AGC grounded.

* Complete SIGNCAP coding for the VHF receiver is included in Appendix A.

7.2.2 Interstage Network Modeling

The purpose of this section is to describe in more depth some experimental techniques which have been developed in modeling receiver interstage networks. The techniques use a combination of insight and experience, and allow the analyst to achieve a good circuit model with very few iterations of the modeling process. By a model of an interstage network we mean a circuit diagram, with explicit component values, such that the predicted effect of the interstage when placed in the remainder of the circuit will be the same as that due to the physical circuit. It is thus necessary not only to model the elements which have been intentionally designed into the circuit, but also the parasitic elements, primarily series inductance and shunt capacitance, which are unintentionally part of the circuit.

In this section we will limit the discussion to two port interstage networks such as illustrated in Fig. 7.7. These networks are assumed to be linear passive and bilateral and available for measurements to be made on. Two basic techniques are discussed in this chapter for characterizing the interstage networks, depending on their intended use. For networks used to couple transistor circuits, where the source and load impedances are typically low, the only measurements which were made are the insertion losses in a 50 ohm system. This has been discussed in the previous section. For networks used to couple vacuum tube circuits, where the source and load impedances are typically high, the input impedance and the voltage insertion ratio between a 50 ohm generator and an open-circuit load can be measured. This will be further discussed in Section 7.9. In both cases, the measurements are made over the entire frequency range it is desired to characterize the network.

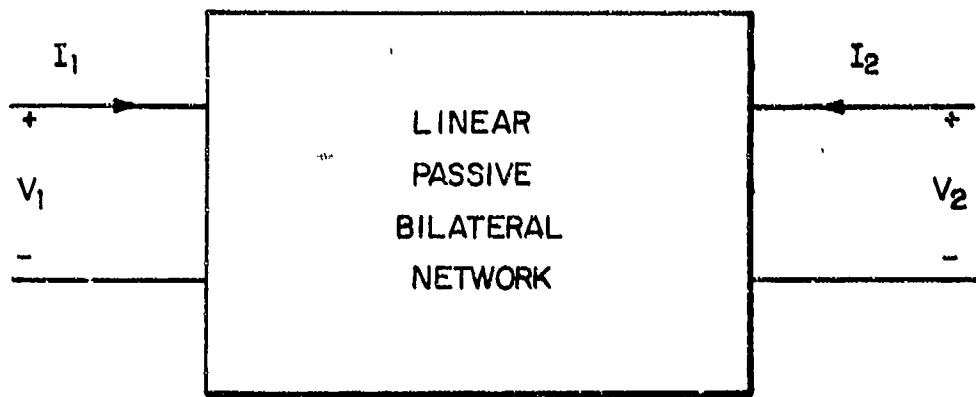


Fig. 7.7. Interstage Network.

Once the measurements are performed, an initial circuit model can be made of the network based on the nominal values of the network's resistors, inductors, and capacitors. There will be, in many cases, unknown parameters due to variable inductors and variable capacitors. Initial guesses can be made of these component values, based on the measured frequency responses, and the theoretical relations between the resonant frequencies and the circuit parameters.

The next step in the circuit modeling is to take the initial circuit model and, using a linear circuit analysis program, predict the same parameters as were measured. The input impedance can be predicted by driving the network with a one-ampere current source; the input impedance is the resulting voltage at the input terminals, in magnitude and phase. The insertion loss of the network in a 50 ohm system can be predicted by driving the network with a two-volt, 50 ohm generator, and terminating the network with a 50 ohm load; the insertion loss in dB is $20 \log_{10}$ times the voltage across the 50 ohm load. The voltage transmission ratio between a 50 ohm generator and an open circuit load is the network's predicted output voltage when driven by a one-volt, 50 ohm generator.

The predicted and measured parameters can then be compared over the entire frequency range. Usually several iterations will have to be made on tuned interstages before the skirt slopes and major resonant frequencies are in agreement. At this point it is appropriate to insert resistance in parallel with inductors so that the resonant circuits will have the proper Q, as indicated by correct parameter values in the vicinity of resonance; usually the Q has little effect away from resonance.

As a final step, the predicted and measured parameters can be examined for the effects of parasitic elements. Generally the most important parasitics are series inductance and shunt capacitance, although one may also need to consider series resistance at times. The effects of parasitics are usually easy to identify; a parasitic inductance in series with a capacitor will cause an increase in transmission if the capacitor is in series with the input-output path, or a decrease in transmission if the capacitor is in shunt between the input-output path and ground. These resonances are usually high Q, and the value of the parasitic can be initially estimated from the resonant frequency and the value of the capacitance. A parasitic capacitance in parallel with an inductance will cause the opposite of the above effects, i.e., a parallel resonance in series with an input-output arm will cause a decrease in transmission, and an increase in transmission when in a shunt arm.

An example of interstage network modeling will now be given to illustrate these principles.

7.2.2.1 Interstage Network Modeling Example

Figure 7.8 is the schematic diagram of the third interstage network in the tuner of the VHF receiver. Inductor L2C and L2D tune the stage over the 30-100 MHz frequency range. Inductors L8 and L9, and capacitors C19 and C22 are trimmers which are adjusted by the manufacturer so that the tracking of the tuner is satisfactory over the frequency range. The primary selectivity of the stage is due to the parallel resonances of C18, C19, L8, L2C, and C22, C23, L9, L2D, with C20 and C21 providing the coupling between the stages. If L8 and L9 were, in fact, zero,

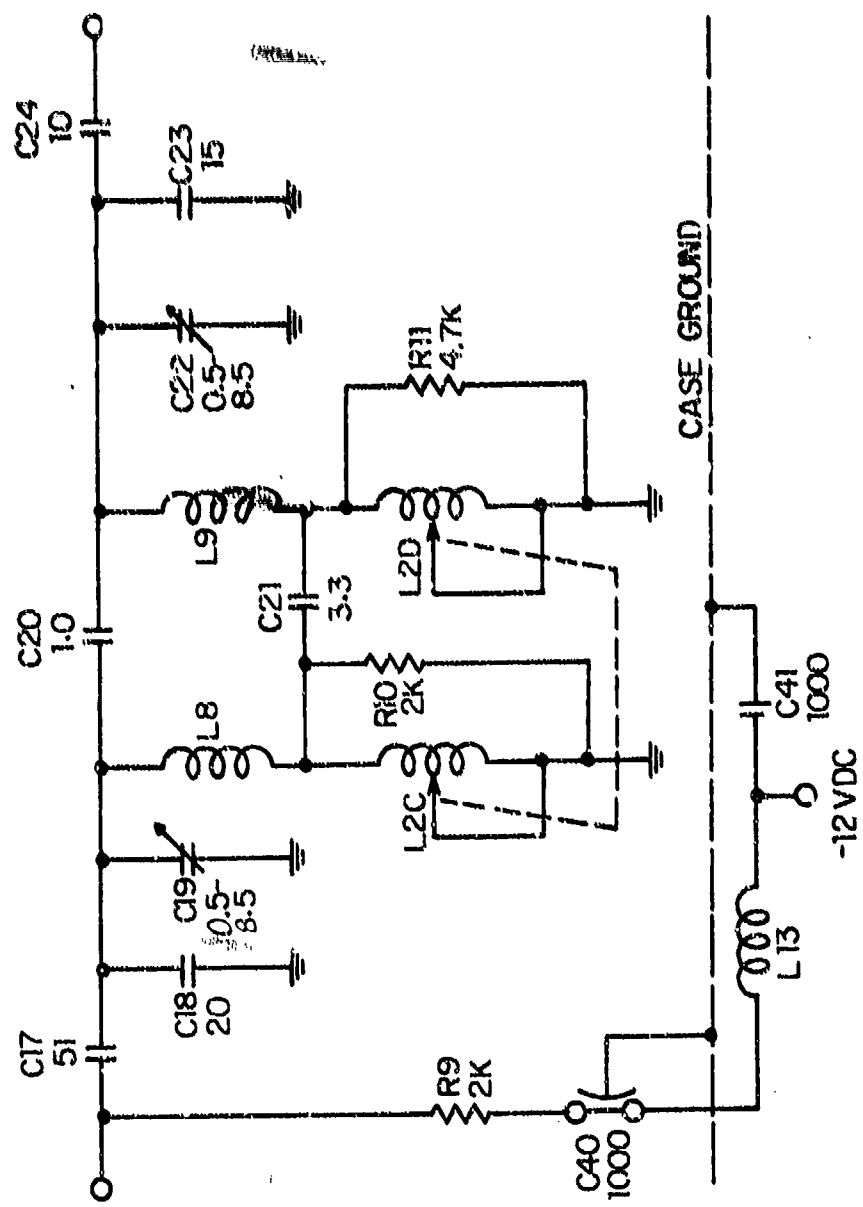


Fig. 7.8 Schematic of VHF Receiver Tuner Interstage Network 3.

the interstage would be a classic capacitance coupled double-tuned interstage network, the insertion gain of which decreases monotonically towards zero at low frequencies, and tends towards a constant value above resonance.

Figure 7.9 shows the insertion gain measured for this network in a 50 ohm system, when the receiver was tuned to 45 MHz on the front panel. The low frequency slope is monotonic, as expected, and the network peaks at 47 MHz. The insertion gain tends towards a constant value of -26 dB in the 60-100 MHz region, but then has an unexpectedly low loss at 245 MHz, and a high loss at 400 MHz.

An examination of the schematic shows that if L8 and L9 are much smaller than L2C and L2D, the possibility exists of a higher-than-tuned-frequency series resonance between L8, L9, and C21, which would account for the low loss at 245 MHz. The high loss at 400 MHz may be due to a series resonance between C18 and a parasitic series inductance, and C23 and a parasitic lead inductance. With these clues, the first step in the modeling is to find network values such that the main response is well modeled. A network for which this is so is shown in Fig. 7.10, and its predicted insertion gain is shown in Fig. 7.11. The network is seen to resonate at the correct frequency, and to have a reasonably constant insertion gain above resonance.

The next step is to reapportion the total inductance of L8 and L2C (and L9 and L2D) so that the main resonance is unchanged, but the second resonance occurs at 245 MHz. It is found that this occurs with L8 equal to 0.0565 μ h, and L2C equal to 0.29 μ h. The series resonance at 400 MHz can be modeled by lumping C18 and C19 together, and C22 and C23 together,

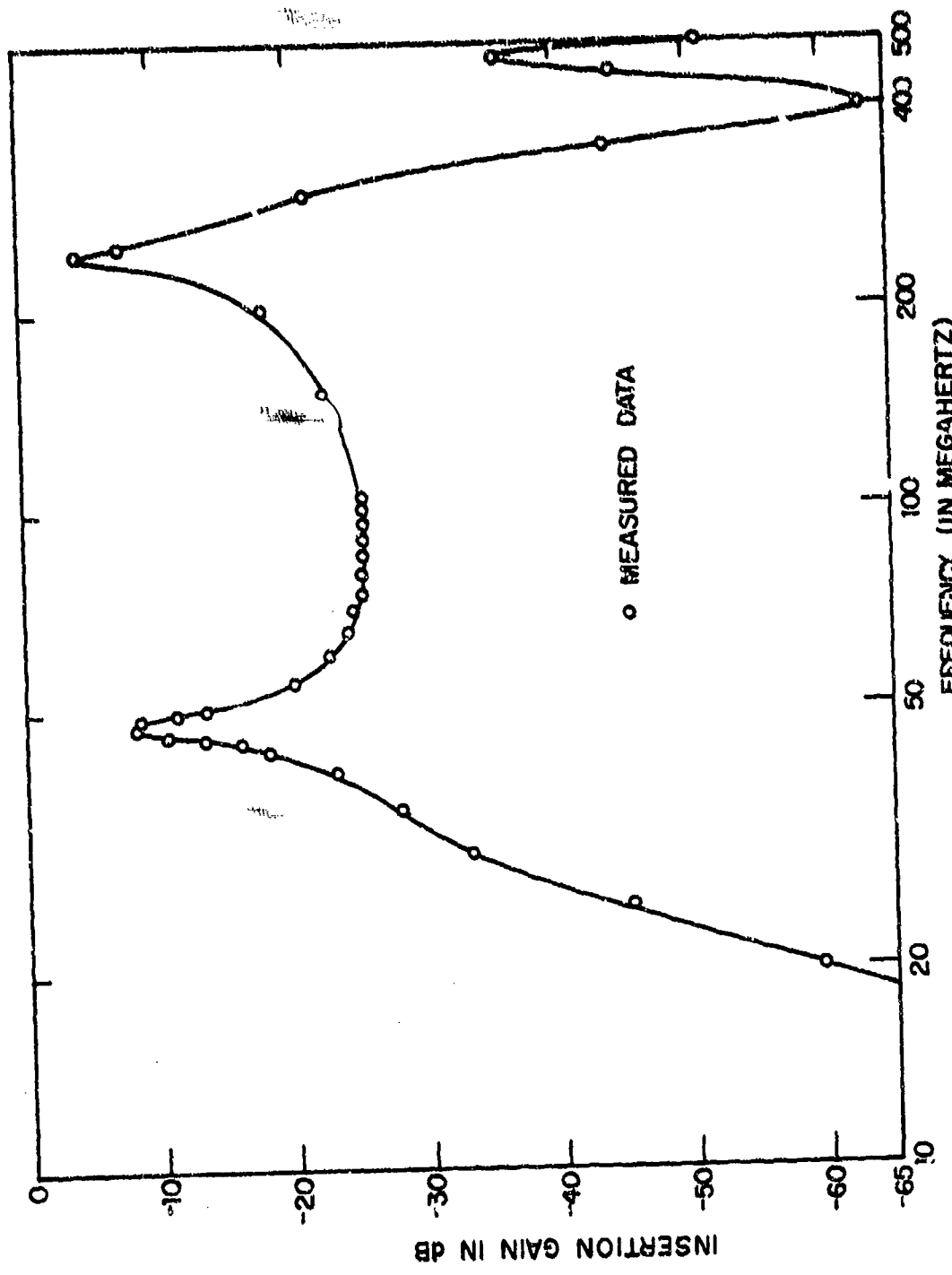


Fig. 7.9 Measured Insertion Gain of Interstage Network 3.

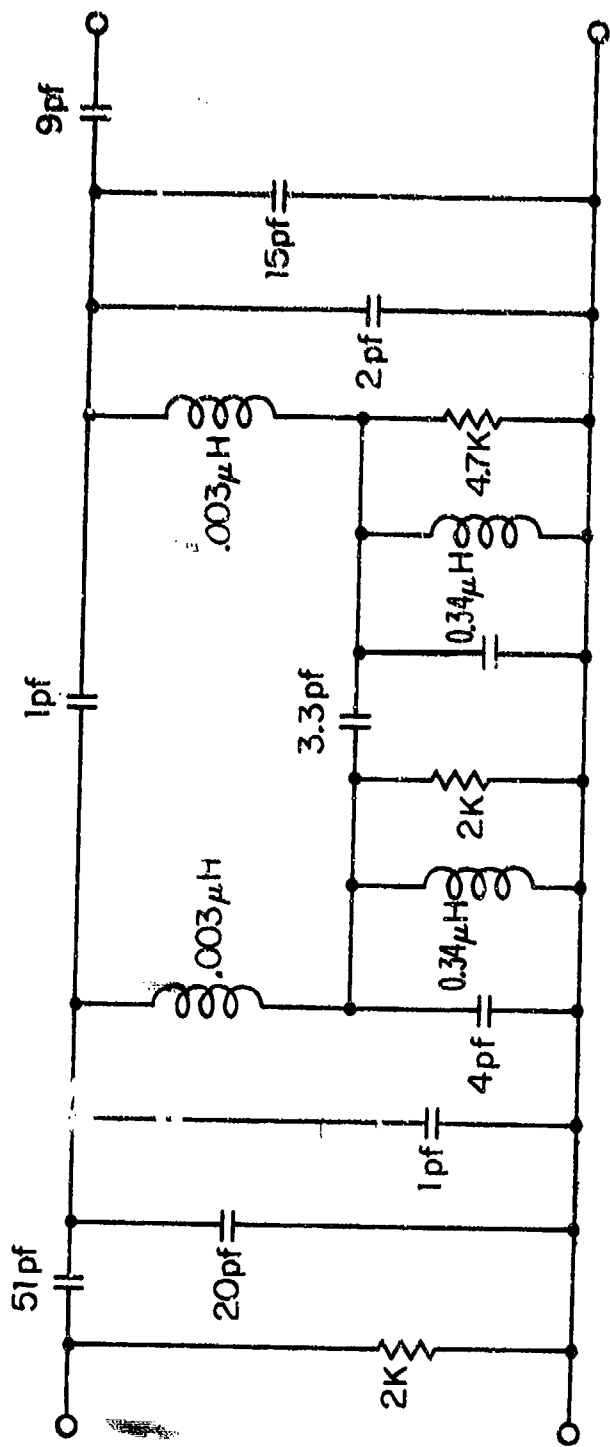


Fig. 7.10. First Cut Circuit Model of Interstage Network 3.

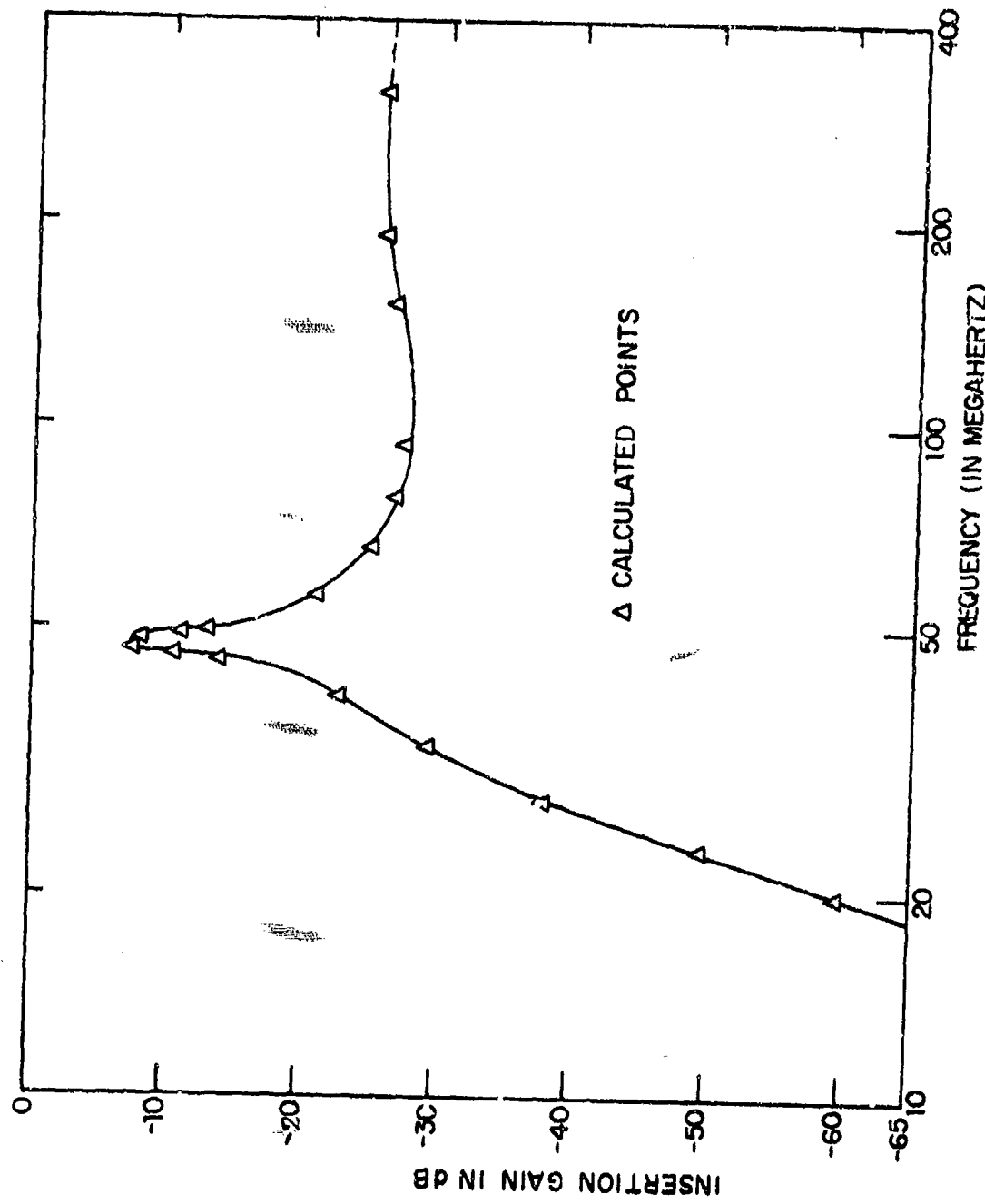


Fig. 7.11. Predicted Insertion Gain of First Cut Interstage Network 3.

and inserting 0.008 μ H in series with each of them. The resulting circuit model is shown in Fig. 7.12, and the measured and predicted insertion gains are shown in Fig. 7.13. It is evident that the circuit model is a good representation of the network. A close look at Fig. 7.12 shows that R11 was changed from 4.7K to 2K. This was done so that the predicted peak insertion gain is the same as the measured insertion gain.

As a final point, it should be noted that there is a slight detuning between the prediction and measurement in the 400 MHz region. If necessary, a slightly different choice of the parasitic inductor values would improve this match. It was not felt necessary, however, for this application.

In Section 7.9 comparisons are shown between predicted and measured network input impedances and voltage transfer ratios for vacuum-tube interstage networks. The network models were formed using the same techniques as described here.

7.3 Tuner Modeling

The analysis of the tuner is from RF inputs at J1 to IF outputs at J2. The mixer was modeled as a small local-oscillator mixer, with the desired difference frequency the result of a second-order mix. The local oscillator was measured to have an amplitude of 2.9 volts rms, which results in a predicted internal base-emitter voltage in the mixer transistor of 29 mV. Thus, the mixer is operating slightly above the 25 mV breakpoint which was taken in Section 6.3 to be the transition from small to large local-oscillator drives. Three nonlinear transfer functions are considered in this section.

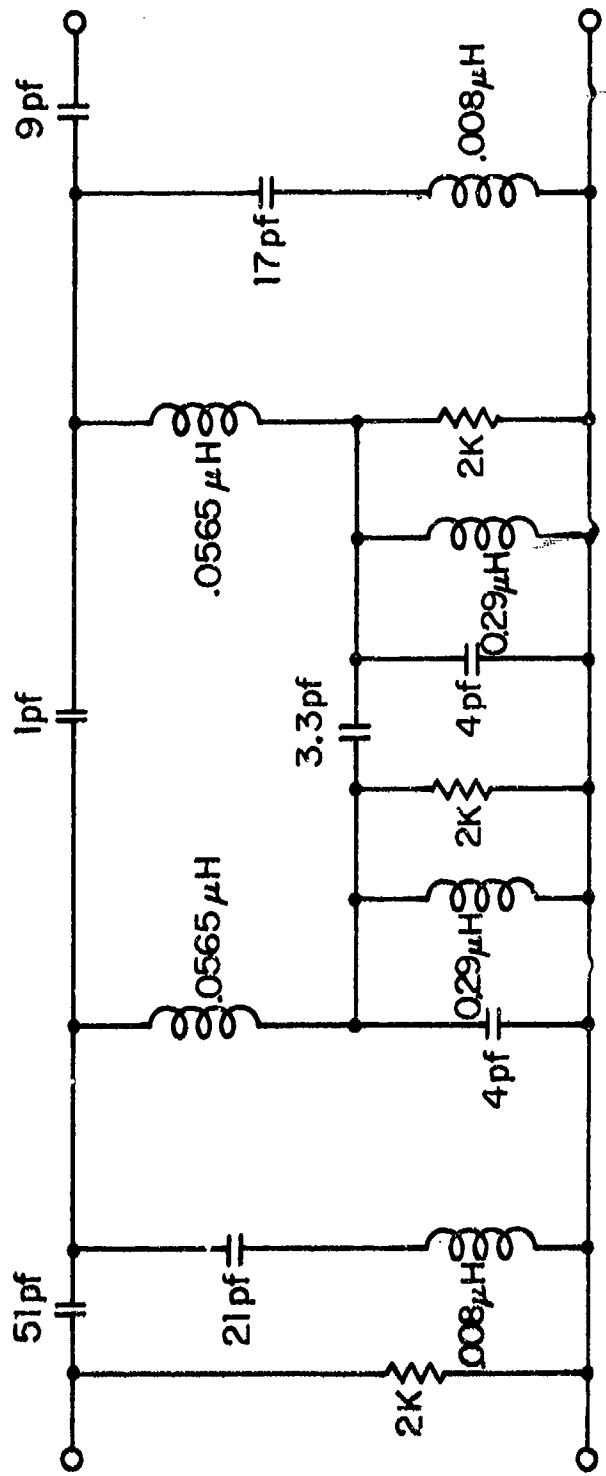


Fig. 7.12. Circuit Model of VHF Receiver Tuner Interstage Network 3.

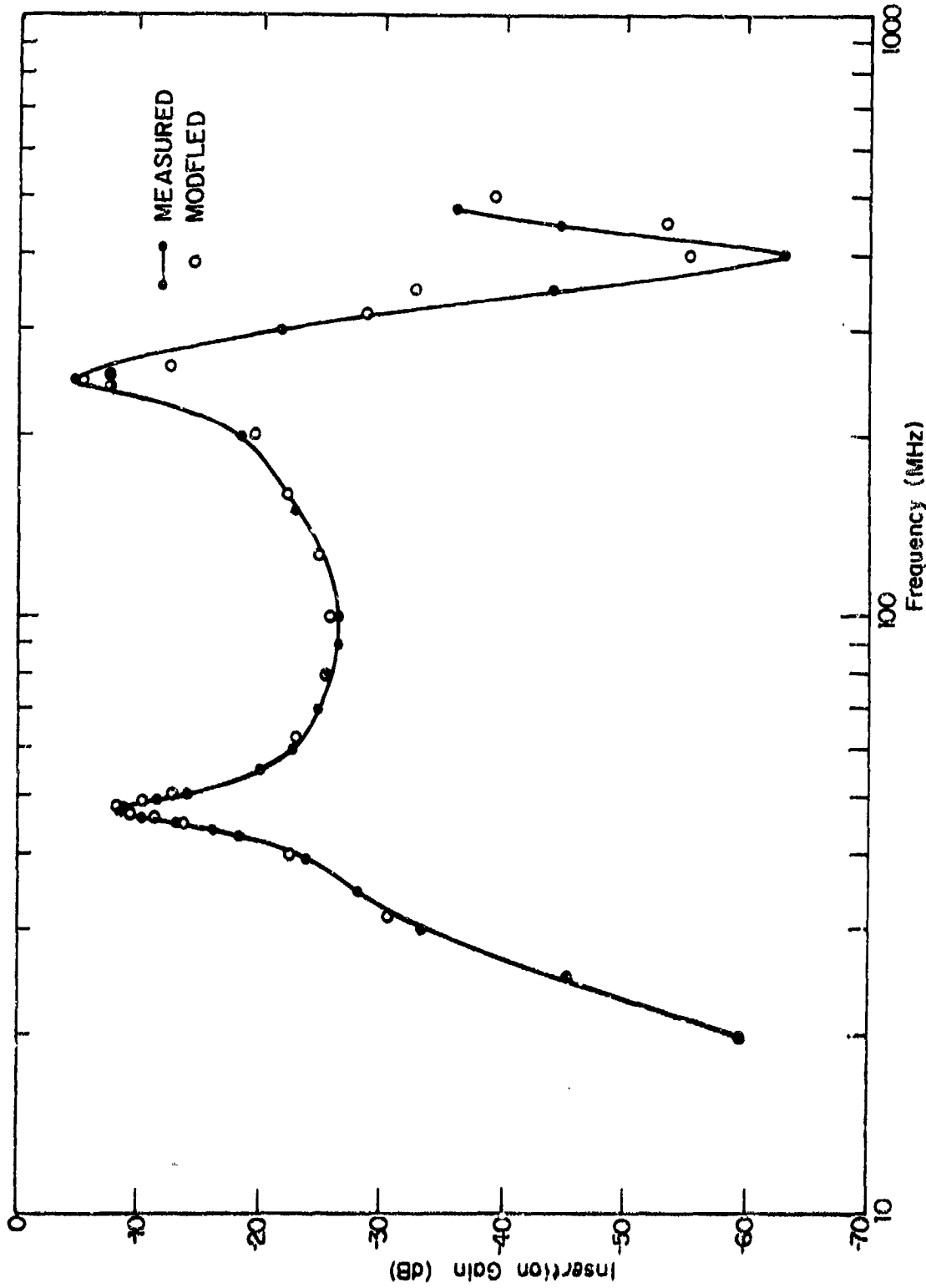


Fig. 7.13. Measured and Predicted Insertion Gain: VHF Receiver Tuner Interstage Network 3.

The second-order nonlinear transfer function describes the mixing of the input signal and the local oscillator to produce the intermediate frequency. In the tuner, the local-oscillator is nominally 21.4 MHz higher in frequency than the signal to give an IF of 21.4 MHz. The receiver will have an image response 21.4 MHz above the local oscillator frequency, or, alternatively, 42.8 MHz above the desired signal frequency. Measurements and predictions of the second-order nonlinear transfer function will be presented. The second-order nonlinear transfer function is described as the equivalent first-order nonlinear transfer function.

The third-order and fourth-order nonlinear transfer functions of the tuner are defined with one frequency equal to the local oscillator frequency, and the remaining two and three frequencies, respectively, variable. Thus, the third-order and fourth-order transfer functions can be measured with conventional two-tone probing signals at f_1 and f_2 . Measurements and predictions will be shown for the case of $f_1 \pm f_2$ and $2f_1 - f_2$ set equal to 45 MHz, the tuned frequency. These inputs result in intermodulation products at the intermediate frequency. The third and fourth-order nonlinear transfer functions are interpreted as the equivalent second and third-order nonlinear transfer functions for the tuner.

7.3.1 Second-Order Nonlinear Transfer Function (Equivalent First-Order Nonlinear Transfer Function)

The second-order response of the tuner is its desired output frequency response. If the input signal is at a frequency f_1 , then the output is at a frequency $f_{LO} - f_1$, which is a second-order mixer response. The equivalent first-order transfer function is:

$$H_1^{eq}(-f_1; f_{LO}) = AH_2(-f_1, f_{LO}), \quad (7.1)$$

where

f_1 = signal frequency,

f_{LO} = local-oscillator frequency,

A = local-oscillator amplitude in peak volts.

The measurement of H_1^{eq} is performed by a single tone test. The input signal available power and the difference frequency delivered power are measured. The difference, in dB, between the two is the (equivalent) insertion conversion gain of the tuner. This is 6 dB higher than the (equivalent) first-order transfer function. Figure 7.14 shows the measured and predicted gains. It is noted that they are in excellent agreement over the measured range 30 to 100 MHz, with the exception of a slightly low prediction at 44 MHz, and high prediction at 48 MHz.

Several points should be noted with regard to the predictions. They cover a 120 dB range, and are in basically good agreement over the entire range. The fourth-order correction term was not included in the predictions. The secondary peak which occurs in the neighborhood of 88 MHz is the image response of the receiver, which occurs when the input signal frequency is $f_{IF} + f_{LO}$. Since $f_{IF} = 21.4$ MHz, and $f_{LO} = 66.6$ MHz, the image frequency should be 88 MHz. The prediction of the image response is quite good. The null at 66.6 MHz is a zero-beat, which occurs when the signal frequency is the same as the local-oscillator frequency.

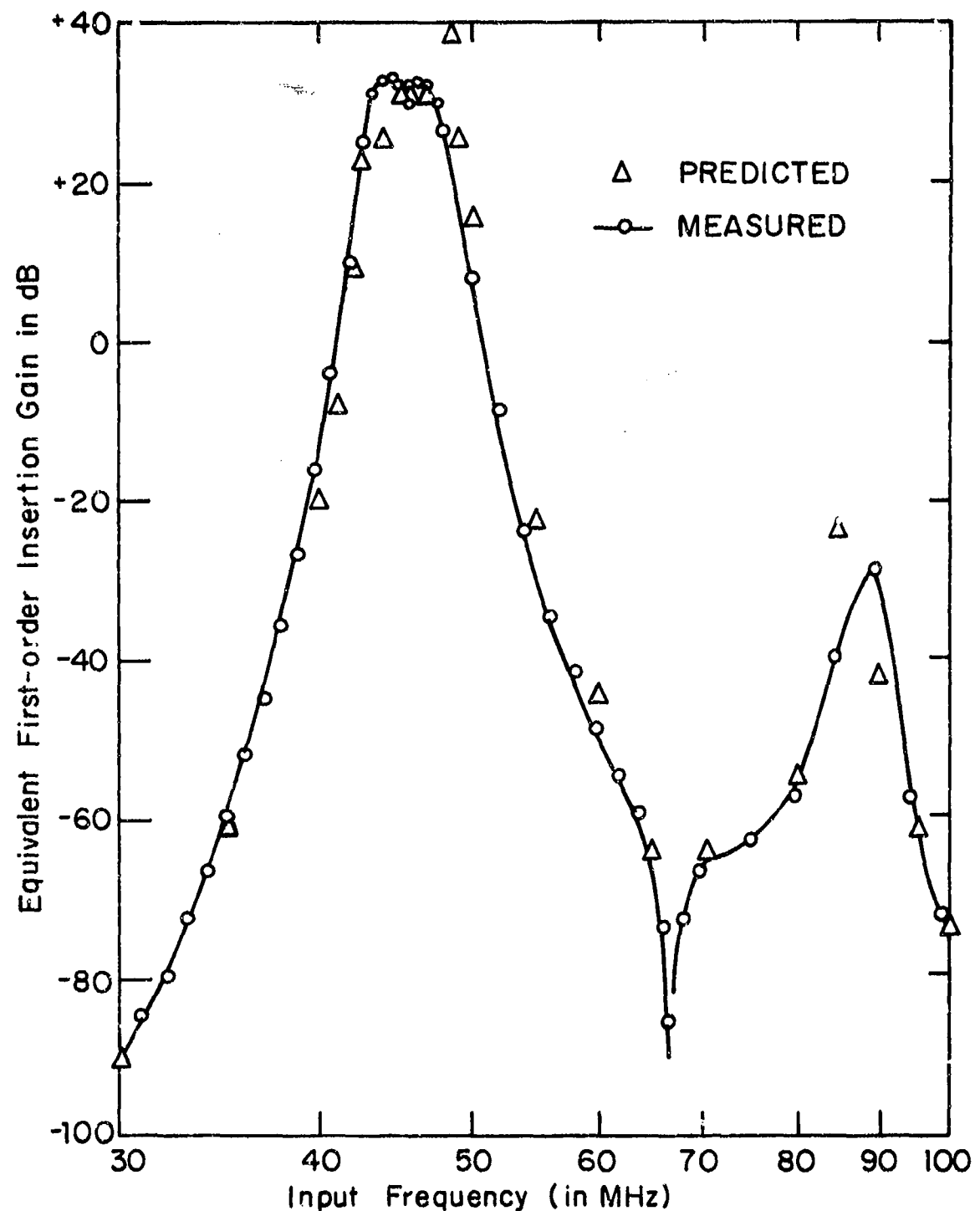


Fig. 7.14. Measured and Predicted First-Order Equivalent Insertion Gain for the VHF Tuner.

7.3.2 Third-Order Nonlinear Transfer Function (Equivalent Second-Order Nonlinear Transfer Function)

The third-order nonlinear transfer function of the tuner was measured in a two-tone test. Two tones, at frequencies f_1 and f_2 , with $f_1 \pm f_2$ equal to 45 MHz, were inputs, and the IF output signal at $f_{LO} - (f_1 \pm f_2)$ was measured. Since the input was a two-tone, with the third frequency being the local-oscillator, it was decided to characterize the third-order nonlinear transfer function as an equivalent second-order nonlinear transfer function, H_2^{eq} , given by:

$$H_2^{eq}(-f_1, \pm f_2; f_{LO}) = \frac{3A}{2} H_3(-f_1, \pm f_2, f_{LO}), \quad (7.2)$$

where A is the peak amplitude of the local-oscillator, and $H_3(-f_1, \pm f_2, f_{LO})$ is the actual third-order nonlinear transfer function of the tuner for the three input frequencies, f_1 , $\pm f_2$, f_{LO} .

The equivalent second-order nonlinear transfer function was measured in the laboratory, and predicted with the SIGNCAP software. The experimental data and predictions are shown in Fig. 7.15. The equivalent second nonlinear transfer function peaks in the 80 to 100 MHz range. Since $f_1 - f_2$ is equal to 45 MHz, f_2 varies from 35 to 55 MHz, which covers a range of peak insertion gain, and causes the peaking of the equivalent second-order nonlinear transfer function. Thus f_2 is an in-band signal over the significant range of the equivalent second-order response, and one might expect the co-channel interference, which is a linear response, to be more significant than the interference due to the equivalent second-order response.

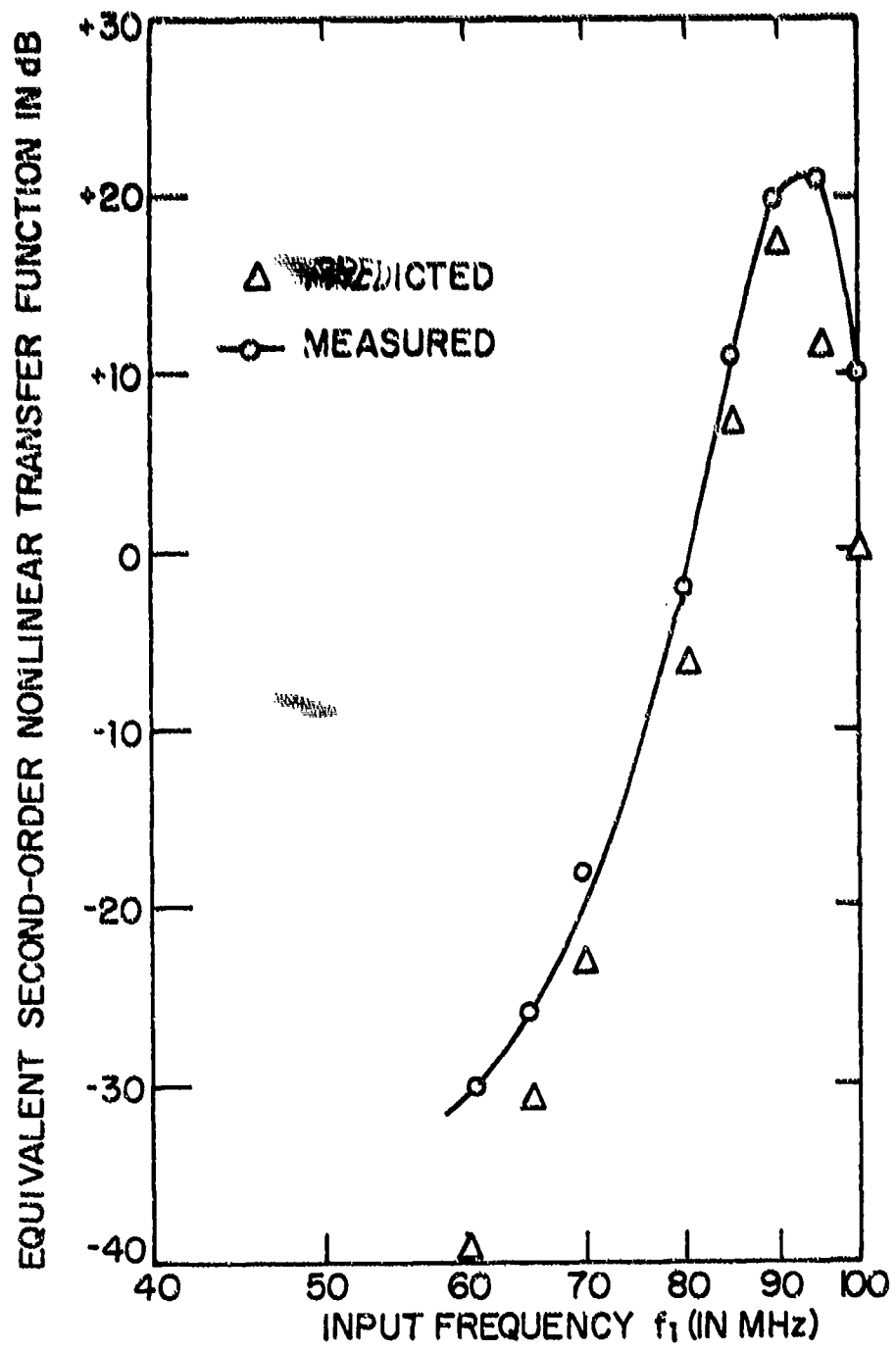


Fig. 7.15 Measured and Predicted Second-Order Equivalent Nonlinear Transfer Function for the VHF Tuner.

It is seen that the equivalent second-order nonlinear transfer function covers a range of about 60 dB for the frequency range of 60 to 100 MHz. The prediction error is in the order of 4 to 6 dB over this range.

7.3.3 Fourth-Order Nonlinear Transfer Function (Equivalent Third-Order Nonlinear Transfer Function)

The final nonlinear transfer function which was measured and predicted is the fourth-order. This transfer function was measured by means of a two-tone test, in which two tones at frequencies f_1 and f_2 , with $2f_1 - f_2 = 45$ MHz, were injected at the receiver input, and the fourth-order intermodulation response at $f_{LO} - (2f_1 - f_2)$ was measured at the IF output. As with the other transfer functions, it is convenient to consider an equivalent third-order nonlinear transfer function, $H_3^{eq}(-f_1, -f_1, f_2, f_{LO})$, instead of the fourth-order transfer function, $H_4(-f_1, -f_1, f_2, f_{LO})$; the two are related by:

$$H_3^{eq}(-f_1, -f_1, f_2, f_{LO}) = 2AH_4(-f_1, -f_1, f_2, f_{LO}) \quad (7.3)$$

The measured and predicted equivalent third-order nonlinear transfer functions are shown in Fig. 7.16. It is seen that the prediction is in good basic agreement with the measurement, aside from a slight frequency shift and the point at 44 MHz. It should also be noted, in evaluating Fig. 7.16, that the frequency of the second tone, f_2 , covers a wide range, as $2f_1 - f_2 = 45$ MHz. Thus, for the range 35 MHz $\leq f_1 \leq 80$ MHz, we find 25 MHz $\leq f_2 \leq 115$ MHz; the equivalent third-order nonlinear transfer function exercises the model over a much wider range than does the equivalent second-order transfer function.

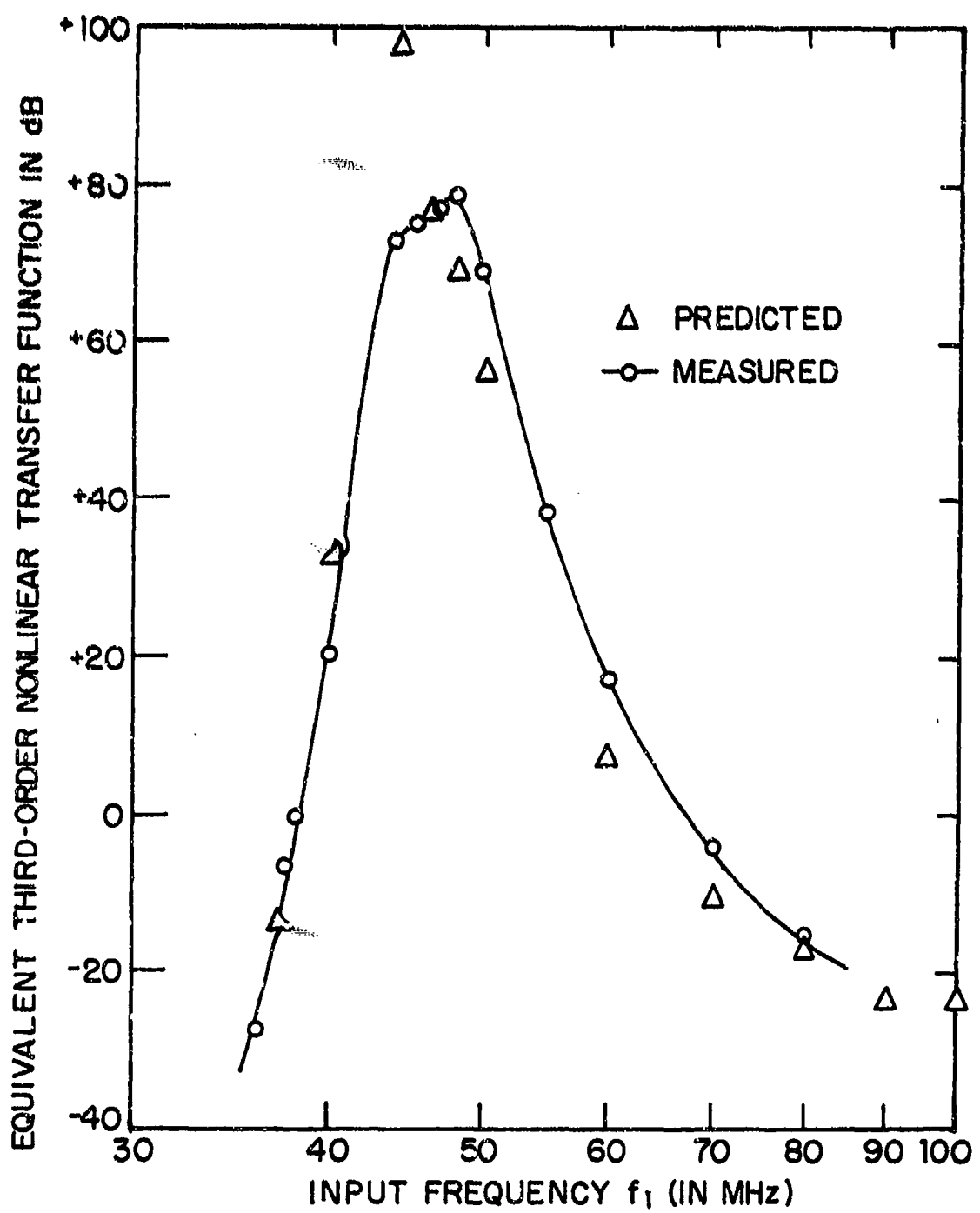


Fig. 7.16 Measured and Predicted Third-Order Equivalent Nonlinear Transfer Function of the VHF Tuner.

7.4 IF Preamplifier Modeling

The response of the IF preamplifier was also measured by means of one and two-tone tests in a 50 ohm system. The one-tone test was used to measure insertion gain, and the two-tone test to measure the second and third-order nonlinear transfer functions.

7.4.1 First-Order Transfer Function Measurement and Prediction

The insertion gain of the preamplifier in a 50 ohm system is 6 dB higher than the first-order nonlinear transfer function. The measured and predicted insertion gains are shown on Fig. 7.17. Observe that the preamplifier has a maximum response around the nominal 21.4 MHz center frequency, and a bandwidth of the order of 2 MHz. The peak insertion gain is 27 dB, with the gain at half and double the tuned frequency of the order of -60 dB. The predicted insertion gain is in good agreement in the frequency range around the intermediate frequency, and somewhat above the measured insertion gain at lower and higher frequencies.

The measurements shown in Fig. 7.17 were made with the limiter diodes, CR1 and CR2 of Figure 7.4, removed from the circuit. Measurements made with the diodes in the circuit show their principal effects to be a slight decrease in the resonant frequency and a lowering of the high-frequency gain by a few dB. Thus the diodes can be well represented simply by fixed capacitors provided they are not being driven by a signal large with respect to kT/q volts.

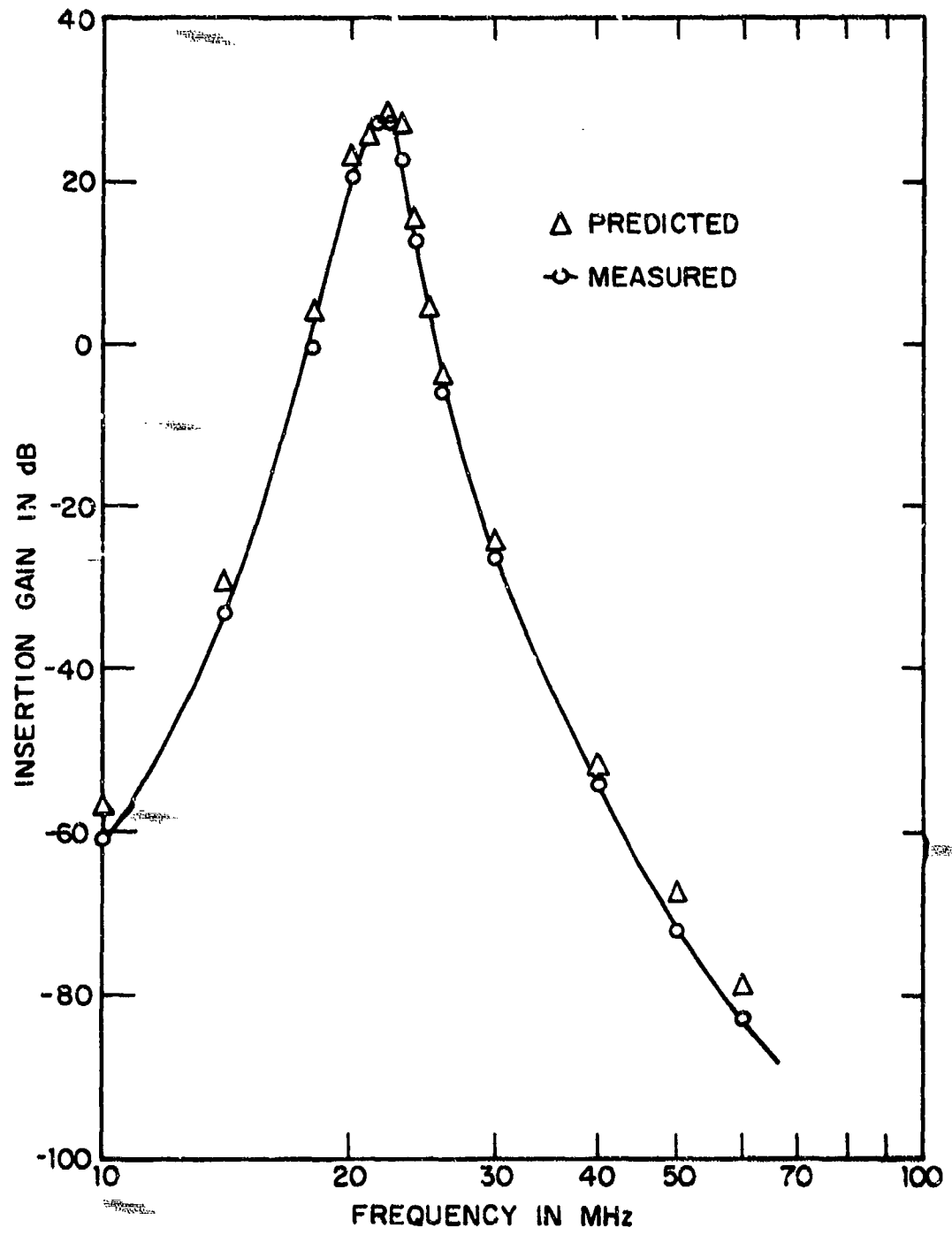


Fig. 7.17 Insertion Gain of the VHF IF Preamplifier.

7.4.2 Second-Order Nonlinear Transfer Function

The second-order nonlinear transfer function was measured by means of a two-tone test. Two tones at frequencies f_1 and f_2 , with $f_1 \pm f_2 = 21.4$ MHz were used as the input signal. The output at 21.4 MHz was measured.

The measured and predicted second-order nonlinear transfer functions are shown on Fig. 7.18. They are seen to be in excellent agreement over the range 3.4 MHz $\leq f_1 \leq 90$ MHz. The transfer function is relatively flat over this wide frequency range, except for the null at the tuned frequency of 21.4 MHz. This response is quite understandable. The input network to Q1 is a broadband resistive network, with a DC decoupling capacitor C1. For all frequencies between the cutoff of this RC network, and the high-frequency limitations of Q1 itself, the distortion produced by Q1 should be relatively constant. Due to the selectivity of the Q2-Q3 interstage, Q3 should generate little second-order distortion. Thus, the main contributor to the second-order nonlinear transfer function of the preamplifier should be Q1, which will result in a constant second-order transfer function except for a null at f_1 near 21.4 MHz, for which f_2 is 0 Hz, and a gradual roll-off at high-frequencies due to the cutoff of Q1.

7.4.3 Third-Order Nonlinear Transfer Function

The third-order nonlinear transfer function was also measured by means of a two-tone test. Two tones of frequency f_1 and f_2 , with $2f_1 \pm f_2 = 21.4$ MHz, were used as the input signal and the output at 21.4 MHz was measured. The third-order nonlinear transfer function was then computed from the measured output power at 21.4 MHz and the known input powers at f_1 and f_2 .

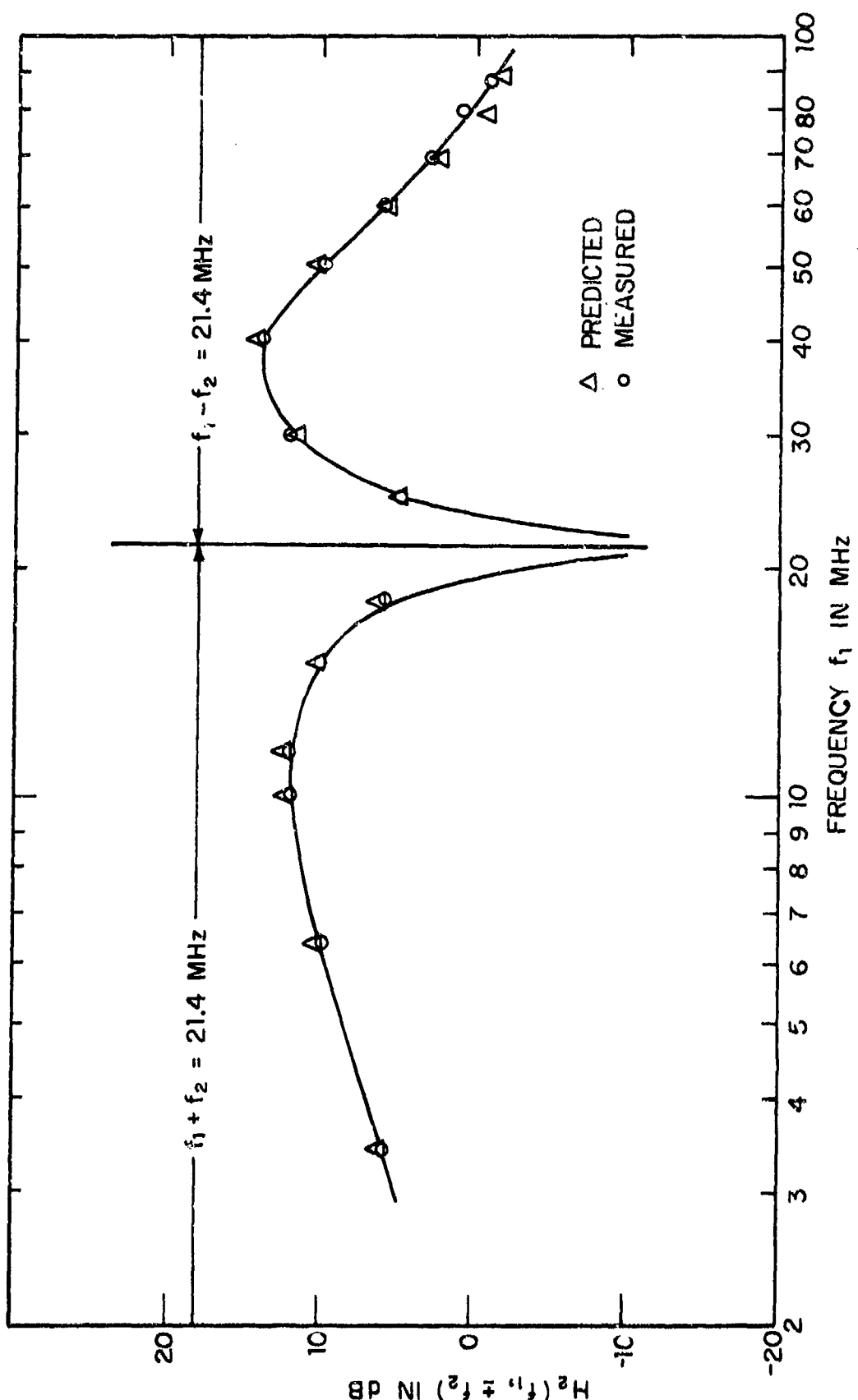


Fig. 7.18. Second order nonlinear transfer function of the VHF IF preamplifier.

Results and theoretical predictions are shown on Fig. 7.19. In contrast to the second-order transfer function, the third-order is extremely frequency sensitive. It peaks at the tuned frequency, and drops sharply on either side. This behavior shows that the second stage, Q3-Q4, is the source of the third-order nonlinear distortion for signals close to the intermediate frequency. The explanation of this is that when the tones are near the center frequency of the preamplifier, they are amplified by the first stage, Q1-Q2. The resulting stronger signals then cause significant third-order intermodulation to be produced in Q3-Q4. When the tones are away from the center frequency, the selectivity of the first stage attenuates the signals applied to the second stage, and thus only the first stage intermodulation is then significant. The agreement between the predicted and measured third-order transfer functions is again good for both in-band and out-of-band interference.

7.5 IF Amplifier Modeling

The measurements and predictions presented in this section are those of the first order (linear) transfer function and the third-order nonlinear transfer function of the IF amplifier. No second-order data are presented, as the receiver selectivity preceding the IF amplifier precludes the generation of significant second-order products in the IF amplifier.

The IF amplifier has the narrowest bandwidth and highest impedance levels and gains of the three receiver modules. As such, the modeling of the IF amplifier presented some problems which were not present in the tuner or IF preamplifier. The two tuned interstage networks were modeled by means of insertion

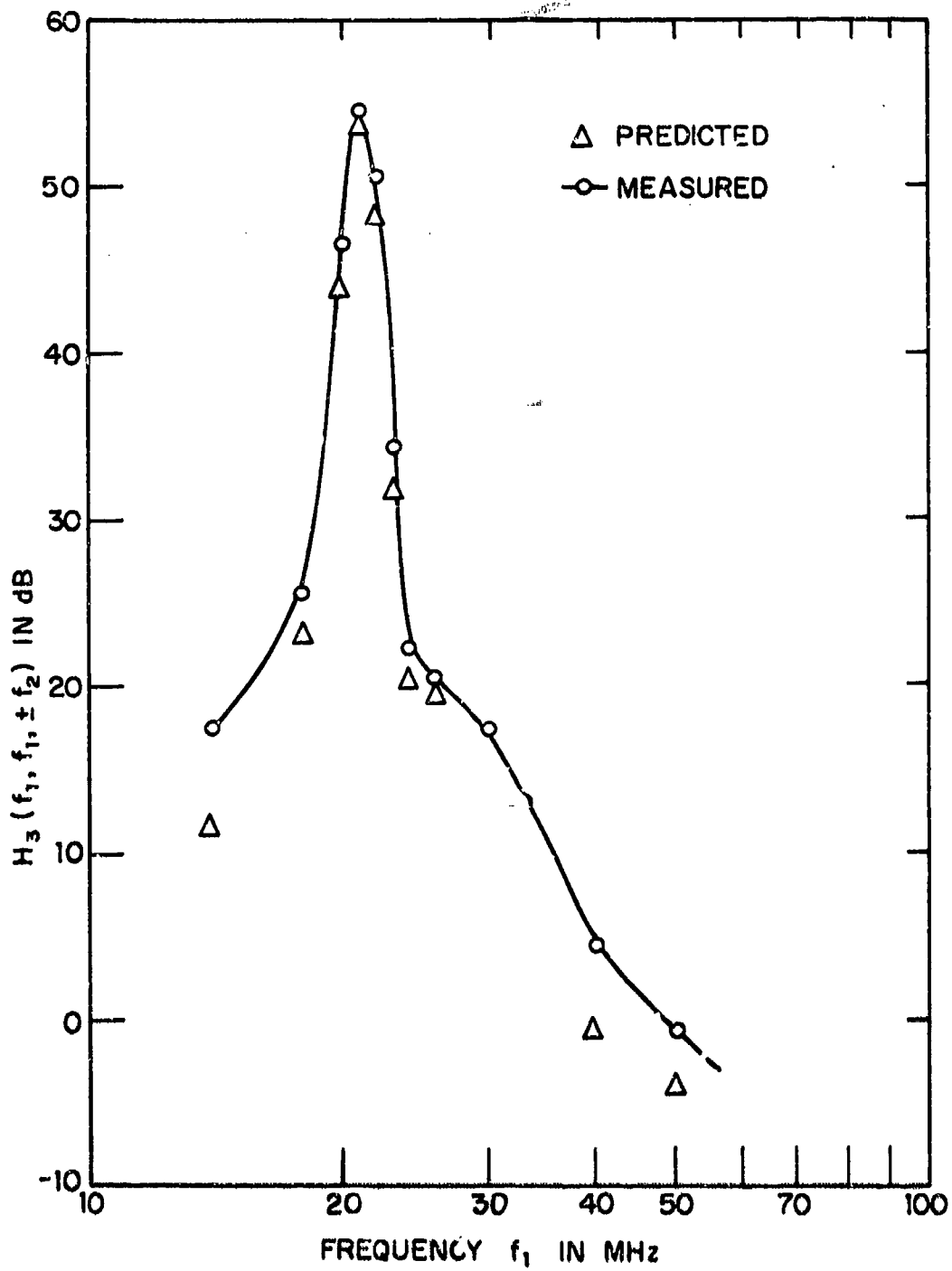


Fig. 7.19 Third order nonlinear transfer function of the VHF IF preamplifier.

loss measurements in a 50 ohm system, followed by transmission measurements in the IF amplifier. The rationale for this two-step modeling is as follows. The networks are high Q, narrow-band networks. Both interstage networks are double-tuned networks, with the two tuned circuits coupled by small capacitors. Each of the interstages has a capacitive divider on its output, used for impedance transformation. For the frequency range of interest, input impedances of the interstage networks are high compared to 50 ohms, and insertion loss measurements in a 50 ohm system serve primarily to model the transfer characteristics of the coupling capacitor and the output tuned circuit. If the network is then driven by a known transistor, the input tuned circuit can be readily modeled. This procedure was followed for the two interstage networks. Figure 7.20 shows the model for the first interstage network.

A comparison of Figure 7.20 with the IF amplifier schematic shows that the schematic diagram alone does not sufficiently model the tuned interstage. It was necessary to shunt the inductors with resistors in order to have the correct resonant impedance; this is simply control of the circuit Q. It was also necessary to model an interesting parasitic effect. Consider Fig. 7.21, the photograph of the IF amplifier circuit board. Two arrows are shown on the figure, one pointing to the input of the first tuned interstage network, and the other to the output of the first tuned interstage network. It is seen that the input and output are quite close together, and are thus effectively coupled together by a small capacitive impedance. Figure 7.20 shows that this capacitor is modeled as being 0.22 pf. Figure 7.22 shows the measured insertion loss of this network.

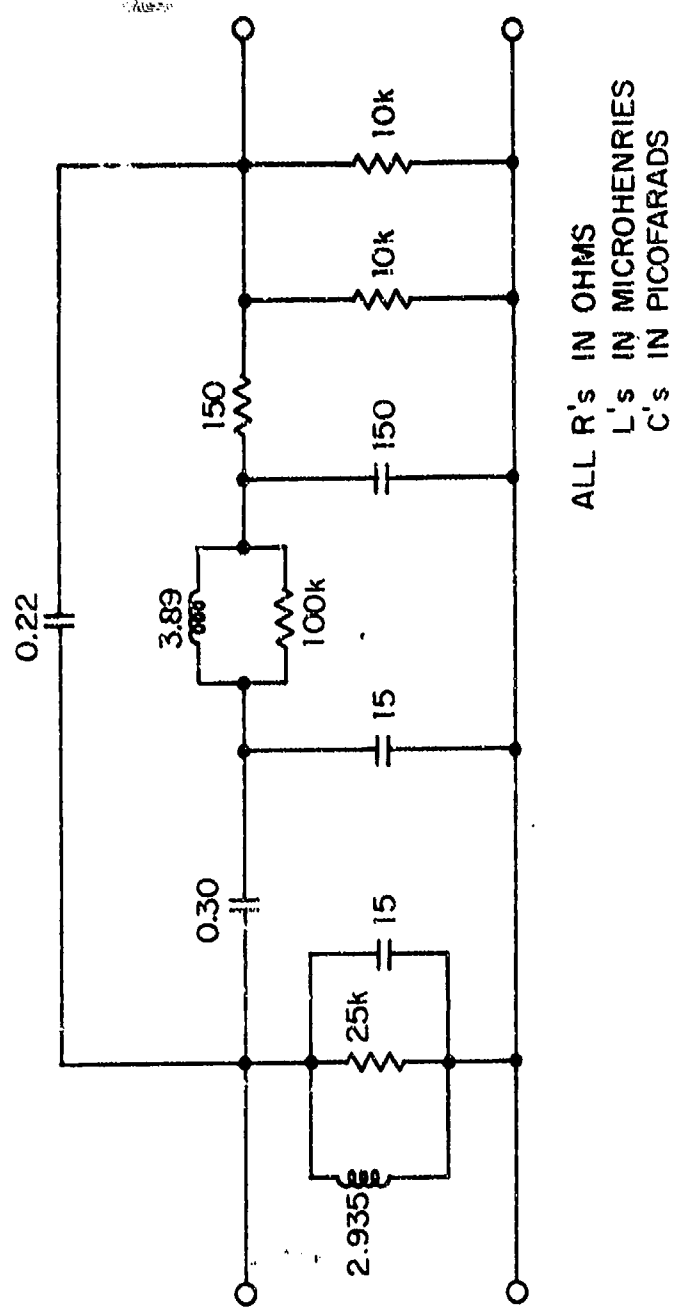
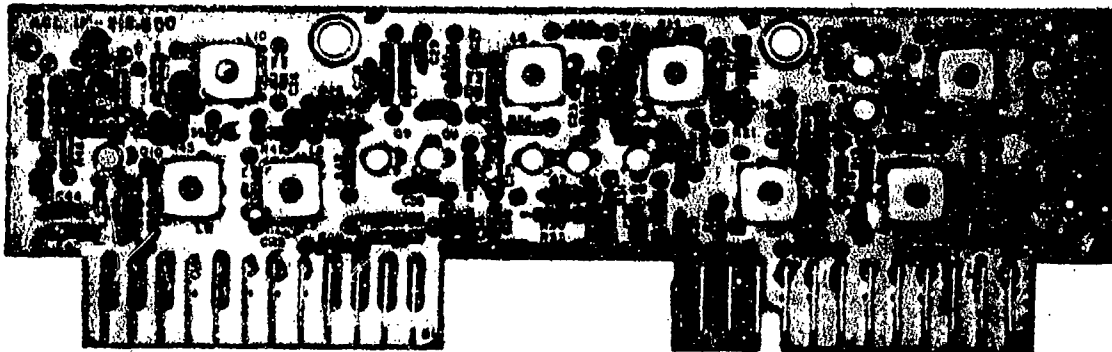


Fig. 7.20 Circuit model of IF interstage network 1.



a. IF Amplifier Card - Component Side

Q_2 Collector Q_3 Base



b. IF Amplifier Card - Printed Circuit
Side Showing Proximity of Q_2 Collector
and Q_3 Base.

Fig. 7.21 IF Amplifier and Detector Card.

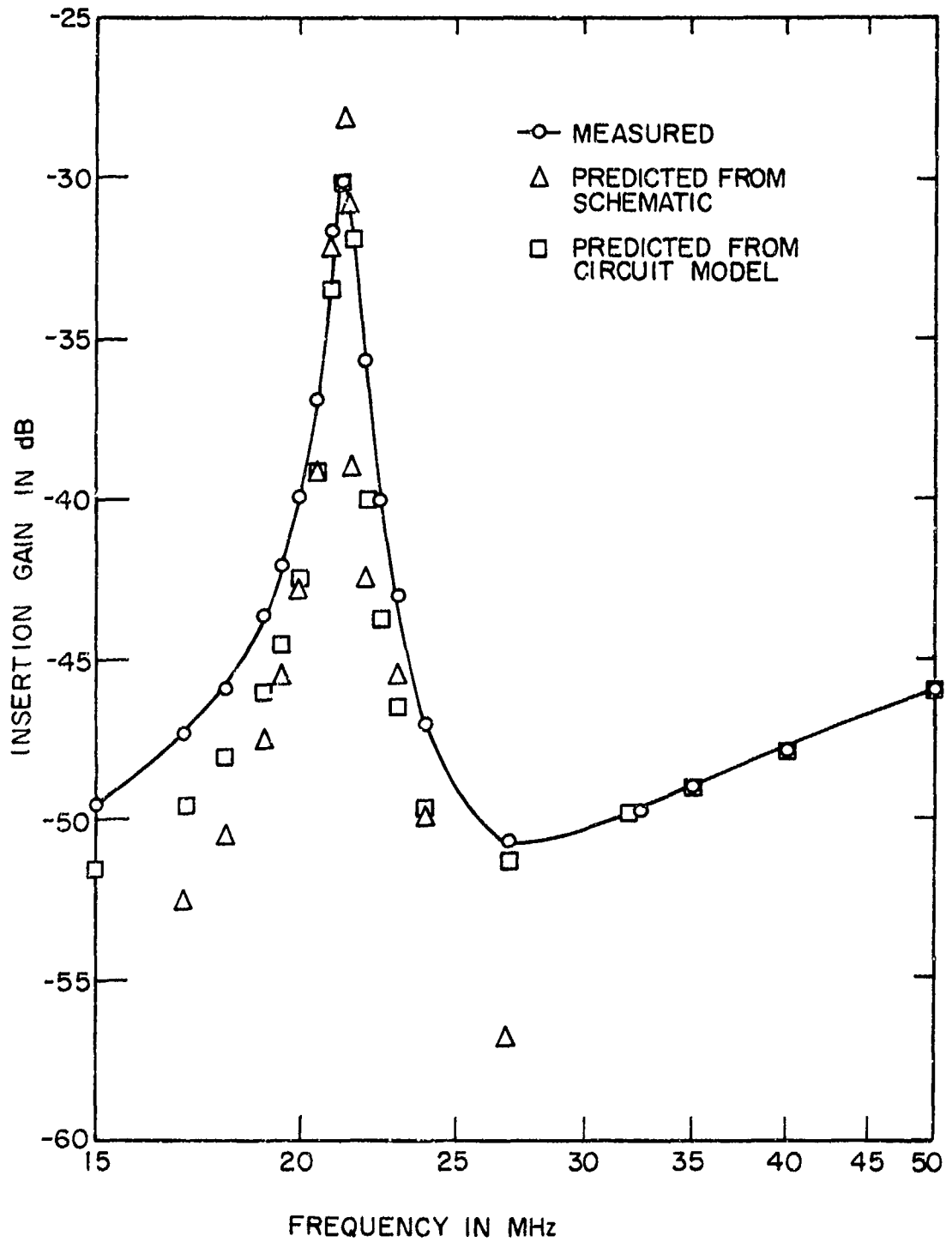


Fig. 7.22 Insertion gain of IF interstage network 1.

Also shown on Fig. 7.22 are two predicted insertion losses for the network, one based on the circuit diagram, and the other on the circuit model of Fig. 7.20, which includes the 0.22 pf parasitic capacitor and the shunt resistors. The effect of the capacitor is striking - without it the high frequency loss increases rapidly with frequency, while with the capacitor the high frequency loss decreases rapidly with frequency. Effects such as this can be readily observed and modeled when working on the circuit level.

In modeling high-Q, narrow-band tuned circuits, it was also found that simply matching transmission gains, while adequate for modeling of the first-order response, might prove inadequate for nonlinear response. This occurs when nonlinearities in the collector circuit enter into the distortion generation. In this case it is also necessary to match the linear response at internal points in the amplifier circuitry, as well as just at the input-output terminals. This matching can be conveniently done by means of a linear circuit analysis program.

7.5.1 First-Order Transfer Function Measurement and Prediction

The measured and predicted insertion gains of the IF amplifier are shown in Fig. 7.23. The IF amplifier appears to be critically tuned, with a 21.4 MHz center frequency, midband-gain of 16 dB, and 500 kHz bandwidth. The frequency range of Fig. 7.23 is 20.5 to 22 MHz and the insertion gain varies over a 40 dB range. The IF amplifier is tuned to its 21.4 MHz center frequency, and the bandwidth is the desired 500 kHz. The agreement between prediction and measurement is considered acceptable over the entire range. It should be noted that the prediction

is across a 50 ohm load at the first limiter (Q6-Q7) input. The input to the AM detector would be approximately 39 dB higher than shown in Fig. 7.23, as the 50 ohm load in series with R27 causes a 15 dB loss, while the C18-C19 capacitive divider causes a 24 dB loss. It should also be noted that the AM detector diode was disconnected when these measurements were made. The AM detector input is a high impedance point and does not provide a convenient monitoring point for the laboratory measurements. The input to Q6, however, is a lower impedance point. Therefore, measurements of the overall IF transfer functions were made with the input at the R1-R2 junction, and the output at the R27-R30-R3 junction with Q6 disconnected. The effect of the diode will be considered in detail in Section 7.7.

7.5.2 Third-Order Nonlinear Transfer Function

A spot check of the $2f_1 - f_2$ transfer function was made at three different values of f_1 , with $2f_1 - f_2$ held constant at 21.4 MHz. Table 7.2 shows the measured and predicted values of the

TABLE 7.2
IF Amplifier Third-Order Nonlinear Transfer Functions

f_1 (MHz)	f_2 (MHz)	$ H_3(f_1, f_1, -f_2) $ (dB)	
		Measured	Predicted
21.3	21.2	84.4	78.9
21.5	21.6	70.4	65.9
22.5	23.6	6.4	6.4

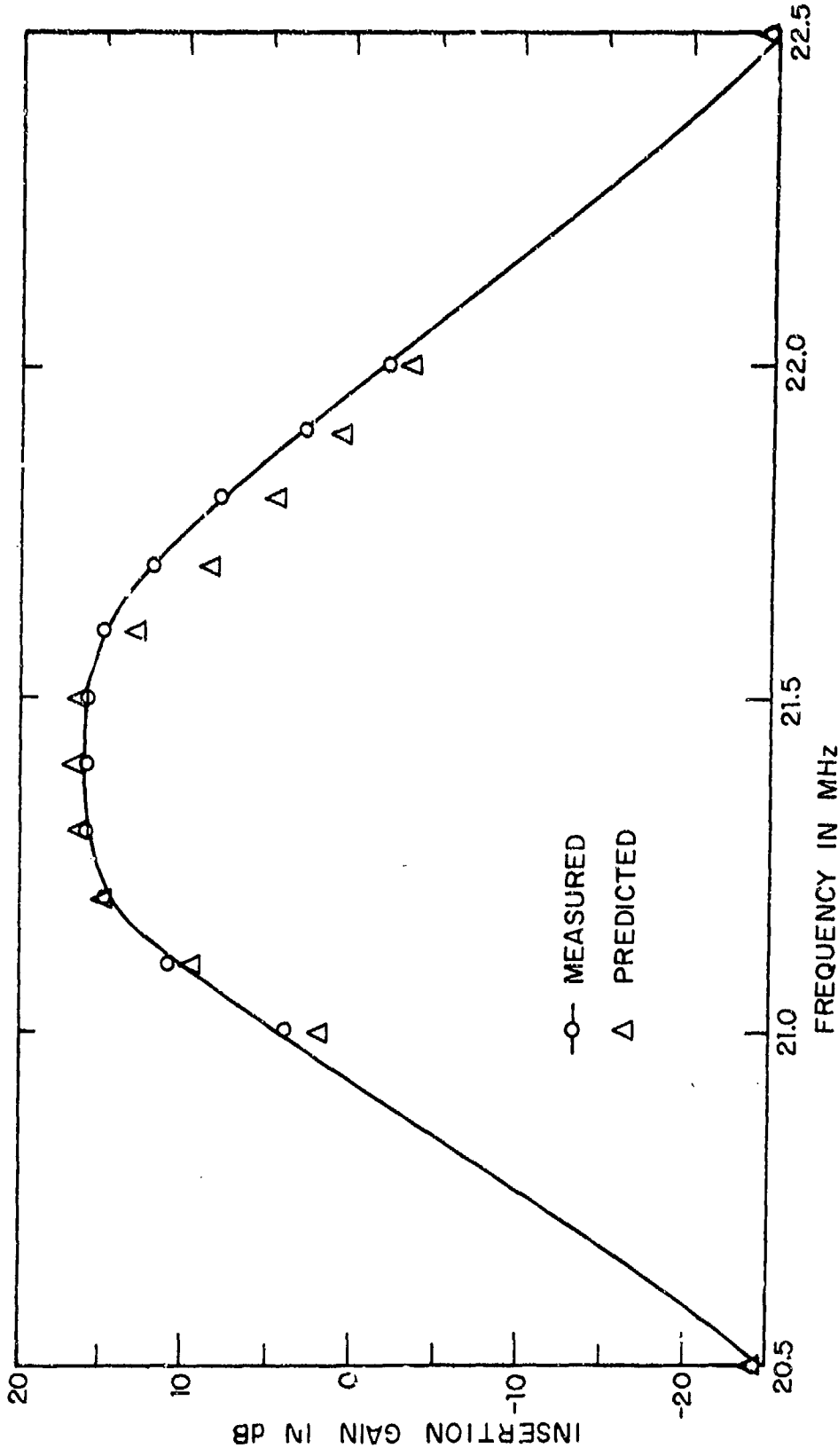


Fig. 7.23 Insertion gain of IF amplifier.

third-order nonlinear transfer function for the three points. The first point, $f_1 = 21.3$ MHz and $f_2 = 21.2$ MHz, is a case of in-band interference. The measured third-order nonlinear transfer function is 84.4 dB; its large magnitude is due to the fact that the distortion is produced in the Q3-Q4 pair, and has the full gain of Q1-Q2 and the first tuned interstage network. The second point, $f_1 = 21.5$ MHz and $f_2 = 21.6$ MHz, is on the edge of the first interstage's passband. While the distortion is still primarily in Q3-Q4 its amplitude is down 14 dB from that of the first point. The final point, $f_1 = 22.5$ MHz, $f_2 = 23.6$ MHz, is out-of-band with respect to the IF tuned circuits, and the distortion is produced in the Q1-Q2 pair. The third-order nonlinear transfer functions are considered to be in sufficiently good agreement with the measured data to confirm the modeling of both the transistors and the passive networks.

7.6 Detector and AGC Effects

In this section we present experimentally determined detector and AGC characteristics. The predictions and measurements of the previous four sections were all made with the AGC circuit grounded, and the AM detector diode disconnected. In actual operation, of course, the detector diode would be connected and the AGC would be operative. Since the SIGNCAP transistor model has, as input parameters, the operating points of the transistors, the effect of varying input levels of signal and interference can be taken into account by an iterative analysis which determines a consistent solution to the closed loop system of the nonlinear receiver and its AGC and detector characteristics.

7.6.1 The AM Detector

The IF amplifier has been analyzed so far with the output taken at the FM limiter input, and CR1, the AM diode detector, disconnected. In actual operation, of course, the diode is in place, and will load the second tuned interstage network. In order to determine the extent of this loading, the diode was reconnected and the IF amplifier measurements repeated. In the course of the measurements it became evident that the insertion gain of the IF amplifier was not a unique, repeatable quantity for a given frequency. Further investigation showed that the insertion gain was, in fact, a function of the amplitude of the signal being detected, with the gain decreasing with smaller signals.

Figure 7.24 shows the measured insertion gain under three conditions, namely (1) the AM detector diode disconnected, (2) the AM detector diode connected and the signal across a 50 ohm load at the Q8 input set at -30 dBm, and (3) the diode connected and the signal set at -50 dBm. It is seen that as the signal level decreases the peak insertion gain decreases both in amplitude and the frequency at which it occurs.

In order to find a physical explanation for this, we return to the circuit diagram, Fig. 7.6. The AM detector diode, CR1, goes between a high impedance point (the junction of L4 and C18), and its filter and buffer amplifier, R24, C20, and Q5. If the input impedance of CR1 were level dependent, then the variable insertion gain would be understood. Table 7.3 shows the DC voltage measured at the cathode of CR1, and the peak AC voltage computed at the anode of CR1 for several power levels defined at the limiter input. The AC voltage was computed, not measured,

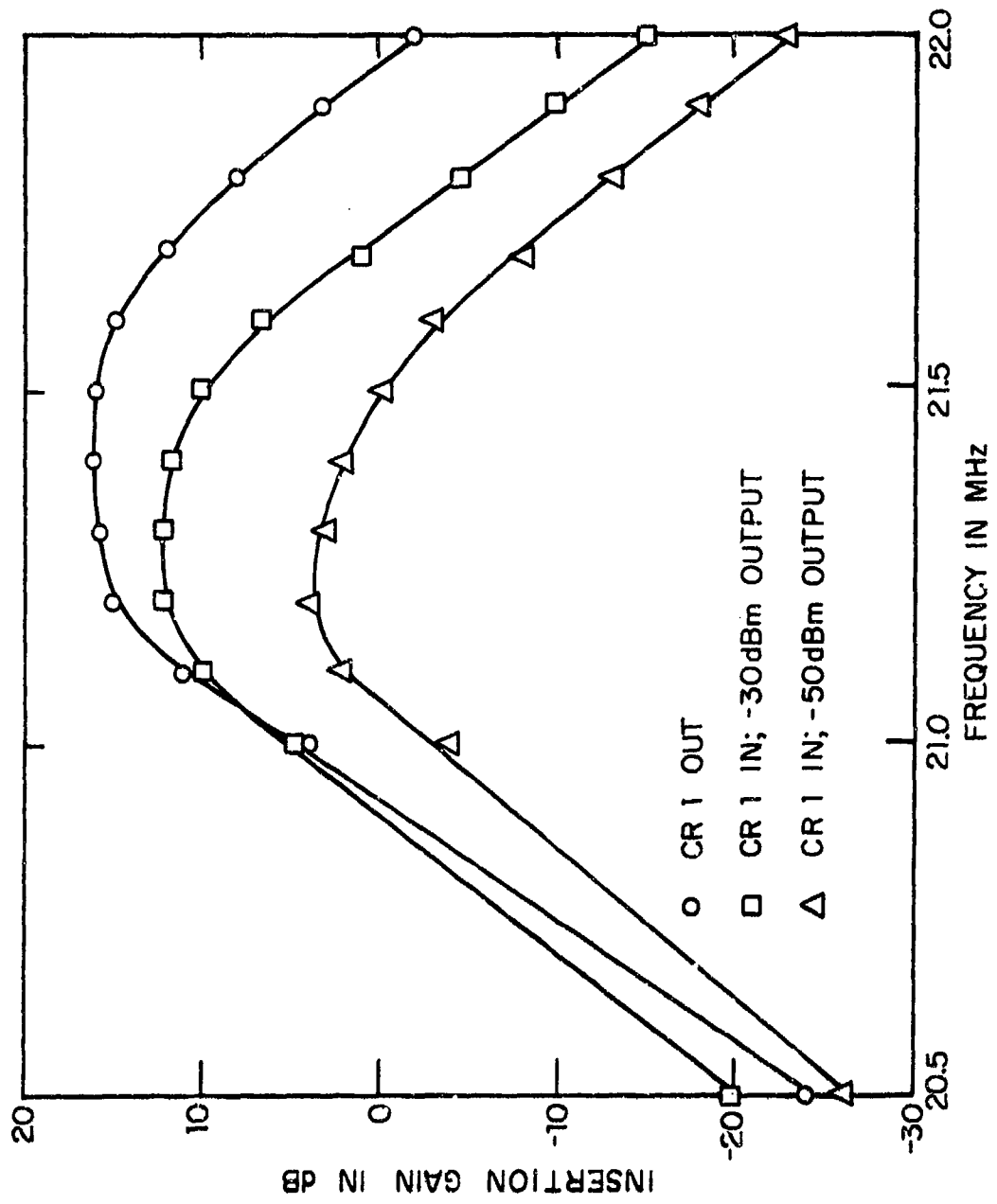


Fig. 7.24. Measured effect of AM detector upon the IF amplifier insertion gain.

TABLE 7.3
CRL DETECTOR VOLTAGES AT 21.4 MHz

Power in 50 ohms at Q6 Input	Peak Anode Voltage, CRL (Computed)	DC Cathode Voltage, CRL (Measured)
None	0.000 V	-0.0964 V
-50 dBm	0.086 V	-0.0890 V
-40 dBm	0.272 V	0.000 V
-30 dBm	0.860 V	+0.4052 V

as the act of measuring would, in itself, change the voltage being measured. The computation was based on the predicted voltage transfer function between the limiter input and the AM detector input. The table shows that at -30 dBm there is a peak forward voltage across the diode of about 0.46 volts. During most of the cycle the voltage is less than this; indeed, the diode is reverse biased for approximately 67% of the cycle. For a -50 dBm level, however, the diode is never reverse biased, and has a peak forward bias of 0.175 volts. It is thus reasonable to expect the detector to present a signal level dependent impedance to the interstage network.

With this insight into the AM detector operating points, we now seek reasonable models for the input terminal behavior of the detector. Figure 7.25 shows the experimental data of Fig. 7.23, along with two predicted curves. In one set of predictions, the detector circuitry is replaced by a parallel combination of 1.25 pF and 10 K ohms to ground; this is seen to model reasonably well the detector behavior at -30 dBm. The second set of predictions are for the detector circuitry replaced by a parallel combination of 2.0 pF and 3.0 K ohms; this is seen to model the -50 dBm results.

The linearity of the AM detector was measured by the following experiment. The IF amplifier was tested as an isolated unit, with an AM signal used as its input. The modulation frequency was kept at 4 KHz, and the input carrier level was kept at -42 dBm; This produces an output carrier level of -30 dBm at the limiter input monitor point. The modulation index was varied over a wide range, and the AM detector output voltage was measured with an audio voltmeter, which was calibrated in dBm relative to a 600 ohm load. Figure 7.26 shows the measured transfer function. It is seen that the detector has at least a 30 dB linear range, corresponding to a modulation index of slightly greater than 30%. In a second test, the modulation index was kept constant at 30%, and the modulation frequency varied from 100 Hz to 60 KHz. The detector output was essentially flat up to 20 KHz, and down 3 dB at 60 KHz.

7.6.2 FM Detector

The FM detector consists of two stages of bandpass limiting in transistors Q6-Q7, and Q8-Q9, followed by a diode discriminator. The discriminator output is buffered by C10, an emitter

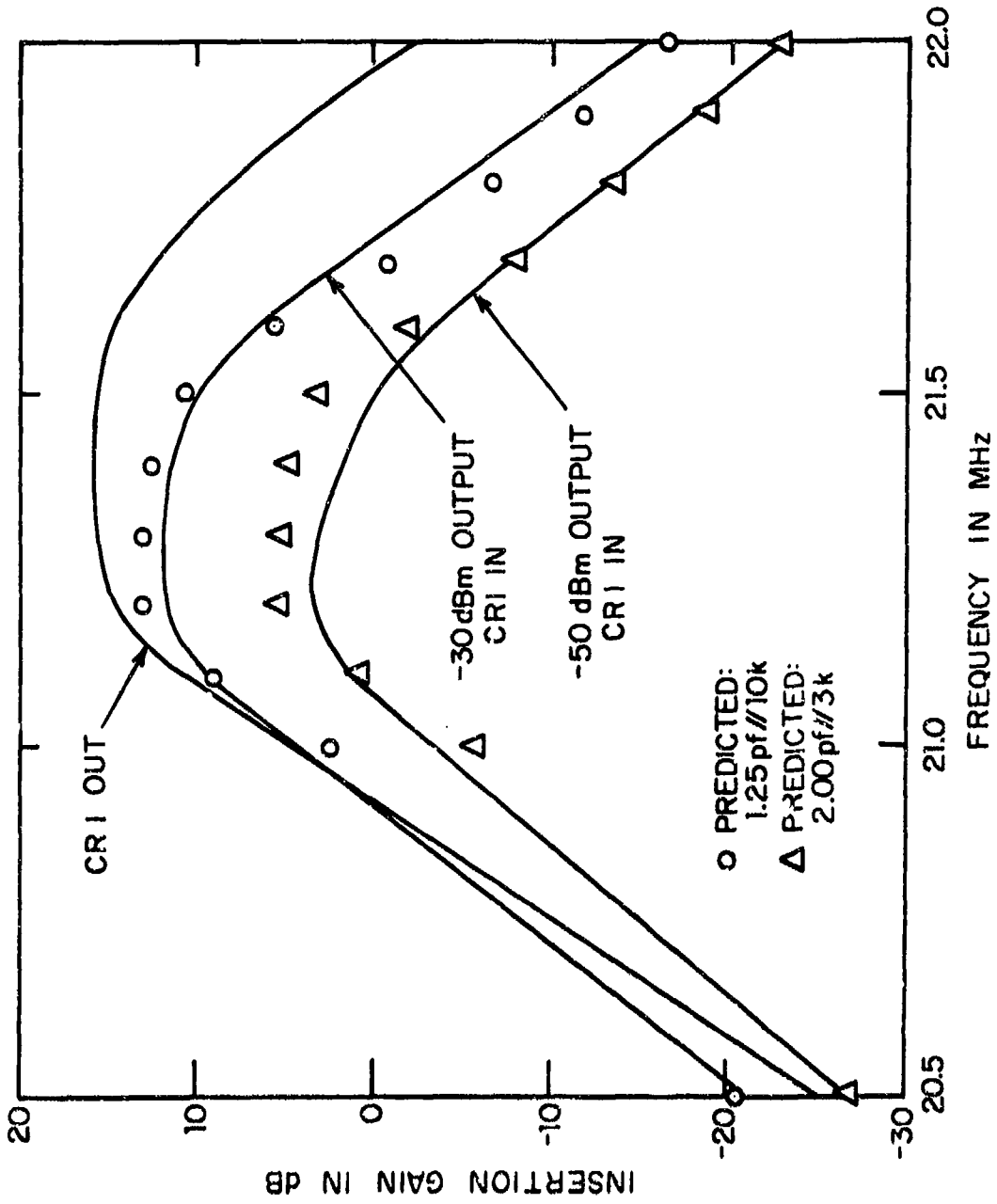


Fig. 7.25. Comparison of IF amplifier insertion gain dependence upon AM detector model.

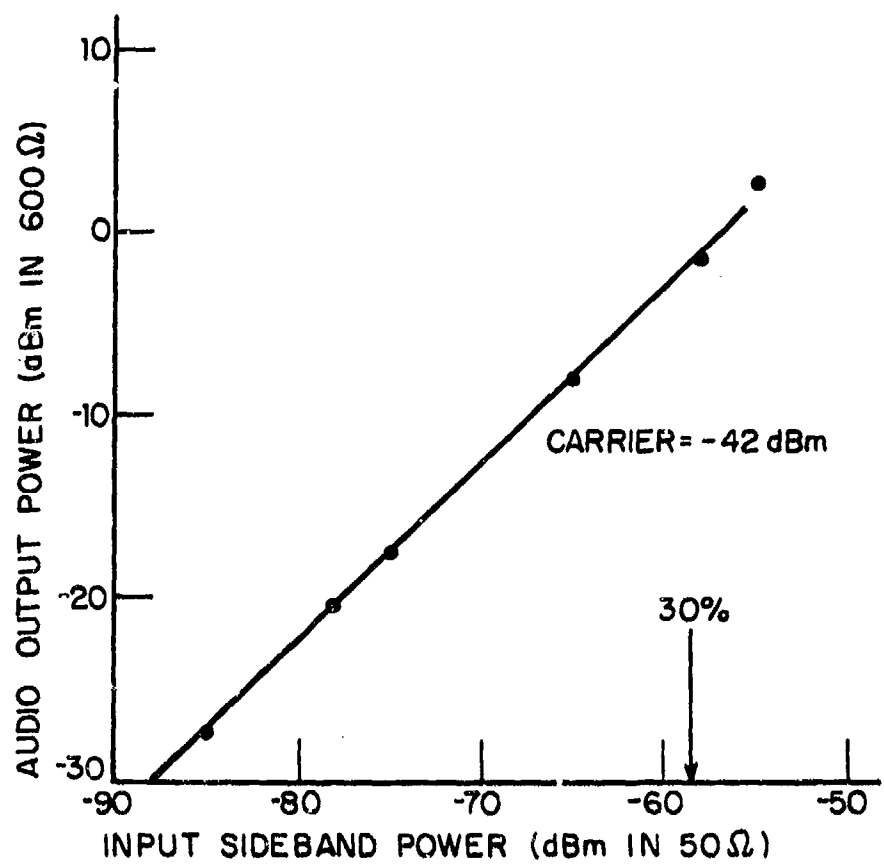


Fig. 7.26. AM detector transfer function.

follower. The measured discriminator response is shown in Fig. 7.27. In taking the data, the input was a tone, kept at a constant amplitude of -30 dBm at the input to Q6. The linear range of the discriminator is seen to be 21.1 to 21.7 MHz, and the sensitivity is 11.6 volts/MHz, or, equivalently, 11.6 mv/KHz.

7.6.3 AGC

The input to the AGC amplifier is the AM detector output of the IF amplifier. The output of the AGC amplifier is the delayed AGC to the RF tuner, and the normal AGC to the pre-IF amplifier. Figure 7.28 shows the measured relevant AGC characteristics of the receiver. The abscissa is available input power, in dBm, to the RF tuner. The left-hand ordinate are the AGC voltages, and the right-hand ordinate is the power measured in 50 ohms at the FM limiter input, our conventional monitoring point. The measurements were made with an input which was a 45.5 MHz tone.

The AGC is inoperative for inputs below approximately -94 dBm. For input levels lower than -94 dBm, the receiver output power increases approximately as the 1.5 power of the input power. This is due to the previously noted level-dependent input impedance of the AM detector diode. For inputs between -94 dBm to about -90 dBm, the receiver is in a transition state, with the AGC beginning to operate. For inputs greater than -90 dBm the output is about -23 dBm. The output cannot be exactly constant, of course, or there would not be an error signal to feed back to the AGC circuitry. The slope of the output curve is approximately 0.0225 dB output/dB input.

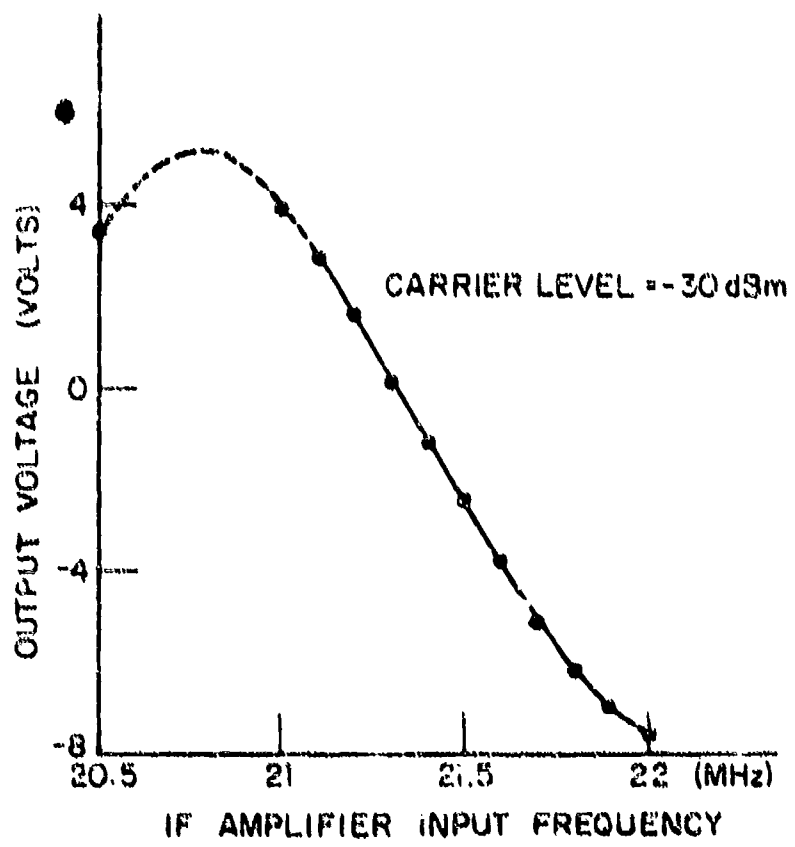


Fig. 7.27. FM discriminator response.

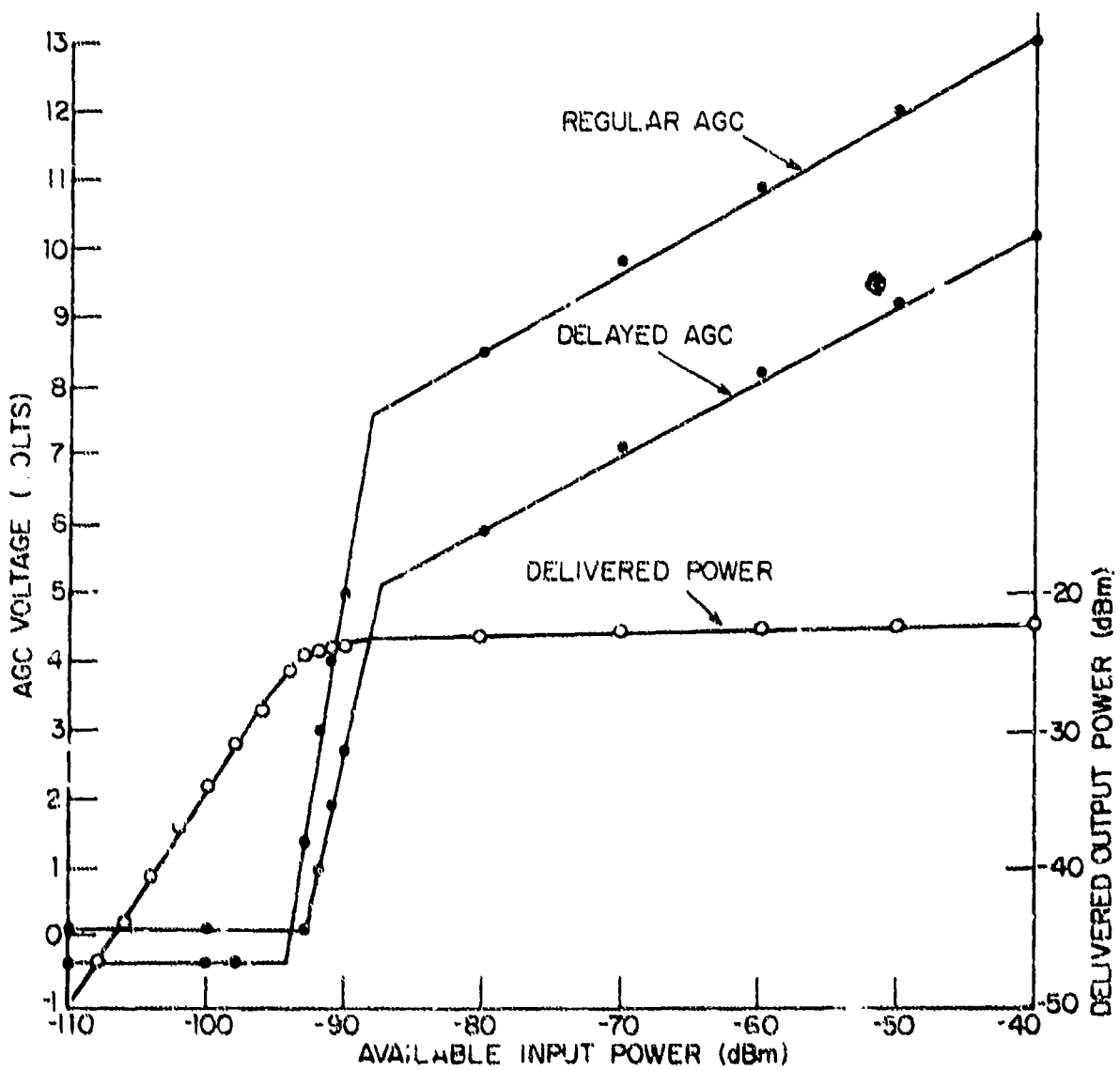


Fig. 7.28. Measured Receiver AGC Characteristics

7.7 Complete Predetection Receiver

The complete predetection portion of the VHF receiver was modeled by considering the RF tuner, pre-IF amplifier, and IF amplifier as separate segments for analysis purposes. These segments, or receiver subsystems, are shown in Fig. 7.29. Source and load impedances as well as interstage output and input impedances are noted in the figure. The three segments were analyzed to determine the overall nonlinear transfer functions by utilizing the cascading theory with linear interaction corrections as discussed in Chapter 2, Section 2.3. This approach conserves computer effort within the limitation of SIGNCAP. The cascade calculation can be either accomplished manually or by using the cascading options in SIGNCAP. Division of the receiver at the interfaces described is natural and can be expected to be quite successful since the tuner, pre-IF, and IF amplifier interfaces all have source and load impedances that are essentially resistive and broadband over the frequency regions of concern.

In the following sections we shall outline the theoretical approach to determining the equivalent first, second, and third-order nonlinear transfer functions. Predictions will be compared with overall measured responses. We shall also write out explicit relationships relating the predetection receiver output to multitone input signals to illustrate the detailed use of transfer functions and their cascades. Table 7.4 summarizes the notation used for the individual nonlinear transfer functions. Observe that we have used the equivalent amplifier concept (See Chapter 1) in describing the RF tuner since it contains the input signal down-conversion process. The local oscillator has been assumed sinusoidal with complex amplitude A .

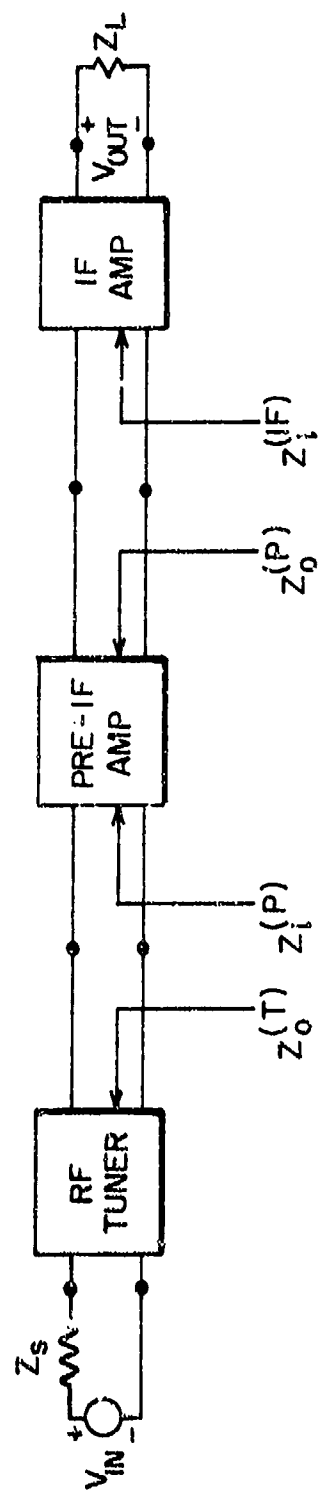


Fig. 7.29. Segments of VHF Receiver Used in Cascading Nonlinear Transfer Functions.

Table 7.4.

Nonlinear Transfer Functions for the
Predetection VHF Receiver Segments

	RF Tuner	Pre-IF Amplifier	IF Amplifier
<u>First-Order</u>	$H_1^{\text{eq}}(T) = AH_2^{(T)}$	$H_1^{(P)}$	$H_1^{(\text{IF})}$
<u>Second-Order</u>	$H_2^{\text{eq}}(T) = \frac{3}{2} AH_3^{(T)}$	$H_2^{(P)}$	$H_2^{(\text{IF})}$
<u>Third-Order</u>	$H_3^{\text{eq}}(T) = 2 AH_4^{(T)}$	$H_3^{(P)}$	$H_3^{(\text{IF})}$

7.7.1 Equivalent First-Order Nonlinear Transfer Function

The predicted and measured equivalent nonlinear transfer functions for the desired and image responses are shown in Figs. 7.30 and 7.31, respectively. The modeling of both the desired and image responses are good in both amplitude and frequency. Note that the peak values of the desired and image responses differ by about 65 dB in both measurement and prediction.

The prediction is based upon the first-order equivalent transfer function given by

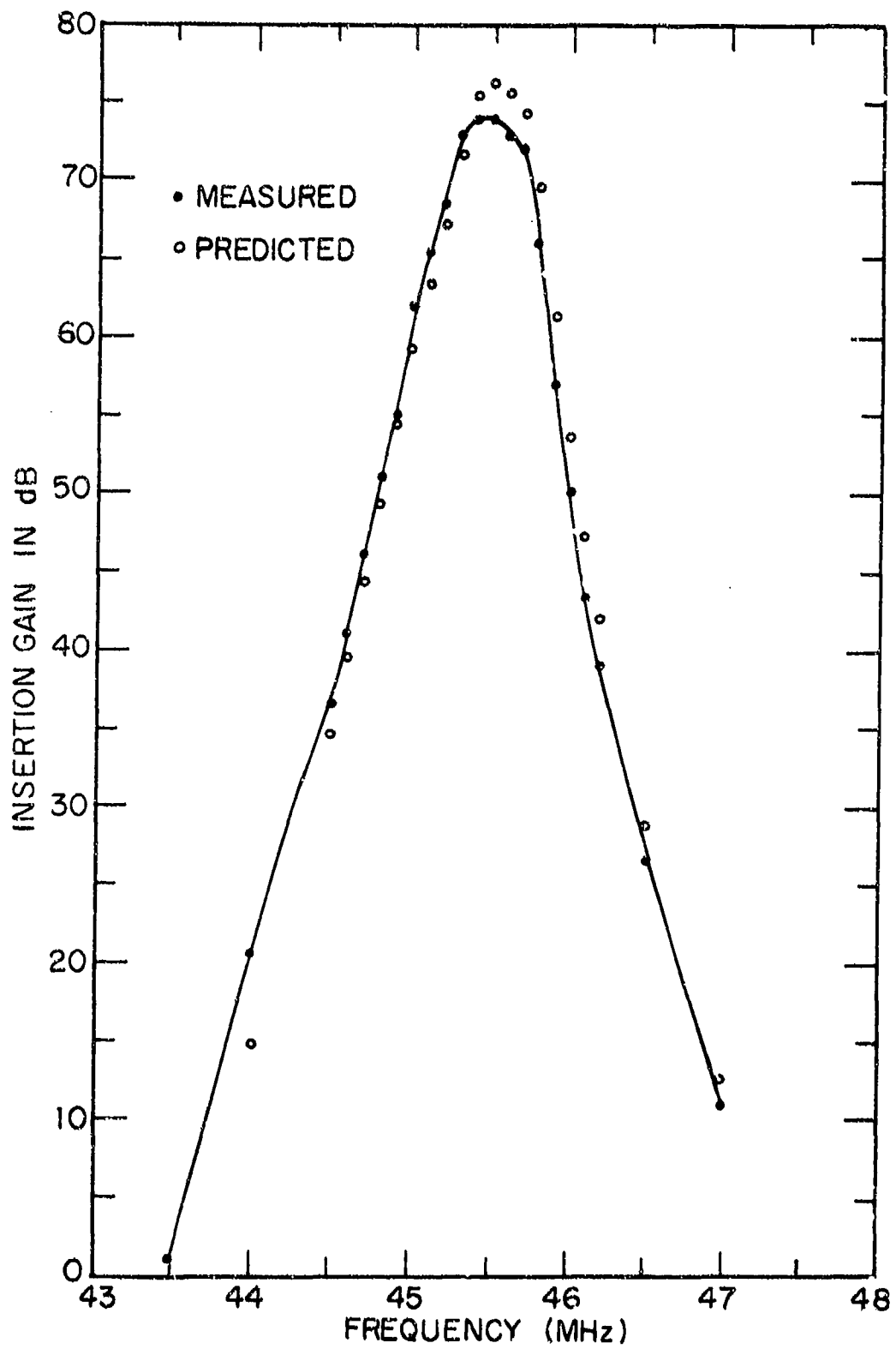


Fig. 7.30. VHF Receiver Equivalent First-Order Transfer Function.

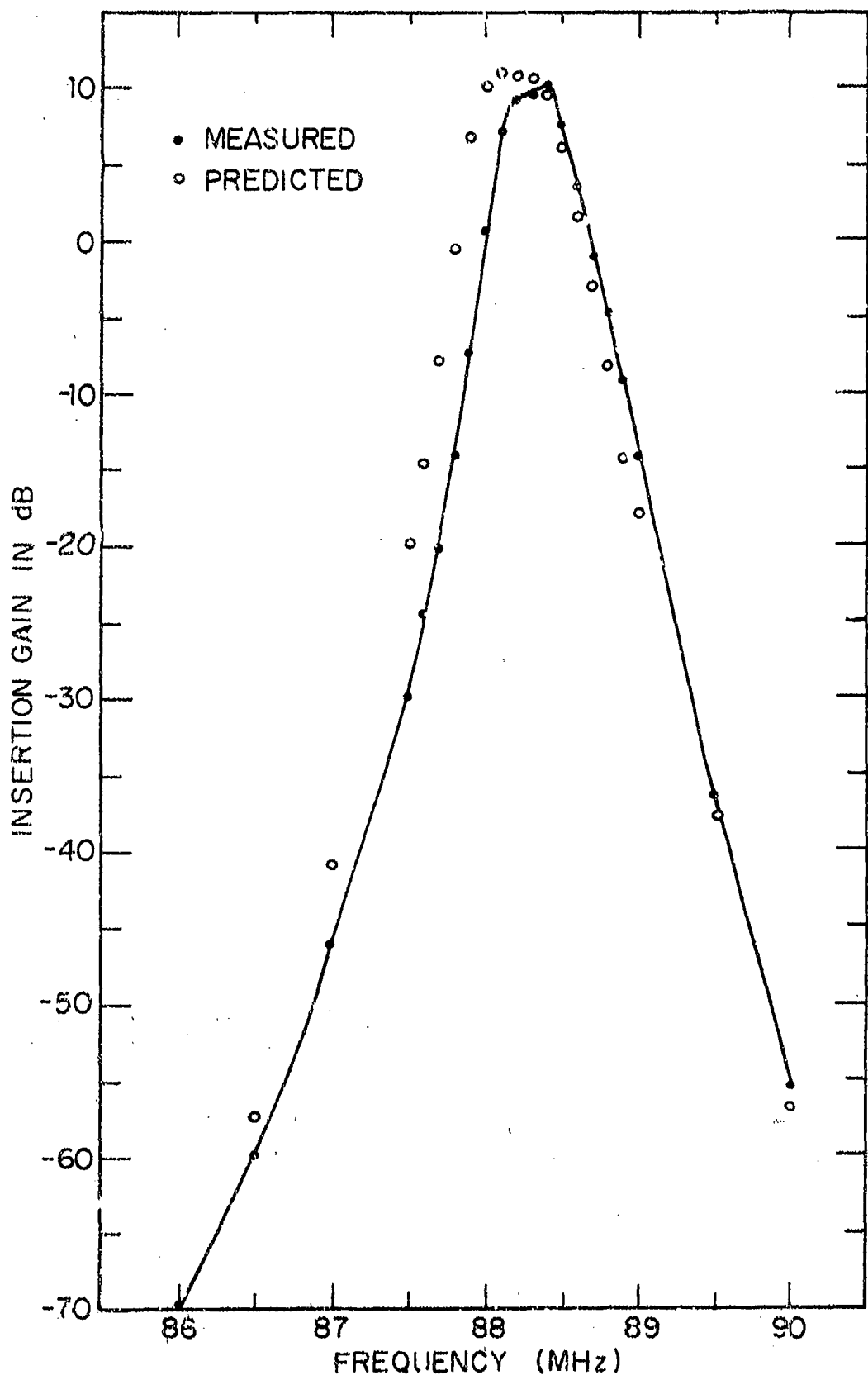


Fig. 7.31. VHF Receiver Equivalent First-Order Transfer Function. Image Response.

$$\begin{aligned}
 H_1^{eq}(-f; f_{LO}) &= H_1^{eq(T)}(-f; f_{LO}) \\
 \cdot \frac{z_0^{(T)}(f_{LO}-f) + z_i^{(P)}(f_{LO}-f)}{z_i^{(P)}(f_{LO}-f)} H_1^{(P)}(f_{LO}-f) \\
 \cdot \frac{z_0^{(P)}(f_{LO}-f) + z_i^{(IF)}(f_{LO}-f)}{z_i^{(IF)}(f_{LO}-f)} H_1^{(IF)}(f_{LO}-f) \quad (7.4)
 \end{aligned}$$

where the impedance ratios account for the linear interaction (See Chapter 2, Section 23.) between the tuner and the pre-amplifier and also between the pre-amplifier and the IF amplifier. It follows that the desired signal at the IF amplifier output is given by the real part of

$$v_{out}^{eq} e^{j2\pi(f_{LO}-f)t} = v(f) H_1^{eq}(-f; f_{LO}) e^{j2\pi(f_{LO}-f)t} \quad (7.5)$$

where $v(f)$ is the amplitude of the input signal. The actual prediction is shown in Fig. 7.30 and was made using SIGNCAP. The image response shown in Fig. 7.31 is predicted by evaluating $H_1^{eq}(f; -f_{LO})$ since the input frequency f is higher than the local oscillator frequency f_{LO} .

7.7.2 Equivalent Second-Order Nonlinear Transfer Function

The predicted and measured equivalent second-order nonlinear transfer function for the complete receiver is shown in Fig. 7.32. As mentioned in previous sections, the response is measured in a

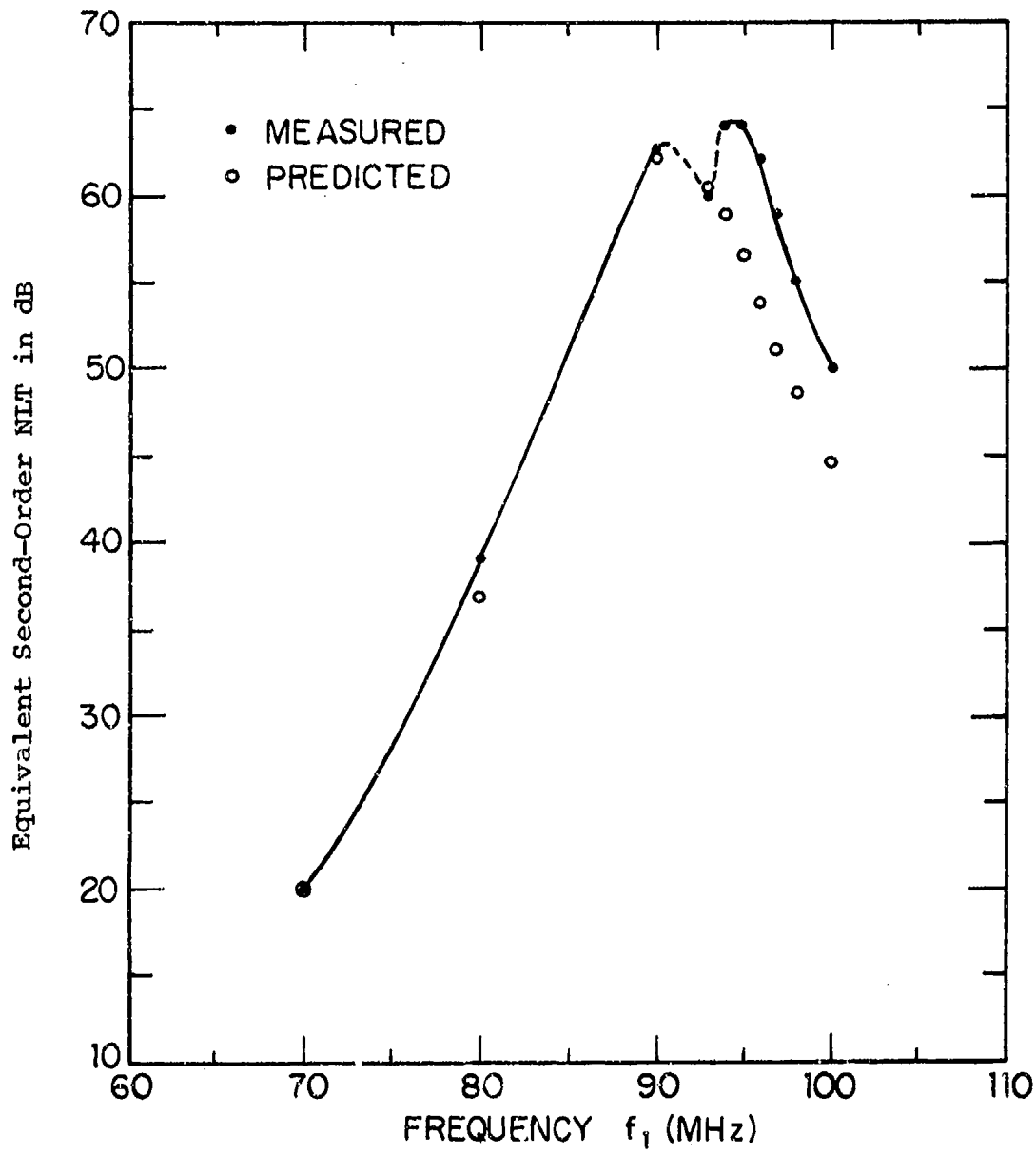


Fig. 7.32. VHF Receiver Equivalent Second-Order Nonlinear Transfer Function.

two-tone test, with $|f_1 - f_2|$ being set equal to the tuned frequency of the receiver. The predicted and measured nonlinear transfer functions are, again, in reasonably good agreement. Again SIGNCAP was used to obtain the theoretical prediction by using its cascading capability.

7.7.3 Equivalent Third-Order Nonlinear Transfer Function

The predicted and measured equivalent third-order nonlinear transfer function for the complete receiver is shown in Fig. 7.33. Although the equivalent first and second-order nonlinear transfer functions were predicted using the SIGNCAP cascade capability, the equivalent third-order nonlinear transfer function was predicted by a manual cascade calculation. The reason for not using SIGNCAP I in its existing form to perform the equivalent third-order prediction is that a complete sixth-order analysis would have been required. It was recognized that the required time to compute all products to sixth-order would not be justified since a manual calculation of the dominant terms should be more than adequate.

The equivalent third-order nonlinear transfer function for the complete predetection receiver relates the receiver IF amplifier output at $f_{LO} - (2f_1 - f_2)$ to the RF tuner inputs at f_1 and f_2 . In particular, the output is given by the real part of

$$v_{\text{OUT}} e^{j2\pi[f_{\text{LO}} - (2f_1 - f_2)]t} = \frac{3}{4} A_1^*{}^2 (f_1) A_2 (f_2) H_3^{\text{eq}} (-f_1, -f_1, f_2; f_{\text{LO}}) e^{j2\pi[f_{\text{LO}} - (2f_1 - f_2)]t}. \quad (7.6)$$

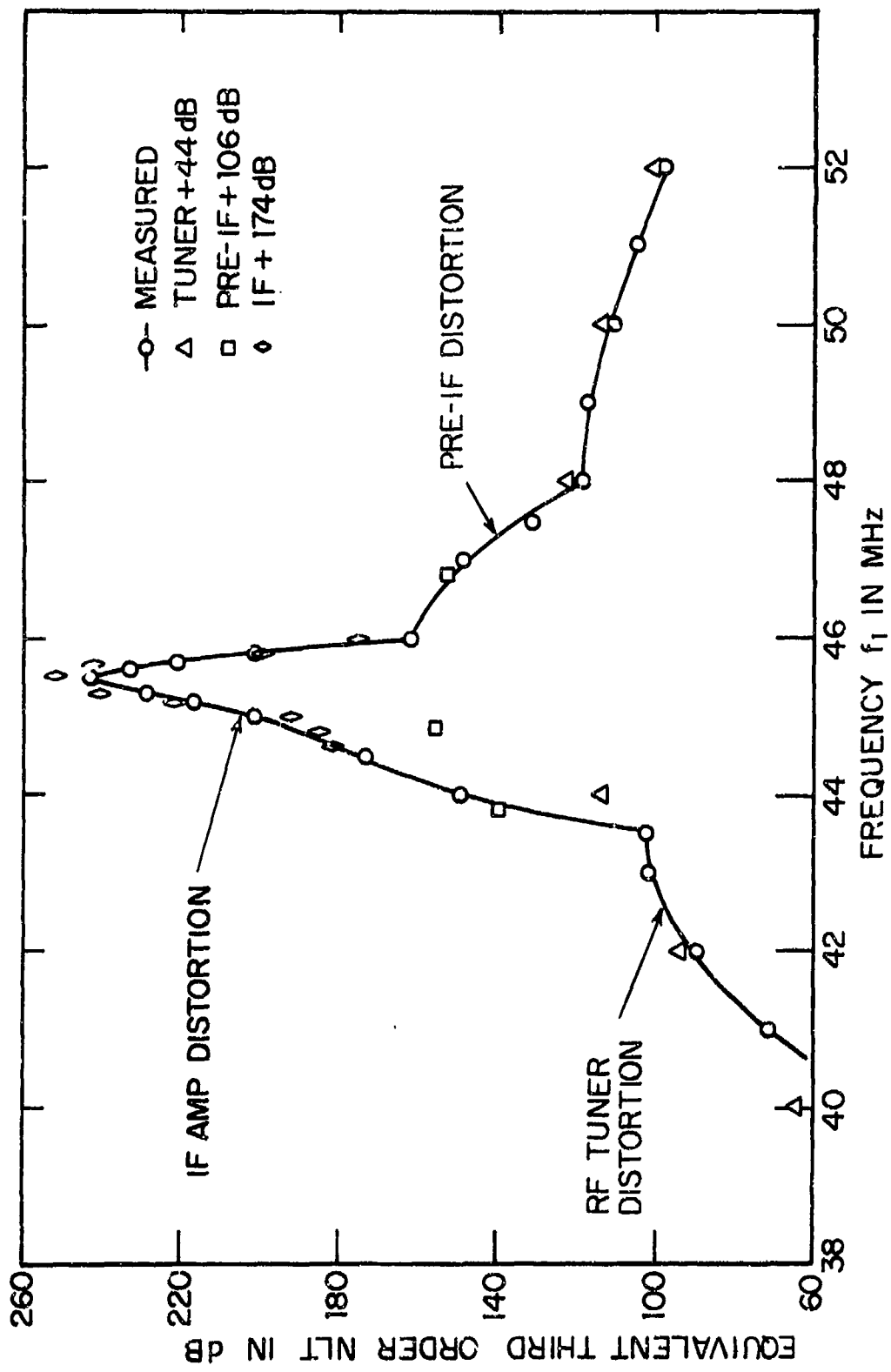


Fig. 7.33. VHF Receiver Equivalent Third-Order Nonlinear Transfer Function.

where H_3^{eq} is to be determined in terms of the nonlinear transfer functions (Table 7.4) of the individual cascaded subsystems appropriately corrected for linear interaction as described in Chapter 2, Section 2.3. The amplitudes of the input tones at f_1 and f_2 are, respectively, given by $A_1(f_1)$ and $A_1(f_2)$.

The experimentally determined third-order equivalent nonlinear transfer function illustrated in Fig. 7.33 strongly suggests a particularly simple approach to evaluating the cascaded third-order intermodulation term. There are many contributing terms that are present but the dominant distortion in the IF amplifier passband arises from the following three principal cascade cases:

1. Equivalent Third-Order RF Tuner - Linear Pre-IF Amplifier - Linear IF Amplifier.
2. Equivalent First-Order RF Tuner - Third-Order Pre-IF Amplifier - Linear IF Amplifier.
3. Equivalent First-Order RF Tuner - Linear Pre-IF Amplifier - Third-Order IF Amplifier.

Case 1 requires a conventional fourth-order analysis while Cases 2 and 3 are specific terms in a sixth-order analysis of the complete receiver.

Case 1: RF Tuner

At RF tuner output frequencies outside the pre-IF and IF amplifier passbands, the dominant nonlinearity in the RF tuner is excited by the two input tones at frequencies f_1 and f_2 . The equivalent third-order intermodulation distortion output at $f_{LO} - (2f_1 - f_2) = f_{IF}$ is then simply amplified by the pre-IF and IF amplifiers. For this situation we have

$$\begin{aligned}
 H_3^{eq}(-f_1, -f_1, f_2; f_{LO}) &= H_3^{eq(T)}(-f_1, -f_1, f_2; f_{LO}) \\
 &\cdot \frac{z_0^T(f_{IF}) + z_i^{(P)}(f_{IF})}{z_i^{(P)}(f_{IF})} H_1^{(P)}(f_{IF}) \\
 &\cdot \frac{z_0^{(P)}(f_{IF}) + z_i^{(IF)}(f_{IF})}{z_i^{(IF)}(f_{IF})} H_1^{(IF)}(f_{IF}). \tag{7.7}
 \end{aligned}$$

where

$$H_3^{eq(T)}(-f_1, -f_1, f_2, f_{LO}) = 2AH_4^{(T)}(-f_1, -f_1, f_2, f_{LO}). \tag{7.8}$$

If we recognize that the interfacing source and load impedances between the subsystems are essentially frequency independent and equal, we may further reduce Eq. (7.7) to

$$H_3^{eq} = H_3^{eq(T)} 2 H_1^{(P)} 2 H_1^{(IF)}. \tag{7.9}$$

Making use of the relationship between insertion gain and the first-order transfer function (See Chapter 6, Section 6.2.1) we obtain

$$\begin{aligned}
 20 \log_{10} |H_3^{eq}| &= 20 \log_{10} |H_3^{eq(T)}| \\
 &+ G_I^{(P)}(f_{IF}) + G_I^{(IF)}(f_{IF}). \tag{7.10}
 \end{aligned}$$

But, the mid-band insertion gain of the pre-IF amplifier is 16 dB while the value for the IF amplifier is 28 dB. Hence, the

contributions from the RF tuner to the output equivalent third-order intermodulation distortion is

$$20 \log_{10} |H_3^{\text{eq}}| = 20 \log_{10} |H_3^{\text{eq}(T)}| + 44 \text{ dB.} \quad (7.11)$$

This result has been plotted in Fig. 7.33 by the triangular data points. Observe that this result fits the measured distortion quite well when input frequency f_1 is outside the range 44-48 MHz.

Case 2: Pre-IF Amplifier

As the RF tuner output frequency moves within the pre-IF amplifier passband, the dominant nonlinearity passes from the RF tuner to the pre-IF amplifier. The third-order intermodulation distortion from the pre-IF amplifier, as excited by the two tones at $f_{\text{LO}} - f_1$ and $f_{\text{LO}} - f_2$, now dominates. This distortion is then simply amplified by the IF amplifier. The receiver input tones at f_1 and f_2 have also been amplified by the RF tuner equivalent amplifier gain. Using the third-order cascade results from Chapter 2, Section 2.3, we can write

$$\begin{aligned} H_3^{\text{eq}}(-f_1, -f_1, f_2; f_{\text{LO}}) &= \\ &\left\{ \frac{z_0^{(T)}(f_{\text{LO}} - f_1) + z_i^{(P)}(f_{\text{LO}} - f_1)}{z_i^{(P)}(f_{\text{LO}} - f_1)} H_1^{\text{eq}(T)}(-f_1, f_{\text{LO}}) \right\}^2 \\ &\cdot \frac{z_0^{(T)}(f_2 - f_{\text{LO}}) + z_i^{(P)}(f_2 - f_{\text{LO}})}{z_i^{(P)}(f_2 - f_{\text{LO}})} H_1^{\text{eq}(T)}(-f_2, f_{\text{LO}}) \\ &\cdot \frac{z_0^{(P)}(f_{\text{IF}}) + z_i^{(\text{IF})}(f_{\text{IF}})}{z_i^{(\text{IF})}(f_{\text{IF}})} H_3^{(P)}(f_{\text{LO}} - f_1, f_{\text{LO}} - f_1, -f_{\text{LO}} + f_2) \cdot H_1^{(\text{IF})}(f_{\text{IF}}) \end{aligned} \quad (7.12)$$

If we now recognize that the interfacing impedances are broad-band resistive and equal, we can simplify further to obtain

$$H_3^{eq} = \left\{ 2 H_1^{eq(T)} \right\}^2 \cdot 2 H_1^{eq(T)} \cdot 2 H_3^{(P)} H_1^{(IF)}. \quad (7.13)$$

Using the insertion gain relationships for linear stages, we can now write

$$\begin{aligned} 20 \log_{10} |H_3^{eq}| &= 2 G_I^{eq(T)} (-f_1; f_{LO}) \\ &\quad + G_I^{eq(T)} (-f_2; f_{LO}) \\ &\quad + G_I^{(IF)} (f_{IF}) \\ &\quad + 20 \log_{10} |H_3^{(P)}|. \end{aligned} \quad (7.14)$$

where $G_I^{eq(T)}$ is the equivalent-amplifier insertion gain (conversion gain) of the RF tuner. If we assume that the two input tones at f_1 and f_2 are within the passband of the RF tuner, whose insertion gain is nearly flat at 30 dB over the region of interest, we have

$$\begin{aligned} 20 \log_{10} |H_3^{eq}| &= 2 \cdot 30 + 30 + 16 + 20 \log_{10} |H_3^{(P)}| \\ &= 20 \log_{10} |H_3^{(P)}| + 106 \text{ dB}. \end{aligned} \quad (7.15)$$

This result has also been shown in Fig. 7.33 by the data points indicated by squares. Observe that these points fit the measured data well in the region indicated as pre-IF distortion.

Case 3: IF Amplifier

As the pre-IF amplifier outputs at $f_{LO} - f_1$ and $f_{LO} - f_2$ move within the IF amplifier passband, the dominant nonlinearity moves from the pre-IF amplifier to the IF amplifier. The third-order intermodulation distortion from the IF amplifier now will dominate. The RF tuner and pre-IF amplifier now serve only to linearly amplify the two input tones at $f_{LO} - f_1$ and $f_{LO} - f_2$. Using the results of cascading analysis and assuming equal resistive broadband interfacing impedances, we can write, by analogy,

$$20 \log_{10} |H_3^{eq}| = 2 \left[G_I^{eq(T)}(-f_1; f_{LO}) + G_I^{(P)}(f_{LO} - f_1) \right] \\ + \left[G_I^{eq(T)}(-f_2; f_{LO}) + G_I^{(P)}(f_{LO} - f_2) \right] \\ + 20 \log_{10} |H_3^{(IF)}|. \quad (7.16)$$

Again assuming $f_{LO} - f_1$ and $f_{LO} - f_2$ are within the passband of the pre-IF amplifier whose insertion gain is 28 dB, we have

$$20 \log_{10} |H_3^{eq}| = 2[30 + 28] + [30 + 28] + 20 \log_{10} |H_3^{(IF)}| \\ = 20 \log_{10} |H_3^{(IF)}| + 174 \text{ dB}. \quad (7.17)$$

This result has been shown as the data points plotted as diamonds in Fig. 7.33. These data points fit the experimental measurements quite well.

We note that the initial assumption regarding the significant contributions to the third-order equivalent nonlinear transfer function have been confirmed. The agreement between the predicted and measured third-order transfer functions are based upon a simple cascade argument with linear interaction corrections is good. The result confirms that there is little nonlinear interaction between the three principal subsystems of the predetection receiver.

We have also shown that, although the receiver is analyzed as an equivalent third-order system, it actually contains significant sixth-order terms when the pre-IF amplifier and the IF amplifier distortion is dominant. The cascade technique used in this section utilizes the significant sixth-order components in deriving the equivalent third-order nonlinear transfer functions.

7.8 Gain Compression/Expansion in the VHF Receiver IF Amplifier

In a linear amplifier, the output signal at the input signal frequency varies linearly with the input signal amplitude, that is, the gain of the amplifier is constant with respect to input amplitude. Gain compression occurs when the odd-order distortion products at the signal frequency subtract from the desired signal, thus apparently decreasing the gain. In broadband circuits, $H_1(f)$ and $H_3(f, f, -f)$ are normally out-of-phase, causing gain compression. It is less known, however, that in frequency-selective circuits the relative phases of $H_1(f)$ and $H_3(f, f, -f)$ may be highly frequency-dependent. In this case, the odd-order products may add to, rather than subtract from, the desired signal, thus causing gain expansion. Experimentally obtained broadband gain compression has been discussed in Section 6.4.5 of Chapter 6. In

this section we illustrate, both theoretically and experimentally, the transition from expansion to compression as a function of frequency by using the VHF receiver IF amplifier model as an example.

Figure 7.34 shows the measured available input-output delivered power characteristics of the IF amplifier at 21.4 MHz. It is seen that expansion occurs for input signal levels below approximately -30 dBm. At higher input signal levels, the amplifier apparently limits, and small-signal analysis is no longer valid. One concludes that in this case, small-signal nonlinear modeling is applicable in the region of expansion, but not of compression.

Figure 7.35 shows the same amplifier input-output measured power for 20.0 MHz operation. In this case it is seen that the system exhibits compression. The compression is gradual, indicating that small-signal nonlinear effects are predominant, and the input signal level can be even higher than -10 dBm without large-signal compression. The large difference in the linearity range at 21.4 MHz and at 20 MHz is due to the frequency selectivity of the amplifier.

Figure 7.36 shows computed gain dependence based on the small-signal nonlinear circuit model of the IF amplifier. These curves were computed using Eq. 6.60 together with nonlinear transfer functions derived from SIGNCAP. Curves are shown for a set of frequencies 100 kHz apart. Note that for the lower frequencies, the nonlinear model predicts expansion, but for the higher frequencies, compression is predicted. This is due to the fact that the angle of $H_3(f, f, -f)$ relative to $H_1(f)$ rotates from a

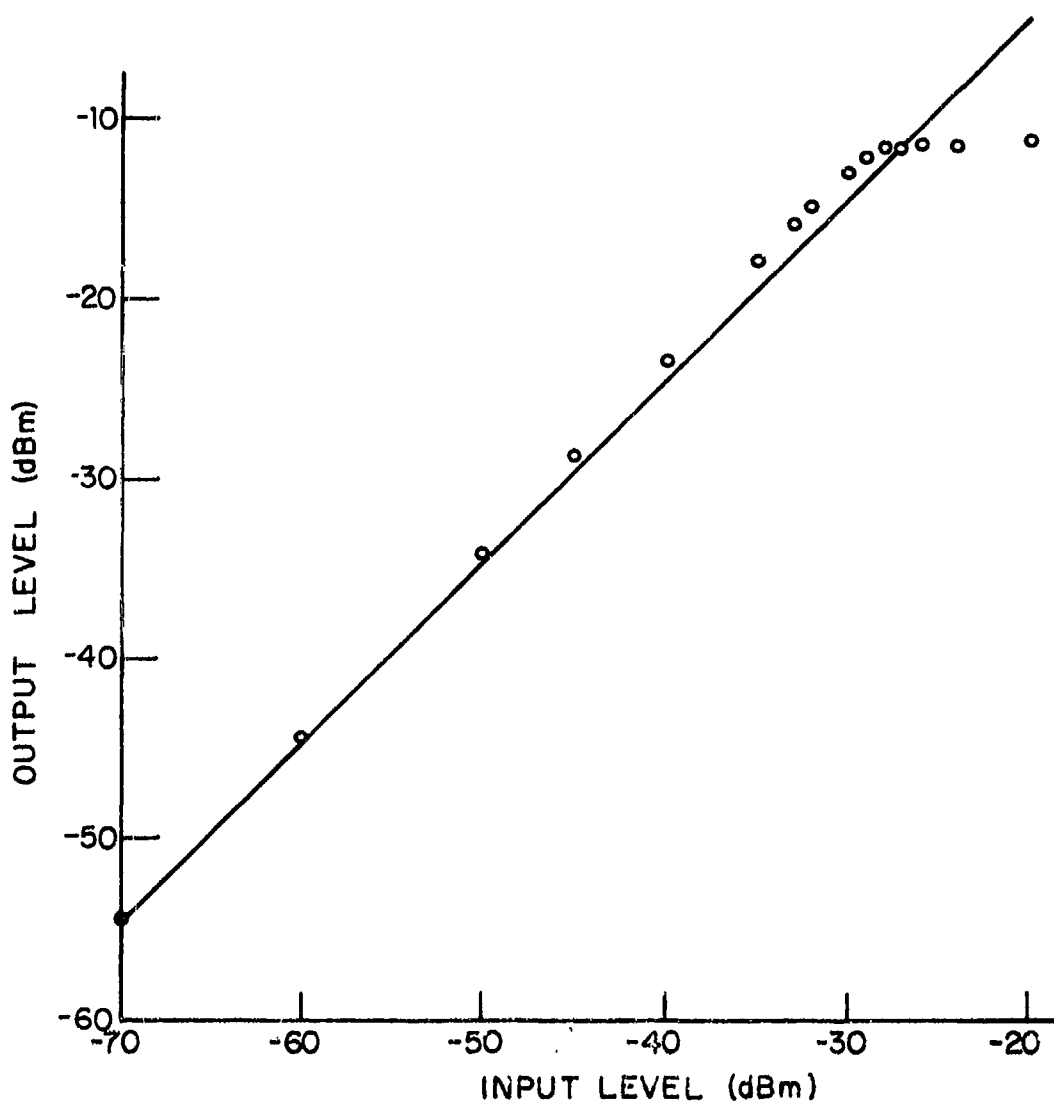


Fig. 7.34. Measured Input-Output Characteristic of the VHF Receiver IF Amplifier at 21.4 MHz.

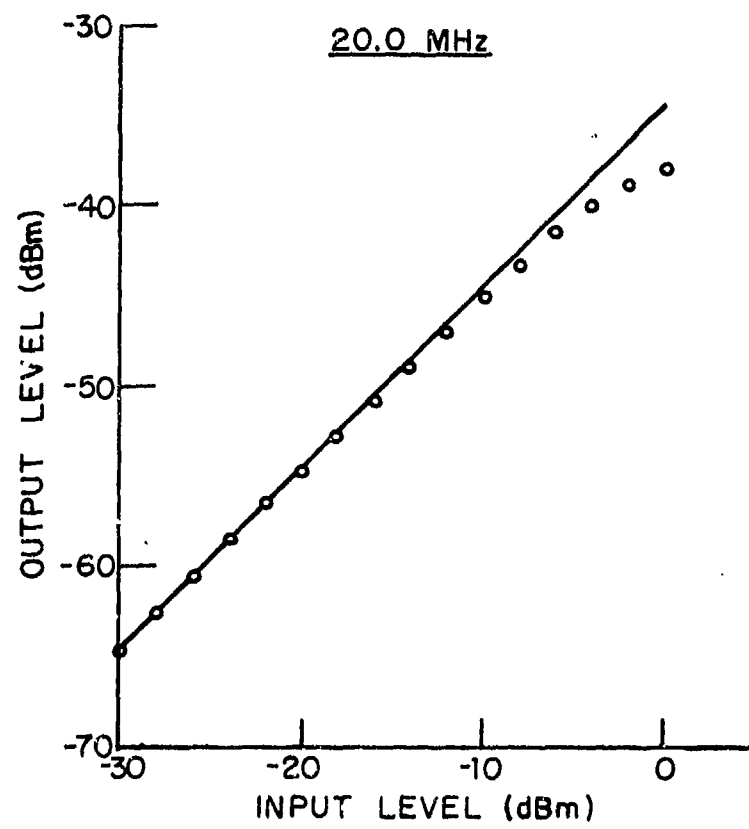


Fig. 7.35. Measured Input-Output Characteristic of the VHF Receiver IF Amplifier at 20.0 MHz.

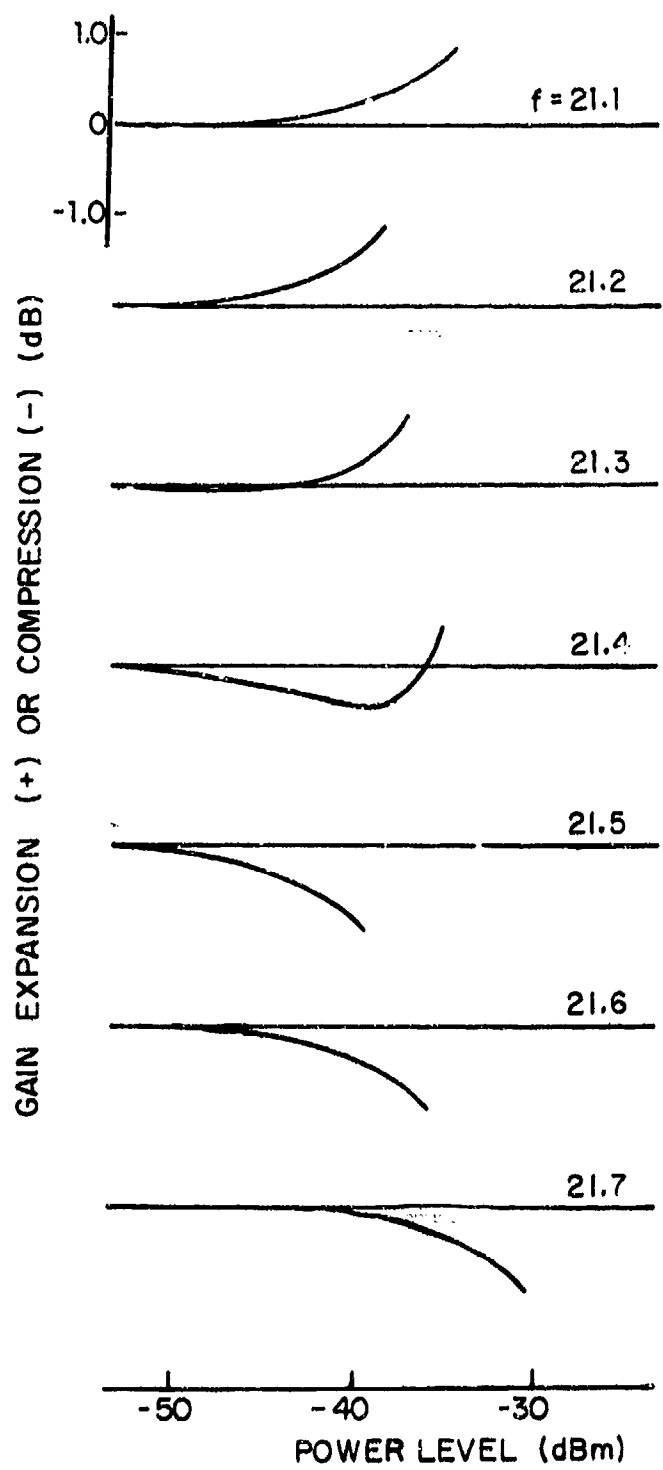


Fig. 7.36. Calculated Gain Compression/Expansion Curves for the VHF Receiver IF Amplifier.

value less than 90° to a value more than 90° . At 21.3 MHz this phase is almost exactly 90° so that the output component due to $H_3(f, f, -f)$ does not significantly modify the output level. Thus, at this frequency, the amplifier input-output characteristic appear to have an extended linear range. The theory thus predicts that both compression and expansion may be observed at a single frequency as the input level is varied. Furthermore, even if the measurement indicates that the receiver appears to be linear at a particular frequency, a two-tone intermodulation distortion measurement might show the receiver to be quite nonlinear. This behavior suggests that intermodulation measurements rather than compression measurements should be used in experimentally determining the region of validity of the small-signal nonlinear model.

7.9 Crossmodulation in the VHF Receiver IF Amplifier

The modeling of the VHF receiver IF amplifier has been presented earlier in this chapter. Both pre- and post-detection crossmodulation experiments have been performed on the IF amplifier, and the measured results compared with predictions based on the first term of the frequency power series canonic model developed in Chapter 3. These results are discussed in this section.

We first consider the predetection experiment. In this case, the desired signal was an unmodulated tone at 21.3 MHz, while the undesired signal was a sinusoidally amplitude modulated signal, with 0.3 modulation index, 4 kHz modulation frequency, and 10 MHz carrier frequency. The amplitude of the desired signal was set to give -30 dBm at the IF amplifier predetection output, thus assuring that the IF amplifier is operated in the small-signal region. The complex envelopes $z_1(t)$ and $z_2(t)$ of the desired and undesired signals are then

$$z_1(t) = A_1 \quad (7.18)$$

and

$$z_2(t) = A_2 (1 + \alpha_2 \cos 2\pi\mu_2 t). \quad (7.19)$$

Since the modulation frequency is small compared to the IF amplifier bandwidth, the derivative terms of the canonic model can be neglected, resulting in the ratio of first crossmodulation sideband amplitude to carrier amplitude given in Chapter 3 by Eq. (3.99), or

$$\frac{3}{2} \alpha_2 |A_2|^2 \left| \frac{H_3(v_1, v_2, -v_2)}{H_1(v_1)} \right|. \quad (7.20)$$

Table 3.3 shows that in addition to the first sideband, located $\mu_2 = 4$ kHz away from the desired carrier, there will be a second sideband located $2\mu_2 = 8$ kHz away from the desired carrier, the amplitude of which is $a_2/4$ times that of the first sideband.

Figure 7.37 shows the measured delivered output power in these crossmodulations sidebands, and the predicted delivered power based on the circuit model and the canonic model. The input is the available carrier power in the undesired signal. It is seen that the measured crossmodulation power has the second-order slope predicted by theory, and that the agreement between predicted and measured crossmodulation power is excellent for both the first and second order sidebands.

Next, we consider the post-detection experiment, for which both the desired and undesired signals were sinusoidally amplitude modulated tones, of complex amplitudes

$$z_1(t) = A_1(1 + a_1 \cos 2\pi\mu_1 t). \quad (7.21)$$

and

$$z_2(t) = A_2(1 + a_2 \cos 2\pi\mu_2 t). \quad (7.22)$$

The desired signal carrier frequency was 21.3 MHz, μ_1 was 1 kHz, and a_1 was 0.2. The undesired signal carrier frequency was varied over the range 10 to 70 MHz, μ_2 was 3 kHz, and a_2 was 0.2. The desired input level A_1 was set to give -30 dBm at the IF amplifier pre-detection test point, while A_2 was set so that the available power from the undesired signal was -10 dBm.

The post detection ratio of the first crossmodulation sideband to the desired signal sideband, as given by Eq. (3.100), is

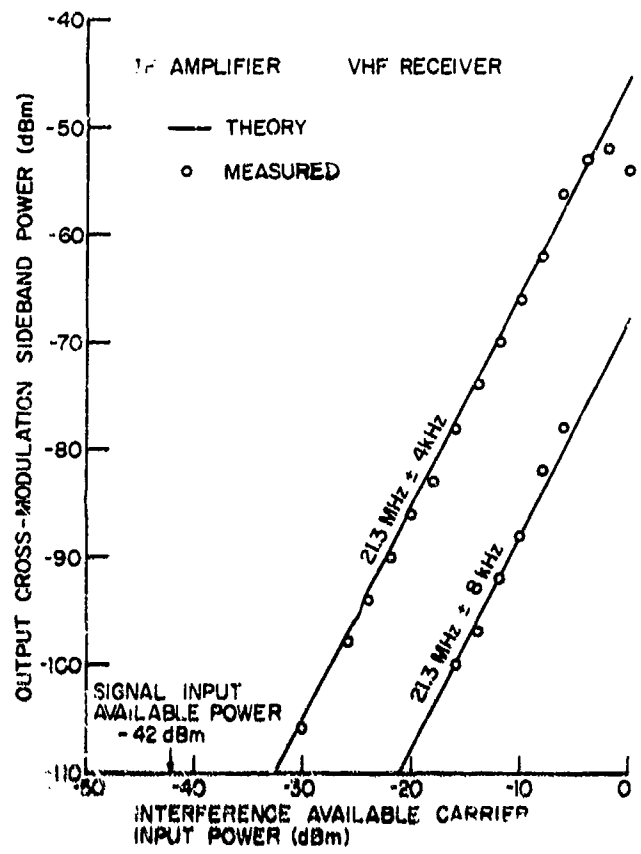


Fig. 7.37. Comparison of Measured and Predicted Crossmodulation Sideband Level.
($f_2 = 10 \text{ MHz}$).

$$3 \frac{\alpha_2}{\alpha_1} |A_2|^2 \operatorname{Re} \left\{ \frac{H_3(v_1, v_2, -v_2)}{H_1(v_1)} \right\}. \quad (7.23)$$

Figure 7.38 shows this ratio, in dB, as a function of the carrier frequency of the undesired signal. The measurement was made with an audio frequency distortion analyzer, and the agreement between theory and measurement is good.

7.10 Waveform Distortion Due to Crossmodulation, VHF Receiver IF Amplifier

The frequency-power-series model can be used to predict crossmodulation distortion of time waveforms. In this section we present two such examples. In both cases the output waveform is calculated and compared to corresponding measured waveforms. The nonlinear circuit is the VHF receiver IF amplifier followed by the AM detector. The input consists of two tones. In the first example one tone is modulated. Both are modulated in the second example.

The IF amplifier described in previous sections is sufficiently wideband that for modulating frequencies in the audio range the first and third-order responses suffice and no derivative terms need be included in the canonic model to obtain accurate predictions. Therefore, the complex envelope of the output may be written

$$q(t) = H_1(v_1)z_1(t) + \frac{3}{2} H_3(v_1, v_2, -v_2)z_1(t)|z_2(t)|^2. \quad (7.24)$$

where $z_1(t)$ and $z_2(t)$ are the complex envelopes of the desired and interfering signals, respectively. As before, $H_1(v_1)$ and

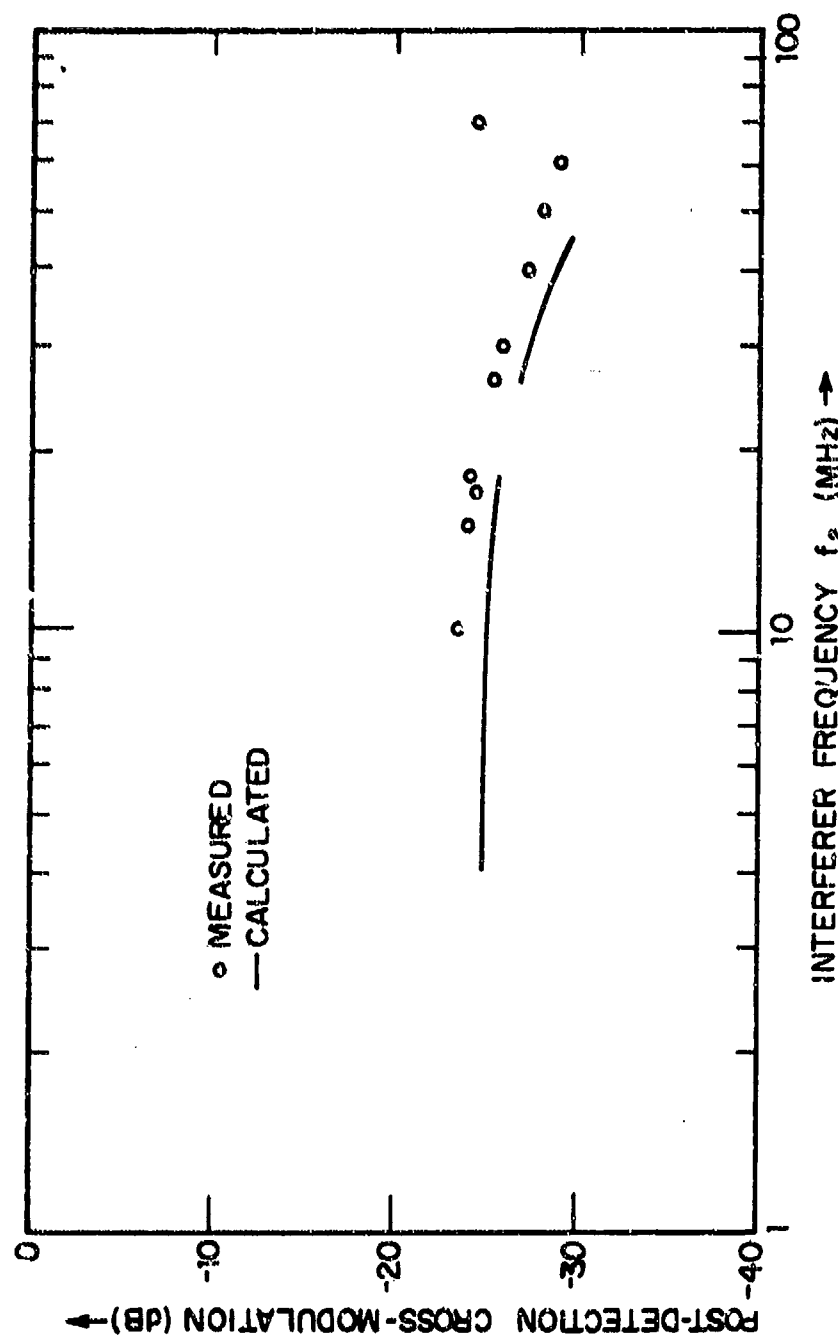


Fig. 7.38. Measured and Calculated Postdetection Cross-modulation, IF Amplifier of a VHF Receiver.

$H_3(v_1, v_2, -v_2)$ are the first and third-order transfer functions evaluated at the appropriate frequencies.

7.10.1 Unmodulated Signal; AM Interference

The first example is that of an unmodulated desired signal and an interferer amplitude modulated by a periodic triangular waveform. The triangular waveform was selected to easily show that distortion of the envelope $z_1(t)$ depends on $|z_2(t)|^2$ as indicated by Eq. (7.24).

The complex envelope of the interferer is

$$z_2(t) = A_2 [1 + \alpha_2 m(t)]. \quad (7.25)$$

The triangular waveform $m(t)$ is shown in Fig. 7.39. Since the modulation waveform is periodic and possesses odd symmetry, it is sufficient to consider $m(t)$ only over its half-period interval $(-T/4, T/4)$:

$$m(t) = \frac{4t}{T} \quad - T/4 \leq t \leq T/4. \quad (7.26)$$

Substituting Eqs. (7.25) and (7.26) into Eq. (7.24) yields

$$q(t) = A_1 H_1(v_1) + \frac{3}{2} A_1 |A_2|^2 H_3(v_1, v_2, -v_2) \left(1 + \frac{8\alpha_2 t}{T} + \frac{16\alpha_2^2 t^2}{T^2} \right),$$

$$- T/4 \leq t \leq T/4. \quad (7.27)$$

The first term contributes a DC term to the AM detector output. This is not of interest. The AM detector output, assuming the second term is small relative to the first term, is, except for a scale factor, given by

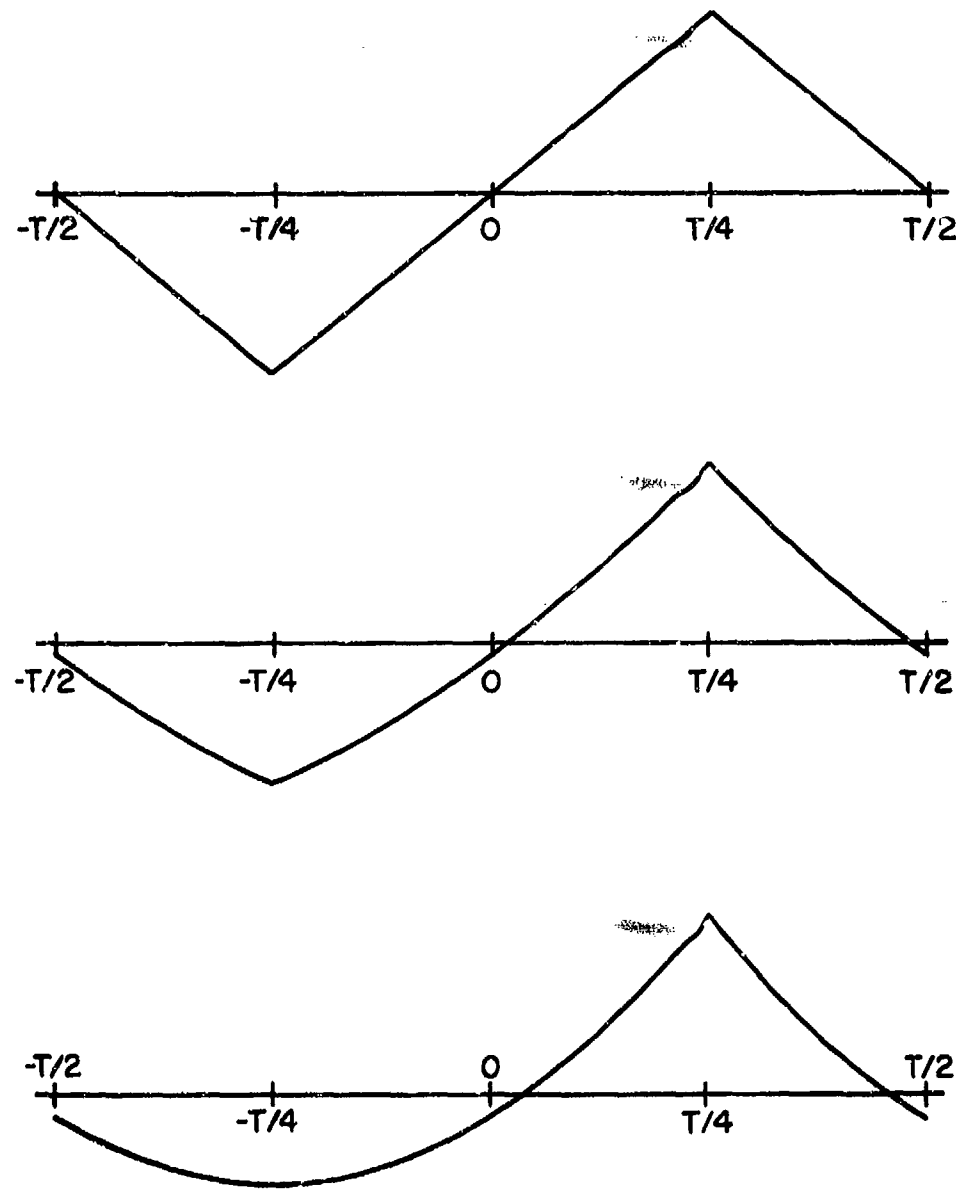


Fig. 7.39. Calculated Waveforms:
Top, Modulation on Interferer;
Middle, Crossmodulation ($\alpha_2 = 0.385$);
Bottom, Crossmodulation ($\alpha_2 = 1.000$).

$$1 + \frac{8\alpha_2 t}{T} + \frac{16\alpha_2^2 t^2}{T^2}; - T/4 \leq t \leq T/4. \quad (7.28)$$

Removing the DC component in Eq. (7.28), (which is $1 + \frac{1}{3} \alpha_2^2$), we find that the crossmodulation time waveform at the AM detector output as predicted by Eq. (7.24) is

$$m_o(t) = -\frac{\alpha_2^2}{3} + \frac{8\alpha_2 t}{T} + \frac{16\alpha_2^2 t^2}{T^2}. \quad (7.29)$$

This result is plotted in Fig. 7.39 for two values of the modulation index, $\alpha_2 = 0.385$ and 1.00 . It can also be seen from Eq. (7.29) that for $\alpha_2 = 1.00$, the waveform has a zero derivative at $t = -T/4$.

An experiment was conducted in which the actual crossmodulation waveform was observed for the values of the modulation index α_2 used in calculating Fig. 7.39. Photographs of the detector output voltage are shown in Figs. 7.40 and 7.41. For this experiment the desired carrier was at 21.3 MHz with output power level at -30 dBm; the interferer was at 26.0 MHz and an input power level of -10 dBm. The repetition rate of the triangular waveform was 1000 Hz.

Comparing Figs. 7.39, 7.40, and 7.41 the observed waveforms are found to be in good agreement with the calculated waveforms. For $\alpha_2 = 1.0$, the case of 100% modulation on the interferer, the zero slope at $t = T/4$ predicted by the theory is, in fact, clearly visible in Fig. 7.41.

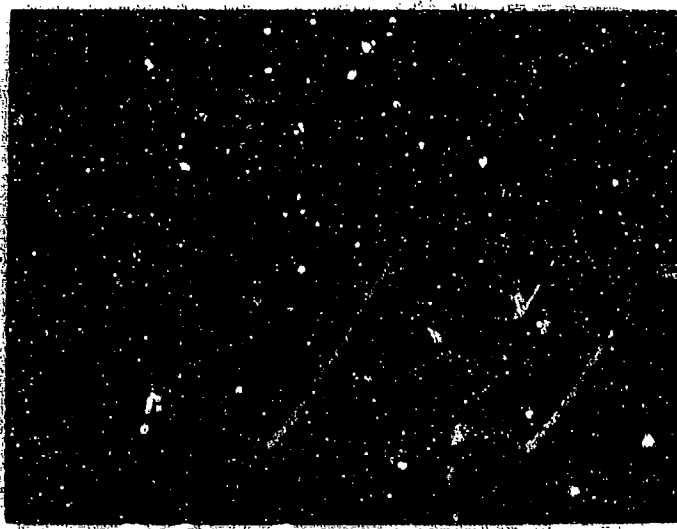


Fig. 7.40. Observed Waveforms

Top: Modulation on Interferer;
Bottom: Crossmodulation ($\alpha_2 = 0.385$)



Fig. 7.41. Observed Waveforms

Top: Modulation on Interferer
Bottom: Crossmodulation ($\alpha_2 = 1.00$)

7.10.2 AM Desired Signal - AM Interference

The second example of a distorted output waveform to be examined is the case of a signal at ν_1 with square-wave AM modulation and an interferer at ν_2 with AM sinusoidal modulation frequency μ_2 . For moderate distortion levels, the resulting detector output will be the desired square-wave modulation with a superimposed crossmodulation distortion which is roughly a sinusoidal waveform. The purpose of using a square-wave modulation is to allow the eye to readily distinguish the effects of cross-modulation when the output deviates from a square-wave. If we let $s(t)$ be the square wave (with amplitudes ± 1) then the complex envelopes of desired and interfering signals are

$$z_1(t) = A_1 [1 + \alpha_1 s(t)] \quad (7.30)$$

$$z_2(t) = A_2 [1 + \alpha_2 \cos 2\pi\mu_2 t] \quad (7.31)$$

Substitution in Eq. (7.24) gives the complex envelope of the output

$$\begin{aligned} q(t) &= A_1 H_1(\nu_1) [1 + \alpha_1 s(t)] + \frac{3}{2} A_1 |A_2|^2 H_3(\nu_1, \nu_2, -\nu_2) \\ &\quad [1 + \alpha_1 s(t)] \left[\left(1 + \frac{\alpha_2^2}{2}\right) + 2\alpha_2 \cos 2\pi\mu_2 t + \frac{\alpha_2^2}{2} \cos 4\pi\mu_2 t \right] \end{aligned} \quad (7.32)$$

Equation (7.32) can be rewritten as

$$q(t) = A_1 H_1(v_1) [1 + \alpha_1 s(t)] \left\{ 1 + \frac{3}{2} |A_2|^2 \frac{H_3(v_1, v_2, -v_2)}{H_1(v_1)} \right. \\ \left. \cdot \left[\left(1 + \frac{\alpha_2^2}{2}\right) + 2\alpha_2 \cos 2\pi\mu_2 t + \frac{\alpha_2^2}{2} \cos 4\pi\mu_2 t \right] \right\}. \quad (7.33)$$

Assuming that the distortion given by the second term in Eq. (7.33) is small, the envelope detector output, $|q(t)|$, is approximately given by

$$|q(t)| \approx A_1 H_1(v_1) [1 + \alpha_1 s(t)] \\ \cdot \left\{ 1 + \frac{3}{2} |A_2|^2 \operatorname{Re} \frac{H_3(v_1, v_2, -v_2)}{H_1(v_1)} \left[\left(1 + \frac{\alpha_2^2}{2}\right) + 2\alpha_2 \cos 2\pi\mu_2 t \right. \right. \\ \left. \left. + \frac{\alpha_2^2}{2} \cos 4\pi\mu_2 t \right] \right\} \\ = \alpha_1 A_1 H_1(v_1) \left\{ \frac{1}{\alpha_1} \left[1 + \frac{3}{2} |A_2|^2 \operatorname{Re} \left\{ \frac{H_3(v_1, v_2, -v_2)}{H_1(v_1)} \right\} \left(1 + \frac{\alpha_2^2}{2}\right) \right] \right. \\ \left. + \left[1 + \frac{3}{2} |A_2|^2 \operatorname{Re} \left\{ \frac{H_3(v_1, v_2, -v_2)}{H_1(v_1)} \right\} \left(1 + \frac{\alpha_2^2}{2}\right) \right] s(t) \right. \\ \left. + \frac{3}{2} |A_2|^2 \frac{\alpha_2}{\alpha_1} \operatorname{Re} \left\{ \frac{H_3(v_1, v_2, -v_2)}{H_1(v_1)} \right\} \left\{ 2 \cos 2\pi\mu_2 t + \frac{\alpha_2^2}{2} \cos 4\pi\mu_2 t \right\} \right. \\ \left. \cdot [1 + \alpha_1 s(t)] \right\}. \quad (7.34)$$

The first term on the right-hand side of Eq. (7.34) is an uninteresting DC term which can be ignored. Similarly, the factor $\alpha_1 A_1 H_1(v_1)$ is common to all terms and will drop out in a cross-modulation ratio calculation. Thus, the output of an envelope detector would be proportional to

$$e_{AM}(t) = \left\{ 1 + \frac{3}{2} |A_2|^2 \operatorname{Re} \left[\frac{H_3(v_1, v_2, -v_2)}{H_1(v_1)} \right] \left(1 + \frac{\alpha_2^2}{2} \right) \right\} s(t)$$

$$+ \left\{ \frac{3}{2} \frac{\alpha_2}{\alpha_1} |A_2|^2 \operatorname{Re} \left[\frac{H_3(v_1, v_2, -v_2)}{H_1(v_1)} \right] \right.$$

$$\left. (2 \cos 2\pi\mu_2 t + \frac{\alpha_2}{2} \cos 4\pi\mu_2 t) \right\} \left[1 + \alpha_1 s(t) \right]. \quad (7.35)$$

The first term of Eq. (7.35) is the desired modulation (square wave) at the output as affected by desensitization while the second is the distortion due to sinusoidal crossmodulation.

It is convenient to examine the peak value and various upper and lower levels of the envelope of the detector output. Assume that the period of the distorting sinusoidal modulation at μ_2 is smaller than the period of the square wave modulation on the desired signal. From Eq. (7.35) it can be seen that the interferer modulation and its second harmonic generate a sinusoidal perturbation on the top and bottom of the square wave envelope $s(t)$. The four amplitude levels (A, B, C, and D) of the detector output waveform are defined in Fig. 7.42. From Eq. (7.35) it is seen that these quantities are given by

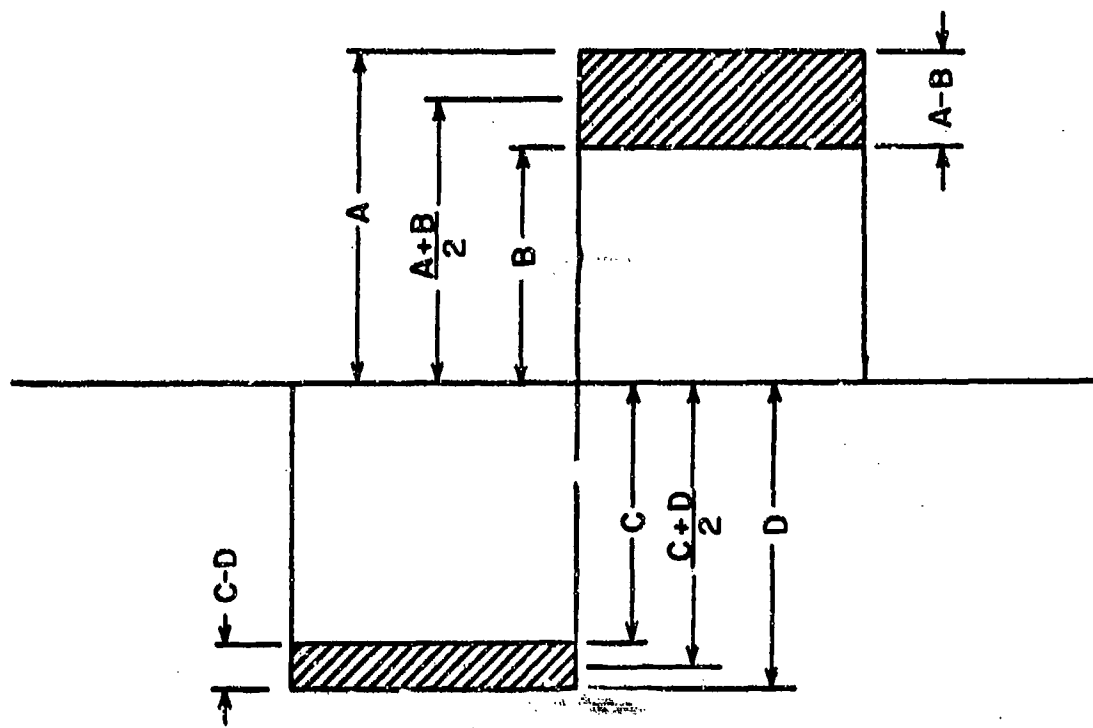


Fig. 7.42. Amplitude Levels of Detector Output Waveform.

$$\frac{A+B}{2} = -\frac{C+D}{2} = 1 + \frac{3}{2} \left(1 + \frac{\alpha_2^2}{2}\right) |A_2|^2 \operatorname{Re} \left[\frac{H_3(v_1, v_2, -v_2)}{H_1(v_1)} \right] \quad (7.36)$$

$$A-B = 3 \frac{\alpha_2}{\alpha_1} (1 + \alpha_1) \left(2 + \frac{\alpha_2^2}{2}\right) |A_2|^2 \operatorname{Re} \left[\frac{H_3(v_1, v_2, -v_2)}{H_1(v_1)} \right] \quad (7.37)$$

$$C-D = 3 \frac{\alpha_2}{\alpha_1} (1 - \alpha_1) \left(2 + \frac{\alpha_2^2}{2}\right) |A_2|^2 \operatorname{Re} \left[\frac{H_3(v_1, v_2, -v_2)}{H_1(v_1)} \right] \quad (7.38)$$

Thus, it is possible to find a ratio of amplitude differences

$$\frac{C-D}{A-B} = \frac{1 - \alpha_1}{1 + \alpha_1}.$$

This ratio is independent of both the interferer level and the non-linear transfer function $H_3(v_1, v_2, -v_2)$. It depends only on the modulation index α_1 . This ratio can be readily measured.

Experimental results were obtained with the VHF receiver IF amplifier using the same carrier frequencies and power levels as in the example of Section 7.10.1. Photographs of the results are shown in Fig. 7.43. The repetition rate of the square wave modulation on the desired signal was 5 kHz and the modulation index α_1 was 1/3. The sinewave modulation on the undesired signal was at 10 kHz with a modulation index $\alpha_2 = 1/3$. For the value of α_1 , the predicted ratio $(C-D)/(A-B)$ is 1/2 which was also observed experimentally.

The accuracy of calculated values of $H_3(v_1, v_2, -v_2)$ may be checked by comparing calculated and measured values of the ratio



Modulation Sources Unsyncronized



Modulation Sources Synchronized

Fig. 7.43. Output Waveforms Showing Crossmodulation Distortion

$$^2 \frac{A-B}{A+B} = \frac{k_1 \operatorname{Re}[H_3(v_1, v_2, -v_2)/H_1(v_1)]}{1 + k_2 \operatorname{Re}[H_3(v_1, v_2, -v_2)/H_1(v_1)]} \quad (7.40)$$

where k_1 and k_2 are constants independent of frequency. The calculated value of this ratio for the IF amplifier was 0.192. The value observed was 0.18.

7.11 Predetection Tapped Delay Line Canonic Modeling, VHF Receiver RF Tuner

In this section we present two examples of the application of the tapped delay line canonic model in computing crossmodulation distortion. The first example is a hypothetical case, for which the crossmodulation distortion can be computed exactly using the frequency power series canonic model. The results are compared with those predicted using the tapped delay line model, thus bringing out some of the practical limitations of the latter canonic model. The second example compares predicted and measured crossmodulation in the RF tuner of the VHF receiver, for an unmodulated desired signal and a frequency modulated undesired signal.

7.11.1 A Known Test Case

The frequency power series canonic model is useful when the Taylor series expansion of the nonlinear transfer function over the signal bandwidths of interest is rapidly convergent. A specific case occurs when the nonlinear transfer function can be exactly represented by a two-term expansion; in this case, an exact computation can be made for the nonlinear effects of the circuit. In particular, consider a circuit with the third-order nonlinear transfer function.

$$H_3(f_1, f_2, f_3) = K_1 + (f_2 - v_2)K_2 + (f_3 + v_2)K_3 \quad (7.41)$$

This transfer function is simple enough so that it is possible to compute analytically an exact prediction of crossmodulation. Observe that this transfer function is independent of f_1 and depends only in a linear fashion on $f_2 - v_2$ and $f_3 + v_2$. Thus the derivatives of the nonlinear transfer function are

$$\frac{\partial H_3}{\partial f_1} = 0, \quad (7.42)$$

$$\frac{\partial H_3}{\partial f_2} = K_2, \quad (7.43)$$

$$\frac{\partial H_3}{\partial f_3} = K_3. \quad (7.44)$$

From Equations (3.54) and (3.42), the complex envelope of the third-order output component referred to $\underline{v} = (v_1, v_2, -v_2)$ has the expansion

$$\begin{aligned} q_3(t; \underline{v}) &= \frac{(3,1,1,1)}{2^2} [H_3(\underline{v}) z_1(t) |z_2(t)|^2 \\ &+ \frac{1}{2\pi j} \left\{ \frac{\partial H_3(\underline{v})}{\partial f_1} \dot{z}_1(t) z_2(t) z_2^*(t) \right. \\ &+ \frac{\partial H_3(\underline{v})}{\partial f_2} z_1(t) \dot{z}_2(t) z_2^*(t) \\ &+ \left. \frac{\partial H_3(\underline{v})}{\partial f_3} z_1(t) z_2(t) \dot{z}_2^*(t) \right\}] \\ &+ \text{higher derivative terms.} \end{aligned} \quad (7.45)$$

Substituting Equations (7.42) - (7.44) into Equation (7.45), and evaluating the multinomial coefficient results in

$$q_3(t; \underline{\nu}) = \frac{3}{2} [K_1 z_1(t) |z_2(t)|^2 + \frac{1}{2\pi j} \{ K_2 z_1(t) \dot{z}_2(t) z_2^*(t) + K_3 z_1(t) z_2(t) \dot{z}_2^*(t) \}]. \quad (7.46)$$

Next, consider that the desired signal is an unmodulated tone at ν_1 and the undesired signal is a sinusoidally frequency modulated tone centered at ν_2 . Therefore,

$$z_1(t) = A_1 \quad (7.47)$$

and
$$z_2(t) = A_2 e^{j \frac{\alpha_2}{\mu_2} \cos 2\pi\mu_2 t}. \quad (7.48)$$

Substituting Equations (7.47) and (7.48) into Equation (7.46), and evaluating the derivative of Equation (7.48) results in

$$q_3(t; \underline{\nu}) = \frac{3}{2} A_1^2 [K_1 A_2^2 + A_2^2 \alpha_2 (K_3 - K_2) \sin 2\pi\mu_2 t] \quad (7.49)$$

The real third-order signal is therefore given by

$$\begin{aligned} \operatorname{Re}\{q_3(t; \underline{\nu}) e^{j 2\pi\nu_1 t}\} &= \frac{3}{2} A_1 A_2^2 K_1 \cos 2\pi\nu_1 t \\ &+ \frac{3}{4} \alpha_2 A_2^2 A_1 (K_3 - K_2) [\cos 2\pi(\nu_1 + \mu_2)t + \cos 2\pi(\nu_1 - \mu_2)t]. \end{aligned} \quad (3.50)$$

The first term on the right-hand side of Equation (7.50) is a desensitization term, while the second term contains the upper and lower crossmodulation sidebands at frequencies $\nu_1 \pm \nu_2$. No other crossmodulation sidebands will be present. In passing, we note again that the predicted FM crossmodulation arises from the derivative terms of the frequency power series canonic model. There is no contribution from the leading term in the series.

As a numerical example, consider the parameters

$$K_1 = (5.0 + j 0.0), \quad (7.51)$$

$$K_2 = (2.5 + j 2.5)/W, \quad (7.52)$$

$$K_3 = (2.5 - j 2.5)/W, \quad (7.53)$$

where $W = 2.8$ MHz. From Equation (7.41) this results in

$$H_3(f_1, f_2, f_3) = 5.0 + 2.5(f_2 + f_3)/W + j 2.5(f_2 - f_3 - 2\nu_2)/W \quad (7.54)$$

$H_3(f_1, f_2, f_3)$ was evaluated numerically for $f_1 = \nu_1 = 45$ MHz, $\nu_2 = 50$ MHz, and $\nu_3 = -\nu_2$. Thus the crossmodulation is centered on ν_1 . Numerical values were computed for H_3 at 100 kHz intervals of f_2 and f_3 , centered on ν_2 and ν_3 , resulting in a frequency domain grid of 33×33 samples of H_3 . This computed H_3 was then weighted along both frequency axes by a simple window function of the form

$$1/4, 3/4, 1, \dots, 1, 3/4, 1/4, \quad (7.55)$$

and the end elements averaged together to form a collapsed 32×32 sampled array of $H_3(v_1, f_2, f_3)$ that had been band-limited in the f_2 and f_3 coordinates. Next a two-dimensional Fourier transformation was used to generate samples of the third-order nonlinear impulse response.

A tapped-delay-line canonic model of the system was then programmed on a digital computer, using as weights the third-order nonlinear impulse response samples. Two computations were run, one for the peak frequency deviation α_2 being 100 kHz, and one for α_2 being 300 kHz. In both cases the modulation frequency μ_2 was 5 kHz. Since $\alpha_2/\mu_2 \gg 1$, the bandwidth of the frequency modulated signal is $2\alpha_2$, or 200 kHz and 600 kHz, respectively. The sideband level given by the tapped-delay-line canonic model for these two cases is shown as a function of the total number of delay-line taps in the model in Figures 7.44 and 7.45. Also shown on the figure is the level of the first and only crossmodulation sideband level, as given by Equation (7.50). With the 100 kHz frequency deviation, the tapped delay line canonic model accurately computes the intermodulation sidebands at $v_1 \pm \mu_2$, (the first sideband in Fig. 7.44) provided seventeen or more taps were used in the model. Equation (7.50) shows that these sidebands should be the only ones present. However, the results generated by the computer indicate the appearance of higher order sidebands that are labeled the second and third-order sidebands in the figure. The levels of these sidebands provide a measure of the model error. The second-order sideband is significant even at the largest number of taps examined. Thus, the model can be considered poor when $\alpha_2 = 100$ kHz.

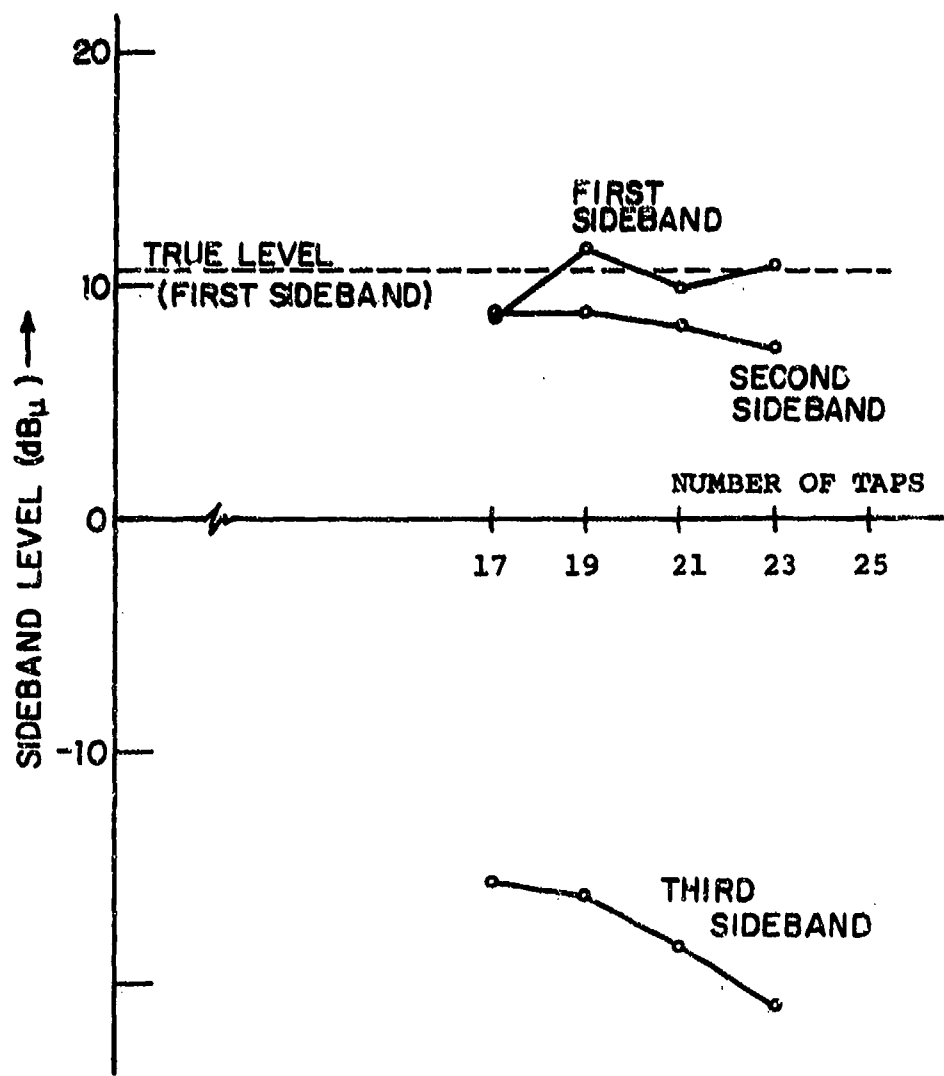


Fig. 7.44. Accuracy of Crossmodulation Sideband Levels computed from a Truncated Tapped Delay Line Model.
Peak Deviation = 100 kHz.

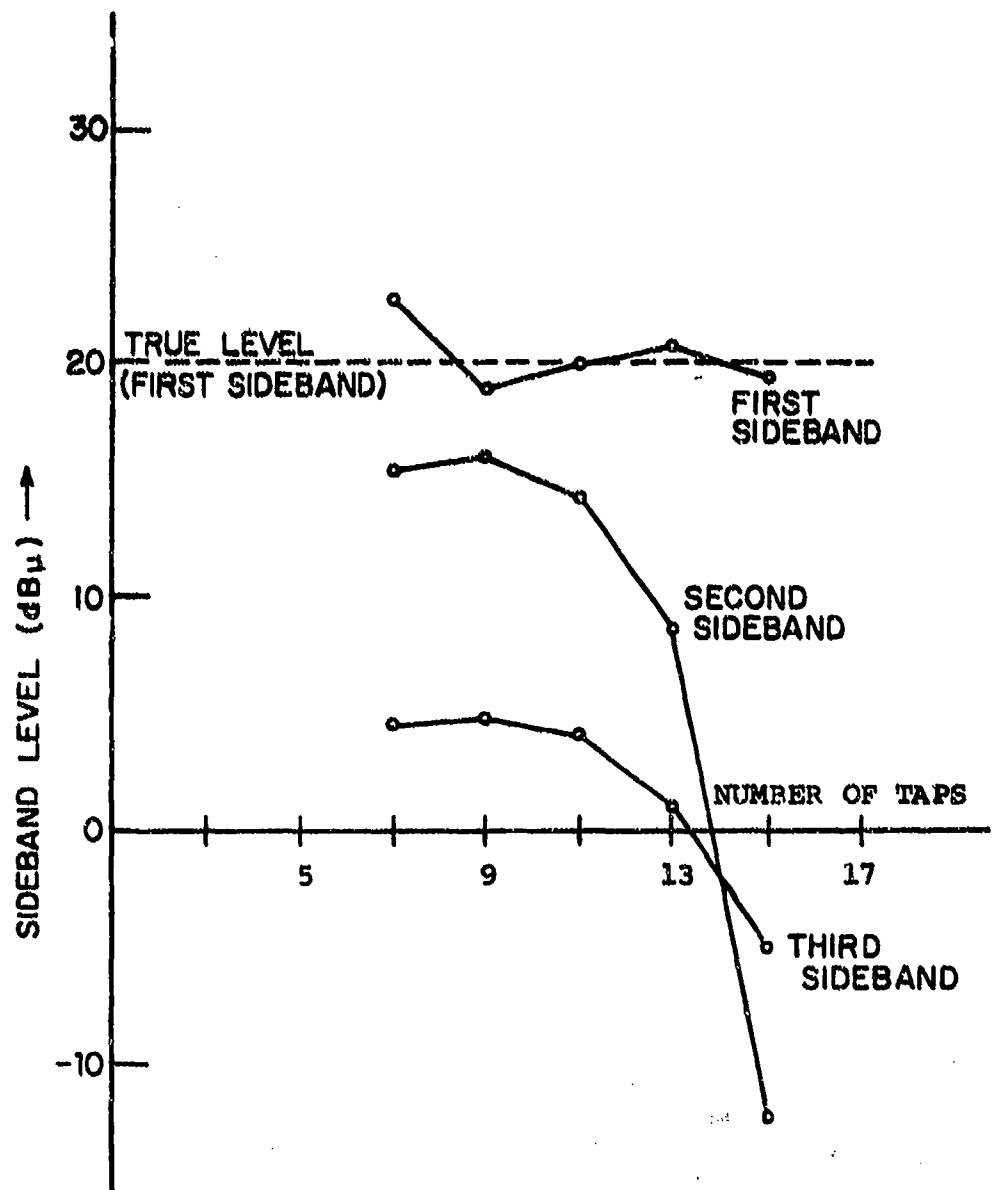


Fig. 7.45. Accuracy of Crossmodulation Sideband Levels
Computed from a Truncated Tapped Delay Line Model
Peak Deviation = 300 kHz

It can be seen, however, that the accuracy improves slowly with the number of taps. In the case of the 300 kHz peak frequency deviation, the higher sidebands decrease much more rapidly. With thirteen taps the higher-order sidebands predicted by the tapped-delay-line model are 20 dB down from the true sideband, and are decreasing rapidly as more taps are added.

7.11.2 Wideband Crossmodulation in the VHF Receiver Tuner

We now consider the case of wideband crossmodulation in the tuner section of the VHF receiver. Companion laboratory measurements have been made and compared with the predictions computed from a tapped delay canonic model. We first describe the predictions and proceed to the measurement. The interfering signal chosen in this example is a 50 MHz carrier, frequency modulated at 5 kHz rate with peak deviation of 1 MHz. The desired signal is at 45 MHz, the nominal frequency at which the tuner has been modeled.

In calculating crossmodulation effects we will be interested in the third-order response $q_3(t; v_1, v_2, -v_2)$, given by Equation (4.71) as

$$q_3(t; v_1, v_2, -v_2) = \frac{3}{2} B_1 B_2 \sum_r \tilde{g}_{3Y}(rT) z_1(t-r_1 T_1) z_2(t-r_2 T_2) z_2^*(t-r_3 T_2) \quad (7.58)$$

where T_i is the sampling interval of the i^{th} signal. For the application this will be further specialized to the case of a sinusoidally-modulated interferer, and an unmodulated desired carrier, so that

$$z_1(t) = A_1 \cdot \quad (7.57)$$

and

$$z_2(t) = A_2 e^{j \frac{a_2}{\mu_2} \cos 2\pi\mu_2 t} \quad (7.58)$$

The interfering signal will be expanded in the familiar Bessel function expansion:

$$z_2(t) = A_2 \sum_{\ell=0}^{\infty} j^{\ell} \epsilon_{\ell} J_{\ell}\left(\frac{a_2}{\mu_2}\right) \cos 2\pi\ell\mu_2 t, \quad (7.59)$$

where

$$\epsilon_{\ell} = \begin{cases} 1 & , \ell=0 \\ 2 & , \ell \neq 0. \end{cases} \quad (7.60)$$

With these substitutions Eq. (7.56) becomes

$$q_3(t; v_1, v_2, -v_2) = \frac{A_1 |A_2|^2}{B_1 B_2} \sum_k \tilde{g}_3 \underbrace{y_k}_{(7.61)} \sum_{\ell=0}^{\infty} \sum_{m=0}^{\infty} j^{\ell-m} \epsilon_{\ell} \epsilon_m J_{\ell}\left(\frac{a_2}{\mu_2}\right) J_m\left(\frac{a_2}{\mu_2}\right) \cos 2\pi\mu_2(t-r_2 T_2) \cos 2\pi\mu_2(t-r_3 T_2).$$

This equation is not in a form suitable for analyzing the spectral structure of the interference. To achieve this it will be necessary to expand the product of trigonometric functions appearing in Eq. (7.61) and collect terms appropriately. To simplify the presentation of the result we make the following definition:

$$q_3(t; v_1, v_2, -v_2) = x_0 + jy_0 + \sum_{n=1}^{\infty} (x_{cn} + jy_{cn}) \cos 2\pi n \mu_2 t \\ + (x_{sn} + jy_{sn}) \sin 2\pi n \mu_2 t. \quad (7.62)$$

After making the necessary substitutions and performing considerable algebra, Eq. (7.61) gives the following spectral decomposition for $n \geq 1$

$$x_{cn} + jy_{cn} = \frac{3j^{-n} |A_1| |A_2|^2}{2B_1 B_2^2} \left\{ \sum_{\ell=0}^{\infty} (-1)^n e_{\ell} J_{\ell} \left(\frac{a_2}{\mu_2} \right) J_{\ell-n} \left(\frac{a_2}{\mu_2} \right) \right. \\ \left. \sum_x \tilde{g}_{3x}(rT) \cos 2\pi \mu_2 T_2 [\ell(r_2 - r_3) + nr_3] \right. \\ \left. + \sum_{\ell=0}^{\infty} e_{\ell} J_{\ell} \left(\frac{a_2}{\mu_2} \right) J_{\ell+n} \left(\frac{a_2}{\mu_2} \right) \sum_x \tilde{g}_{3x}(rT) \right. \\ \left. \cos 2\pi \mu_2 T_2 [\ell(r_2 - r_3) - nr_3] \right\} \quad (7.63)$$

$$x_{sn} + jy_{sn} = \frac{3j^{-n} |A_1| |A_2|^2}{2B_1 B_2^2} \left\{ \sum_{\ell=0}^{\infty} (-1)^n e_{\ell} J_{\ell} \left(\frac{a_2}{\mu_2} \right) J_{\ell-n} \left(\frac{a_2}{\mu_2} \right) \sum_x \tilde{g}_{3x}(rT) \right. \\ \left. \sin 2\pi \mu_2 T_2 [\ell(r_2 - r_3) + nr_3] \right. \\ \left. + \sum_{\ell=0}^{\infty} e_{\ell} J_{\ell} \left(\frac{a_2}{\mu_2} \right) J_{\ell+n} \left(\frac{a_2}{\mu_2} \right) \sum_x \tilde{g}_{3x}(rT) \right. \\ \left. \sin 2\pi \mu_2 T_2 [\ell(r_2 - r_3) - nr_3] \right\}. \quad (7.67)$$

Basically, this is the result which will be used for calculations. However, it is possible to significantly reduce the necessary computation by replacing $\tilde{g}_{3Y}(x_1)$ with an equivalent two-dimensional transform.

We have assumed an unmodulated desired signal, occupying zero spectral width. Therefore the variation of $\tilde{G}_{3Y}(f_1, f_2, f_3)$ for changes in f_1 will not affect the result. In fact we may represent this function by its value at $f_1=0$,

$$\tilde{G}_{3Y}(f_1, f_2, f_3) = \text{Rect}\left(\frac{f_1}{B_1}\right)\tilde{G}_{3Y}(0, f_2, f_3) \quad (7.65)$$

where the bandwidth B_1 is arbitrary but non-zero. Transforming this gives

$$\tilde{g}_{3Y}(\tau_1, \tau_2, \tau_3) = \frac{\sin \pi B_1 \tau_1}{\pi \tau_1} \tilde{g}_{3Y}^*(\tau_2, \tau_3) \quad (7.66)$$

where the function $\tilde{g}_{3Y}^*(\tau_2, \tau_3)$ is defined as the two-dimensional transform of $\tilde{G}_{3Y}(0, f_2, f_3)$. Now if we allow B_1 to become infinitely large in Eq. (7.66) we have

$$\frac{1}{B_1} \tilde{g}_{3Y}(\tau_1, \tau_2, \tau_3) = \begin{cases} \tilde{g}_{3Y}^*(\tau_2, \tau_3), & \tau_1=0 \\ 0, & \tau_1 \neq 0. \end{cases} \quad (7.67)$$

When this is substituted into Eqs. (7.63) and (7.64) the triple summations reduce to double summations:

$$\begin{aligned}
 x_{cn} + jy_{cn} = & \frac{3j^{-n} A_1 |A_2|^2}{2B_2^2} \left\{ \sum_{l=0}^{\infty} (-1)^n e_l J_l \left(\frac{\alpha_2}{\mu_2}\right) J_{l-n} \left(\frac{\alpha_2}{\mu_2}\right) \right. \\
 & \left. \Sigma \tilde{g}_{3,y}^* (xT) \cos 2\pi\mu_2 T_2 [l(x_2 - x_3) + nx_3] \right. \\
 & \left. + \sum_{l=0}^{\infty} e_l J_l \left(\frac{\alpha_2}{\mu_2}\right) J_{l+n} \left(\frac{\alpha_2}{\mu_2}\right) \right. \\
 & \left. \Sigma \tilde{g}_{3,y}^* (xT) \cos 2\pi\mu_2 T_2 [l(x_2 - x_3) - nx_3] \right\}. \quad (7.68)
 \end{aligned}$$

$$\begin{aligned}
 x_{sn} + jy_{sn} = & \frac{3j^{-n} A_1 |A_2|^2}{2B_2^2} \left\{ \sum_{l=0}^{\infty} (-1)^n e_l J_l \left(\frac{\alpha_2}{\mu_2}\right) J_{l-n} \left(\frac{\alpha_2}{\mu_2}\right) \right. \\
 & \left. \Sigma \tilde{g}_{3,y}^* (xT) \sin 2\pi\mu_2 T_2 [l(x_2 - x_3) + nx_3] \right. \\
 & \left. - \sum_{l=0}^{\infty} e_l J_l \left(\frac{\alpha_2}{\mu_2}\right) J_{l+n} \left(\frac{\alpha_2}{\mu_2}\right) \right. \\
 & \left. \Sigma \tilde{g}_{3,y}^* (xT) \sin 2\pi\mu_2 T_2 [l(x_1 - x_3) - nx_3] \right\}. \quad (7.69)
 \end{aligned}$$

The amplitude of the sideband at $\nu_1 + n\mu_2$ is given by

$$\frac{1}{2} \sqrt{(x_{cn} + y_{sn})^2 + (x_{sn} - y_{cn})^2} \quad (7.70)$$

while

$$\frac{1}{2} \sqrt{(x_{cn} - y_{sn})^2 + (x_{sn} + y_{cn})^2}. \quad (7.71)$$

The crossmodulation components in the tuner arise from the fourth-order nonlinear response, which we consider as an equivalent third-order response. In order to apply the tapped-delay-line canonic model, we again begin with the nonlinear transfer function, with

$$\left. \begin{aligned} f_1 &= v_1 = 45 \text{ MHz}, \\ f_2 &= 50 \text{ MHz} + k_1 f_m; k_1 \text{ integer.} \\ f_3 &= 50 \text{ MHz} + k_2 f_m; k_2 \text{ integer.} \\ f_4 &= v_4 = f_{\text{LO}} = 45 \text{ MHz} + f_{\text{IF}}, \\ u_2 &= 5 \text{ kHz,} \\ a_2 &= 1 \text{ MHz.} \end{aligned} \right\} \quad (7.72)$$

The crossmodulation products to be examined occur at the frequencies

$$f_{\text{IF}} + k_1 f_m - k_2 f_m \quad (7.73)$$

with the first pair of sidebands at $f_{\text{IF}} \pm 5 \text{ kHz}$. The nonlinear transfer function of interest in this case is the fourth-order transfer function

$$H_4(-v_1, f_2, f_3, f_{\text{LO}}) \quad (7.74)$$

It is this transfer function which predicts the crossmodulation components at $f_{IF} \pm k_3$ 5 kHz ($k_3 = 1, 2, \dots$). Using SIGNCAP, the fourth-order transfer function of the tuner was evaluated at 64 points over a two-dimensional frequency region extending 1.4 MHz to either side of the interfering frequency, and then interpolated to a 32×32 windowed grid. The magnitude of the transfer function over this region before windowing is plotted in Figure 7.46. This data was processed, and the first four crossmodulation sideband levels ($k_3 = 1, 2, 3, 4$) calculated. The results corresponding to 0 dBm desired and interfering signals are shown in Fig. 7.47.

Laboratory measurements of the first two sidebands were made for a range of interferer input levels, with the desired signal now held constant at -50 dBm. These are plotted in Figs. 7.48 and 7.49. Third and higher sidebands were not at a level great enough to permit accurate measurement. In each case the predicted values have also been plotted. Fig. 7.48 shows the data for the first set of sidebands, and Fig. 7.49 the second set. Both figures show similar results. For interferer available power lower than -45 dBm, the measured sidebands have a second-order slope, which is the correct slope for crossmodulation. For input signals greater than -45 dBm, the behavior of all sidebands becomes anomalous, the slopes change, large separations open between upper and lower sidebands, etc. The significance of -45 dBm input power can be explained by referring to the desensitization values shown with the curves in Fig. 7.48 and 7.49. At -45 dBm, -40 dBm, and -35 dBm, the measured desensitization of the desired 45 MHz signal by the 50 MHz interference is 0.1 dB, 0.3 dB, and 0.8 dB, respectively.

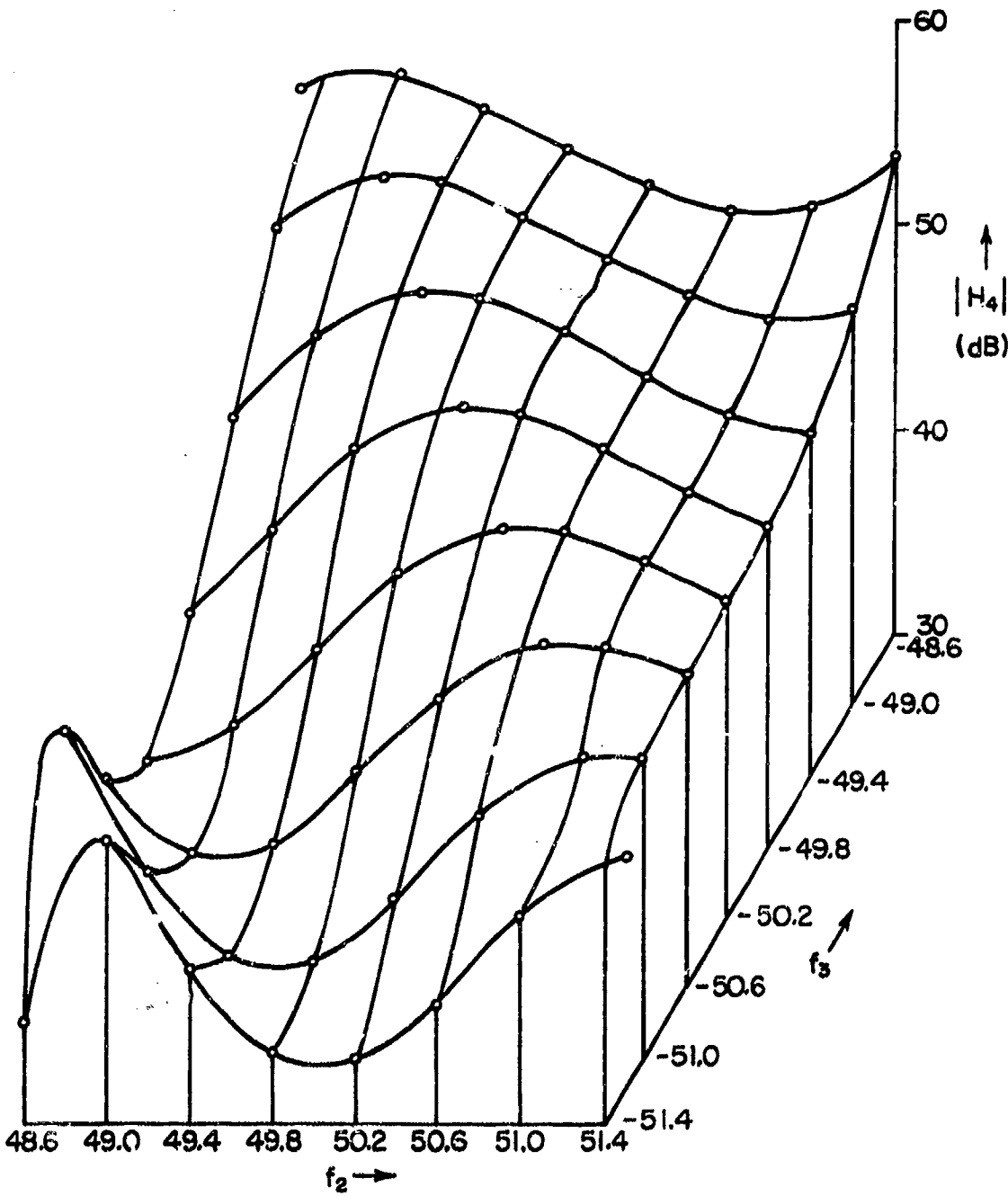


Fig. 7.46. Magnitude of the Nonlinear Transfer Function $H_4(-45, f_2, f_3, f_{LO})$.

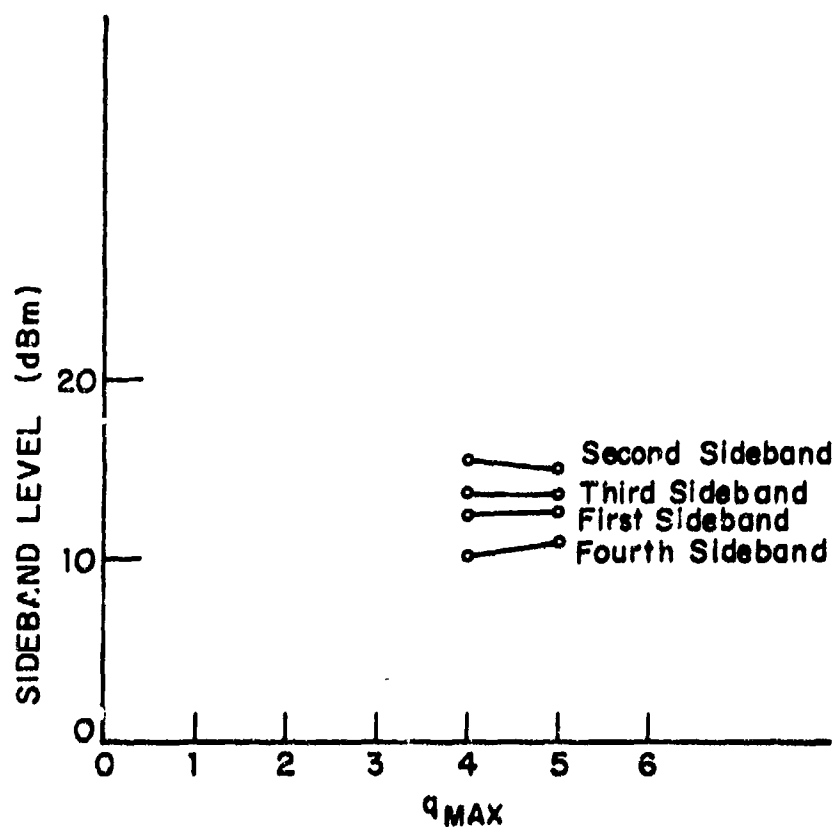


Fig. 7.47. Calculated Crossmodulation Sideband Levels.
 Interferer = 0 dBm, 50 MHz FM, $f_m = 5$ kHz,
 Peak Deviation = 1 MHz.

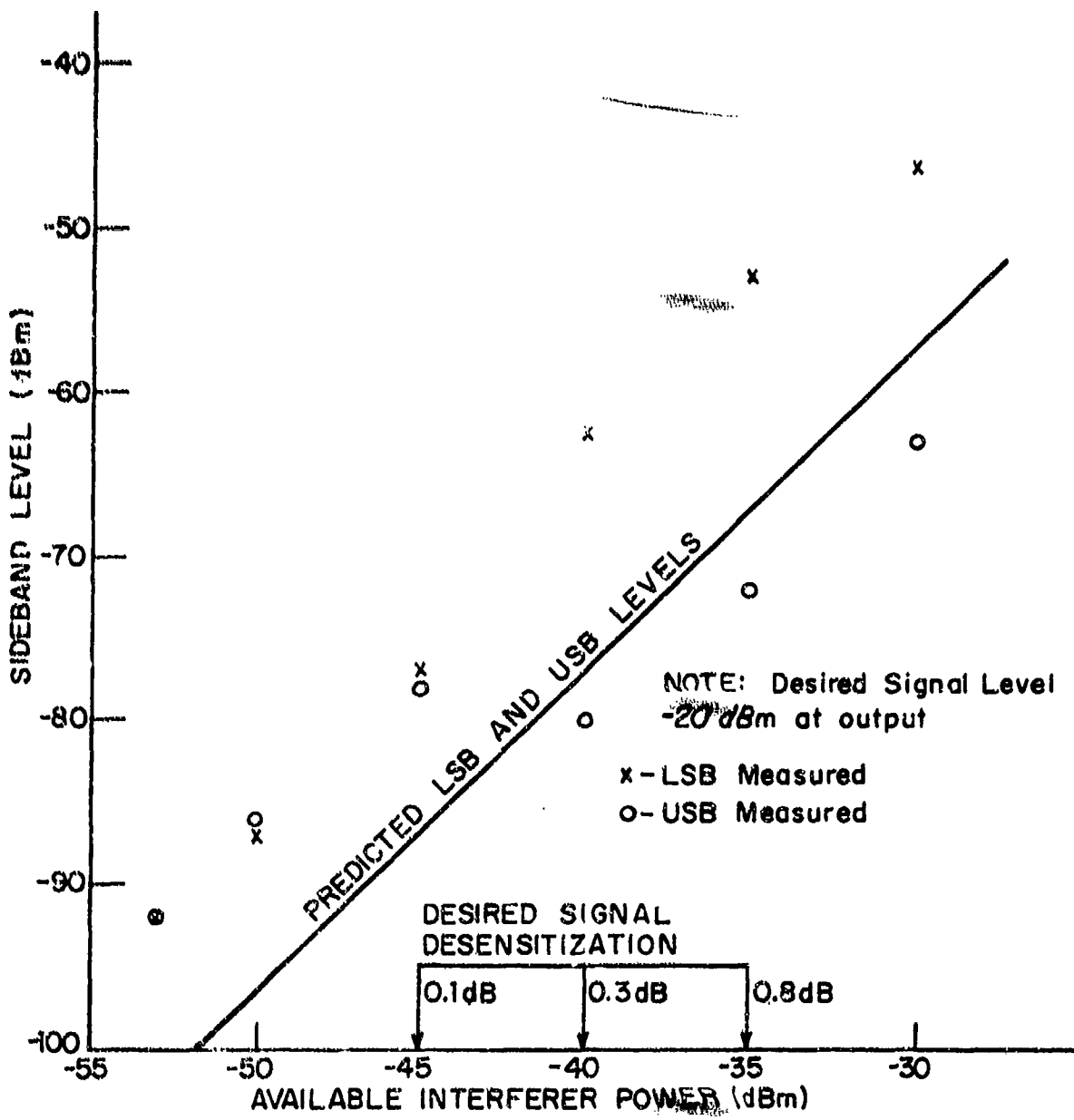


Fig. 7.48. Predicted and Measured Levels for First Cross-modulation Sidebands.

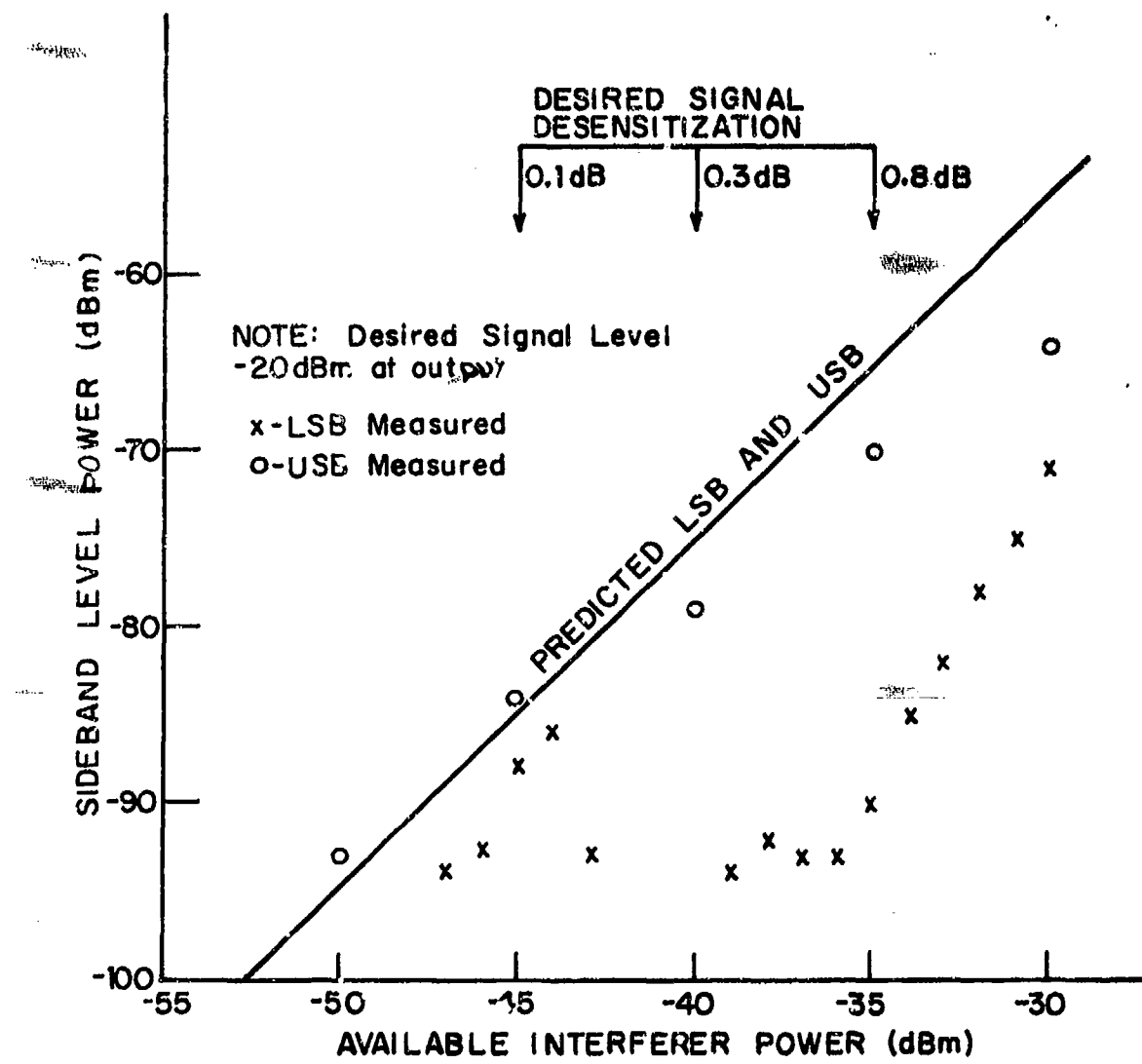


Fig. 7.49. Predicted and Measured Levels for Second Cross-modulation Sidebands.

Thus, the anomalous crossmodulation is correlated with the onset of desensitization and can be attributed to large signal effects.

It is seen that the tapped delay line model provides a reasonable prediction of crossmodulation in the small signal region, but is not accurate in the large signal region. It should be noted that at 45 MHz the insertion gain is 30 dB, and the -50 dBm input signal causes a -20 dBm output signal. At the 0.1 dB compression point, the crossmodulation sideband power is about -85 dBm, 65 dB lower than the desired carrier. Thus the crossmodulation in this case can only be predicted accurately by the third-order model when it causes a small interference effect. Similar effects have been found on desensitization experiments, which result from the same form of the nonlinear transfer function.

7.12 Nominal Receiver Modeling

It may be necessary, in certain practical applications, to model a communication receiver without having a receiver physically available for experimental purposes. In this case, it is necessary to use available material such as is found in a manufacturer's manual or a military technical order to parameterize the circuitry. A receiver which is modeled in this fashion is known as a nominal receiver. In this section we apply the nominal receiver concept to the VHF tuner described in Section 7.3. The data in this section come from Spina et. al., (1972).

7.12.1 Parameterizing of the Nominal Tuner

Two sources of data were used to find the circuit parameters for the nominal tuner. The first source was the manufacturer's instruction manual, which contained schematic diagrams

of the tuner circuitry, operating point information and detailed alignment procedures for the bench testing of the tuner. The second source was measurements performed on samples of the same type of transistors as were in the tuner. The parameters found in this manner could be expected to be representative of the type tuner, but not to represent any specific serial numbered tuner.

The alignment procedure specified in the instruction manual called for an input frequency of 100 MHz, corresponding to a local-oscillator frequency of 121.4 MHz. Inductors L_{2A} through L_{2D} are used for variable tuning in the receiver, while capacitors C_3 , C_5 , C_{19} , C_{22} are fine-tuning components used to obtain symmetry in the tuner response. Inductors L_5 and L_6 tune the mixer collector circuit to the 21.4 MHz intermediate frequency. The alignment procedure was simulated on the computer, using SIGNCAP to predict the desired second-order response. According to the manual, the tuner should have a nominal 3 dB bandwidth of 5 MHz, but this may vary from 3 to 7 MHz, depending on the frequency. The nominal receiver had a bandwidth of 6 MHz after alignment. Figure 7.50 shows the resulting predicted equivalent (first-order) insertion gain of the nominal tuner at 100 MHz.

7.12.2 Nominal Tuner Results

Once the tuner was aligned at 100 MHz, inductors L_{2A} through L_{2D} were retuned together to an input frequency of 45 MHz, and the local oscillator was changed to a frequency of 66.4 MHz. The retuning was accomplished by varying L_{2A} through L_{2D} together for a maximum 21.4 MHz response at the IF output port J2. This did not, in fact, guarantee a symmetric response at 21.4 MHz. SIGNCAP was then run to predict the second through fourth nonlinear transfer functions, and the predictions were

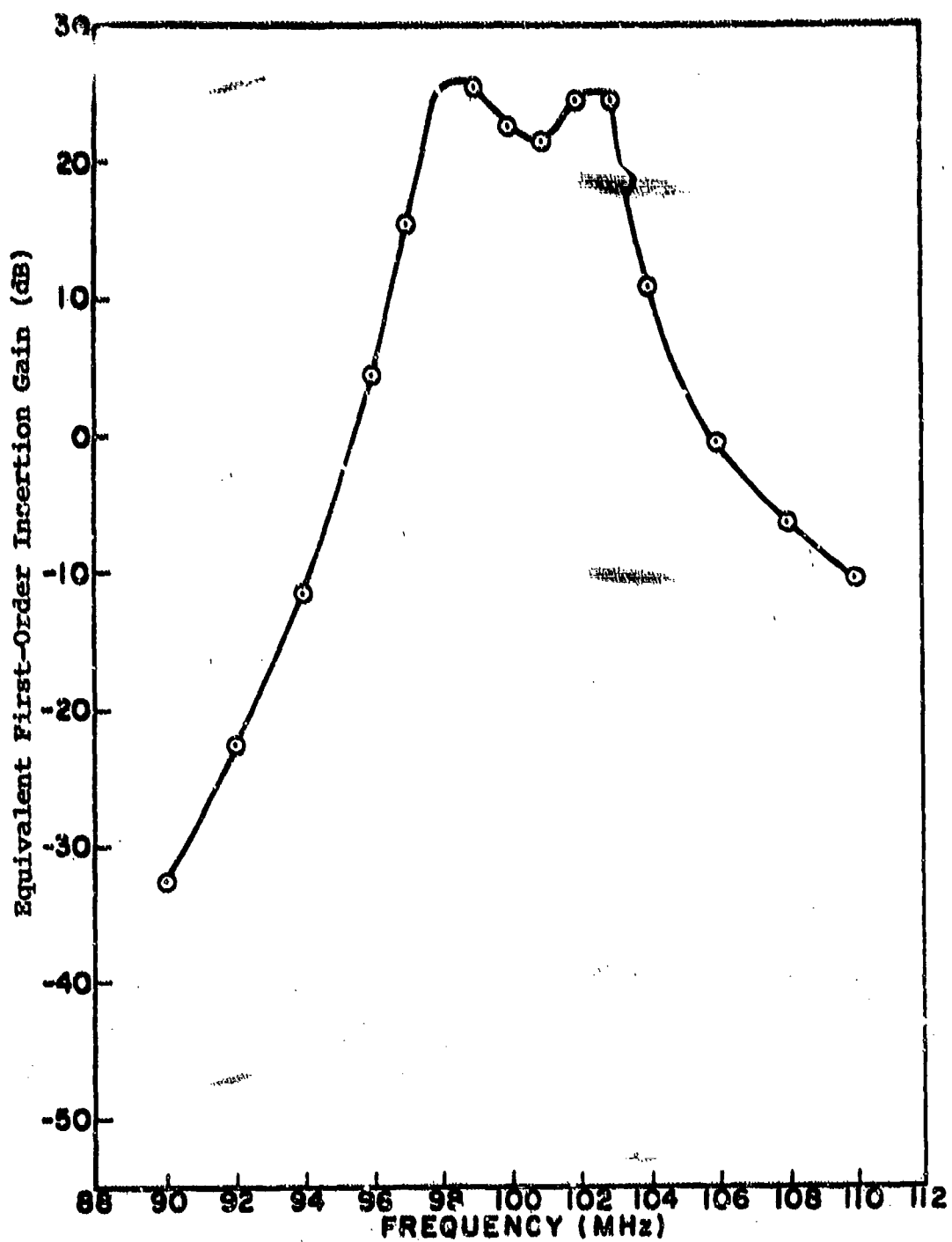


Fig. 7.50. Computer VHF RF Tuner Response via Alignment Procedure.

compared with the measured nonlinear transfer functions. Figures 7.51 through 7.53 show the nominal predicted and actual measured equivalent nonlinear transfer functions.

The equivalent insertion gain, which is due to the second order nonlinear transfer function, is shown in Fig. 7.51. The prediction is quite good in terms of the skirts and the image response, but the predicted peak gain is about 4 dB too high, and the predicted pass-band response does not have the flat response found in the measured data. This is probably due to the fact that when the tuner was "retuned" to 45 MHz, it was tuned for a peak at 45 MHz, instead of a flat response in the 45 MHz region.

The equivalent second-order nonlinear transfer function, caused by the tuner's third-order nonlinearities, is shown in Fig. 7.52. The nominal predicted response is about 10 dB high, and at a slightly lower frequency than the measured transfer function.

The equivalent third-order nonlinear transfer function, caused by the tuner's fourth-order nonlinearities, is shown in Fig. 7.53. The nominal predicted response is about 20 dB too high, and, as with the first and second order transfer functions, occur at a slightly lower frequency than the measured equivalent third-order nonlinear transfer function.

To summarize the comparisons between the nominal predictions and the measured responses, one could expect, based on this case, that a meaningful nominal model could be formed from limited design data. The quality of the model would depend in some degree on the experience which the analyst has with the actual receiver.

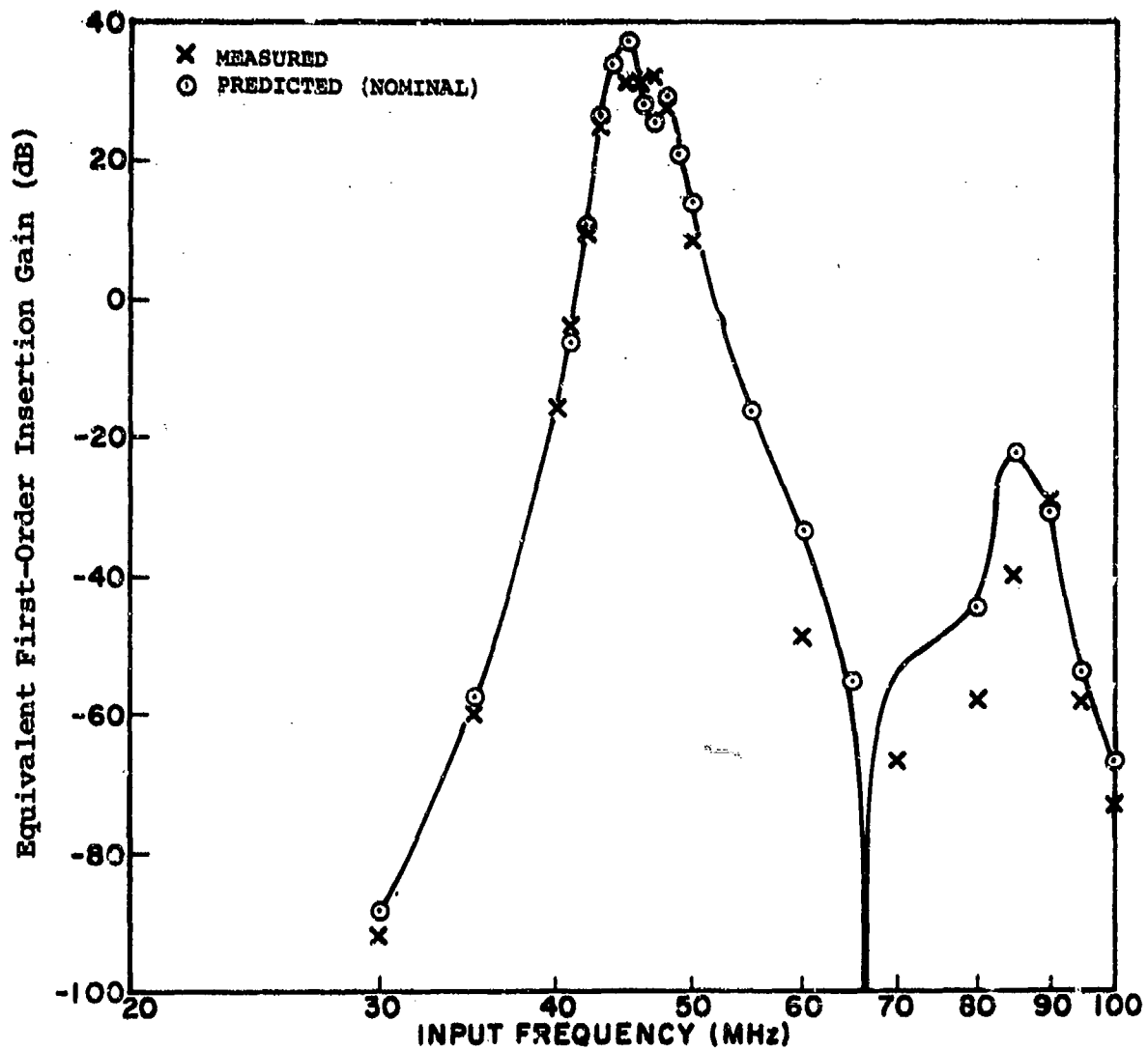


Fig. 7.51. Nominal vs. Measured 2nd Order Transfer Function.

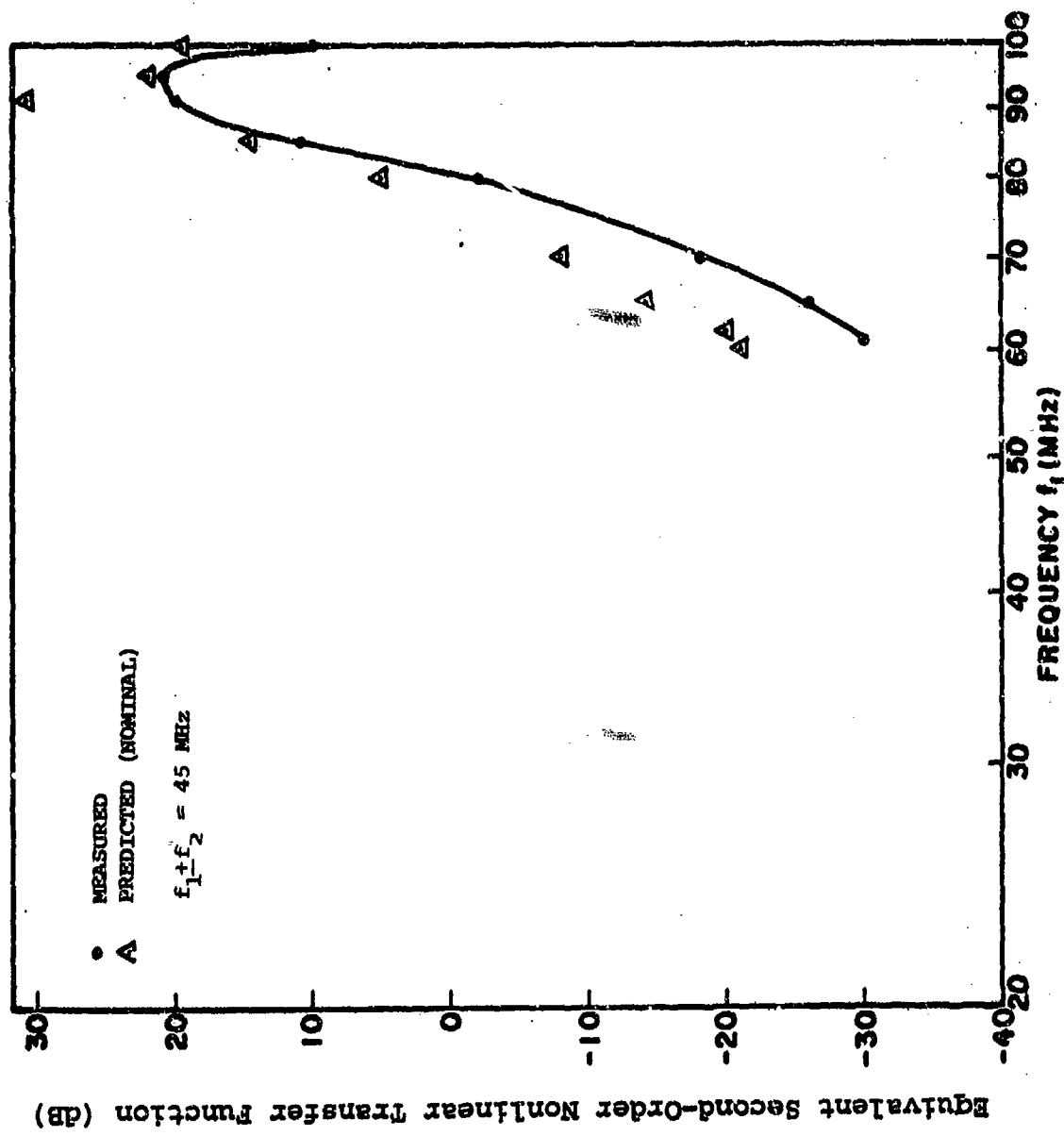


Fig. 7.52 Nominal vs. Measured 3rd Order Transfer Function.

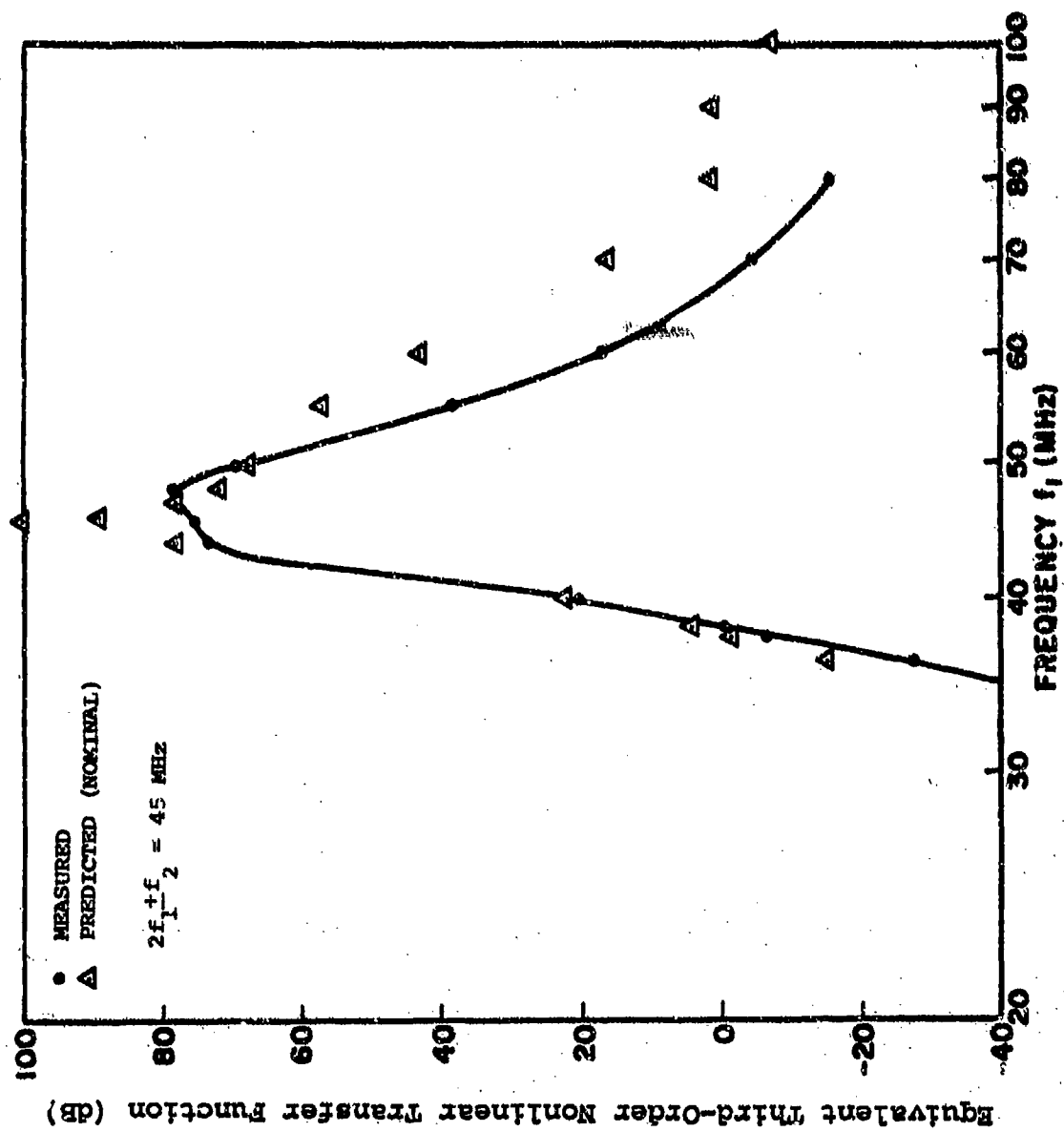


Fig. 7.53. Nominal vs. Measured 4th Order Transfer Function.

7.12.3 Nominal Receiver Parameter Variations

As part of the nominal receiver study, systematic changes were made in various linear and nonlinear parameters of the tuner, and their effects on the several nonlinear transfer functions noted. Table 7.5 summarizes the results of this study. The amount of data in the table is limited, but it indicates that the excessive accuracy in parameter values, i.e., 1% knowledge of the parameter, is not necessary for reasonable prediction purposes; a 5% accuracy would seem to give acceptable results. This is encouraging, as a scatter is to be expected in the parameter of various receivers of the same type.

Table 7.5.
VHF Tuner Parameter Variation

Parameter Varied	Nonlinear Transfer Function Computed	Changes in Nonlinear Transfer Function for a:		
		1% Variation	5% Variation	10% Variation
B-E Resistive Nonlinearity	H_2	0.2 dB	1.0 dB	
	H_4	0.2 dB	2.0 dB	
B-E Capacitive Nonlinearity	H_2		1.0 dB	1.5 dB
	H_4		2.0 dB	4.0 dB
H_{FE} Nonlinearity	H_2		2.0 dB	0.4 dB
	H_4		0.4 dB	1.0 dB
All Resistor	H_2		±0.2 dB	

7.13 HF Receiver Modeling

7.13.1 Introduction

The remainder of this chapter is concerned with the modeling of the RF Translator, a part of the front-end of a vacuum-tube type HF receiver. This translator consists of several amplification and mixing stages including both pentodes and triodes. Additionally, six high-Q linear interstage networks interconnect the vacuum tubes.

The modeling of the linear passive interstages follows the procedures used for the solid-state receiver. The modeling of the vacuum tube amplifier stages is based on the small-signal time-invariant Volterra series using the 3/2 power-law models. However, the vacuum tube mixers of this receiver operate in regions where the small-signal theory is not valid. Thus, the mixers require a large-signal approach; they were characterized by frequency-invariant power series coefficients measured with the tubes operating with broadband resistive loads. The overall response of the translator was predicted by using SIGNCAP to predict the non-linear transfer functions of the RF stages, and non-interacting cascade theory to predict the response of the mixer stages. The predicted and measured nonlinear transfer functions of the complete translator are shown to be in good agreement.

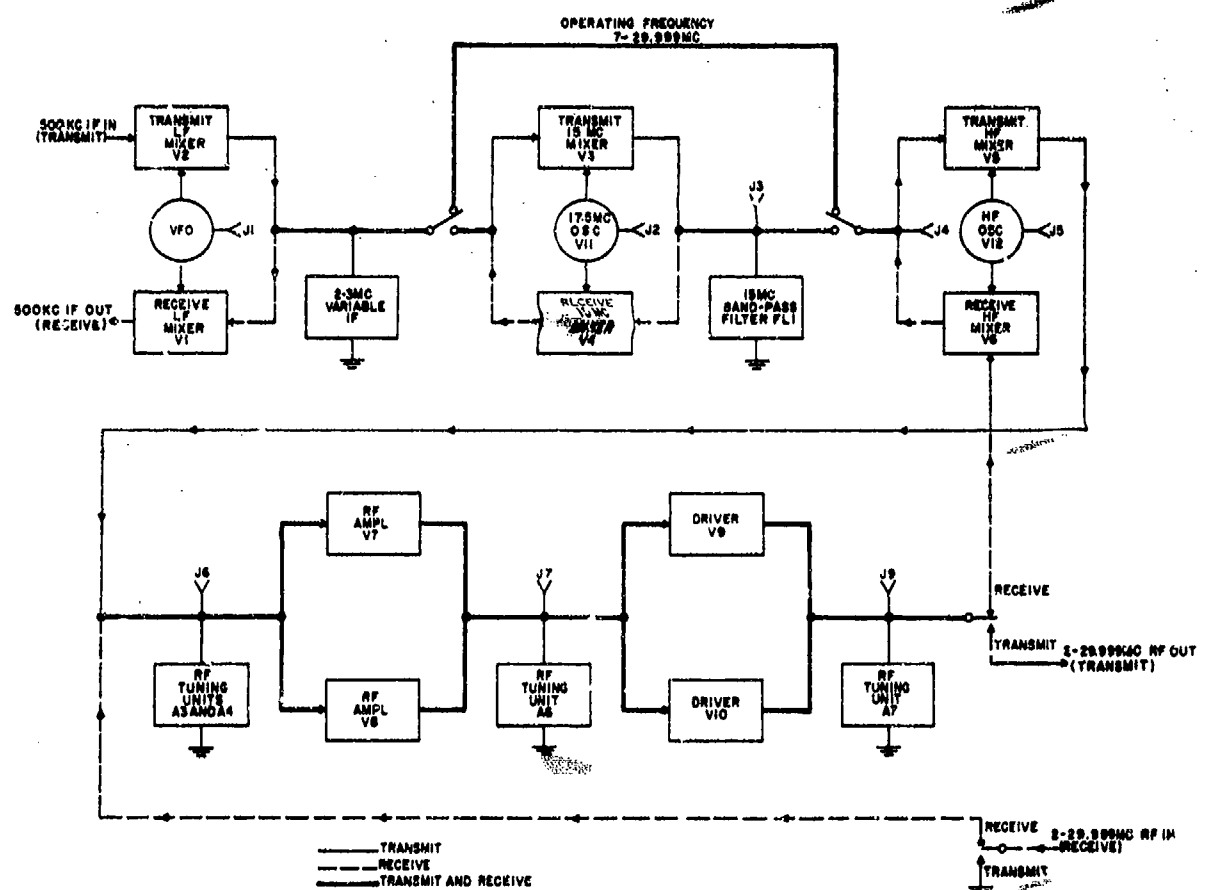


Fig. 7.54. Block Diagram, RF Tuner Module

7. 15 MHz bandpass filter F11 is the load of V6. It is centered at 15 MHz and has a 1 MHz bandwidth. Its output is connected to the grid of V4.
8. Receive 15 MHz mixer V4 is a 6AH6 pentode. The input signal is applied to the grid, and the local oscillator to the cathode. Its output frequency lies between 2.001 MHz and 3.000 MHz.
9. 2-3 MHz variable IF is the load of V4. It is tuned to the output frequency of V4. Its output is connected to the grid of V1.
10. Receive LF mixer V1 is a 6AH6 pentode. The input signal is applied to the grid, and the local oscillator to the cathode. Its output frequency is 500 kHz, which is the input to the IF module.

The nominal characteristics of the translator are listed in Table 7.6.

7.13.2 Circuit Model of the Translator

The modeling of the translator was divided into two parts, namely:

- (a) Modeling of vacuum tubes.
- (b) Modeling of the linear passive interstages.

The vacuum tubes were removed from the unit and their characteristics measured. These data are summarized in Chapter 5 and Section 6.6. The major portion of this section covers the results of modeling the linear interstages. The operating point measurements and local oscillator waveforms are presented in this section. All tests and modeling reported in this chapter are for the translator tuned to a received frequency of 5.000 MHz.

Table 7.6
RF Translator Characteristics

Frequency range	2.000 to 29.999 megacycles
Number of channels	28,000
Channel spacing	One kilocycle apart on integral kilocycles
Frequency control	Phase locked to frequency standard. Standard may be either internal or 100-kc external.
Passband response	Within 1.0 dB for ± 6 kc from selected frequency in transmit and receive.
Sensitivity	AM: $2.5\mu V$ for not less than 10 dB s+n/n ratio.
Image response	(Receive) Not less than 80 dB below response to selected frequency below 20.0 mc; 60 dB, below 20.0 mc.
Spurious response	(Receive) Not less than 60 dB below response to in-band signals.
Intermodulation distortion	(SSB Receive) All intermodulation products at IF output not less than 45 dB down from one of two equal test signals applied to antenna terminal at $100-\mu V$ level.

The interstage network measurements were made with all vacuum tubes removed. To model an interstage, two sets of measurements were made. First, the input impedances of the networks were measured. Next, each network was excited by a 50 ohm generator, and the open-circuit output voltages of the networks were measured. Based on these measurements and the data available in the instruction manual, the networks were modeled using a linear circuit analysis program, and the input impedances and voltage transfer ratios compared with the measurements. It is to be noted that the interstage network modeling procedures differed between the VHF solid-state receiver, and the HF vacuum-tube receiver. The VHF receiver interstages were modeled by only measuring their insertion losses, while, for the HF receiver interstages, both input impedance and voltage transfer ratio were measured. The reason for the extra measurements in the case of the HF receiver is the higher Q associated with vacuum tube circuitry; in order to properly characterize the networks near resonance, their impedance levels must be established. The impedance measurement is of greater importance for networks which couple high-impedance devices, such as vacuum tubes and FETs, than for low-impedance devices, such as bipolar junction transistors.

Following the network measurements, operating point measurements were made on all signal processing vacuum tubes, and the amplitudes and spectra of all local-oscillator outputs were measured under both unloaded and loaded conditions. One and two-tone measurements were made to find the first-, second-, and third-order transfer functions of individual stages and then of the complete translator.

7.13.2.1 Linear Passive Interstages

There are six passive interstages to be modeled from the antenna to the receiver IF amplifier. With reference to Fig. 7.54, these interstages are:

- Interstage 1: antenna input to grid of V7/V8 parallel pentode amplifier.
- Interstage 2: V7/V8 to V9/V10 parallel pentode amplifier.
- Interstage 3: V9/V10 to V6 triode first mixer.
- Interstage 4: V6 to V4 pentode second mixer.
- Interstage 5: V1 to V1 pentode third mixer.
- Interstage 6: V1 to receiver IF.

The results of modeling each interstage, following the two step procedure described above, are presented next.

The first network to be analyzed connects the antenna input to the grid of V7. It couples to the antenna via an autotransformer, and has a low source impedance. Therefore, in modeling it, only the voltage transfer ratio was measured.

The measured and predicted transmission characteristic for this interstage is shown in Fig. 7.55. The interstage is seen to be sharply tuned, peaking at 5.2 MHz to a peak transmission 5 dB higher than at 5.0 MHz. The predicted transmission is in good agreement with the measurements except for the region below 1.5 MHz. Here, the prediction is monotonic with frequency, while the measurement is oscillatory. It is interesting to note that the predictions are in good agreement with the minima of the transmission ripple.

The second interstage network connects V7/V8 with V9/V10. The input impedance of the network is shown in Fig. 7.56. The impedance

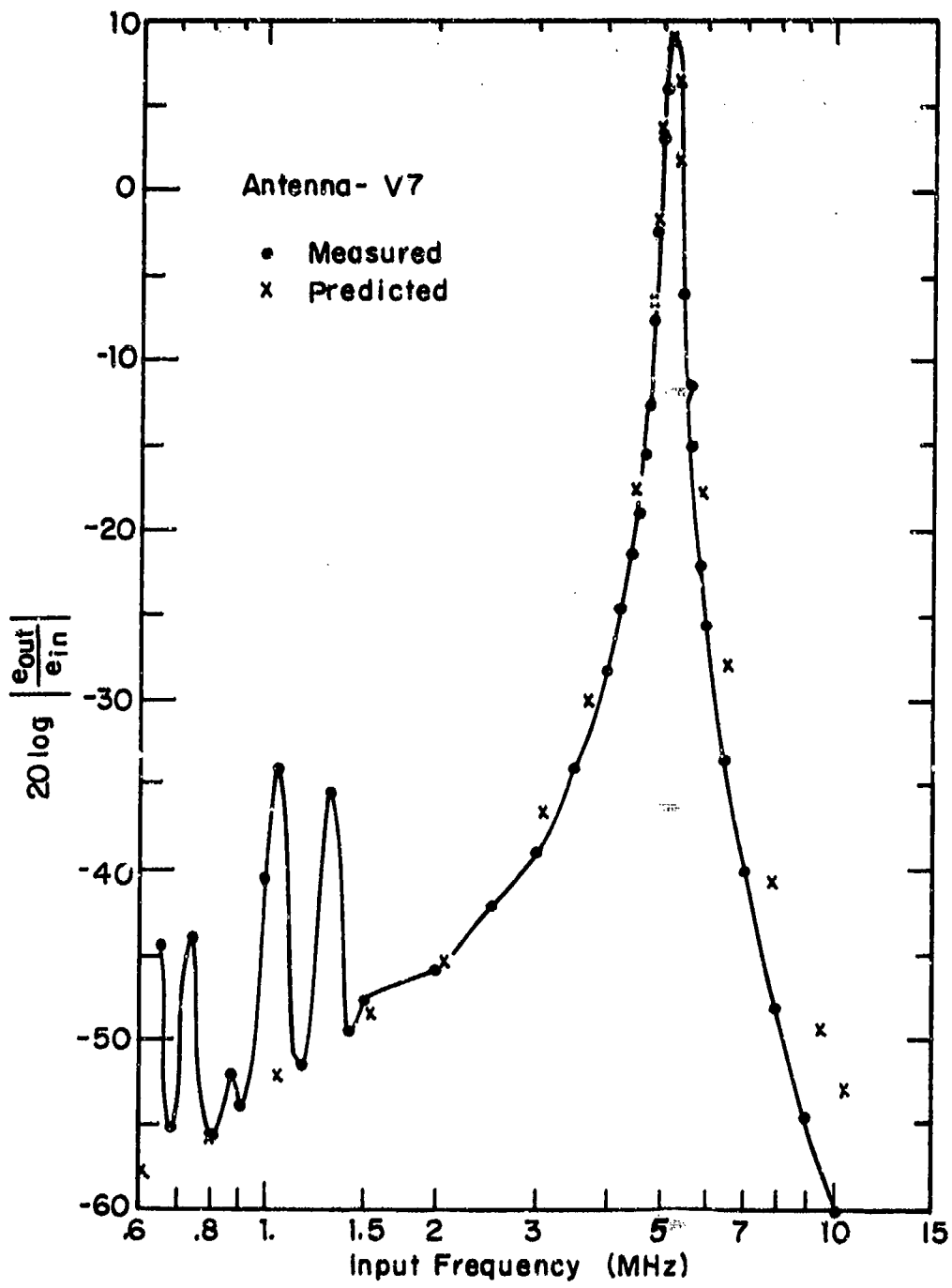


Fig. 7.55. Interstage #1 Transmission Characteristic (Antenna-V7)

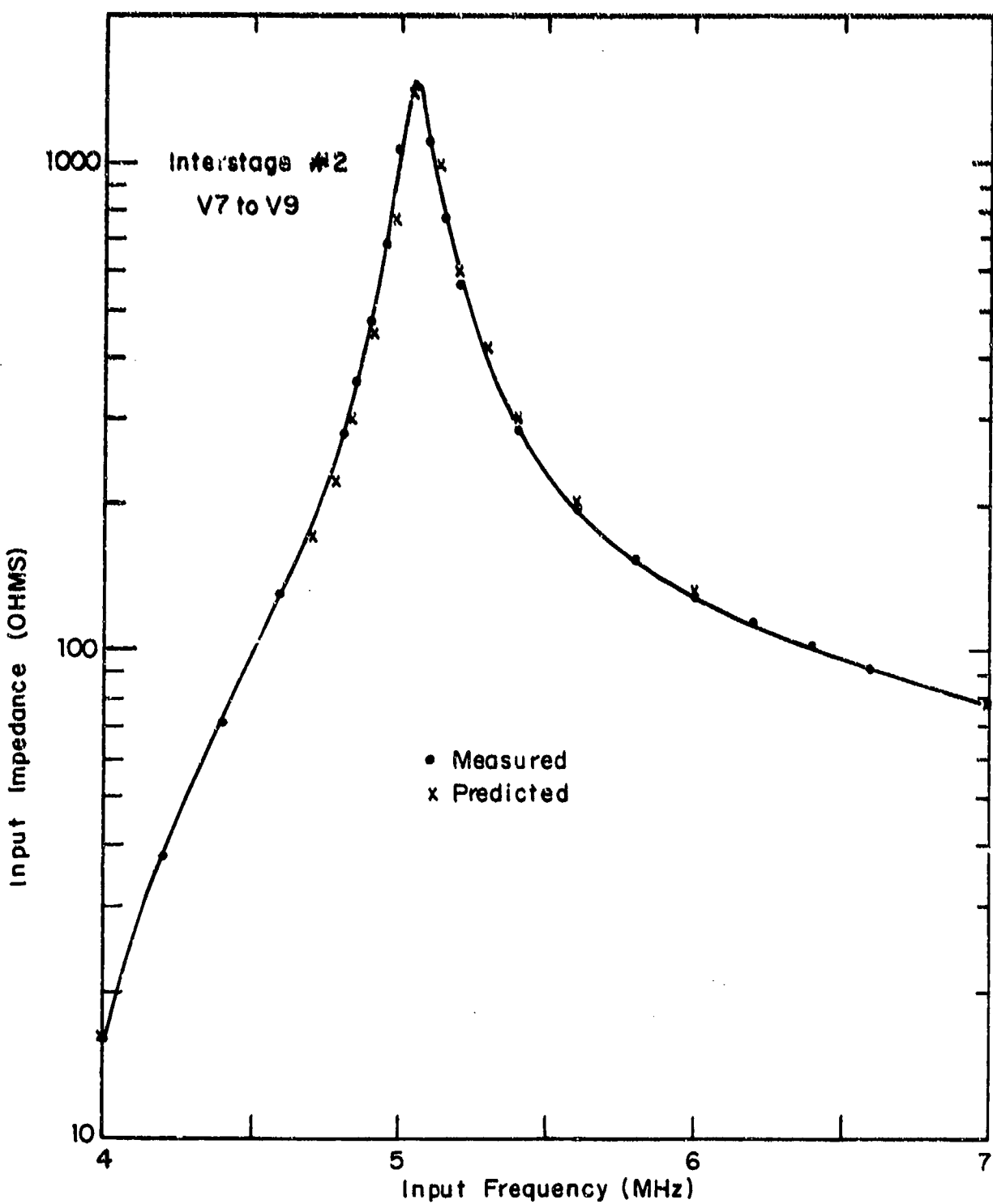


Fig. 7.56. Interstage Network #2: Input Impedance
(V7 to V9)

peaks at 4.05 MHz, and decreases monotonically on both sides. It should be particularly noted that the input impedance is quite low at 4 MHz, and, indeed, is still decreasing; this is due to an input circuit series resonance which occurs at about 3.3 MHz. The voltage transfer characteristic of the network is shown in Fig. 7.57. Here the input resonance is quite evident, with a sharp null appearing at 3.3 MHz. The circuit has a broad transmission maximum around 5 MHz, and then another null near 230 MHz. Both figures show excellent agreement between prediction and measurement.

The third interstage network connects V9/V10 to the first mixer, V6. The input impedance is shown in Fig. 7.58. It is seen to peak at about 5.3 MHz. The transmission characteristic is shown in Fig. 7.59. The transmission is seen to be broad, nearly flat from 4 to 6 MHz. There is a sharp null at about 35 MHz, caused by a series resonance to ground of capacitor and a parasitic inductor in series with it. The predicted and measured input impedances are seen to be in good agreement. The predicted transmission is in good agreement with the measured above about 1.5 MHz, but somewhat high below 2.5 MHz.

The fourth interstage network interconnects the first and second mixers, V6 and V4. It is an interesting network, in that it contains two transformers and therefore provides a distinctly different modeling problem than the other interstages. In the model, the transformers were replaced by their pi equivalent circuits. The circuit parameters were determined through impedance measurements made at the transformer terminals, as well as by using a linear circuit analysis program to match input impedance and transfer characteristics of the entire interstage.

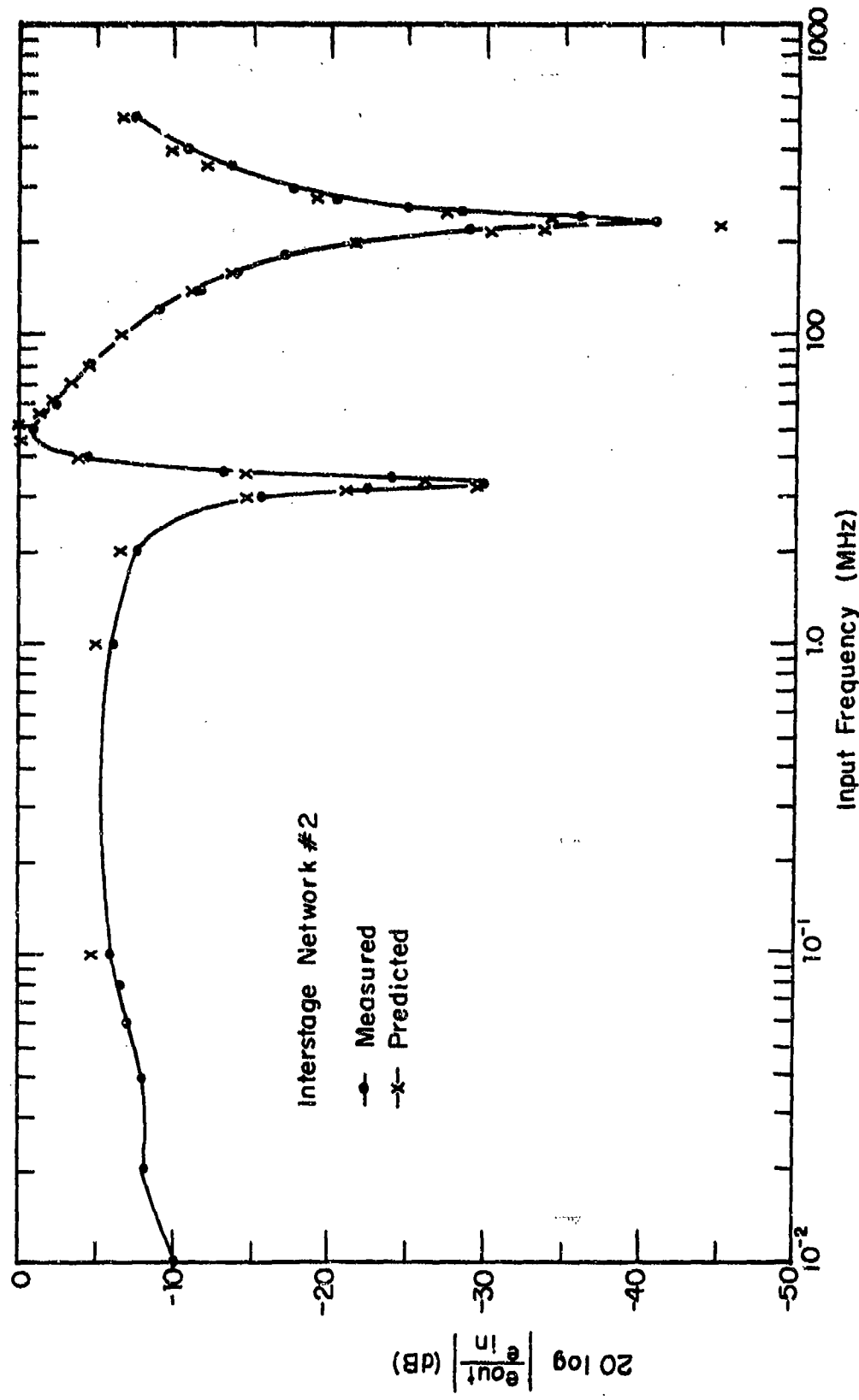


Fig. 7.57. Interstage Network #2 voltage Transmission Ratio (V7 to V9)

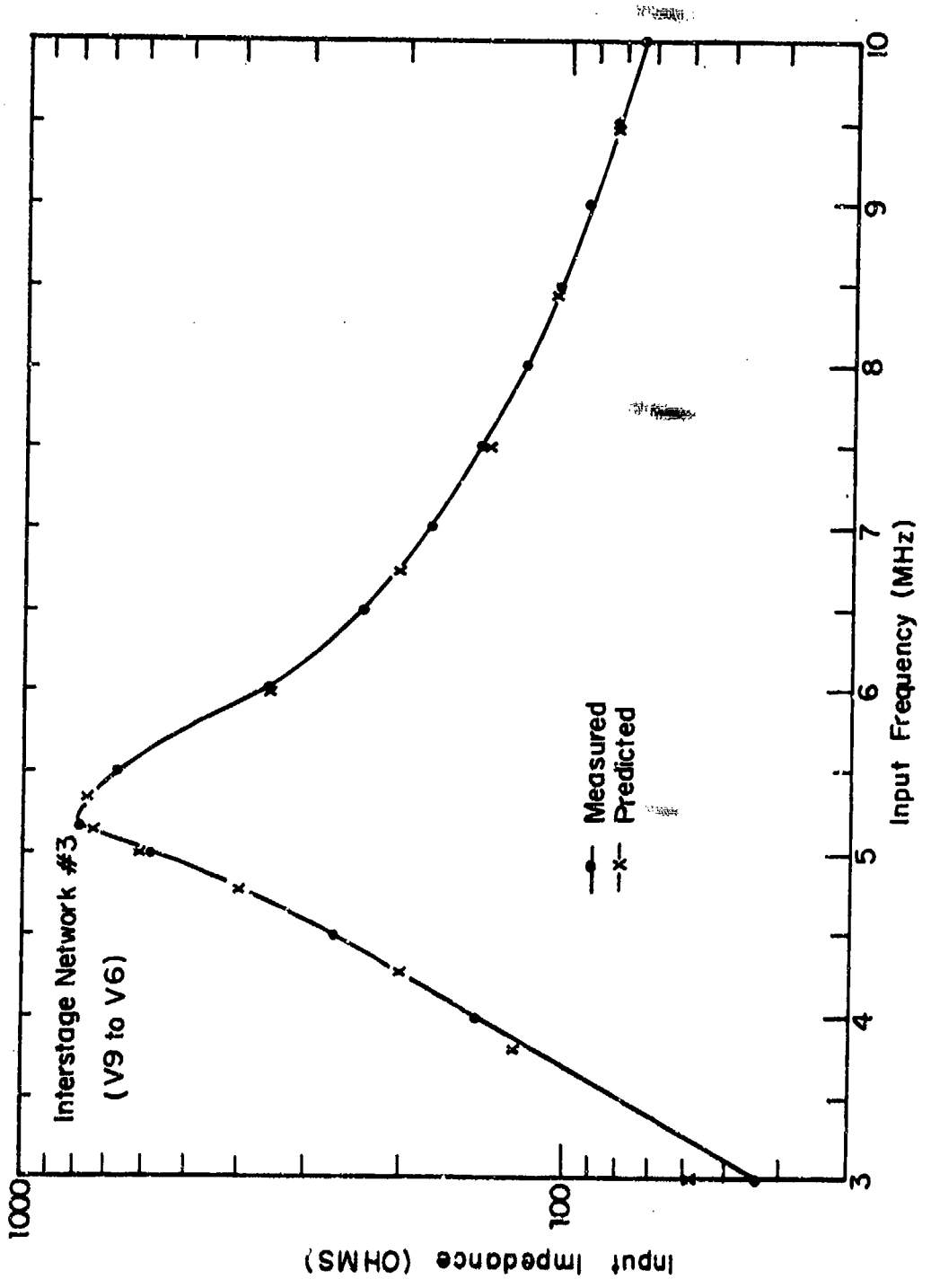


Fig. 7.58. Interstage Network #3 Input Impedance (v9 to V6)

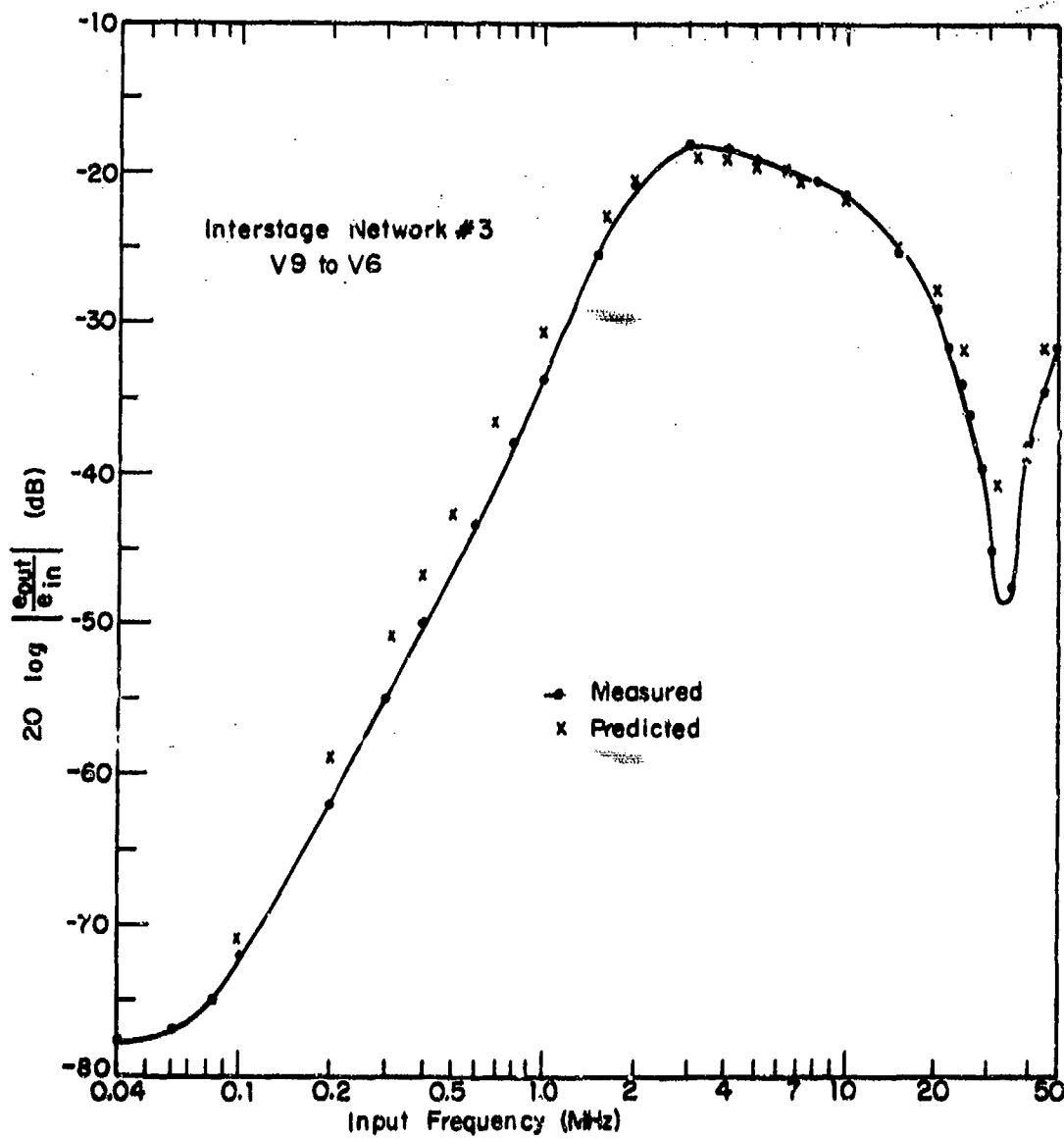


Fig. 7.59. Voltage Transfer Ratio Interstage Network #3: V9~V6

The input impedance of the interstage network is shown in Fig. 7.60. The single maximum in the input impedance should be noted. Normally, the input impedance of a double-resonant transformer has a double-hump; in this filter, the lower maximum is suppressed by a series resonance between the mutual inductance and a coupling capacitor.

The voltage transfer characteristic of the interstage network is shown in Fig. 7.61. It has a 1 MHz bandwidth and a 15 MHz center frequency. It is seen that the network is overcoupled, as the response has a double-hump. The response does not fall off rapidly at higher frequencies, i.e., in the 18 - 24 MHz range. This is due to the fact that the measurements were made with V6 and V4 removed from the receiver. If V4 were in the receiver, its input capacity would cause a more rapid fall off in the high frequency characteristic, as well as slightly increasing the peak value of the transfer characteristic.

Interstage network 5 is a variable-tuned network which connects the second and third mixers, V4 and V1. For the 5 MHz input signal, the network is tuned to 3 MHz, and has a bandwidth of about 100 kHz. The input impedance of the network is shown in Fig. 7.62. The network is seen to have an input impedance zero at about 1.5 MHz, and a peak at about 3 MHz. Details of the peak impedance are shown in more detail in the insert on the figure.

The voltage transmission characteristic is shown in Figs. 7.63 and 7.64. Figure 7.63 shows the transfer characteristic over the range 1-10 MHz. The network is seen to have an extremely sharp resonance, the details of which are shown in Fig. 7.64. From these figures it is seen that the circuit model is quite good.

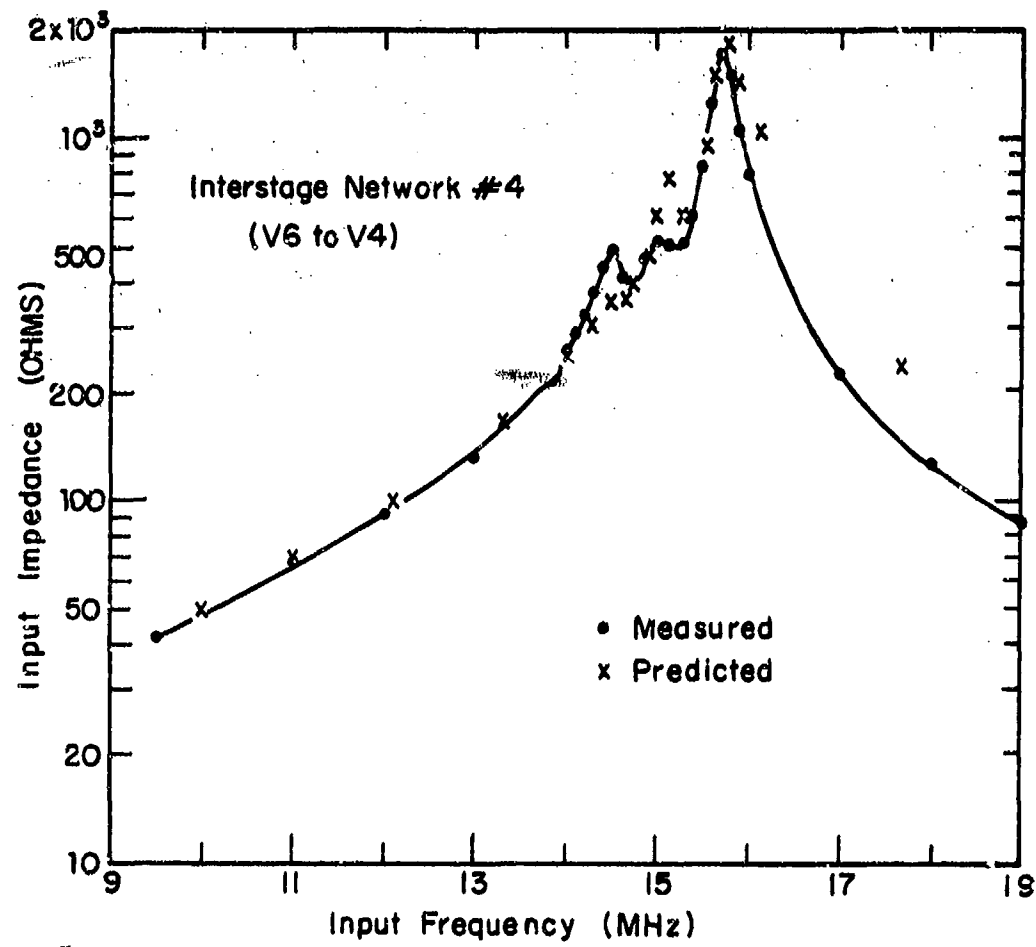


Fig. 7.60. Input Impedance Interstage Network #4
(V6 to V4)

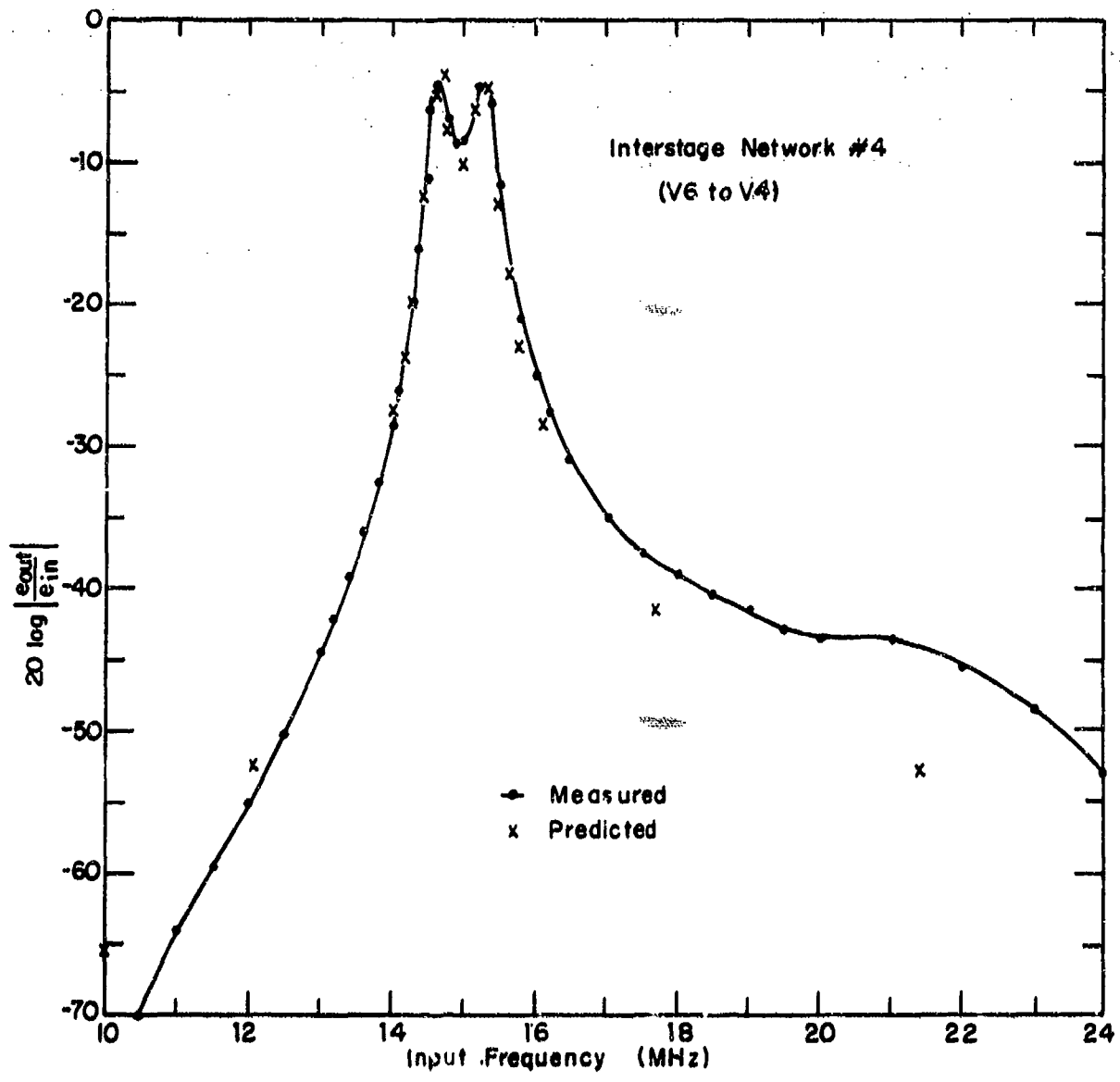


Fig. 7.61. Voltage Transfer Ratio Interstage Network #4: V6-V4

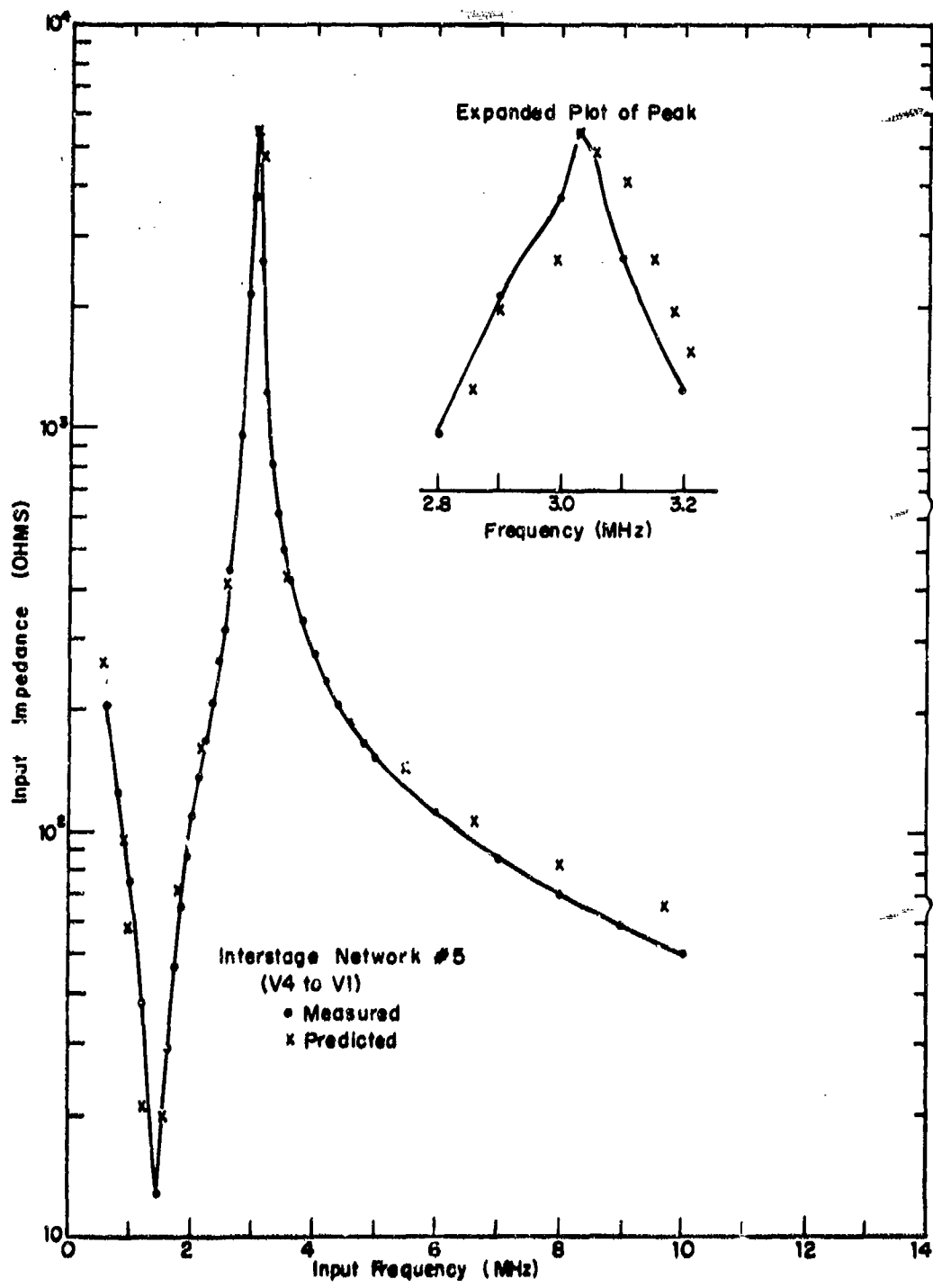


Fig. 7.62. Input Impedance Interstage #5 (V4 to V1)

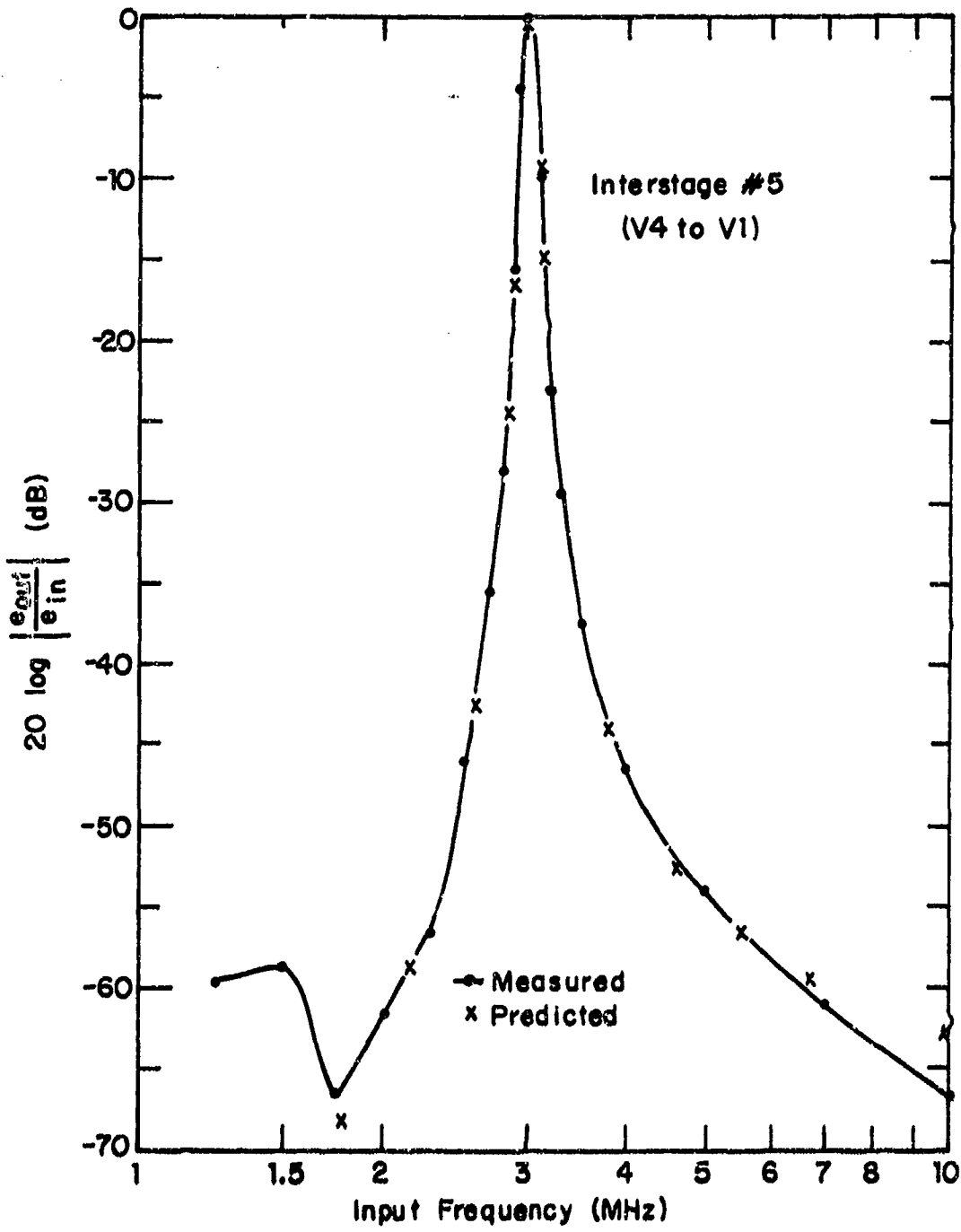


Fig. 7.63. Voltage Transmission Ratio Interstage #5 (V4 to V1)

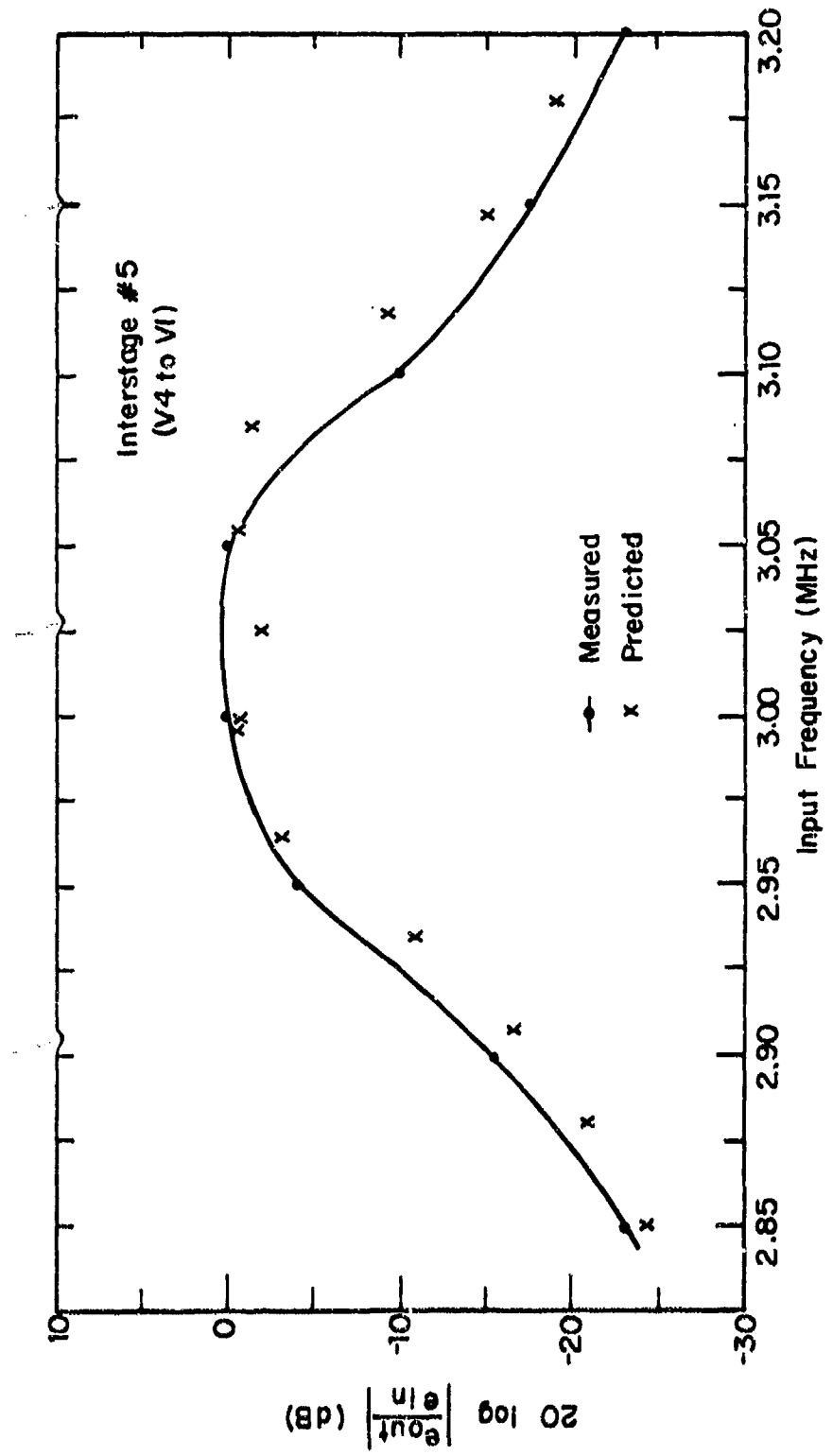


Fig. 7.64. Voltage Transmission V4-V1 Interstage

The final interstage network connects the third mixer to the receiver's IF amplifier. The interstage is fixed-tuned as the 500 kHz IF is constant, independent of input frequency. It is made up of a pair of capacitively coupled high-Q tuned networks, with a capacitive divider on the output. The capacitive divider allows the network to feed a 50 ohm load with no further impedance matching required. The input impedance of the network is shown in Fig. 7.65, and the transfer characteristic is shown in Fig. 7.66. Good agreement exists between measurement and prediction in this network.

7.13.2.2 Operating Point Data

The purpose of this section is to collect, in one place, data pertaining to measured operating points and local-oscillator signals which have been measured in the RF translator. These data were used in deriving the circuit parameters for the translator. The vacuum tube parameters have been given previously.

The vacuum tube operating points are given in Table 7.7. Mixer operating points were measured with the mixer tubes being driven by their local-oscillators. Note that the 6AH6 mixers, V1 and V4, have the same DC bias on the screen as on the plate.

TABLE 7.7.
VACUUM TUBE OPERATING POINTS (VOLTAGE)

Voltage	V1	V4	V6A	V6B	V7	V8	V9	V10
Plate	116.5	118.3	115.6	115.6	96.9	96.9	235.0	235.2
Screen	116.5	118.3	-	-	99.1	99.4	223.0	223.3
Grid #1	-3.32	-3.05	-1.95	-2.00	-1.33	-1.33	-6.25	-5.94

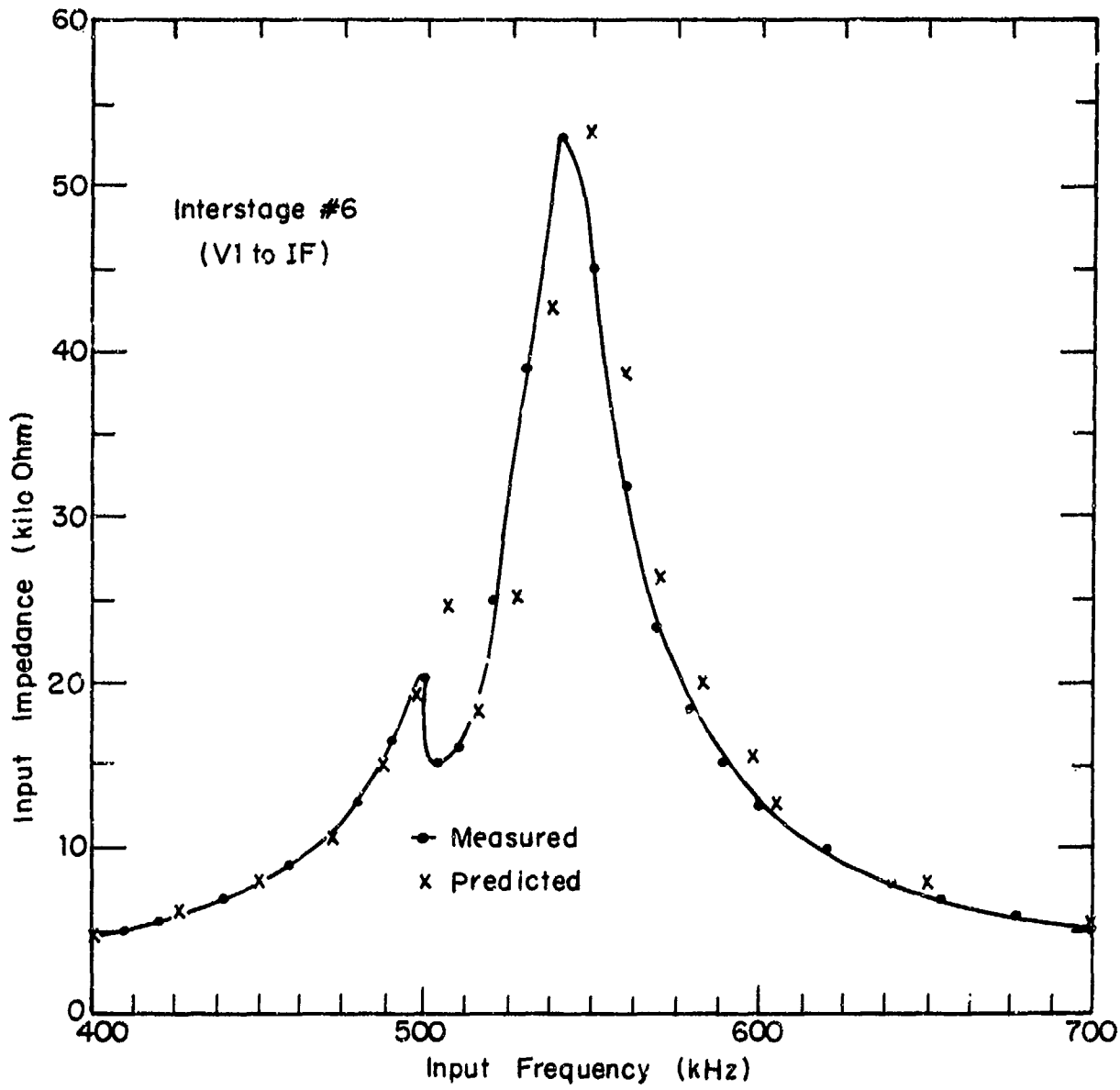


Fig. 7.65. Input Impedance Interstage #6
(V1 to IF)

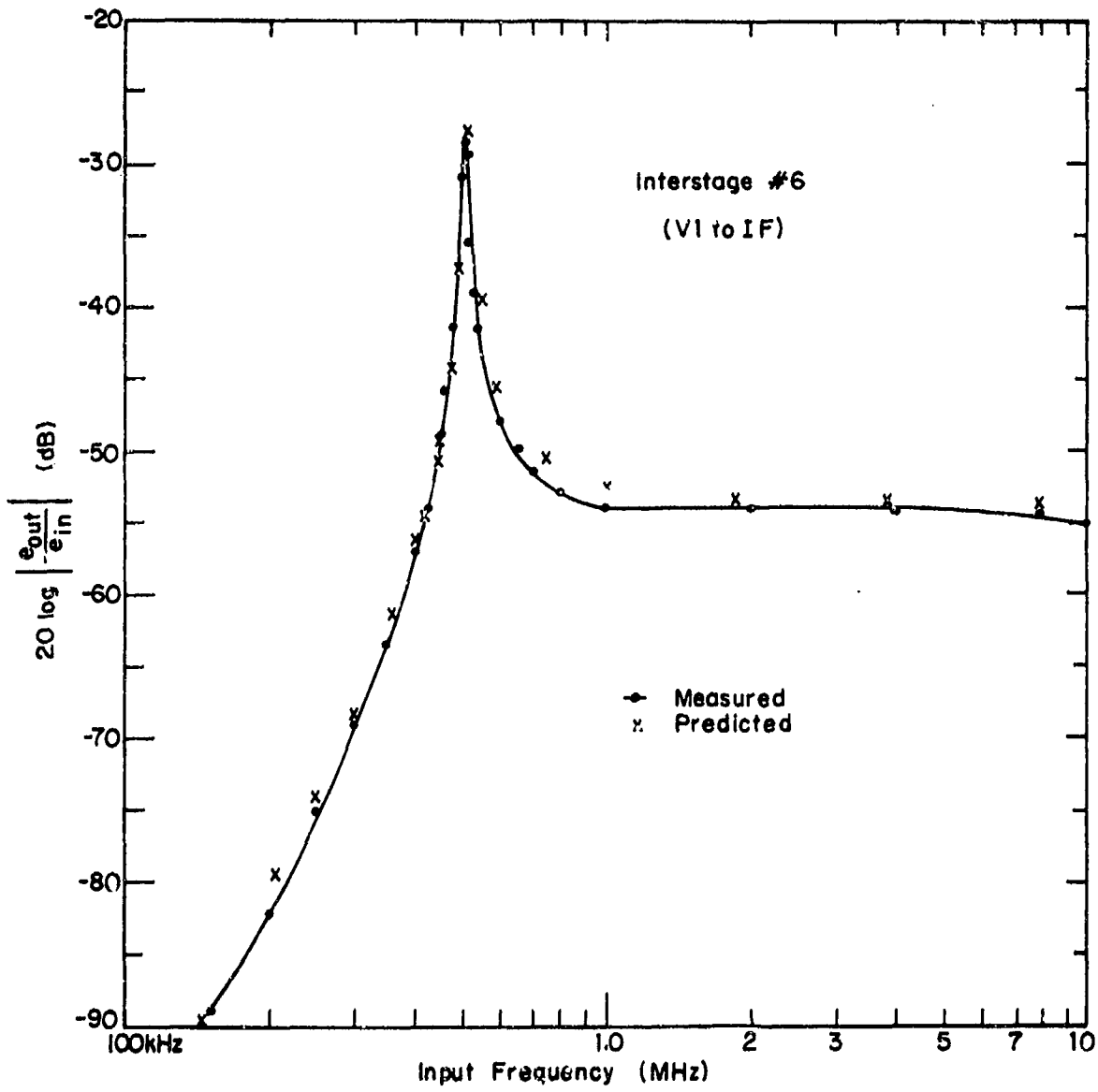


Fig. 7.66. Voltage Transfer Ratio Interstage #6 (V1 to IF)

The spectral data for the local-oscillator are given in Table 7.8. These data were measured with the mixers being driven by the local-oscillators. Voltages were measured at the cathode of the mixers, which is the local-oscillator injection point, and are rms voltages. Spectral data were taken at the referenced test points, using a 50 ohm input impedance spectrum analyzer connected in series with a 20K resistor; the spectral data in the table are therefore 52 dB below the level existing at the test points. The local-oscillator drives to V6, the HF mixer, and V4, the 15 MHz mixer, are both relatively clean, with second harmonics 20 dB below the fundamental. The local-oscillator for V1, the LF mixer, is however, not as good, with significant harmonic distortion.

Table 7.8.
LOCAL OSCILLATOR HARMONIC POWER IN dBm

Mixer Harmonic	V6 9.5 MHz 0.79V rms J5 (dBm)	V4 17.5 MHz 0.99V rms J2 (dBm)	V1 3.5 MHz 1.40V rms J1 (dBm)
1	-39.5	-36.5	-34.0
2	-61.0	-59.5	-49.0
3	-70.5	-70.0	-57.0
4	-92.5	-82.0	-68.0
5	-94.0	-88.0	-70.0
6	-86.5		-69.0
7	-82.0		-74.0
8	-85.5		-77.5
9	-41.0		-83.0
10			-83.0
11			-86.5

7.13.3 Mixer Performance

The nonlinear performance of the three mixers in the receiver were measured with the mixers functioning in the receiver and the receiver tuned to 5.000 MHz. In the tests the mixer control grids were excited by one and two-tone inputs, and the outputs were measured by means of resistive divider networks connected across specified points in the mixer plate networks. The three mixers are operated in regions where the small-signal theory is not valid, and therefore the SIGNCAP 3/2 power-law vacuum-tube software is not applicable. There is thus little likelihood of the mixers being characterized analytically, by the 3/2 power law which is applicable to the vacuum tube amplifiers.

However, it was shown through measurements that the current delivered by the vacuum tube mixers can be characterized by means of a zero-memory power series, that is, one can write the plate-current, grid-voltage by the series:

$$i_p = a_1^{eq} e_g + a_2^{eq} e_g^2 + a_3^{eq} e_g^3 \dots, \quad (7.75)$$

where

i_p = incremental plate current

e_g = incremental grid voltage

a_i^{eq} = is the equivalent i -th order mixer power series coefficient for a given Local Oscillator (L.O.) waveform $e_{LO}(t)$

The equivalent i -th order nonlinearity, a_i^{eq} is actually due to the $(i+1)$ -th order nonlinearity a_{i+1} of the mixer if the L.O. is considered as external to the mixer. That is, if the mixer tube is truly zero-memory, then for a sinusoidal local oscillator for

small enough signal and local-oscillator levels a_i^{eq} will be proportional to $V_{LO} a_{i+1}$. However, here we do not attempt to present a relation between L.O. waveform and a_i^{eq} ; the equivalent nonlinear coefficients for the given L.O. waveforms, simply written as a_i^{eq} with an L.O. waveform implicit.

In Table 7.9 the a_i^{eq} for the three mixers in the receiver are given. These coefficients were determined through measurements of intermodulation output power for sinusoidal signal inputs. The zero-memory assumption for a_i^{eq} was experimentally shown to be valid by observing little variation in output distortion with signal frequency. The determination of the a_i^{eq} through measurement is a departure from the purely theoretical approach used with the transistor circuits and the vacuum tube circuits operating in the well-behaved region. It is, however, a legitimate approach, due to both the wide bandwidths of the vacuum tubes, and the isolation between stages provided by the vacuum tubes.

Table 7.9.
Mixer Equivalent Power-Series Coefficients

Tube	a_1^{eq} (mho)	a_3^{eq} (mho/ v^2)
12AT7, V6	1.16×10^{-3}	5.5×10^{-5}
6AH6, V4	1.15×10^{-3}	2.4×10^{-4}
6AH6, V1	3.96×10^{-4}	4.16×10^{-5}

7.13.4 RF Amplifier Performance

The RF amplifier portion of the translator consists of the portion of the translator between the antenna output and the grid of V6, the first mixer. The circuitry and components which make up the RF amplifier consist of four pentodes and the first three interstages. One and two-tone tests were performed to measure the first three nonlinear transfer functions of the RF amplifier, and predictions of these transfer functions were made using the 3/2 power law SIGNCAP model. The measurements and predictions are presented in this section. The measurements and predictions were made at a $5\text{K}\Omega - 50\Omega$ divider on the grid of V6.

The predicted and measured insertion gain of the RF stages are shown in Fig. 7.67. The agreement is quite good below resonance, and seen to be somewhat high at and above resonance. The interpretation which should be given to this data is that there are two simultaneous effects being observed. First, the overall predicted gain is several dB too high. Second, above resonance the predicted transmission of the linear networks, particularly the antenna -V7 network, is some 5 dB too high. The latter is confirmed by Fig. 7.55.

The predicted and measured third-order nonlinear transfer functions are shown in Fig. 7.68. The agreement is good over the range 4.8 MHz - 5.4 MHz for f_1 covering an 80 dB variation in amplitude and being off only 10 dB in the peak value. In the 4.0 - 4.8 MHz range the prediction is for a continually decreasing nonlinear transfer function, while the measurement shows much less variation. This is attributed to the modeling of the first two pentodes in the RF amplifier which are the 6DC6's shown

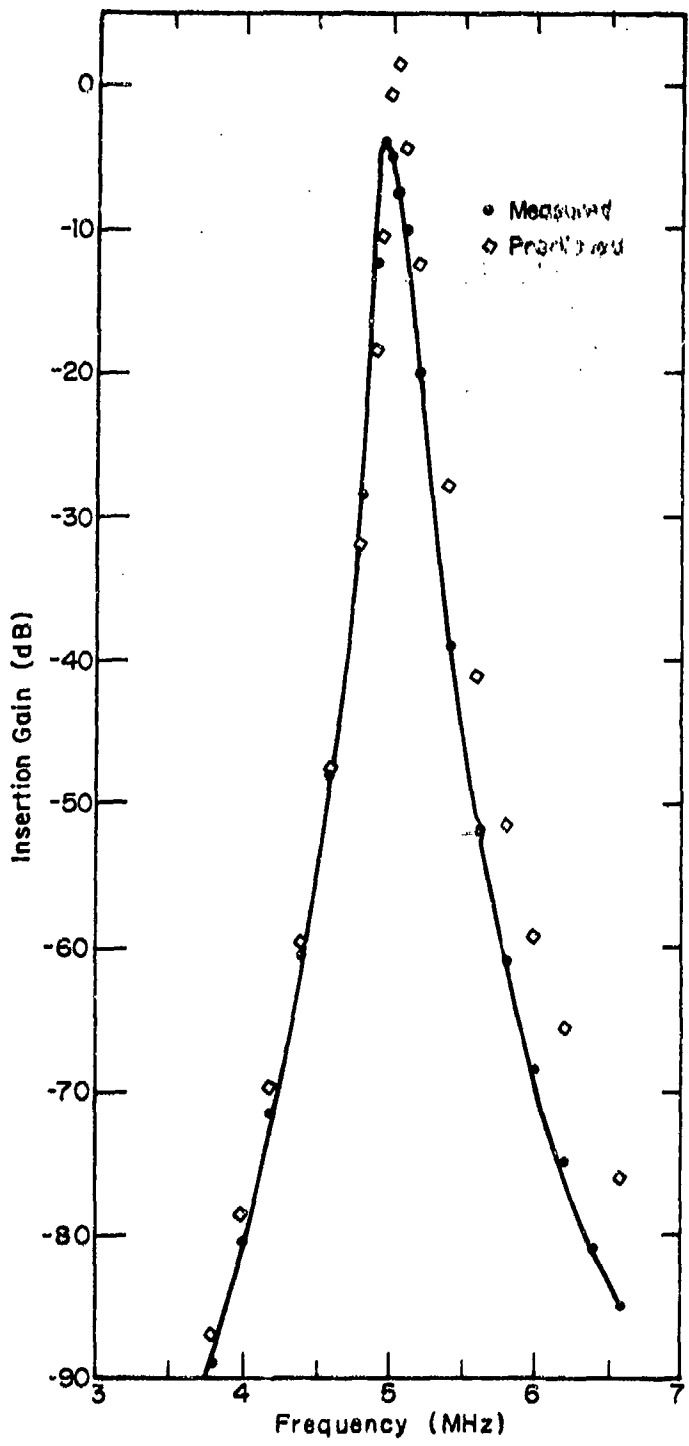


Fig. 7.67. RF Translator: First-Order Transfer Function of RF Stages

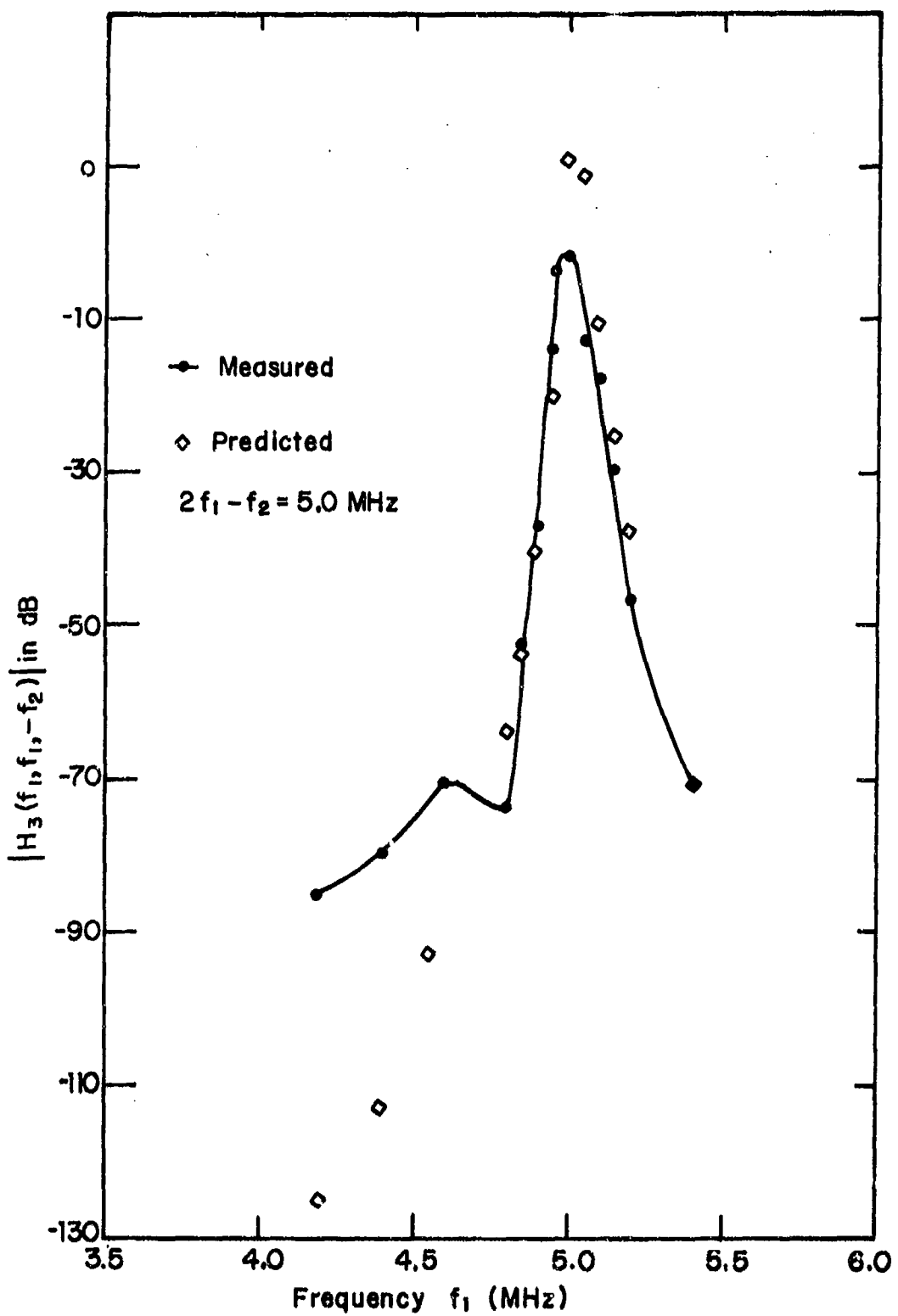


Fig. 7.68. RF Translator Third-Order Response of RF Stages

in Section 6.6 to predict lower than measured third-order nonlinear transfer functions. If the frequency range below 4.8 MHz corresponds to the range in which the primary distortion comes from the first-two pentodes (6DC6's), while the range above 4.8 MHz corresponds to the primary distortion coming from the second two pentodes (5763's), then the behavior is explainable in terms of the known pentode model behavior.

7.13.5 Complete RF Translator Response

With the modeling of all of the parts of the RF translator completed, we now present the measured and predicted nonlinear transfer functions of the entire RF translator section. The measurements were made with inputs applied to the antenna input, and outputs measured at the third mixer output with a spectrum analyzer. The first and third-order nonlinear transfer functions were measured by means of one and two-tone tests, with the available power per tone being -40 dBm in all cases. The second-order nonlinear transfer function was too small to be measured. The predictions presented in this section were made with the RF section analyzed by means of SIGNCAP's 3/2 power pentode model, and the mixers modeled by means of the a_1^{eq} and a_3^{eq} power series coefficients from Table 7.9 and the interstage network models.

7.13.5.1 Simplified Power-Series Modeling of Vacuum Tube Stages

To illustrate the use of equivalent power-series coefficients and the simplified network models to vacuum-tube receiver modeling consider the circuit shown in Fig. 7.69. This is a typical stage in a cascaded vacuum tube receiver. The voltage v_o is the input voltage across a very high input impedance. The vacuum-tube electron device is characterized as a zero-memory nonlinear incremental current generator, $i_p(v_o)$ which drives the linear interstage network, the z parameters of which are z_{11} , z_{12} , z_{21} , and

z_{22} . These relationships are shown in Fig. 7.69b. The interstage network input and output voltages v_1 , v_2 , and currents i_1 , i_2 are related by

$$\begin{bmatrix} v_1 \\ v_2 \end{bmatrix} = \begin{bmatrix} z_{11} & z_{12} \\ z_{21} & z_{22} \end{bmatrix} \begin{bmatrix} i_1 \\ i_2 \end{bmatrix}. \quad (7.76)$$

The voltage v_2 is the input voltage to the next vacuum tube. Since vacuum tube input impedances are assumed infinite, $i_2 \stackrel{\Delta}{=} 0$, and

$$v_2 = z_{21} i_1. \quad (7.77)$$

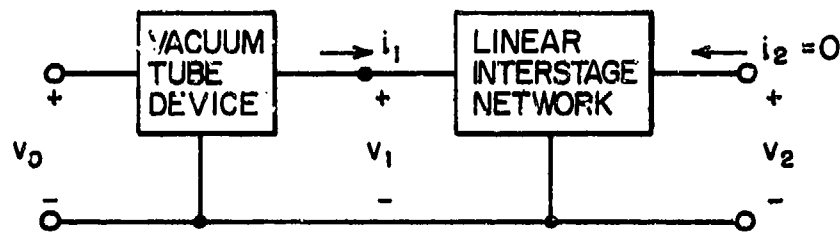
The interstage network input current i_1 is given in terms of a_1^{eq} and a_3^{eq} by the power series for the vacuum tube as

$$i_1 = -i_p = -a_1^{\text{eq}} v_o - a_3^{\text{eq}} v_o^3, \quad (7.78)$$

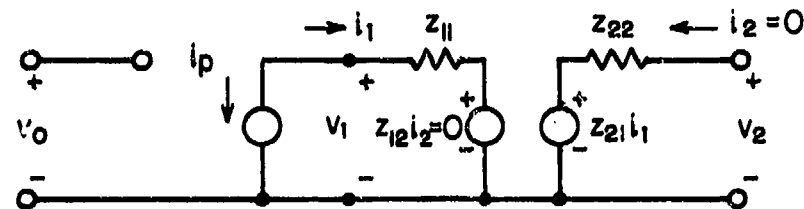
where it has been assumed that the vacuum tube is adequately modeled as a nonlinear current source. Thus, v_2 , the output voltage at the infinite impedance load ($i_2=0$) is given by

$$v_2 = -z_{21} i_p = -g_{21} a_1^{\text{eq}} v_o + a_3^{\text{eq}} v_o^3, \quad (7.79)$$

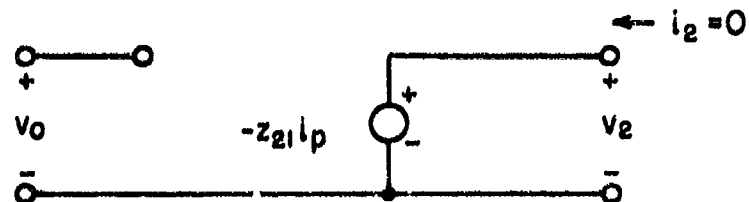
since there is no drop in z_{22} . Equation (7.79) can be applied on a stage-by-stage basis, using the correct power series coefficients for each stage. The transfer impedance z_{21} must be evaluated at the frequency combinations of interest.



a. Typical Vacuum-Tube Network Interstage



b. Incremental Nonlinear Equivalent Interstage



c. Effective Nonlinear Incremental Model

Fig. 7.69. Simplified Nonlinear Incremental Model for a Vacuum Tube Stage.

The complete nonlinear analysis of the mixers in the HF receiver translator was computed by a systematic application of Eq. (7.79). Only the equivalent first and third-order responses were calculated, as the equivalent second-order responses were found experimentally to be so small as to be unmeasurable.

7.13.5.2 Translator Nonlinear Transfer Functions

The desired RF translator output is centered around the 500 kHz intermediate frequency. Since the receiver is a triple conversion system, the response is actually a third-order response at the frequency $f_s + f_{L01} - f_{L02} - f_{L03}$, where f_s is the signal frequency and the remaining frequencies are the three local oscillator frequencies. However, consistent with our use of equivalent power-series coefficients, (a_1^{eq} and a_3^{eq}), the desired response is interpreted as an equivalent first-order response. Thus, we can also refer to the equivalent insertion gain of the complete translator as the difference between the output delivered and available input powers at the output and input frequencies. The predicted and measured equivalent insertion of the RF translator are shown on Fig. 7.70. The figure covers the frequency range 4.88-5.18 MHz, and shows good agreement between the predictions and measurements. The insertion gain varies over a 30 dB range, and the primary difference between the prediction and measurement is a slight detuning of the peak region of the predicted insertion gain.

The predicted and measured equivalent third-order nonlinear transfer functions of the translator, $H_3^{eq}(f_1, f_1, -f_2, f_{L01}, -f_{L02}, -f_{L03})$, are shown in Fig. 7.71. Again we find good agreement with the primary difference being a detuning effect. The parameters of the receiver are such that, over the frequency range

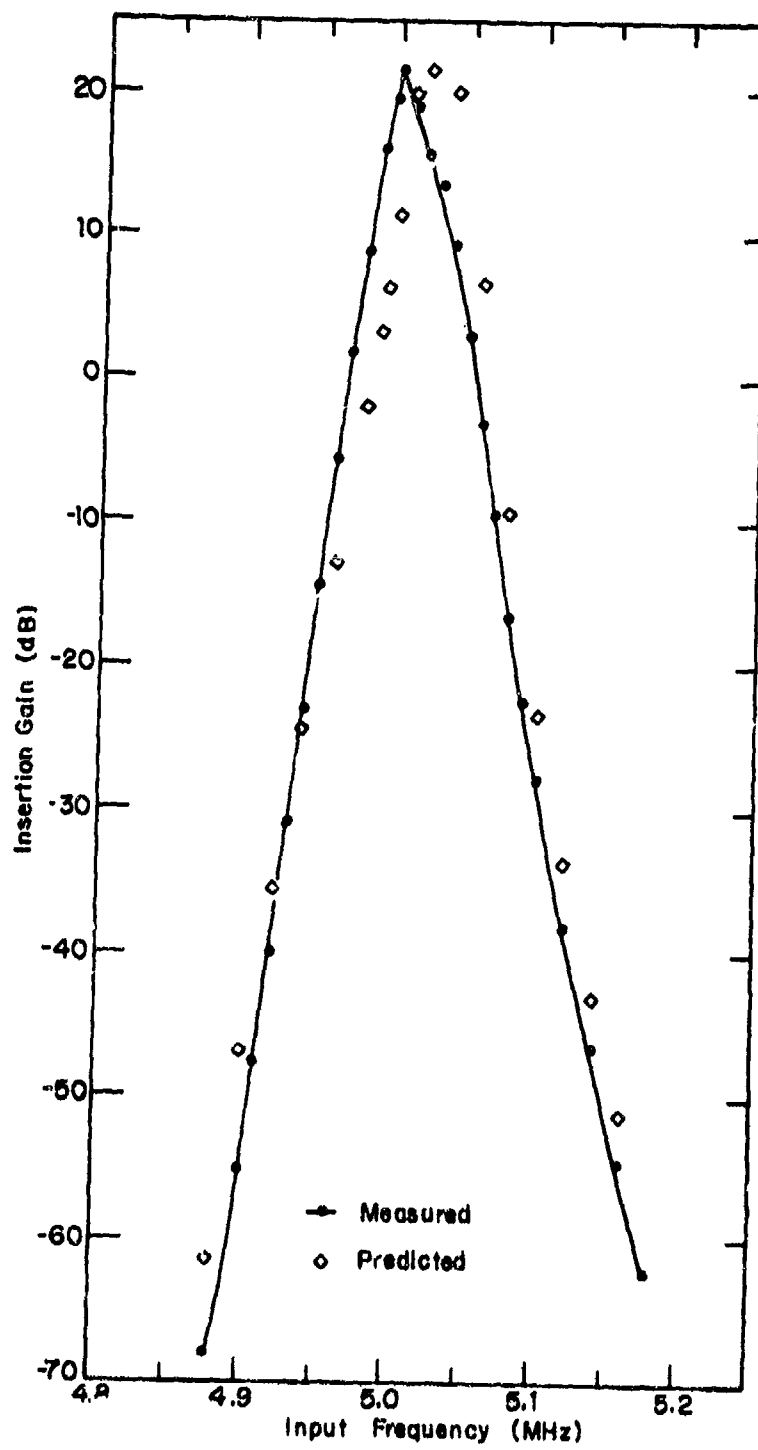


Fig. 7.70. RF Translator First-Order Response.

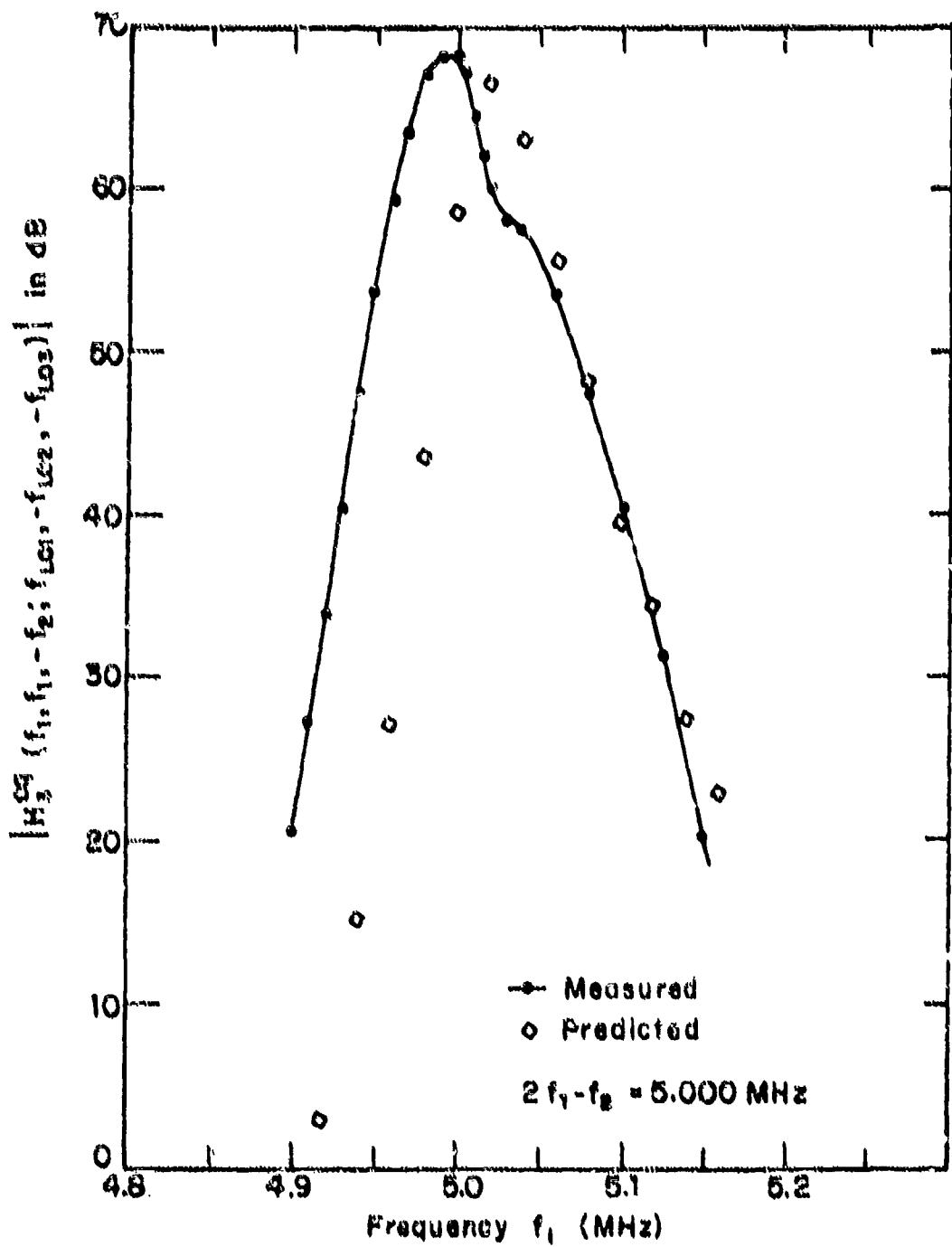


Fig. 7.21. RF Translator Equivalent Third-Order Nonlinear Transfer Function

shown, the source of the third-order intermodulation distortion is the first mixer, V6. The second and third mixers do not cause significant intermodulation distortion, and the third-order distortion of the RF stages is sufficiently small that it also does not contribute significantly to the RF translator distortion in this frequency range.

APPENDIX A

SIGNCAP I - NONLINEAR CIRCUIT ANALYSIS COMPUTER PROGRAM

A.1 Introduction

The SIGNATRON Nonlinear Circuit Analysis Program, known as SIGNCAP I, allows the engineer to determine the nonlinear transfer functions of an electronic circuit. SIGNCAP utilizes a set of standard electric circuit elements, and can analyze networks made up of interconnections of these elements.

SIGNCAP is written in FORTRAN IV, and has been implemented on two computers, the IBM 1130 with 8K of core and the Honeywell 635. The IBM 1130 version can directly analyze networks containing up to 30 nodes, while the Honeywell 635 version can directly analyze networks containing up to 50 nodes. Larger networks can be analyzed by segmenting the network into subnetworks, and then utilizing SIGNCAP's cascading option.

Structurally, SIGNCAP solves the nonlinear network problem by forming both the nodal admittance matrix (Y matrix) for the entire network, and the first-order generator (current-source) excitation vector, for all of the linear sources in the entire network. The generators can be located at any node in the network, and can have any desired frequency, amplitude, and phase. The usual procedure of premultiplying the generator vector by the inverse Y matrix results in the first-order nodal voltage vector for the network, the elements of which are the first-order transfer functions at all nodes in the network at the given excitation frequency. In the event that there is more than one generator at a

given frequency, the first-order transfer function will be the total transfer function due to the superposition of the generators since the first-order transfer function is a linear function. The higher-order transfer functions are solved iteratively, using the analysis techniques described in Chapter 2.

SIGNCAP is simple to employ. The user enters a description of the circuit to be analyzed, as well as the frequencies and order of the analysis. SIGNCAP interprets the input statements, performs the nonlinear analysis, and outputs the results in printed form. There are five types of inputs which are needed to describe a given circuit. The input statements define the topology of the circuit, the circuit element values, the linear and nonlinear devices used in the circuit, the circuit excitation and the order of the analysis, and the desired output.

This appendix is designed so that the reader will be able to use SIGNCAP after reading it. It does not contain an in-depth discussion of the various subroutines which make up SIGNCAP, nor does it contain detailed program flow charts or program listings, as they are not necessary for an understanding of SIGNCAP. Section A.2 provides a user-oriented discussion of the SIGNCAP analysis techniques and program interaction. The circuit elements and models which are used in SIGNCAP are described in Section A.3, and the input statement structure is described in Section A.4. Section A.5 deals with the use of SIGNCAP in typical examples. Examples are also given in the other sections when a particular point is to be illustrated.

A.2 SIGNCAP Analysis Techniques

A.2.1 Nodal Admittance Analysis

The purpose of SIGNCAP is to determine the nonlinear transfer function of a network. We use the convention that the nonlinear transfer functions are voltage transfer functions, that is, they relate an output response voltage to one or more input excitation voltages. It is thus both natural and convenient to perform the nonlinear circuit analysis on a nodal basis, where the independent variables are the known voltages and the dependent variables are the unknown nodal voltages. As a simple example, consider the linear Pi network of Fig. A.1a. The nodal equations for this network are:

$$v_1 \left(\frac{1}{z_1} + \frac{1}{z_2} \right) - v_2 \frac{1}{z_2} = I_1, \quad (\text{A.1a})$$

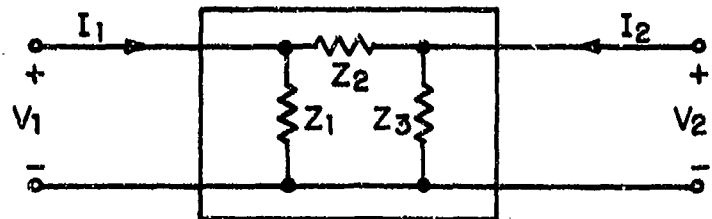
$$-v_1 \frac{1}{z_2} v_2 \left(\frac{1}{z_2} + \frac{1}{z_3} \right) = I_2, \quad (\text{A.1b})$$

which can be written in matrix form as:

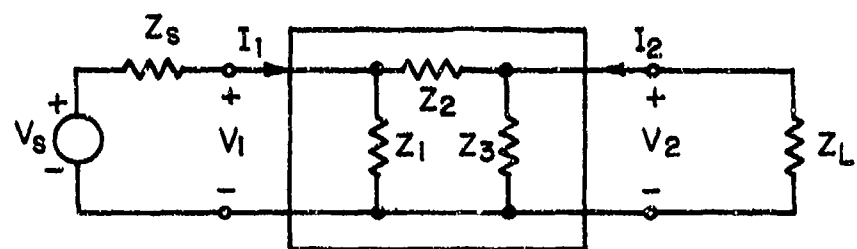
$$\begin{bmatrix} \frac{1}{z_1} + \frac{1}{z_2} & -\frac{1}{z_2} \\ -\frac{1}{z_2} & \frac{1}{z_2} + \frac{1}{z_3} \end{bmatrix} \begin{bmatrix} v_1 \\ v_2 \end{bmatrix} = \begin{bmatrix} I_1 \\ I_2 \end{bmatrix}. \quad (\text{A.2})$$

Equation (A.2) is conventionally written as:

$$[V] [v] = [I]. \quad (\text{A.3})$$



(a) A Passive Linear Pi Network



(b) An Excited Linear Pi Network

Fig. A.1. Illustrating Nodal Analysis.

where:

[Y] = nodal admittance matrix,

[V] = nodal voltage vector,

[I] = nodal current vector.

The nodal admittance matrix is a property of the network itself, and can be constructed independently of external source and load constraints. It is a square matrix, the elements of which are equal to:

$y_{ij} \Big|_{i \neq j}$ = negative of admittance between node i and node j

y_{ii} = sum of all admittances between node i and all other nodes including ground.

If the passive network of Fig. A.1a is embedded in a larger network, constraints are placed on the terminal voltages and currents. In particular, consider the embedding of Fig. A.1b, where node 1 is driven by a voltage source V_S with Thevenin impedance Z_S , and node 2 is terminated in a passive impedance Z_L .

The terminal constraints are:

$$I_1 = (V_S - V_1) \frac{1}{Z_S}, \quad (A.4a)$$

$$I_2 = -V_2 \frac{1}{Z_L}. \quad (A.4b)$$

Substituting (A.4) into (A.1) results in:

$$v_1 \left(\frac{1}{z_1} + \frac{1}{z_2} + \frac{1}{z_s} \right) - v_2 \frac{1}{z_2} = v_s \frac{1}{z_s}, \quad (A.5a)$$

$$-v_1 \frac{1}{z_2} + v_2 \left(\frac{1}{z_2} + \frac{1}{z_3} + \frac{1}{z_L} \right) = 0, \quad (A.5b)$$

which can be written in matrix form as:

$$\begin{bmatrix} \frac{1}{z_1} + \frac{1}{z_2} + \frac{1}{z_s} & -\frac{1}{z_2} \\ -\frac{1}{z_2} & \frac{1}{z_2} + \frac{1}{z_3} + \frac{1}{z_L} \end{bmatrix} \begin{bmatrix} v_1 \\ v_2 \end{bmatrix} = \begin{bmatrix} v_s \frac{1}{z_s} \\ 0 \end{bmatrix}. \quad (A.6)$$

Equation (A.6), the current-voltage matrix equation for the embedded pi network, is seen to be closely related to Eq.(A.2), the current-voltage matrix equation for the isolated pi network. The differences are:

1. The admittance between node 1 and ground has been increased by $\frac{1}{z_s}$, the source admittance.
2. The admittance between node 2 and ground has been increased by $\frac{1}{z_L}$, the load admittance.
3. I_1 has been replaced by the Norton current source $v_s \cdot \frac{1}{z_s}$, and I_2 has been set equal to zero.

Thus, the network equations are now in the form of a known voltage excitation, v_s , and two unknown response voltages, v_1 and v_2 . The unknown voltages can be solved for by matrix inversion:

$$\begin{bmatrix} v_1 \\ v_2 \end{bmatrix} = \begin{bmatrix} \frac{1}{z_1} + \frac{1}{z_2} + \frac{1}{z_s} & -\frac{1}{z_2} \\ -\frac{1}{z_2} & \frac{1}{z_2} + \frac{1}{z_3} + \frac{1}{z_L} \end{bmatrix}^{-1} \begin{bmatrix} v_s & \frac{1}{z_s} \\ 0 \end{bmatrix}. \quad (\text{A.7})$$

In the case of a linear network, Eq. (A.7) is the desired result. It shows that the desired nodal response can be found in terms of the known current source vector and the admittance matrix of the embedded network. In fact, if $v_s = 1$, v_1 and v_2 are numerically equal to the first-order nonlinear transfer functions at nodes 1 and 2, respectively. This can be written in matrix form as:

$$[H_1] = [Y]^{-1}[I], \quad (\text{A.8})$$

where:

$[H_1]$ = first-order nonlinear transfer function vector,

$[Y]$ = nodal admittance matrix of entire network,
including source and load impedances

$[I]$ = current excitation vector.

If the voltage excitation can be written as the sum of n sinusoids, and the \underline{Y} matrix is frequency selective over their frequencies, Eq. (A.8) must be solved n times in order to determine the first-order nonlinear transfer functions at all n frequencies.

The solution of the linear network problem is, given the \underline{Y} matrix, seen to be straightforward. We now turn our attention to the nonlinear network problem. We have shown in Chapter 2 that the method of solution of the small-signal nonlinear network is centered around the Taylor's series expansion of the network's nonlinear element's current-voltage relation around their operating points, that is:

$$i = a_1 v + a_2 v^2 + a_3 v^3. \quad (\text{A.9})$$

For a linear element, a_1 is the element's admittance, and all the a_i are zero for i greater than one. The incremental voltage, v , can be either the nonlinear element's terminal voltage for an independent nonlinearity, or the voltage across some other point in the circuit, for a dependent nonlinearity. The solution for the first-order nonlinear transfer function, at a frequency f_i , is, from (A.8), given by:

$$[H_1(f_i)] = [\underline{Y}(f_i)]^{-1} [I(f_i)]. \quad (\text{A.10})$$

In Eq. (A.10) we have explicitly shown the frequency dependence of the \underline{Y} matrix. The current vector I is made up of all independent sources of frequency f_i , and all nonlinear elements in the circuit are replaced by the first term in their Taylor's series for

the first-order analysis. If an n^{th} order nonlinear analysis is to be performed, and the input is given by

$$v_s(t) = \sum_{i=1}^n A_i \exp(j2\pi f_i t). \quad (\text{A.11})$$

Equation (A.10) must be evaluated for all combinations of the n input frequencies, taken one at a time, or $\binom{n}{1}$ times to find the set of n first-order nonlinear transfer functions, $\{H_1(f_1), H_1(f_2), \dots, H_1(f_n)\}$.

Once the first-order nonlinear transfer functions have been evaluated, the second-order nonlinear transfer functions can be evaluated. This can be represented in matrix form as:

$$[H_2(f_i, f_j)] = [Y(f_i + f_j)]^{-1} [I_2(H_1(f_i), H_1(f_j))]. \quad (\text{A.12})$$

Equation (A.12) says that the second-order nonlinear transfer function vector, H_2 , evaluated at the sum frequency $f_i + f_j$, is the product of a second-order current vector I_2 , and the inverse of the Y matrix, both evaluated at $f_i + f_j$. I_2 is a function of $H_1(f_i)$ and $H_1(f_j)$, the first-order transfer functions evaluated at frequencies f_i and f_j . The exact functional form of I_2 is determined by the types and locations of the nonlinearities, as described in Chapter 2. In an n^{th} -order analysis, the input is again the sum of n exponentials and Eq. (A.12) must be evaluated for all combinations of n frequencies taken two at a time, or $\binom{n}{2}$ times.

The third-order nonlinear transfer function can be represented in terms of the first and second-order nonlinear transfer functions as:

$$\begin{aligned} [H_3(f_i, f_j)] &= [Y(f_i + f_j + f_k)]^{-1} [I_3(H_1(f_i), H_1(f_j), H_1(f_k))] \\ &\quad + I_{23}(H_1(f_i)H_2(f_j + f_k)). \end{aligned} \quad (\text{A.13})$$

Equation (A.13) is in the same form as Eq. (A.12). Specifically the third-order nonlinear transfer function vector, H_3 , evaluated at frequency $f_i + f_j + f_k$, is the product of a third-order current vector, $I_3 + I_{23}$, and the inverse of the \underline{Y} matrix, both evaluated at frequency $f_i + f_j + f_k$. The current vector is made up of two types of terms, namely the direct third-order currents given by I_3 , and the third-order currents given by an interaction of first-order and second-order terms, I_{23} . The exact functional form of $I_3 + I_{23}$ is determined by the types and locations of the nonlinearities, as described in Chapter 2. In an n^{th} -order analysis, Eq. (A.13) must be evaluated for all combinations of the n input frequencies taken three at a time, or $\binom{n}{3}$ times.

The solution for higher-order nonlinear transfer functions follows the same form as described above. In general, the solution for the m^{th} -order nonlinear transfer function in an n^{th} -order analysis, $m \leq n$, requires the solution of $\binom{n}{m}$ equations of the form of Eq. (A.13). Thus, in a complete n^{th} -order analysis, the number of matrix inversions which are required is:

$$\binom{n}{1} + \binom{n}{2} + \dots + \binom{n}{n} = 2^n - 1 \quad (\text{A.14})$$

Equation (A.14) provides a fundamental insight into the solution time of SIGNCAP's nonlinear transfer function analysis. As a general rule, an n^{th} -order analysis of a given circuit will require $2^n - 1$ times the running time of a first-order analysis of the circuit. To give a benchmark speed, the analysis of a 27 node, 4 transistor, IF amplifier on the Honeywell 635 required 9.35 seconds per output frequency term. Thus a fourth-order analysis of this circuit would take approximately 140 seconds.

A.2.2 Segmentation and Cascade Analysis

As is shown in Eq. (A.3), the nodal admittance matrix for a r node network has r^2 elements. Since these are in general complex elements, the storage of the matrix in the computer requires $2r^2$ words, e.g., 200 words for a ten node circuit and 20,000 words for a hundred node circuit. It is evident that for any size computer there will be a maximum size circuit which can be analyzed as a single unit. For circuits which exceed this size, it is convenient to break the circuit up into smaller circuits, called segments, analyze each segment separately, and then determine the nonlinear transfer functions of the complete circuit through the use of the cascade equations of Chapter 2.

The procedure of segmentation and cascading is familiar in linear circuit theory, where the Thevenin source is the open-circuit output voltage of a segment, and the Thevenin impedance is the output impedance of a segment. In the case of nonlinear transfer function analysis, the nonlinear transfer functions of each segment are computed with each segment driven by a source which has the same impedance as the Thevenin impedance of the previous segment, and loaded by an impedance equal to the input impedance of the succeeding segment. Both the input and output impedance are evaluated at the frequency combination used for the nonlinear transfer function being evaluated.

SIGNCAP allows the circuit analyst to arbitrarily divide the circuit into segments, and then performs the computation of the input and output impedances of each segment for all frequency combinations. The analyst must make sure that the number of nodes in

each segment is no greater than the maximum number of nodes which the particular SIGNCAP implementation can analyze. It is best to avoid segmenting at a point where significant nonlinear interaction is present, so reasonable common-sense should be used in choosing the segmentation points.

A secondary advantage of segmentation and cascading is there is a decrease in running time for a given circuit. The matrix inversion in SIGNCAP I uses the standard Gauss-Jordan method of inversion, which, for a matrix of order r has a computation time proportional to r^3 . Now, consider the analysis of a r node circuit which has been segmented into S segments, each containing r/S nodes. For this we see that the matrix inversion computation time per segment is decreased by S^3 , and, since there are S segments, the matrix inversion computation time for the complete circuit is decreased by S^2 . While the full decrease of S^2 will not be realized due to subsidiary computations, it is seen that segmentation should be computationally efficient. To give a benchmark, a cascaded second-order analysis of a complete communications receiver containing 85 nodes and twelve transistors was performed on the Honeywell 635. The receiver was segmented into three segments. The analysis took 70 seconds per output frequency. Based on the 9.35 seconds per frequency benchmark for the 27 node circuit, the analysis of a single 85 node network would take 280 seconds. Thus the segmenting decreased the running time by a factor of 4, as compared to a maximum possible decrease of 9. This shows that segmentation is, indeed, efficient in terms of running time.

A.2.3 SIGNCAP Processing

SIGNCAP contains over 90 subroutines, and nothing would be gained in this section by showing their interactions. However, the SIGNCAP user should have some idea of the concept of the processing which takes place in SIGNCAP. In this section we therefore discuss the processing which takes place in SIGNCAP independently of the actual flow of subroutines.

The processing flow shown in Fig. A.2, is made up of nine phases, numbered from zero to eight. The first phase, phase 0, is the data input phase. The circuit coding is read into the computer, and a disk data file is set up which contains all of the circuit elements and parameters. At the end of the data input phase, control is passed to phase 1, in which the order of the analysis, the $2^n - 1$ analysis frequencies, and the parameters of all of the nonlinear elements are computed. The partial Y matrices, which are the Y matrices less the input and output impedances, are formed in phase 2; $2^n - 1$ partial Y matrices are formed for each segment, one for each of the analysis frequencies, and they are all stored on disk. The input and output impedances of each segment at each of the $2^n - 1$ frequencies are computed in phase 3 and stored on disk. These impedances are added to the partial Y matrices in phase 4, and the resulting Y matrices are inverted and stored on disk. All of the Y matrices for all of the segments are inverted at this time. The computation of the nonlinear transfer functions takes place in phase 5. Cascading is performed in phase 6 and printout in phase 7. If any parameters are to be modified, the bookkeeping for the modification is computed in phase 8, and control is returned to phase 1. If there are no modifications, the program exits after phase 8.

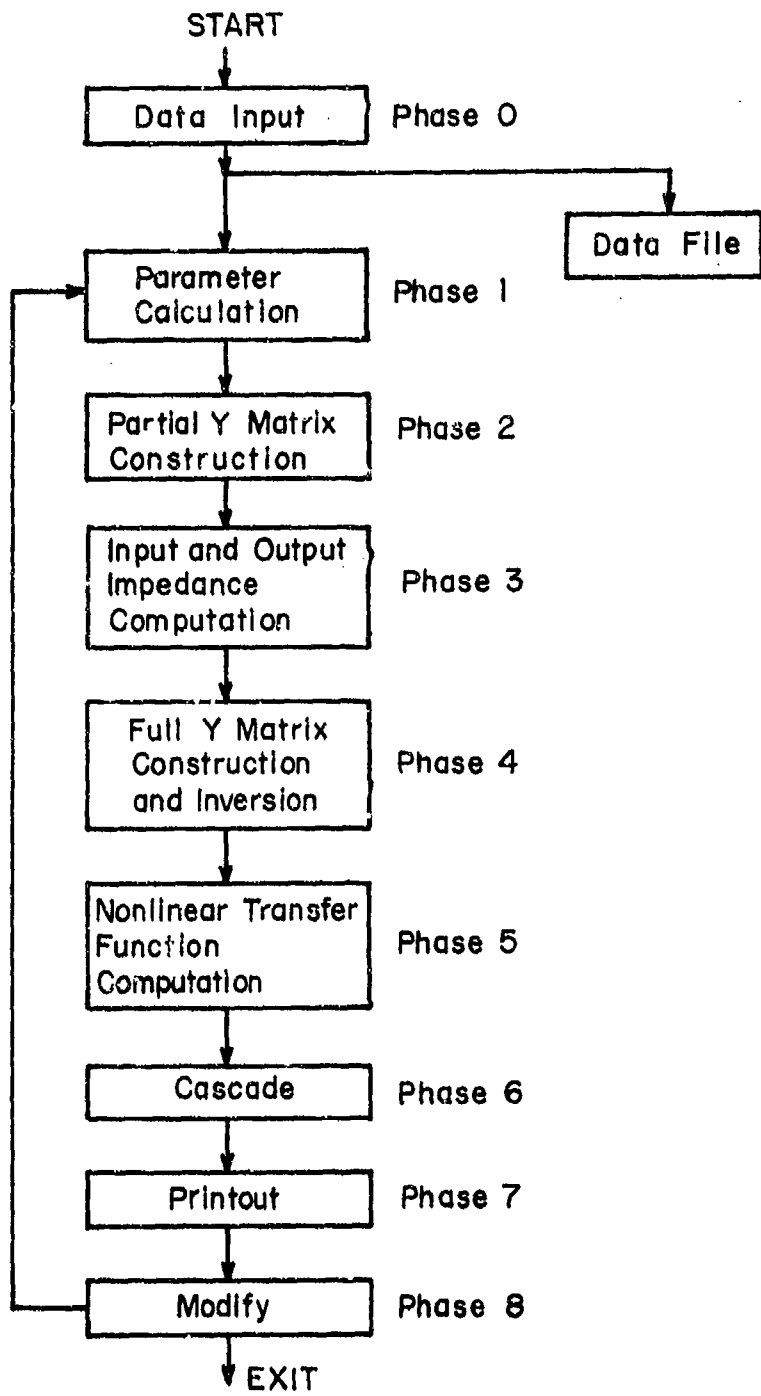


Fig. A.2. SIGNCAP Processing.

It should be noted that SIGNCAP makes use of disk storage for communication between phases, as well as for data storage. Sufficient disk space must be allocated by the user to store the $2^n - 1$ Y matrices for each segment, plus the requirements for storing printout and data files. The latter two requirements are small compared to the Y matrix storage requirements; for example, the fourth-order analysis of a fifty node network requires seventy-five thousand words of disk to store the fifteen Y matrices. The use of disk storage is dynamically controlled by the program, and, provided the user has sufficient disk space allocated, the program handles all allocation problems.

A .2.4 SIGNCAP Data Preparation

The nonlinear transfer function analysis performed by SIGNCAP requires the user to specify the circuit to be analyzed and the order of and frequencies at which the nonlinear analysis will be performed. SIGNCAP recognizes the following circuit elements:

- Resistor
- Capacitor
- Inductor
- Y Parameter Passive Networks
- Bipolar Junction Transistor
- Semiconductor Diode
- Vacuum Diode
- Vacuum Triode
- Vacuum Pentode
- Voltage Sources

SIGNCAP can analyze any circuit made up of interconnections of these basic elements.

As has been noted earlier, the SIGNCAP analysis is performed on a nodal basis. The input data structure has been designed with this in mind. The first step in the analysis of a circuit is the drawing of its complete circuit model. This model should include all of the parasitic circuit elements which can be identified. Next, the circuit nodes are identified and numbered. The signal ground is defined as node 0, and the numbering of the remaining nodes starts with 1 and continues sequentially until the last node has been numbered. There is no requirement that adjacent nodes be assigned sequential node numbers, but no numbers in the sequence can be skipped. The node numbering of SIGNCAP elements which have more than two nodes, namely the bipolar junction transistor, vacuum triode, and vacuum pentode, is done according to a specific convention described in detail in Section A.3. Once the node numbers have been assigned, the circuit elements can be coded for entry into SIGNCAP, as described in Section A.4.

As nonlinear transfer functions are defined in terms of voltages, the SIGNCAP software includes independent voltage sources. Their definitions include the nodes they are connected to, their impedances, frequencies, and amplitudes of their real and imaginary components. Voltage sources can be connected to any node in the circuit, and a single source can generate an arbitrary number of frequencies. The order of the analysis which will be performed on a given segment is equal to the total number of frequencies generated by all the generators in the segment. The analysis will be performed at all of the $2^n - 1$ frequency combinations of the n input frequencies. For example, if it is desired to perform a third-order analysis, with input frequencies f_1 , f_2 , f_3 , and peak amplitudes E_1 , E_2 , E_3 , SIGNCAP will analyze and printout the seven scaled nonlinear transfer functions given by:

<u>Scaled Nonlinear Transfer Function</u>	<u>Frequency</u>
$E_1 H_1 (f_1)$	f_1
$E_2 H_1 (f_2)$	f_2
$E_3 H_1 (f_3)$	f_3
$E_1 E_2 H_2 (f_1, f_2)$	$f_1 + f_2$
$E_1 E_3 H_2 (f_1, f_3)$	$f_1 + f_3$
$E_2 E_3 H_2 (f_2, f_3)$	$f_2 + f_3$
$E_1 E_2 E_3 H_3 (f_1, f_2, f_3)$	$f_1 + f_2 + f_3$

These nonlinear transfer functions are called "scaled" because they are premultiplied by the input signal amplitudes or products of the amplitudes. If the input amplitudes are all set to unity, the scale factors become unity, and the SIGNCAP output is the actual nonlinear transfer function. Scaling may be desired, for example, in the analysis of receivers which include mixers. The local oscillator amplitude is a fixed value for the receiver, and can be automatically included in the analysis by entering it as the amplitude of the local-oscillator generator in the circuit model.

SIGNCAP also has a modify feature, as shown by phase 8 of Fig. A.2. By using this feature, circuit element values or analysis frequencies can be changed, and the same circuit re-analyzed without re-inputting the entire circuit description. As many modifications as desired can be made. Thus, for example, a given nonlinear circuit can be analyzed for a number of input frequencies in one computer run, greatly decreasing the amount of time needed to analyze a circuit.

A.3 Circuit Elements and Models

The circuit elements which SIGNCAP recognizes are shown in Table A.1, along with either their defining characteristics or

Table A.1
SIGNCAP Elements Definitions

Element	Symbol	Current-Voltage Relation
Resistor		$I = \frac{e_m - e_n}{R}$
Capacitor		$I = j\omega C(e_m - e_n)$
Inductor		$I = \frac{1}{j\omega L} (e_m - e_n)$
Y-Parameter (bilateral)		$\begin{bmatrix} i_m \\ i_n \end{bmatrix} = \begin{bmatrix} y_{11} & y_{12} \\ y_{21} & y_{22} \end{bmatrix} \begin{bmatrix} e_m \\ e_n \end{bmatrix}$
Bipolar Junction Transistor		See Ch. 5
Semiconductor Diode		See Ch. 5 for AC. Exponential diode for DC.
Vacuum Diode		$I = Ge_b^{3/2}$ See Ch. 5
Vacuum Triode		Generalized 3/2 power law See Ch. 5
Vacuum Pentode		Generalized 3/2 power law See Ch. 5
Voltage Source		Frequency = f Hz Amplitude = $E_{Re} + jE_{Im}$ Impedance = $R + jX$
(m) is node number m		

references to the chapter in which they are fully discussed. All nodes are shown on the chart as (m) , where m is the node number.

The first three elements are the conventional linear resistor, inductor and capacitor. A linear circuit made up of an arbitrary interconnection of these can be analyzed with SIGNCAP. However, linear circuit theory tells us that from an input-output point of view, a complex RLC network, containing many nodes can be replaced by a pi network. SIGNCAP accepts the Y parameters of the pi network. The use of the pi network can thus result in a large saving in the effective number of nodes in a circuit, as an interstage pi network goes between two already defined active device nodes. However, for an n^{th} -order analysis, $2^n - 1$ sets of pi parameters must be entered, whereas the RLC input description is frequency independent and need be entered only once. The input and output nodes of the R, L, C, and pi need not be sequentially numbered.

The nonlinear devices which SIGNCAP utilizes are the next four elements of Table A.1. The bipolar junction transistor model is the four-node nonlinear T described in Chapter 5. Three of the nodes are external, and the fourth, the base-emitter junction, is internal. The convention is used that the base, collector, and emitter nodes are numbered m , $m+2$, $m+3$, respectively. Thus only the base node number need be given when specifying the location of a transistor in a circuit.

The semiconductor diode uses the model described in Chapter 5. It can be either forward biased, in which case it is represented by a nonlinear resistor in parallel with a diffusion capacitance, or back biased, in which case it is represented by a varactor capacitor in parallel with a fixed resistance. The two nodes need not be sequentially numbered.

The vacuum diode, triode, and pentode models use the generalized 3/2 power law vacuum tube models of Chapter 5. They are represented as two, three and four node devices, respectively. The node numbering on the diode need not be sequential. The triode grid, plate and cathode nodes are numbered m, m+1, m+2, respectively. The pentode signal grid, screen grid, plate, and cathode are numbered m, m+1, m+2, m+3, respectively. The pentode suppressor grid is assumed to be at cathode potential.

The last circuit element which SIGNCAP uses is the independent voltage generator. It is defined by the terminals it is between, the magnitude of its in-phase and quadrature Thevenin voltage components, output impedance, and frequency in Hertz. The frequency can be set equal to zero, in which case the generator becomes a battery. The generator impedance is specified by its real and imaginary parts, R and X.

A.4 SIGNCAP Data Input Structure

A.4.1 The SIGNCAP Input

The user communicates with SIGNCAP through the SIGNCAP data input structure. The input allows the circuit configuration, order of and frequencies of analysis, and output format, to be specified by the analyst. There are six categories of input data. These are:

1. Comment
2. Command
3. Linear Elements
4. Nonlinear Elements
5. Solution Control
6. Output Control

The input data are punched on cards, or an equivalent time-sharing input, according to a specific, easy to learn, format. In this section we discuss the data categories and describe their individual formats. In the description, all formats are given in terms of punched card inputs.

A.4.1.1 Comment

The comment card can be introduced at any place in the data input. It is printed on the computer output for informational purposes, but is not processed further by the program. The comment card has an asterisk in columns 1 and 2, and can have any desired text in the remaining columns. An example of the comment card is:

** THIS IS A COMMENT CARD

A.4.1.2 Command

The command cards control the segmenting and length of the circuit being analyzed. All control cards start with an asterisk and are immediately followed by one or more alphabetical words. There is no space between the asterisk and the start of the first word, but successive words on a control card are separated by blanks. The control cards are described as follows.

*START SEGMENT

This card is a delimiter which indicates that all cards following until the appearance of *END SEGMENT are to be processed as one segment of an analysis.

*END SEGMENT

This card is a delimiter, which indicates that all cards between it and the previous *START SEGMENT card are to be processed as one segment of an analysis.

***CASCADE**

This card is the first input card in the cascade analysis of a circuit. It alerts the software that there will be more than one data segment to be analyzed, and that after all their nonlinear transfer functions are found separately, they should be cascaded to determine the nonlinear transfer functions of the complete circuit. In a cascade analysis it is necessary to indicate the input and output nodes of each segment. This is done by means of two control cards, each of which is followed by a card which gives the number of the input or output node. The two cards are:

***OUTPUT**

This card is followed by a NODE card which gives the number of the node which is to be the output node of the segment. The two cards may appear anywhere in the segment. The asterisk is in column 1, and OUTPUT starts in column 2. The NODE card which follows the *OUTPUT card has NODE in columns 1 through 4, and the node number in integer format, I5, right justified in column 10.

***GENERATOR**

This card is used in all segments except the first to indicate the input node of a segment. It is followed by a NODE card which gives the number of the node which is to be the input node of the segment. Computations will be made at the frequencies associated with the previous segment, with the output impedances of the previous stage at these frequencies

and GENERATOR starts in column 2. The NODE card which follows

the *GENERATOR card has NODE in columns 1 through 4, and the node number in I5 format, right justified in column 10. The two cards may appear anywhere in the segment.

*END

This card is the last card in any SIGNCAP data input. It indicates the end of all data, and switches the program from Phase 0 to Phase 1.

A.4.1.3 Linear Elements

SIGNCAP recognizes four types of linear elements, the resistor, capacitor, inductor, and pi network. The program recognizes that the linear elements are either one of the first three or a pi network by means of two cards, each starting with an asterisk, namely *PASSIVE COMPONENTS and *PI. These cards, in turn, are followed by cards which contain the R,L,C component values, or the pi parameters. The details of these cards are:

*PASSIVE COMPONENTS

This card indicates that all cards following until the next card starting with an asterisk denote resistive, inductive, or capacitive linear components. The asterisk is in column 1, and PASSIVE starts in column 2.

Following the *PASSIVE COMPONENTS card are cards which describe the connection of a particular resistor, inductor, or capacitor to a pair of circuit nodes. These cards all take the form:

R			
L	xx	yy	zz
C			

where R, L, or C denotes a resistor, inductor, or capacitor, going from node xx to yy, and of value zz ohms, henrys, or farads. If yy is blank it is interpreted as being node 0, the reference or ground node; xx cannot be blank. R,L, or C appears in column 1, the (integer) node numbers are right justified in columns 5 and 10, and the component value is in real format, E10.5, in columns 11 to 20.

*PI

This card indicates that all the cards following until the next card starting with an asterisk contain the Y parameters of a pi network. The asterisk is in column 1, and PI starts in column 2. Following the *PI card are cards which describe the nodes to which the pi is connected and give the parameters of the pi.

The card used to define the nodes to which a pi network is connected takes the form:

NODE xx yy

where xx and yy, the two nodes which define the pi input and output, are right justified integer format in columns 10 and 15. This card follows the *PI control card. The common node of the pi is assumed to go to AC ground.

The Y parameter cards contain the values of Y₁₁, Y₁₂, and Y₂₂ used in a Y parameter analysis. Since the Y parameters are in general frequency dependent, there must be one Y parameter card for each frequency in the analysis. As has been shown, for N frequencies, $2^N - 1$ Y parameter cards will be required. These cards follow immediately after the node card for the particular pi network. The format of the Y parameter cards is:

YP xx Y₁₁ Y₁₂ Y₂₂

where YP appear in columns 1 - 2, xx defines the frequency combinations and is integer format, 15, right justified in column 10, and Y₁₁, Y₁₂, Y₁₃ are the three Y parameters. Y₁₁, Y₁₂, and Y₁₃ are in polar form and appear in columns 11 - 20, 21 - 30 for Y₁₁, 31 - 40, 41 - 50 for Y₁₂, and 51 - 60, 61 - 70 for Y₂₂.

A.4.1.4 Nonlinear Elements

SIGNCAP recognizes five types of nonlinear elements, the semiconductor diode, bipolar junction transistor, vacuum diode, triode, and pentode. The mathematical models for these elements are those described in Chapter 5. These models are built into SIGNCAP. The data input structure of SIGNCAP calls up the desired model and inputs the required parameters. The structure of these data inputs are all similar. The appropriate model is called up by a card starting with an asterisk. This is then followed by cards which contain node numbering data and model parameter data. The details of these cards follow.

A.4.1.4.1 Semiconductor Diode

The semiconductor diode has been incorporated into SIGNCAP with a forward-biased diode being represented by an exponential resistive non-linearity in parallel with a diffusion capacitance, and a reverse biased diode by a varactor, or nonlinear capacitor, in parallel with a resistor. Four cards are required to define a semiconductor diode, the first being a control card, the second a NODE card, and the remaining two being diode parameter cards. They are, respectively:

*SEMICONDUCTOR DIODE

NODE XX YY

I_o	N	C_j	C'_j
V	K	μ	R

The asterisk is in column 1, SEMICONDUCTOR starts in column 2, and there is a single space between SEMICONDUCTOR and DIODE. NODE starts in column 1, and XX and YY the plate and cathode nodes numbers, are in I5 format right justified in columns 10 and 15. The third and fourth cards contain the diode parameters. The third card has the forward-biased diode parameters -- the bias current I_o , non-ideality factor N, forward-biased junction capacitance extrapolated to zero current C_j , and derivative of junction bias with current C'_j . If the diode is reverse biased, the third card is blank. The fourth card has the reverse biased diode parameters. The varactor capacitance is defined as

$$C(V) = KV^{-\mu},$$

where K is the value of the varactor capacitor at 1 volt reverse bias. K, V, and μ are the first three entries on the fourth card, and R, the parallel reverse biased leakage resistance of the diode, is the fourth entry. If the diode is forward biased, the fourth card is blank. Both the third and fourth cards are in real format, E10.5, when non-blank.

A.4.1.4.2 Bipolar Junction Transistor

The bipolar junction transistor is modeled as a nonlinear T. Since the node numbering convention is built into the transistor model, the location of the transistor in the circuit is defined by giving the number of the external base terminal, XX. The circuit coding must be such that each of the external terminals, i.e., XX, XX+2, XX+3, is connected to some other node in the circuit. The transistor parameters are given on five cards. The card sequence for defining the bipolar junction transistor is:

*TRANSISTOR

NODE XX

-5 Parameter Cards -

The *TRANSISTOR Card indicates that the six cards between it and the next card starting with an asterisk describe a bipolar junction transistor. The base node, is number xx in the card NODE xx, and the five following cards, excluding comment cards, give transistor linear and non-linear parameters. The NODE card is standard, with NODE appearing in columns 1 - 4, and XX, the number of the base node, in integer format, I5, right justified in column 10. The data on the five cards are in E10 format, structured as follows:

<u>Card</u>	<u>Column</u>	<u>Parameter</u>	<u>Usage</u>
1	1 - 10	η	avalanche exponent
1	11 - 20	V_{CB}	collector-base bias voltage
1	21 - 30	V_{CBO}	avalanche voltage
1	31 - 40	μ	collector capacitance exponent
2	1 - 10	I_c	Collector bias current
2	11 - 20	$I_{c\max}$	collector current at maximum D.C. current gain
2	21 - 30	a	h_{FE} nonlinearity coefficient
2	31 - 40	$h_{FE\max}$	maximum D.C. current gain
3	1 - 10	k	collector capacitor scale factor
3	11 - 20	n	diode nonideality factor
3	21 - 30	C_{je}	base-emitter junction space charge capacitance
3	31 - 40	C'_2	derivative of base-emitter diffusion capacitance
4	1 - 10	r_b	base resistance
4	11 - 20	r_c	collector resistance
5	1 - 10	C_1	base-emitter capacitance
5	21 - 30	C_3	base-collector and overlap capacitance

A.4.1.4.3 Vacuum Diode

Three cards are required to define a vacuum diode. The first is a control card, the second a NODE card, and the last is a tube parameter card. They are, respectively,

*VACUUM	DIODE		
NODE	XX	YY	
	G	E_{bo}	C_{pk}

The asterisk is in column 1, VACUUM starts in column 2, and there is a single space between VACUUM and DIODE. NODE starts in column 1, and XX and YY, the plate and cathode node numbers, are in I5 format, right justified in columns 10 and 15. On the third card, the perveance G, plate-cathode bias voltage E_{bo} , and plate-cathode capacitance C_{pk} , are in E10 format.

A .4.1.4.4 Vacuum Triode

The coding for the vacuum triode is defined by the five card sequence:

*VACUUM TRIODE

NODE XX

G_o	MU	$E_{c_{max}}$
E_{co}	E_{bo}	ϕ
C_{gk}	C_{pg}	C_{pk}

The asterisk is in column 1, VACUUM starts in column 2, and there is a single space between VACUUM and TRIODE. NODE starts in column 1, and XX, the grid node number, is in I5 format, right justified in column 10. The parameters on the remaining cards are in E10 format.

A .4.1.4.5 Vacuum Pentode

The coding for the vacuum pentode is defined by the six card sequence:

***VACUUM PENTODE**

NODE XX

G _o	MU	D	M
E _{co}	E _{Cmax}	*	
E ₂₀	E _{bo}		
C _{gk}	C _{pg}	C _{pk}	

The asterisk is in column 1, VACUUM starts in column 2, and there is a single space between VACUUM and PENTODE.

NODE starts in column 1, and XX, the signal grid (grid number 1) node number, is in I5 format, right justified in column 10. The parameters on the remaining cards are in E10 format.

A .4.1.5 Solution Control

A .4.1.5.1 Frequency Control

In order to determine a nonlinear transfer function it is necessary to define the parameters of the input signals and the frequencies at which the analysis is to be performed. The input signals are considered to be generated by sinusoidal voltage generators, defined by their impedance, peak amplitude phase, and frequency. They are entered on 2+n cards, for an n'th order analysis, as follows:

***GENERATOR**

This card indicates that all cards between it and the next control card describe a Thevenin voltage generator which is connected between a specified node and ground. The asterisk is in column 1, and GENERATOR starts in column 2. The next card is

a NODE card, telling to which node the generator is connected. The node card takes the form:

NODE xx

The word NODE appears in columns 1 - 4, and xx, the node number, in integer format, I5, right justified in column 10.

The definition of a generator includes the specification of the generator's frequency and amplitude. These are provided on frequency cards. There must be one frequency card for each frequency which a generator generates, and there must be as many frequency cards as there are total defined frequencies. Each defined frequency is assigned an identification number, which the software uses to keep track of frequency combinations in the processing. If there are N frequencies, the identification numbers run from 1 through N, with their assignment being arbitrary. The frequency cards follow directly after the node card for a given generator. The format of the frequency card is:

FR xx yy REA IMA

where FR appears in columns 1 - 2, xx is the identification number, an integer right-justified in column 10, yy is the generator frequency, in E format right justified in columns 11 - 30, and REA and IMA are the (signed) peak amplitudes of the in-phase and quadrature generator voltages, in E format right justified in columns 31 - 50 and 51 - 70 respectively. As a default, if REA and IMA are left blank, a one-volt in-phase generator with no quadrature component is

assumed. It is important to note and understand that the order of the nonlinear analysis which the program will carry out is equal to N, the total number of defined frequencies in the circuit. For example, if there are three defined frequencies, f₁, f₂ and f₃, the program will carry out the following analysis:

first order	f ₁ , f ₂ , f ₃
second order	f ₁ +f ₂ , f ₁ +f ₃ , f ₂ +f ₃
third order	f ₁ +f ₂ +f ₃

In general, there will be $2^N - 1$ frequencies at which the nonlinear transfer functions will be analyzed. If n'th harmonic analysis is desired, there must be n frequency cards, each containing the fundamental frequency, and each defined as a different frequency. Thus, for example, a second harmonic analysis of a frequency of 1 MHz would have frequency cards:

FR 1 1.0E6
FR 2 1.0E6

while for a third-order intermodulation analysis of two tones at 1 MHz and 1.5 MHz, where the product of interest is twice the first frequency minus the second frequency (0.5 MHz = $2 \times 1.0 \text{ MHz} - 1.5 \text{ MHz}$), the frequency cards would be:

FR 1 1.0E6
FR 2 1.0E6
FR 3 -1.5E6

In these examples, the 1 volt default values have been used.

Two more points must be made concerning the frequency cards. First, in certain circumstances, coherent generators may appear at different nodes of the network. In this case, the frequency in hertz going with a particular identification number need only be defined the first time the identification number appears. Thereafter, only the identification number need be used. Secondly, a given circuit may have several generators, located at different nodes. This occurs, for example, in the analysis of multiple conversion receivers, where each local oscillator is modeled as a separate generator with its own distinct frequency or frequencies. If there are I separate generators in the circuit, each generating N_i separate frequencies, then the order of the analysis will be $\sum_{i=1}^I N_i$.

The final specification of a generator is its Thevenin impedance. This is provided for by the impedance cards. Impedance cards follow the frequency cards. There must be one impedance card for each frequency at which the circuit is being analyzed. Thus, for N generator frequencies, there must be 2^{N-1} impedance cards. The format of the impedance card is:

IM xx yy zz

where IM is in columns 1-2, xx, denoting the frequency combinations for this impedance, is an integer variable right justified in column 10, and yy and zz are the real and imaginary parts of the generator impedance in E format in columns 11 - 20 and 21 - 30 respectively. The integer variable defining the frequency combinations is defined quite simply; if the frequency is made up of the combination of fm+fn+fp, then the frequency

combination is mnp. Thus, for example, for the third-order frequency $f_1+f_2+f_3$, the quantity xx would be the integer variable 123.

As a default, if the generator impedance is constant for all frequencies, only one impedance card need be used, and the parameter xx should be left blank. This default option finds wide use in the case where a standard signal generator is the signal source. In this case the impedance is the signal generator's impedance, typically 50 ohms.

A.4.1.5.2 Solution Modification

In most nonlinear modeling applications it is necessary to analyze a basic circuit over many frequencies or frequency combinations. It is also often desired to rerun a circuit analysis with certain component values changed, in order to determine the circuit sensitivity to component variation. In SIGNCAP solution modification is performed by means of the *MODIFY cards which allows a set of data to be changed, and then an analysis automatically rerun with all unmodified parameters as they were in the previous run. Both component values and generator frequencies can be modified. The format card is:

*MODIFY

The asterisk is in column 1, and MODIFY begins in column 2. The *MODIFY card can be followed by R,L,C,PI,FR, and IM cards. If there are multiple *MODIFY cards in a given circuit analysis, they will be processed sequentially, that is, first all the modifications associated with the first *MODIFY will be performed, then those associated with the second *MODIFY, and so on.

Modification is destructive, in that any modified parameter retains its last modified value, and does not return to its originally defined value subsequent to the modification. Furthermore, in order to modify a parameter, the parameter must have been defined in the original circuit; new circuit elements cannot be inserted in the middle of an analysis.

A.4.1.6 Output Control

The output of SIGNCAP, printed on the computer's line printer, contains a large amount of information. The output structure is divided into three main groups, namely:

1. Images of all input cards
2. All circuit parameters, both linear and nonlinear
3. All scaled nonlinear transfer functions

of all frequencies and orders, for all nodes. The scaled nonlinear transfer functions are printed, one node to a line, in two forms, namely cartesian, and log polar. The Cartesian form consists of the real and imaginary parts of the scaled nonlinear transfer functions while the log polar form consists of $20 \log_{10}$ of the magnitude of the scaled nonlinear transfer function and its angle in degrees.

In the event the *MODIFY option is used, the original printout is followed by a listing of the modified parameters, and all scaled nonlinear transfer functions are again printed out, one node to a line, for all frequencies, orders, and nodes.

In the event the *CASCADE option is used, the printout occurs for each segment.

It is evident that an analysis of a large network can generate an inordinate large amount of printout. The PRINT SELECT control cards allow the analyst to specify the nodes and orders which are to be printed out, and suppress the remaining ones. The card structure is as follows. The control card is:

*PRINT SELECT

with the asterisk in column 1, PRINT starting in column 2, and a space between PRINT and SELECT. To print selected nodes, the *PRINT SELECT card is followed by a multiple node card:

NODE XX YY ZZ ...

where NODE starts in column 1, and the nodes to be printed, XX, YY, ZZ, etc., are in I5 format, right justified and ~~starting~~ in field 11-15. As many NODE cards as desired can be used sequentially, but the first blank field ends the node definition. The order to be printed use the same format as the NODE card, but the first ten columns are blank, i.e., NODE is omitted. The *PRINT SELECT control cards may appear anywhere in a segment. If *PRINT SELECT control cards do not appear in a segment, but do appear in a prior segment, then the printing will be controlled by the cards in the prior segment. Absence of either or both card(s) in all segments will, by default, cause a complete printout of all nodes and/or non-linear transfer functions of all orders. Regardless of what *PRINT SELECT cards are used in the segments of a cascade analysis, the non-linear transfer functions of all orders are printed for the output node of the cascade.

One more output control option is available to the analyst, namely the capability of suppressing the printout of all circuit data except for the parameters associated with the generators. This is accomplished by inserting the following card:

OFF

where OFF starts in column 1, directly after the *PRINT SELECT card. The use of the OFF card does not affect the selection of the nodes and orders it is desired to print out.

A.5 Examples

In this section two examples of SIGNCAP coding and output are presented. The first example, in Section A.5.1, is similar to the single-stage 2N2950 transistor amplifier analyzed in Chapter 6. In this example, the complete input and output are shown. The second example is the coding of the complete VHF receiver of Chapter 7. This coding shows the use of multiple generators, cascading, and printout control.

A.5.1 Single-Stage Transistor Amplifier

In this section we show the use of SIGNCAP in analyzing a 2N2950 transistor amplifier with a high impedance load. The example was run on the Honeywell 635 computer, under the CARDIN system. Figure A.3 shows the circuit model used in the analysis. It is similar to the circuit of Fig. 6.7, with the coupling capacitors replaced by AC short circuits and a 5.1 kilohm resistor inserted between the collector and the 50 ohm output. The node numbering is shown on the figure, and the transistor parameters are given in Chapter 5.

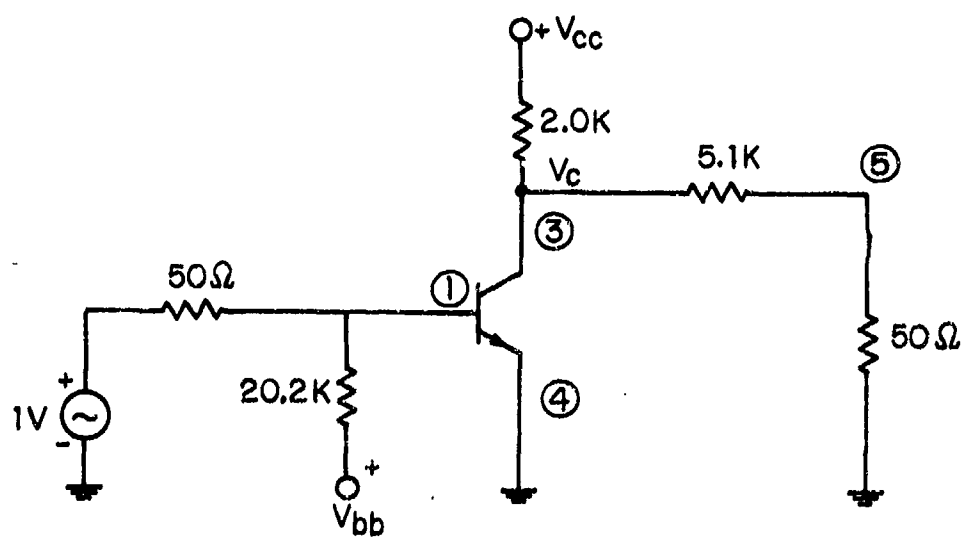


Fig. A.3. A 2N2950 Transistor Circuit.

In running SIGNCAP, all output was put into a file named GUTPTO. Table A.2 shows the first 66 lines of this file, which constitute the input data for the problem. Line 4 is a comment line, which identifies the problem. Line 6 is the *START SEGMENT statement, and line 64 is the *END SEGMENT statement; all lines in between them define the circuit and analysis of the segment. As only one segment is to be analyzed, line 64 is followed by line 66, *END. Returning now to the intermediate coding, lines 8 and 9 show that only the output at Node 5 is to be printed. Lines 11, 12, and 16 show that there is a 50 ohm generator at node 1. Lines 13, 14, and 15 show that a third-order analysis is to be performed at frequencies $f_1 = 4.5$ MHz, $f_2 = 4.5$ MHz, and $f_3 = -5.0$ MHz, resulting in an intermodulation product at 4.0 MHz. This set of frequencies is followed by six *MODIFY statements, each defining a new set of frequencies; these statements run from lines 18 through 46. Lines 48 through 54 define the passive components of the circuit, while lines 56 through 62 define the transistor parameters; node 1 is given as the base node. Lines 53 and 54 are of interest. Line 53, a 0.001 ohm resistor between the emitter and ground, is a default value. No node of either the transistor or the vacuum tubes can be grounded directly, so that if a node is grounded in the physical circuit, a small resistor is inserted in the model. Line 54 is a parasitic collector-to-ground capacitance of the 2N2950, discussed in Chapter 5. It is coded as a separate element.

Table A.3 shows the next step in the SIGNCAP output, which is an analysis of input data and a printout of parameter data for the analysis being performed. Line 68 indicates that the

Table A.2
2N2950 Input Coding

```
SYSTEM ?SCAN
FILE?U@0UTPTO
FORM?U
CODE?
EDIT?Y
?P A
#0001
#0002
#0003
** HIGH IMPEDANCE 2N2950 #0004
#0005
*START SEGMENT #0006
#0007
*PRINT SELECT #0008
N0 5 #0009
#0010
*GENERATOR #0011
NODE 1 #0012
FR 1 4.5E6 #0013
FR 2 4.5E6 #0014
FR 3 -5.0E6 #0015
IM 50. #0016
#0017
*M0 #0018
FR 1 6.5E6 #0019
FR 2 6.5E6 #0020
FR 3 -7.0E6 #0021
#0022
*M0 #0023
FR 1 9.5E6 #0024
FR 2 9.5E6 #0025
FR 3 -10.0E6 #0026
#0027
*M0 #0028
FR 1 19.5E6 #0029
FR 2 19.5E6 #0030
FR 3 -20.0E6 #0031
#0032
*M0 #0033
FR 1 29.5E6 #0034
FR 2 29.5E6 #0035
FR 3 -30.0E6 #0036
#0037
*M0 #0038
FR 1 39.5E6 #0039
FR 2 39.5E6 #0040
FR 3 -40.0E6 #0041
```

~~Table A.2~~ (Continued)

#0042
*M0 #0043
FR 1 49.5E6 #0044
FR 2 49.5E6 #0045
FR 3 -50.0E6 #0046
#0047
*PASSIVE COMPONENTS #0048
R 1 0 20.2E3 #0049
R 3 0 2.0E3 #0050
R 3 5 5.1E3 #0051
R 5 0 50. #0052
R 4 0 .001 #0053
C 3 0 4.E- 12 #0054
#0055
*TRANSISTOR #0056
NODE 1 #0057
4.6 5.2 140. .348 #0058
.0024 .150 .125 8.2 #0059
21.E-12 1.0 340.E-12 59.E-9 #0060
10.1 635.E 3 #0061
0.0 1.5E-12 #0062
#0063
*END SEGMENT #0064
#0065
*END #0066

Table A.3
Interpretation of Input Coding

```

#0067
SEGMENT 1 #0068
#0069
#0070
#0071
GENERATOR, NODE 1 #0072
#0073
#0074
FREQUENCY AMPLITUDE #0075
#0076
1 0.4500000E 07 0.1000000E 01 0. #0077
2 0.4500000E 07 0.1000000E 01 0. #0078
3 -0.5000000E 07 0.1000000E 01 0. #0079
#0080
FREQUENCY ADMITTANCE #0081
0 0.2000000E-01 0. #0082
#0083
#0084
#0085
#0086
COMPONENTS #0087
NODE 1, 0 R = 0.2020000E 05 #0088
NODE 3, 0 R = 0.2000000E 04 #0089
NODE 3, 5 R = 0.5100000E 04 #0090
NODE 5, 0 R = 0.5000000E 02 #0091
NODE 4, 0 R = 0.1000000E-02 #0092
NODE 3, 0 C = 0.4000000E-11 #0093
#0094
#0095
#0096
TRANSISTOR, NODE 1 #0097
#0098
N = 4.60 VCB = 5.2 VCB0 = 140.0 MU = 0.348 #0099
IC = 0.0024 ICMAX = 0.1500 A = 0.1250 HFEMAX = 8.2 #0100
K = 0.2100000E-10 REF = 1.00000 C(J) = 0.3400E-09 C(PKIME) = 0.59
00E-07 #0101
RB = 10.10 RC = 635000.0 SCC = 0. #0102
C1 = 0. C2 = 0.5058298E-09 C3 = 0.1500000E-11 #0103
#0104
#0105
HMO = 0.1000000E 01 #0106
HM1 = 0.2334431E-06 ALPHA1 = 0.8715839E 00 K1 = 0.1081029E 00 GAM
MA1 = 0.1183178E-10 #0107
HM2 = 0.8080729E-07 ALPHA2 = 0.2486754E 01 K2 = 0.2078901E 01 GAM
MA2 = -0.3959096E-12 #0108
HM3 = 0.1346791E-07 ALPHA3 = -0.3828569E 03 K3 = 0.2665258E 02 GAM
MA3 = 0.3421065E-13 #0109
#0110
IC/HMO = 0.2399999E-02 KE1 = 0.9250449E 01 IE = 0.2810674E-02 #0111
RBI = 0.9900989E-01 RCI = 0.1574803E-05 #0112
SC0 = 0. C(2,0) = 0.5058298E-09 C(2,1) = 0.5900000E-07 #0113
#0114

```

data are associated with segment 1, which is the only segment in this example. Lines 72 through 82 define the generator in the analysis, which is connected to node 1, of frequencies 4.5, 4.5, and -5.0 MHz, amplitudes $1 + j0$ volts, and admittances 0.02 mhos for all frequencies. The components and their node connections are echoed in lines 87 through 93, and the transistor and its input parameters echoed in lines 97 through 103. Lines 106 through 113 print various nonlinear coefficients derived by the program. The HMs are the Taylor series coefficients of the avalanche nonlinearity, the ALPHAs of the HFE nonlinearity, the Ks of the base-emitter resistive diode nonlinearity, the GAMMAs of the collector capacitance nonlinearity, and the C(2,0) and C(2,1) on line 113, the emitter capacitance. The remaining parameters of lines 111 and 112 are the collector bias current divided by the zero-order avalanche coefficient IC/HMO, the linearized emitter resistance REI, the emitter bias current IE, and the reciprocals of the base and collector resistances RBI and RCI. The parameter SC0 of line 113 is not used in the present transistor model.

Table A.4 shows lines 115 through 163 of the output. Lines 116 through 155 give the seven nonlinear transfer functions of node 5, namely $H_1(f_1)$, $H_1(f_2)$, $H_1(f_3)$, $H_2(f_1, f_2)$, $H_2(f_1, f_3)$, $H_2(f_2, f_3)$ and $H_3(f_1, f_2, f_3)$. The format of all of these is the same, and only one transfer function will be discussed. Lines 134 through 137 pertain to $H_2(f_1, f_2)$, at a frequency of 9 MHz. This is shown by the data on line 134. Line 136 shows the meaning of the numerical data printed on line 137, namely that they are successively:

- (a) node number
- (b) real part of nonlinear transfer function

Table A.4
Nonlinear Transfer Function Output

```

#0115
ORDER = 1 FREQUENCY = 0.450001E 07 (1) #0116
#0117
NODE REAL IMAG. MAG. DB ANGLE #0118
5 0 -0.5630833E-01 0.2400222E 00 -0.1216230E 02 0.1032026E 03 #0119
#0120
#0121
ORDER = 1 FREQUENCY = 0.450001E 07 (2) #0122
#0123
NODE REAL IMAG. MAG. DB ANGLE #0124
5 0 -0.5630833E-01 0.2400221E 00 -0.1216230E 02 0.1032026E 03 #0125
#0126
#0127
ORDER = 1 FREQUENCY = -0.500001E 07 (3) #0128
#0129
NODE REAL IMAG. MAG. DB ANGLE #0130
5 0 -0.4086849E-01 -0.2203612E 00 -0.1299043E 02 -0.1005068E 03 #0131
#0132
#0133
ORDER = 2 FREQUENCY = 0.900001E 07 (1,2) #0134
#0135
NODE REAL IMAG. MAG. DB ANGLE #0136
5 0 0.1039890E-01 0.7696153E-01 -0.2219595E 02 0.8230491E 02 #0137
#0138
#0139
ORDER = 2 FREQUENCY = -0.500001E 06 (1,3) #0140
#0141
NODE REAL IMAG. MAG. DB ANGLE #0142
5 0 -0.6971810E 00 -0.2104628E 00 -0.2754325E 01 -0.1632022E 03 #0143
#0144
#0145
ORDER = 2 FREQUENCY = -0.500001E 06 (2,3) #0146
#0147
NODE REAL IMAG. MAG. DB ANGLE #0148
5 0 -0.6971811E 00 -0.2104629E 00 -0.2754325E 01 -0.1632021E 03 #0149
#0150
#0151
ORDER = 3 FREQUENCY = 0.400001E 07 (1,2,3) #0152
#0153
NODE REAL IMAG. MAG. DB ANGLE #0154
5 0 0.3442190E 00 -0.1161751E 01 0.1667711E 01 -0.7349580E 02 #0155
#0156
SEGMENT 1 #0157
#0158
#0159
#0160
GENERATOR, NODE 1 #0161
#0162
#0163

```

- (c) imaginary part of nonlinear transfer function
- (d) $20 \log_{10}$ (magnitude of nonlinear transfer function)
- (e) phase of nonlinear transfer function in degrees.

If the *PRINT SELECT statement had not been used, the nonlinear transfer functions for all nodes would have been printed; by using the statement, only node 5 was printed.

Line 157 is the beginning of the printout for the second set of frequencies. Instead of repeating all of the printout, the computer was interrupted and returned to the monitor level after line 163. Table A.5 shows the output printed by using the EDIT feature of the time-sharing system to print only those lines pertaining to node 5. The 49 nonlinear transfer functions (seven nonlinear transfer functions per frequency set, for seven frequency sets) are printed in compact form. After the last transfer function is printed on line 503, the system reaches an end-of-file, and the printout is finished.

A.5.2 VHF Receiver

Table A.6 shows the input coding used to analyze a complete VHF receiver. The analysis in the table is a fourth-order analysis, using two generators. The first generator, at node 1, has three input frequencies, $f_1 = f_2 = 30$ MHz, and $f_3 = -15$ MHz. The second generator, at node 28, is the local-oscillator at $f_4 = -66.4$ MHz. The fourth-order intermodulation product is at -21.4 MHz, which is in the receiver's IF passband. The node 1 generator has a 50 ohm impedance, while the local-oscillator, which was known to have a low output impedance, was given a default value of 0.1 ohm impedance.

Table A.5
All Nonlinear Transfer Functions at Node 5

```

ZONE
SYSTEM TSCAN
FILETYPE=PTU
FORMATU
ODEP= 5
EDITTY
TP A
5 0 -0.5630833E-01 0.2400822E 00 -0.1216830E 02 0.1038026E 03 #0119
5 0 -0.5630833E-01 0.2400821E 00 -0.1216830E 02 0.1038026E 03 #0125
5 0 -0.4086849E-01 -0.2203612E 00 -0.1299043E 02 -0.1005068E 03 #0131
5 0 0.1039890E-01 0.7696153E-01 -0.2219595E 02 0.8230491E 02 #0137
5 0 -0.6971810E 00 -0.2104688E 00 -0.2754325E 01 -0.1638028E 03 #0143
5 0 -0.6971811E 00 -0.2104689E 00 -0.2754325E 01 -0.1638028E 03 #0149
5 0 0.3448190E 00 -0.1161781E 01 0.1667711E 01 -0.7349580E 02 #0155
5 0 -0.1837528E-01 0.1745513E 00 -0.1513977E 02 0.9405535E 02 #0177
5 0 -0.1837529E-01 0.1745512E 00 -0.1513977E 02 0.9405536E 02 #0183
5 0 -0.6464934E-02 -0.1686736E 00 -0.1576680E 02 -0.9227584E 02 #0189
5 0 -0.3528295E-02 0.8306884E-01 -0.2160342E 02 0.9843007E 02 #0195
5 0 -0.4986940E 00 -0.1395462E 00 -0.5813333E 01 -0.1641862E 03 #0201
5 0 -0.4986940E 00 -0.1395463E 00 -0.5813333E 01 -0.1641862E 03 #0207
5 0 0.8284718E-01 -0.5837046E 00 -0.4889518E 01 -0.6190177E 02 #0213
5 0 0.1053746E-01 0.1192700E 00 -0.1843561E 02 0.8495105E 02 #0235
5 0 0.1053745E-01 0.1192700E 00 -0.1843561E 02 0.8495105E 02 #0241
5 0 0.1245689E-01 -0.1128490E 00 -0.1889745E 02 -0.8370118E 02 #0247
5 0 0.7169647E-02 0.7132268E-01 -0.2289178E 02 0.8485968E 02 #0253
5 0 -0.3710643E 00 -0.1009288E 00 -0.8301043E 01 -0.1647838E 03 #0259
5 0 -0.3710643E 00 -0.1009289E 00 -0.8301042E 01 -0.1647838E 03 #0265
5 0 -0.2000128E-02 -0.8984552E 00 -0.1050222E 02 -0.9038397E 02 #0271
5 0 0.2208241E-01 0.4914355E-01 -0.2537195E 02 0.6580347E 02 #0293
5 0 0.2208240E-01 0.4914355E-01 -0.2537195E 02 0.6580347E 02 #0299
5 0 0.2204044E-01 -0.4736790E-01 -0.2563917E 02 -0.6504728E 02 #0305
5 0 0.2304287E-01 0.3044717E-01 -0.2836241E 02 0.5288102E 02 #0311
5 0 -0.2439992E 00 -0.6374652E-01 -0.1196548E 02 -0.1653583E 03 #0317
5 0 -0.2439992E 00 -0.6374652E-01 -0.1196548E 02 -0.1653583E 03 #0323
5 0 -0.3417670E-01 -0.8403915E-01 -0.2084567E 02 -0.1121304E 03 #0329
5 0 0.1908637E-01 0.2511525E-01 -0.3002148E 02 0.5276694E 02 #0351
5 0 0.1908636E-01 0.2511525E-01 -0.3002148E 02 0.5276694E 02 #0357
5 0 0.1888233E-01 -0.2435509E-01 -0.3022408E 02 -0.5221383E 02 #0363
5 0 0.1905159E-01 0.9991785E-02 -0.3334608E 02 0.2767519E 02 #0369
5 0 -0.1806439E 00 -0.4644466E-01 -0.1458554E 02 -0.1655812E 03 #0375
5 0 -0.1806439E 00 -0.4644466E-01 -0.1458554E 02 -0.1655812E 03 #0381
5 0 -0.2516239E-01 -0.3093341E-01 -0.2798597E 02 -0.1291262E 03 #0387
5 0 0.1507226E-01 0.1409378E-01 -0.3370786E 02 0.4307853E-02 #0409
5 0 0.1507226E-01 0.1409378E-01 -0.3370786E 02 0.4307854E 02 #0415
5 0 0.1488569E-01 -0.1371760E-01 -0.3387474E 02 -0.4266149E 02 #0421
5 0 0.1260604E-01 -0.7932773E-02 -0.3788751E 02 0.8716773E 01 #0427
5 0 -0.1352901E 00 -0.3442339E-01 -0.1710225E 02 -0.1657245E 03 #0433
5 0 -0.1352901E 00 -0.3442339E-01 -0.1710224E 02 -0.1657245E 03 #0439
5 0 -0.1519329E-01 -0.1201329E-01 -0.3425789E 02 -0.1416667E 03 #0445
5 0 0.1174016E-01 0.8436053E-02 -0.3679857E 02 0.3569965E 02 #0467
5 0 0.1174016E-01 0.8436052E-02 -0.3679857E 02 0.3569965E 02 #0473
5 0 0.1159589E-01 -0.8234082E-02 -0.3694080E 02 -0.3537803E 02 #0479
5 0 0.7918963E-02 -0.7544041E-03 -0.4198740E 02 -0.5441890E 01 #0485
5 0 -0.1027375E 00 -0.2595229E-01 -0.1949678E 02 -0.1658232E 03 #0491
5 0 -0.1027375E 00 -0.2595229E-01 -0.1949678E 02 -0.1658232E 03 #0497
5 0 -0.8838752E-02 -0.4944226E-02 -0.3988984E 02 -0.1507782E 03 #0503
EOF

```

TABLE A.6
COMPONENTS RECEIVED
SIGNACAP CODING

SCASCADE				
** IF TUNER				000
** FIRST TWO STAGES		TUNER TUNED TO 43 MHZ		001
** STANT SEGMENT				002
** GENERATOR				003
NODE				004
FR	1	30.00		005
FR	2	30.00		006
FR	3	-10.00		007
TH		00.		008
GENERATOR				009
NODE				010
** LOCAL OSCILLATOR FOR A 43 MHZ RECEIVER				011
FR	4	66.4 EB		012
IM				013
RESISTIVE COMPONENTS				014
R	1	1.0E0		015
C	1	27.0E-12		016
C	1	21.0E-12		017
C	2	8.0E-12		018
L	2	3.0E-0		019
L	1	32.0E-0		020
C	3	6.0E-12		021
C	2	4.0E-12		022
C	3	4.0E-12		023
L	4	3.0E-0		024
C	4	4.0E-12		025
L	1	32.0E-0		026
Q	4	20.0E03		027
C	4	6.0E-12		028
C	4	47.0E-12		029
C	6	39.0E-12		030
R	6	96.0E+3		031
Q	6	33.0E+3		032
TRANSISTOR				033
NODE				034
** RECEIVER Q1				035
G.0	7.00	900.	214	036
.0020	.003	6458	187.	037
		1.0	2.00E-9	038
400.	920.29			039
** END	RECEIVER Q1	1.5E-12		040
				041

***PASSIVE COMPONENTS**
 R 9 3000.
 C 9 1.0E-9
 C 9 3.3E-12
 L 9 13 110.E-9
 C 14 6.0E-12
***TRANSISTOR**
NODE 10
**** RECEIVER Q2**
 5.00 5.70 200. 209
 .00193 .006 1.14 75.
 1.0 2.80E-9
 400. 1.14E6 1.0E-12
**** END OF RECEIVER Q2**
***PASSIVE COMPONENTS**
 R 11 .01
 R 12 2.0E+3
 C 12 14 31.0E-12
 C 14 21.0E-12
 L 14 15 3.0E-9
 C 15 4.0E-12
 L 15 32.0E-9
 C 15 2.0E+3
 C 16 16 1.0E-12
 L 16 17 3.0E-9
 C 17 4.0E-12
 L 17 32.0E-9
 C 15 17 3.0E-12
 R 17 4.7E3
 C 18 17.0E-12
 C 18 18 9.0E-12
 C 18 2.0E-13
 C 18 2.0E-12
 C 19 2.0E-12
 C 17 4.0E-12
**** SECOND TWO STAGES TUNER TUNED TO 45 MHZ**
 C 19 28 9.0E-12
 R 19 3.3E+03
 C 19 6.0E+03
***TRANSISTOR**
NODE 18
**** RECEIVER Q4**
 4.00 8.86 140. 340
 .00649 .190 .125 R.2
 31.2E-12 1.0 240.E-12 59.1E-09
 10.1 1.0E9 1.E-4
 0. 1.09E-9 1.0E-12
**** END OF RECEIVER Q4**

*PASSIVE COMPONENTS		092		
R 21	470.	093		
C 21	1.0E-09	094		
C 20	27.E-12	095		
C 20 25	.32E-12	096		
L 20 25	97.E-08	097		
*TRANSISTOR		098		
NODE 23		099		
** Q3 PARAMETERS		100		
4.5	8.73	50.	.086	101
.00359	.02	.30	51.4	102
1.4E-12	1.0	25.E-12	7.5E-9	103
.00.	2.0E9			104
				105
** END OF Q3 PARAMETERS.		106		
*PASSIVE COMPONENTS		107		
R 22	.01	108		
C 24 26	1.5E-12	109		
L 24 29	3.00E-6	110		
C 24	20.0E-12	111		
L 26 29	3.00E-6	112		
R 24 29	1.0E+04	113		
C 26 27	20.E-12	114		
C 27	91.E-12	115		
C 29	175.E-12	116		
R 29	1.0E+3	117		
C 24 29	1.0E-12	118		
C 26 29	2.0E-12	119		
*PRINT SELECT		120		
VO	27	121		
*OUTPUT		122		
NODE 27		123		
** OUTPUT NODE IS ***** 27 ***		124		
*END SEGMENT		125		
** PREAMPLIFIER		126		
** INPUT NODE IS ***** 1 *****		127		
*START SEGMENT		128		
*GENERATOR		129		
NODE 1		130		
*PASSIVE COMPONENTS		131		
R 1 2	20.	132		
R 2 0	100.	133		
R 2 0	50.	134		
Q 1 0	150.	135		
R 1 3	330.	136		
R 2 0	150.	137		
C 3 4	1.E-9	138		
R 4 0	4700.	139		

```

*TRANSISTOR
NODE 4
**Q1 PREAMPLIFIER
** Q1 IF PREAMPLIFIER
5.0 8.37 200. .33
4.45 F-35.9 E-30.0 145.
.25F-121.0 0.0 3.5E-9
250. 12.4E+6
C.0 .99F-12
**END Q1 PREAMPLIFIER
*PASSIVE COMPONENTS
R 7 0 2400.
C 7 0 1.E-9
Q 8 0 1040.
C 4 8 1.E-9
R 9 12 220.
R 12 0 3300.
*TRANSISTOR
NODE 9
** Q2 PREAMPLIFIER
** Q2 IF PREAMPLIFIER
5.0 7.20 200. .33
4.45 F-34.2 E-30.0 72.
.25F-121.0 0.0 2.5E-9
220. 1.44E+6
C.0 .99F-12
**END Q2 PREAMPLIFIER
*PASSIVE COMPONENTS
R 9 0 .01
Q 11 26 3300.
L 11 26 2.8E-6
Q 26 0 1500.
C 26 0 1.E-9
C 11 0 18.E-12
C 11 13 2.2E-12
R 13 0 4700.
L 13 0 2.8E-6
C 13 14 22.E-12
C 14 0 68.E-12
Q 14 15 470.
Q 15 0 4700.
*TRANSISTOR
NODE 15
** Q3 PREAMPLIFIER
** Q3 IF PREAMPLIFIER
5.0 1.90 200. .33
4.45 F-34.9 E-30.0 114.
.25F-121.0 0.0 5.5E-9
200. 5.2E+6
C.0 .99F-12
**END Q3 PREAMPLIFIER

```

```

*PASSIVE COMPONENTS 191
R 18 0 2400. 192
C 18 0 1.E-9 193
Q 17 0 1000. 194
C 17 19 1.E-9 195
R 19 23 470. 196
R 23 0 3300. 197
*TRANSISTOR 198
NODE 20 199
**Q4 PREAMPLIFIER 200
** Q4 IF PREAMPLIFIER 201
5.0 6.81 200. 202
3.17 E-38.0 F-30.0 A2. 203
.25F-121.0 0.0 2.9E-09 204
230. 1.62E+6 205
0.0 1.89E-12 206
**END Q4 PREAMPLIFIER 207
*PASSIVE COMPONENTS 208
Q 20 0 .01 209
C 22 0 15.E-12 210
L 22 27 2.85-6 211
R 22 27 10000. 212
R 27 0 1500. 213
C 27 0 1.E-9 214
C 22 24 2.4E-12 215
C 24 0 22.E-12 216
Q 24 25 4700. 217
L 24 25 2.85-6 218
C 25 0 1.E-10 219
*POINT SELECT 220
NODE 26 221
*OUTPUT 222
NODE 25 223
** OUTPUT NODE IS ***** 25 ***** 224
*END SEGMENT 225
** 21.4 MHZ IF AMPLIFIER 226
** INPUT NODE IS ***** 1 ***** 227
*START SEGMENT 228
*GENERATOR 229
NODE 1 230
*PASSIVE COMPONENTS 231
R 1 0 100. 232
R 1 2 68. 233
R 2 0 100. 234
C 2 3 1.0E-9 235
R 3 0 1.0E4 236
R 3 0 1.0E4 237
*TRANSISTOR 238
** IF AMPLIFIER Q1 239
NODE 3 240
** IF AMPLIFIER Q1 241
5.0 4.64 200. 242
1.52E-3 1.2F-2 0.294B 243
4.05F-12 1.0R. 2.08E-11 2.4E-8 244
45.79 2.3E6 245
0.0 1.62E-12 246
** END IF AMPLIFIER Q1 247
** END IF AMPLIFIER Q1 248

```

*PASSIVE COMPONENTS	249
R 6 7 47.	250
R 7 0 2.2E3	251
C 7 0 1.0E-8	252
R 5 11 .01	253
*TRANSISTOR	254
** IF AMPLIFIER Q2	255
NODE 1 0	256
** IF AMPLIFIER Q2	257
R 5 10.6E2 200. .33	258
1.5E-3 8.E-3 .2203 44.4	259
4.39E-12 1.08 2.98E-11 2.4E-9	260
25.8 2.5E6	261
0. 1.39E-12	262
** END IF AMPLIFIER Q2	263
** END IF AMPLIFIER Q2	264
*PASSIVE COMPONENTS	265
R 8 0 .01	266
C 10 15 .22E-12	267
L 12 12 2.935E-6	268
Q 10 12 25.E3	269
C 10 12 15.E-12	270
C 10 13 0.30E-12	271
C 12 0 1.0E-8	272
R 12 0 1.0E+3	273
C 13 0 15.E-12	274
L 14 14 3.98E-6	275
R 14 14 1.0E5	276
C 14 0 150.E-12	277
Q 14 15 150.	278
Q 14 0 1.E+4	279
R 14 0 1.E+4	280
** END OF FIRST HALF OF IF AMPLIFIER	281
*TRANSISTOR	282
** IF AMPLIFIER Q3	283
NODE 15	284
** IF AMPLIFIER Q3	285
R 5 4.73 200. .33	286
1.65E-3 .0130 .2463 41.8	287
4.69E-12 1.08 3.24E-11 2.4E-9	288
42.41 2.5E6	289
0. 1.05E-12	290
** END IF AMPLIFIER Q3	291
** END IF AMPLIFIER Q3	292
*PASSIVE COMPONENTS	293
R 18 19 47.	294
R 10 0 2000.	295
C 10 0 1.E-8	296
R 17 23 .01	297
*TRANSISTOR	298
** IF AMPLIFIER Q4	299
NODE 20	300
** IF AMPLIFIER Q4	301
R 5 12.00 200. .33	302
1.64E-3 1.62E-2 .7562 42.3	303
4.97E-12 1.08 3.6E-11 2.4E-9	304
94.88 2.5E6	305
0. 1.36E-12	306
** END IF AMPLIFIER Q4	307
** END IF AMPLIFIER Q4	308

CAPACITIVE COMPONENTS			
R	28	0	0.1
R	29	24	100.
L	24	25	2.97E-6
C	24	25	20.E-9
C	24	25	13.E-12
R	24	0	1000.
C	24	0	1.0E-8
C	24	26	0.24E-12
L	24	0	3.70E-6
R	24	0	30.E3
C	26	27	13.0E-12
C	27	0	220.E-12
R	27	28	270.
R	28	0	4700.
R	28	0	30.
INPUT SELECT			
NODE	28		
OUTPUT			
NODE	28		
** INPUT NODE IS ***** 30*****			
*END SEGMENT			
*END			
			309
			310
			311
			312
			313
			314
			315
			316
			317
			318
			319
			320
			321
			322
			323
			324
			325
			326
			327
			328
			329
			330
			331
			33
			33

The receiver analysis uses the SIGNCAP cascade software.

The first data card is the *CASCADE. Cards 1 through 125 define the first segment, 126 through 225 the second segment, and 226 through 331 the third segment. The *END card, 332, terminates the data input. Each segment has a *PRINT SELECT, which selects the output node as the only one to be printed, and an *OUTPUT card to define the output node. These are coded in lines 120-123, 220-223, and 320-323, for segments 1, 2, and 3, respectively. Segments 2 and 3 have their inputs defined by the *GENERATOR cards, lines 129-130, and 229-230, respectively.

The remainder of the coding is straightforward, being divided into passive components and transistors.

APPENDIX B

NONLINEAR MODELING FROM TRANSISTOR SPECIFICATION DATA

Much of the information needed to parameterize a transistor model is available in the specification sheets for the transistor. It must be recognized from the outset that the quality of specification sheets is variable, some being exhaustive and some containing virtually no useful modeling information. It must also be recognized that a specification sheet represents a "typical" transistor of a certain family, and there is no reason to assume that a given transistor of this type will conform to the typical in detail.

In addition to specification sheets, parameter information is available in specialized handbooks. One such source is the Transistor and Diode Model Handbook, compiled for the Air Force Weapons Laboratory by IBM (Cordwell, 1969).

In this appendix we will model a 2N918 NPN bipolar transistor using typical specification data. Specification data is shown in Figs. B.1 - B.4. These data are an example of specification data containing a large amount of useful information. From the data one can model almost the complete transistor. The model parameters derived from the specification data will be compared with 2N918 parameters listed in the Transistor and Diode Handbook. Where parameters are not available from the specification data but are available in the handbook, the handbook values will be used.

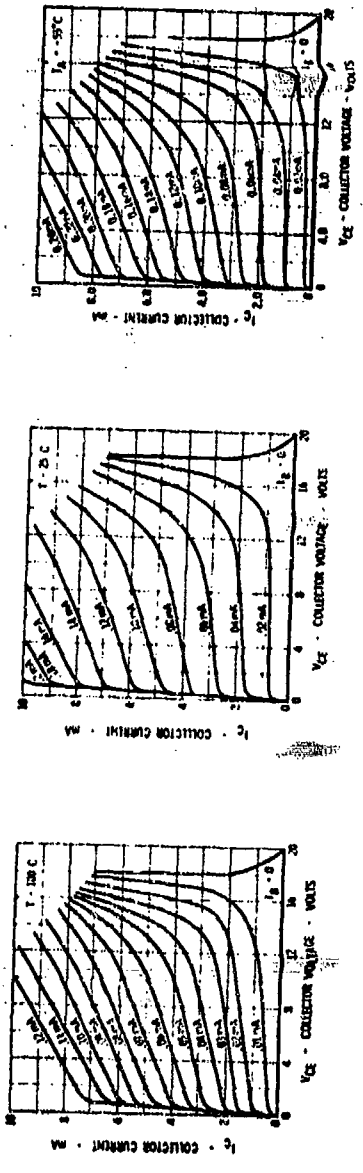


Fig. B.1 Collector Characteristics of 2N918 (From Fairchild, 1970).

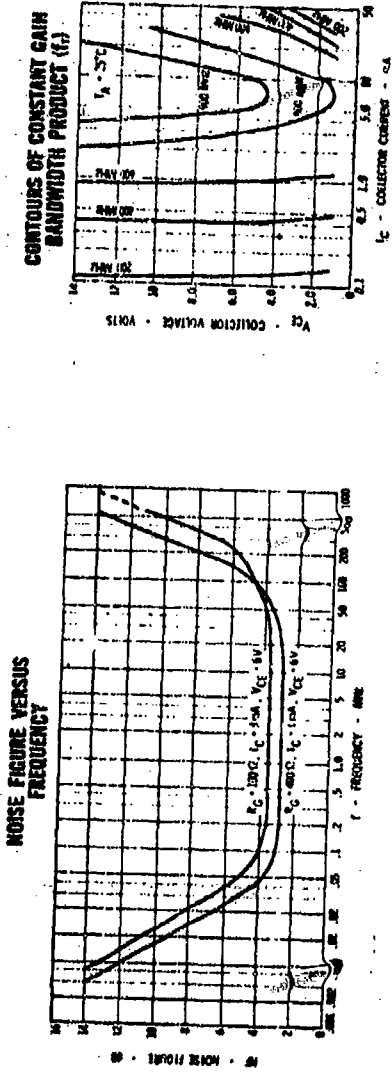


Fig. B.2 Noise Figure and Gain Bandwidth Characteristics of 2N918. (From Fairchild, 1970).

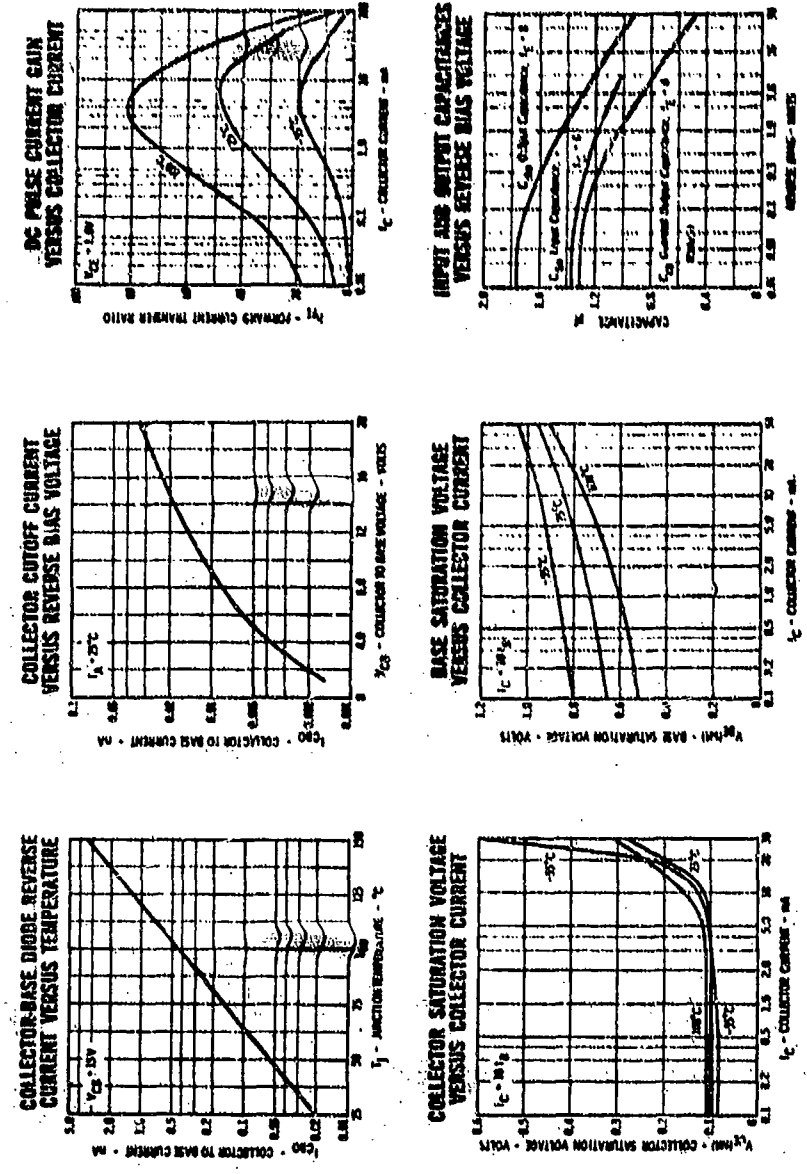


Fig. B.3 Electrical Characteristics of 2N518
(From Fairchild, 1970).

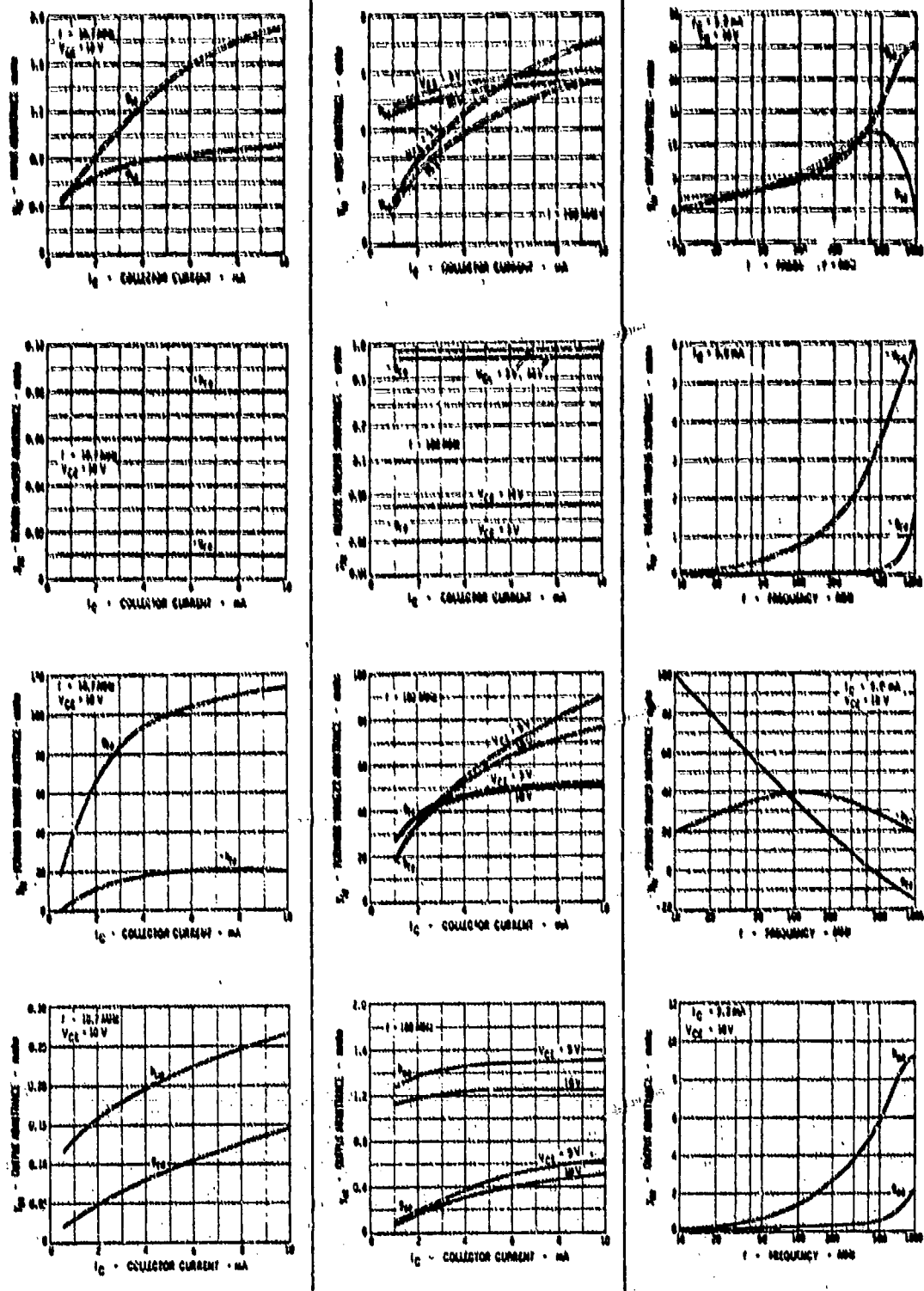


Fig. B.4 Small-Signal Common-Emitter "Y" Parameters of 2N918 (From Fairchild, 1970).

B.1 Base-Emitter Exponential Non-Linearity

The specification data does not give the base-emitter diode current-voltage curve, so the diode non-ideality factor cannot be derived. As a default value it can be set equal to unity. The handbook has the relationship

$$\frac{fI}{nkT} = 37.9 \text{ v}^{-1}, \quad (\text{B.1})$$

taking the temperature T to be 25°C , $kT/q = 25.9 \text{ mV}$ and

$$n = 1.02. \quad (\text{B.2})$$

The default value of unity can also be used.

B.2 h_{FE} Nonlinearity

Curves of h_{FE} vs. I_C are shown for temperatures of -55°C , 25°C , and 100°C on Figure B.3. At 25°C it is seen that

$$h_{FE_{max}} = 49. \quad (\text{B.3})$$

$$I_{C_{max}} \approx 7 \text{ mA}. \quad (\text{B.4})$$

$$h_{FE} \approx 38 \text{ at } I_C = 1.0 \text{ mA}. \quad (\text{B.5})$$

Based on these values from Eq. (5.54),

$$a = \frac{1}{\log^2 \left(\frac{I_C}{I_{C_{max}}} \right)} \left(\frac{h_{FE_{max}}}{h_{FE}} - 1 \right) = 0.405. \quad (\text{B.6})$$

The value of h_{FE} is also 49 at I_C _{max}, and, from Eq. (5.55), 49.3 at 1 mA. The handbook reference (Cordwell, 1969) gives $\alpha_0 = 0.9777$, which implies an h_{FE} of 44. Table B.1 shows the values of h_{FE} taken from Figure B.3 and computed using Eq. (5.54). The match is seen to be good over the range 0.1 mA to 10 mA.

B.3 Avalanche Nonlinearity

From Eqs. (5.49) through (5.52),

$$I_C = \frac{I_B \alpha_N}{1 - \alpha_N} \frac{1}{1 - \left(\frac{V_{CB}}{V_{CEO}}\right)^\eta}. \quad (B.7)$$

where V_{CEO} is the common-emitter sustaining voltage and V_{CB} is the collector-to-base voltage. Assuming V_{CB} to be equal to V_{CE} , Equation (B.7) can be rewritten as

$$I_C = \frac{I_B \alpha_N}{1 - \alpha_N} \frac{1}{1 - \left(\frac{V_{CE}}{V_{CEO}}\right)^\eta}. \quad (B.8)$$

The data needed to solve Eq. (B.8) for η are found on the common emitter collector curves in Figure B.1. The sustaining voltage is seen to be about 18 volts. Furthermore, at 16 volt V_{CE} , the ratio of the collector current to the extrapolated collector current at 0 volt V_{CE} , for a constant base current, is approximately 2.72. Therefore:

$$\frac{1}{1 - \left(\frac{16}{18}\right)^\eta} = 2.72. \quad (B.9)$$

$$\eta = 3.88. \quad (B.10)$$

Table B.1.

2N918 h_{FE} Values.(a = 0.405, I_C _{max} = 7 mA.)

<u>Collector Current</u>	<u>h_{FE} from Fig. B.3</u>	<u>h_{FE} from Eq. (5.54)</u>
.1 mA.	18	20.6
.5	30	32
1	38	38
5	48	45
7	49	49
10	48	45

B.4 Collector Capacitance Nonlinearity

The collector-base capacitance is shown as a function of collector bias on Figure B.3; the curve marked "guarded measurement" is the desired junction capacitance. It is seen to have a low-voltage value of 1.3 pF, a 0.3 volt value of 1.2 pF, and a 30 volt value of 0.5 pF. Using Equation (5.14)

$$C(V) = \frac{C(0)}{\left[1 - V/\theta\right]^\mu}, \quad (B.11)$$

results in

$$C(0) = 1.3 \text{ pF}. \quad (B.12)$$

Furthermore, it can be seen that for voltages greater than 1 Volt, the slope of the capacitance-voltage curve is constant. Therefore, we find:

$$\mu = 0.26, \quad (B.13)$$

with $C(0)$ and μ known, θ can be determined by using the 0.3 Volt capacitance value, or

$$\theta = \frac{0.3}{\left[\frac{C(0.3)}{C(0)}\right]^{1/\mu} - 1} = 0.78 \text{ Volt}. \quad (B.14)$$

Cordwell (1969) has $\mu = 0.2$, $\theta = 1.0$ V, and $C(0) = 2.4$ pF.

B.5 Emitter Capacitance Non-Linearity

Figure B.2 has contours of constant f_T , plotted as a function of I_C and V_{CE} . From Equations (5.81) and (5.42),

$$C_2 = \frac{1}{2\pi f_T r_e} = \frac{I_E}{f_T} \frac{q}{2\pi kT} = \frac{6.14 \times 10^{-3}}{f_T} I_E, \quad (B.15)$$

where I_E is in milliamperes. C_2 can be found directly from the f_T data, and is shown as a function of I_C for $V_{CE} = 10$ volts on Figure B.5. From this it is seen that

$$C_{je} = 4 \text{ pF}, \quad (B.16)$$

$$C_C' = 6.57 \text{ pF/mA}. \quad (B.17)$$

For currents greater than 16 mA the increase of C_2 is faster than linear, and higher-order terms would have to be added to the C_2 Taylor series to model the C_2 nonlinearity in this region.

B.6 Base Resistance r_b

The base resistance can be found from the y_{ie} data in Figure B.4. At low frequencies

$$y_{ie} \approx \frac{1}{r_b + h_{fe} r_e}. \quad (B.18)$$

From Figure B.4, at 10.7 MHz and 10 mA, g_{ie} is 1.9 Mho. Since h_{fe} is approximately 50

$$r_b = \frac{1}{y_{ie}} - h_{fe} \frac{kT}{qr_e} \quad (B.19)$$

$$= 395 \text{ ohms}. \quad (B.20)$$

Cordwell (1969) has $r_b = 280$ ohms.

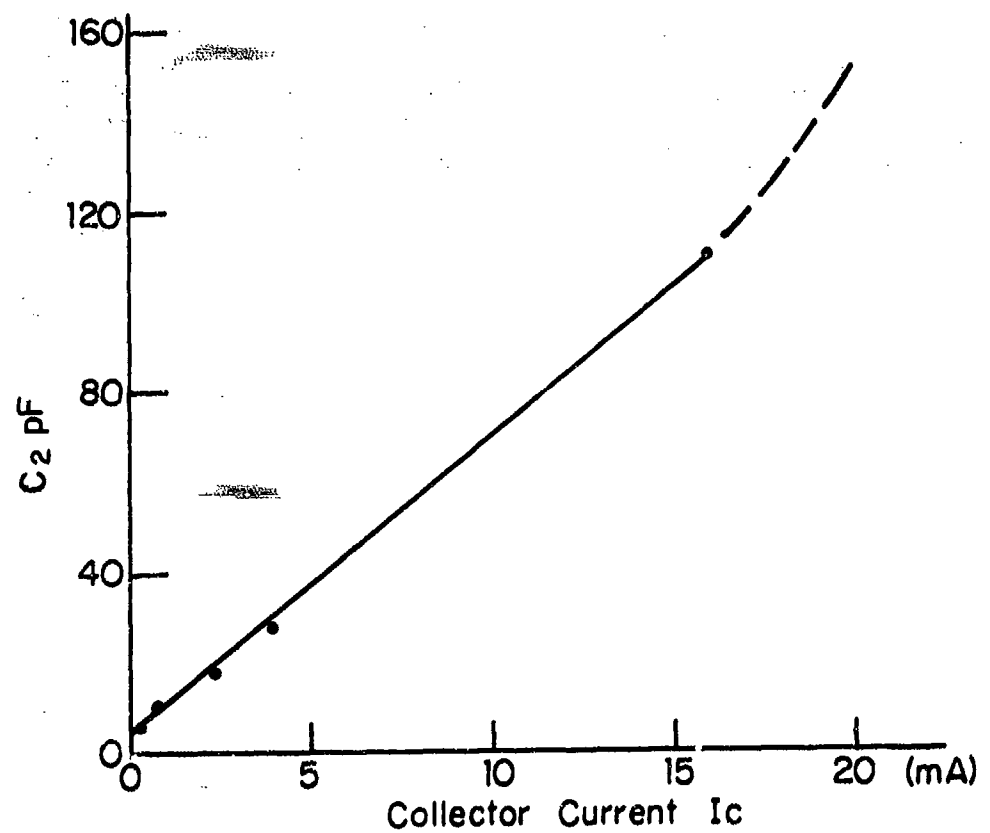


Fig. B.5. C_2 Nonlinearity of 2N918 at $V_{CE} = 10$ Volt.

B.7 Collector Resistance

The collector resistance can be found from the common-emitter collector curves. In the absence of avalanche effects, the slope of the common emitter family is $r_c(1-\alpha_o)$ ohms. While r_c is assumed to be independent of the operating point, it actually is operating point dependent. As a typical value, taking α_o to be .98, which is consistent with an h_{fe} of 50, the .02 mA base-current common-emitter curve of Figure B.1 gives:

$$r_c = 1.5 \text{ Megohms.} \quad (\text{B.21})$$

B.8 Capacitances C_1 and C_3

These parasitic capacitances can be found from the y-parameter data. Using the 500 MHz data and Equations (5.86) and (5.88)

$$C_3 \approx \frac{-\text{Im}(y_{12e})}{2\pi f} \Big|_{f=5 \times 10^8} \quad (\text{B.22})$$

$$= 1.1 \text{ pF,} \quad (\text{B.23})$$

$$C_1 + C_3 = \frac{\text{Im}(y_{11e})}{2\pi f} \Big|_{f=5 \times 10^8} \quad (\text{B.24})$$

$$= 3.82 \text{ pF.} \quad (\text{B.25})$$

Therefore:

$$C_1 = 2.72 \text{ pF.} \quad (\text{B.26})$$

B.9. Summary of 2N918 Parameters

A summary of the 2N918 parameters derived in this Appendix is shown in Table B.2.

Table B.2
 Table of 2N918 Model Parameters for Nonlinear and Linear Incremental Model
 at $T_A = 25^\circ\text{C}$ and $V_C = 10\text{V}$, $I_C = 10 \text{ mA}$.

Description	Nonlinear Parameters	Linear Parameters
Emitter Junction Forward Biased		
Conductance	$I_E = 10 \text{ mA}$; $n = 1.02$	$r_e = 2.6 \text{ ohms}$
Capacitance	$C_{je} = 4 \text{ pF}$; $C_d = 6.57 \text{ pF/mA}$	$C_2 = 69.7 \text{ pF}$
Collector Junction Reverse Biased		
Conductance	$r_c = 1.5 \text{ Megohms}$	$r_c = 1.5 \text{ Megohms}$
Capacitance	$C(0) = 1.3 \text{ pF}$; $\phi = 0.78V$; $\mu = 0.26$	$C_c = 0.69 \text{ pF}$
Dependent Source		
h_{FE}	$a = 0.405$	
Avalanche	$h_{FE_{max}} = 49$; $I_{C_{max}} = 7 \text{ mA}$	$h_{fe} = 49$
	$V_{CEO} = 18 \text{ Volt}$; $\gamma = 3.88$	
Base	$r_b = 395 \text{ ohms}$	$v_b = 395 \text{ ohms}$
Emitter-to-Base Capacitance	$C_1 = 2.72 \text{ pF}$	$C_1 = 2.72 \text{ pF}$
Collector-to-Base Capacitance	$C_3 = 1.1 \text{ pF}$	$C_3 = 1.1 \text{ pF}$

BIBLIOGRAPHY

- Aaronson, G., and Schilling, R.B., 1972. "A Comparison of Two Transistor Models." IEEE Trans. on Elec. Dev., Vol. ED-19, No. 1, pp 1-3, Jan. 1972.
- Abramowitz, M., and Stegun, I., 1954, editors, Handbook of Mathematical Functions, National Bureau of Standards Applied Math. Series No. 55, Washington, D.C., 1964.
- Adler, R.B., A.C. Smith, and R.L. Longini. 1964. Introduction to Semiconductor Physics, SEE Vol. 1, John Wiley & Sons., Inc., New York, 1964.
- Akima, H., 1970. "A New Method of Interpolation and Smooth Curve Fitting Based on Local Procedures," Journal of the ACM, Vol. 17, No. 4, pp. 589-602, October 1970.
- Allen, R.H., 1969. Efficient Computer Aided Analysis of Non-Linear Electronic Circuits, Information Sciences Report No. 35, Boeing Scientific Research Labs., Seattle, August 1969 (AD No. 694306).
- . 1969b. Numerically Stable Explicit Integration Techniques Using A Linearized Runge-Kutta Extension, Boeing Scientific Research Lab., Document D1-82-0929, October 1969.
- Anderson, D.R., and Leon, B.J., 1965. "Nonlinear Distortion and Truncation Errors in Frequency Converters and Power Amplifiers," IEEE Trans. on Circ. Th., Vol. CT-12, No. 3, pp. 314-321, September 1965.
- Aprille, T.J..Jr., 1971. "Two Computer Algorithms For Obtaining the Periodic Response of Nonlinear Circuits," University of Illinois Coordinate Sciences Laboratory Report R-540, Urbana, Illinois, 1971.
- Aprille, T.J. Jr., and Trick, T.N., 1972. "Steady-State Analysis of Nonlinear Circuits with Periodic Inputs," Proc. IEEE, Vol.60, No.1, January 1972.
- Aracil, J., 1970. "Measurement of Wiener Kernels with Binary Random Signals," IEEE Trans. on Auto. Control, pp. 123-125, February 1970.
- Bailey, R.L., 1970. "Large-Signal Nonlinear Analysis of a High-Frequency Junction Transistor," IEEE Trans. on Elec. Dev., Vol. ED-17, No. 2, pp. 108-119, February 1970.
- Barrett, J.F., 1963. "The use of Functionals in the Analysis of Nonlinear Physical Systems," Journal of Electronics and Control, Vol. 15, pp. 567-611, 1963.
- Bashkow, T.R., 1957. "The Λ -Matrix, New Network Description," IRE Trans. Circuit Theory, Vol. CT-4, pp. 117-119, September 1957.
- Bedrosian, E., and Rice, S.O., 1971. "The Output Properties of Volterra Systems (Nonlinear Systems with Memory) Driven by Harmonic and Gaussian Inputs," Proc. IEEE, Vol. 59. No. 12, pp. 1688-1707, December 1971.
- Bello, P.A., 1963. "Characterization of Randomly Time-Variant Linear Channels," IEEE Trans. on Comm. Systems, Vol. CS-11,

- pp. 360-393, December 1963.
- Bello, P.A., L. Ehrman, J.W. Graham, and S.A. Meer, 1971. Communications Receiver Interference Modeling: Nonlinear Canonic Models and Small-Signal Nonlinear Transfer Function Analysis, 1971 IEEE International Electromagnetic Compatibility Symposium Record, Philadelphia, Pa., p. 183, July 1971.
- Bello, P.A., "Nonlinear Canonic Models of Receivers," International Conference on Communications, Philadelphia, Pa., pp. 30-2-30-9, June 19-21, 1971.
- Berry, R.D., 1971. "An Optimal Ordering of Electronic Circuit Equations for a Sparse Matrix Solution," IEEE Trans. on Circuit Theory, Vol. CT-18, pp. 40-50, January 1971.
- Bose A.G., 1956. "A Theory of Nonlinear Systems," Tech.Rpt. No. 309, Research Lab. of Electronics, Mass. Inst.of Technology, Cambridge, Mass., May 15, 1956
- Brayton, R.K., and Gustavson, F.G., 1969. "Some Results on Sparse Matrices," IBM Report 2332, Yorktown, N.Y., 1969.
- Brilliant, M.B., 1958. "Theory of the Analysis of Nonlinear Systems," Tech. Report No. 345, M.I.T. Research Labs of Electronics, 1958.
- Bryant, P.R., "The Explicit Form of Bashkow's A Matrix," IRE Trans. Circuit Theory, Vol. CT-9 pp. 303-306, September 1962.
- Calahan, D.A., 1968. "A Stable Accurate Method of Numerical Integration For Non-Linear Systems," Proc. IEEE, p.744, April 1968.
- Calahan, D.A., and Gear, C.W., 1970. "An Ill-Conditioning Problem With Implicit Integration," AFOSR-70-1472TR, E.E. Dept., University of Michigan, May 1970 (AD 706913).
- Calahan, D.A., 1970. "Numerical Techniques for Fast and Accurate Transient Analysis of Non-Linear Circuits," AFOSR-70-1470TR, E.E. Dept. University of Michigan, May 1970 (AD 706914).
- . 1972. Computer-Aided Network Design, McGraw Hill, Inc., New York, 1972.
- Calahan, D.A., T.E. Grapes, J. Donahey, and N. Orlandea, 1971. "Description of a Sparse Matrix Compiler with Applications," Systems Engineering Laboratory, University of Michigan, Ann Arbor, Michigan, October 11, 1971.
- Cobbold, R.S.C., 1970. Theory and Application of Field- Effect Transistors, Wiley-Interscience, New York, 1970.
- Cochran, W.T., 1967. et. al., "What Is the Fast Fourier Transform?", Proc. IEEE, Vol. 55, No. 10, pp. 1664-1674, October 1967.
- Coddington, E.A., and Levinson, N., 1955. Theory of Ordinary Differential Equations, McGraw Hill, New York, 1955.

- Cooke, H.F., RN, 1971. "Microwave Transistors: Theory and Design," Proc. IEEE, Vol. 59, No. 8, pp.1163-1181, August 1971.
- Cooley, J.W., and Tukey, J.W., 1965. "An Algorithm for the Machine Computation of Complex Fourier Series," Math Comput., Vol. 19, pp. 297-301, April 1965.
- Cordwell, W.A., 1969. "Transistor and Diode Model Handbook," Air Force Weapons Laboratory, Kirtland Air Force Base, New Mexico, October 1969.
- Coniglione, J., 1966. "Preferred Circuit Techniques for Crystal-Diode Mixers," RADC-TR-66-610, November 1966.
- Crawford, R.H., 1967. Mosfet in Circuit Design, McGraw Hill Book Co., New York, 1967.
- Dahlquist, Germund, 1963. "A Special Stability Problem for Linear Multistep Methods," BIT (Nordisk Tidskrift for Informations-Behandling), Vol.3, pp. 27-43, 1963.
- Deutsch, R., 1962. Non-Linear Transformations of Random Processes, Section 6.5, Prentice-Hall, Inc., New Jersey, 1962.
- Duff, W.G., 1969. "EMC Figure of Merit for Receivers," IEEE 1969 Electromagnetic Compatibility Symposium Proceedings, pp. 257-262, Asbury Park, New Jersey, 1969.
- Ebstein, B., R.G. Huenemann, and R. Sea, 1967. "Third Order Intermodulation Study," RADC-TR-67-344, July 1967.
- Ehrman, Leonard, and Meer, S. Ahmed, 1972. "Communication Receivers Interference Modeling: Nonlinear Transfer Functions from Circuit Analysis: Mild Excitations," International Conference on Communications, Philadelphia, Pa., June 19-21, 1972, pp. 30-10 to 30-15.
- Eimberger, J., 1968. Linear Integrated Circuits: Theory and Applications, John Wiley & Sons, Inc., New York, 1968.
- Fair, R.B., 1972. "Harmonic Distortion in the Junction Field-Effect Transistor with Field-Dependent Mobility," IEEE Trans. on Elect. Dev., Vol. ED-19, No.1, pp.9-13, Jan. 1972.
- Fairchild Semiconductor Co., Fairchild Semiconductor Transistor and Diode Data Catalog 1970.
- Feller, W., 1950. An Introduction to Probability Theory and its Applications, Vol. 1, John Wiley & Sons, Inc., New York, 1950.
- Flake, R.H., 1963. "Volterra Series Representation of Nonlinear Systems," Trans. AIEEE, Vol. 64, pp. 330-335, 1963.
- Fowler, M.E., and Warten, R.M., 1967. "A Numerical Technique For Ordinary Differential Equations With Widely Separated Eigenvalues," IBM Journal Res. and Dev., Vol. 11, pp.537-543, September 1967.
- Gardiner, J.G., and Ghobrial, S.I., 1971. "Distortion Performance of the Abrupt-Junction Current-Pumped Varactor Frequency Converter," IEEE Trans. on Microwave Theory and Technique, Vol. MTT-19, No. 9, pp. 741-749, September 1971.

- Gartner, W.W., 1960. Transistors, Principles, Design and Applications, D. Van Nostrand Co., Inc., New York, 1960.
- Gear, C.W., 1968a. "The Automatic Integration of Stiff Ordinary Differential Equations," Proc. 1968 IFIPS Congress, pp. A81-A85.
- . 1968b. "The Control of Parameters In The Automatic Integration of Ordinary Differential Equations," Dept. Computer Science, University of Illinois, May 17, 1968.
- . 1971a. "The Simultaneous Numerical Solution of Differential-Algebraic Equations," IEEE Trans. on Circuit Theory, Vol. CT-18, January 1971.
- . 1971b. Numerical Initial Value Problems in Ordinary Differential Equations, Prentice-Hall, Inc., New Jersey, 1971.
- George, C.A., "BELAC User's Manual," General Electric Co. Technical Information Series, No. R69EML11, 1 August 1969, Utica, New York.
- George, D.A., 1959. "Continuous Nonlinear Systems," Technical Report 355, Massachusetts Institute of Technology, Research Lab. of Electronics, Cambridge, Mass., July 24, 1959.
- Gershoff, A.J., 1963. "Characterization of Time-Varying Linear Systems," Proc. IEEE (Correspondence), Vol. 51, p.238, January 1963.
- Gold, B. and Rader, C.M., 1969. Digital Processing of Signals, Chapter 7, McGraw-Hill Book Co., New York, 1969.
- Graham, J.W. and Bello, P.A., 1972. "Communication Receivers Interference Modeling," International Conference on Communications, Philadelphia, Pa., June 19-21, 1972, p. 30-1.
- Graham, J.W. and Ehrman, L., 1972. "Experimental Validation of the Nonlinear Transfer Function Approach to Receiver Modeling," International Conference on Communications, Philadelphia, Pa., June 19-21, 1972, pp.30-22 to 30-28
- Gray, P.E., D. DeWitt, A.R. Boothroyd and J.F. Gibbons, 1964. Physical Electronics and Circuits Models of Transistors, SEEC Vol.2, John Wiley & Sons, Inc., New York, 1964.
- Gray, P.E. and Searle, C.L., 1969. Electronic Principles Physics, Models, and Circuits, John Wiley & Sons, Inc., New York, 1969.
- Gretsch, W.R., 1966. "The Spectrum of Intermodulation Generated in Semiconductor Diode Junction," Proc. IEEE, Vol. 54, No. 11, pp. 1528-1535, November 1966.
- Grim, W.M., Jr., 1961. "The Voice Interference Analysis of a Communication Channel," Proceedings 7th Conference on Radio Interference Reduction and Electronic Compatibility, pp. 597-608, November 1961.

- Gummel, H.K., 1970. "A Charge Control Relation for Bipolar Transistors," BSTJ, Vol. 49, pp. 115-120, January 1970.
- Gummel, H.K. and Poon, H.C., 1970. "An Integral Charge Control Model of Bipolar Transistors," BSTJ, pp. 827-852, May-June 1970.
- Gustavsen, F.G., 1971. "Some Basic Techniques for Solving Sparse Systems of Linear Equations," Proc. of the Sparse Matrix Symposium, pp. 41-52, Plenum, 1971.
- Hachtel, G.D., R.K. Brayton and F.G. Gustavson, 1971. "The Sparse Tableau Approach to Network Analysis and Design," IEEE Trans. Circuit Theory, Vol. CT-18, pp. 101-113, January 1971.
- Hamilton, D.J., F.A. Lindholm, and J.A. Narud, 1964. "Comparison of Large-Signal Models for Junction Transistors," Proc. IEEE, Vol. 52, No. 3, pp. 239-248, March 1964.
- Harris, J.N., 1966. Digital Transistor Circuits, SEEC Vol. 6, John Wiley & Sons, Inc., New York, 1966.
- Henrici, P., Discrete Variable Methods In Ordinary Differential Equations, John Wiley & Sons, Chapter 5, 1962.
- . 1963. Error Propagation for Difference Methods, John Wiley & Sons, New York 1963.
- Herskowitz, G.T., and Schilling, R.B., 1972. eds., Semiconductor Device Modeling For Computer-Aided Design, McGraw-Hill Book Co., Inc., New York, 1972.
- Hewitt, H., J. Richards, C. Teacher, 1970. "The Applicability of Speech Recognition to Automatic Intelligibility Testing," Paper Presented at Spring 1970 Meeting of Acoustical Society of America, Atlantic City, New Jersey, 1970.
- Hewlett-Packard Corp., Application Note 907, "The Hot Carrier Diode Theory, Design, and Application." undated.
- . Application Note 913, "Step Recovery Diode Frequency Multiplier Design." undated.
- . Application Note 95, "S-Paramenters... Circuit Analysis and Design."
- Hsieh, H.Y., and Ghausi, M.S., "On Optimal-Pivoting Algorithms in Sparse Matrices," IEEE Trans. on Circuit Theory, Vol. CT-19, pp. 93-96, January 1972.
- . 1972. "A Probabilistic Approach to Optimal Pivoting and Prediction of Fill-In for Random Sparse Matrices," IEEE Trans. on Circuit Theory, CT-19, pp. 329-336, July 1972.
- IBM Corp., 1965. "1620 Electronic Circuit Analysis Program (ECAP) (1620-EE-02X) User's Manual," Data Processing Division, White Plains, New York, 1965.

Jensen, R.W., 1966. "Charge Control Transistor Model for the IBM Electronic Circuit Analysis Program," IEEE Trans. on Circuit Theory, Vol. CT-13, No.4, pp. 428-432, December 1966.

Kailath, T., 1959. "Sampling Models for Linear Time-Variant Filters," M.I.T. Research Lab. of Electronics, Cambridge, Mass., Rept. No. 352; May 25, 1959.

Kim, W., and Meadows, H., 1971. Modern Network Analysis, John Wiley & Sons, Chapter 4, New York, 1971.

Kornfeld, D., et. al., 1967. "Preferred Circuit Techniques For Transistor Amplifiers," RAD-C-TR-67-15, February 1967.

Kuo, F.F., and Magnuson, W.G., Jr., Ed., 1969. Computer Oriented Circuit Design, Prentice-Hall, Inc., New Jersey, 1969.

Kuo, Y.L., and Witkowski, J.D., 1972. "Computer-Aided Distortion Analysis of Bipolar Transistor Circuits," Bell Telephone Laboratories, Inc., North Andover, Mass., 1972.

Lange, J., and Carr, W.N., 1972. "An Application of Device Modeling to Microwave Power Transistors," IEEE Journal of Solid State Circuits, Vol. SC-6, No. 4, pp. 71-80, January 1972.

Lee, Y.W. and Schetzen, M., "Measurement of the Wiener Kernels of a Nonlinear System by Cross-Correlation," International J. of Control, Vol. 2, No.3, pp. 237-354, 1965.

Lenkowsky, J., 1962. "Some Aspects of Perturbational Analysis of Time-Varying Circuits," IEEE Trans. on Circuit Theory, Vol. CT-9, pp 13-18, March 1962.

Lindholm, F.A., 1971, "Unified Modeling of Field-Effect Devices," IEEE Journal of Solid-State Circuits, Vol. SC-6, No.4. pp.250-259, August 1971.

Liniger, W., and Willoughby, R.A., 1970. "Efficient Integration Methods For Stiff Systems of Ordinary Differential Equations," SIAM J. Anal., Vol. 7. pp. 47-66, March 1970.

Lomax, H., "An Operational Unification of Finite Difference Methods For The Numerical Integration of Ordinary Differential Equations," NASA TR R-262, Ames Research Center, May 1967.

Lotsch, H.K.V., 1968. "Theory of Nonlinear Distortion Produced in a Semiconductor Diode," IEEE Trans. on Electronic Dev., Vol. ED-15, No. 5, pp. 294-307, May 1968.

Lubbock, J.K. and Bansal, V.S., 1969. "Multidimensional Laplace Transforms for Solution of Nonlinear Equations," Institution of Electrical Engineers, (Great Britain) Proc. Vol. 116, 1969.

Lynn, D.K., C.S. Meyer and D.J. Hamilton, 1968. Analysis and Design of Integrated Circuits, McGraw-Hill Book Co., New York, 1968.

- Macnee, Alan F., 1967. Computational Utility of Non-Linear Transistor Models. Technical Report ECOM-01870-17, Cooley Electronics Lab., University of Michigan, November 1967 (AD 824300).
- Malmberg, Allan F., 1969. Net-2 Network Analysis Program, Braddock, Dunn & McDonald, Inc., El Paso Texas, December 1969 (AD 863797).
- Mathers, H.W., S.R. Sedore, and J.R. Sentz, "Automated Digital Computer Program for Determining Responses of Electronic Circuits to Transient Nuclear Radiation (SCEPTRE), Vol. I, IBM Electronics Systems Center, Owego, New York, February 1967.
- M.I.T., E.E. Staff, 1943. Applied Electronics, Chapter IV, John Wiley & Sons, New York, 1943.
- Maurer, R.E., and Narayanan, S., 1968. "Noise Loading Analysis of a Third-Order Nonlinear System with Memory," IEEE Trans. on Communication Techniques, Vol. COM-16, No.5, pp. 701-712, October 1968.
- Mayher, R., 1966, "Basic Performance Thresholds", ESD-TR-66-9, December 1966.
- Meyer, R.G., M.J. Shensa, and R. Eschenbach, 1972. "Cross Modulation and Intermodulation in Amplifiers at High Frequencies," IEEE Journal of Solid-State Circuits, Vol. SC-7, No.1, pp. 16-23, February 1972.
- Miller, S.L., 1955. "Avalanche Breakdown in Germanium," Phys. Rev., 99, p. 1234, August 15, 1955.
- Miller, D.M. and Meyer, R.G., 1971. "Nonlinearity and Cross Modulation in Field-Effect Transistors," IEEE Journal of Solid-State Circ., Vol. SC-6, No.4, pp. 244-251, August 1971.
- Milliman, L.D., W.A. Massena and R.H. Dickhaut, 1967, "CIRCUS—A Digital Computer Program for Transient Analysis of Electronic Circuits—User's Guide," The Boeing Co., Seattle, Wash., Harry Diamond Laboratories Report AD-346-1, January 1967.
- Narayanan, S., 1967 "Transistor Distortion Analysis Using Volterra Series Representation," BSTJ, Vol. 46, p. 991, May-June 1967.
- _____. 1969. "Intermodulation Distortion of Cascaded Transistors," IEEE Journal Solid-State Circuits, Vol. SC-4, No. 3, June 1969.
- _____. 1970. "Application of Volterra Series to Intermodulation Distortion Analysis of Transistor Feedback Amplifiers," IEEE Trans. on Circuit Theory, Vol. CT-17, No.4, pp. 518-527, November 1970.
- Nordsieck, A., 1962. "On Numerical Integration of Ordinary Differential Equations," Math. of Computation, Vol. 16, pp. 22-49, 1962.
- Norin, R.S., and Pottle, C., 1971, "Effective Ordering of Sparse Matrices Arising from Nonlinear Electrical Networks," IEEE Trans. on Cir. Theory, Vol. CT-18, pp.139-145, Jan. 1971.

- O'Donnell, J., 1972. "Communication Receivers Interference Modeling: Nonlinear Transfer Functions from Circuit Analysis: Strong Excitation," International Conference on Communications, Philadelphia, Pa., pp. 3-16-3-21, June 19-21, 1972.
- Orloff, L.M., 1964. "Intermodulation Analysis of Crystal Mixer," Proc. IEEE, Vol. 52, No. 3, pp. 173-179, March 1964.
- Parente, R.B., "Functional Analysis of Systems Characterized by Nonlinear Differential Equations," M.I.T. Res. Lab. of Electronics, Tech. Report 444, July 15, 1966.
- Penfield, P., 1966. "Circuit Theory of Periodically-Driven Nonlinear Systems," Proc. IEEE, Vol. 54, No. 2, pp. 266-280, February 1966.
- Peterson, D.P., Middleton, D. (1962), "Sampling and Reconstructing of Wave-Number-Limited Functions in N-Dimensional Euclidian Spaces", Information and Control, Vol. 5, No. 4, Dec. 1962, pp. 279-323.
- Peterson, E. and Hussey, L.W., 1939. "Equivalent Modulation Circuits," BSTJ, Vol. 18, pp. 32-34, January 1939.
- Peterson, L.C., and Llewellyn, 1945. "The Performance and Measurement of Mixers in Terms of Linear Network Theory," Proc. IRE, Vol. 33, No. 7, pp. 458-476, July 1945.
- Polak, E., and Wong, ~~E.~~, 1970. Notes for a First Course in Linear Systems, Chapter 1, Van Nostrand Reinhold, N.Y., 1970.
- Poon, H.C., and Meckwood, J.C., 1972. "Modeling of Avalanche Effects in Integral Charge Control Model," IEEE Trans. on Elec. Dev., Vol. ED-19, No. 1, pp. 90-97, January 1972.
- . 1972. "Modeling of Bipolar Transistor Using Integral Charge-Control Model with Applications to Third-Order Distortion Studies," IEEE Trans. on Elec. Dev., Vol. ED-19, No. 6, pp. 719-731, June 1972.
- Pope, D.A., 1963. "An Exponential Method of Numerical Integration of Ordinary Differential Equations," Comm. of the ACM, Vol. 6, pp. 491-493, August 1963.
- Pottle, C., 1966. "State-Space Techniques for General Active Network Analysis," Chapter 3, Systems Analysis By Digital Computer, F.F. Kuo, and J.F. Kaiser, ed. John Wiley & Sons, New York, 1966.
- Rafuse, R.P., and Steinbrecher, D.H., 1969. "Interference Reduction Techniques," RADC-TR-68-576, January 1969.
- Ralston, A., 1965. A First Course in Numerical Analysis, McGraw-Hill Book Co., New York, 1965.
- Reid, J.H., Editor, 1971. Large Sparse Sets of Linear Equations, Academic Press, 1971.
- Rome Air Development Center, 1966. "Interference Notebook," RADC-TR-66-1, Chapter 5, Vol. 2, 1966.
- Rose, D.J., and Willoughby, R.A., 1972. "Sparse Matrices and their Applications," September 9-10, 1971, Proc. of Symposium Held at IBM Thomas J. Watson Research Center, Yorktown Heights, New York, Plenum, 1972.

- Saaleh, A.A.M., "Theory of Resistive Mixers," Sc.D. Thesis, M.I.T., January 1970.
- Sandberg, 1964. "On Truncation Techniques in the Approximate Analysis of Periodically Time-Varying Non-Linear Networks," IEEE Trans. on Circuit Theory, pp. 195-201, June 1964.
- Sandberg, I.W., and Shichman, H., 1968. "Numerical Integration of Systems of Stiff Non-Linear Differential Equations," BSTJ, Vol. 47, No.4, pp. 511-527, April 1968.
- Schwarz, R., and Friedland, B., 1965. Linear Systems, McGraw-Hill Book Co., Chapters 2,4, New York , 1965.
- Searle, C.L., A.R. Boothroyd, E.J. Angelo, Jr., P.E. Gray, and D.O. Pederson, 1964. Elementary Circuit Properties of Transistors, SEEC, Vol.3, John Wiley & Sons, Inc., New York, 1964.
- Sevin, L.J. Jr., 1965, Field Effect Transistors, McGraw-Hill Book Co., New York, 1965.
- Shichman, H., 1970. "Integration System of a Non-Linear Network-Analysis Program," IEEE Trans. on Circuit Theory, Vol. CT-17, No.3, pp. 378-386, August 1970.
- Shimbo, O., 1971. "Effects of Intermodulation, AM-PM Conversion, and Additive Noise on Multicarrier TWT Systems," Proc. IEEE Vol.59, No.2, pp.230-238, February 1971.
- Spangenberg, K.R., Vacuum Tubes, McGraw-Hill Book Co., New York, 1948.
- Spina, J.F., A.W. Fitch and D.D. Weiner, 1972. "Computer Modeling of a Solid-State VHF Tuner Using the Nonlinear Transfer Function Approach," Proc. of the IEEE 1972 International Conference on Communications, pp. 29-30, June 1972.
- Steinbrecher, D., J.P. Curtis and R.E. Snyder, "Intermodulation Distortion In Amplifiers and Broadband Mixers," Undated 1969 Conference Report Supported in Part by Contract F30603-68-C-0023, Project 4540.
- Steiner, J.W., 1964. "An Analysis of Radio Frequency Interference Due to Mixer Intermodulation Products," IEEE Trans. on Electromagnetic Compatibility, pp. 62-68, January 1964.
- Thornton, R.D., D.O. Pederson, C.L. Searle, E.J. Angelo Jr., and J. Willis, 1965. Multistage Transistor Circuits, SEEC Vol. 5, John Wiley & Sons, Inc., New York, 1965.
- Thornton, R.D., D. De Witt, E.R. Chenette, P.E. Gray, 1966. Characteristics and Limitations of Transistors, SEEC Vol.4, John Wiley & Sons, Inc., New York, 1966.
- Thornton, R.D., J.G. Linvill, E.R. Chenette, H.L. Ablin, J.N. Harris and A.R. Boothroyd, 1966. Handbook of Basic Transistor Circuits and Measurements, SEEC, Vol. 7, John Wiley & Sons, Inc., New York, 1966.

- van der Ziel, A., 1970. "Noise in Solid-State Devices and Lasers," Proc. IEEE, Vol. 58, pp. 1178-1206, August 1970.
- Van Trees, H.L., 1962. Synthesis of Optimum Nonlinear Control Systems, M.I.T. Press, Cambridge, Mass., 1962.
- Volterra, V., 1930. Theory of Functionals and of Integral and Integro-Differential Equations, Blackie and Sons Ltd., London, 1930.
- Wass, C.A.A., 1949. "A Table of Intermodulation Products," IEEE Journal, Vol. 95, Part 3, pp. 31-39, January 1949.
- Wathen-Dunn, W., and Lipke, D.W., 1959. "On the Power Gained by Clipping Speech in the Audio Band," JASA, Vol. 30, No. 1, pp. 36-40, January 1959.
- Watson, H.A., ed. 1969. Microwave Semiconductor Devices and their Circuit Applications, McGraw-Hill Book Co., New York, 1969.
- Wedlock, B.D., 1968. "On the Field-Effect Transistor Characteristics," IEEE Trans. Elect. Dev., Vol. ED-15, pp. 181-2, March 1968.
- . 1970. "Static Large-Signal Field-Effect Transistor Models," Proc. IEEE, Vol. 58, No. 4, pp. 593-595, April 1970.
- Weiner, D.D., J.F. Spina, and A. Fitch, 1971. Towards An Improved Methodology For Mathematically Modeling Communications Receivers, 1971 IEEE International Electromagnetic Compatibility Symposium Record, Philadelphia, Pa., pp. 175-182, June 1971.
- Wiener, N., 1942. "Response of a Non-Linear Device to Noise," M.I.T. Radiation Laboratory Report V-16S, April 1942.
- . 1958. Nonlinear Problems in Random Theory, John Wiley & Sons, M.I.T. Press, New York, 1958.
- Willoughby, R.A., ed. 1968. "Proceedings of the IBM Symposium on Sparse Matrices and their Applications," IBM, Yorktown Heights, New York, September 9-10, 1968.
- Wilson, R.L. and Massena, W.A., 1965. "An Extension of Bryant-Baskow A Matrix," IEEE Trans. Circuit Theory, pp. 120-122, March 1965.
- Zadeh, L.A., 1950. "Frequency Analysis of Variable Networks," Proc. IRE, Vol. 38, pp. 291-299, March 1950.
- Zadeh, L.A., and Desoer, C.A., 1963. Linear System Theory, McGraw-Hill, New York, 1963.
- Zames, G., 1960. "Nonlinear Operators for System Analysis," Tech. Report No. 370, M.I.T. Research Lab. of Electronics, August 1960.

GLOSSARY OF PRINCIPAL SYMBOLS

Following is a list of the principal symbols that appear in this book, along with identification as to where the symbol is first used. Most of the symbols appear throughout the book. Certain symbols which are used only in the development of more general relations in one section are not included. A few conventions followed throughout the book are:

1. \sum_k indicates summation over the index k
2. \prod_k indicates multiplication over the index k
3. * indicates a complex conjugate
4. \sim indicates bandlimiting of a function
5. an underbar, , indicates a vector quantity.

In addition to this glossary, Table 3.7, pp 201-204, lists the key symbols used in Chapter 3, Canonic Models for Nonlinear Systems.

GLOSSARY OF PRINCIPAL SYMBOLS

\underline{A}	a constant matrix	(Eq. 4.84)
$A_n(f_1, f_2 \dots f_n)$	a nonlinear transfer function of order n	(Eq. 2.29)
A_1, A_2	amplitudes of interfering tones	(Eq. 1.3)
a	nonlinearity parameter	(Eq. 5.54)
$a(t)$	in-phase component of a complex signal	(Sec. 3.2)
a_n	power-series coefficient	(Eq. 1.1)
a_n^{eq}	equivalent n^{th} -order power series coefficient	(Eq. 7.78)
a_{pq}	Fourier expansion amplitude of $a_q(t)$	(Eq. 4.24)
α	diode exponential parameter	(Eq. 4.2)
α_j	integration rule coefficient	(Eq. 4.131)
α_o	transistor small-signal common-base linear current gain	(Sec. 5.3.1)
a_1, a_2	modulation amplitudes	(Eq. 3.81)
B	bandwidth of a signal	(Eq. 3.56)
$B_n(f_1, f_2 \dots f_n)$	a nonlinear transfer function of order n	(Eq. 2.30)
$B_n(m)$	nonlinear product coefficient	(Eq. 1.50)
$b(t)$	quadrature component of a complex signal	(Sec. 3.2)
β_j	integration rule coefficient	(Eq. 4.131)
c	a numerical coefficient	(Eq. 2.3)
C_1	transistor base-emitter header capacitance	(Sec. 5.3.1)

C_3	transistor fixed collector-base capacitance	(Sec. 5.3.1)
C_c	transistor collector capacitance	(Sec. 5.3.2)
C_p	transistor diffusion capacitance	(Sec. 5.3.1)
C_d'	derivative of C_2 with respect to I_E	(Eq. 5.82)
C_{je}	transistor space charge layer capacitance	(Sec. 5.3.1)
$C_n(f_1, f_2 \dots f_n)$	a nonlinear transfer function of order n	(Sec. 2.2.2)
$C_n^{\alpha\alpha}$	n^{th} -order transfer function of α stage	(Eq. 2.174)
$C_n^{\beta\beta}$	n^{th} -order transfer function of β stage	(Eq. 2.174)
c.c.	complex conjugate	(Eq. 2.6)
D	pentode current division ratio	(Eq. 5.116)
$\delta(\)$	unit impulse	(Eq. 1.35)
e	plate-cathode voltage	(Eq. 5.95)
$E_{C_{\max}}$	a permeance cutoff voltage	(Eq. 5.110)
$E_n(f_1, f_2 \dots f_n)$	n^{th} -order nonlinear transfer function	(Eq. 2.154)
η	avalanche coefficient	(Eq. 5.4)
$F_n[\]$	regular homogeneous functional of degree n	(Eq. 1.9)
$F_n(f_1, f_2 \dots f_n)$	n^{th} -order nonlinear transfer function	(Eq. 2.155)
f	frequency in hertz	(Eq. 1.30)

\underline{f}_{mn}	two-input frequency vector	(Eq. 2.203)
$\underline{f}(\underline{x}, \underline{u})$	a nonlinear matrix	(Eq. 4.84)
f_a	transistor common-base half-power frequency	(Sec. 5.3.1)
f_{Σ}	general output frequency	(Eq. 1.47)
f_T	transistor common-emitter half-power frequency	(Sec. 5.3.1)
G	perveance	(Eq. 5.95)
G_I	insertion gain	(Eq. 6.7)
$G_{nv}(f-y)$	narrowband lowpass nonlinear transfer function	(Eq. 3.28)
$G(v_2, v_3)$	zero-memory voltage dependent nonlinearity	(Eq. 2.22)
$G[x(t)]$	functional series expansion	(Eq. 1.10)
g_m	transconductance	(Eq. 5.107)
g_{mn}	zero-memory voltage dependent nonlinearity coefficients	(Eq. 2.22)
\hat{g}_n	n^{th} -order current source	(Eq. 2.71)
\hat{g}_{nm}	m^{th} -order interaction current source	(Eq. 2.72)
$g_{nv}(t)$	narrowband lowpass nonlinear impulse response	(Eq. 3.27)
g_T	transducer gain	(Eq. 6.1)
γ_n	charge power series coefficients	(Eq. 2.84)
H_{m+n}	$m+n$ order two-input nonlinear transfer function	(Eq. 2.201)
\hat{H}_n	n^{th} -order current source	(Eq. 2.81)
$H_n(f_1, f_2 \dots f_n)$	nonlinear transfer function of order n	(Eq. 1.30)

\hat{H}_{nm}	m^{th} -order interactive current source	(Eq. 2.80)
$H_n(t, f)$	n^{th} -order time-varying nonlinear transfer function	(Eq. 4.42)
$H_n^{\text{eq}}(f_1, f_2, \dots, f_o)$	equivalent n^{th} -order nonlinear transfer function	(Eq. 1.59)
h	integration step size	(Eq. 4.131)
h_{FE}	ratio of DC collector-to-base current	(Eq. 5.44)
h_{fe}	transistor small-signal linear common-emitter current gain	(Sec. 5.3.1)
h_i, h_r, h_f, h_o	H parameters	(Eq. 5.26)
h_{mn}	$m+n^{\text{th}}$ -order two-input nonlinear impulse response	(Eq. 2.200)
$h_n(t, \tau)$	n^{th} -order time-varying nonlinear impulse response	(Eq. 4.39)
$h_n(\tau_1, \tau_2, \dots, \tau_3)$	n^{th} -order nonlinear impulse response	(Eq. 1.12)
I	identity matrix	(Eq. 4.162)
$I_{C_{\max}}$	collector current for maximum h_{FE}	(Eq. 5.54)
I_n	n^{th} -order intercept	(Fig. 6.3)
I_s	diode saturation current	(Eq. 4.2)
$I_1(t), I_2(t)$	interfering signals	(Eq. 1.2)
$I_2^{\alpha\beta}$	Norton current source	(Eq. 2.179)
i_o	operating-point current	(Eq. 4.9)
i_r	resistor current	(Eq. 1.15)
i_s	space charge current	(Eq. 5.95)
$i(t)$	perturbation current	(Eq. 4.9)
j	loop current	(Eq. 4.1)

K_n	zero-memory voltage nonlinearity coefficients	(Eq. 2.14)
\hat{K}_n	n^{th} -order current source	(Eq. 2.40)
\hat{K}_{nm}	m^{th} -order interactive current source	(Eq. 2.46)
$K(V)$	zero-memory voltage nonlinearity	(Eq. 2.13)
k	Boltzman's constant	(Eq. 5.1)
k_n	nonlinear resistor coefficients	(Eq. 1.15)
$k(x, u)$	a nonlinear matrix	(Eq. 4.85)
$k_n(\xi_1, \xi_2 \dots \xi_n)$	n^{th} -order Volterra kernel	(Eq. 1.9)
λ	Eigenvalue	(Eq. 4.132)
M	avalanche multiplication factor	(Eq. 5.4)
m	pentode parameter	(Eq. 5.116)
\underline{m}	vector of index variables	(Eq. 1.49)
m_i	index variable	(Eq. 1.48)
$m(t)$	amplitude modulation	(Eq. 1.5)
μ	semiconductor capacitance exponent	(Eq. 5.2)
μ	vacuum tube amplification factor	(Eq. 5.102)
μ_1, μ_2	modulation frequencies	(Eq. 3.82)
n	diode ideality factor	(Eq. 5.5)
n	order of a nonlinearity	(Eq. 1.1)
$(n; m_1, m_2 \dots m_M)$	multinomial coefficient	(Sec. 2.1.2)
ν	a center frequency	(Eq. 3.21)
$\underline{\nu}$	a vector of center frequencies	(Sec. 3.2)
ν_k	center frequency of a narrowband signal	(Sec. 3.2)

ω_i	radian frequency	(Eq. 1.3)
P_n^t	n^{th} -order delivered power, dBm	(Eq. 6.5)
P_n^o	n^{th} -order output power for 0 dBm inputs	(Eq. 6.72)
$P(t; y)$	intermodulation waveform	(Eq. 3.17)
p_a	source available power	(Eq. 6.1)
P_n	n^{th} -order delivered power (watts)	(Eq. 6.1)
P_r	a reference power	(Eq. 6.3)
(p, q)	mixer (p, q) response index	(Sec. 1.9.2)
Φ	flux	(Eq. 2.62)
$\Phi(t, \tau)$	transition matrix	(Eq. 4.159)
ϕ	internal diode barrier potential	(Eq. 5.2)
ϕ	a vacuum tube potential	(Eq. 5.101)
ϕ_o	phase	(Sec. 3.5.2.2)
ϕ_n	flux power series coefficients	(Eq. 2.85)
ϕ_{pq}	Fourier expansion phase of $a_q(t)$	(Eq. 4.24)
Q_b	charge control model base charge	(Eq. 5.90)
$Q_{n\gamma}(f)$	spectrum of $q_{n\gamma}(t)$	(Eq. 3.32)
$Q(v)$	capacitance charge	(Eq. 2.84)
q	electron charge	(Eq. 5.1)
$q_n(t)$	complex envelope of $y_n(t)$	(Eq. 3.24)
$q_{n\gamma}(t)$	complex envelope of $y_{n\gamma}(t)$	(Eq. 3.25)

$\text{Re} \{ \}$	the real-part of { }	(Eq. 2.2)
$R(I)$	zero-memory current nonlinearity	(Eq. 2.16)
R_n	zero-memory current nonlinearity coefficients	(Eq. 2.18)
r_b	transistor base spreading resistance	(Sec. 5.3.1)
r_c	transistor collector resistance	(Sec. 5.3.1)
r_e	transistor base-emitter resistance	(Sec. 5.3.1)
r_p	plate resistance	(Eq. 5.107)
s	elastance	(Eq. 5.3)
s_1	amplitude of desired tone	(Eq. 1.3)
$s_{11}, s_{12}, s_{21},$ s_{22}	S parameters	(Eq. 5.35)
$s_1(t)$	desired signal	(Eq. 1.2)
σ	time-domain variable	(Eq. 1.22)
T	absolute temperature	(Eq. 5.1)
$T_{\alpha\beta}$	impedance correction factor	(Eq. (2.178))
τ	time-domain variable	(Eq. 1.12)
U_n	n^{th} order quadratic functions	(Eq. 2.97)
\underline{U}_n	n^{th} order quadratic function vector	(Eq. 2.98)

u	large-signal source voltage	(Eq. 4.1)
u_d	voltage across a diode	(Eq. 4.1)
$u_d(i_o)$	operating-point diode voltage	(Eq. 4.10)
V_{BD}	avalanche breakdown voltage	(Eq. 5.4)
V_{CBO}	sustaining voltage	(Eq. 5.45)
v	element voltage	(Eq. 1.15)
v_d	diode perturbation voltage	(Eq. 4.10)
$v_g(t)$	Thevenin generator voltage	(Eq. 2.19)
$X(f)$	voltage spectrum of $x(t)$	(Eq. 1.32)
x_o, x_{ck}, x_{sk}	spectral amplitudes	(Eq. 3.85)
$x(t)$	system time-domain input	(Eq. 1.1)
$Y(f)$	voltage spectrum of $y(t)$	(Eq. 1.33)
$Y(p)$	admittance operator	(Eq. 2.25)
$[Y(p)]$	admittance operator matrix	(Eq. 2.27)
y_i, y_r, y_f, y_o	Y parameters	(Eq. 5.23)
y_o, y_{ck}, y_{sk}	spectral amplitudes	(Eq. 3.85)
$y(t)$	system time-domain output	(Eq. 1.1)

$Z(f)$	spectrum of $z(t)$	(Eq. 3.7)
Z_i^β	input impedance of β stage	(Sec. 2.3.3.2)
Z_o^α	output impedance of α stage	(Eq. 2.178)
$z(t)$	complex envelope of $x(t)$	(Eq. 3.3)

SUBJECT INDEX

- Adjacent channel, 5, 153
Admittance matrix, 55
AGC, 5, 277, 537, 544
Alpha, 309
Analytic system, 46
Antenna, 5
A-stable, 262
Avalanche breakdown, 283, 324
Avalanche nonlinearity,
 transistor, 85, 324
- Base resistance, 342
Branch, 239
Breakdown voltage, 283
- Cascade, 99, 552, 636
Canonic model, 2, 41, 139,
 583
Frequency power series,
 140, 149, 194, 583
 AM-FM, 172
 FM-AM, 184
 AM-FM, 190
 FM-FM, 190
Tapped delay line,
 140, 161, 590
- Circuit analysis, small
 signal, 40, 48, 73
- Cochannel, 5, 153
Coherency, 38
Collector capacitance, 337
Collector resistance, 343
Communications receiver, 3
 HF, 609
 Equivalent power
 series, 631
 Interstage networks,
 614
 Mixers, 630
 Operating points, 627
 RF amplifier, 633
- VHF, 492, 537
Detector, 537
IF amplifier, 498, 528, 561,
 567, 570
Image response, 549
Modeling, 501
Pre-IF amplifier, 496, 524
RF tuner, 492, 514, 590
SIGNCAP coding, 689
- Complex signal, 27, 41
Compression, 9, 10, 31, 153, 435, 561
Convolution, 19
Corrector, 259
Crossmodulation, 9, 11, 153, 170, 567,
 570, 590
Current controlled nonlinearity, 64
Cutoff frequency, 309
- Demodulator, 3
Detector, 537, 538, 541
Dependent nonlinearity, 53, 68
Depletion layer capacitance,
 278, 308
Desensitization, 9, 10, 31, 170, 450
Diffusion capacitance, 285, 307
Diode, 208, 277
 Ideality factor, 297, 322
 Junction, 277, 288
 Vacuum, 356
- Ebers-Moll, 303, 319
Eigenvalue, 261
Emitter capacitance, 338, 340
Equivalent nonlinear transfer
 function, 37, 517, 549, 631
Excess elements, 239
Explicit integration, 259
Exponential nonlinearity, 85, 318, 411

Fourier transform, 1, 25, 147, 163, 258
Functional, 13
Frequency conversion, 36
Frequency domain, 52, 506

H parameters, 310
Hysteresis, 47
hFE nonlinearity, 85, 328
hfe, 309, 330

IF, 37
Image response, 549
Impedance, 5
Implicit integration, 259
Inband, 5
Incremental model, 276
Input impedance, 614
Insertion gain, 394, 505, 524, 534
Interaction, 99
Intercept, 405, 423
Intermodulation, 9, 12, 31, 43, 144, 153, 423, 445, 458, 459
Interstage network modeling, 505

Jacobian, 251

Kirchoff's voltage law, 208

Large signal, 2, 47, 205, 208, 210, 465, 609
Link, 239
Local oscillator, 38, 219, 504
Loop equation, 208

Memory, 7, 9, 13, 25, 49
Memory nonlinearity, 53, 71
Mixer, 3, 36, 403, 430
(p,q) response, 37
Multinomial, 44, 60, 97
Multiple input nodes, 128
Multiple signals, 5, 8, 30

Narrowband, 5
Signal, 140
Newton-Raphson, 205, 263
Nominal receiver, 601, 697
Nonlinear
Capacitance, 85
Circuit, 1, 8, 15
Conductance, 53, 54
Current generator, transistor, 332
Differential equations, 207
Impulse response, 1, 8, 20, 23, 142
Inductance, 67
Resistor, 16, 53, 65
System, 1
Transfer function, 1, 8, 55, 105, 142, 421, 445, 517, 526, 535, 549, 609
Numerical integration, 1, 210, 258

Operator, 54
Operating point, 227
Equation, 213, 248
Order, 15, 259
Out-of-band, 5

Parasitic parameters, 510
Periodic solution, 206, 270
Perturbation, 206, 212
Perturbation equation, 213, 224, 248, 270
Phase, 38

Power

Available, 392
Delivered, 392, 403, 409
Series, 7, 9, 26, 210, 636
Small signal limit, 403,
 411

Recurrence, 90

Reversion of series, 218, 335

Sampling theorem, 162

S-parameters, 313
SIGNCAP, 38, 552, 609, 643
Small signals, 2, 47, 403, 411,
 425

Specification sheet modeling, Unit impulse, 25, 27
 697

Spectrum, 24, 147

 Signature, 9

Stability, 260

State equation, 207, 236

Step size, 259

Stiff equations, 207, 261

Strongly drive, see large
 signal

Sustaining voltage, 327

Symmetric, 45, 62

Taylor series, 23, 49, 64, 154,
 211, 276

Thevenin, 114

Time

 domain, 205

 varying coefficients, 217

 varying linear differen-
 tial equation, 225

 varying Volterra series,
 205, 223, 226, 265

Total model, 276, 467

Transducer gain, 392

Transistor, 3, 303

Amplifier

large-signal, 465
single-stage, 415
two-stage, 440

Model

charge-control bipolar, 350
field effect, 349
bipolar nonlinear T, 83, 305,
 316, 344

Parameters

2N918, 708
2N2950, 345, 415
SA395, 444

Tree, 239

Truncation, 47

Vacuum tube, 3, 356

Amplifier

 triode, 453
 pentode, 459

Diode, 359

Parameters, 390, 456, 461

Pentode, 374

Triode, 359

Vector-matrix differential
 equation, 238, 268

Volterra series, 7, 14, 24, 46, 205

Waveform distortion, 570

Wideband, 5

y parameters, 310

Z parameters, 637